

**Studies on the Decomposition of Selected Brominated
Flame Retardants (BFRs) and Formation of
Polybrominated Dibenzo-*p*-dioxins and Dibenzofurans
(PBDD/Fs) and Mixed Halogenated Dibenzo-*p*-dioxins and
Dibenzofurans (PXDD/Fs)**

**A Thesis Submitted for the Degree of
Doctor of Philosophy in Chemical Engineering**

Anam Saeed

M.Sc. Chemical Engineering

B.Sc. Chemical Engineering



MURDOCH
UNIVERSITY
PERTH, WESTERN AUSTRALIA

October, 2016

School of Engineering and Information Technology

Murdoch University

DECLARATION

I hereby declare that the material embodied in this thesis is my own account of my research and contains as its main content work which has not previously been submitted for a degree or diploma at any tertiary education institution. To the best of my knowledge and belief this thesis is the result of original research, contains no material previously published or written by another person, except where due reference has been made in the text.

Signature: _____

Date: _____

6/10/2016

Anam Saeed

STATEMENT OF CONTRIBUTION OF OTHERS

We, the undersigned, attest that Research Higher Degree candidate, Anam Saeed, has carried out the experiments, result analysis, computational work and writing in all papers included in this thesis.



Dr Mohammednoor Altarawneh

6/10/2016

Date:



Professor Bogdan Dlugogorski

6/10/2016

Date:

ABSTRACT

Brominated flame retardants (BFRs) are bromine-bearing hydrocarbons added or applied to materials to increase their fire resistance. As thermal treatment or recycling activities are common disposal methods for BFR-laden objects, it is essential to determine the precise decomposition chemistry of BFRs at elevated temperatures, and their transformation pathways into hazardous pollutants. Sunlight can trigger the photodecomposition of BFRs, either during the life cycle of treated objects, or when emitted to the environment after disposal. Therefore, knowledge of the geometric and electronic structures of BFRs is of chief importance when tracking their fate in the ambient environment.

Although BFR decomposition mainly occurs in a condensed phase, gas phase reactions also contribute significantly to their overall decay and subsequent fragmentation into brominated pollutants. Thermal degradation of BFRs often proceeds in the presence of bromine atoms which inhibit complete combustion. Therefore, under thermal conditions such as smouldering, municipal waste incineration, pyrolysis, thermal recycling, uncontrolled burning and fires, BFRs degrade to form brominated products of incomplete combustion (BPICs). Thermal degradation of BFRs produces potent precursors to polybrominated dibenzo-*p*-dioxins and dibenzofurans (PBDD/Fs). Co-combustion of BFR-containing objects with a chlorine source (e.g., polyvinyl chlorides) results in the emission of significant concentrations of mixed halogenated dibenzo-*p*-dioxins and dibenzofurans (i.e., PXDD/Fs; X = Br, Cl).

In this thesis, we investigated the thermochemical parameters of bromochlorophenols (BCPhs) and the photodecomposition properties of major BFRs and their derived brominated phenols (BPhs). We scrutinised the formation of brominated and non-brominated products that evolved during the thermal decomposition of major BFR i.e., tetrabromobisphenol A (TBBA), through experimental measurements coupled with accurate quantum chemical calculations. We acquired thermo-kinetic parameters as well as mechanistic routes pertinent to the destruction of TBBA. We illustrated reaction networks for the synthesis of PXDD/Fs from BPhs and chlorinated phenols (CPhs). Similarly, we described pathways leading to the formation of PBDFs and polybrominated diphenylethers (PBDEs) from brominated benzenes (BBzs).

We critically reviewed the literature on BFR thermal decomposition with specific foci on underlying mechanisms, decomposition products, the influence of the polymeric matrix, metallic content and operational conditions.

As BCPs are direct building blocks for the formation of PXDD/Fs, we computed the thermochemical parameters of their complete series. We calculated standard enthalpies of formation, entropies, heat capacities and bond dissociation enthalpies (BDHs) of O-H bonds for the complete series of BCPs. Values of the acid dissociation constant (pK_a) were estimated based on an accurate thermodynamic cycle incorporating solvation and protonation energies. Calculated values of BDHs of O-H bonds in BCPs vary slightly with the change in degree and pattern of halogenation. Gibbs energies of solvation of BCPs in water are highly exergonic, with their values increasing with the degree of halogen substitution. Values of pK_a dictate that BCPs characterised by high degrees of halogenation display stronger acidity and dissociate more easily in aqueous media (i.e., they are stronger acids than lower substituted phenols).

Photolysis and photochemical decomposition are important channels for the degradation of halogenated organic pollutants in the environment. Therefore, we performed density functional theory (DFT) and time-dependent density functional theory (TDFT) calculations in order to derive the photodecomposition properties of major deployed BFRs and congeners of BPhs in both gaseous and aqueous media. We clarified the effect of degree and pattern of bromination on the photodebromination of selected brominated aromatic compounds based on several molecular descriptors; namely, geometries of the ground (S_0) and electronically first excited (S_1) states, values of the HOMO-LUMO energy gap (E^{H-L}) and atomic charges on bromine atoms (q_{Br}). Molecules exhibit different geometries in the S_0 and S_1 states and C-Br bonds elongate upon $S_0 \rightarrow S_1$ transitions. In agreement with the recent findings on PBDEs, we found that the photoreactivity of bromine atoms in investigated BFRs and BPhs followed the sequence of *ortho* > *meta* > *para*. The bromine atom connected to the *ortho*-position holds the highest positive atomic charge and, thus, experiences the greatest lengthening of C-Br bonds in the S_1 state, in both gaseous and an aqueous media, prompting their reductive debromination. Excitation energies decrease linearly with increasing numbers of bromine substituents, and congeners with a high degree of bromination photodecompose more readily than lower brominated isomers. Computed values of E^{H-L} for major BFRs and their non-brominated

molecules inferred that the number of bromine substituents and the nature of the structure (aromatic/non-aromatic) contributes significantly towards the photoreactivity of molecules.

We conducted gas phase thermal decomposition of TBBA using a laboratory-scale tubular reactor. Our main focus was to identify pollutants arising in the temperature range of 673 – 1123 K following evaporation of TBBA in the gas phase. The identification and quantitation involved the use of a gas chromatograph – triple quadrupole mass spectrometer (GC-QQQMS) instrument, functioning in multiple reaction monitoring (MRM) and total ion current (TIC) modes. Product analysis revealed that thermal decomposition of TBBA commenced at 723 K. The major decomposition products were HBr, di-tribrominated bisphenols, benzene, phenol, mono-tribrominated congeners of benzene and phenol, brominated and non-brominated alkylated benzenes, benzofuran, bromobenzofuran, dibenzofuran, bromine substituted polyaromatic hydrocarbons (PAHs), biphenyl and biphenylene. We observed that, most of the decomposition products evolved in trivial concentrations at a temperature of 773 K and peaked at around 923 – 973 K. Higher temperatures favour the generation of non-brominated products. In this chapter, we have performed quantum chemical calculations to derive the degradation pathways of TBBA and to illustrate routes for the formation of brominated and non-brominated species.

We constructed formation mechanisms related to the emission of PBDD/Fs in systems involving BFRs. In particular, we investigated formation corridors of (i) PXDD/Fs from the coupling reactions of 2-chlorophenoxy (2-CPhxy) and 2-bromophenoxy (2-BPhxy) radicals, (ii) PBDFs and PBDEs synthesis from the condensation reaction of monobromobenzene (MBBz) and a 2-BPhxy radical. The coupling reactions of 2-BPhxy and 2-CPhxy radicals produce keto-ether (through the additions of a phenoxy O at *ortho* C(H), C(Cl) and C(Br) sites) and diketo (at *ortho* positions to C–C bridges) structures. Keto-ethers act as direct intermediates for the formation of dioxin moieties such as dibenzo-*p*-dioxin (DD), 1-monochlorodibenzo-*p*-dioxin (1-MCDD), 1-monobromodibenzo-*p*-dioxin (1-MBDD), 1-bromo-6-chlorodibenzo-*p*-dioxin (1-B,6-CDD) and 1-bromo-9-chlorodibenzo-*p*-dioxin (1-B,9-CDD) molecules. Diketo adducts initiate the formation of furan species, i.e., 4-monochlorodibenzofuran (4-MCDF), 4-monobromodibenzofuran (4-MBDF) and 4-bromo-6-chlorodibenzofuran (4-B,6-CDF) compounds, through interconversion and rearrangement reactions. We found that, these mechanisms of formation, commencing from halogenated phenoxy radicals, are largely insensitive to patterns and degrees of halogenation on *meta* and

para sites. It follows that, our developed mechanistic and kinetic factors of reactions involving 2-BPhxy and 2-CPhxy should also apply to higher halogenated phenoxy radicals.

We explored the initial oxidative decomposition pathways of monobromobenzene (MBBz) in the generation of BPhxy radicals and examined the possible dimerisation reactions of MBBz and 2-BPhxy. It was found that, the coupling of MBBz and 2-BPhxy results in the generation of twelve pre-PBDF intermediates, of which four can also serve as building blocks for the synthesis of PBDEs. The resonance-stabilised structure of the *o*-BPhxy radical accumulates more spin density character on its phenoxy O atom (30.9 %) in reference to *ortho*-C and *para*-C sites. Thus, the formation of the pre-PBDE/pre-PBDF structures via O/*o*-C couplings advances faster, as it requires lower activation enthalpies (79.2 – 84.9 kJ mol⁻¹) than the pre-PBDF moieties, which arise via pairing reactions involving *o*-C(H or Br)/*o*-C(H or Br) sites (97.2 – 180.2 kJ mol⁻¹). Kinetic analysis indicates that the O/*o*-C pre-PBDE/pre-PBDF adducts self-eject the out-of-plane H atoms to produce PBDEs, rather than undergo a three-step mechanism that forms PBDFs. Since the formation mechanisms of PBDFs and PBDDs are typically only sensitive to the bromination at *ortho* positions, the results reported herein also apply to higher brominated isomers of BBzs.

Overall, this thesis provides novel and comprehensive information on the thermochemical properties of the complete series of BCPhs (potential precursors to PXDD/Fs) and the electronic/structural characteristics of BFRs and their derived BPhs, with regards to their photodecomposition. To gain an insight into the degradation of TBBA once it has evaporated, this thesis examines the pure gas phase decomposition of TBBA and suggests mechanisms by which the experimentally-detected volatile organic compounds (VOCs) and semi-volatile organic compounds (SVOCs) are generated. Furthermore, this thesis explores the role of BPhs and CPhs as building blocks for the formation of PXDD/Fs, and computes their parameters. We also elucidate reaction pathways and thermo-kinetic parameters for PBDFs and PBDEs produced by the oxidation of BBzs.

PUBLICATIONS RELATED TO THE CURRENT RESEARCH

INTERNATIONAL JOURNAL ARTICLES

1. **Saeed, A.**, Altarawneh, M., Dlugogorski, B.Z. Formation of mixed halogenated dibenzo-*p*-dioxins and dibenzofurans (PXDD/Fs). *Chemosphere* **2015**, 137, 149-156.
2. **Saeed, A.**, Altarawneh, M., Hefter, G., Dlugogorski, B.Z. Thermodynamic parameters including acid dissociation constants for bromochlorophenols (BCPs). *J. Chem. Eng. Data* **2016**, 61, 160-172.
3. **Saeed, A.**, Altarawneh, M., Dlugogorski, B.Z. Photodecomposition of bromophenols. *Chemosphere* **2016**, 150, 749-758.
4. **Saeed, A.**, Altarawneh, M., Jansson, S., Dlugogorski, B.Z. Formation of polybrominated dibenzofurans (PBDFs) and polybrominated diphenyl ethers (PBDEs) from oxidation of brominated flame retardants (BFRs). *Environ. Sci. Technol.* Submitted.
5. **Saeed, A.**, Altarawneh, M., Siddique, K., Dlugogorski, B.Z. Properties of brominated flame retardants (BFRs) at the verge of their photodecomposition. In progress.
6. Altarawneh, M., **Saeed, A.**, Dlugogorski, B.Z. Thermal decomposition of brominated flame retardants (BFRs): Products and mechanisms. In progress.
7. **Saeed, A.**, Dlugogorski, B.Z., Sakai, S., Ortuño, N., Conesa, J.A., Font, R., Altarawneh, M. Thermal Decomposition of Tetrabromobisphenol A (TBBA). In progress.

CONFERENCE PAPERS

1. **Saeed, A.**, Altarawneh, M., Dlugogorski, B.Z. Reactions of 2-chlorophenol and 2-bromophenol: mechanisms of formation of mixed halogenated dioxins and furans (PXDD/Fs). *Organohalogen Compd.* **2015**, 76, 345-348.
2. **Saeed, A.**, Altarawneh, M., Dlugogorski, B.Z. Formation of PBDFs and PBBs from bromobenzenes. *Organohalogen Compd.* **2015**, 77, 606-609.
3. **Saeed, A.**, Altarawneh, M., Dlugogorski, B.Z. Formation of brominated and non-brominated species from gas-phase thermal decomposition of TBBA. 14th International Congress on Combustion By-Products and their Health Effects. PIC**2015**.A. 149.

4. **Saeed, A.**, Dlugogorski, B. Z., Altarawneh, M. Formation of PBDD/Fs precursors in gas-phase decomposition of tetrabromobisphenol A (TBBA). *Organohalogen Compd.* Accepted.

TABLE OF CONTENTS

DECLARATION	II
ABSTRACT.....	IV
PUBLICATIONS RELATED TO THE CURRENT RESEARCH.....	VIII
TABLE OF CONTENTS.....	X
ACKNOWLEDGEMENTS.....	XV
CHAPTER 1 INTRODUCTION	1
1.1. Research background	2
1.2. Project objectives	3
1.3. Thesis outline	5
CHAPTER 2 LITERATURE REVIEW	10
2.1. Introduction.....	12
2.2. Methodologies.....	15
2.2.1. Experimental apparatus	15
2.2.1.1. Thermogravimetry (TG)	15
2.2.1.2. Differential scanning calorimetry (DSC)	16
2.2.1.3. Pyrolysis gas chromatography mass spectrometry (Py-GC/MS)	16
2.2.1.4. Tubular reactor assembly.....	17
2.2.1.5. Incinerators	18
2.2.2. Analytical methodologies.....	18
2.2.2.1. Volatile and semi-volatile organic compounds	18
2.2.2.2. HBr emissions.....	19
2.2.2.3. Analysis of CO ₂ , CO and nitrogen content.....	19
2.2.3. Theoretical modelling	20
2.3. Thermal decomposition of major BFRs.....	21
2.3.1. Thermal decomposition of TBBA.....	21
2.3.1.1. Overall decay of pure TBBA	21
2.3.1.2. Decomposition products	24
2.3.1.3. Mechanisms of thermal decomposition of pure TBBA.....	29
2.3.1.4. Kinetic modelling	35
2.3.1.5. Decomposition of polymeric materials laden with TBBA	37
2.3.1.6. Fixation of Br content in TBBA via introducing metal oxides	42
2.3.2. Thermal decomposition of HBCDs.....	43
2.3.3. Thermal decomposition of PBDEs and polybrominated biphenyls (PBBs)	46

2.3.3.1. Degradation of pure PBDEs	49
2.3.3.2. Effects of polymers on the generation of PBDD/Fs from PBDEs	51
2.3.3.3. Decomposition of PBBs	53
2.3.4. Decomposition of 1,2-Bis-(2,4,6-tribromophenoxy)ethane (BTBPE).....	55
2.4. Combustion behaviour of bromine	56
2.4.1. Speciation of bromine during decomposition of BFRs	56
2.4.2. Bromine reactions with H/O species	58
2.4.3. Bromine reactions with hydrocarbon species.....	60
2.5. Formation of PBDD/Fs	61
2.5.1. Pathways to PBDD/Fs from bromophenols	63
2.5.1.1. Homogenous formation of PBDD/Fs from bromophenols.....	66
2.5.1.2. Formation of PBDD/Fs from catalytic-assisted coupling of bromophenols	71
2.5.2. De novo synthesis of PBDD/Fs.....	72
2.5.3. Bromination mechanisms	74
2.6. Formation of PXDD/Fs.....	77
2.6.1. Formation of PXDD/Fs from mixed halogenated phenols.....	77
2.6.2. Formation of PXDD/Fs from BFRs-containing materials	79
2.6.3. De novo formation of PXDD/Fs	87
References.....	89
CHAPTER 3 RESEARCH METHODOLOGY	110
3.1. Experimental methodology	111
3.1.1. Experimental apparatus	111
3.1.1.1. Solid vaporiser	112
3.1.1.2. Tubular reactor	112
3.1.1.3. Product collection system	117
3.1.2. Chemicals	117
3.1.3. Methods.....	118
3.1.3.1. Experimental procedure.....	118
3.1.3.2. Product analysis	119
3.2. Computational methodology.....	126
3.2.1. Ab initio calculations	126
3.2.2. Hartree-Fock method.....	127
3.2.2. Density functional theory	128
3.2.2.1. The Thomas-Fermi model	128
3.2.2.2. The Hohenberg-kohn theorem.....	129

3.2.2.3. Kohn-sham DFT	130
3.2.2.4. The exchange-correlation functional	131
3.2.3. Computational tools	134
3.2.3.1. Gaussian09.....	134
3.2.3.2. Dmol ³	135
3.2.3.3. ChemRate	135
3.2.3.4. KiSThelP	135
CHAPTER 4 THERMODYNAMIC PARAMETERS INCLUDING ACID DISSOCIATION CONSTANTS FOR BROMOCHLOROPHENOLS (BCPhs)	143
Abstract.....	144
4.1. Introduction	145
4.2. Computational details.....	146
4.3. Results and discussion.....	147
4.3.1. Optimised geometries	147
4.3.2. Heat capacities and standard entropies	147
4.3.3. Standard enthalpy of formation of BCPhs and their radicals	155
4.3.4. Bond dissociation enthalpies	160
4.3.5. Gibbs energies of formation of BCPhs and their anions in gaseous and aqueous phases.....	162
4.3.6. Acid dissociation constants (p <i>K</i> _a).....	163
4.4. Conclusions	168
Supporting information.....	168
References.....	169
CHAPTER 5 PHOTODECOMPOSITION OF BROMOPHENOLS.....	179
Abstract.....	180
5.1. Introduction	181
5.2. Computational details.....	182
5.3. Results and discussion.....	183
5.3.1. Optimised geometries for BPhs in ground and first excited states.....	183
5.3.2. Effect of degree and pattern of bromination on the photoreactivity.....	187
5.3.3. UV-Vis absorption.....	191
5.4. Conclusions.....	199
Acknowledgments.....	199
References.....	201
CHAPTER 6 PROPERTIES OF BROMINATED FLAME RETARDANTS (BFRs) ON THE VERGE OF THEIR PHOTODECOMPOSITION	207

Abstract.....	207
6.1. Introduction.....	209
6.2. Computational details	211
6.3. Results and discussion	213
6.3.1. Optimised structures in ground and excited states for selected BFRs	213
6.3.2. Frontier molecular orbitals; the HUMO-LUMO energy gap	217
6.3.3. Charge distribution.....	219
6.3.4. Optical properties including UV-Vis absorption spectra, excitation energies and oscillation strengths.....	221
6.4. Conclusion	230
Acknowledgments.....	230
References.....	231
CHAPTER 7 THERMAL DECOMPOSITION OF TETRABROMOBISPHENOL A (TBBA)	239
Abstract.....	240
7.1. Introduction.....	241
7.2. Methodology	244
7.2.1. Materials.....	244
7.2.2. Experimental setup and procedure	245
7.2.2.1 Blanks and replicates	248
7.2.3. Computational methodology	249
7.3. Results and discussion	249
7.3.1. TBBA decomposition.....	249
7.3.2. Formation of brominated bisphenols and HBr	251
7.3.3. Formation of brominated phenols, brominated alkylated phenols, brominated benzenes and brominated alkylated benzenes	253
7.3.4. Formation of polyaromatic hydrocarbons (PAHs).....	257
Supporting information.....	261
Acknowledgements.....	261
CHAPTER 8 FORMATION OF MIXED HALOGENATED DIBENZO-<i>P</i>-DIOXINS AND DIBENZO FURANS (PXDD/F_S)	267
Abstract.....	268
8.1. Introduction.....	269
8.2. Computational details	271
8.3. Results and discussion	271
8.3.1. Formation of 2-chlorophenoxy and 2-bromophenoxy radicals.....	272

8.3.2. Reactions of 2-chlorophenoxy and 2-bromophenoxy radicals.....	272
8.3.3. Formation of DD, 1-MBDD, 1-MCDD, 1-B,6-CDD and 1-B,9-CDD	273
8.3.4. Formation of 4-MCDF, 4-MBDF and 4-B,6-CDF.....	276
8.3.5. Reaction rate constant calculations	277
8.4. Conclusion	282
Supporting information.....	283
Acknowledgments.....	283
References.....	284
CHAPTER 9 FORMATION OF POLYBROMINATED DIBENZOFURANS (PBDFs) AND POLYBROMINATED DIPHENYL ETHERS (PBDEs) FROM OXIDATION OF BROMINATED FLAME RETARDANTS (BFRs)	291
Abstract.....	292
9.1. Introduction.....	293
9.2. Computational details	295
9.3. Results and discussion	296
9.3.1. Formation of pre-PBDFs and pre-PBDEs.....	296
9.3.2. Formation of PBDFs and DBDEs	298
9.3.3. Reaction rate constants.....	303
9.4. Conclusions.....	307
Acknowledgments.....	307
Supplementary material	308
References.....	309
CHAPTER 10 CONCLUSION AND RECOMMENDATIONS	315
10.1. Conclusion	316
10.2. Recommendations for future work	320
APPENDICES	323
APPENDIX A (CHAPTER 3).....	324
APPENDIX C (CHAPTER 6)	325
APPENDIX D (CHAPTER 7).....	328

ACKNOWLEDGEMENTS

First and foremost, I would like to express my profound gratitude to my supervisors, Dr Mohammednoor Altarawneh and Prof. Bogdan Z. Dlugogorski, for their sound advice, encouragement, patience and continuous support during my doctoral study. I genuinely appreciate their guidance and their contributions of time, ideas and funding, which have made my research inspiring and productive. Their useful comments during my research write-up have greatly improved my writing skills, which is a huge achievement for me. I would also like to thank Murdoch University, Australia, for awarding me a postgraduate research scholarship. I also acknowledge the support provided by the Australian Research Council (ARC) and the computing time granted by the National Computational Infrastructure (NCI), Australia, and the Pawsey Supercomputing Centre in Perth.

I am sincerely grateful to Dr Juita for her assistance and useful suggestions for my experimental work. The members of Fire Safety and Combustion Kinetics group, Kamal Siddique, Ibukun Oluwoye, Zhe Zeng, Niveen Assaf and Nassim Zeinali have been a source of insightful discussions that helped me in my project. Their company taught me the virtues of teamwork. I would also like to acknowledge all staff at the Department of Engineering and Information Technology for their administrative assistance.

I would like to thank my parents (Mr and Mrs Anwar Saeed Khan) for their love, encouragement and support throughout my life. They gave me the strength and opportunity to chase my dreams and to be what I am today. I especially appreciate my brother (Talha) and sisters (Anza and Huriya) for their generous love and support. I am grateful to my in-laws for their prayers. A special thanks to my daughter Hoorain for her patience and love. Last, but not least, the person who was with me throughout my PhD journey and made completion possible was my husband and colleague, Kamal Siddique. Enormous thanks are due to all my friends who encouraged me to fulfil this project. I thank you all.

DEDICATION

I would like to dedicate my thesis to my beloved parents

(Anwar Saeed Khan and Awaisa Saeed)

LIST OF ABBREVIATION

BFRs	brominated flame retardants
PBDD/Fs	polybrominated dibenzo- <i>p</i> -dioxins and dibenzofurans
PXDD/Fs	mixed halogenated (brominated chlorinated) dibenzo- <i>p</i> -dioxins and dibenzofurans
PCDD/Fs	polychlorinated dibenzo- <i>p</i> -dioxins and dibenzofurans
BPICs	brominated products of incomplete combustion
PBDEs	polybrominated diphenyl ethers
HBCD	hexabromocyclododecane
TBBA	tetrabromobisphenol A
POPs	persistent organic pollutants
NBFRs	novel brominated flame retardants
FRs	flame retardants
e-waste	electronic waste
TGA	thermogravimetric analysis
DSC	differential scanning calorimetry
Py-GC/MS	pyrolysis-gas chromatography mass spectrometry
FTIR	fourier transform infrared spectroscopy
VOC	volatile organic compounds
SVOC	semi-volatile organic compounds
STDS	system of thermal diagnostic studies
PAH	polyaromatic hydrocarbons
ASE	accelerated solvent extractor
PLE	pressurised liquid extraction
DCM	dichloromethane
EI	electron impact
SIM	selective ion monitoring
ECNI	electron capture negative ion
ECD	electron capture detector
FID	flame ionisation detector
GLC	gas liquid chromatograph
MSW	municipal solid wastes
CEM	continuous emission monitor
TIC	total ion current
BDHs	bond dissociation enthalpies
BPhs	bromophenols
CPhs	chlorophenols
HBr	hydrogen bromide
PBBs	polybrominated biphenyls
PBT	polybutylene terephthalate polymers
MRM	multiple reactions monitoring
DD	dibenzo- <i>p</i> -dioxin
DF	dibenzofuran
CPhxy	chlorophenoxy
BPhxy	bromophenoxy

PXDEs	mixed halogenated congeners of diphenyl ether and biphenyl
PXBs	mixed halogenated biphenyls
DFT	density functional theory
TDDFT	time dependant density functional theory
COSMO	conductor-like screening model
S ₀	ground state
S ₁	first excited state
ALDA	local exchange density functional approximation
HOMO	highest occupied molecular orbital
LUMO	lowest unoccupied molecular orbital
HF	Hartree-Fock
SCF	self-consistent field approach
MCSCF	multi-configuration self-consistent field theory
LDA	local density approximation
GGA	generalised gradient approximation
VASP	Vienna ab initio simulation package
ADF	Amsterdam density functional
PE	polyethylene
ABS	acrylonitrile butadiene styrene
E _a	activation energy
A	pre-exponential factor/arrhenius parameter
PVC	polyvinyl chloride
I.D.	inner diameter
O.D.	outer diameter
B ₂ O ₃	boron trioxide
GC	gas chromatograph
MS	mass spectrometer
QQQ	triple quadruple
<i>m/z</i>	mass to charge ratio
CID	collision induced dissociation
S/N	signal to noise ratio
CE	collision energy
$\Delta_f H^\circ_{298}$	standard gas-phase enthalpy of formation
S°_{298}	standard gas-phase entropy
$C_p^\circ(T)$	heat capacity
ΔG^*_{solv}	gibbs energy of solvation
BCPh	bromochlorophenol
$\Delta_{R1} H^\circ_{298}$	reaction enthalpy
p <i>K</i> _a	acid dissociation constants
$E^{\text{H-L}}$	HOMO-LUMO energy gap
<i>q</i> _{Br}	charge on bromine atom
IRC	intrinsic reaction coordinate
TST	transition state theory
KiSThelP	kinetic and statistical-thermodynamic program
TS	transition state

BBzs	bromobenzenes
MBBz	monobromobenzene
PBDEs	polybrominated diphenylethers
TST	transition state theory
GC-QQMS	gas chromatograph triple quadruple mass spectrometer

CHAPTER 1 INTRODUCTION

Table of Contents

1.1. Research background	2
1.2. Project objectives	3
1.3. Thesis outline	5

1.1. Research background

Brominated flame retardants (BFRs) denote a group of chemicals, added to various consumer products (namely; polymeric materials, furniture and carpets, electric and electronic equipments, fabrics and building insulations) to reduce their flammability and delay their ignition. Owing to their cost effectiveness, low decomposition temperatures and minimal influence on the mechanical properties of treated objects, BFRs have gradually substituted other types of flame retardants (FRs); including inorganic FRs, chlorinated FRs and nitrogen containing FRs. Therefore, high global market demand over the past few decades has dramatically raised the production of BFRs. BFRs are typically added to materials at high loads, for example, BFRs may constitute 5.0 – 10.0 % (by weight) of treated plastics and 19.0 % (by weight) of printed circuit boards.

Thermal degradation of BFRs releases bromine which acts as an active agent to trap dynamic free O/H radicals, thereby interrupting the chemical chain reactions present in the fire. This inhibits the complete combustion process and it facilitates the production of a wide range of toxic products of incomplete combustion (PICs). Major PICs include brominated benzenes and phenols, in addition to a wide range of brominated aromatics. Brominated benzenes and brominated phenols serve as direct building blocks for the formation of polybrominated dibenzo-*p*-dioxins and dibenzofurans (PBDD/Fs); a group of chemicals that shares similar notorious properties with their chlorinated counterparts (PCDD/Fs). The co-existence of BFRs and polyvinyl chlorides (PVCs) in fires of household, electrical and electronic wastes establishes a unique environment for the generation of mixed chlorinated and brominated dibenzo-*p*-dioxins and furans (PXDD/Fs; X = Br, Cl).

Along with their harmful decomposition products (range of volatile and semi-volatile organic compounds), BFRs themselves are introduced to the environment from many thermal systems, including uncontrolled fires, recycling facilities and municipal waste incinerators. Once emitted into air and water bodies, BFRs exhibit a profound tendency to undergo long-range atmospheric transport to remote areas and tend to bioaccumulate in the food chain. Consequently, these compounds have been detected

at alarming rates in several environmental matrices, including air samples, water bodies, sewage sludge and sediments.

Thus, it is important to understand the combustion chemistry of BFRs and to reveal the mechanistic pathways that operate in their transformation into phenols, benzenes, PBDD/Fs and PXDD/Fs. Via combined theoretical and experimental approaches, this thesis broadly aims to: (i) compute thermodynamic and kinetic parameters that govern the environmental and combustion behaviour of BFRs, (ii) report the electronic and structural properties of BFRs and their derived brominated phenols (BPhs) on the verge of their photodecomposition, in gaseous and aqueous media, (iii) explore the formation of brominated and non-brominated pollutants from the gas phase pyrolysis of the most commonly deployed BFR i.e., tetrabromobisphenol A (TBBA), (iv) illustrate the complex mechanistic pathways operating in the generation of brominated and non-brominated pollutants from the destruction of TBBA, (v) elucidate mechanisms and thermo-kinetic parameters for the generation of PXDD/Fs from BPhs and chlorophenols (CPhs), and (vi) report the mechanistic steps involved in the synthesis of PBDFs and polybrominated diphenylethers (PBDEs) from the oxidation of bromobenzenes (BBzs).

1.2. Project objectives

While there is mounting evidence of the effects of BFRs on human health as well as on the environment, the major environmental and health burden of BFRs are associated with their decomposition and transformation into more notorious chemicals. Once emitted into the environment, BFRs are decomposed under the influence of strong ultraviolet (UV) light, in a process that is catalysed by potent photocatalysts such as carboxylic acids. The continuous increase in the measured level of BFRs and their hazardous decomposition products in the environmental media prompted the scientific community to examine the chemical and physical phenomena that control their occurrence, distribution, and fate. Accordingly, knowledge of the combustion chemistry, transformation mechanisms and environmental behaviour of BFRs and their intermediate products is important in order to minimise their emissions and effects on the environment.

In the present work, our combined theoretical and experimental work has led to:

1. An informative understanding of the environmental fate and transformation chemistry of bromochlorophenols (BCPhs; dynamic precursors for PXDD/Fs generation). This has been accomplished via estimating the thermochemical properties of the complete series of BPhs (including their acid dissociation constants, pK_a).
2. Illustration of elimination corridors of BPhs and selected BFRs in the environment via photodecomposition. From this perspective, the present contribution reports geometrical parameters of the complete series of BPhs and selected BFRs in their ground (S_0), as well as in their first singlet excited (S_1) states and computes their electronic absorption spectra. We calculated excitation energies for $S_0 \rightarrow S_1$ transitions within the framework of the time-dependent density functional theory (TDDFT). We estimated and discussed charges on bromine atoms and HOMO-LUMO energy gaps as molecular descriptors for the photoreactivity of BPhs and selected BFRs.
3. Exploration of the gas phase degradation of TBBA as a function of reaction temperature under an inert atmosphere. The objective is to decouple the gas-phase route from the overall decomposition of TBBA that often includes complex reactions occurring in the condensed medium. We quantitated the yields of numerous species under the varying effect of temperature to illustrate the dependence of their formation on temperature. We deployed quantum chemical calculations to build a reliable framework along with thermo-kinetic data for the destruction of TBBA into a series of brominated and non-brominated products.
4. Construction of the mechanistic routes operating in the gas phase formation of PXDD/Fs from halogenated phenols. We obtained the reaction enthalpies and activation barriers of all individual reactions (reactants, products and intermediates).

5. Generation of PBDFs and PBDEs corridors from the oxidation reactions of monobromobenzene (MBBz). BBzs evolve as an important entity in appreciable quantities from the decomposition of most commonly applied BFRs. The mechanisms and the kinetic parameters presented in this study explain the formation of PBDEs and PBDFs from the oxidation of BBzs and should facilitate the development of relevant kinetic models.

In view of the above tasks, the thesis is organised as follows:

1.3. Thesis outline

Chapter 2 reviews the literature pertinent to the thermal decomposition of BFRs. Specifically, it 1) critically summarises the methodologies and mechanisms relevant to the thermal decomposition of BFRs; 2) assesses the contribution of gas phase versus heterogeneous routes in the overall decomposition of BFRs; 3) reports available kinetic modelling describing the decay and fragmentation routes of BFRs; 4) examines the speciation of bromine during BFR decomposition, and its reactions with H/O species and hydrocarbons; 5) analyses the competing pathways of PBDD/Fs and PCDD/Fs formation; 6) presents the mechanistic pathways for the effects of polymeric materials on the decomposition of BFRs and surveys literature data relating to the emissions of volatile organic compounds (VOCs), semi-volatile organic compounds (SVOCs) and PBDD/Fs from several BFRs, such as TBBA, hexabromocyclododecane (HBCD), polybrominated biphenyls (PBBs), PBDEs and BPhs.

Chapter 3 reviews the experimental and theoretical methodologies applied throughout the research project. It provides a comprehensive description of the experimental facility designed and constructed to study the gas phase thermal decomposition of TBBA, including feed preparation, reaction and product collection systems. This chapter sets out the analytical techniques (e.g., sampling methods and product analysis protocols) used to capture and analyse the combustion products. For the quality assurance of our experimental measurements, we regularly performed replicates and blank tests and introduced internal and surrogate standards. This chapter also

summarises the theoretical approaches and concepts behind the deployed quantum chemical methods along with a brief description of Dmol³, Gaussian09, ChemRate and KiSTheIP codes.

Chapter 4 reports the theoretically calculated thermochemical properties and acid dissociation constants for the complete series of BCPs. The estimated thermochemical parameters should be instrumental for a better understanding of the relative stability of isomers in each homologue profile. This is an important aspect in the pursuit to formulate a robust rationale in regard to thermodynamic control of the final yield of PBDD/Fs. Overall, the results suggest that, aromatic compounds substituted bromine decompose faster for more brominated species.

Chapter 5 evaluates the photodecomposition properties of BPhs. In this chapter, we deploy the TDDFT formalism to predict the geometrical and electronic properties for the complete series of BPhs in the ground and first excited states. The analysis indicates that higher brominated congeners of phenols photodecompose more readily than lower brominated congeners. We find that the position of bromine substituents on the aromatic ring presume a strong effect on the process of photolysis following the sequence of debromination at *ortho* > *meta* > *para* sites.

Chapter 6, with the aim to acquire an insight into the phototransformation of the most common BFRs found in the environment, this chapter computes geometric and electronic parameters for the studied BFRs. Computed properties include optimised geometries, frontier molecular orbitals, electron density distribution, atomic charge partition and UV-Vis absorption spectra, in the ground and first excited states, for both gaseous and aqueous media. The findings of this chapter indicate that, halogenated aromatic compounds absorb UV light. The bromine atoms connected to *ortho*-C (with regard to C-C and C-O bonding or the hydroxyl group) hold the highest positive atomic charges and therefore, experience the highest bond elongation in their first excited state. Rupture of C-Br bonds occurs first at *ortho* positions, and higher brominated compounds consequently transform into lower brominated species.

Chapter 7 presents a comprehensive experimental study on the pyrolysis of TBBA to reveal its decomposition behaviour, particularly focusing on the identification and quantitation of toxic species. This study discloses the effects of reaction temperatures (673 – 1123 K) on the gas-phase thermal degradation of TBBA and maps out product distribution. This chapter illustrates our in-house developed multiple reaction monitoring (MRM) methods for the careful identification and quantitation of toxic species using gas chromatograph - triple quadrupole mass spectrometer (GC-QQQMS) instrument. In addition to the experimental results, quantum chemical calculations construct reaction pathways that describe the formation of the experimentally- obtained products. Results conclude that the thermal degradation of TBBA commences at 723 K. TBBA undergoes complete pyrolysis, generating a variety of by-products (brominated and non-brominated aromatic compounds). We observed that, most of the decomposition products arise in trivial concentrations at temperatures of 773 K and peak at around 923 K and 973 K. Generally, higher temperatures favour the formation of non-brominated species.

Chapter 8 elucidates the mechanistic routes involved in the formation of PXDD/Fs from the gas phase coupling of 2-bromophenoxy (2-BPhxy) and 2-chlorophenoxy (2-CPhxy) radicals. In this chapter, we describe the formation of BPhxy/CPhxy radicals from their corresponding bromo/chlorophenol molecules. The coupling of radicals affords fifteen distinct isomers in which six could serve as direct building blocks for the formation of PXDFs and four for the generation of brominated, chlorinated dehalogenated dioxins. We find that two phenoxy radicals, each with one available *ortho*-substituted halogen atom, may combine to form keto-ether species that act as prerequisites for the generation of PXDD congeners. Whereas, two phenols, each with one available *ortho*-substituted hydrogen, may react to form diketo species that transform into PXDFs.

Chapter 9 maps out the formation routes of PBDFs and PBDEs from MBBz reactions. It aims to fill the literature gap on the formation mechanisms of halogenated dibenzofurans from halogenated benzenes under an oxidative environment. We acquire reaction and activation enthalpies for the steps leading to the production of PBDEs and PBDFs. Initial oxidative decomposition of MBBz affords bromophenoxy

CHAPTER 1 Introduction

radicals. We show that direct ring-cyclisation of several MBBz/*ortho* 2-BPhxy products generates pre-PBDF isomers from either via O/*o*-C or *o*-C/*o*-C coupling. However, the bimolecular coupling reactions of MBBz and BPhxy radicals produce stable molecules such as PBDEs.

Chapter 10 offers the concluding remarks of the thesis and provides hints and suggestions for future directions.

Figure 1.1 presents the structure of the thesis.

CHAPTER 1 Introduction

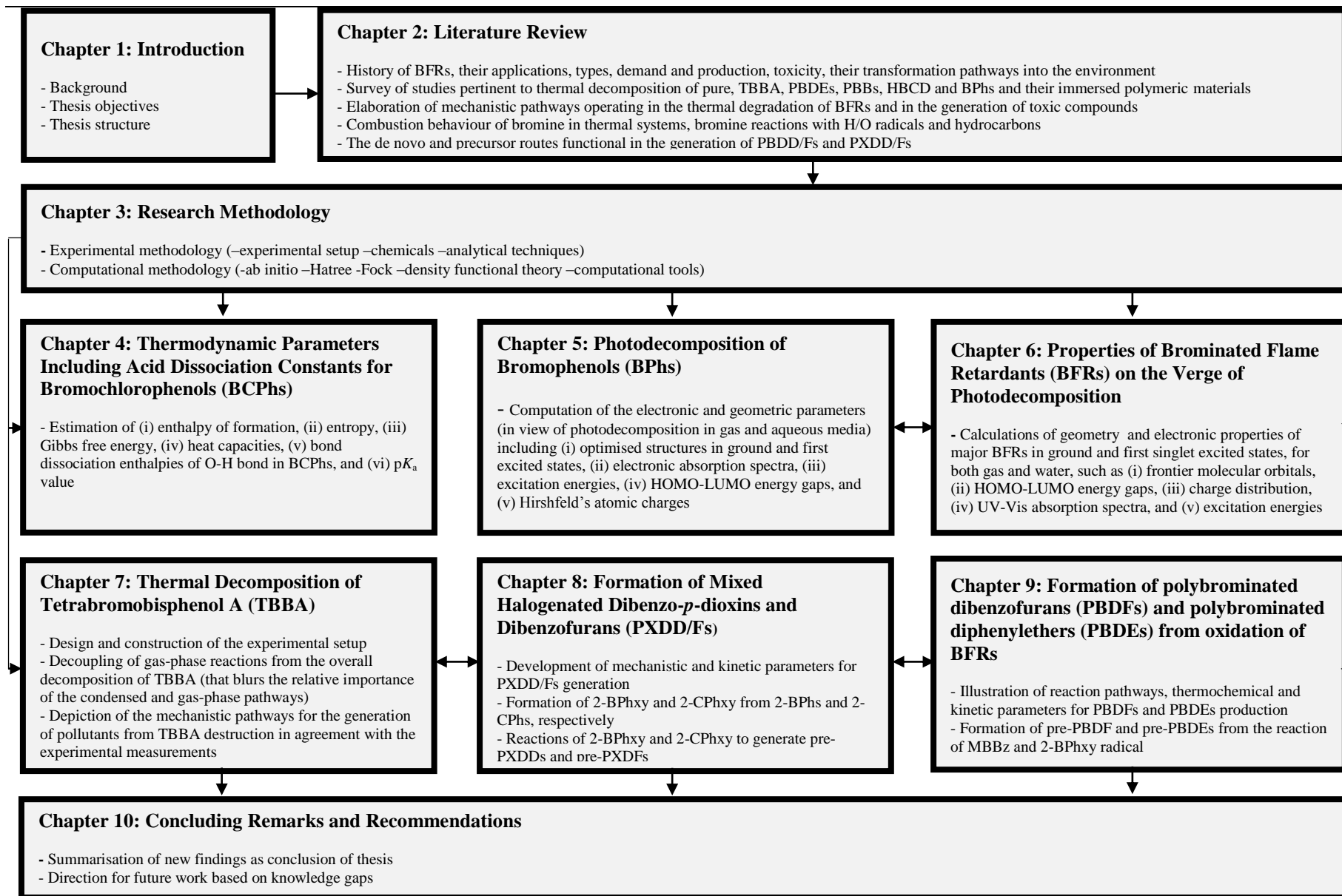


Figure 1.1. Thesis structure.

CHAPTER 2 LITERATURE REVIEW

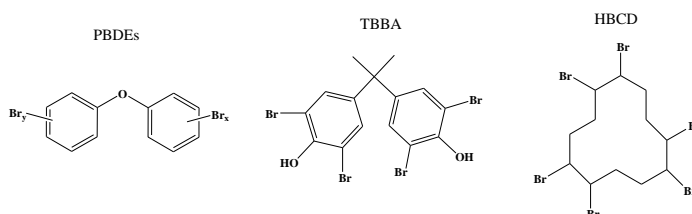
Table of Contents

2.1. Introduction	12
2.2. Methodologies	15
2.2.1. Experimental apparatus	15
2.2.1.1. Thermogravimetry (TG)	15
2.2.1.2. Differential scanning calorimetry (DSC).....	16
2.2.1.3. Pyrolysis gas chromatography mass spectrometry (Py-GC/MS)	16
2.2.1.4. Tubular reactor assembly	17
2.2.1.5. Incinerators	18
2.2.2. Analytical methodologies	18
2.2.2.1. Volatile and semi-volatile organic compounds	18
2.2.2.2. HBr emissions.....	19
2.2.2.3. Analysis of CO ₂ , CO and nitrogen content.....	19
2.2.3. Theoretical modelling.....	20

2.3. Thermal decomposition of major BFRs	21
2.3.1. Thermal decomposition of TBBA	21
2.3.1.1. Overall decay of pure TBBA	21
2.3.1.2. Decomposition products	24
2.3.1.3. Mechanisms of thermal decomposition of pure TBBA	29
2.3.1.4. Kinetic modelling	35
2.3.1.5. Decomposition of polymeric materials laden with TBBA	37
2.3.1.6. Fixation of Br content in TBBA via introducing metal oxides.....	42
2.3.2. Thermal decomposition of HBCDs	43
2.3.3. Thermal decomposition of PBDEs and polybrominated biphenyls (PBBs)	46
2.3.3.1. Degradation of pure PBDEs	49
2.3.3.2. Effects of polymers on the generation of PBDD/Fs from PBDEs.....	51
2.3.3.3. Decomposition of PBBs.....	53
2.3.4. Decomposition of 1,2-Bis-(2,4,6-tribromophenoxy)ethane (BTBPE)	55
2.4. Combustion behaviour of bromine	56
2.4.1. Speciation of bromine during decomposition of BFRs	56
2.4.2. Bromine reactions with H/O species	58
2.4.3. Bromine reactions with hydrocarbon species.....	60
2.5. Formation of PBDD/Fs	61
2.5.1. Pathways to PBDD/Fs from bromophenols	63
2.5.1.1. Homogenous formation of PBDD/Fs from bromophenols.....	66
2.5.1.2. Formation of PBDD/Fs from catalytic-assisted coupling of bromophenols	
71	
2.5.2. De novo synthesis of PBDD/Fs.....	72
2.5.3. Bromination mechanisms	74
2.6. Formation of PXDD/Fs	77
2.6.1. Formation of PXDD/Fs from mixed halogenated phenols.....	77
2.6.2. Formation of PXDD/Fs from BFRs-containing materials	79
2.6.3. De novo formation of PXDD/Fs	87
References	89

2.1. Introduction

Brominated flame retardants (BFRs) represent a broad group of chemicals added to polymeric components in numerous consumer products such as plastics, textiles, electronic equipments and furniture's to enhance their fire resistance. Close to 75 distinct BFRs have been produced commercially [1]. Technical mixtures of polybrominated diphenyl ethers (PBDEs) were the most utilised BFRs over the last few decades. Serious health and environmental concerns have led to the usage and production of PBDEs being discontinued worldwide. Hexabromocyclododecanes (HBCDs) and tetrabromobisphenol A (TBBA) are currently the two most commonly-deployed BFRs, with TBBA accounting for more than half the world's total BFR production.



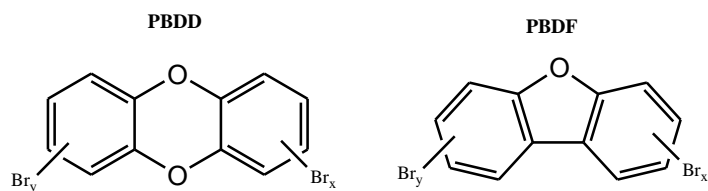
HBCDs and TBBA have been linked with toxic characteristics and classified as persistent organic pollutants (POPs). This, in turn, has prompted the formulation and use of the next generation of BFRs, known as novel BFRs (NBFRs).

The BFRs are cost-effective, have low decomposition temperatures, have little effect on the mechanical properties of polymers, and have significant potential for delaying ignition [1-2]. BFRs have gradually substituted different types of flame retardants (FRs), including inorganic FRs, chlorinated FRs, and phosphorous and nitrogen-containing FRs. High global market demand over the past few decades has led to dramatic increases in the production of BFRs. According to world market reviews, the estimated global demand for BFRs in 2008 was more than 690,000 tons/year in comparison to reported production of 20,000 tons/year in 2000 [3]. BFRs typically encompass 5– 10 % and 19 % by weight (wt) of treated plastics and printed circuit boards, respectively [4-5].

Based on their intended applications, BFRs could be incorporated into polymeric materials either as additive or reactive constituents [1, 6]. Additive BFRs are blended

with the hydrocarbon constituents and, thus, do not react with the polymer. These BFRs are also called *backbone BFRs*. As a consequence, additive BFRs could leach out of the treated objects during their lifespans. This phenomenon is the main source of “indoor exposure” to BFRs. Reactive BFRs are covalently bonded to the polymer. Indoor exposure to reactive BFRs could occur if an excessive amount was reacted with the polymer during production. TBBA and HBCD are common examples of reactive and additive BFRs, respectively. Based on their physico-chemical properties, BFRs are bio-accumulative and can endure long range atmospheric transport [7-9]. As a result, concentrations of several BFRs have consistently been detected in various environmental matrices [10-11], including air and dust [12-13], soil [14], biological samples [15] and the food chain [16-18].

Used BFRs-treated bodies of domestic, industrial and commercial sectors are commonly discarded into regular municipal waste streams at the end of their lifecycles. Thermal treatment represents a mainstream strategy for disposal of materials laden with BFRs. For example, pyrolysis has become the most advantageous recycling system for thermosetting resins laden with BFRs [19]. In this regard, several BFRs were reported to act as potent precursors for the formation of polybrominated dibenzo-*p*-dioxins and dibenzofurans (PBDD/Fs); i.e., a group of chemicals that shares similar notorious behaviour [20-23] with their chlorinated counterparts (PCDD/Fs). The toxicity profile of each PBDD/Fs depends on the number and position of bromine around the two phenyl rings. Experimental studies have established inventories of the emission of PBDD/Fs from incineration of BFR-containing fuels, such as from the combustible fraction of residential waste [8], electronic waste [9] and discarded plastic resins [10]. These studies have illustrated phenomena governing the generation of PBDD/Fs from BFRs. When subjected to heat (i.e. pyrolysis, combustion and thermal stress), materials laden with BFRs readily degrade and have a high tendency to form brominated products of incomplete combustion (BPICs) [24-27]. Accidental spontaneous fires of polymeric materials laden with BFRs often result in the emission of PBDD/Fs, PCDD/Fs in addition to mixed polybrominated chlorinated dibenzo-*p*-dioxins, and furans (PXDD/Fs; X= Cl, Br) [28-30]. Owing to the high bromine and chlorine contents in electrical and electronic wastes (e-waste), thermal recycling of e-waste often pollutes surrounding areas with large loads of PBDD/Fs and PXDD/Fs [31-32].



Experimental studies have addressed the thermal decomposition of pure BFRs and/or BFR-laden polymers under oxidative and pyrolytic environments, typically in the temperature range of 553 – 1173 K. As it is the case of the homogenous formation of PCDD/Fs, the formation of PBDD/Fs from BFRs occurs along two general pathways: 1) coupling of structurally-related gas phase precursors, and 2) via so-called “de novo synthesis” (i.e. burning off the carbon matrix) [33-40]. Weber and Kuch [39] reported that under insufficient oxygen content, the precursor-derived pathway prevails over de novo synthesis. In contrast, Vehlow et al. [41] argued that the de novo pathway is significantly more important under well-controlled combustion conditions. It has also been confirmed that the presence of metals, especially CuO, has a strong positive catalytic effect that enhances the thermal breakdown of BFRs considerably [42-43]. In real combustion conditions, several factors affect the overall thermal decomposition of BFRs. These factors include the chemical composition of the fuel, the polymer matrix, the residence time of present metallic species, bromine input, oxygen concentration and temperature.

Review articles of BFRs have mainly focussed on their environmental occurrence, spatial distributions, toxicological effects and progress in analytical chemical detections [1, 15-44]. Weber and Kuch [39] present a definitive account of the pathways leading to the formation of PBDD/Fs from BFRs. The present review updates Weber and Kuch’s [39] review and presents the research that has been carried out since its publication in 2003. Herein, we survey literature studies on the thermal decomposition of BFRs with emphasis on the yields and formation routes of PBDD/Fs. This review is organised as follows. First, we briefly present the theoretical modelling methods commonly deployed to study the decomposition of BFRs, before describing decomposition products and pathways of major BFRs. Next, we examine bromine combustion chemistry, then analyse the competing pathways of PBDD/F and PCDD/F formation. While we elaborate on plausible future research directions in each section of this review, we devote the

conclusion section to a summary of the most focal, outstanding issues pertinent to the degradation of BFRs in thermal systems.

2.2. Methodologies

2.2.1. Experimental apparatus

Major experimental techniques commonly deployed to study the thermal decomposition of BFRs include thermogravimetric analysis (TGA), differential scanning calorimetry (DSC), pyrolysis-gas chromatography-mass spectrometry (Py-GC/MS) and tubular flow reaction. The identification and quantification of decomposition product arrays involve coupling each experimental apparatus with appropriate analytical methods.

2.2.1.1. Thermogravimetry (TG)

Thermogravimetry apparatus measures the variations in a sample's mass as a function of temperature or time [45].

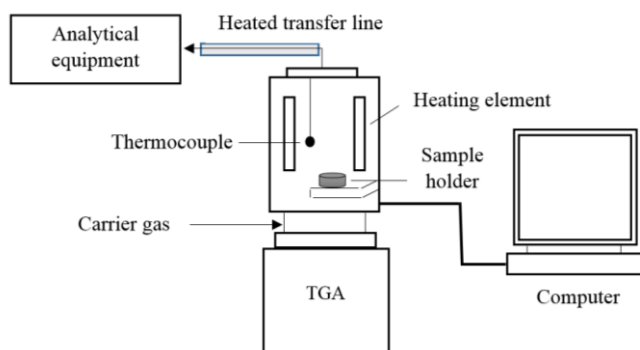


Figure 2.1. Schematic diagram of a typical thermogravimetric analyser (TGA).

Then, TGA reports mass loss curves to provide global kinetic parameters at each step of the decomposition process [46-48]. To operate TGA, a small quantity of sample is introduced into thermobalance by placing it in an alumina crucible that is positioned in a preheated temperature-programmed furnace with a nitrogen or helium atmosphere. Figure 2.1 shows a schematic diagram of a TG apparatus. The TG apparatus is connected with Fourier transform infrared spectroscopy (FTIR) through a heat transfer line for the

classification and quantification of the light gaseous and volatile organic compounds (VOCs) emitted during the weight loss stages of the sample [49-51].

2.2.1.2. Differential scanning calorimetry (DSC)

Differential scanning calorimetry is a thermo-analytical technique used to measure thermal transition phases of test samples. It estimates the difference in heat required to elevate the temperature of a sample (linearly with time) compared with a reference material. Both test and reference materials are maintained at the same temperature. In a typical DSC analysis, the test mixture is placed in a sample pan to carry out the heating process. Figure 2.2 depicts a DSC instrument setup. As the temperature changes, DSC measures the amount of heat radiated or absorbed by the sample in comparison to the temperature difference between the sample and blank [52]. Synchronisation of TGA and DSC methods provides simultaneous thermogravimetric and calorimetric data.

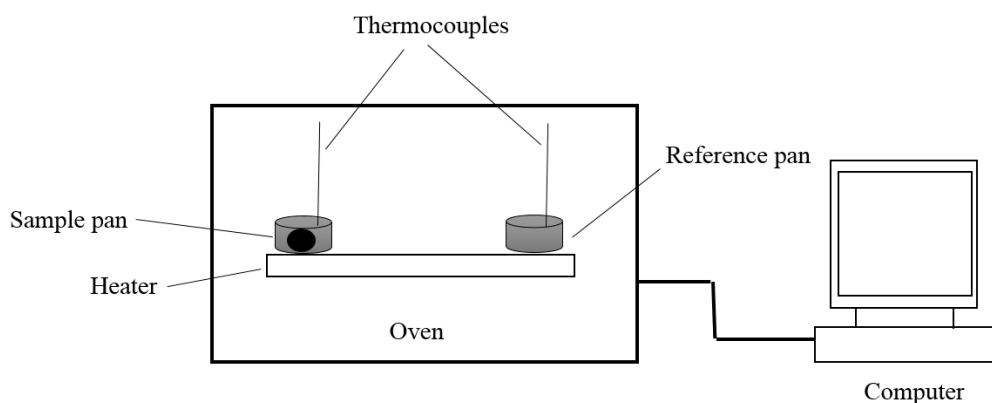


Figure 2.2. Differential scanning calorimeter (DSC) apparatus.

2.2.1.3. Pyrolysis gas chromatography mass spectrometry (Py-GC/MS)

In Py-GC/MS experiments, a Curie-point pyrolyser is connected directly to a gas chromatograph mass spectrometer (GC/MS) or is mounted on the injector of a GC column configured with an MS detector [53-54]. The temperature of the pyrolyser is regulated by the material's Curie point [55]. Py-GC/MS can operate at constant temperatures to work isothermally, or ramp up to high temperature at a specific heating rate. Analysing for products with Py-GC/MS necessitates using short residence times for analysis. This

ensures that the effects of secondary reactions on the decomposition of initially formed products are minimal [5, 56].

2.2.1.4. Tubular reactor assembly

Tubular reactors are often deployed as an approximation to plug flow reactors, in which reacting gases are mixed radially, with no temperature drop in radial directions. The reaction zone of the tubular reactor operates isothermally. This enables the study of degradation behaviour at a constant temperature. In the experimental configuration, the tubular reactor tube (constructed with quartz or ceramic material) is aligned with the centre line of a precisely temperature-controlled furnace. Figure 2.3 portrays a typical schematic diagram of a tubular reactor experimental setup. In this configuration, the quartz tube reactor is placed horizontally inside the oven [57-58]. This design is comparable to fixed-bed reactors commonly employed in combustion experiments [25, 29, 59-61]. In the tube furnace setup, the reactor tube is supported in a horizontal furnace, whereas, the sample is placed outside the furnace. The sample is then introduced to the combustion zone at a controlled speed by a carrier gas [61-63].

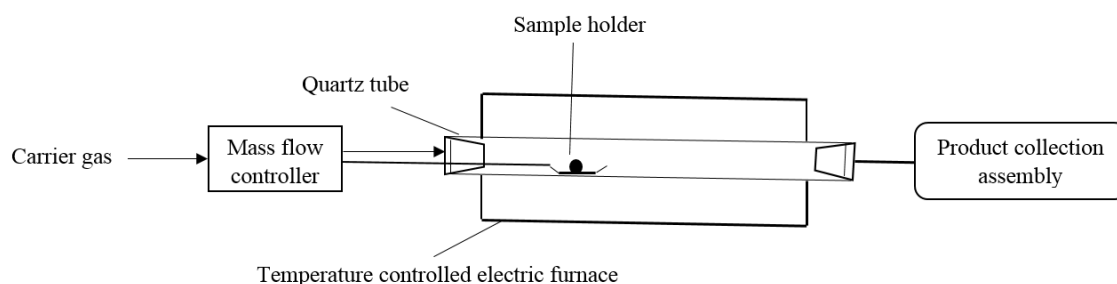


Figure 2.3. Schematic diagram a tubular reactor.

Dillinger's group [34, 35, 42-43] developed a closed and continuous system named the "system of thermal diagnostic studies" (STDS). The thermal compartment of an STDS incorporates a high-temperature, fused silica tubular reactor in a horizontal, temperature-programmed Lindberg furnace connected online to GC/MS. An external syringe pump assembly which feeds and controls the flow of liquid sample in the reaction zone.

2.2.1.5. Incinerators

The incineration behaviour of fuels is investigated in rotary kiln furnaces or pilot-scale incinerators. These incinerators are composed of a primary combustion chamber coupled with a secondary combustion chamber followed by a flue gas cooling duct [64-65]. The operating temperature conditions for the first and second combustion chambers are between 773 – 1173 K and 1073 – 1473 K, respectively. The flue gas cooling duct is integrated with a scrubber and an activated carbon chamber to trap different categories of products. The incinerated residue and flue gas samples are removed from the secondary combustion chamber for further analysis [66].

2.2.2. Analytical methodologies

Studies on the thermal decomposition of pure BFRs and BFR-containing polymeric materials provide a brief summary on the analytical methodologies used for the detection of a wide range of decomposition products, both qualitatively and quantitatively. In the following sections, we will examine and summarise reported analytical techniques employed for sampling several brominated and non-brominated products, most notably, 1) PBDD/Fs, 2) hydrogen bromide (HBr), 3) poly aromatic hydrocarbons (PAH), volatile organic compounds (VOCs) and semi-volatile products (SVOCs), and 4) CO, CO₂, water content and non-condensable gases.

2.2.2.1. Volatile and semi-volatile organic compounds

Gaseous VOCs and SVOCs flow from the reactor are typically captured through high molecular weight resin cartridges, i.e., XAD-2 or tenax, which afford a significant capacity to adsorb VOC and SVOC products. VOCs and SVOCs could be extracted from resin cartridges by a mixture of dichloromethane/acetone (1:1) using an ASE method. The fraction attained from ASE is analysed with HRGC/MS, GC-FID (flame ionisation detector) or MSD detectors [67]. Barontini et al. [69] utilised a series of cold trap systems maintained at a low temperature (about 253 K) in a sodium chloride/ice bath to trap VOC entities from the exhaust flue gas stream that were emitted by the thermal degradation of BFRs. Trapped VOC products were extracted by solvent and injected in the chromatographic analyser for identification and quantification. Another study evaluated

a wide range of VOCs released from combustion systems by using an online GC instrument [78]. A review of the literature reveals that pyrolysis GC/MS systems operated in EI mode present a powerful analytical technique for the identification of VOCs [70].

2.2.2.2. HBr emissions

Evolved HBr gas generally accounts for 40 – 80 % of initial bromine content in BFRs. HBr is commonly collected in a dilute alkaline solution of either NaOH, Na₂CO₃ or NaHCO₃ prior to its quantification by several means with different detectors [71-77]. Quantification of HBr is usually accomplished by monitoring the diluted NaOH-HBr solution in an ion chromatogram [67, 73, 75-77]. Larsen et al. measure the HBr concentration in a gas liquid chromatograph flame ionisation detector (GLC- FID) [72]. Titration of alkaline solutions containing HBr is also an important technique for the estimation of HBr yield [74, 78]. TG-FTIR runs allow direct measurement of HBr quantities based on FTIR absorption peaks. Concentrations of HBr are obtained from specific calibration curves developed from laboratory-prepared water-HBr solutions of varying concentrations [54, 78-82]. ICP-MS can also be used to measure the Br content.

2.2.2.3. Analysis of CO₂, CO and nitrogen content

GC-FID detector measures light hydrocarbon series, whereas non-condensable gases such as carbon dioxide (CO₂), carbon monoxide (CO), oxygen and nitrogen are quantified by a gas chromatogram thermal conductivity detector (GC-TCD) [75, 83]. Marsanich et al. used FTIR analysis to measure CO and CO₂ components from the thermal decomposition of TBBA [78]. Experimental findings interrelated to the thermal decomposition of BFRs and BFR-laden materials applied FTIR technology for the determination of nitrogen, water and CO fractions [54, 81, 84-85]. These compounds are readily identified with FTIR based on their characteristic absorbance curves. Soderstrom et al. placed an IR instrument on the product flue gas line of a pilot-scale fluidised bed reactor to simultaneously monitor the concentrations of CO₂ and CO [24]. Similarly, Lemieux et al. [65, 68] in their experiments on combustion of municipal solid wastes (MSWs), placed a continuous emission monitor (CEM) instrument on the gas effluents from the reactor to monitor the in-line concentrations of O₂, CO₂, CO and N₂ simultaneously. A TGA study

on the pyrolysis of laminated printed circuit boards treated with TBBA reported water and CO₂ product profiles using an MS detector by analysing their differential thermal analysis and total ion current (TIC) curves [73].

In previous investigations, researchers deployed quantum chemical calculations to study the different aspects of BFRs in view of the photo and thermal decomposition. Our research group used quantum chemical approach (ab initio molecular orbital theory and density functional theory computations) to explore the accurate properties of molecular systems that include mechanistic pathways, thermochemical and kinetic parameters presented in the next sections of this review.

2.2.3. Theoretical modelling

Computational chemistry has emerged as a powerful tool in combustion chemistry. It provides accurate results for a large number of properties of interest, most notably bond dissociation enthalpies (BDHs), reaction rate constants, mechanisms, p*K*_a values, vibrational frequencies and NMR shifts [86-89]. Intermediates, radicals and transition states are often too transient for the experimental measurements. Computational chemistry provides a robust description of these structures. The underlying principle in all computational methods is to provide a solution for the time-dependent Schrödinger equation [90]. The basis of all numerical solutions to this equation is the Hartree-Fock (HF) self-consistent field approach (SCF) which forms the foundation for the more elaborate electronic structure methods. The HF theory relies on several simplifications, including the Born-Oppenheimer approximation, the independent electron approximation and the linear combination of atomic orbitals approximation.

Post-HF methods or ab initio methods afford a more realistic account for the electronic system by decomposing energies into Coulomb repulsion, exchange and correlational components. Ab initio methods differ in the approaches they use to compute the correlation energy [90]. These methods are generally grouped into three categories: configuration interaction (CISD, CISD (T), Møller-Plesset perturbation theory (MP*n* methods), and multi-configuration self-consistent field theory (MCSCF). Calculations based on ab initio methods are computationally expensive but very accurate for general

applications. Density functional theory (DFT) methods afford reasonably satisfactory results with less computational time. DFT methods universally focus on the electron density and differ in the way they present exchange and correlation functionals [91]. There are two main DFT methods: local density approximation (LDA), and the generalised gradient approximation (GGA), of which the B3LYP functional is the most widely-used method. There has been rapid progress in formulating new DFT functionals by parameterising exchange and correlation functionals against experimental measurements and ab initio calculated values [92].

In carrying out these quantum chemical calculations, there is a balance between the desired accuracy of results and the size of the system (i.e. number of molecules or unit cells). When available, calculated quantities (i.e. bond lengths, equilibrium constants, lattice parameters, BDH, etc.) are contrasted with corresponding experimental measurements in order to provide a benchmark or level of accuracy. Quantum chemical calculations are performed with the aid of several packages, each with unique applications, such as Gaussian09 [93], Dmol³ [94], Vienna ab initio simulation package (VASP) [95], and Amsterdam density functional (ADF) [96].

2.3. Thermal decomposition of major BFRs

2.3.1. Thermal decomposition of TBBA

The thermal decomposition of TBBA is very complex, due to competing physical processes and chemical reactions. Experimental studies on the thermal degradation of TBBA focus on various aspects, namely: 1) overall decay of TBBA, 2) degradation versus evaporation routes, 3) selective analysis of brominated phenols (BPhs) and PBDD/Fs, 4) distribution of Br across brominated products and emission of HBr, 5) quantitative analysis of all products, 6) deriving reduced and detailed kinetic models, 7) suggesting mechanisms based on linking product profiles with plausible reaction networks, 8) the effect of epoxy resins and other polymeric materials on the decomposition behaviour of TBBA, and 9) the effect of metal oxides as HBr scavengers.

2.3.1.1. Overall decay of pure TBBA

Experiments using TGA-FTIR and DSC-FTIR investigated the pyrolysis of TBBA at different heating rates/modes and temperatures [97-102]. These studies observed very similar degradation behaviour and provided curves of total weight loss, data relevant to the thermal stability of TBBA, gaseous product profiles, differential scanning calorimetric analyses, mechanistic insights into primary decomposition steps, and evaporation rates. Figure 2.4 shows the reported curves of TBBA weight loss from selected studies. Luda et al. [101] used TGA at a heating rate of 10 K/min in an inert medium to reveal that the decomposition of TBBA proceeds in two stages of weight loss, 473 – 563 K and 563 – 773 K. The first stage consumed nearly 60% of the initial TBBA weight. The onset of the second stage, according to Barontini et al. [99] using similar operating conditions, extends to nearly 623 K. In both studies, 20% of stable TBBA residue is left above 723 K. In contrast to TBBA, the degradation of unbrominated TBBA, i.e. bisphenol A, occurs in one step interval (473 – 543 K) without leaving any residue [101]. Although thermal degradation could start at temperatures as low as 458 K, it only becomes significant above 503 K [97].

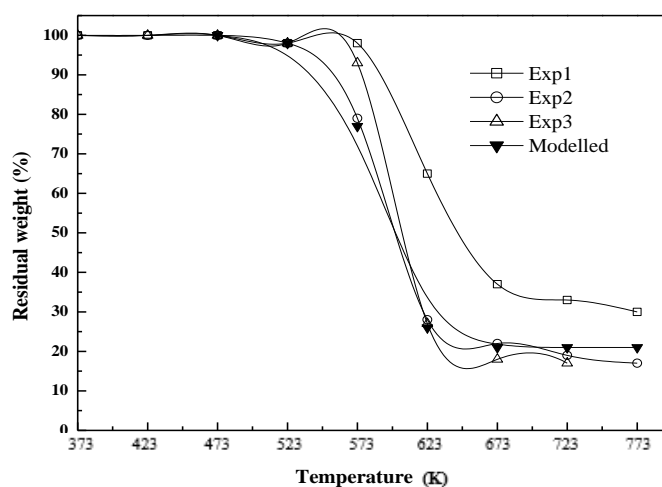


Figure 2.4. TBBA residual weight (%) from thermal decomposition of TBBA heated at 10 K/min. Curves refer to experimental results ($-\Delta$ -[47], $-\square$ -[123], $-o$ -[102]) and predicted results from a kinetic model [114].

A longer residence time of isothermal heating promotes condensation reactions over degradation reactions. As a result, isothermal TGA runs leave a larger residue when compared with dynamic runs [99]. These aforementioned studies were carried out in

open flow systems, allowing for the minimisation of the effects of secondary gas phase reactions on the degradation of solid TBBA. Indeed, pyrolysis of TBBA under closed-vessel conditions (i.e. quartz ampoules) results in 100% weight loss [101].

IR spectra measured before heating and at the end of the first stage of weight loss give valuable information on structural modifications and prominent plausible initiation reactions [101]. Displacement of the aromatic wagging vibrations and disappearance of stretched phenol-OH bonds suggest that fissions of H₃C-aromatic and O-H bonds are likely to be significant initial decomposition corridors. Isothermal TGA runs in a tubular reactor over the temperature range of 453 – 543 K discloses that the overall decomposition of TBBA could effectively be described by a single-step kinetic model [99]. Values of the pre-exponential (*A*) factor and the activation energy (*E_a*) are assigned $3.76 \times 10^{13} \text{ s}^{-1}$ and $179.1 \text{ kJ mol}^{-1}$, respectively.

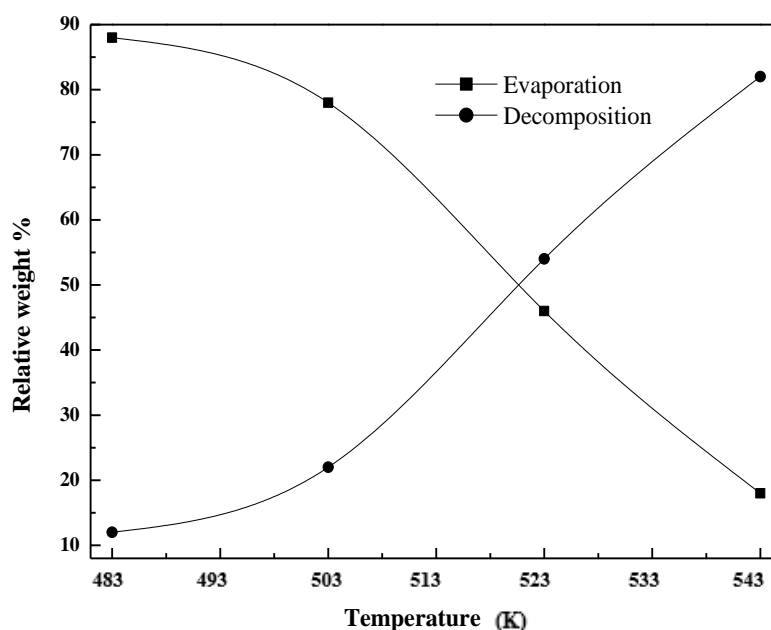


Figure 2.5. Relative weight of TBBA evaporated and decomposed at temperatures between 483 - 543 K [108].

Profiles of TBBA thermal degradation in a batch reactor and TGA can provide a quantitative assessment of the contribution of evaporation versus degradation to overall TBBA decomposition. Heating TBBA samples in crucibles with different surface areas (and hence different evaporation rates) alters the overall decomposition rate of TBBA

[100]. The amount of volatiles from TGA data is related to the mass transfer principles and quasi-steady-state assumptions, permits the approximate estimation of evaporation rates and vapour pressure parameters for TBBA. These data allow evaluation of the relative contributions of concurrent TBBA evaporation and thermal degradation in the aqueous medium [97]. Figure 2.5 depicts evaporative and degradation components. It is evident from this figure that the evaporation channel predominantly causes TBBA decay up to 503 K, and still contributes significantly at slightly higher temperatures (i.e. ~ 18% at 543 K).

2.3.1.2. Decomposition products

Studies on the thermal degradation of TBBA report qualitative, semi-quantitative and quantitative data on the decomposition products [24, 99-100, 103-111]. The literature's consensus is that the primary degradation products from the pyrolysis of TBBA include HBr, brominated phenols, and brominated derivatives of bisphenol A, in addition to the solid residue (char). Figure 2.6 shows the yields of major products measured at a constant heating rate of 10 K/min. Para-alkylated BPhs also form in low concentrations. Formation of BPhs and their alkylated substituents indicate that cleavages of isopropylidene linkages act as prominent initiation channels in the overall decomposition of TBBA. As will be discussed in Section 3.1.3, the literature provides conflicting views on the mechanisms of HBr formation. FTIR results indicate that evolved HBr accounts for 52 – 59 % of the bromine initially present in TBBA samples [112]. The presence of oxygen merely changes the quantities of bromine converted to HBr relative to pure pyrolytic conditions [112]. Closing bromine balance reveals that nearly 45% of the initial bromine content transforms into condensable (VOCs and SOVCs), leaving only 1% in the char [97]. The implications of bromine-deficient char on the de novo formation of PBDD/Fs will be elaborated in Section 5.4.

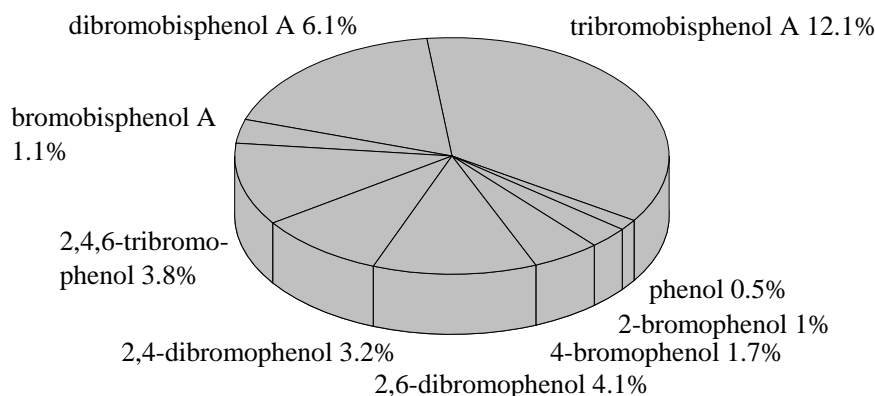


Figure 2.6. Weight yields (%) of the major products of TBBA decomposition at a constant heating rate of 10 K/min [45].

The recent study by Ortuño et al. [103] is perhaps the only contribution that provides quantitative data on all TBBA decomposition products. The authors carried out pyrolysis and combustion runs on TBBA inside a tubular reactor at 873 K and 1123 K. GC/MS confirmed the formation of more than one hundred SVOCs. The isotope dilution method was used to identify and quantitate each compound. Non-brominated products included PAHs, partially-oxygenated compounds, alkanes and alkylated benzenes. In addition to the major brominated products reported in other studies (BPhs and brominated BA), numerous brominated alkanes, brominated benzenes and brominated PAHs also evolved. The obtained profiles of BPhs matched analogous profiles from other studies and were dominated by 2,4,6-tribromophenols and 2,4-/2,6-/dibromophenols.

The majority of studies on the thermal decomposition of pure TBBA or TBBA-laden materials have aimed to investigate the possible formation of PBDD/Fs and BPhs. Table 2.1 shows a summary of experimental investigations into the formation of PBDD/Fs from thermal treatments of TBBA, and polymers laden with TBBA, under various operational conditions. Several congeners of PBDD/Fs exist in the gas phase, albeit in the ppm range. The most toxic 2,3,7,8-substituted congeners appear at a ppb level or were not detected. Combustion of TBBA generally yields more PBDD/Fs relative to pyrolytic conditions. This is evident from data by Ortuño et al. [103] and Thoma et al. [111], who reported the total yields of PBDD/Fs at 1073 K to be around 20 ppm and 25 ppb under oxidative and pyrolytic conditions, respectively.

Table 2.1. Thermal decomposition of TBBA and TBBA-laden polymeric materials.

BFRs	Reactor type/operating conditions	Thermal decomposition products	Max. concentration of PBDD/Fs at T (K)	References
TBBA	TGA (453 – 543 K)	HBr, phenol, mono- tribromophenol, mono- tribromobisphenol A, other brominated products	No values were reported	[78]
TBBA- containing paper, laminated printed circuit boards	TGA (313 – 1273 K)	HBr, brominated aromatics, mono- tribromophenol	No values were reported	[73]
TBBA	TGA	Monobrominated cyclic and aliphatic compounds, bromopentane, dibromomethylbenzene, mono-tribromophenol, HBr, char	No values were reported	[71]
TBBA	TGA	HBr, Tribromobisphenol, Phenol, mono- tribromophenols,	No values were reported	[82]
TBBA	TGA	HBr, mono- Tribromobisphenol A, phenol, mono- tribromophenol, char	No values were reported	[102]

CHAPTER 2 Literature Review

TBBPA	Quartz tube reactor Combustion (873 K and 1123 K)	Gases, volatile compounds, PAHs, brominated phenols, tetra- to hexa- BDFs, tetra- to penta-BDDs	1123 K (ppt) Σ PBDFs(962260) Σ PBDDs (20440)	[103]
TBBPA	Quartz tube reactor Pyrolysis (873 K and 1123 K)	Gases, volatile compounds, PAHs, brominated phenols, Tetra- to penta- BDFs, Tetra-BDDs	1123 K (ppt) Σ PBDFs (12710) Σ PBDDs(12530)	[103]
TBBA Printed circuit boards	Pyrolysis TGA	Bromophenols, bisphenol, ketones, aldehyde, carbonization, char, H ₂ O, CH ₄ , HBr, CO ₂ and CH ₃ COCH ₃	No values were reported	[104]
TBBA contained in printed circuit boards	Quartz tube reactor pyrolysis (278 – 1073 K) (heating rate 10 K min ⁻¹)	Aromatic products i.e mono- to tribromophenols, methylated phenols, methylated hexanes, HBr, char and dioxin	No values were reported	[105]
TBBA	Tubular reactor Pyrolysis (303 – 873 K)	HBr, CO, CO ₂ , Brominated bisphenol A, Mono- to tetra- BPhs, bisphenol	No BDD/Fs	[99]
TBBA	Pyrolysis (453 K and 543 K)	HBr, mono-tri-BPhs,	No values were reported	[100]

CHAPTER 2 Literature Review

TBBA	Closed-vessel pyrolysis (873 K) $\tau = 10$ s, 30 s, 2min, 5 min, 30 min, 1 hr	Brominated phenols (mono- tri-), monobrominated cyclic and acyclic aliphatic compounds, bromopentane, benzenes, naphthanes, dibromomethyl phenol, PBDD/Fs	Not analysed BDD/Fs	[106]
TBBA with polyethylene (PE)	Oxidation Quartz reactor tube $\tau = 3-4$ s	PBDD/Fs, PBBz, PBPhs	(ppm) PBDD (2.2) PBDF (15.3)	[107]
Various artificial municipal waste samples combusted with DBDE, HBCD, TBBA	Pilot scale fluidised bed reactor 1013 – 1093 K $\tau = 2-3$ s	HCl, Cl ₂ , HBr, Br, BrCl, PBCDD/Fs , DBDDs/Fs, PBDD/Fs,	(ng/m ³) PBCDFs (1731) TBDF (153) PBCDDs (68)	[24]
TBBP-A	Oven (873 K)	mono-to penta BPh, Tri- to hexa-BBz mono- to penta-BDDs, mono- to penta-BDFs	(ppm) Σ PBDD (116) Σ PBDF (99)	[108]
TBBP-S	Oven 873 K	mono-to penta BPh, Tri- to hexa-BBz, mono-to hexa-BDDs, di- to hexa-BDFs	(ppm) Σ PBDD(2090) Σ PBDF(260)	[108]
TBBA with ABS additive	Quartz tube reactor Oxidation (5%)	Analysed dioxin/furan products mono- to penta-BDFs mono- to penta-BDDs	Σ PBDFs (ppb) (2700 at 973 K) Σ PBDDs (ppb) (403 at 873 K)	[109]

		(673 – 973 K)		
		$\tau = 20$ min		
TBBA with ABS additive	Quartz tube reactor	Analysed dioxin/furan products	873 K (ppb) Σ PBDFs(340)	
	Pyrolysis (673 – 973 K)	mono- to penta-BDFs mono- to penta-BDDs	Σ PBDDs (9)	[109]
	$\tau = 20$ min			
TBBA with epoxidlamine	Oven Pyrolysis (873 – 1073 K)	PBDFs \gg PBDDs	1073 K (ppm) PBDD (>2) PBDF (10)	[110]
TBBPA	Pyrolysis (973 – 1173 K)	mono-to tetra-BDDs mono- to tetra- BDFs	(ppm) Σ PBDDs (498) Σ PBDFs (1150)	[111]

2.3.1.3. Mechanisms of thermal decomposition of pure TBBA

As discussed above, the decomposition of TBBA occurs in three phases: a gas phase ($T \geq 723$ K), a condensed phase upon melting of TBBA ($513 \text{ K} \leq T \leq 723 \text{ K}$), and during further charring of residue if longer residence time permits. Prominent decomposition reactions in the condensed media are fundamentally different from the corresponding reactions prevailing in the gas phase. In the latter, unimolecular-derived pathways dominate the decomposition of TBBA, whereas, bimolecular condensation-type reactions are expected to be of significant importance. Based on evaporation rates reported by Marsanich et al. [100] and the IR spectrum measured by Luda et al. [101], TBBA starts to evaporate just above its melting point (i.e. 453 K). Thus, products reported at temperatures below 453 K are most likely to be produced from the decomposition of the evaporated component of TBBA.

Altarawneh and Dlugogorski [113] detailed the mechanisms of the thermal decomposition of TBBA in the gas phase. Investigated reactions included unimolecular decompositions of TBBA and its bimolecular reactions with important radicals existing in the pyrolytic medium, namely, H, CH₃ and Br. Derived pathways in the gas phase mimic the more complex equivalent processes occurring in the condensed medium. Figure 2.7 illustrates a theoretically developed mechanism for the self-decomposition of

TBBA as a gas phase molecule. Unimolecular fragmentation of TBBA branches into seven initial exit pathways. These channels are characterised by: fission of C-CH₃ bonds (pathway A), unimolecular transfer from the phenolic H leading to elimination of a Br atom (pathway B), direct rupture of C-Br bonds (pathway C), cleavage of isopropylidene linkages accompanied by hydrogen migration (pathway D), fission of phenolic O-H bonds (pathway E), splitting of (H₃C)₂C-aromatic bonds (pathway F) and loss of H atoms from methyl moieties (pathway G). Pathway A has lower energetic requirements than the other channels.

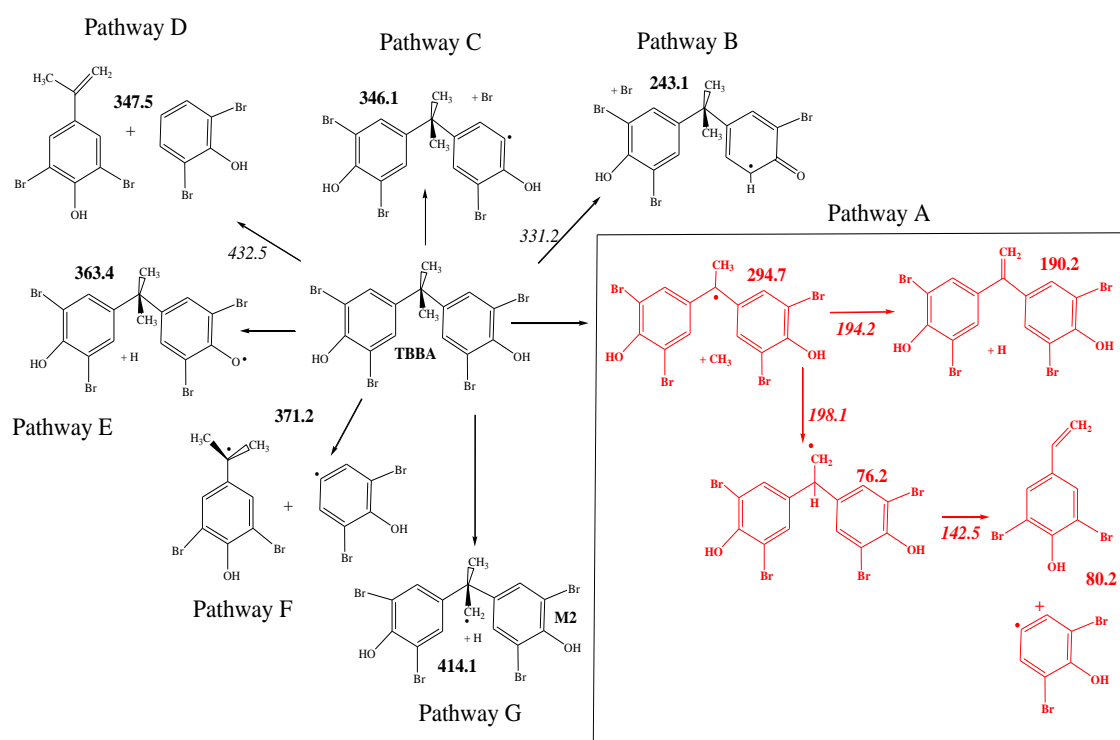


Figure 2.7. Pathways encountered in the gas-phase decompositions of TBBA [113].

Calculated reaction rate constants for the pathways (Figure 2.7) demonstrate that the fission of C-CH₃ bonds is the sole important initiation channel in the unimolecular decomposition of TBBA in the gas phase. The most plausible products from the initial gas-phase decomposition of TBBA are 4,4'-(ethene-1,1-diyl)bis(2,6-dibromophenol), 2,6-dibromo-4-vinylphenol and 2,6-dibromophenol. However, the latter two compounds appear in the product profiles of TBBA pyrolysis, formation of 4,4'-(ethene-1,1-diyl)bis(2,6-dibromophenol) has never been reported. However, it should be noted that

the literature provides no examples of experiments on pure gas pyrolysis of TBBA. All relevant studies investigated the heating of solid TBBA samples. Performing these experiments is challenging, due to the very high boiling point of TBBA (453 K). Bimolecular reactions of H and Br atoms with TBBA lead exclusively to the generation of H₂ and HBr. Br atoms prefer to exclusively extract phenolic H-atoms. This, in turn, indicates that any initially-formed Br atoms transform into HBr.

Apart from a few studies, the majority of investigations describe TBBA decomposition using gas phase-like reactions [98] similar to those described in Figure 2.7. Marongiu et al. [114] presented a detailed mechanistic study that accounted for the degradation of TBBA in a condensed medium. Their mechanism combined gas phase reactions and key mechanistic steps governing the decomposition of aqueous polymers [115-116]. Figure 2.8 provides a qualitative description of reaction networks and processes encountered in the thermal decomposition of TBBA. In this mechanism, several reaction categories control the decomposition of TBBA:

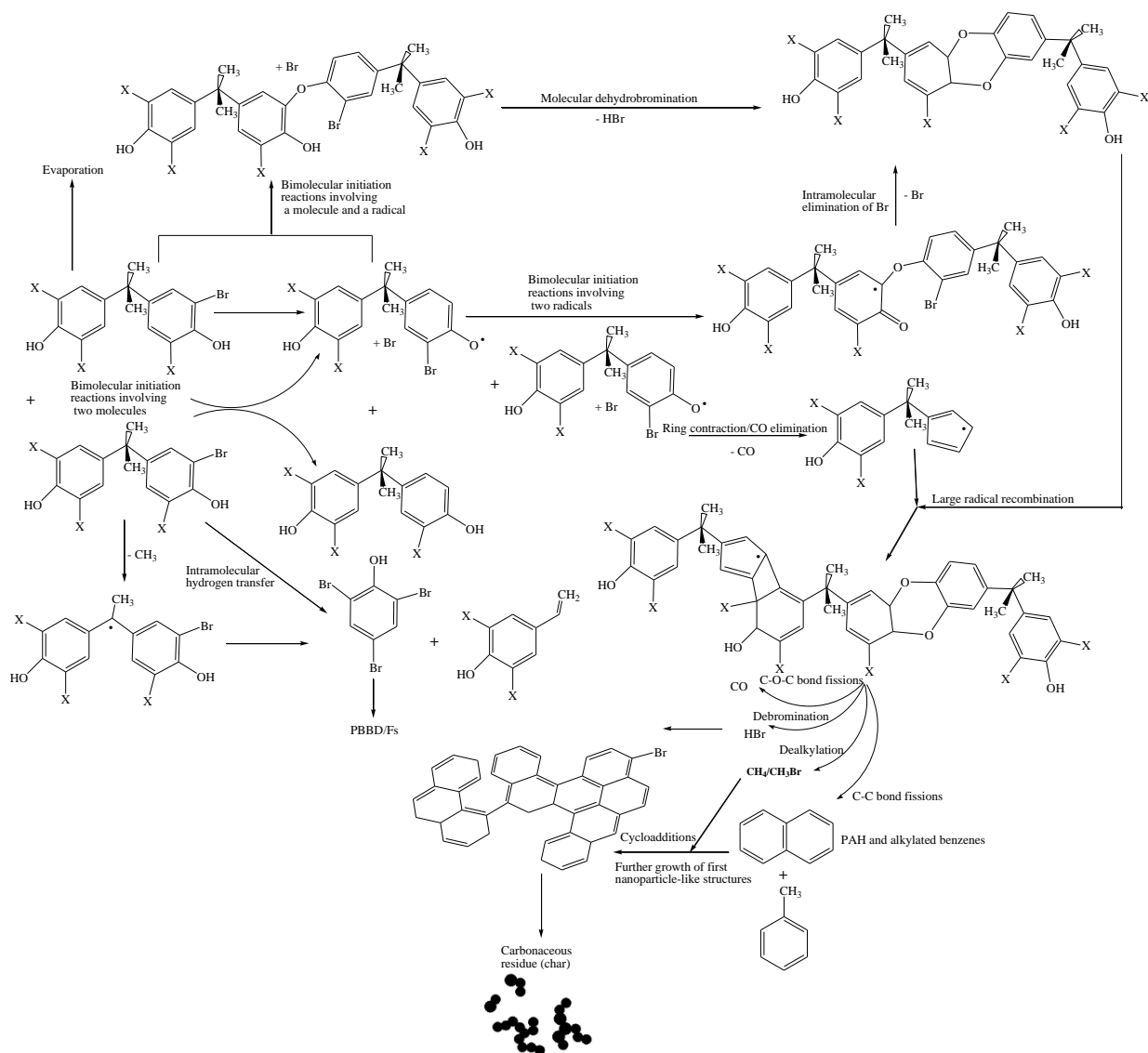
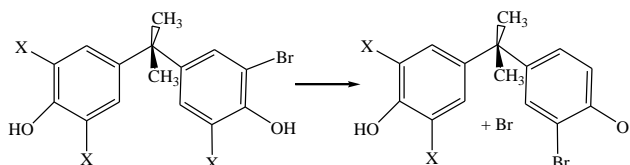
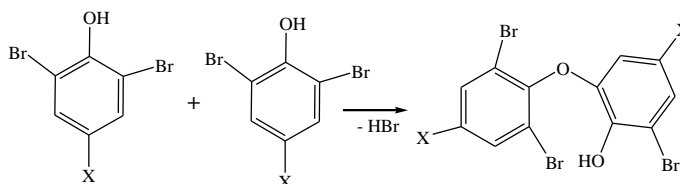


Figure 2.8. Decomposition pathways of TBBA in an aqueous medium [114].

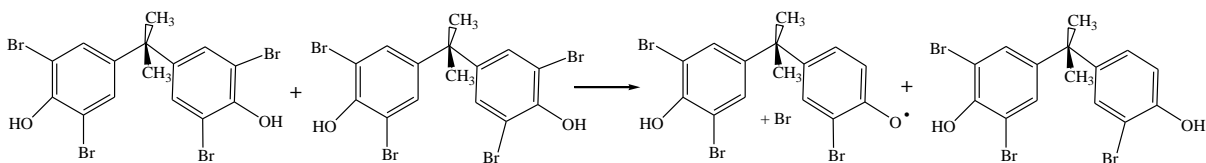
- Elimination of HBr:** Release of HBr/Br leads to the formation of lower brominated bisphenol A derivatives through a complex C-Br fission mechanism and is the most important initiation reaction. Loss of HBr could occur via different modes, most notably through intramolecular H migration from phenolic'H or bimolecular condensation reactions involving molecule/molecule, molecule/radical and radical/radical initiation reactions. Among all plausible HBr elimination reactions, keto-enolic tautomerisation resembles a rate-determining step for the initial decomposition of TBBA:



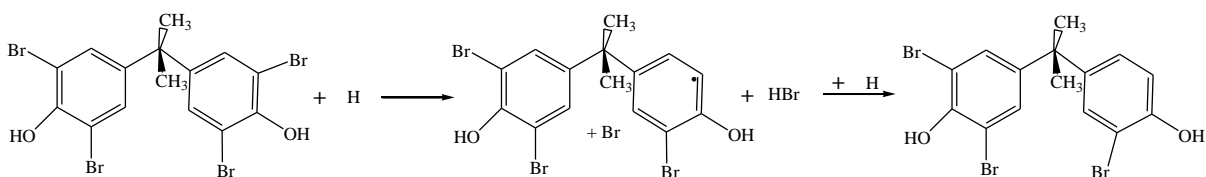
The most important initiation reaction in the gas phase (i.e. elimination of CH_3) is insignificant in the condensed phase. As shown in Figure 2.8, debromination reactions eventually lead to the growth of heavy intermediates via radical- and molecular-substitutive additions. Along the same line of enquiry, Luda et al. [101] demonstrated that HBr elimination occurs via bimolecular displacement of Br atoms with phenolic H atoms:



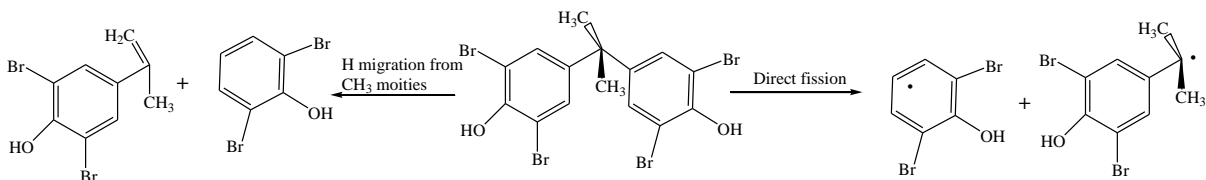
Consecutive HBr elimination/condensation reactions produce carbonaceous residue. HBr elimination from bimolecular reactions involving bromophenols and/or bromophenoxy radicals requires considerable endothermicity when occurring in the gas phase [117]. If HBr elimination/condensation reactions occur readily in the aqueous medium, this suggests that the energetic requirements for this process in the condensed phase differ significantly from corresponding values in the gas phase. The presence of trapped TBBA-like structures in the condensed medium (and in the residue) might entail a steric hindrance between C-Br and O-H bonds, thereby facilitating the expulsion of HBr. The absence of any residue from pyrolysis of bisphenol A highlights the importance of HBr elimination in the formation of char during pyrolysis of TBBA [101]. Bimolecular reactions of two TBBA moieties in the condensed phase yield other brominated congeners of bisphenol A:



In a pyrolytic environment, abundant H atoms selectively abstract Br atoms and occupy the resulting radical site. This process provides another route for the formation of lower brominated isomers of bisphenol A:



- *Scissions of isopropylidene bonds:* Significant concentrations of bromophenols above 573 K form fissions of isopropylidene linkages through different reactions:



Detection of 2,6-dibromophenol as the most abundant bromophenol congener supports the fission of isopropylidene bridges as being the most direct and important corridor for TBBA decomposition. What remains unclear is to what extent such reactions happen in the gas phase. The fact that ruptures of isopropylidene linkages are minor channels in the gas phase [113] implies that scissions of aromatic- $(\text{H}_3\text{C})_2\text{C}$ bonds occur in the condensed phase via a different pathway; possibly catalysed by neighbouring aromatic rings. The release of bromophenols follows rupture of isopropylidene bridges.

- *Reactions leading to the evolution of soot:* The well-known HACA mechanism [118] determines the formation of soot from the pyrolysis and combustion of fuel (e.g. hydrocarbon liquid, biomass, coal, etc.). Initially-formed PAH species continue to grow via polymerisations, coagulations and surface reactions to form soot. Formation of

several PAH compounds from TBBA pyrolysis [103] contributes partially to the generation of residue. However, the largest fraction of residue most likely originates from further growth of heavy components formed by molecular/radical substitutive additions. C-C and C-O bond fissions in these components release CO, alkanes and alkylbenzenes. Further decomposition of the residue may occur by polymerisation of double isopropylidene bonds and condensation of phenolic H bonds. Radical addition to double bonds in heavy components increases the rate of formation of larger molecules, i.e. nucleolus for char. As explained by Marongiu et al. [114], the formation of char from pyrolysis of TBBA should consider analogous process occur during the pyrolysis of heavy distillation residues, namely, diffusion-controlled radical and effective collision recombination.

2.3.1.4. Kinetic modelling

Available kinetic models of TBBA decomposition include single-step global apparent kinetics [99], a detailed model by Marongiu et al. [114], and a correlational and simplified mechanistic model by Font et al. [119]. The comprehensive model by Marongiu et al. [114] incorporates about 60 components (real and lumped molecules/radicals) and 900 reactions. Validating this model against experimental data obtained under isothermal and dynamic TGA runs satisfactorily reproduces many aspects of TBBA degradation and vaporisation, including overall decay of TBBA, relative yields of HBr and carbonaceous residues, evaporation rates of TBBA, and relative distributions of gas phase products (bromophenols and brominated isomers of bisphenol A). Reaction rate constants in this model are mainly based on matching gas phase reactions while taking into account their inversion or transposition into the liquid phase. In this approach, E_a values are corrected (i.e. lowered) by subtracting the condensation heats of reactants. Correction in values of A factors reflects the loss of degree of freedoms (i.e. translational and rotational contributions) from a gas phase molecule to a condensed phase. Reaction rate constants for char formation utilise analogous values in the mechanism for PVC [116]. Table 2.2 summarises the kinetic parameters of Marongiu et al.'s model [114]. Figure 2.4 and 2.9 compare modelled and experimentally-observed values of overall TBBA decay and major brominated decomposition product yields.

Table 2.2. Kinetic parameters for stages in the thermal decomposition of TBBA.^a

CHAPTER 2 Literature Review

Reaction type	A	n	E_a
Initiation reactions and bromine radical	$Y \times 10^{13}$	0	180,000
Initiation reactions of heavy components during char growth	$Z \times 10^{14}$	0	143,000
Bimolecular initiation reactions	10^{13}	0	172,000
Bromine radical substitutive addition	4×10^8	0	25,000
Radical intramolecular addition	$B \times 10^8$	0	146,000
Carbon monoxide elimination	2.5×10^{11}	0	184,000
Decomposition of radicals	2.3×10^{13}	0	126,000
Molecular dehydrobromination	$C \times 10^{12}$	0	190,000
Termination reaction	$E \times 10^8$ to 10^9	1	8400

The value of each variable depends on the type of reactants taking part in the reaction. $Y = 2$ to 8 , $Z = 2$ to 3 , $B = 1$ to 2 , $E = 1$ to 2 , $C = 1$ to 7 . The rate constant parameters expressed in terms of Arrhenius equation with units ($\text{cm}^3 \text{mol}^{-1} \text{s}^{-1}$, J) [114].

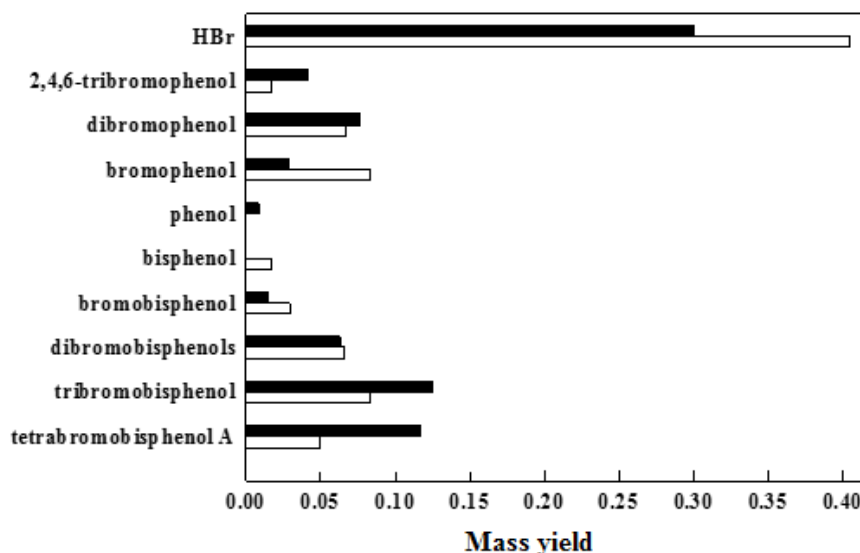
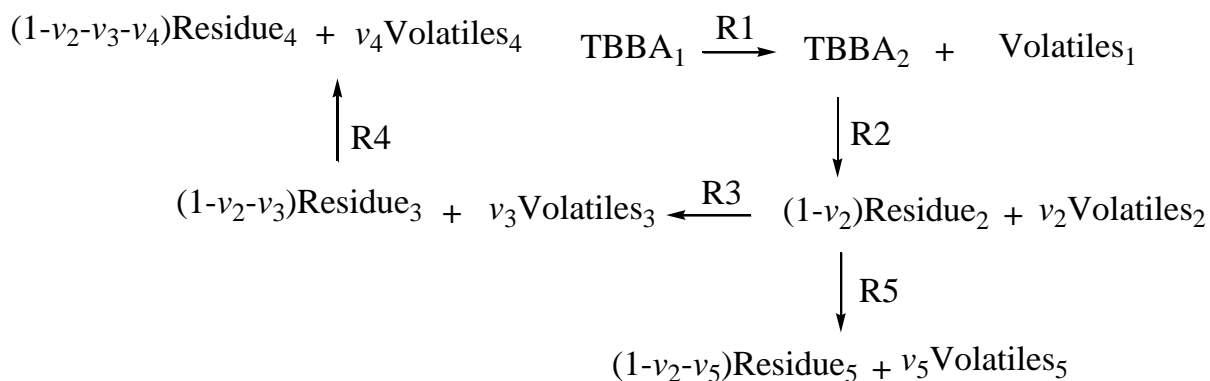


Figure 2.9. Mass yield of major brominated decomposition products of TBBA. White bars = model values [114], black bars = experimental values [45].

The correlation model of Font et al. [119] fits the characteristics of TBBA weight loss, obtained by several isothermal and dynamic TGA runs, to a unique set of kinetic parameters. The underlying idea behind this model is that TBBA decomposition occurs simultaneously with vaporisation through five consecutive global reactions:

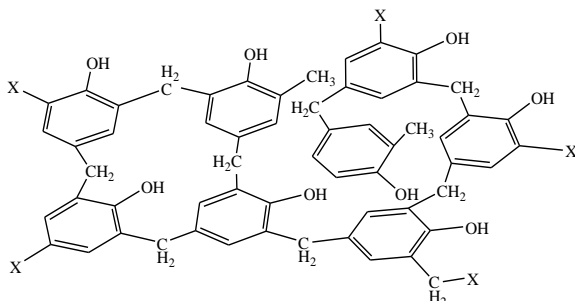


Using an optimisation procedure to model the experimentally-observed weight losses produces apparent kinetic parameters for global reactions R1 - R5. Font et al. [119] simplified the detailed kinetic model of Marongiu et al. [114] to consider only initiation and primary recombination reactions. In this simplified mechanistic model, the five global reactions covered by the correlation model describe decomposition behaviour after the growth of the first heavy molecules (i.e. more than 30 carbon atoms). The main shortcoming of Font et al.'s [119] models is that they only account for TBBA weight loss, vaporisation rate and the average molecular weight of the evolved volatiles. In this regard, a more robust kinetic model of TBBA thermal decomposition would be expected to account quantitatively for the formation of all decomposition products, most notably those reported recently by Ortuño et al. [103].

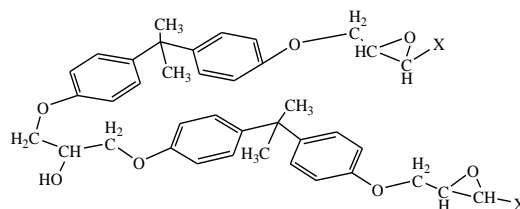
2.3.1.5. Decomposition of polymeric materials laden with TBBA

Co-pyrolysis of TBBA with polymeric constituents can simulate real scenarios relevant to accidental fires involving materials laden with TBBA, or their thermally-based recycling processes. Studies on the pyrolysis of TBBA-containing polymers have investigated the degradation behaviour of four structural categories, namely, neat non-brominated polymers, neat brominated polymers, modified (or hardened) non-brominated polymers and modified (or hardened) brominated polymers. In general, the presence of TBBA units in phenolic materials impairs their thermodynamic stability and increases the amount of residue relative to non-brominated polymers. The initial stage in the weight loss curves of many polymers treated with TBBA mainly corresponds to the evaporation of their TBBA content. Decomposition behaviour of TBBA-treated polymers is dependent on the type of polymeric building block present (i.e. epoxy, phenol, etc.) and the presence of hardening agents (amine groups, aliphatic anhydride, etc.)

Epoxy and phenol resins (below) are the most widely employed plastics in electric and electronic equipment [120]:



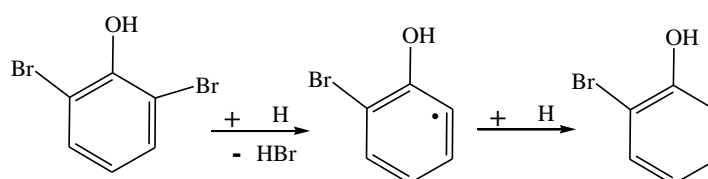
Phenolic resins



Epoxy resins

Results from an interesting study by Grause et al. [105] on the pyrolysis of phenolic resin-containing TBBA highlighted the remarkable differences in the decomposition behaviour of pure TBBA and phenolic resins treated with TBBA:

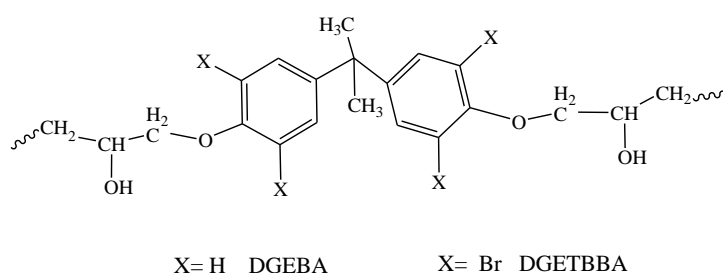
- Pyrolysis of phenolic resin laden with TBBA does not produce brominated or non-brominated congeners of bisphenol A. On the contrary, these compounds account for ~25% of total brominated products produced from the decomposition of pure TBBA [97]. A plausible explanation is that TBBA exists as a co-monomer in phenolic resins, and thus it is trapped in the polymeric material. This has the potential to shut down direct evaporation as a route for the emission of TBBA and its other lower brominated isomers.
- Decomposition of pure TBBA produces higher yields of BPhs (as the mass fraction relative to TBBA initial mass) than phenolic resins containing TBBA. Pyrolysis of polymers produces a hydrogen-rich environment. Abundant H atoms preferentially abstract bromine atoms, thereby lowering total BPh yields, as follows:



- In the pyrolysis of pure TBBA, ~ 55 % of the initial bromine content transforms into HBr. Formation of HBr arises from initial H migration from the OH group and, most importantly, through bimolecular condensation reactions (Figure 2.8). Emission of HBr from the thermal degradation of phenolic-resin treated with TBBA contributes approximately 87 % of the initial bromine content and occurs within two main temperature intervals: either below or above 673 K. Nearly 50 % of HBr is released in the first temperature interval, while the remaining 37 % is emitted in the temperature range of 673 – 973 K. Emission of HBr in the first interval corresponds to the decomposition of TBBA. Decomposition of phenolic resins commences above 673 K and thus, the formation of HBr in the higher temperature interval most likely stems from Br abstraction by H radicals. The latter is produced from the fragmentation of phenolic resins.

- Similar to the decomposition of free TBBA, the formation of brominated aromatics from the pyrolysis of phenolic resins laden with TBBA completes at 643 – 673 K.

Diglycidyl ether bisphenol A (DGEBA) and diglycidyl ether tetrabromobisphenol A (DGETBBA) epoxy resins constitute the basic building blocks of TBBA-epoxy types (the epoxy group \triangle experiences rapid enolisation into a C-OH moiety):

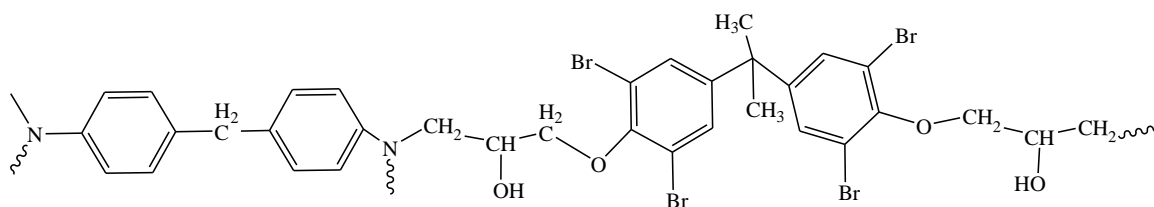


Quan et al. [104] and Luda et al. [121] present two distinct weight loss curves for the decomposition of DGETBBA based on a heating rate of 10 K min⁻¹. Quan et al. [104] found that the degradation curve of DGETBBA proceeds with one stage of weight loss in range of 543 – 673 K, leaving a solid residue equal to 64.0% of the original mass. A faster TGA heating rate of DGETBBA of 20 K min⁻¹ reduces the amount of residue to 17% [121]. Barontini et al. [112] also highlighted the dependence of residues on heating.

Faster heating rates produced lower amounts of residues under oxidative and pyrolytic operating conditions.

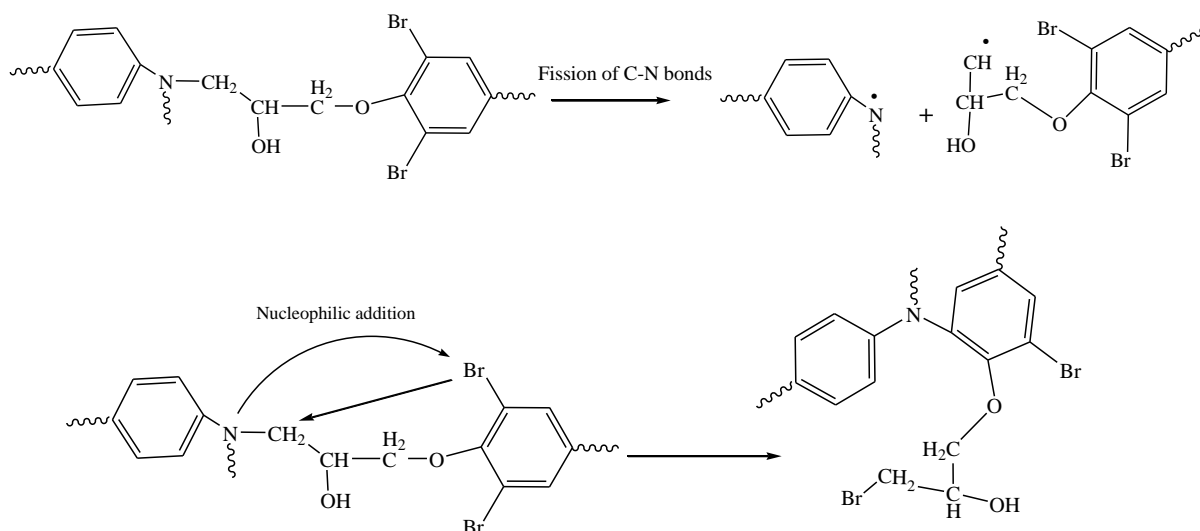
Evaporation of DGEBA and DGETBBA commences at 528 K and 547 K, respectively. Formation of TBBA and bisphenol A from pyrolysis of both DGEBA and DGETBBA suggests fission of O-CH₂- bonds and the occurrence of parallel bromination reactions [104]. Products of DGETBBA decomposition span all species evolved from pure TBBA pyrolysis, i.e. bromophenols, bisphenol A, *p*-isopropenylphenol and PBDD/Fs [97]. Covalently-bonded and additively incorporated TBBA in epoxy resins produce very similar homologue profiles of PBDD/Fs [107]. In both cases, mono bromo dibenzofurans congeners dominate the isomer distributions of PBDD/Fs. This infers that the formation of BPhs from TBBA is not satirically hindered due to the covalent fixation of TBBA in the epoxy backbone. Oxidative and pyrolytic decomposition of TBBA-epoxy types has nearly the same conversion rate of bromine into HBr (i.e. 57.1% and 53.6 %, respectively) [112].

Brominated epoxy resins often incorporate amine-containing co-monomers as hardening agents [122]. Cured DGETBBA with 4,4'-diaminodiphenyl represents one of the most widely deployed epoxy resins in printed circuit boards [123]:

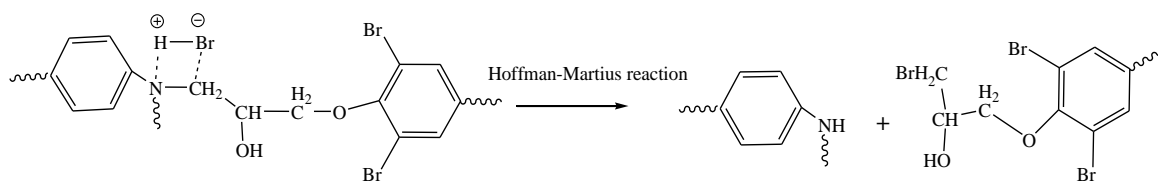


TBBA-containing resin cured with a nitrogen-hardener

Weak allylic C-N bonds, and the property of the amine group as being a good nucleophilic attacking group, combine to control the initial decomposition of nitrogen-cured, TBBA-based epoxy resins [124]:



Further degradation of brominated epoxy resins cured with amine-containing compounds occurs via HBr addition through the Hofmann-Martius reaction [125]:



Brominated epoxy resins cured with amine groups start to decompose at around 553 K [124], which is similar to that for pure TBBA [97]. In contrast, degradation of non-brominated epoxy resins commences at ~ 653 K. The presence of N-C bonds in both brominated and non-brominated resins suggests that reactions derived by HBr (nucleophilic addition) cause a rapid decomposition of brominated epoxy resins (which occurs at lower temperatures than in non-brominated epoxy resins). The HBr-catalysed decomposition of epoxy resins has serious implications for the safe pyrolytic recycling of TBBA-containing wastes and should receive prior consideration.

The degradation of cured brominated epoxy ester with phthalic anhydride [121] shares very similar characteristics with the analogous decomposition of brominated amine hardened epoxies [122, 124]. In comparison with non-brominated phthalic anhydride epoxy, its brominated counterpart loses weight more steeply at temperatures higher than 613 K, manifesting as thermal instability with increasing temperature. Unimolecular re-

arrangements of the oxirane ring and elimination of a glycidyl group starts the decomposition of phthalic anhydride epoxy [121]. It will be essential to develop kinetic models of the decomposition of TBBA-laden polymers.

2.3.1.6. Fixation of Br content in TBBA via introducing metal oxides

Interest in the effects of metal oxides on the thermal decomposition of TBBA originates from their profound capacity to act as halogen absorbers or fixers [126-129]. While adding metal oxides does not significantly change the decomposition profile of pure TBBA, it greatly suppresses formation of HBr and brominated phenols. Figure 2.10 compares bromination speciation for different types and loads of metal oxides [129]. XRD measurements prove that part of the bromine in TBBA is converted into metal bromides and oxybromides. Further reduction of metal oxides into metallic species is accompanied by enhanced CO₂ yield. The exact mechanism for the action of metal oxides is not known. A rise in concentrations of benzene suggests that metal oxides abstract a Br atom, either from the original TBBA or any other brominated species. The Deacon reaction may contribute to the reduction in HBr concentrations; however, simultaneous FTIR measurements of Br₂ are not available to support this.

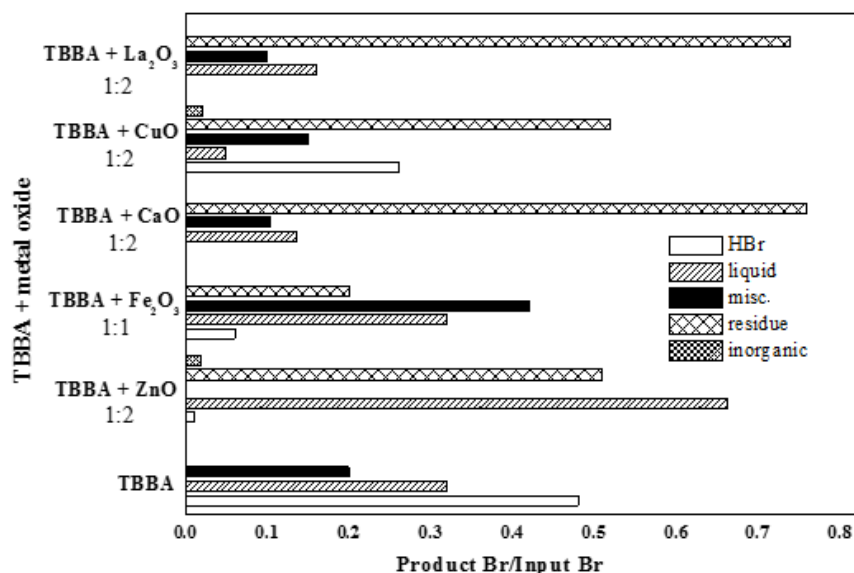
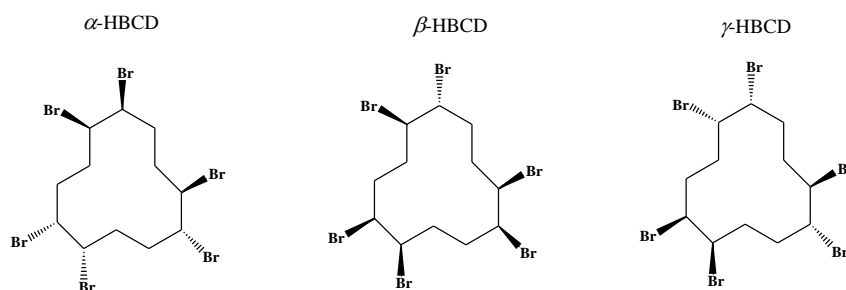


Figure 2.10. Distributions of bromine mass produced by pyrolysis of TBBA-metal oxide mixtures (molar ratio) at 673 K [129].

Thermodynamic considerations greatly favour direct reactions between metal oxides and HBr. Although metal oxides perform as HBr scavengers, they could potentially promote the formation of PBDD/Fs. As a consequence, the overall merit of deploying metal oxides as an abatement technology for bromine emissions during thermal treatment of TBBA warrants further investigation.

2.3.2. Thermal decomposition of HBCDs

Depending on the achiral positioning of bromine atoms with respect to the C₁₂ ring, there exist 16 theoretically possible stereoisomers of HBCDs [130]. Among these, the labelled α -, β - and γ -HBCD enantiomers dominate all technical mixtures of HBCDs [131]:



Melting temperatures for these three isomers are reported to be 445 K, 442 K and 482 K, respectively [132]. Samples of HBCDs with different isomeric compositions exhibit very similar degradation profiles. Decomposition occurs mainly in the narrow temperature range of 503 – 543 K [4, 133]. This observation could be explained by a rapid equilibrium being established between isomers of HBCDs at elevated temperatures [134].

Earlier studies on the thermal decomposition of HBCDs focused on its thermal stability and provided very similar weight loss curves [132, 135-136]. Isothermal TGA runs indicated that the decomposition of HBCDs commences at 513 K, after which a HBCD ring undergoes dramatic decomposition in one stage, assuming an S shape [136]. This, in turn, suggests that the overall decomposition of HBCDs is governed by an autocatalytic process derived from initially formed radical species. Reported apparent activation energy for the overall decomposition of HBCDs is in the range 90 – 120 kJ mol⁻¹. These estimates are considerably lower than the activation energies required for the unimolecular elimination of HBr from brominated gas phase linear alkanes, i.e. ~ 240 kJ/mol [137]. This indicates that the first HBr elimination is not a rate-determining step

in the overall decomposition of HBCDs and supports the occurrence of an autocatalytic, sustained, reaction chain. However, it is worthwhile noting that the literature does not provide kinetic or thermochemical data on HBr loss from brominated cycloalkanes for comparison.

At a constant heating rate of 10K min^{-1} , rapid decomposition of HBCD consumes 94% of its initial content [133, 136]. Formed HBr accounts for $\sim 73\%$ of the initial bromine load. The inability of FTIR to detect Br_2 impedes attempts to provide conclusive evidence regarding its formation. GC/MS analysis of the pyrolysis residue identifies a wide range of brominated/non-brominated $\text{C}_8 - \text{C}_{12}$ products. Detected species include lower brominated congeners of cyclododecadiene, brominated biphenyls, brominated methyl-naphthalene and brominated cyclododecatriene. Detection of these products by Barontini et al. [133, 138] provides an experimental verification of the decomposition mechanism originally proposed by Larsen and Ecker [136]. This mechanism mainly involves successive dehydrobromination reactions, unimolecular arrangement, C-C bond breakage reactions, Diels-Alder reactions and radical-derived reactions. The occurrence of these reactions implies that intramolecular reactions hold more importance than intermolecular reactions. Formation of mono-, di- and tri- brominated biphenyls and alkyl naphthalene exclusively suggests that these compounds come from tetrabromocyclododecadiene (TBCD). The latter forms after three subsequent HBr elimination reactions from the parent HBCD. Figure 2.11 portrays an overall mechanism for the decomposition of HBCDs. Note that this mechanism has no analogous mechanistic validation with quantum chemical calculations. Constructing a simplified kinetic model based on global reaction steps will be instrumental in providing further insight into HBCD decomposition. Introducing oxygen does not affect the decomposition behaviour of HBCD nor does it influence the product profiles [133, 136]. On the other hand, the presence of impurities in HBCD samples seems to greatly enhance its thermal decomposition.

Studies on the thermal decomposition of HBCDs point out that two important aspects require further investigation: the effect of polymeric matrices and the contribution of a gas phase decomposition route. As the overall degradation of HBCDs is governed by an autocatalytic process, the presence of C_xH_y radical species may potentially cause the decomposition of HBCDs to commence prior to its melting. This would have important implications for the operational requirements of safe HBCD deployment, as well as for

its thermal recycling. All pyrolysis studies on HBCDs demonstrate that HBCD decomposition occurs in one stage, corresponding to its degradation in the aqueous phase. Nevertheless, HBCDs share a defining physical feature with VOCs [139]. They can emit to the atmosphere from treated objects at ambient temperatures, with a reported 40-fold increase when the temperature rises to 353 K [140]. The latter temperature could easily be reached within a landfill, due to heat release by biodegradation [141]. Investigating the decomposition of HBCDs in the gas phase will help to better understand its behaviour under ambient conditions.

Oxidation of pure HBCDs does not yield any congeners of PBDD/Fs. On the contrary, controlled incineration of polystyrene and extruded polystyrene with HBCD in a pilot-scale plant resulted in the formation of 0.028 ng g^{-1} of PBDD/Fs [142]. Nonetheless, the addition of HBCD did not change the yield or pattern of formed PBDD/Fs, suggesting that these brominated pollutants form from the breakdown of the polymeric constituents, via de novo synthesis rather than through a precursor pathway. However, as discussed in the next section, brominated biphenyls (major products of HBCD pyrolysis), act as building blocks for PBDFs.

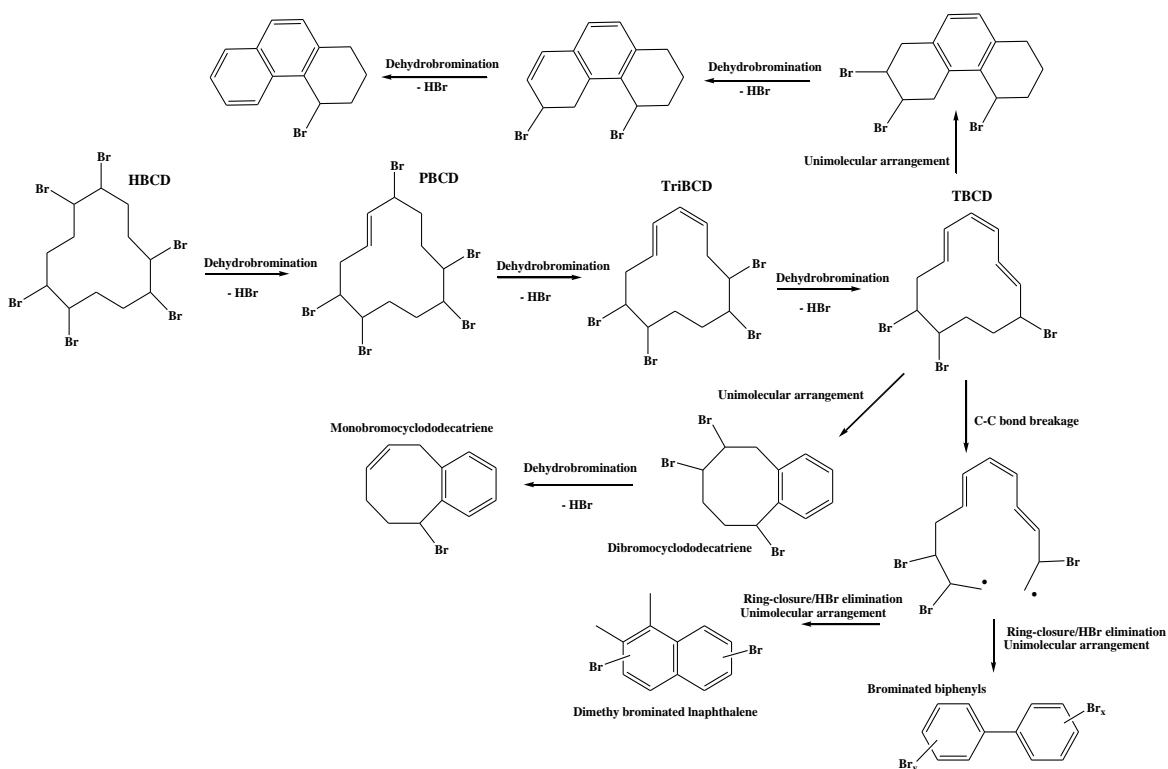


Figure 2.11. Proposed mechanism for the decomposition of HBCD [133, 136].

2.3.3. Thermal decomposition of PBDEs and polybrominated biphenyls (PBBs)

Earlier studies on the thermal decomposition of BFRs (1970's – 1990's) focused mainly on the degradation of PBDEs and PBBs in laboratory-scale pyrolysis experiments [109, 143-150]. Investigated aspects included 1) decomposition behaviour of pure PBDEs and PBBs, 2) the effect of polymeric materials, 3) potential for the formation of PBDD/Fs, and 4) degradation during extrusion (i.e. compounding) with polymers. Table 2.3 summarises the operational conditions used in these studies, the major decomposition products, and associated PBDD/F emission profiles.

Table 2.3. Thermal decomposition of PBDEs, PBBs, PBDEs and PBB-laden polymeric materials.

BFRs	Reactor type/operating conditions	Thermal decomposition products	Max. concentration of PBDD/Fs at T (K)	References
DBDE	Oven Oxidation (673 – 1073 K)	HBBz, PBDD/Fs, CO ₂ , HBr, Br ₂	773 K (ppm) PBDD/F (3000)	[149]
DBDE with polymer matrix	Oven Oxidation (673 – 1073 K)	HBBz, PBDD/Fs, CO ₂ , HBr, Br ₂ , TBDFs	873 K (ppm) PBDD/Fs (124000) PBDFs>>PBDDs	[149]
Decabromodiphenyl with polybutylene terephthalate	Quartz tube reactor Oxidation (5% O ₂) (673 – 973 K) $\tau = 20$ min	Tri- to octa- BDFs tetra- to octa- BDDs	873 K (ppm) Σ PBDFs (82) Σ PBDDs (218 ppb)	[109]

CHAPTER 2 Literature Review

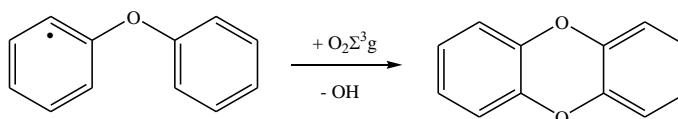
Decabromodiphenyl with polybutylene terephthalate	Quartz tube reactor Pyrolysis (673 – 973 K) $\tau = 20$ min	Tri- to octa- BDFs	873 K (ppm) PBDFs (20.1)	[109]
DBDE	Oven Pyrolysis (673 – 1073 K)	PBDFs>>PBDD (hexa- to octa- BDD/Fs)	773 K (ppm) Σ PBDF (2756)	[143]
DBDE with polystyrene and 4% antimony oxide	DIN Oven Pyrolysis 873 – 1073 K	Analysed dioxin/furan products PBDFs>> PBDDs	873 K (ppm) PBDF (>100000)	[110]
OBDE immersed ABS (6% antimony oxide)	Oven, Pyrolysis (873 – 1073 K)	PBDFs>> PBDDs	873 K (ppm) PBDDs (1000) PBDFs (>300000)	[110]
Penta-BDE with polyurethane	oven Pyrolysis (873 K)	di- to tetra- BDDs di- to penta- BDFs	(ppm) Σ PBDFs (50000) Σ PBDDs (>70000)	[110]
Technical mixture of HBBs	Quartz tube reactor (1073 K)	Tri- to hepta- BDF	(ppm) PBDFs (2070)	[150]
Penta-BDE	Quartz tube reactor Pyrolysis (973 – 1173 K) τ =10 min	PBDFs>> PBDDs (mono- to penta-BDD/Fs)	973 K (ppm) Σ PBDD (254700) Σ PBDF (614800)	[148]
DBDE	Quartz tube reactor Pyrolysis	PBDFs>> PBDDs (tetra- to octa- BDD/Fs)	1173 K (ppm) Σ PBDD (2774) Σ PBDF (15586)	[148]

CHAPTER 2 Literature Review

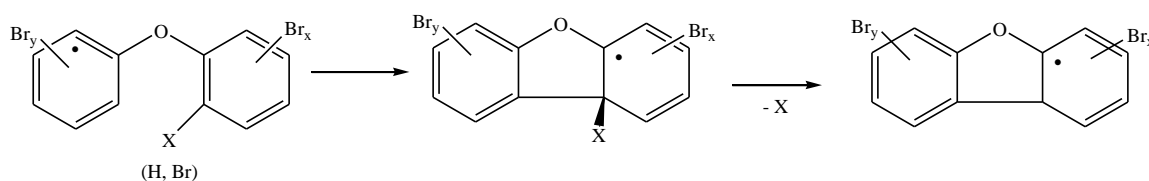
	(973 – 1173 K)			
	$\tau = 10$ min			
HBBs with polystyrene (PS)	Quartz tube reactor Pyrolysis (973 K, 1073 K, 1173 K) $\tau = 10$ min	di to hepta-BDFs	1073 K (ppm) PBDFs (8900)	[148]
HBBs with polyethylene (PE)	Quartz tube reactor pyrolysis (973 K, 1073 K, 1173 K) $\tau = 10$ min	di to hepta-BDFs	973 K (ppm) PBDFs (43000)	[148]
PBDE	Thermolysis Quartz minivals (783 K) $\tau = 60$ s	HBr, PBBz, Tri- and tetra-BPh, BFs, naphthalenes, mono- to hexa-BDD/Fs	(ppm) \sum PBDD/Fs (100000)	[147]
OBDE	Quartz minivals Thermolysis (903 K) $\tau = 60$ s	PBBz, Tri- to hepta-BDD/Fs	(ppm) \sum PBDD/Fs (50000)	[147]
PBBs	Quartz minivals Thermolysis (903 K) $\tau = 60$ s	tetra- to octa-BDD/Fs	(ppm) \sum PBDD/Fs (10000)	[147]
PBBs	Glass tube, pyrolysis (653 – 673 K)	tetra- to penta-BDFs	(ppm) \sum PBDFs (44)	[157]

2.3.3.1. Degradation of pure PBDEs

Starting with the decomposition of pure PBDEs, the highest yields of PBDD/Fs under condensed phase conditions occur at around 873 K, in total yields of up to ~ 10 % [147]. This temperature coincides with the analogous optimal range for the formation of PBDD/Fs during PBDE pyrolysis in a gas phase process, i.e. 873 K – 973 K [146]. Luijk and Grovers suggest PBDD/F formation is a combination of homogenous and heterogeneous pathways [151]. Altarawneh and Dlugogorski [152] have recently constructed a gas phase mechanism for the synthesis of PBDD/Fs from PBDEs. Figure 2.12a depicts the principal pathways of this mechanism (based on 2,2'-dibromodiphenyl ether as a representative compound for the PBDE family). Central to these pathways is the abstraction of an *ortho* H/Br substituent, followed by addition of an oxygen molecule to the vacant radical site. As Figure 2.12a shows, the formed peroxy adduct (ROO \cdot) evolves in a very exothermic and complex corridor to yield PBDDs congeners. DFT molecular modelling predicts that the overall reaction:



is exothermic by $242.1 \text{ kJ mol}^{-1}$, with a net activation energy of 48.5 kJ mol^{-1} residing below the separated initial reactants. Isomers of PBDF result from a direct C-C bridging:



Reactions comprising this mechanism incur substantially lower energy requirements than other proposed pathways that lead to the formation of BPhs [39], such as the unimolecular elimination of HBr ($340.0 \text{ kJ mol}^{-1}$ at 298.15 K) and direct fission of C-O bonds (337.0

kJ mol^{-1} at 298.15 K). The simple nature of the mechanism shown in Figure 2.12a supports the experimentally detected high yield of PBDD/Fs from PBDE oxidative decomposition. Altarawneh and Dlugogorski demonstrate that the degree of bromination has little influence on the calculated thermochemical and kinetic parameters and that all congeners of PBDEs form PBDD/Fs at very comparable rates. However, this finding contradicts the experimental observation [145] that lower brominated PBDEs (e.g. Penta-BDE) form PBDD/Fs better than higher brominated isomers do (e.g. Octa-BDE). To provide a plausible explanation, it was suggested that HBr elimination (i.e. the first step in the conversion of PBDEs into PBDD/Fs) becomes more sterically hindered as the degree of bromination increases [153].

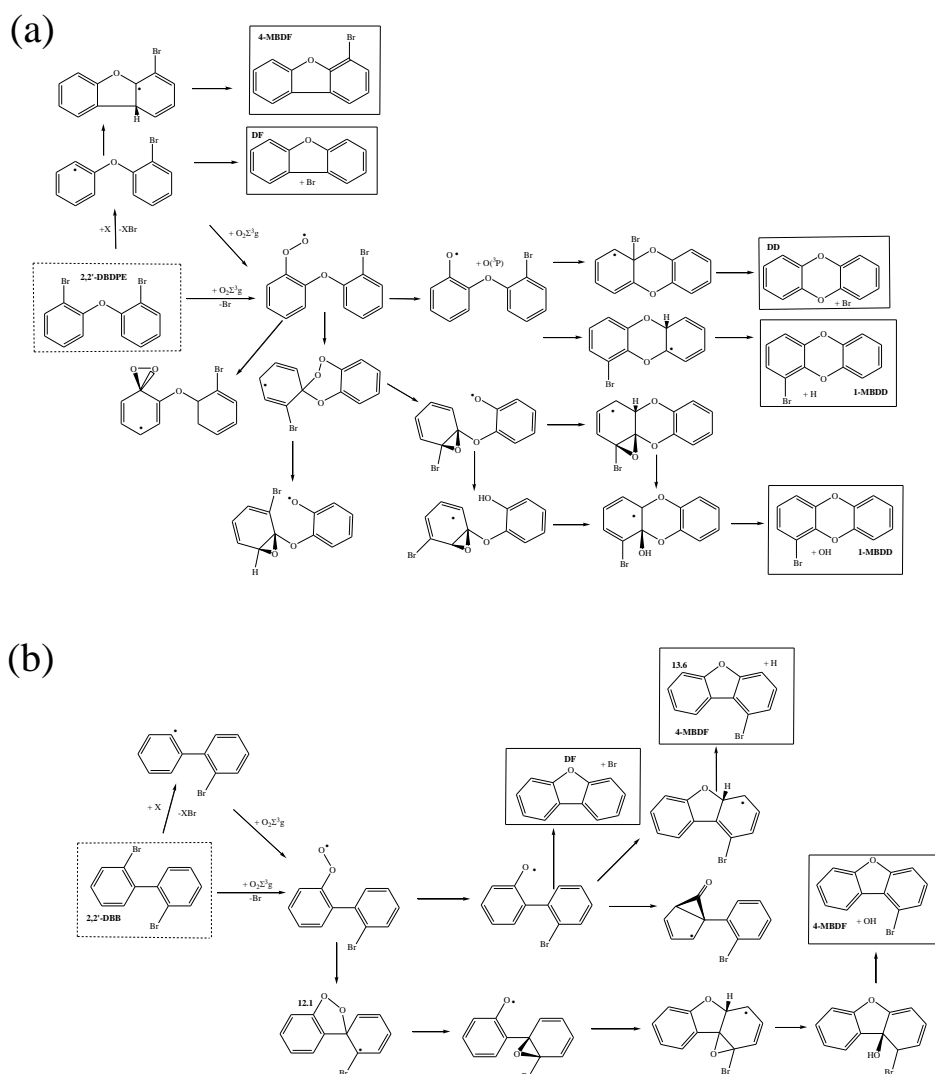


Figure 2.12. Mechanism of gas phase formation of (a) PBDD/Fs from PBDEs [152], and (b) PBDFs from PBBs [158].

If the formation of PBDD/Fs occurs via the mechanism presented in Figure 2.12a, the low yield of PBDD/Fs from higher brominated PBDEs merits further clarification. A plausible explanation might partially originate from the inverse relationship between PBDE isomer vapour pressures and bromination degree [154]. At 293 K, the vapour pressure for a penta-BDE is two orders of magnitude lower than for a hepta-BDE congener. Consequently, it is sensible to assume that the evaporation of PBDEs decreases considerably with increasing degrees of bromination. In other words, the potential for PBDE congeners to undergo oxidative transformation into PBDD/Fs is influenced by their evaporation rates. It will be informative to test this argument experimentally by measuring the PBDD/F yields of comparable concentrations of gaseous PBDEs, with different degrees of bromination, at the same temperature.

2.3.3.2. Effects of polymers on the generation of PBDD/Fs from PBDEs

Four observations demonstrate the effects of polymeric materials on the formation of PBDD/Fs produced by the decomposition of PBDE-laden polymeric materials, compared with those produced from pure PBDEs [145]:

- Reduction in the optimal temperature window for PCDF formation, from ~ 873 K to 623 – 673 K.
- Profound selectivity towards PCDF formation. Luijk et al. [145] explained that addition of polymeric materials to pure PBDEs results in a 7-fold increase in the formation of PCDFs.
- Significant enhancement of total PBDF yield.
- Shifting homologue patterns toward lower brominated congeners.

Figure 2.13 [110] contrasts the temperature profiles for PBDF formed from pure PBDE (in a condensed phase) with the profiles of various PBDE-containing polymer blends. The underlying mechanism, in which polymeric materials increase the rate at which PBDF is formed from PBDE, is still a matter of discussion. It is suggested that hydrogen atoms in the condensed phase replace bromine atoms via hydrogen/bromine exchange reactions, leading to lower brominated congeners of PBDEs [109]. This is followed by

evaporation of PBDE isomers. Similarly, Luijk et al. [151] suggested that PBDEs abstract hydrogen atoms from polymeric chains during their melting phase; a process which also shifts the homologue profile toward lower brominated congeners.

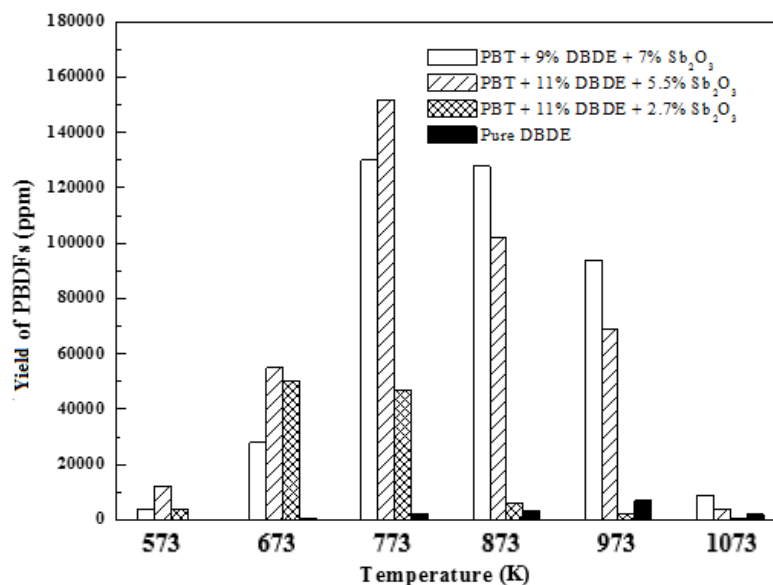
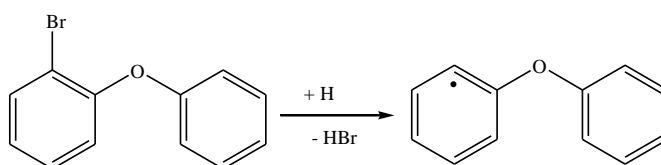


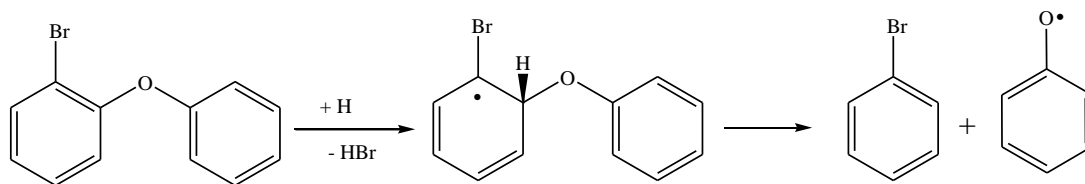
Figure 2.13. Comparison of temperature profiles for the formation of PBDFs from pure DBDE and different polymer blends containing PBDE + Sb₂O₃. PBT denotes polybutylene-terephthalate [110]

As demonstrated in the preceding section, loss of *ortho* H/Br substituents from PBDE isomers initiates their simple conversion into PBDFs. Pyrolysis or oxidation of polymers proceeds in a hydrogen-rich environment. Hydrogen atoms selectively abstract aromatic Br atoms via a trivial reaction barrier (37.3 kJ mol⁻¹) [152]:



In the condensed phase, an intramolecular movement could lead to the expulsion of a Br atom or unimolecular loss of an HBr molecule. Reactions of PBDEs with H atoms could potentially generate potent building blocks for the formation of PBDD/Fs [152]. Addition

of an H atom to the pivot bridge in a PBDE produces a brominated phenoxy radical and a brominated benzene molecule:



Indeed, the absence of any PBDD congeners from the pyrolysis of pure PBDEs or polymer-containing PBDEs does not enable verification of the occurrence of this H-derived splitting of the ether linkage [110]. It is anticipated that carrying out a thermolysis study on PBDEs under highly reducing conditions would be instrumental in revealing the extent of H-induced splitting. The analogous breakage of ether linkages by ipso addition of Br atoms has been confirmed experimentally [155] and theoretically [152].

The observed debromination of PBDEs by polymeric materials seems to overlap with the functionality of BFRs in scavenging the propagating H/Br radicals [151]. For example, Br atoms released during the scavenging process readily abstract an aromatic H atom [152]. Brauman and Chen explained that the decomposition of hydrocarbon chains initiates an autocatalytic debromination of PBDEs, i.e. the first step in transforming PBDDs into PBDFs [156]. It will be interesting to explore the mechanisms of PBDE and polymeric hydrocarbon chain interactions. One of the most intriguing unanswered questions in this regard is whether $-C_xH_y-$ chains can mediate ring-closure reactions toward PBDFs, in addition to their established role in the debromination process.

All of the aforementioned studies were carried out in laboratory-scale reactors (i.e. quartz tubes). The study by Sakai et al. [155] is perhaps the only investigation reporting levels of PBDD/Fs produced from PBDEs and polymer-containing PBDEs under combustion-like conditions. The broad conclusion is that adequate, well-controlled combustion conditions greatly reduce the input concentrations of PBDEs and PBDD/Fs. However, there are no studies of the behaviour of PBDEs or PBDE-laden polymers under real fire scenarios.

2.3.3.3. Decomposition of PBBs

Studies of the thermal decomposition of PBBs are very limited. The oxidation of 2,2',4,4',5,5'-hexabromobiphenyl (the so-called FireMaster FF-1) at 653 – 673 K in open and closed glass tubes produces 40 ppm tetra-BDFs (TBDFs) and 4 ppm penta-BDFs, respectively [157]. While glass tubes likely involve a catalytic wall effect, the dominant formation of TBDF congeners and absence of any PBDD congeners serves as confirmatory evidence of a gas phase process that converts PBBs into PBDFs through a simple, exothermic mechanism [158]. Figure 2.12b features the most important reaction in this O₂-initiated mechanism. Similar to the mechanism governing the formation of PBDDs from PBDEs, this mechanism involves a unimolecular arrangement of the initially-formed RO₂ adduct leading to the formation of PBDFs. Other previously suggested mechanisms [39] are deemed to be unfeasible from a mechanistic point of view (insertion of O₂ into the structure of PBBs) or are energetically prohibited (fission of C-C bridge).

In spite of pure pyrolytic conditions, the co-pyrolysis of PBBs with polybutylene terephthalate polymers (PBT) produces PBDF congeners at 10 ppm in the temperature window 673 – 773 K, without detection of any PBDD congeners [109]. The source of oxygen in formed PBDFs must originate from oxygen contained in the PBT polymer. Introducing oxygen increases concentrations of PBDFs up to 70 ppm for certain PBDFs isomers. Concentrations of PBDDs under oxidative conditions are lower than those of PBDFs by at least two orders of magnitude [109]. The addition of PBBs does not exert any influence on the decomposition behaviour of pure PBT. Considering that PBT starts to melt at 653 K, and formation of PBDD/Fs peaks at 873 K, two important pivotal points can be concluded:

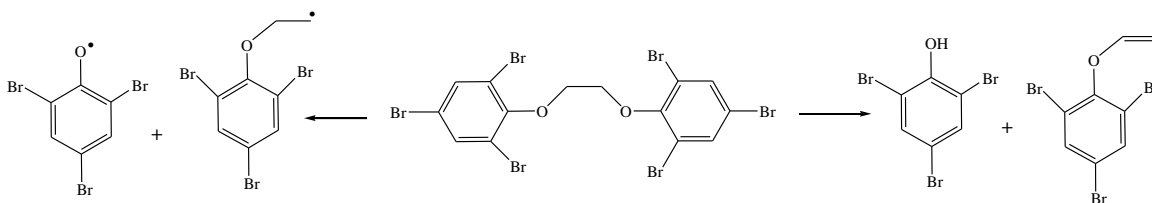
- Evaporation of PBBs occurs during polymer breakdown in the condensed phase.
- Formation of PBDFs from PBBs follows a gas phase mechanism; i.e. the oxidative transformation mechanism shown in Figure 2.12b.

Concentrations of PBBs can still be detected in the environment decades after their use and production was prohibited. Uncontrolled burning or incineration of materials laden with PBBs is an ongoing environmental and health burden. Owing to their simple structure, PBBs could potentially combust or pyrolyse with any aromatic-containing

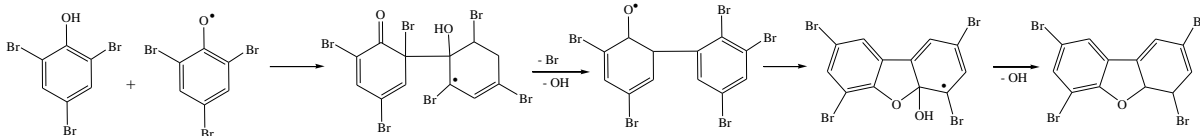
BFRs. However, PBB formation has not yet been confirmed experimentally from the thermal decomposition of any BFRs. Biphenyl constitutes a major product from pyrolysis of benzene [159] and other simple aromatic compounds. In other words, PBBs could form as unwanted by-products from combustion/pyrolysis of any aromatic-containing fuels if bromine is present.

2.3.4. Decomposition of 1,2-Bis-(2,4,6-tribromophenoxy)ethane (BTBPE)

Studies on the thermal decomposition of BTBPE provide a very consistent picture. Balabanovich et al. [160] found that BTBPE, initially in powder form, evaporates unaltered at 513 K before it completely decomposes at 613 K in the gas phase. Striebich et al. [146] investigated gas phase decomposition of BTBPE in inert and oxidative media and found very similar stability behaviour under both oxidation and pyrolytic conditions. In both studies, major products included an equivalent amount of two compounds, 2,4,6-tribromophenol and 2,4,6-tribromophenyl ether. Altarawneh and Dlugogorski [117] reported that these two products arise from the two most important channels in the unimolecular decomposition of the BTBPE molecule. These two channels characterise a 1,3-hydrogen shift from a CH₂ site to an O site and a direct scission of CH₂-O bonds:



These two reactions require very similar energetic requirements: 266.8 kJ mol⁻¹ (1,3-hydrogen shift) and 276.0 kJ mol⁻¹ (fission of CH₂-O bond). Formation of several congeners of tetra-BDDs (TBDDs) indicates coupling of 2,4,6-tribromophenol molecules or their derived 2,4,6-tribromophenoxy radicals. In the first instance, double bromination of *ortho* sites in 2,4,6-tribromophenoxy radicals hinders the formation of PBDFs, which is consistent with the experiments of Balabanovich et al. [160]. Nonetheless, theoretical modelling suggests that the formation of PBDFs could occur from bimolecular reactions involving 2,4,6-tribromophenol and 2,4,6-tribromophenoxy molecules.



The absence of any PBDF compounds in Balabanovich et al.'s experiments could be due to the use of a single quadrupole mass spectrometer. This allows no attenuation of the baseline noise that would have been possible with a MS/MS (triple quadrupole) machine, using the multiple reactions monitoring (MRM) technique commonly applied for PBDF detection. Clearly, future work on BTBPE decomposition should carefully screen for the formation of PBDFs.

2.4. Combustion behaviour of bromine

2.4.1. Speciation of bromine during decomposition of BFRs

Bromine content in typical MSWs varies in the range of 20 - 520 mg kg⁻¹ [41, 161-163]. Concentrations of bromine in MSWs loaded with BFRs could reach as high as few wt % [162, 164]. As such, it became imperative to study bromine speciation during the thermal treatment of waste streams containing BFRs. Vehlow and Mark [41, 165] observed bromine branching into gas, fly ash and bottom ash during combustion of flame-retarded extruded polystyrene in a pilot incinerator at 1173 K. Figure 2.14 shows the bromine inventory in these three phases following the thermal treatment of e-waste. Two key points can be concluded from reported bromine phase speciation:

- The amount of bromine in bottom ash remains nearly constant if the amount of input bromine increases. Input bromine is of an organic nature that decomposes into gaseous HBr and smaller brominated species at relatively low temperatures.
- The majority of initial, organic-bonded bromine disintegrates into the gas phase.

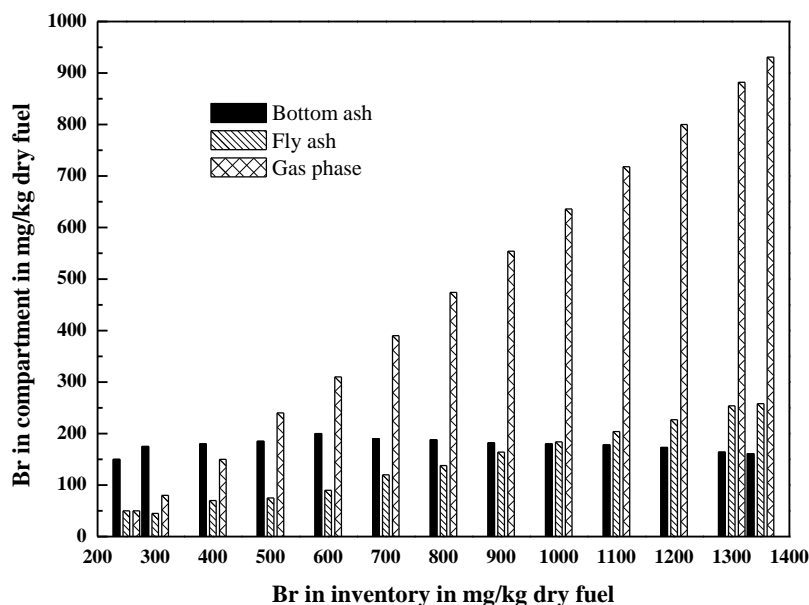


Figure 2.14. Speciation of bromine from combustion of e-waste-containing fuels at 1223 K [41, 165].

Figure 2.15 depicts the partitioning of gaseous Br into HBr and Br₂. The striking feature in this figure is that elemental bromine starts to appear only when the total bromine gaseous content exceeds 250 mg m⁻³. The share of Br₂ reaches 50% of the total gaseous fraction at higher bromine loads. The high Br₂ contribution in real incineration systems is in line with thermodynamic equilibrium models which predict a predominance of Br₂ during combustion [35] and pyrolysis of bromophenols [34]. In chlorinated systems, HCl is by far the dominant species [166]. This noticeable difference between chlorinated and brominated systems could be partly due to HBr being oxidised by OH radicals at a higher rate than HCl would be. The reaction rate constant for OH + HBr → H₂O + Br is faster than its chlorinated counterpart by 3 orders of magnitude at 298 K [167]. Released Br atoms could readily convert HBr into Br₂ via the reaction Br + HBr → H + Br₂.

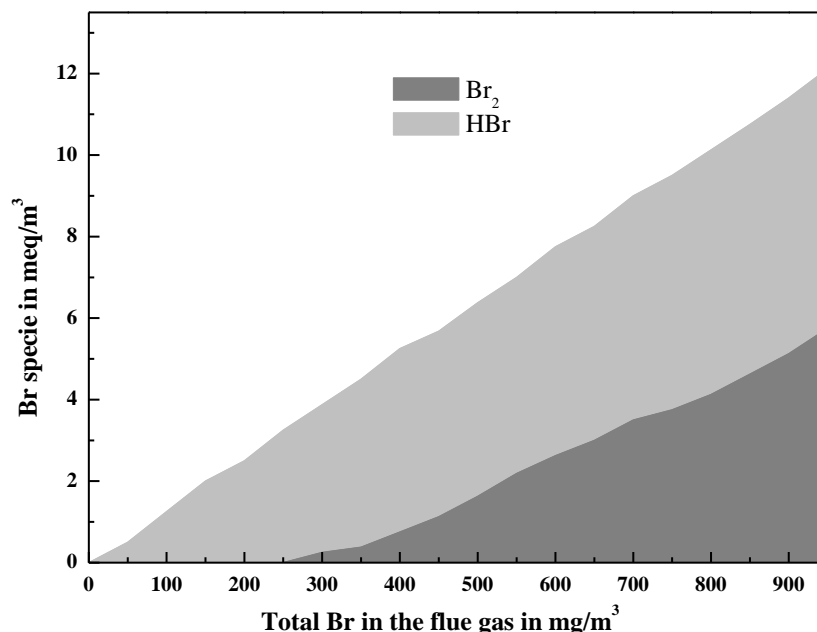


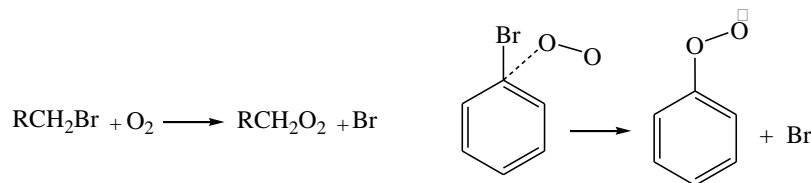
Figure 2.15. Bromine distribution in the raw gas of combusting e-waste [41, 165].

Other studies have reached similar conclusions by finding that under pyrolysis (823 K) and gasification (1503 K) conditions, most bromines exist in the form of HBr, with smaller fractions of Br₂ and metal bromides [168-170]. Ni et al. [171] analysed the occurrence of bromine as HBr and Br₂ produced by the combustion of waste printed circuit boards. They analysed the effects of temperature, residence time and excess air on the conversion of bromine into HBr/Br₂. The effect of temperature was much stronger than residence time on bromine speciation in solid and gas phases. At higher temperatures, most of the bromine transfers to the fly ash in the form of HBr and Br₂. In the temperature range of 1073 – 1673 K, the ratio of HBr to Br₂ becomes greater than 1.0, while it drops below unity under 1073 K. At 1473 K, about 99.9% of raw bromine shifts to the flue gas and 0.1% persists in the remaining solid residue [171]. Similar results were obtained by Bientinesi et al. [172], who reported that the majority of co-combusted waste bromine existed in the flue gas, with only a minor part remaining in char [172].

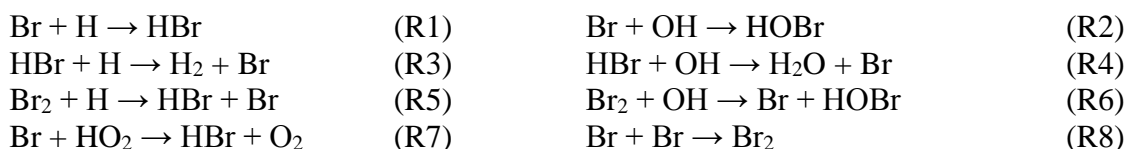
2.4.2. Bromine reactions with H/O species

Relatively weak aromatic and aliphatic C-Br bonds in BFRs motivate the release of Br atoms in the early stages of the combustion process. The principal functionality of

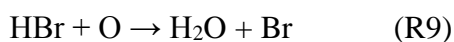
bromine in BFRs is to trap active radicals from combustion media [173]. Adding molecular oxygen to brominated hydrocarbons also releases Br atoms directly via inversion substitution:



The three forms of gaseous bromine (Br_2 , HBr and Br) operate effectively in the termination stage of oxidising agents, i.e. OH^\cdot and H radicals:



Of particular importance is the consumption of OH radicals by HBr , which also suppresses further oxidation of CO into CO_2 , thereby enhancing the formation of incomplete combustion products. Atomic oxygen regenerates Br atoms from HBr in a highly exothermic reaction ($258.7 \text{ kJ mol}^{-1}$) [174]:



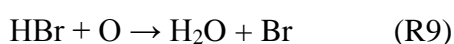
Dixon-Lewis et al. [175] re-examined high-temperature bromine chemistry to update the inhibition mechanism involving HBr/Br_2 -doped flames. Table 2.4 lists rate constants for these reactions as considered in Dixon-Lewis et al.'s mechanism [175]. They found that HBr and Br_2 act differently as inhibitors. For example, R3 is rapidly equilibrated and depletes HBr in favour of atomic Br . In contrast, R5 is far from equilibrium and consumes H atoms from the reaction zone via competition with the chain-propagating reaction $\text{H} + \text{O}_2 \rightarrow \text{O} + \text{OH}$. The most prominent chain-breaking reactions are R1, R7 and R8. Reactions involving HOBr are of negligible importance for removing or generating chain carriers in $\text{H}/\text{O}/\text{Br}$ flames. Flame speed increases rapidly if the inlet concentration of molecular bromine exceeds 20%.

Table 2.4. Reaction rate constant parameters for the H/Br inhibition cycle. $A \times n$ values are $\text{cm}^3 \text{mol}^{-1} \text{s}^{-1}$. E_a values are J mol^{-1} [175].

Reaction	A	n	E_a
$\text{Br} + \text{H} \rightarrow \text{HBr}$	1.9×10^{21}	-1.87	0.00
$\text{HBr} + \text{H} \rightarrow \text{H}_2 + \text{Br}$	1.3×10^{10}	1.05	682
$\text{HBr} + \text{OH} \rightarrow \text{H}_2\text{O} + \text{Br}$	4.0×10^{12}	0.00	-1290
$\text{Br}_2 + \text{H} \rightarrow \text{H}_2 + \text{Br}$	4.6×10^7	2.05	-7553
$\text{Br}_2 + \text{OH} \rightarrow \text{Br} + \text{HOBr}$	1.1×10^{15}	-0.66	0.00
$\text{Br} + \text{HO}_2 \rightarrow \text{HBr} + \text{O}_2$	8.6×10^{09}	1.00	1960
$\text{Br} + \text{Br} \rightarrow \text{Br}_2$	1.5×10^{14}	0.00	-7118

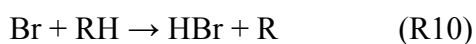
2.4.3. Bromine reactions with hydrocarbon species

Decomposition of polymeric constituents produces a wide spectrum of hydrocarbons, ranging from short C_1 - C_3 species to PAHs. Babushok and Tsang [176] demonstrated that the effect of the bromine inhibition cycle on the oxidation process was very similar regardless of the initial C_1 - C_4 alkane fuel. They found that burning velocity is only sensitive to the set of reactions in Table 2.4, in addition to the reaction of Br atoms with HCO, which is an end product of combustion of nearly all hydrocarbons:

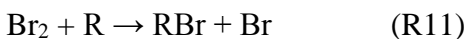


Apart from significant decreases in the fuel's burning velocity, introducing bromine to the combustion system does not alter the profile of products relative to pure fuel, as bromine-bearing species only react significantly with the end-products of fuel combustion.

Interest in Br atom-hydrocarbon reactions stems mainly from atmospheric applications. Abstractions of H by Br atoms from alkanes are very fast, and equilibrate rapidly with the reverse reaction [177]:



Activation energies for reaction R10 correlate with the C-H BDH values for H atom abstraction. On the other hand, abstractions of Br atoms from bromine molecules [178] by alkyl radicals are irreversible and often incur negative activation energies:



For aromatic compounds, Bierbach et al. [179] attempted to measure a rate constant for the reaction $\text{Br} + \text{C}_6\text{H}_6$ at 298 K. However, they could not establish a measurable decay of benzene. An upper limit for the reaction was assigned a value of $1.0 \times 10^{-14} \text{ cm}^3 \text{ molecule}^{-1} \text{ s}^{-1}$ at ambient conditions. Altarawneh and Dlugogorski [152] found that reaction of Br atoms with the aromatic ring proceeds via H abstraction at all temperatures, with no contribution from an addition/substitution channel. The activation energy for the abstraction of aromatic H atoms by Br is significantly higher (100 kJ mol^{-1}) [152] than corresponding barriers for abstractions of secondary H atoms from alkanes (40 kJ mol^{-1}) [177].

2.5. Formation of PBDD/Fs

Congener profiles of PCDD/Fs measured during various combustion and metallurgical thermal processes exhibit very similar specific isomer patterns [40]. This implies that the majority of PCDD/Fs, especially at low temperatures (i.e. 523 – 673 K) form via a common mechanism, i.e. de novo synthesis. It is estimated that 70% of PCDD/F emission is due to de novo synthesis [166]. In contrast, the corresponding isomeric profiles of PBDD/Fs show significant discrepancies among emission sources [40]. In principle, several mechanisms could potentially contribute to the formation of PBDD/Fs from BFR-containing fuels:

- Direct transformation of BFRs into PBDD/Fs: Very high yields of PBDFs from pyrolysis and oxidation of PBDEs and PBBs proposes the direct conversion of these BFRs into PBDD/Fs prior to their decomposition. As demonstrated in Section 3.3, theoretical calculations can construct a very simple mechanism for the formation of PBDD/Fs from PBDEs and PBBs. In these mechanisms, unimolecular rearrangement reactions of ROO' species are more plausible than

pathways involving rupturing of C-C/C-O linkages and closed-shell elimination of H₂/HBr.

- Homogenous or catalyst-assisted coupling of bromophenols: decomposition of several BFRs, such as TBBA, PBDEs and BTBPE, produce appreciable amounts of BPhs. BPhs are potent building blocks for the formation of PBDD/Fs through homogenous and heterogeneous corridors.

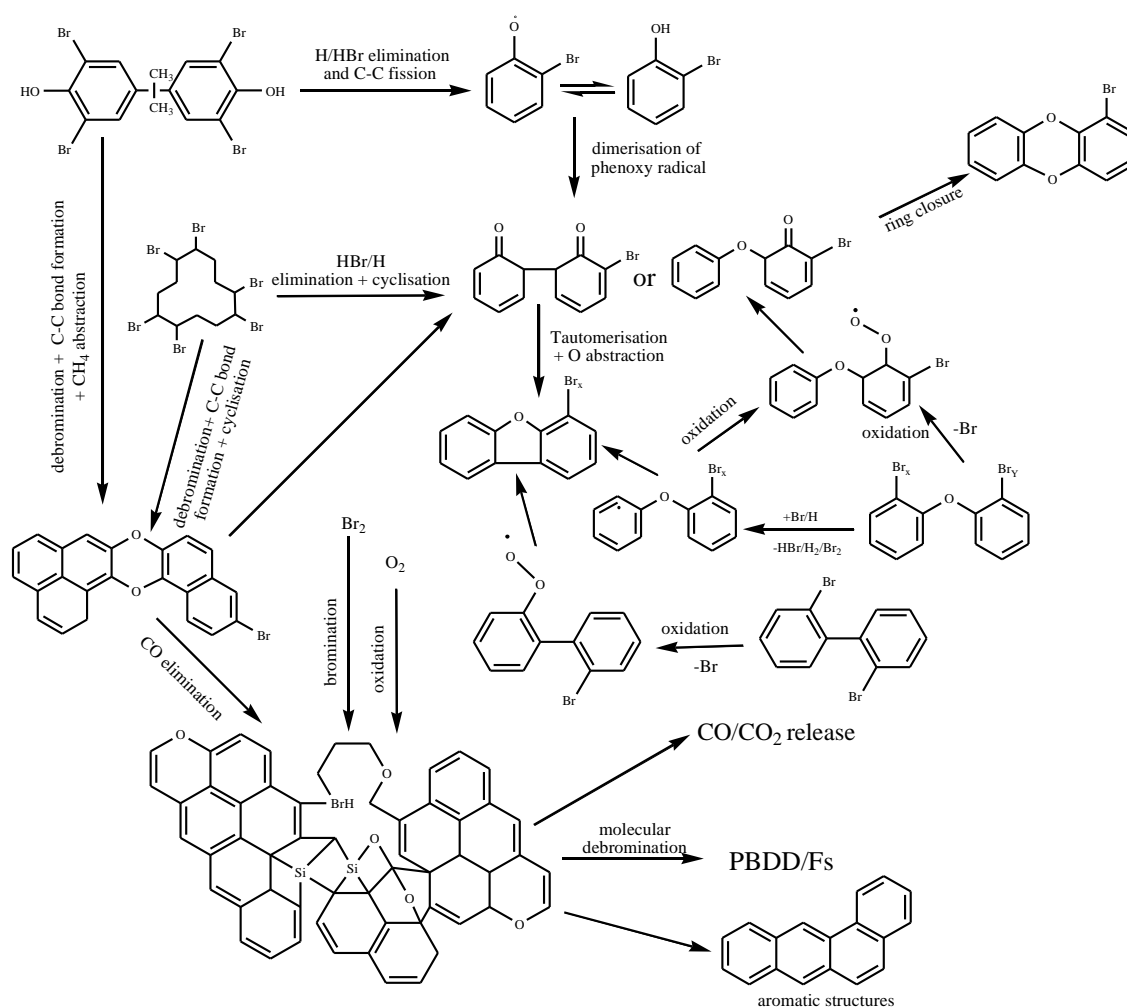


Figure 2.16. General decomposition pathways leading to PBDD/F formation in the thermal breakdown of different BFRs.

- De novo synthesis: Partial oxidation of organic residual carbon and PAHs in fly ash denote so-called “de novo” synthesis. While the precursor pathway is generally more prevalent in forming PBDD/Fs from BFRs, the de novo pathway

is anticipated to contribute significantly in two cases. Sufficient combustion conditions completely degrade BFRs into short hydrocarbons. As is the case for PCDD/F formation, these species initiate formation of PBDD/Fs via the de novo route [180]. On the other hand, BFRs with no aromatic rings in their structures, i.e. HBCDs, do not decompose to give high concentrations of bromophenols or bromobenzenes. As a result, the formation of PBDD/Fs from these BFRs most likely arises from the build-up of their fragmented smaller hydrocarbons.

Figure 2.16 summarises the pathways leading from the thermal decomposition of BFRs to PBDD/F formation.

2.5.1. Pathways to PBDD/Fs from bromophenols

While certain BFRs, such as BBDEs and PBBs, could serve as direct intermediates for the formation of PBDD/Fs, BPhs, commonly-suggested precursors for PBDD/Fs, form as major products from the decomposition of several BFRs, like TBBA and BTBPE. In contrast to chlorinated phenols, studies on the combustion or pyrolysis of BPhs are rather minimal. Table 2.5 summarises studies on thermal decomposition and combustion of BPhs or mixtures of BPhs and chlorophenols, with emphasis on the investigated BPh congeners, operational conditions (oxygen content, temperature residence time) and emission profiles of PBDD/Fs [34, 35, 42, 43, 57, 67, 81, 181-184].

Table 2.5. Thermal decomposition studies of bromophenol congeners.

Compound	Reactor type/operating conditions	Thermal decomposition products	Max. concentration of PBDD/Fs at T (K)	References
2,4-Dibromophenol	Quartz reactor tube Pyrolysis (473 – 773 K)	1-BDD, 2,7-diBDD, 2,8-diBDF, 1,3,8-triBDD, 2,4,8-triBDF	673 K 2,7-diBDDs	[182]
2,6-Dibromophenol	Quartz reactor tube	1,6-diBDD, 1,9-diBDD, 1-BDD,	673 K 1,9/1,6-diBDDs	

CHAPTER 2 Literature Review

	Pyrolysis (473 – 773K)	TriBDDs, 2,7- diBDD, 2,8-diBDF, pentaBDDs		[182]
2,4,6- Tribromophenol	Quartz reactor tube Pyrolysis (473 – 773 K)	1,3,6,8-TBDDs, 1,3,7,9-TBDDs, Tri- BDDs, penta-BDDs, mono-tri benzenes	673 K TBDDs	[182]
2-bromophenol	Fused silica reactor Oxidation on CuO/silica surface (523 – 823 K)	DD, 1-MBDD, DBDD, TriBDD, 4- MBDD, di- triBPhs, polybrominated benzenes	723 K, DD (14.4%), 1-MBDD (5.1%), DBDD (6.4%), TrBDD (1.8%), 4- MBDD (0.2%)	[42]
Mixture of 2- chlorophenol and 2- bromophenol	Fused silica tubular reactor Oxidation (573 – 1273 K) $\tau = 2$ s	DD, 4-B,6- CDF, phenol, 4,6- DBDF, 2,6 –diBPh, 4,6-DCDF, 2-B,4- CP, 2,4-diBPh, 2- C,4-BPh, 4-MBDF, 4-MCDF, DF, 1- MBDD, 1-MCDD	MBDD (0.07% at 623 K) diBDF (0.53 % at 873 K) MBDF (0.15% at 873 K)	[184]
2-bromophenol	Fused silica tubular reactor Oxidation $\tau = 2$ s (573 – 1373 K)	DD, 4,6-DBDF, DF, MBDD/Fs, naphthalene, bromonaphthalene, 2,4-diBPh, 2,6- diBPh, phenol, Bromobenzene, and benzene	DD (22.2% at 873 K) MBDD (0.15% at 823 K) 4-MBDF (0.82% at 923 K) 4,6-DBDF (2.40 % at 923 K)	[35]
2-bromophenol	Fused silica reactor	DD, 1-MBDD, DBDD, TriBDD, 4- MBDD, DF, di-	623 K	[43]

CHAPTER 2 Literature Review

	Pyrolysis on CuO/silica surface (523 – 823 K)	triBPhs, polybrominated benzenes	DD (1.90%), 1- MBDD (1.66%), DBDD (2.98%), 4-MBDF (0.004% at 673 K) DF (0.04% at 723 K)	
Mixture of 2- chlorophenol and 2- bromophenol	Fused silica tubular reactor Pyrolysis (573 – 1273 K) $\tau = 2$ s	Naphthalene, DD, phenol, DF, BBz, Chloronaphthalene, 4-B,6-CDF, bromonaphthalene, benzene, 4,6-DCDF, chlorobenzene, 4- MBDF, 4-MCDF, 1- MBDD, 2-C,4-BPh, 2,4-diBPh, 2-B,4-CP	MBDD (0.02% at 1023 K) MBDF (0.06% at 973 K)	[183]
2-bromophenol	Tubular reactor Pyrolysis (573 – 1273 K)	DD, MBDD, diBDF DF, naphthalene, chloronaphthalene, phenol, chlorobenzene, benzene	MBDD and two PBDD (0.15 %, 22.2% at 823 K) MBDF, diBDF (0.82%, 2.40 % at 923 K)	[34]
<i>o</i> -bromophenol	Pyrolysis quartz ampoule 873 K	DD, phenol, DF, DD, Dibenzofuranol, dihydroDBF	DD at 873 K	[57]
<i>p</i> -bromophenol	Pyrolysis quartz ampoule 873 K	Bromopentane, bromobenzene, phenol, dibromobenzene, DF, dihydroDBF, DBDF	diBDF at 873 K	[57]

CHAPTER 2 Literature Review

2,4,6-Tribromophenol	Tubular flow reactor Oxidation (573 – 1073 K)	1,3,6,8-TBDD, 1,3,7,9-TBDD, Tri-BDD,	773 K 1,3,6,8-TBDD (31%), 1,3,7,9-TBDD (25%)	[181]
2,4,6 tri-bromophenol	Quartz reactor tube Oxidation (573 – 1073 K) $\tau = 2$ s	DiBPhs, TBDDs, Dibromomethylphenol	773 K TBDD, No PBDF	[146]
2,4,6 tri-bromophenol	Quartz reactor tube Pyrolysis (573 – 1073 K) $\tau = 2$ s	HBr, diBPh, benzene, no PBDD/Fs	898 K No PBDD/Fs,	[146]
2,4,6-tribromophenol	Quartz tube reactor Combustion (873 – 1173 K)	Brominated benzenes, DD, TriBDD	TriBDD (1073 K)	[181]
Pentabromophenol	Quartz tube reactor pyrolysis (873 – 1173 K)	Brominated naphthalenes, brominated benzenes, BDD	Bromodioxins (973 K)	[181]

2.5.1.1. Homogenous formation of PBDD/Fs from bromophenols

Evans and Dellinger investigated slow pyrolysis [34] and oxidation [35] ($\tau = 2.0$ s) of 2-bromophenol (2-BPh) in a fused-silica flow reactor at 573 – 1273 K. They compared the temperature-product profiles with their previous results on thermal pyrolytic and oxidative degradation of 2-chlorophenol (2-CPh). Figure 2.17 presents temperature-product profiles from the degradation of 2-BPh under pyrolytic and oxidative decomposition.

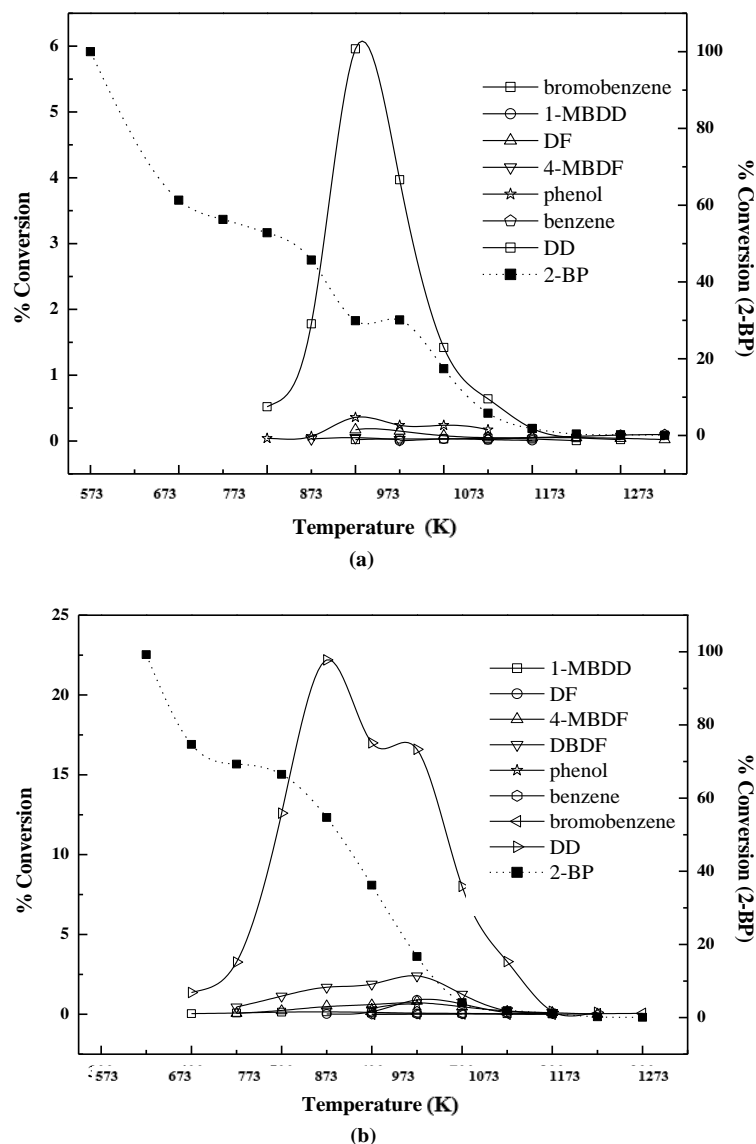
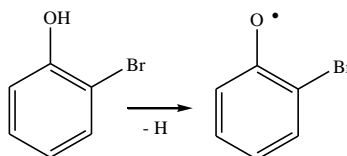
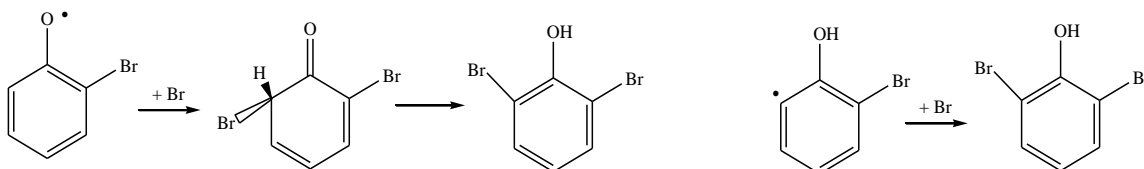


Figure 2.17. Temperature product profile for % conversion of 2-bromophenol into subsequent products in (a) an inert atmosphere [34], and (b) an oxidising atmosphere [35].

Observed products in both cases included lower brominated (i.e. di- or mono-) PBDD/Fs, phenols, naphthalene and benzenes. As Figure 2.17 depicts, thermal degradation of the 2-BPh molecule starts at nearly 623 K and achieves complete destruction at 1073 K. The unexpected low onset decomposition temperature prompted the author to consider heterogeneous wall reactions as assisting in the rupture of the hydroxyl O-H bond (360 kJ mol^{-1}):



Reactions of H atoms with the parent 2-BPh molecule are all exothermic and branches to the abstraction of a hydroxyl' H atom, abstraction of a Br atom, or displacement of a Br atom. The latter reaction is more favourable than addition at an *ipso* site, leading to the expulsion of the OH group. Hence, phenol forms with a higher yield and at a lower temperature than bromobenzene. The yield of brominated product under oxidative conditions is higher than that under a pyrolytic atmosphere. According to pseudo-equilibrium calculations [34-35], oxygen molecules create OH radicals which convert HBr into the water and the strong brominating agent, Br atoms. Bromination of the 2-BPh molecule into di-brominated congeners could occur either by addition of a bromine atom to a 2-bromophenoxy radical or addition of a bromine atom to a vacant radical site in a phenyl-type radical:



BPhs form more PBDD/Fs when compared with the yield of PCDD/Fs formed from chlorophenols. In fact, addition of bromine enhances the formation of PCDD/Fs from chlorophenols [67, 181]. This interesting observation could be rationalised by considering:

- Aromatic C-Br bonds are weaker than corresponding C-Cl bonds by 62.8 kJ mol^{-1} [185]. Formed Br atoms contribute to further decomposition of chlorophenols by abstraction of phenolic and aromatic H atoms.
- The predominant bromine in BPh systems is Br_2 , versus HCl in chlorophenols systems. HCl is largely unreactive (i.e. BDH amounts to 340 kJ mol^{-1}) and does not participate in further destruction or chlorination reactions, which contrasts

with active Br_2 molecules which readily dissociate into Br atoms (i.e. BDH amounts to $223.0 \text{ kJ mol}^{-1}$). Released Br atoms accelerate the formation of chlorophenoxy radicals from chlorophenols, which is a crucial step in PCDD/F generation.

Formation of PBDD/Fs from bromophenols follows well-documented steps analogous to the synthesis of PCDD/Fs from chlorophenols [186].

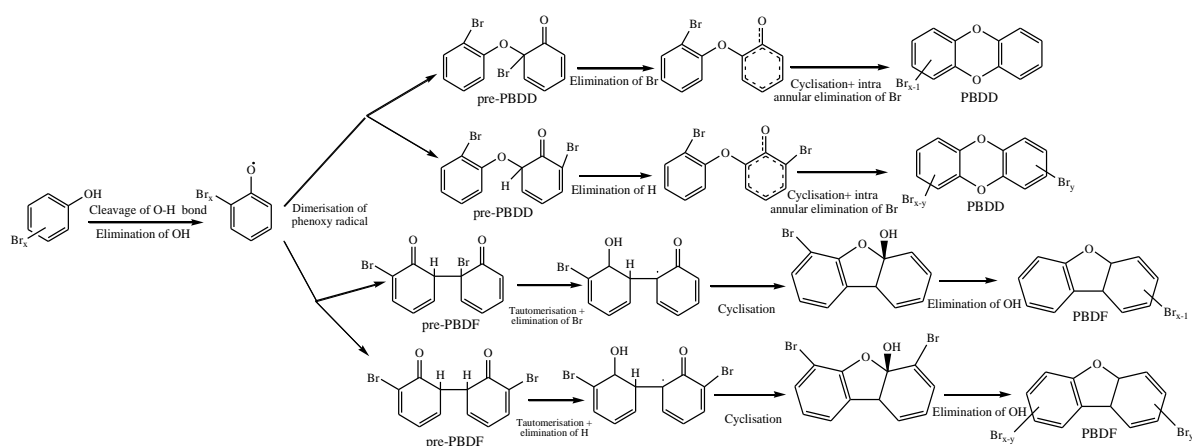


Figure 2.18. Proposed mechanism for the formation of PBDD/Fs from bromophenols [187, 188].

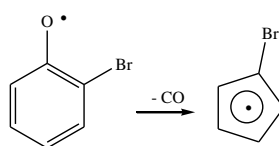
Figure 2.18 shows the formation mechanism of PBDD/Fs, which occurs via the coupling of two 2-bromophenoxy radicals. Principal reactions include:

- Coupling or self-condensation of bromophenol molecules or bromophenoxy radicals, leading to the formation of pre-PBDD/F intermediates. Formation of pre-PBDF intermediates requires coupling of two bromophenoxy radicals, each with at least one *ortho* C(H) site. The addition of a phenolic 'O' atom to an *ortho* position at another bromophenoxy radical produces pre-PBDF intermediates.
- Cyclisation of pre-PBDD intermediates into PBDDs accompanied with the unimolecular elimination of Br atoms or HBr molecules.

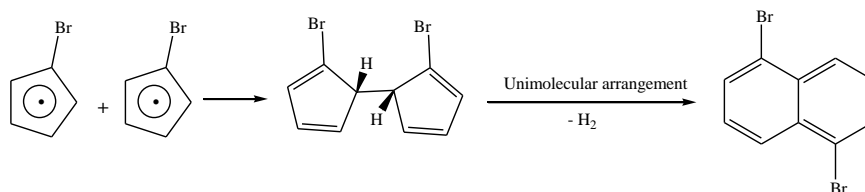
- Single or double enolisation of keto-keto pre-PBDE intermediates into PBDFs. This reaction is followed by a ring-closure reaction leading to the expulsion of a water molecule.

Rate-determining steps in closed-shell corridors (i.e. an overall activation barrier of 240 - 300 kJ mol⁻¹) are ring-cyclisation reactions that lead to the expulsion of HBr (for PBDDs) and H₂O (for PBDFs) [187-188]. Open-shell pathways afford significantly lower overall activation barriers and are initiated by abstraction of H or Br atoms from C-C or C-O bridges in the pre-PBDD/F intermediates. Theoretical studies predict the reaction and activation energies for the formation of PBDD/Fs from bromophenoxy radicals [187-188] to be very similar to corresponding mechanisms forming PCDD/Fs from chlorophenoxy radicals [186]. It follows that the difference in dioxin product distributions between BPh and chlorophenol systems must arise from factors mentioned above (i.e. weaker C-Br bonds and higher reactivity of Br₂), rather than from their distinct thermochemical and kinetic parameters. Formation of phenylethyne and diphenylethyne at temperatures higher than 973 K [34] suggests an addition of C₁-C₃ species (radicals and molecules) to benzene and bromobenzene.

Bimolecular self-reactions of bromophenoxy radicals constitute a rather minor exit channel compared with unimolecular decomposition (via ring contraction/CO elimination) into bromocyclobentadiene radicals:



Recombination of bromocyclobentadiene radicals is regarded as a main source for the formation of bromonaphthalene molecules:



Naphthalene often acts as the first PAH nucleolus for soot formation [189]. As such, other proposed pathways for naphthalene molecule formation include condensation from

smaller alkane/alkene chains at higher temperatures; i.e. HACA- and Diels-Alder-type mechanisms. Several simplified and kinetic models describe the homogeneous gas phase decomposition of chlorophenol molecules and subsequent formation of PCDD/Fs [166]. In contrast, corresponding kinetic models of the thermal/oxidative degradation of bromophenols are absent from the literature.

2.5.1.2. Formation of PBDD/Fs from catalytic-assisted coupling of bromophenols

In practical scenarios, metals and their oxides could potentially act as potent catalysts in the formation of PBDD/Fs from BPhs. In this regard, atmospheric oxygen could readily oxidise the high portion of elemental Cu in printed circuit boards [19] into CuO [190]. Surface CuO mediates the rupture of hydroxyl' O-H bonds and facilitates PBDD/F formation. Figure 2.19 shows proposed pathways for the catalyst-mediated formation of PBDD/Fs from bromophenol molecules. A Langmuir-Hinshelwood mechanism (reactions between two adsorbed species) operates in the formation of PBDD/Fs, while generation of PBDD/Fs occurs via an Eley-Rideal mechanism (reactions between gaseous and adsorbed species). These two mechanisms also participate in the formation of higher brominated congeners of benzenes and phenols. Under oxidative [42] and pyrolytic [43] conditions, the surface-mediated formation of PBDD/Fs from BPhs was significantly higher than the equivalent formation of PCDD/Fs from chlorophenols. This has been attributed [43] to the ease of formation of Br atoms in BPh systems compared with the formation of Cl atoms from chlorophenols. However, the exact role of Cu surfaces in generating halogen atoms is not yet fully elucidated. For example, it is not clear whether these Cu-surfaces assist in generating halogen atoms from hydrogen halides or merely act as catalysts for electrophilic substitution. Several hypotheses on the role of Cu/Fe-based catalysts in facilitating the halogenation of organic pollutants could be tested by observing the pattern and degree of halogenation in mixtures of hydrogen halides/halides/phenol (with varying relative loads) over Cu-containing surfaces.

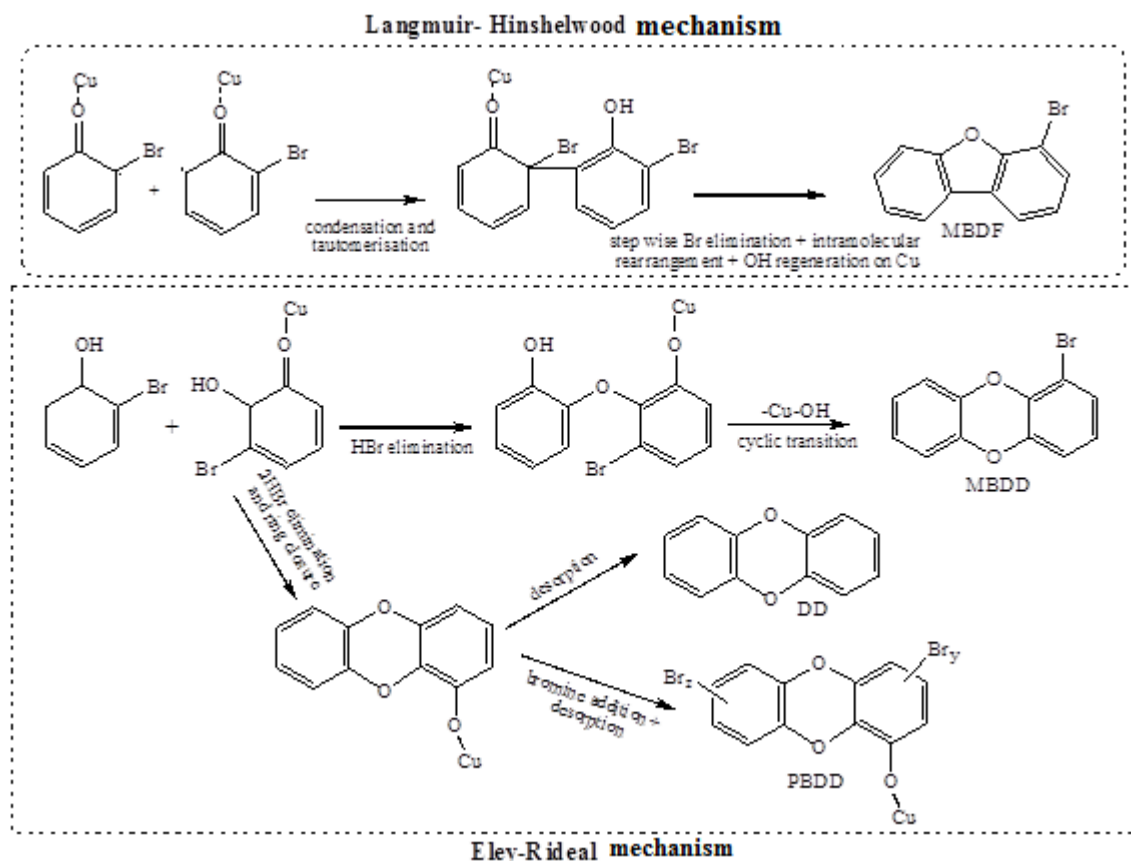


Figure 2.19. Suggested pathways for formation of PBDD/Fs from catalyst-assisted coupling of bromophenols over a CuO surface [43].

2.5.2. De novo synthesis of PBDD/Fs

Experiments on the thermal heating of MSWs enriched with ^{13}C -carbon proved the formation of dibenzo-*p*-dioxin (DD) and dibenzofuran (DF) rings via de novo synthesis [191]. Condensation of two aromatic rings initiates PAH formation. The addition of oxygen molecules to the surfaces of formed PAHs results in their oxidation and formation of DD and DF backbones. Cosentino et al. [192] theoretically investigated de novo synthesis of DF from pyrene and benzodibenzofuran. They found that the rate-determining step corresponded to the elimination of CO molecules, with an energy barrier in the range of 105.0 – 125.0 kJ mol⁻¹. Stanmore [193] and Altarawneh et al. [166] reviewed and analysed kinetic factors controlling PCDD/F formation in thermal systems by the de novo process. Salient mechanistic aspects relevant to de novo synthesis are still not fully understood. Yields by de novo synthesis seem also to be affected not only by fly ash content but also by the constituents in the gas phase. Some interpretations [194]

propose that de novo synthesis of halogenated DD/DF compounds forms non-halogenated DD/DF compounds, but major halogenation is due to gas phase reactions and back-adsorption on the partially halogenated carbon surfaces.

Heinbuch and Stieglitz demonstrated that the formation of halogenated compounds by de novo synthesis is not restricted to chlorinated molecules [195]. They substituted inorganic chloride with bromide in MSW fly ash to find analogous halogenation effects. Yields of brominated products correlated with the amount of bromine added. However, only lower brominated congeners of PBDFs were found. This was attributed to the low volatility of higher brominated PBDFs. Lower brominated congeners can readily evaporate and thus escape destruction by the fly ash.

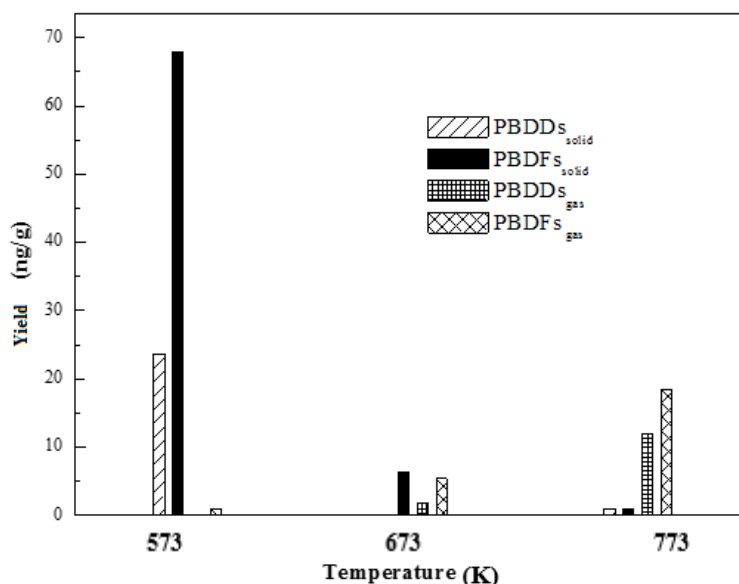


Figure 2.20. Concentration of PBDD/Fs in solid and gas phases at different reaction temperatures [196]

Ortuño et al. [196] studied de novo formation of PBDD/Fs by heating mixtures of activated carbon with different loads of CuBr_2 . The addition of CuBr_2 greatly accelerated the oxidative breakdown of carbonaceous structures. Decomposition of CuBr_2 started at ~ 423 K and produced CuBr and gaseous Br_2 . DSC runs estimated the overall activation energies for the decompositions of a pure carbon mixture, and a mixture containing 50 % wt CuBr_2 , as being $158.4 \text{ kJ mol}^{-1}$ and 78.7 kJ mol^{-1} , respectively. These two values correlate well with the differences in bond energy between C-C and C-Br bonds. Formed

PBDD/Fs reached a maximum yield of 91.7 ng g^{-1} at 573 K. Once again, the amount of PBDFs significantly overshoot that of PBDDs, confirming the occurrence of de novo synthesis. Figure 2.20 shows the total concentrations of PBDDs and PBDFs in the gas phase and in solid residue at different temperatures. The significant decline in evolved concentrations of PBDFs with temperature indicates that oxidative breakdown of the carbon matrix is favoured at lower temperatures; where the carbonaceous surface still retains its definite structure [196]. The same temperature-product trends were also observed by Heinbuch and Stieglitz [195], who found that the yield of brominated compounds by de novo formation reaches its maximum at 623 K.

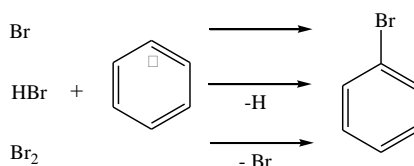
The dominance of 1,2-dibromobenzene in the homologue group of dibromobenzenes assumes a two-step process in the de novo formation of brominated species [197]. The first step characterises bromination of the carbon surface in a side-by-side orientation. This is followed by oxidative decomposition of the carbon surface in a mechanism similar to pathways suggested by Cosentino et al [192]. The total yield of PBDD/Fs was approximately 10 times higher when compared with de novo synthesis of PCDD/Fs. Similarly, Schuler and Jager [180] observed that rates of PBDD/F formation in a pilot incineration plant were 4 – 20 times higher than for their chlorinated counterparts.

Bearing in mind that the complete destruction of BFRs leads to the formation of small brominated species, it will be helpful to investigate PBDD/Fs generation from the oxidative degradation of bromo alkanes or alkenes. Likewise, pyrolysis of HBCD produces several PAHs [133]. The literature provides no comparable combustion studies. Decomposition of HBCDs in the presence of oxygen may promote PBDD/F formation. This assumption warrants further investigation.

2.5.3. Bromination mechanisms

The majority of bromine produced by BFR thermal decomposition comes from organic sources, i.e. it was originally bonded in BFR structures. The prevailing heterogeneous chlorinating pathways are not as important as the bromination pathways that produce PBDD/Fs from BFRs. In addition to the presence of bromine in parent BFRs and their fragmented products, gaseous reactions are expected to play a major role in the

bromination of PBDD/Fs. Reactions of Br, HBr and Br₂ with phenyl-type radicals are crucial bromination routes in the gas phase:



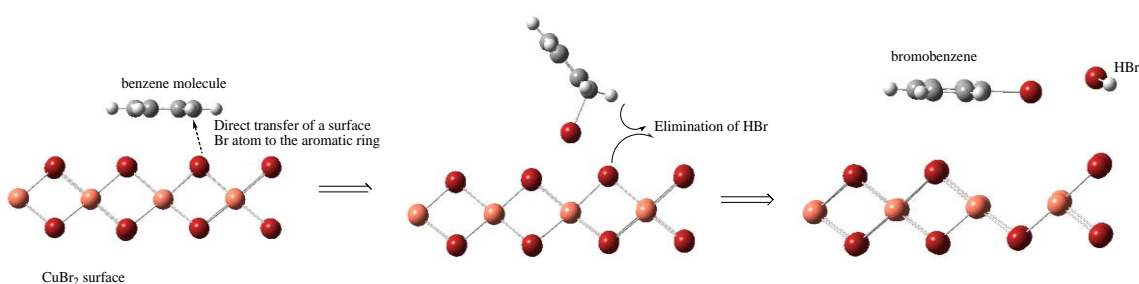
Since Br₂ exists in appreciable amounts in brominated systems, in contrast to the very dilute concentrations of Cl₂ in a chlorine-bearing environment, gas phase bromination by Br₂ is more prevalent than chlorination by elemental chlorine.

Most studies on the halogenation of organic pollutants have focused on chlorination mechanisms. There is a clear disparity with studies on bromination pathways. The high metallic Cu content in e-waste [198] could, in principle, promote the occurrence of heterogeneous bromination routes similar to those operating in the chlorination of PCDD/Fs, most notably [166]:

- Gaseous bromination
- Surface dehydrogenation
- Transfer of inorganic bromine to residue carbon during or prior to de novo synthesis
- Deacon reactions

Several studies have assessed the efficiency of metal oxides in forming Cl₂ from HCl via the Deacon process [199]; however, there are no analogous studies that consider HBr. Nevertheless, experimental measurements from a pilot-scale plant [41], as well as thermodynamic equilibrium models [34], confirm the presence of high concentrations of Br₂ during the decomposition of brominated aromatics without assistance by the Deacon process. Formation of PBDD/Fs via de novo synthesis, where the source of bromine was of an inorganic nature [146], indicates a transfer of bromine from inorganic materials to the carbon matrix.

Adsorption of HBr on metal oxides produces volatile metal halides and molecular bromine [127]. In this context, metal oxides regenerate the active bromination agent, Br₂, and metal halides. The exact mechanism of this process and its associated limiting kinetics are not yet recognised. The role of CuBr₂ as a direct bromination agent for organic pollutants has not been thoroughly assessed. Nonetheless, CuBr₂ is often utilised as a bromination agent in organic synthesis due to its excellent coordination capability [200]. Experimental studies point out that CuCl₂ is a very effective chlorination agent [201-202]. CuCl₂ has been viewed as a shuttle that transfers inorganic chlorine from fly ash to PCDD/F moieties [193]. Due to the very similar structures of CuCl₂ [203] and CuBr₂ [204], the latter could operate by direct heterogeneous transmission of bromine into gaseous PBDD/F compounds. This occurs via the presumed two-step surface-catalysed mechanism:



Neither kinetics parameters nor the mechanistic steps are precisely known. Experimental proof for the occurrence of surface bromination comes from the observation of the reduction of CuBr₂ into CuBr during de novo synthesis of PBDD/Fs [196]. It is sensible to assume that DD and DF moieties are formed via de novo synthesis, followed by surface bromination. Altarawneh and Dlugogorski [205] demonstrated that the halogenation patterns of many persistent organic pollutants are in accord with Fukui electrophilic indices. Sovocool et al. [206] and Munslow et al. [207] compared the experimentally measured signatures of the electrophilic aromatic substitution of PBDDs and PBDFs in the aqueous phase.

Many aspects of the homogenous and heterogeneous bromination routes of PBDD/Fs require further attention. For example, co-pyrolysis/oxidation of benzene with Br₂ and/or HBr could highlight the extent to which pure gas phase bromination proceeds.

2.6. Formation of PXDD/Fs

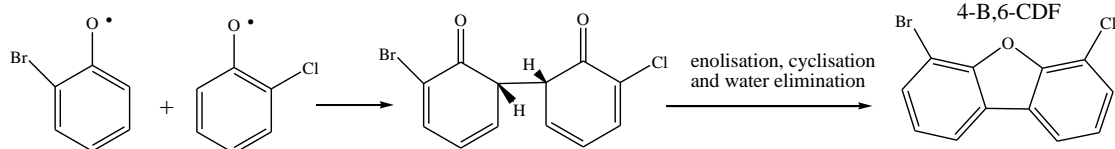
Bromine concentration in a typical MSW is ~ 200 times lower than that of chlorine, i.e. around 300 ppm [208]. Only very small amounts of mono- and di-bromo polychloro DD/DF are formed compared with PCDD/Fs [41]. However, sufficient amounts of BFR-containing materials in thermal processes such as metallurgical operations [209], uncontrolled burning of plastics [210] and recycling of e-waste [32] produce considerable concentrations of bromine in ash and flue gas. Consequently, these processes represent hot spots for PXDD/F formation. PXDD/Fs actually form wherever a source with trace amounts of bromine is available [211]. The carbon skeleton of PXDD/Fs must form via the same mechanisms operating in the formation of PCDD/Fs and PBDD/Fs (i.e. homogenous or catalyst-assisted coupling of halogenated phenols or benzenes, oxidative/pyrolytic transformation of certain BFRs and de novo synthesis). Nevertheless, PXDD/F formation mechanisms are still not completely understood. The most intriguing remaining questions are related to the relationship between initial bromine input and formed PXDD/Fs, the nearly universal dominance of PXDFs over PXDDs, and the relative contribution of de novo synthesis versus the precursor pathway which normally dominates PBDD/Fs formation.

2.6.1. Formation of PXDD/Fs from mixed halogenated phenols

Evans and Dellinger expanded their studies on the oxidation and pyrolysis of pure 2-CPh and 2-BPh to study the co-pyrolysis [183] and co-combustion [184] of an equimolar mixture of these two compounds. Under both operational conditions, 4-bromo-6-chlorodibenzofuran (4-B,6-CDF) was the only detected PXDD/F product [183, 184]. As was the case with pyrolysis and oxidation of pure 2-CPh [212] and 2-BPh [35], non-halogenated DD constituted the most abundant species. The maximum yields of DD under co-pyrolysis of 2-CPh and 2-BPh [183] were 4 times greater than that of pure 2-CPh [213], and 5 times lower than that of 2-BPh [34], respectively. Formation of more DD from pyrolysis of a mixture containing 2-CPh and 2-BPh, compared with pyrolysis of pure 2-CPh, suggests assistance by bromine atoms [183]. This observation is consistent with the general consensus that adding bromine to chlorophenol systems increases the yield of PCDD/Fs. This increase is partially due to the reaction of Br atoms with Cl₂ molecules; $\text{Br} + \text{Cl}_2 \rightarrow \text{BrCl} + \text{Cl}$ [34]. Pseudo-equilibrium thermodynamic calculations

of a pyrolytic 50:50 2-BPh/2-CPh mixture confirms the formation of trace concentrations of Cl atoms, where Cl atoms were not present upon considering a neat 2-CP system [183]. Oxidation of a 2-CPh and 2-BPh mixture [184] produces more 4,6-DBDF and 4,6-DCDF than the oxidation of individual 2-CPh and 2-BPh components. Under oxidative conditions, abundant OH radicals accelerate the rupture of phenolic O-H bonds and produce Br atoms from HBr (i.e. $\text{OH} + \text{HBr} \rightarrow \text{H}_2\text{O} + \text{Br}$) [184].

Pathways for the formation of PXDD/Fs from mixed halogenated phenols are similar to the corresponding pathways producing PCDD/Fs and PBDD/Fs (Figure 2.18) from their corresponding pure halogenated phenols. Clearly, DD could form from the coupling of two phenoxy radicals, or a phenoxy radical with either a 2-chlorophenoxy (2-CPhxy) or a 2-bromophenoxy (2-BPhxy) radical. A recent quantum chemical study [214] revealed that the formation of pre-PXDD and pre-PXDF intermediates incurred comparable exothermicity, in the ranges of $72.8 \text{ kJ} - 120.0 \text{ kJ mol}^{-1}$ and $59.8 - 107.6 \text{ kJ mol}^{-1}$, respectively. 4-B,6-CDF forms via an *ortho* C(H)//*ortho* C(H) coupling involving 2-BPhxy and 2-CPhxy radicals:



The absence of any PXDD isomers from co-pyrolysis/oxidation of 2-CPh and 2-BPh mixtures is surprising. Theoretical calculations predict that 1-bromo-6-chlorodibenzo-*p*-dioxin (1-B,6-CDD) forms at rates comparable to DD, 1-MBDD and 1-MCDD. A profound wall-catalytic effect in Evans and Dellinger's experiments [183-184] may have contributed to the destruction of any formed PXDDs. The potential for the formation of PXDD/Fs from mixtures of 2-BPh and 2-CPh molecules demands additional re-examination under pure gas phase conditions (i.e. ultra-pure quartz reactors). Nevertheless, a limiting case scenario for investigating the formation of PXDD/Fs from mixed halogenated phenols requires considering different halogenation types on the two *ortho* positions of the phenol ring. Bearing in mind that halogenation on *meta* and *para* sites does not exert an influence on steps governing the formation of PXDD/Fs, a 2-B,6-C-phenol molecule represents an excellent candidate for this case. Preliminary theoretical

results indicate that the kinetics parameters [214] of the final ring-closure reaction are not sensitive to halogenation type. Figure 2.21 shows the effect of halogenation type on the kinetics of final cyclisation reactions.

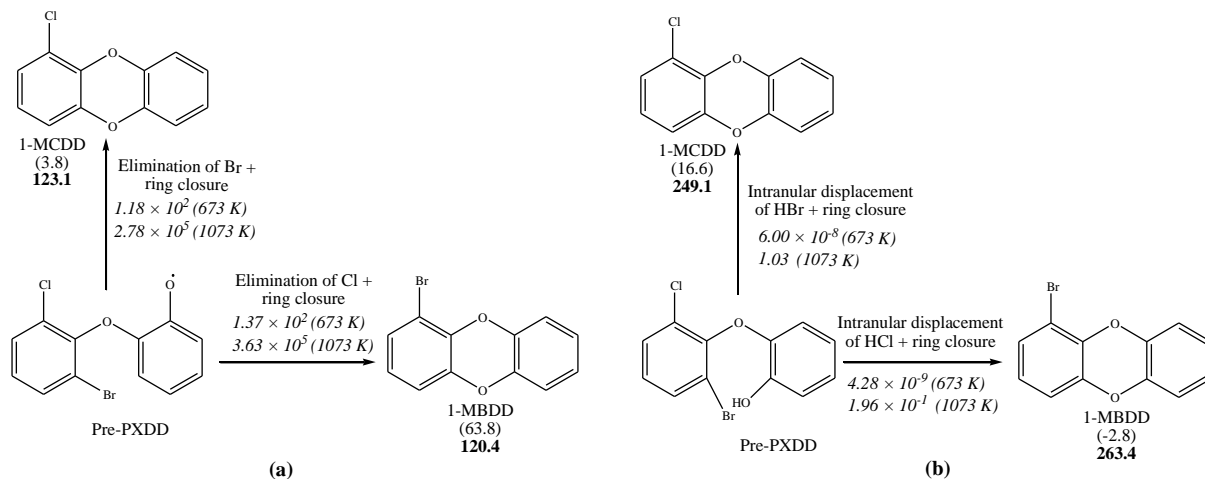


Figure 2.21. Effect of halogenation type on the kinetics of final cyclisation reactions involved in the formation of PXDD from pre-PXDD structures. Values in brackets and bold type denote reaction and activation energies, respectively (kJ mol^{-1}) at 298 K. Values in italics represent reaction rate constants at the given temperature [214].

2.6.2. Formation of PXDD/Fs from BFRs-containing materials

Several bench- and pilot-scale experiments have investigated the formation of PXDD/Fs from BFR-containing fuels. Table 2.6 summarises the major findings of these studies [41, 83, 209, 215-228].

Table 2.6. Summary of studies of PXDD/F formation.

Systems	Reactor type/ operating conditions	Thermal decomposition products	Max. concentration of PXDD/Fs	References
Fly ash with bromine	Pyrex ampoule placed on	PXDD (penta- hexa halogenated)	PXDF:PXCD >9 (PXDF congeners)	[215]

CHAPTER 2 Literature Review

and chlorine content	GC oven at 423 K, 573 K, 623 K	PXDF (tri – tetra halogenated)	Br ₁ Cl ₃ >Cl ₄ >Br ₂ Cl ₂ >Br ₃ C I ₁ >Br ₄ (623 K)
Flue gas analysis	Waste incinerator	PXDD (tetra- octa halogenated) PXDF (tetra- octa halogenated)	PXDD (6.2 ng m ⁻³ N ⁻¹) Br ₁ Cl ₃ (0.04), Br ₂ Cl ₂ (0.043), X ₄ (2.2), Br ₁ Cl ₄ (0.088), X ₅ (2.7), Br ₁ Cl ₅ (0.0051), X ₆ (0.45), Br ₁ Cl ₆ (0.15), X ₇ (0.64), Br ₁ Cl ₇ (0.14), X ₈ (0.21) PXDF (11ng m ⁻³ N ⁻¹) Br ₁ Cl ₃ (0.11), X ₄ (7.7), X ₅ (2.5), X ₆ (0.14), X ₇ (0.39), X ₈ (0.13)
Flue gas analysis	Industrial waste incinerator	PXDD (tetra- octa halogenated) PXDF (tetra- octa halogenated)	PXDD (0.82 ng m ⁻³ N ⁻¹) Br ₁ Cl ₃ (0.0086), Br ₂ Cl ₂ (0.0028), X ₄ (0.29), Br ₁ Cl ₄ (0.014), X ₅ (0.42), X ₆ (0.028), Br ₁ Cl ₆ (0.0076), X ₇ (0.061), Br ₁ Cl ₇ (0.016), X ₈ (0.016) PXDF (1.1 ng m ⁻³ N ⁻¹) Br ₁ Cl ₃ (0.016), X ₄ (1.0), X ₅ (0.042), X ₇ (0.021), X ₈ (0.015)
Flue gas analysis	Sewage sludge sample	PXDD (hepta halogenated) PXDF (penta halogenated)	PXDD (0.0039 ng m ⁻³ N ⁻¹) Br ₁ Cl ₆ (0.0009), X ₇ (0.0039) PXDF (0.002 ng m ⁻³ N ⁻¹)

CHAPTER 2 Literature Review

			X ₅ (0.002)	
BFR-containing municipal waste incinerator	Municipal waste incinerator 1073 – 1123 K	TeXDD, TeXDF	PXDD (Cl ₄ , Br ₁ Cl ₃ , Br ₂ Cl ₂ , Br ₄) PXDF (Cl ₄ , Br ₁ Cl ₃ , Br ₂ Cl ₂ , Br ₃ Cl ₁ , Br ₄)	[217]
Stack gas emission	Industrial thermal process	PBCDD/PBCDF	PBCDF (1.7-3740 pmol Nm ⁻³) tetra-hexa halogenated, B ₁ C ₆ and B ₁ C ₇ PBCDD (0.2-582 pmol Nm ⁻³) (tetra-hexa halogenated)	[209]
PVC with TBDDs	Quartz tube reactor	PBCDD	TCDD, Br ₁ Cl ₃ , Br ₂ Cl ₂ , Br ₃ Cl ₁ , TBDD	[148]
Fly ash	Municipal waste incinerator	PBCDD/Fs	Monobromotricloro to monochlorotribromo dibenzo- <i>p</i> -dioxins	[234]
Artificial waste with BFR	Pilot Reactor Combustion at 1073 K	PBCDD/Fs	Br ₂ Cl ₂ DD Br ₂ Cl ₂ DF TeBCDD/F PeBCDD/F	[218]
Artificial waste with BFR	Flue gas cooling at 523 K	PBCDD/Fs	Br ₂ Cl ₂ DD Br ₂ Cl ₂ DF TeBCDD/F PeBCDD/F	[218]
Municipal waste incinerator or fly	Laboratory borosilicate reactor at 573 K	PBCDD	Br ₃ Cl ₁ DD, Br ₂ Cl ₂ DD, Br ₁ Cl ₃ DD	[219]

CHAPTER 2 Literature Review

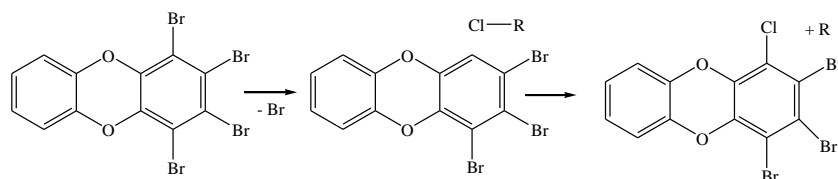
ash sample				
BFR with PCDD/F s	Gamma irradiation technique	PXDD/Fs	PXDD/F (mono to hepta halogenated)	[220]
Ash sample	Wood fired boiler	BCDD/Fs	Br ₁ Cl ₃ DD, Br ₁ Cl ₄ DD, Br ₁ Cl ₅ DD	[221]
Electrica l and electroni c waste with municip al solid waste	Incinerator	BCDD/Fs	MonobromopolychloroD D/Fs BCDF>>BCDD	[222]
Fly ash sample	Municipal waste incinerator	Monobromopolychloro to dibromopolychloroDD/ Fs	TetrahalogenatedDFs (Cl ₄ DF, BrCl ₃ DF, Br ₂ Cl ₂ DF, Br ₃ Cl ₁ DF and Br ₄ DF)	[223]
Fly ash sample	Municipal incinerator	PBCDD/Fs	PBCDD (ppb) BrCl ₃ (7), BrCl ₄ (24), BrCl ₅ (48) BrCl ₆ (21), BrCl ₇ (8) PBCDF (ppb) BrCl ₃ (7), BrCl ₄ (2), BrCl ₅ (0.5) BrCl ₆ (0.1), BrCl ₇ (0.2)	[229]
Raw gas	TAMARA incinerator	PXDD/Fs	50 ng m ⁻³	[41]

CHAPTER 2 Literature Review

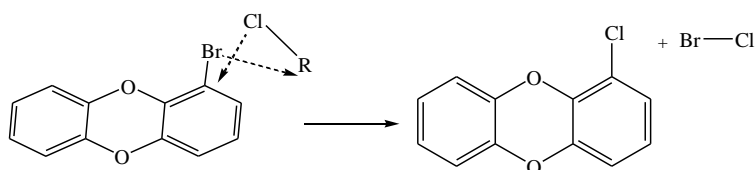
Municipal waste sample	Waste Incinerator	PXDD/Fs	23 ng m ⁻³	[224]
Flue gas sample	Waste incineration	Mixed halogenated dibenzo- <i>p</i> -dioxins/furans	PXDD (ng m ⁻³) BrCl ₃ (1.3), Br ₂ Cl ₂ (<0.5) PXDF (ng m ⁻³) BrCl ₃ (1.3)	[225]
Clean gas	Waste incineration	Mixed halogenated dibenzo- <i>p</i> -dioxins/furans	PXDD/F (ng m ⁻³) BrCl ₃ DD (0.15) BrCl ₃ DF (4.5)	[225]
Printed circuit boards	Rotary kiln furnace	polybromomonochloro DD/DFs	9.5 ng g ⁻¹	[226]
Fly ash samples	Municipal waste incinerator	PXDD/Fs	PXDD (ppb) BrCl ₃ (16), BrCl ₄ (25), BrCl ₅ (17), BrCl ₆ (16), BrCl ₄ (13) PXDF (ppb) BrCl ₃ (5), BrCl ₄ (6), BrCl ₅ (15), BrCl ₆ (20), BrCl ₇ (1)	[228]
Fly ash sample	Industrial waste incinerator	PXDD/F	PXDD BrCl ₄ , BrCl ₅ , BrCl ₆ , BrCl ₇ PXDF BrCl ₄ , BrCl ₅ , BrCl ₆ , BrCl ₇	[228]

Co-combustion/pyrolysis of the few chlorine and bromine-containing components provides important mechanistic information on PXDD/F formation [229]. Three

reactions are proposed to control the final yields of PXDD/Fs; chlorine-bromine exchange, bromination of PCDD/Fs, and formation by de novo synthesis. Commencing with the chlorine-bromine exchange reactions, Thoma et al. co-pyrolysed 1,2,3,4-TBDD and materials with three distinct chlorine donors: PVC, HCl and NaCl [230]. Pyrolysis of 1,2,3,4-TBDD with PVC, HCl and NaCl at 1173 K yielded 34.7 %, 20.5 % and 0.3 % 1,2,3,4-TCDD, respectively. It follows that inorganic chlorine content (i.e. the predominant chlorine form in typical MSW) does not contribute significantly to chlorine incorporation in PBDD/Fs. Pyrolysis of PVC with PBDEs and PBBs at 1073 K [72], produced several mixed halogenated congeners of diphenyl ether (PXDE) and biphenyl (PXB). While the two experimental studies by Thoma et al. [72, 230] confirm the formation of mixed halogenated species, intermediate reactions are still not clear. At temperatures as high as 1073 – 1173 K, rupture of C-Br bonds occurs readily, leaving radical sites. Addition of chlorine to the apparent radical site could take place via a simple gas-phase abstraction reaction:



Gradual and slow increases in temperature offer a better verification of the occurrence of the presumed bromine-chlorine exchange prior to the rupture of C-Br bonds:



Söderström and Marklund [217] investigated the effects of BFR type (TBBA, HBCD and decabromodiphenyl ether (DeBDE)) and bromine load (Br/Cl ratios in initial fuel of 1:1 or 2:1) on the formation of PXDD/Fs from artificial solid waste in a pilot-scale, fluidised bed incinerator at temperatures of 1073 – 1093 K. All chlorine-bromine containing fuels produced PXDD/F congeners, especially tetra mixed halogenated dibenzofuran (TXDD/Fs where $n_{Cl} + n_{Br} = 4$) isomers. Figure 2.22 compares yields of TXDFs with

those of TCDFs and TBDFs for different types of BFRs and bromine loads. Söderström and Marklund [217] demonstrated that no obvious trend could be deduced with regard to the dependency of the total yield of PXDF isomers on the type of added BFRs and the bromine load. However, careful inspection of their TXDF profiles reveals that the significant yield of Σ Di-Br, di-CDF isomers, when using DeBDE as a source of bromine, originated from a simple conversion of DeBDE to PBDFs. Chlorination reactions of TBDF isomers transform them into TXDF congeners (Figure 2.22). It is also plausible to assume that feed PBDEs experience chlorination substitution [231] prior to their conversion into PXDF congeners. The high furan/dioxin ratios from various incineration/metallurgical processes [209] indicate the presence of PBDEs in initial fuels.

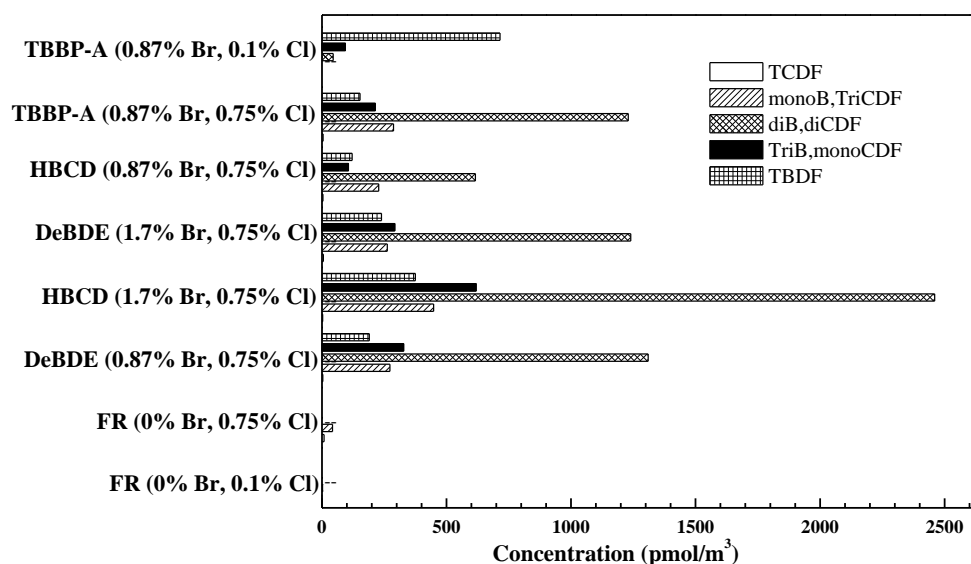


Figure 2.22. Product profiles for different PXDF congeners evolved from the thermal degradation of BFRs, along with chlorine contents [24].

When chlorine and bromine are present, the yields of PXDD/Fs were always greater than their chlorinated or brominated counterparts (i.e. diBr, diCDF versus TCDD and TBDD) [217]. Total concentrations of TXDF isomers were 10 times higher than those of TCDF congeners formed in a pure chlorine environment but were comparable to PBDF congeners formed in a pure bromine environment. Overall, PXDD/F formation is a complex process, and the final halogenation degree does not rely only on the structure of

present BFRs, but also depends on the interplay between Cl- and Br-containing gaseous species (HCl, HBr, BrCl, etc.).

As an important mechanistic fingerprint, Söderström and Marklund measured the fractions of bromine incorporated into PXDD/Fs at high (1073 K) and low (523 K) temperatures [218]. Initial fuels contained equal molar amounts of chlorine and bromine (introduced as comparable ratios of DeBDE, TBBA and HBCD). Figure 2.23 presents the fraction of Br in formed PXDD/F homologue groups as a proportion of total halogen content (Br + Cl). As depicted in this figure, there is a shift toward more brominated compounds as the temperature increases. Thermodynamic factors aid the formation of brominating species (Br, Br₂ and BrCl) at all temperatures. The authors [218] stated that highly chlorinated compounds have greater thermodynamic stability at lower temperatures and, hence, they appear at higher concentrations than higher brominated compounds. If this holds true, highly chlorinated congeners must also form in greater concentrations at higher temperatures too. Preference toward chlorination at lower temperatures might be kinetically driven. The absence of a kinetic model describing mixtures of Br₂/Cl₂/O₂/H₂ hinders conclusions regarding the prevalence of kinetic considerations at low temperatures.

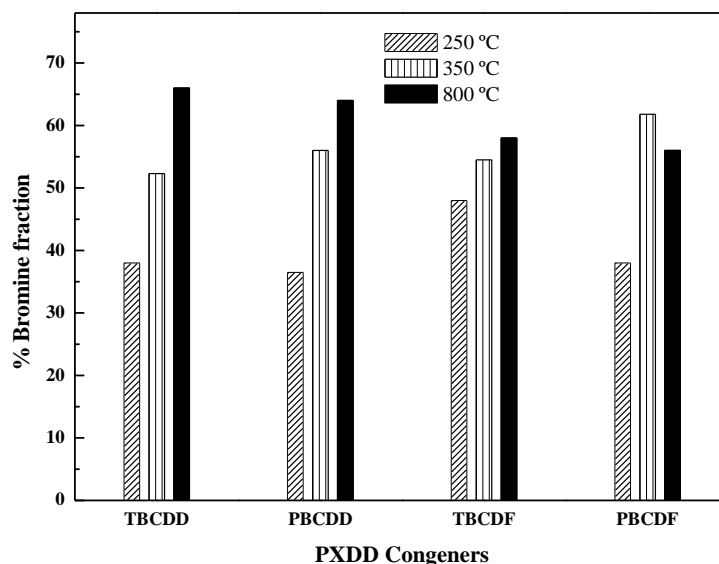


Figure 2.23. Comparison of % bromine fractions (Br/(Br + Cl)) prevailing in PXDD congeners at various temperatures [218].

2.6.3. De novo formation of PXDD/Fs

The majority of PCDD/Fs evolve in the post-combustion zone of MSW incinerators. The less stable BFR materials are expected to be decomposed completely under sufficient combustion conditions. This practice concentrates Br in the fly ash. The co-existence of bromine and chlorine in the fly ash alongside potent metal-based catalysts serves as a perfect recipe for the formation of PXDD/Fs through the de novo corridor. There is a paucity of experimental studies on de novo synthesis of PXDD/Fs. Stieglitz et al. [197] demonstrated that annealing a mixture of fly ash with inorganic Cl, Br donors produces several congeners of PXDD/F. It is worthwhile noting that data were presented qualitatively. As such, no attempts were made to correlate yields of formed PXDD/Fs with chlorine and bromine inputs.

Weber et al. [215] investigated the formation of PXDD/Fs from oxidative decomposition of model fly ash loaded with equimolar concentrations of inorganic chlorine and bromine (potassium salts). At 623 K, the yield of PXDD/Fs reached as high as 5.0 % wt of the initial carbon input. Concentrations of PXDF congeners were at least 9 times higher than those of PXDDs, at all considered temperatures. Decreases in temperature enhanced bromine substitution in PXDD/F isomers, whereas increases in time resulted in an average enhancement of chlorine substitution. Total PCDD/Fs amounted to only 20 % of total PXDD/Fs on a molar basis. The dominance of PXDF congeners over PXDD/Fs and the high yield of PXDD/Fs compared with PCDD/Fs has also been reported in the oxidation of fly ash with BFRs. Isomer patterns in the homologue groups of PXDDs and PXDFs showed very similar trends, suggesting similar bromination and chlorination mechanisms during de novo synthesis. Kawamoto and Ishikawa [232] found that heating an ash sample with an added bromine load (in the form of TBBA) substantially increased its PXDD/F content and clearly changed its homologue distribution pattern. The authors considered this to be strong evidence of de novo synthesis. According to a statistical model developed by Funke et al. [233], PXDF isomers yielded by de novo synthesis correlated very well with input Br/(Br + Cl) ratios. This model also enabled the estimation of input bromine content in the fly ash from known PXDD/F gas concentrations.

A comprehensive understanding of PXDD/F formation via de novo synthesis requires the consideration of several factors:

- In all published experiments on the de novo formation of PXDD/Fs, bromine donors were of an inorganic nature. Complete degradation of BFRs produces brominated short alkanes and alkenes. Consequently, it is of more relevance to deploy brominated C₁-C₃ species as bromine donors in de novo formation of PXDD/Fs.
- As Cu is the main metal used in printed circuit boards, the formation of CuBr₂ during thermal recycling of electronic wastes is very plausible. It will be interesting to study competing chlorination and bromination processes during de novo synthesis when equimolar amounts of CuCl₂ and CuBr₂ are used in model fly ashes.
- If BFRs are used as the source of bromine in fly ashes, it is difficult to trace the source of bromine partaking in de novo synthesis. Does bromine come from the original input BFRs or from brominated species formed during BFR decomposition? Comparing the yields and halogenation patterns of PXDD/Fs at low temperatures (prior to BFR degradation) and high temperatures (after the complete destruction of BFRs) could provide some fingerprints of the source of bromine participating in de novo synthesis.
- It is generally believed that chlorinated C₁-C₃ species go through complex addition and oxidation reactions to yield PCDD/Fs, in a similar fashion as the de novo pathway. It will be interesting to assess the potential for the formation of PXDD/Fs from mixed halogenated C₁-C₃ species.

References

- [1] Alae, M., Arias, P., Sjödin, A., Bergman, A. An overview of commercially used brominated flame retardants, their applications, their use patterns in different countries/regions and possible modes of release. *Environ Int* **2003**, 29, 683-639.
- [2] Birnbaum, L.S., Staskal, D.F. Brominated flame retardants: cause for concern? *Environ Health Perspect* **2004**, 112, 9-17.
- [3] Flame retardant chemicals. A world market review. BizAcumen (ed.), November **2009**.
- [4] Lassen, C., Løkke, S., Hansen, E., Andersen, L.I. Brominated flame retardants: Substance flow analysis and assessment of alternatives. Project No. 494. Danish Environmental Protection Agency (DEPA), Copenhagen. 240. **1999**.
- [5] Galletti, C.G., Bocchini, P. Pyrolysis/gas chromatography/mass spectrometry of lignocellulose. *Rapid Commun Mass Spectrom* **1995**, 9, 815-826.
- [6] Brominated Diphenyl Ethers Environ Health Criteria, Geneva. World Health Organization,. **1994**, 162.
- [7] Watanabe, I., Sakaib, S. Environmental release and behavior of brominated flame retardants. *Environ Int* **2003**, 29, 665-82.
- [8] Gustafsson, K., Björk, M., Burreau, S., Gilek, M. Bioaccumulation kinetics of brominated flame retardants (polybrominated diphenyl ethers) in blue mussels (*Mytilus edulis*). *Environ Toxicol Chem* **1999**, 18, 1218-1224.
- [9] Law, K., Halldorson, T., Danell, R., Stern, G., Gewurtz, S., Alae, M., Marvin, C., Whittle, M., Tomy, G. Bioaccumulation and trophic transfer of some brominated flame retardants in a Lake Winnipeg (Canada) food web. *Environ Toxicol Chem* **2006**, 25, 2177-2186.
- [10] Hyötyläinen, T., Hartonen, K. Determination of brominated flame retardants in environmental samples. *TrAC* **2002**, 21, 13-30.
- [11] Law, R.J., Allchin, C.R., de Boer, J., Covaci, A., Herzke, D., Lepom, P., Morris, S., Tronczynski, J., de Wit, A. C. Levels and trends of brominated flame retardants in the European environment. *Chemosphere* **2006**, 64, 187-208.
- [12] Takigami, H., Suzuki, G., Hirai, Y., Ishikawa, Y., Sunami, M., Sakai, S. Flame retardants in indoor dust and air of a hotel in Japan. *Environ Int* **2009**, 35, 688-6893.

- [13] Karlsson, M., Julander, A., van Bavel, B.L.H. Levels of brominated flame retardants in blood in relation to levels in household air and dust. *Environ Int* **2007**, 33, 62-69.
- [14] Eljarrat, E., Barceló, D. Sample handling and analysis of brominated flame retardants in soil and sludge samples. *TrAC* **2004**, 23, 727-736.
- [15] Covaci, A., Voorspoels, S., de Boer, J. Determination of brominated flame retardants, with emphasis on polybrominated diphenyl ethers (PBDEs) in environmental and human samples -a review. *Environ Int* **2003**, 29, 735-756.
- [16] Ohta, S., Ishizuka, D., Nishimura, H., Nakao, T., Aozasa, O., Shimidzu, Y. Comparison of polybrominated diphenyl ethers in fish, vegetables, and meats and levels in human milk of nursing women in Japan. *Chemosphere* **2002**, 46, 689-696.
- [17] Sormo, E.G., Salmer, M.P., Jenssen, B.M., Hop, H., Baek, K., Kovacs, K.M. Biomagnification of polybrominated diphenyl ether and hexabromocyclododecane flame retardants in the polar bear food chain in Svalbard, Norway. *Environ Toxicol Chem.* **2006**, 25, 2502-2511.
- [18] Morris, S., Allchin, C.R., Zegers, B.N., Haftka, J.J., Boon, J.P., Belpaire, C. Distribution and fate of HBCD and TBBPA brominated flame retardants in North Sea estuaries and aquatic food webs. *Environ Sci Technol* **2004**, 38, 5497-5504.
- [19] Guo, J., Guo, J., Xu, Z. Recycling of non-metallic fractions from waste printed circuit boards: A review. *J Hazard Mater* **2009**, 168, 567-590.
- [20] Birnbaum, L.S., Staskal, D.F., Diliberto, J.J. Health effects of polybrominated dibenzo-*p*-dioxins (PBDDs) and dibenzofurans (PBDFs). *Environ Int* **2003**, 29, 855-860.
- [21] Mennear, J.H., Lee, C.C. Polybrominated dibenzo-*p*-dioxins and dibenzofurans: literature review and health assessment. *Environ Health Perspect* **1994**, 102, 265-274.
- [22] Hornung, M.W., Zabel, E.W., Peterson, R.E. Toxic equivalency factors of polybrominated dibenzo-*p*-dioxin, dibenzofuran, biphenyl, and polyhalogenated diphenyl ether congeners based on rainbow trout early life stage mortality. *Toxicol Appl Pharmacol* **1996**, 140, 227-234.

- [23] Weber, L.W., Greim, H. The toxicity of brominated and mixed-halogenated dibenzo-*p*-dioxins and dibenzofurans: an overview. *J Toxicol Environ Health* **1997**, 50, 195-215.
- [24] Soderstrom, G., Marklund, S. PBCDD and PBCDF from incineration of waste-containing brominated flame retardants. *Environ Sci Technol* **2002**, 36, 1959-1964.
- [25] Barontini, F., Marsanich, K., Petarca, L., Cozzani, V. Thermal degradation and decomposition products of electronic boards containing BFRs. *Ind Eng Chem Res* **2005**, 44, 4186-4199.
- [26] Gullett, B.K., Linak, W.P., Touati, A., Wasson, S.J., Gatica, S., King, C.J. Characterization of air emissions and residual ash from open burning of electronic wastes during simulated rudimentary recycling operations. *J Mater Cycles Waste Manage* **2007**, 9, 69-79.
- [27] Lai, Y.C., Lee, W.J., Li, H.W., Wang, L.C., Chang-Chien G.P. Inhibition of polybrominated dibenzo-*p*-dioxin and dibenzofuran formation from the pyrolysis of printed circuit boards. *Environ Sci Technol* **2006**, 41, 957-962.
- [28] Estrellan, C.R., Lino, F. Toxic emissions from open burning. *Chemosphere* **2010**, 80, 193-207.
- [29] Tame, N.W., Dlugogorski, B.Z., Kennedy, E.M. Formation of polychlorinated dibenzo-*p*-dioxins and polychlorinated dibenzofurans (PCDD/F) in fires of arsenic-free treated wood: role of organic preservatives. *Environ Sci Technol* **2007**, 41, 6425-6432.
- [30] Litten, S., McChesney, D.J., Hamilton, M.C., Fowler B. Destruction of the world trade center and PCBs, PBDEs, PCDD/Fs, PBDD/Fs, and chlorinated biphenylenes in water, sediment, and sewage sludge. *Environ Sci Technol* **2003**, 37, 5502-5510.
- [31] Tue, N.M., Takahashi, S., Subramanian, A., Sakai, S., Tanabe, S. Environmental contamination and human exposure to dioxin-related compounds in e-waste recycling sites of developing countries. *Environ Sci Process Impacts* **2013**, 15, 1326-1331.
- [32] Yu, X., Zennegg, M., Engwall, M., Rotander, A., Larrson, M., Wong, M.H. E-waste recycling heavily contaminates a chinese city with chlorinated, brominated and mixed halogenated dioxins. *Organohalogen Compd* **2008**, 70, 813-816.

- [33] Huang, H., Buekens, A. On the mechanisms of dioxin formation in combustion processes. *Chemosphere* **1995**, 31, 4099-4117.
- [34] Evans, C.S., Dellinger, B. Mechanisms of dioxin formation from the high-temperature pyrolysis of 2-bromophenol. *Environ Sci Technol* **2003**, 37, 5574-5580.
- [35] Evans, C.S., Dellinger, B. Mechanisms of dioxin formation from the high-temperature oxidation of 2-bromophenol. *Environ Sci Technol* **2005**, 39, 2128-2134.
- [36] Stieglitz, L., Zwick, G., Beck, J., Roth, W., Vogg, H. On the de-novo synthesis of PCDD/PCDF on fly ash of municipal waste incinerators. *Chemosphere* **1989**, 18, 1219-1226.
- [37] Lorenz, W., Bahadir, M. Recycling of flame retardants containing printed circuits: A study of the possible formation of polyhalogenated dibenzodioxins/-furans. *Chemosphere* **1993**, 26, 2221-2229.
- [38] Luijk, R., Dorland, C., Smit, P., Jansen, J., Govers, H.A.J. The role of bromine in the de novo synthesis in a model fly ash system. *Chemosphere* **1994**, 28, 1299-1309.
- [39] Weber, R., Kuch, B. Relevance of BFRs and thermal conditions on the formation pathways of brominated and brominated-chlorinated dibenzodioxins and dibenzofurans. *Environ Int* **2003**, 29, 699-710.
- [40] Du, B., Zheng, M., Tian, H., Liu, A., Huang, Y., Li, L. Occurrence and characteristics of polybrominated dibenzo-*p*-dioxins and dibenzofurans in stack gas emissions from industrial thermal processes. *Chemosphere* **2010**, 80, 1227-1733.
- [41] Vehlow, J., Bergfeldt, B., Jay, K., Seifert, H., Wanke, T., Mark, F.E. Thermal treatment of electrical and electronic waste plastics. *Waste Manage Res* **2000**, 18, 131-140.
- [42] Evans, C.S., Dellinger, B. Surface-mediated formation of PBDD/Fs from the high-temperature oxidation of 2-bromophenol on a CuO/silica surface. *Chemosphere* **2006**, 63, 1291-1299.
- [43] Evans, C.S., Dellinger, B. Surface-mediated formation of polybrominated dibenzo-*p*-dioxins and dibenzofurans from the high-temperature pyrolysis of 2-bromophenol on a CuO/silica surface. *Environ Sci Technol* **2005**, 39, 4857-4863.

- [44] Covaci, A., Harrad, S., Abdallah, M.A.E., Ali, N., Law, R.J., Herzke, D. Novel brominated flame retardants: A review of their analysis, environmental fate and behaviour. *Environ Int* **2011**, 37, 532-556.
- [45] Introduction to Thermal Analysis: Techniques and Applications. ed. M.E. Brown. **2001**, Netherland: Kluwer Academic Publishers.
- [46] Milosavljevic, I., Suuberg, E.M. Cellulose thermal decomposition kinetics: global mass loss kinetics. *Ind Eng Chem Res* **1995**, 34, 1081-1091.
- [47] Teng, H., Wei, Y.C. Thermogravimetric studies on the kinetics of rice hull pyrolysis and the influence of water treatment. *Ind. Eng. Chem. Res.* **1998**, 37, 3806-3811.
- [48] Peterson, J.D., Vyazovkin, S., Wight, C.A. Kinetics of the thermal and thermo-oxidative degradation of polystyrene, polyethylene and poly(propylene). *Macromol Chem Phys* **2001**, 202, 775-784.
- [49] Su, W., Ma, H., Wang, Q., Ma, L.J. Thermal behavior and gaseous emission analysis during co-combustion of ethanol fermentation residue from food waste and coal using TG–FTIR. *J Anal Appl Pyrolysis* **2013**, 99, 79-84.
- [50] Xu, T., Huang, X. A TG-FTIR investigation into smoke suppression mechanism of magnesium hydroxide in asphalt combustion process. *J Anal Appl Pyrolysis* **2010**, 87, 217-223.
- [51] Liu, Q., Wang, S., Zheng, Y., LuoK, C.Z. Mechanism study of wood lignin pyrolysis by using TG–FTIR analysis. *J Anal Appl Pyrolysis* **2008**, 82, 170-177.
- [52] Haines, P.J., Wilburn, F.W. Differential thermal analysis and differential scanning calorimetry. ed. Handbook of Thermal Analysis and Calorimetry, ed. I.B. ME. Vol. 1. 1998, Netherlands: Elsevier Science BV.
- [53] Moldoveanu, S.C. Pyrolysis GC/MS, present and future (recent past and present needs). *J Microcolumn Sep* **2001**, 13, 102-125.
- [54] Quan, C., Li, A., Gao, N. Research on pyrolysis of PCB waste with TG-FTIR and Py-GC/MS. *J Therm Anal Calorim* **2012**, 110, 1463-1470.
- [55] Luda, M.P., Balabanovich, A.I., Zanetti, M.G.D. Thermal decomposition of fire retardant brominated epoxy resins cured with different nitrogen containing hardeners. *Polym Degrad Stab* **2007**, 92, 1088-1100.
- [56] Fahmi, R., Bridgwater, A.V., Thain, S.C., Donnison, I.S., Morris, P.M., Yates, N. Prediction of Klason lignin and lignin thermal degradation products by Py–

- GC/MS in a collection of lolium and festuca grasses. *J Anal Appl Pyrolysis* **2007**, 80, 16-23.
- [57] Lenoir, D., Zier, B., Bieniek, D.K.A. The influence of water and metals on PBDD/F concentration in incineration of decabrombiphenyl ether in polymeric matrices. *Chemosphere* **1994**, 28, 1921-1928.
- [58] Moghtaderi, B., Meesri, C., Wall, T.F. Pyrolytic characteristics of blended coal and woody biomass. *Fuel* **2004**, 83, 745-750.
- [59] Sricharoenchaikul V., Atong, D. Thermal decomposition study on *Jatropha curcas* L. waste using TGA and fixed bed reactor. *J Anal Appl Pyrolysis* **2009**, 85, 155-162.
- [60] Duan, H., Li, J., Liu, Y., Yamazaki, N., Jiang, W. Characterization and inventory of PCDD/Fs and PBDD/Fs emissions from the incineration of waste printed circuit board. *Environ Sci Technol* **2011**, 45, 6322-6338.
- [61] Ledesma, E.B., Marsh, N.D., Sandrowitz, A.K., Wornat, M.J. An experimental study on the thermal decomposition of catechol. *Proc Combust Inst* **2002**, 29, 2299-2306.
- [62] Chen, K., Wojtalewicz, D., Altarawneh, M., Mackie, J.C., Kennedy, E.M., Dlugogorski, B.Z. Formation of polychlorinated dibenzo-*p*-dioxins and dibenzofurans (PCDD/F) in oxidation of captan pesticide. *P Combust Inst* **2011**, 33, 701-708.
- [63] Summoogum, S.L., Mackie, J.C., Kennedy, E.M., Delichatsios, M.A., Dlugogorski, B.Z. Thermal Decomposition of alpha-cypermethrin under non-oxidative conditions. *Chemosphere* **2011**, 85, 143-150.
- [64] Lemieux, P.M., Ryan, J.V. Enhanced formation of chlorinated PICs by the addition of bromine. *Combust Sci Tech* **1998**, 134, 367-387.
- [65] Lemieux, P.M., Stewart, E.S., Ryan, J.V. Pilot-scale studies on the effect of bromine addition on the emissions of chlorinated organic combustion by-products. *Waste Manag* **2002**, 22, 381-389.
- [66] Sakai, S., Watanabe, J., Honda, Y., Takatsuki, H., Aoki, I., Futamatsu, Masayuki, F., Shiozaki, K. Combustion of brominated flame retardants and behavior of its byproducts. *Chemosphere* **2001**, 42, 519-531.
- [67] Ortuño, N., Moltó, J., Conesa, J.A., Font, R. Formation of brominated pollutants during the pyrolysis and combustion of tetrabromobisphenol A at different temperatures. *Environ Pollut* **2014**, 191, 31-37.

- [68] Lemieux, P.M., Ryan, J.V. Enhanced formation of dioxins and furans from combustion devices by addition of trace quantities of bromine. *Waste Management* 1998, 18, 361-370.
- [69] Barontini, F., Cozzani, V. Formation of hydrogen bromide and organobrominated compounds in the thermal degradation of electronic boards. *J Anal Appl Pyrolysis* 2006, 77, 41-55.
- [70] Blazsó, M., Czégény, Z., Csoma, C. Pyrolysis and debromination of flame retarded polymers of electronic scrap studied by analytical pyrolysis. *J Anal Appl Pyrolysis* 2002, 64, 249-261.
- [71] Borojovich, E.J.C., Aizenshtat, Z. Thermal behavior of brominated and polybrominated compounds I: closed vessel conditions. *J Anal Appl Pyrolysis* 2002, 63, 105-128.
- [72] Larsen, E.R., Ecker, E.E. Thermal stability of fire retardants III, decomposition of pentabromochlorocyclohexane and hexabromocyclododecane under processing conditions. *J of Fire Sci* 1988, 6, 139-159.
- [73] Grause, G., Furusawa, M., Okuwaki, A.Y.T. Pyrolysis of tetrabromobisphenol-A containing paper laminated printed circuit boards. *Chemosphere* 2008, 71, 872-878.
- [74] Öberg, T., Warman, K., Bergström, J. Brominated aromatics from combustion. *Chemosphere* 1987, 16, 2451-2465.
- [75] Font, R., Moltó, J., Ortuño, N. Kinetics of tetrabromobisphenol A pyrolysis. Comparison between correlation and mechanistic models. *J Anal Appl Pyrolysis* 2012, 94, 53-62.
- [76] Ni, M., Xiao, H., Chi, Y., Yan, J., Buekens, A., Jin, Y. Lu, S. Combustion and inorganic bromine emission of waste printed circuit boards in a high temperature furnace. *Waste Manag* 2012, 32, 568-574.
- [77] Uddin, M.A., Bhaskar, T., Kaneko, J., Muto, A., Sakata, Y. Matsui, T. Dehydrohalogenation during pyrolysis of brominated flame retardant containing high impact polystyrene (HIPS-Br) mixed with polyvinylchloride (PVC). *Fuel* 2002, 81, 1819-1825.
- [78] Marsanich, K., Zanelli, S., Barontini, F. Cozzani, V. Evaporation and thermal degradation of tetrabromobisphenol A above the melting point. *Thermochimica Acta* 2004, 421, 95-103.

- [79] Barontini, F., Cozzani, V., Petarca, L. Thermal stability and decomposition products of hexabromocyclododecane. *Ind Eng Chem Res* **2001**, 40, 3270-3280.
- [80] Barontini, F., Cozzani, V., Petarca, L. The influence of aluminum on the thermal decomposition of hexabromocyclododecane. *J Anal Appl Pyrolysis* **2003**, 70: 353-368.
- [81] Barontini, F., Marsanich, K., Petarca, L., Cozzani, V. The thermal degradation process of tetrabromobisphenol A. *Ind Eng Chem Res* **2004**, 43, 1952-1961.
- [82] Luda, M.P., Balabanovich, A.I., Hornung, A., Camino, G. Thermal degradation of a brominated bisphenol a derivative. *Polymer Adv Tech* **2003**, 14, 741-748.
- [83] Ortuño, N., Moltó, J., Conesa, J.A., Font, R. Production of brominated dioxins and furans and other compounds during thermal degradation of tetrabromobisphenol A.
- [84] Barontini, F., Marsanich, K., Cozzani, V. The use of TG-FTIR technique for the assessment of hydrogen bromide emissions in the combustion of BFRs. *J Therm Anal Calorim* **2004**; 78, 599-619.
- [85] Barontini F, Cozzani V, Marsanich K, Raffa, V. Petarca, L. An experimental investigation of tetrabromobisphenol A decomposition pathways. *J Anal Appl Pyrol* **2004**, 72, 41-53.
- [86] Altarawneh, M., Dar, T., Dlugogorski, B.Z. Thermochemical parameters and pK_a values for chlorinated congeners of thiophenol. *J Chem Eng Data* **2012**, 57, 1834-1842.
- [87] Altarawneh, M., Dlugogorski, B.Z., Kennedy, E.M., Mackie, J.C. Theoretical study of unimolecular decomposition of catechol. *J Phys Chem A* **2009**, 114, 1060-1067.
- [88] Altarawneh, M., Dlugogorski, B.Z., Kennedy, E.M., Mackie, J.C. Thermochemical properties and decomposition pathways of three isomeric semiquinone radicals. *J Phys Chem A* **2009**, 114, 1098-1108.
- [89] Rayson, M.S., Altarawneh, M., Mackie, J.C., Kennedy, E.M., Dlugogorski, B.Z. Theoretical study of the ammonia hypochlorous acid reaction mechanism. *J Phys Chem A* **2010**, 114, 2597-2606.
- [90] Szabo, A., Ostlund, N.S. Modern Quantum Chemistry: Introduction to Advanced Electronic Structure Theory. ed. **1996**, McGraw-Hill Inc.
- [91] Parr, R.G. Density functional theory. *Annu Rev Phys Chem* **1984**, 34, 631-656.

- [92] Zhao, Y., Lynch, B.J., Truhlar, D.G. Doubly hybrid meta DFT: New multi-coefficient correlation and density functional methods for thermochemistry and thermochemical kinetics. *J Phys Chem A* **2004**, 108, 4786-4791.
- [93] Frisch, M.J., Trucks, G.W., Schlegel, H.B., Scuseria, G.E., Robb, M.A., Cheeseman, J.R., Scalmani, G., Barone, V., Mennucci, B., Petersson, G.A., Nakatsuji, H., Caricato, M., Li, X., Hratchian, H.P., Izmaylov, A.F., Bloino, J., Zheng, G., Sonnenberg, J.L., Hada, M., Ehara, M., Toyota, K., Fukuda, R., Hasegawa, J., Ishida, M., Nakajima, T., Honda, Y., Kitao, O., Nakai, H., Vreven, T., Montgomery, J.A., Peralta, J.E., Ogliaro, F., Bearpark, M., Heyd, J.J., Brothers, E., Kudin, K.N., Staroverov, V.N., Kobayashi, R., Normand, J., Raghavachari, K., Rendell, A., Burant, J.C., Iyengar, S.S., Tomasi, J., Cossi, M., Rega, N., Millam, N.J., Klene, M., Knox, J.E., Cross, J.B., Bakken, V., Adamo, C., Jaramillo, J., Gomperts, R., Stratmann, R.E., Yazyev, O., Austin, A.J., Cammi, R., Pomelli, C., Ochterski, J.W., Martin, R.L., Morokuma, K., Zakrzewski, V. G., Voth, G.A., Salvador, P., Dannenberg, J.J., Dapprich, S., Daniels, A.D., Farkas, O., Foresman, J.B., Ortiz, J.V., Cioslowski, J., Fox, D.J. **2009**, Gaussian09, Revision D.01; Gaussian Inc: Wallingford, CT.
- [94] Delly, B. From molecules to solids with the DMol3 approach. *J Chem Phys* **2000**, 113, 7756-7764.
- [95] Kresse, G., Furthmüller, J. Efficient iterative schemes for ab initio total-energy calculations using a plane-wave basis set. *Phys Rev B* **1996**, 54, 11169-11186.
- [96] te Velde, G., Bickelhaupt, F.M., Baerends, E.J., Guerra, F.C., van Gisbergen, S.J.A., Snijders, J.G., Ziegler, T. Chemistry with ADF. *J Comput Chem* **2001**, 22, 931-967.
- [97] Barontini F, Cozzani V, Marsanich K, Raffa V, Petarca L. An experimental investigation of tetrabromobisphenol A decomposition pathways. *J Anal Appl Pyrol* **2004**, 72, 41-53.
- [98] Borojovicha, E.J.C., Aizenshtata, Z. Thermal behavior of brominated and polybrominated compounds II: Pyroproducts of brominated phenols as mechanistic tools. *J Anal Appl Pyrolysis* **2002**, 63, 129-145.
- [99] Barontini, F., Marsanich, K., Petarca, L., Cozzani, V. The thermal degradation process of tetrabromobisphenol A. *Ind Eng Chem Res* **2004**, 43, 1952-1961.

- [100] Marsanich, K., Zanelli, S., Barontini, F., Cozzani, V. Evaporation and thermal degradation of tetrabromobisphenol A above the melting point. *Thermochim Acta* **2004**, 421, 95-103.
- [101] Luda, M.P., Balabanovich, A.I., Hornung, A., Camino, G. Thermal degradation of a brominated bisphenol a derivative. *Polymer Adv Tech* **2003**, 14, 741-748.
- [102] Factor, A. Thermal decomposition of 4,4'-isopropylidene bis-2,6-dibromophenol (tetrabromobisphenol-A). *J Polym Sci A Polym Chem* **1973**, 11, 1691-701.
- [103] Ortuño, N., Moltó, J., Conesa, J. A., Font, R. Formation of brominated pollutants during the pyrolysis and combustion of tetrabromobisphenol A at different temperatures. *Environ Pollut* **2014**, 191, 31-37.
- [104] Quan, C., Li, A., Gao, N. Research on pyrolysis of PCB waste with TG-FTIR and Py-GC/MS. *J Therm Anal Calorim* **2012**, 110, 1463-1470.
- [105] Grause, G., Furusawa, M., Okuwaki, A., Yoshioka, T. Pyrolysis of tetrabromobisphenol-A containing paper laminated printed circuit boards. *Chemosphere* **2008**, 71, 872-878.
- [106] Borojovich, E.J.C., Aizenshtat, Z. Thermal behavior of brominated and polybrominated compounds I: closed vessel conditions. *J Anal Appl Pyrolysis* **2002**, 63, 105-28.
- [107] Wichmann, H., Dettmer, F.T., Bahadir, M. Thermal formation of PBDD/F from tetrabromobisphenol A—a comparison of polymer linked TBBP A with its additive incorporation in thermoplastics. *Chemosphere* **2002**, 47, 349-355.
- [108] Dettmer, F.T. Bromorganische Flammenschutzmittel Analytische Anforderungen und Thermische Bildung Von Polybromierten Dibenzo-*p*-dioxinen und Dibenzofuranen University of Braunschweig; **2001**.
- [109] Luijk, R., Govers, H.A.J. The formation of polybrominated dibenzo-*p*-dioxins (PBDDs) and dibenzofurans (PBDFs) during pyrolysis of polymer blends containing brominated flame retardants. *Chemosphere* **1992**, 25, 361-374.
- [110] Dumler, R., Thoma, H., Lenoir, D., Hutzinger, O. PBDF and PBDD from the combustion of bromine containing flame retarded polymers: A survey. *Chemosphere* **1989**, 19, 2023-2031.
- [111] Thoma, H., Rist, S., Hauschulz, G., Knorr, E., Hutzinger, O. Polybrominated dibenzodioxins and furans from the pyrolysis of some flame retardants. *Chemosphere* **1986**, 15, 649-952.

- [112] Barontini, F., Marsanich, K., Cozzani, V. The use of TG-FTIR technique for the assessment of hydrogen bromide emissions in the combustion of BFRs. *J Therm Anal Calorim* **2004**, 78, 599-619.
- [113] Altarawneh, M., Dlugogorski, B.Z. Mechanism of thermal decomposition of tetrabromobisphenol a (TBBA). *J Phys Chem A* **2014**, 118, 9338-9346.
- [114] Marongiu, A., Bozzano, G., Dente, M., Ranzi, E., Faravelli, T. Detailed kinetic modeling of pyrolysis of tetrabromobisphenol A. *J Anal Appl Pyrolysis* **2007**, 80, 325-345.
- [115] Dente, M., Bozzano, G., Bussani, G. A comprehensive program for visbreaking simulation: product amounts and their properties prediction. *Comput Chem Eng* **1997**, 21, 1125-1134.
- [116] Marongiu, A., Faravelli, T., Bozzano, G., Dente, M., Ranzi, E. Thermal degradation of polyvinyl chloride. *J Anal Appl Pyrolysis* **2003**, 70, 519-553.
- [117] Altarawneh, M., Dlugogorski, B.Z. Thermal decomposition of 1,2-bis(2,4,6-tribromophenoxy)ethane (BTBPE), a novel brominated flame retardant. *Environ Sci Technol* **2014**, 48, 14335-14343.
- [118] Shukla, B., Koshi, M. A novel route for PAH growth in HACA based mechanisms. *Combust Flame* **2012**, 159, 3589-3596.
- [119] Font, R., Moltó, J., Ortuño, N. Kinetics of tetrabromobisphenol A pyrolysis. Comparison between correlation and mechanistic models. *J Anal Appl Pyrolysis* **2012**, 94, 53-62.
- [120] Fink, J.K. Chapter 3 - Epoxy resins. In: Fink JK, editor. *Reactive Polymers Fundamentals and Applications (Second Edition)*. Oxford: William Andrew Publishing; **2013**, 95-153.
- [121] Luda, M.P., Balabanovich, A.I., Zanetti, M. Pyrolysis of fire retardant anhydride cured epoxy resins. *J Anal Appl Pyrolysis* **2010**, 88, 39-52.
- [122] Luda, M.P., Balabanovich, A.I., Zanetti, M., Guaratto, D. Thermal decomposition of fire retardant brominated epoxy resins cured with different nitrogen containing hardeners. *Polym Degrad Stab* **2007**, 92, 1088-1100.
- [123] Luda, M.P., Balabanovich, A.I., Camino, G. Thermal decomposition of fire retardant brominated epoxy resins. *J Anal Appl Pyrolysis* **2002**, 65, 25-40.
- [124] Balabanovich, A.I., Hornung, A., Merz, D., Seifert, H. The effect of a curing agent on the thermal degradation of fire retardant brominated epoxy resins. *Polym Degrad Stab* **2004**, 85, 713-723.

- [125] March J. Advanced organic chemistry: reactions, mechanisms, and structure. 4th ed. New York: John Wiley & Sons; **1992**.
- [126] Oleszek, S., Grabda, M., Shibata, E., Nakamura, T. TG and TG-MS methods for studies of the reaction between metal oxide and brominated flame retardant in various atmospheres. *Thermochimica Acta* **2012**, 527, 13-21.
- [127] Grabda, M., Oleszek-Kudlak, S., Shibata, E., Nakamura, T. Vaporization of zinc during thermal treatment of ZnO with tetrabromobisphenol A (TBBPA). *J Hazard Mater* **2011**, 187, 473-479.
- [128] Terakado, O., Ohhashi, R., Hirasawa, M. Bromine fixation by metal oxide in pyrolysis of printed circuit board containing brominated flame retardant. *J Anal Appl Pyrolysis* **2013**, 103, 216-221.
- [129] Terakado, O., Ohhashi, R., Hirasawa, M. Thermal degradation study of tetrabromobisphenol A under the presence metal oxide: Comparison of bromine fixation ability. *J Anal Appl Pyrolysis* **2011**, 91, 303-309.
- [130] Becher, G. The stereochemistry of 1,2,5,6,9,10-hexabromocyclododecane and its graphic representation. *Chemosphere* **2005**, 58, 989-991.
- [131] Law, R.J., Kohler, M., Heeb, N.V., Gerecke, A.C., Schmid, P., Voorspoels, S. Hexabromocyclododecane challenges scientists and regulators. *Environ Sci Technol* **2005**, 39, 281A-287A.
- [132] Peled, M., Scharia, R., Sondack, D. Thermal rearrangement of hexabromocyclododecane (HBCD). Desmurs JR, Gerard B, Goldstein MJ (Ed.), *Advances in Organobromine Chemistry* Amsterdam: Elsevier; **1995**, 92-99.
- [133] Barontini, F., Cozzani, V., Petarca, L. Thermal stability and decomposition products of hexabromocyclododecane. *Ind Eng Chem Res* **2001**, 40, 3270-3280.
- [134] Köppen, R., Becker, R., Jung, C., Nehls, I. On the thermally induced isomerisation of hexabromocyclododecane stereoisomers. *Chemosphere* **2008**, 71, 656-662.
- [135] Larsen, E.R., Ecker, E.L. Thermal stability of fire retardants III, decomposition of pentabromochlorocyclohexane and hexabromocyclododecane under processing conditions. *J of Fire Sci* **1988**, 6, 139-159.
- [136] Larsen, E.R., Ecker, E.L. Thermal stability of fire retardants: I, hexabromocyclododecane (HBCD). *J Fire Sci* **1986**, 4, 261-275.
- [137] Ahubelem, N., Altarawneh, M., Dlugogorski, B.Z. Dehydrohalogenation of ethyl halides. *Tetrahedron Lett* **2014**, 55, 4860-4868.

- [138] Barontini, F., Cozzani, V., Cuzzola, A., Petarca, L. Investigation of hexabromocyclododecane thermal degradation pathways by gas chromatography/mass spectrometry. *Rapid Commun Mass Spectrom* **2001**, 15, 690-698.
- [139] Stubbings, W.A., Harrad, S. Extent and mechanisms of brominated flame retardant emissions from waste soft furnishings and fabrics: A critical review. *Environ Int* **2014**, 71, 164-75.
- [140] Kajiwara, N., Takigami, H. Emission behavior of hexabromocyclododecanes and polybrominated diphenyl ethers from flame-retardant-treated textiles. *Env Sci Process Impact* **2013**, 15, 1957-1963.
- [141] Peter, Kjeldsen., Morton, A., Barlaz, A., Rooker, P., Baun, A., Ledina, A., Christensen, T.H. Present and long-term composition of MSW landfill leachate: a review. *Crit Rev. Environ Sci Technol* **2002**, 32, 297-336.
- [142] Takigami, H., Watanabe, M., Kajiwara, N. Destruction behavior of hexabromocyclododecanes during incineration of solid waste containing expanded and extruded polystyrene insulation foams. *Chemosphere* **2014**, 116, 24-33.
- [143] Dumler, R., Lenoir, D., Thoma, H., Hutzinger, O. Thermal formation of polybrominated dibenzofurans and dioxins from decabromodiphenyl ether flame retardant: Influence of antimony(III) oxide and the polymer matrix. *Chemosphere* **1990**, 20, 1867-1873.
- [144] Thoma, H., Hutzinger, O. Pyrolysis and GC/MS-analysis of brominated flame retardants in on-line operation. *Chemosphere* **1989**, 18, 1047-1050.
- [145] Luijk, R., Wever, H., Olie, K., Govers, H.A.J, Boon, J.J. The influence of the polymer matrix on the formation of polybrominated dibenzo-*p*-dioxins (PBDDs) and polybrominated dibenzofurans (PBDFs). *Chemosphere* **1991**, 23, 1173-1183.
- [146] Striebich, R.C., Rubey, W., Tirey, D. A., Dellinger, B. High temperature degradation of polybrominated flame retardant materials. *Chemosphere* **1991**, 23, 1197-1204.
- [147] Buser, H.R. Polybrominated dibenzofurans and dibenzo-*p*-dioxins: thermal reaction products of polybrominated diphenyl ether flame retardants. *Environ Sci Technol* **1986**, 20, 404-408.

- [148] Thoma, H., Hauschulz, G., Hutzinger, O. PVC-induced chlorine-bromine exchange in the pyrolysis of polybrominated diphenyl ethers, -biphenyls, -dibenzodioxins and dibenzofurans. *Chemosphere* **1987**, 16, 297 – 307.
- [149] Lenoir, D., Kampke-Thiel, K. Formation of polybrominated dibenzodioxins and dibenzofurans in laboratory combustion processes of brominated flame retardants, in fire and polymers II. *J Am Chem Soc.* **1995**, 377-392.
- [150] Zacharewski, T., Harris, M., Safe, S., Thoma, H., Hutzinger, O. Applications of the in vitro aryl hydrocarbon hydroxylase induction assay for determining 2,3,7,8- tetrachlorodibenzo-*p*-dioxin equivalents: Pyrolyzed brominated flame retardants. *Toxicology* **1988**, 51, 177-189.
- [151] Luijk, R., Govers, H.A.J., Nelissen, L. Formation of polybrominated dibenzofurans during extrusion of high-impact polystyrene/decabromodiphenyl ether/antimony(III) oxide. *Environ Sci Technol* **1992**, 26, 2191-2198.
- [152] Altarawneh, M., Dlugogorski, B.Z. A mechanistic and kinetic study on the formation of PBDD/Fs from PBDEs. *Environ Sci Technol* **2013**, 47, 5118-5127.
- [153] Lindahl, R., Rappe, C., Buser, H.R. Formation of polychlorinated dibenzofurans (PCDFs) and polychlorinated dibenzo-*p*-dioxins (PCDDs) from the pyrolysis of polychlorinated diphenyl ethers. *Chemosphere* **1980**, 9, 351-361.
- [154] Wong, A., Lei, Y.D., Alae, M., Wania, F. Vapor pressures of the polybrominated diphenyl ethers. *J Chem Eng Data* **2000**, 46, 239-242.
- [155] Wiater, I., Louw, R. Reactions of diphenyl ether with chlorine and bromine atoms around 750 K – relevance for gas-phase “dioxin” formation. *Eur J Org Chem* **1999**, 261-265.
- [156] Brauman, S.K., Chen, I.J.J. Influence of the fire retardant decabromodiphenyl oxide- Sb₂O₃, on the degradation of polystyrene. *Fire Retard Chem* **1981**, 8, 28-36.
- [157] O' Keefe, W. Formation of brominated dibenzofurans from pyrolysis of the polybrominated biphenyl fire retardant, firemaster FF-1. *Environ Health Perspect* **1978**, 23, 347-350.
- [158] Altarawneh, M., Dlugogorski, B.Z. Formation of polybrominated dibenzofurans from polybrominated biphenyls. *Chemosphere* **2015**, 119, 1048-1053.
- [159] Saggese, C., Frassoldati, A., Cuoci, A., Faravelli, T., Ranzi, E. A wide range kinetic modeling study of pyrolysis and oxidation of benzene. *Combust Flame* **2013**, 160, 1168-1190.

- [160] Balabanovich, A.I., Luda, M.P., Camino, G., Hornung, A. Thermal decomposition behavior of 1,2-bis-(2,4,6-tribromophenoxy)ethane. *J Anal Appl Pyrol* **2003**, 67, 95-107.
- [161] Vainikka, P. Occurrence of Bromine in Fluidised Bed Combustion of Solid Recovered Fuel. Turku, Finland: Åbo Akademi University **2011**.
- [162] Vainikka, P., Silvennoinen, J., Frantsi, A., Taipale, R., Yrjas, P., Hannula, J. Bromine and chlorine in aerosols and fly ash when co-firing solid recovered fuel, spruce bark and paper mill sludge in a 80 MWTH CFB boiler. The 20th international conference on fluidized bed combustion. China **2009**, 5, 18-20.
- [163] Vainikka, P., Hupa, M. Review on bromine in solid fuels – Part 2: Anthropogenic occurrence. *Fuel* **2012**, 94, 34-51.
- [164] Vehlow, J., Bergfeldt, B., Hunsinger, H., Jay, K., Seifert, H., Mark, F. E., Tange, L., Drohmann, D. Energy and material recovery by co-combustion of WEEE and MSW. EBFRIIP, Geneva (Switzerland) **2002**.
- [165] Vehlow, J., Mark, F.E. Influence of bromine on metal volatilization in waste combustion. *J Mater Cycles Waste Manage* **2000**, 2, 89-99.
- [166] Altarawneh, M., Dlugogorski, B.Z., Kennedy, E.M., Mackie, J.C. Mechanisms for formation, chlorination, dechlorination and destruction of polychlorinated dibenzo-*p*-dioxins and dibenzofurans (PCDD/Fs). *Prog Energy Combust Sci* **2009**, 35, 245-274.
- [167] Bryukov, M.G., Dellinger, B., Knyazev, V.D. Kinetic study of the gas-phase reaction of OH with Br₂. *J Phys Chem A* **2006**, 110, 9169-9174.
- [168] Boerrigter, H. Implementation of thermal processes for feedstock recycling of bromine, with energy recovery, from plastics waste of electrical and electronic equipment (WEEE) - Phase 2” report ECN-C-01-0110. Energy research Centre of the Netherlands (ECN), Petten (the Netherlands), **2001**.
- [169] PBKD. Recovery of bromine & energy from waste electrical & electronic equipment containing bromine in European Union”, PB Kennedy & Donkin Ltd. PB Kennedy & Donkin Ltd, Report BECCH0741071, **1999**.
- [170] Boerrigter, H, Oudhuis, A.B.J., Tange, L. Bromine recovery from the plastics fraction of waste electric and electronic equipment (WEEE) with staged gasification. Report from: Netherlands Energy Research Foundation (ECN). **2001b**.

- [171] Ni, M., Xiao, H., Chi, Y., Yan, J., Buekens, A., Jin, Y. Combustion and inorganic bromine emission of waste printed circuit boards in a high temperature furnace. *Waste Manag* **2012**, 32, 568-5674.
- [172] Bientinesi, M., Petarca, L. Comparative environmental analysis of waste brominated plastic thermal treatments. *Waste Manage* **2009**, 29, 1095-1102.
- [173] Walravens, B., Battin-Leclerc, F., Côme, G.M., Baronnet, F. Inhibiting effect of brominated compounds on oxidation reactions. *Combust Flame* **1995**, 103, 339-342.
- [174] Takacs, G.A., Glass, G.P. Reaction of atomic oxygen with hydrogen bromide. *J Phys Chem A* **1973**, 77, 1182-1186.
- [175] Dixon-Lewis, G., Marshall, P., Ruscic, B., Burcat, A., Goos, E., Cuoci, A. Inhibition of hydrogen oxidation by HBr and Br₂. *Combust Flame* **2012**, 159, 528-540.
- [176] Babushok, V., Tsang, W. Inhibitor rankings for alkane combustion. *Combust Flame* **2000**, 123, 488-506.
- [177] Seakins, P.W., Pilling, M.J., Niiranen, J.T., Gutman, D., Krasnoperov, L.N. Kinetics and thermochemistry of R+ hydrogen bromide .dblarw. RH + bromine atom reactions: determinations of the heat of formation of ethyl, isopropyl, sec-butyl and tert-butyl radicals. *J Phys Chem A* **1992**, 96, 9847-9855.
- [178] Timonen, R.S., Seetula, J.A., Gutman, D. Kinetics of the reactions of alkyl radicals (CH₃, C₂H₅, i-C₃H₇, and t-C₄H₉) with molecular bromine. *J Phys Chem A* **1990**, 94, 3005-3008.
- [179] Bierbach, A., Barnes, I., Becker, K.H. Rate coefficients for the gas-phase reactions of bromine radicals with a series of alkenes, dienes, and aromatic hydrocarbons at 298 ± 2 K. *Int J Chem Kinet* **1996**, 28, 565-577.
- [180] Schüler, D., Jager, J. Formation of chlorinated and brominated dioxins and other organohalogen compounds at the pilot incineration plant VERONA. *Chemosphere* **2004**, 54, 49-59.
- [181] Sidhu, S.S., Maqsd, L., Dellinger, B., Mascolo, G. The homogeneous, gas-phase formation of chlorinated and brominated dibenzo-*p*-dioxin from 2,4,6-trichloro- and 2,4,6-tribromophenols. *Combust Flame* **1995**, 100, 11-20.
- [182] Na, Y.C., Hong, J.K., Kim, K.J. Formation of polybrominated dibenzo-*p*-dioxins/furans (PBDDs/Fs) by the pyrolysis of 2,4-dibromophenol, 2,6-

- dibromophenol, and 2,4,6-tribromophenol. *Bull Korean Chem Soc* **2007**, 28, 547-551.
- [183] Evans, C.S., Dellinger, B. Formation of bromochlorodibenzo-*p*-dioxins and furans from the high-temperature pyrolysis of a 2-chlorophenol/2-bromophenol mixture. *Environ Sci Technol* **2005**, 39, 7940-7948.
- [184] Evans, C.S., Dellinger, B. Formation of bromochlorodibenzo-*p*-dioxins and dibenzofurans from the high temperature oxidation of a mixture of 2-chlorophenol and 2-bromophenol. *Environ Sci Technol* **2006**, 40, 3036-3042.
- [185] Afeefy, H.Y., Liebman, J.F., Stein, S.E., Linstrom, P.J., Mallard, W.G. NIST Chemistry WebBook, NIST Standard Reference Database Number 692005.
- [186] Altarawneh, M., Dlugogorski, B.Z., Kennedy, E.M., Mackie, J.C. Theoretical study of reaction pathways of dibenzofuran and dibenzo-*p*-dioxin under reducing conditions. *J Phys Chem A* **2007**, 111, 7133-7140.
- [187] Yu, W., Hu, J., Xu, F., Sun, X., Gao, R., Zhang, Q. Mechanism and direct kinetics study on the homogeneous gas phase formation of PBDD/Fs from 2-BPh, 2,4-DBPh, and 2,4,6-TBPh as precursors. *Environ Sci Technol* **2011**, 45, 1917-1925.
- [188] Yu, W., Li, P., Xu, F., Hu, J., Zhang, Q., Wang, W. Quantum chemical and direct dynamic study on homogeneous gas-phase formation of PBDD/Fs from 2,4,5-tribromophenol and 3,4-dibromophenol. *Chemosphere* **2013**, 93, 512-520.
- [189] Kislov, V.V., Islamova, N.I., Kolker, A.M., Lin, S.H., Mebel, A.M. Hydrogen abstraction acetylene addition and diels–alder mechanisms of PAH formation: a detailed study using first principles calculations. *J Chem Theory Comput* **2005**, 1, 908-924.
- [190] Li, L., Mi, X., Shi, Y., Zhou, G. Precursor to the onset of the bulk oxidation of Cu(100). *Phys Rev Lett* **2012**, 108, 176101.
- [191] Hell, K., Stieglitz, L., Dinjus, E. Mechanistic aspects of the de-novo synthesis of PCDD/PCDF on model mixtures and MSWI fly ashes using amorphous ¹²C- and ¹³C-labeled carbon. *Environ Sci Technol* **2001**, 35, 3892-3898.
- [192] Cosentino, U., Pitea, D., Moro, G. Computational modelling of de novo synthesis of dibenzofuran: oxidative pathways of pyrene and benzodibenzofuran. *Theor Chem Acc* **2012**, 131, 1-12.
- [193] Stanmore, B.R. The formation of dioxins in combustion systems. *Combust Flame* **2004**, 136, 398-427.

- [194] Stanmore, B.R. Modeling the formation of PCDD/F in solid waste incinerators. *Chemosphere* **2002**, 47, 565-573.
- [195] Heinbuch, D., Stieglitz, L. Formation of brominated compounds on fly ash. *Chemosphere* **1993**, 27, 317-324.
- [196] Ortuño, N., Conesa, J.A., Moltó, J., Font, R. De novo synthesis of brominated dioxins and furans. *Environ Sci Technol* **2014**, 48, 7959-7965.
- [197] Stieglitz, L., Zwick, G., Beck, J., Bautz, H., Roth, W. Carbonaceous particles in fly ash -a source for the de-novo-synthesis of organochloro compounds. *Chemosphere* **1989**, 19, 283-290.
- [198] Khaliq, A., Rhamdhani, M.A., Brooks, G., Masood, S. Metal extraction processes for electronic waste and existing industrial routes: A review and australian perspective. *Resources* **2014**, 3, 152-179.
- [199] Hisham, M.W.M., Benson, S.W. Thermochemistry of the deacon process. *J Phys Chem A* **1995**, 99, 6194-6198.
- [200] Levere, M.E., Nguyen, N.H., Percec, V. No reduction of CuBr₂ during Cu(0)-catalyzed living radical polymerization of methyl acrylate in DMSO at 25 °C. *Macromolecules* **2012**, 45, 8267-8274.
- [201] Ryu, J.Y. Formation of chlorinated phenols, dibenzo-*p*-dioxins, dibenzofurans, benzenes, benzoquinones and perchloroethylenes from phenols in oxidative and copper (II) chloride-catalyzed thermal process. *Chemosphere* **2008**, 71, 1100-1109.
- [202] Ryu, J.Y., Mulholland, J.A., Takeuchi, M., Kim, D.H., Hatanaka, T. CuCl₂-catalyzed PCDD/F formation and congener patterns from phenols. *Chemosphere* **2005**, 61, 1312-1326.
- [203] Altarawneh, M., Jiang, Z.T., Dlugogorski, B.Z. The structures and thermodynamic stability of copper(II) chloride surfaces. *Phys Chem Chem Phys* **2014**, 16, 24209-24215.
- [204] Altarawneh, M., Dlugogorski, B.Z. Structures, electronic properties and stability phase diagrams for copper (I/II) bromides surfaces. *Phys Chem Chem Phys* **2015**, 17, 9341-9351.
- [205] Altarawneh, M., Dlugogorski, B.Z. Formation and chlorination of carbazole, phenoxazine, and phenazine. *Environ Sci Technol* **2015**, 49, 2215-2221.
- [206] Sovocool, G.W., Munslow, W.D., Donnelly, J.R., Mitchum, R.K. Electrophilic bromination of dibenzofuran. *Chemosphere* **1987**, 16, 221-224.

- [207] Chandler, A.J., Eighmy, T.T., Hjelmar, O., Kosson, D.S., Se, S., Vehlouw, J. Municipal solid waste incinerator residues. Amsterdam, The Netherlands Elsevier; **1997**.
- [208] Saeed, A., Altarawneh, M., Dlugogorski, B.Z. Formation of mixed halogenated dibenzo-p-dioxins and dibenzofurans (PXDD/Fs). *Chemosphere* **2015**, 137, 149–156.
- [209] Du, B., Zheng, M., Huang, Y., Liu, A., Tian, H., Li, L. Mixed polybrominated/chlorinated dibenzo-*p*-dioxins and dibenzofurans in stack gas emissions from industrial thermal processes. *Environ Sci Technol* **2010**, 44, 5818-5823.
- [210] Lemieux, P.M., Ryan, J.V. Enhanced formation of dioxins and furans from combustion devices by addition of trace quantities of bromine. *Waste Manage* **1998**, 18, 361-370.
- [211] Hagenmaier, H., She, J., Benz, T., Dawidowsky, N., Dusterhoft, L., Lindig, C. Analysis of sewage sludge for polyhalogenated dibenzo-*p*-dioxins, dibenzofurans, and diphenylethers. *Chemosphere* **1992**, 25, 1457–1462.
- [212] Evans, C.S., Dellinger, B. Mechanisms of dioxin formation from the high-temperature oxidation of 2-chlorophenol. *Environ Sci Technol* **2004**, 39, 122-127.
- [213] Evans, C.S., Dellinger, B. Mechanisms of dioxin formation from the high-temperature pyrolysis of 2-chlorophenol. *Environ Sci Technol* **2003**, 37, 1325-1330.
- [214] Saeed, A., Altarawneh, M., Dlugogorski, B.Z. Reaction of 2-chlorophenol and 2-bromophenol: mechanisms of formation of mixed halogenated dioxins and furans (PXDD/Fs). *Organohalog Compd* **2014**, 76, 345-348.
- [215] Weber, R., Kuch, B., Ohno, T., Sakurai, T. De novo synthesis of mixed brominated-chlorinated PXDD/PXDF. *Organohalogen compd* **2002**, 56, 181-184.
- [216] Nakao, T., Ohta, S., Aozasa, O., Miyata, H. Investigation of PCDD/DF, PXDD/DF, PBDD/DF, and nitro-PAH detected on flue gas from waste incinerator. *Organohalogen compd* **2002**, 56, 349-352.
- [217] Soderstrom, G., Marklund, S. PXDD and PXDF from combustion of bromoflameretardant containing MSW. *Organohalogen Compd* **2000**, 47, 225-228.

- [218] Soderstrom, G., Marklund, S. Formation of PBCDD and PBCDF during flue gas cooling. *Environ Sci Technol* **2004**, 38, 825-830.
- [219] Zier, B., Lenoir, D., Lahaniatis, E.S., Kettrup, A. Surface catalyzed halogenation-dehalogenation reactions of aromatic bromine compounds adsorbed on fly ash. *Chemosphere* **1991**, 22, 1121-1129.
- [220] Buser, H.R. Brominated and brominated/chlorinated dibenzodioxins and dibenzofurans: potential environmental contaminants. *Chemosphere* **1987**, 16, 713-732.
- [221] Harless, L.R., Lewis, R.G., McDaniel, D.D., Jr Dupuy, A.E. Identification of bromo/chloro dibenzo-*p*-dioxins and dibenzofurans in ash samples. *Chemosphere* **1989**, 18, 201-208.
- [222] Vehlow, J., Wanke, T., Bergfeldt, B., Mark, F.E. Co-combustion of E&E waste plastics in the TAMARA test plant. 5th Annual North American Waste-to-Energy Conference. Research Triangle Park, N.C. **1997**, 291 – 305.
- [223] Schwind, K.H., Hosseinpour, J., Thoma, H. Brominated/chlorinated dibenzo-*p*-dioxins and dibenzofurans: Part 1: Brominated/chlorinated and brominated dibenzo-*p*-dioxins and dibenzofurans in fly ash from a municipal waste incinerator. *Chemosphere* **1988**;17:1875-84.
- [224] Vehlow, J., Mark, E.F. Electrical and electronic plastic waste co-combustion; with municipal solids waste for energy recovery. Technical Paper, APME. **1997**.
- [225] Oberg, T., Warman, K., Bergström, J. Brominated aromatics from combustion. *Chemosphere* **1987**, 16, 2451-2465.
- [226] Sakai, S., Watanabe, J., Honda, Y., Takatsuki, H., Aoki, I., Futamatsu, M. Combustion of brominated flame retardants and behavior of its byproducts. *Chemosphere* **2001**, 42, 519-531.
- [227] Tong, H.Y., Monson, S.J., Gross, M.L., Huang, L.Q. Monobromopolychlorodibenzo-*p*-dioxins and dibenzofurans in municipal waste incinerator flyash. *Anal Chem.* **1991**, 63, 2697-2705.
- [228] Schafer, W., Ballschmiter, K. Monobromo-polychloro-derivatives of benzene, biphenyl, dibenzofurane and dibenzodioxine formed in chemical-waste burning. *Chemosphere* **1986**, 15, 755-763.
- [229] Sovocool, G.W., Mitchum, R.K., Tondeur, Y., Munslow, W.D., Vonnahme, T.L., Donnelly, J.R. Bromo- and bromochloro-polynuclear aromatic

- hydrocarbons, dioxins and dibenzofurans in municipal incinerator fly ash. *Biomed Environ Mass Spectrom* **1988**, 15, 669-676.
- [230] Thoma, H., Hauschulz, G., Hutzinger, O. Chlorine-bromine exchange during pyrolysis of 1,2,3,4-tetrabromo-dibenzodioxin with various chlorine donors. *Chemosphere* **1987**, 16, 1579-1581.
- [231] Rupp, S., Metzger, J.W. Brominated–chlorinated diphenyl ethers formed by thermolysis of polybrominated diphenyl ethers at low temperatures. *Chemosphere* **2005**, 60, 1644-1651.
- [232] Kawamoto, K., Ishikawa, N. Experimental evidence for de novo synthesis of PBDD/PBDF and PXDD/PXDF as well as dioxins in the thermal processes of aash samples. *Organohalog Compd* **2005**, 67, 2219-2221.
- [233] Funcke, W., Hemminghaus H.J., Mark F.E., Vehlow J. PXDF/D in flue gas from an incinerator charging wastes containing Cl and Br and a statistical description of the resulting PXDF/D combustion profiles. *Organohalogen Compd* **1997**, 31, 93-98.
- [234] Luijk, R., Dorland, C., Smit, P., Jansen, J., Govers H.A.J. The role of bromine in the de novo synthesis in a model fly ash system. *Chemosphere* **1994**, 28, 1299–1309.

CHAPTER 3 RESEARCH METHODOLOGY

Table of Contents

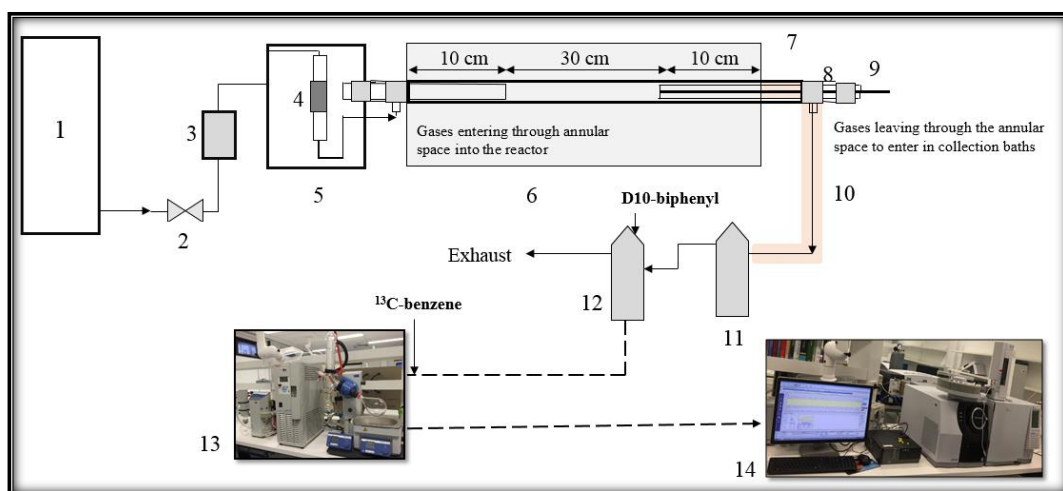
3.1. Experimental methodology	111
3.1.1. Experimental apparatus	111
3.1.1.1. Solid vaporiser	112
3.1.1.2. Tubular reactor.....	112
3.1.1.2.1. Reactor tube coating.....	116
3.1.1.3. Product collection system	117
3.1.2. Chemicals	117
3.1.3. Methods	118
3.1.3.1. Experimental procedure	118
3.1.3.2. Product analysis	119
3.1.3.2.1. Analysis of HBr.....	119
3.1.3.2.2. Analysis of condensable products.....	119
3.2. Computational methodology	126
3.2.1. Ab Initio calculations	126
3.2.2. Hartree-Fock method.....	127
3.2.2. Density functional theory	128
3.2.2.1. The Thomas-Fermi model	128
3.2.2.2. The Hohenberg-Kohn theorem	129
3.2.2.3. Kohn-Sham DFT.....	130
3.2.2.4. The Exchange-Correlation functional.....	131
3.2.3. Computational tools	134
3.2.3.1. Gaussian09.....	134
3.2.3.2. Dmol ³	135
3.2.3.3. Chem rate	135
3.2.3.4. KiSTheLP.....	135

In this thesis, we applied experimental and theoretical approaches to investigate the decomposition behaviour of selected brominated aromatic compounds. This chapter provides a detailed description of the experimental apparatus, procedures, chemicals and analytical techniques applied in this research. Furthermore, we briefly explain our computational methodologies and the theory underpinning the principal calculations.

3.1. Experimental methodology

3.1.1. Experimental apparatus

Gas phase pyrolysis and oxidation experiments involve laboratory-scale bench-type apparatus. The experimental assembly incorporates three main sections: (i) a solid vaporiser, (ii) a horizontal isothermal tubular reactor, and (iii) a product collection setup. Figure 3.1 is a schematic diagram of the experimental setup. The features of each section are described in the following paragraph.



- | | |
|--|--|
| 1. Nitrogen generator | 9. K-type thermocouple |
| 2. Flow regulator | 10. Transfer line with wound heating tape |
| 3. Mass flow controller | 11. Alkaline bath |
| 4. TBBA sample holder | 12. DCM bath cooled by sodium chloride/ice mixture |
| 5. Vaporiser oven | 13. Rotary evaporator |
| 6. 3-zone temperature-controlled furnace | 14. GC-QQQMS |
| 7. Quartz tube reactor | |
| 8. Quartz rod, closed at one end | |

Figure 3.1. Schematic diagram of the experimental setup.

3.1.1.1. Solid vaporiser

Solid fuel is charged in the form of vapour in the reactor to conduct gas phase experiments. For this, we loaded the powdered reactant tetrabromobisphenol A (TBBA) at ambient temperature in a pure quartz vaporiser tube of 10 mm inner diameter (I.D.), as depicted in Figure 3.2.

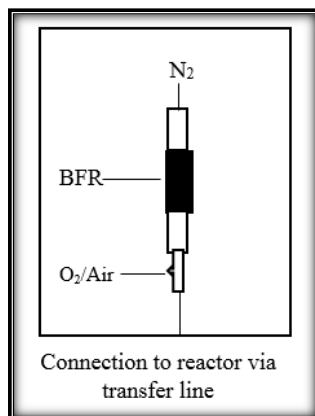


Figure 3.2. Vaporiser assembly.

A high-temperature oven (S.E.M Pty Ltd, 35FD-forced convection oven, digital PID control, with vertical draught) was equipped with a vaporiser tube connected to the inlet and outlet gas flow lines and an accurate temperature controller. Clean glass wool was placed at the inlet and outlet points of the vaporiser tube, for two purposes. Firstly, as a plug to ensure the uniform mixing of the reactant with carrier gases prior to entering the reactor tube. Secondly, to prevent the entrainment of solid, powdered reactant into the reaction system. The oven temperature was programmed to the desired value of 450 K (based on the vapour pressure of the reactant). A stream of nitrogen flowed through the vaporiser at a rate of $705 \text{ cm}^3 \text{ min}^{-1}$, as metered at standard temperature pressure (STP), to entrain TBBA evaporating at 0.06 mg min^{-1} and all preheated mixtures entered the reaction chamber at a known flow rate. The vaporiser outlet was connected to the reactor tube as an input feed line.

3.1.1.2. Tubular reactor

The reaction system comprised an isothermal quartz tubular reactor. Tubular reactors are the most suitable kind for studying the chemistry of combustion/pyrolysis processes [1-6]. In most recent studies, researchers used them to investigate the formation mechanisms of various kind of pollutants. In our experimental measurements, we deployed a high purity (>99.995 %) quartz tube reactor sourced from H. Baumbach & Co Ltd, USA (12.7 mm O.D., 10 mm I.D., 960 mm length, 235 mm³ volume). The quartz reactor tube contained a few transition metals as impurities in ppm (Table 3.1).

Table 3.1. Impurities in the quartz reactor tube (in ppm).

Al ^a	B	Ca	Cu ^b	Fe ^b	Li	K	Mg	Mn ^b	Na	Ni	P	Ti ^{a,b}	Zr ^b	OH
14	<0.2	0.4	<0.05	0.2	0.6	0.6	0.1	<0.05	0.7	<0.1	<0.2	1.1	0.8	<5

a: oxides have a catalytic effect

b: typical transition metals

As illustrated in Figure 3.1 the reactor tube constituted the central part of a tube that was positioned along the centre line of an electrically heated horizontal tubular furnace (Labec HTFS40/300-3, three zones horizontal split tube furnace, 40 mm I.D., 500 mm heated zone length). The temperature of each zone was set independently by accurate temperature controllers (UDAIN 708, accuracy 0.2 %, Australia).

We calibrated the furnace up to 1123 K and checked its isothermal zone (uniform temperature region), by using an external thermocouple inserted and moved horizontally along the centre line of the furnace. Furnace calibration data (temperature range 673 - 1123 K) is given in Table 3.2 and the temperature profile (at 873 K, 923 K, 973 K and 1023 K) is shown in Figure 3.3.

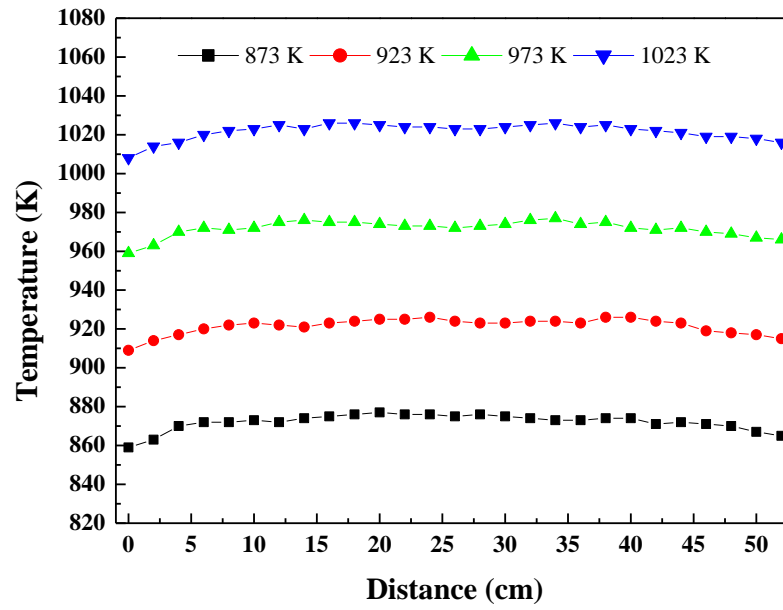


Figure 3.3. Temperature profile of the horizontal tubular furnace.

CHAPTER 3 Research Methodology

Table 3.2. Furnace calibration data.

T (K)	Distance (cm)																										
	0	2	4	6	8	10	12	14	16	18	20	22	24	26	28	30	32	34	36	38	40	42	44	46	48	50	52
623	611	618	621	623	627	626	354	626	597	623	624	623	623	622	621	621	623	624	625	624	623	622	623	623	622	622	618
673	651	662	669	670	668	673	674	676	675	673	674	674	400	400	645	644	672	673	401	402	400	401	672	398	398	397	667
723	704	712	720	721	722	723	725	724	725	724	723	723	723	724	722	723	722	721	724	725	724	723	721	719	718	718	717
773	750	761	770	772	773	773	774	775	776	775	773	774	773	822	773	776	776	775	774	771	770	770	769	769	768	767	766
823	809	813	816	820	822	823	824	825	826	825	826	823	824	823	823	822	822	821	823	824	822	821	822	821	820	818	817
873	859	863	870	872	872	873	872	874	875	876	877	876	876	875	876	875	874	873	873	874	871	872	871	869	868	869	865
923	909	914	917	920	922	923	922	921	923	924	925	925	926	924	923	923	924	924	923	926	926	924	923	919	918	917	915
973	959	963	970	972	971	972	975	976	975	975	974	973	973	972	973	974	976	977	974	975	972	971	972	970	969	967	966
1023	1008	1014	1016	1020	1022	1023	1025	1023	1026	1026	1025	1024	1024	1023	1023	1024	1025	1026	1024	1025	1023	1022	1021	1019	1019	1018	1016
1073	1049	1054	1066	1069	1071	1075	1076	1073	1079	1076	1077	1078	1079	1078	1078	1077	875	1075	1075	1075	1074	1073	1073	1071	1069	1069	1067
1123	1104	1112	1116	1119	1122	1125	1125	1123	1126	1126	1125	1124	1124	1123	1123	1125	1125	1125	1126	1126	1123	1122	1121	1120	1118	1118	1117
1173	1146	1154	1162	1167	1172	1174	1174	1173	1173	1175	1175	1175	1176	1176	1176	1175	1174	1173	1173	1174	1173	1171	1170	1169	1168	1167	1166

Note: isothermal zone at 12 – 40 cm.

Two high purity hollow quartz rods (9.5 mm O.D.), with one end closed, were inserted from opposite ends of the reactor tube to serve three purposes. Firstly, they contained an external thermocouple which provided a point for accurate measurement of reaction zone temperatures. Secondly, they ensured the rapid transport of reactant/product streams through the annular space between the quartz tube and the rods in the isothermal zone. Thirdly, they allowed the execution of experiments at different reaction temperatures; by varying the length of the rods, which alters the reaction chamber volume, the flow rate of carrier gases was kept constant. The tubular reactor flow assembly is shown in Figure 3.4.

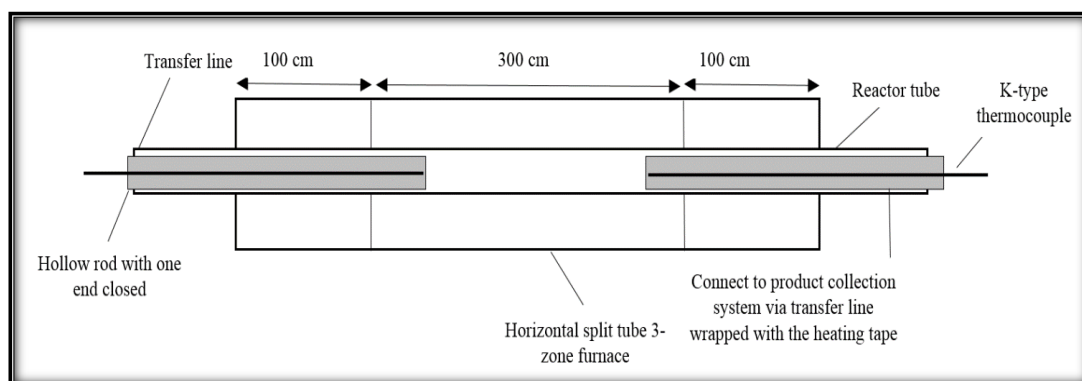


Figure 3.4. Tubular flow reactor assembly.

3.1.1.2.1. Reactor tube coating

Although high purity, the quartz reactor surface could still contain impurities (transition metals) that act as catalysts for the experimental reaction. To minimise this, and to eradicate the conversion of triplet oxygen into singlet oxygen, we applied a B_2O_3 coating to the internal walls of the reactor [7-9]. We prepared a saturated solution of boric acid (99.995 %) in ethanol solvent on a hot plate at <323 K. The inner walls of the reactor tube were carefully rinsed with a saturated solution of boric acid in ethanol and positioned in the reactor that had been preheated to 473 K. After initial heating at 473 K for at least one hour, the temperature was then increased at $2 - 4$ K min^{-1} up to 773 K. Once baked at 773 K for at least 3 h, the boric acid converted into a thin film of boron trioxide (B_2O_3) that appeared as a uniform transparent layer.

Prior to experiments, the reactor tube was purged with a stream of nitrogen in order to prevent the reactor tube's inner wall from coming into contact with moisture, which could decrease the lifespan of the B_2O_3 layer. After experiments, if we observed the B_2O_3 coating falling off the reactor tube wall in the form of white lumps, we considered the reactor tube to require cleaning and recoating.

3.1.1.3. Product collection system

The exit line of the reactor tube was coupled to a product collection system. The experiments were designed to collect HBr, volatile organic compounds (VOCs), semi-volatile organic compounds (SVOCs) and non-condensable gaseous products. The product sampling time was set to 5 h, with a residence time of 2 s. All connection lines were made of PTFE material (Plasma Tech, USA) which can withstand elevated temperatures and is considered chemically inert.

The exhaust gases from the reactor tube were passed through a sampling train that combined an alkaline trap filled with a solution of NaOH, then another solvent trap cooled by a sodium chloride/ice bath, to capture HBr and all VOCs/SVOCs, respectively. The line connecting the product collection train to the reactor tube was wrapped with heating tape (HTC-030), which kept the transfer line temperature at 453 K to avoid product condensation and possible secondary reactions.

3.1.2. Chemicals

This research investigated the thermal decomposition of tetrabromobisphenol A (97 %), a white, solid powder purchased from Sigma Aldrich (Australia). All solvents for trace analysis were supplied from Chem Supply and Merck Millipore (Australia). We acquired pure nitrogen (99.998 %) from a nitrogen generator installed at our laboratory (Peak Scientific, Australia) with an outlet pressure of 80 psi. This was used as a reaction carrier gas. Helium was sourced from BOC Australia at a purity of 99.999 %, and was used as a carrier gas in a gas chromatogram triple quadrupole mass spectrometer (GC-QQQMS). We purchased high purity internal standards (added to solvent bath prior to product collection to estimate % of product recovery) and surrogate standards (introduced prior

to sample preparation for analysis), including D10 biphenyl and ^{13}C -benzene, from Novachem and Sigma Aldrich, respectively. We also bought pure chemical standards to prepare calibration solutions, including phenol, 4-bromophenol (100 $\mu\text{l ml}^{-1}$ of toluene), 2-bromophenol, 2,4-dibromophenol (neat), 2,6-dibromophenol, 2,4,6-tribromophenol (6.0 mg ml^{-1} of methanol), benzene, 1-bromobenzene, 1,2-/1,4-/1,3-dibromobenzene, 1,3,5-tribromobenzene, naphthalene, 2-bromonaphthalene, acenaphthylene, benzofuran, dibenzofuran, 2,6-dibromo-4-methylphenol, 2,6-dibromo-4-tertbutylphenol, 3,5-dibromo-4-hydroxybenzaldehyde, 2,2',5-tribromobiphenyl, 1-bromo-3-ethylbenzene, 3-bromostyrene, biphenylene and bisphenol A from Novachem (distributor for Cambridge Isotope Laboratories, LGC, AccuStandard and Cerilliant).

3.1.3. Methods

3.1.3.1. Experimental procedure

Each experiment commenced by loading a reactant (TBBA powder) into a quartz tube vaporiser and filling the NaOH and solvent traps. The oven, reactor and transfer lines were preheated to the selected temperature prior to turning on the mass flow controllers for the carrier gas supply. Once the temperatures were stabilised for the entire experimental setup (oven, reactor and transfer line), the nitrogen and oxygen supplies were turned on, as per the values given in Table 3.S1 in Appendix A. Subsequently, a mixture of reactant vapours and carrier gases was passed through the reactor and sustained for a residence time of 2 s (for decomposition to occur). The mixture then exited via a product collection unit where the combustion products were sampled from the exhaust gases. HBr was encapsulated in a NaOH solution (alkaline trap), while VOCs and SVOCs were trapped in the solvent bath cooled by sodium chloride and ice (the condenser).

At the conclusion of the experiment, the cold bath and NaOH trap were disconnected and subjected to a sample preparation process. The reactor tube setup was disassembled and rinsed with dichloromethane (DCM) to collect products condensed on the surface of the reactor tube and PTFE transfer lines. The solution from the experimental setup washes undergoes pre-treatment and analysed by GC-QQQMS. Finally, all glassware and transfer lines were washed thoroughly using detergent and acetone, then dried at 333 K in a pre-

heated oven. After each experiment, we flushed our setup with a nitrogen stream overnight and ran blank experiments very frequently to monitor the NaOH and solvent traps.

3.1.3.2. Product analysis

Non-condensable gases were identified using FTIR. VOCs and SVOCs were identified and quantified by GC-QQQMS. HBr contents were estimated by standard potentiometric titration.

3.1.3.2.1. Analysis of HBr

The HBr that evolved from the thermal decomposition of TBBA was trapped in 75 mL of a 0.1 N solution of sodium hydroxide (NaOH) in a 6 h experimental run. For HBr analysis, we prepared a 0.1 N HCl solution and titrated it against a NaOH solution. During titration, we monitored the pH of the solution constantly and estimated the weight % of HBr.

3.1.3.2.2. Analysis of condensable products

Before the experiment, we introduced biphenyl-D10 to the DCM trap as a pre-sampling (or surrogate) standard for calculating the percentage recovery of VOCs and SVOCs. On the basis of biphenyl-D10, we estimated the correction factor needed for quantitation of product species that absorb partially on the product collection system. At the end of the experiment, we transferred the DCM trap condensate very carefully into the pot/rotary bottle of a rotary evaporator. Here, we added benzene-13C to calculate the percentage recovery of light VOCs that might evaporate with the solvent from the rotary evaporator.

In a rotary evaporator, we concentrated the condensate to a small volume of about 1 mL. Since the boiling point of the products was higher than that of the solvent (DCM), we vaporised the solvent and concentrated the trace products for basic analysis. We kept the rotary evaporator at 306 K with 740 kPa of pressure to concentrate the DCM solvent. Then, 1 μ L of the concentrated sample was injected into GC-QQQMS for analysis.

The GC-QQQMS was equipped with two different columns; (i) Rxi-5Sil: (0.25 mm I.D., 0.25 μm film thickness, 30 m length), and (ii) Rxi-5Sil MS, equivalent to DB5-MS: (0.25 mm I.D., 0.25 μm film thickness, 15 m column length). It has been reported that brominated compounds may degrade when passing through a long GC column. Therefore, we used a shorter column (Rxi-5Sil MS, 15 m length) for the detection and quantitation of the brominated organic compounds. For the quantitation and identification of benzene- ^{13}C , we employing a (Rxi-5Sil, 30 m) column in order to measure the peak area of benzene- ^{13}C that may overlap with the DCM peak in shorter column.

Shimadzu GC-QQQMS is an advanced instrument that combines a gas chromatograph (GC) unit for the separation of components (GC-2010 plus) with a triple quadrupole mass analyser (QQQMS) for quantitation of components masses (QQQMS-TQ8040 series, Shimadzu Japan). The GC unit includes a temperature-controlled capillary column for separating a mixture into its individual components. The GC column includes a mobile (inert and unreactive helium or nitrogen) and a stationary phase (microscopic layer of liquid or polymer). The mixture is introduced by an injector at approximately 473 – 573 K, evaporates immediately, travels through the column by the carrier gas, and interacts with the stationary phase of the column. Components with small molecular weights (most volatile) travel faster and elute before then, the components with high molecular weights (high boiling points). The time at which component peak elute is called the retention time. The retention time at which each component elutes depends on the type of column, its dimensions, and the temperature program applied. Column degradation, and the presence of any contaminants in the column, also affect retention time. At the end of the GC column, the components travel to MS via a transfer line, as depicted in the schematic diagram of the GCMS.

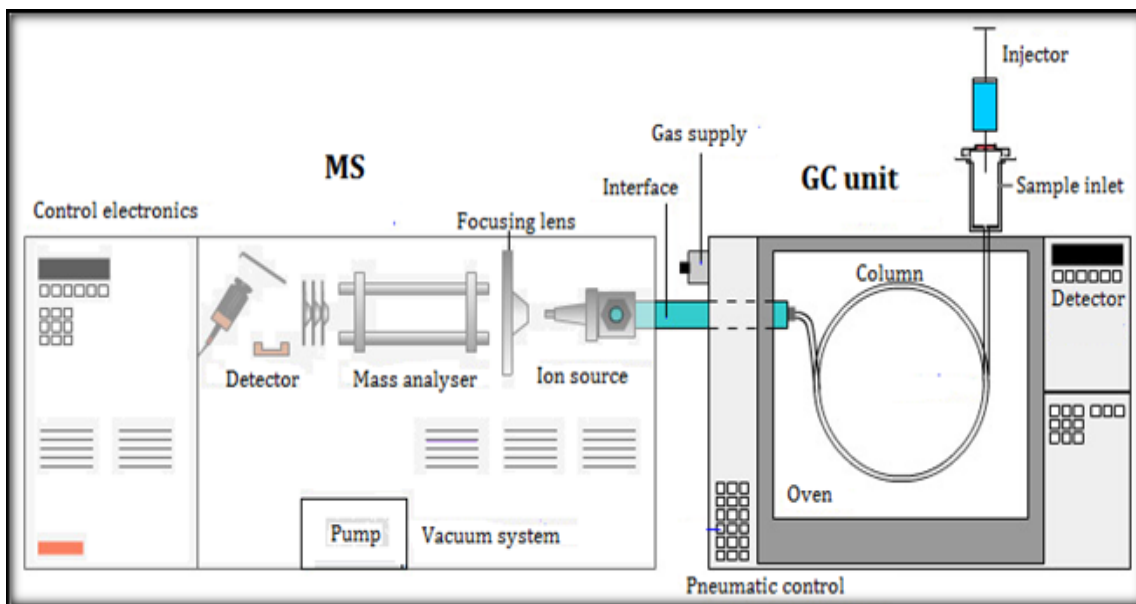


Figure 3.5. Schematic of GCMS system.

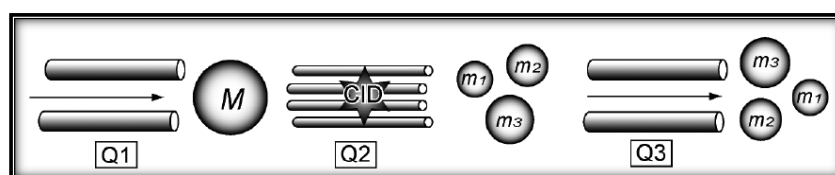
The mass analyser (MS) scans the mass spectra of each component based on the measurements of mass to charge ratio (m/z). The MS captures, ionises, accelerates, deflects and detects the ionised molecules to identify their fragments using m/z ratios. The MS has five main components: the (i) ion source, (ii) focusing lens, (iii) mass analyser (quadruple mass filters), (iv) vacuum system, and (v) a detector (Figure 3.5). The species get ionised when entering the MS, the lens then forces the ions into the mass filter which effectively filters the ions onto the detector, which generates a signal proportional to the number of ions collected. The detector sends this mass spectral information to a computer for processing. During the detection process, a good vacuum is necessary for the MS chamber to maintain a free run path for the ions (i.e. without hitting air molecules).

In QQQMS, the mass analyser incorporates two types of mass filters (such as Q1 and Q3) and a collision cell (Q2). By changing the setting of the quadruple mass filters, we can obtain different mass spectra, as given in Table 3.3. In Q3 scan and selected ion monitoring (SIM) mode, the sample ions are transmitted by Q1 and Q2 quadruples, while the Q3 quadruple performs the scan and SIM function. In our analytical measurements, we deployed Q3 scans, product ion scans, SIM and multiple reaction monitoring (MRM) modes (Table 3).

Table 3.3. Analysis mode and quadruple mass filters.

Analysis mode	Q1	Q2 (Collision cell)	Q3
Q3 scan	Transmission mode (ion transmission)	Transmission mode (ion transmission)	Scan
Q3 SIM	Transmission mode (ion transmission)	Transmission mode (ion transmission)	SIM
Product ion scan	SIM	Collision induced dissociation (CID)	Scan
MRM	SIM	Collision induced dissociation (CID)	SIM

In product ion scan mode, Q1 was fixed to a specific m/z value (m), the collision induced dissociation (CID) cell produced m_1 , m_2 and m_3 ions that were measured by the Q3 quadruple (Figure 3.6). The product ion scan was used favourably for investigating the structures of precursor ions selected with Q1, and to search for optimal MRM measurement conditions (transition and collision energies).

**Figure 3.6.** Product ion scan.

For MRM analysis, the m/z value was fixed for both Q1 and Q3 quadruples and transitions were measured. The Q1 quadruple selected the precursor ion, while the CID cell produced daughter ions that was selected with the Q3 quadruple (Figure 3.7).

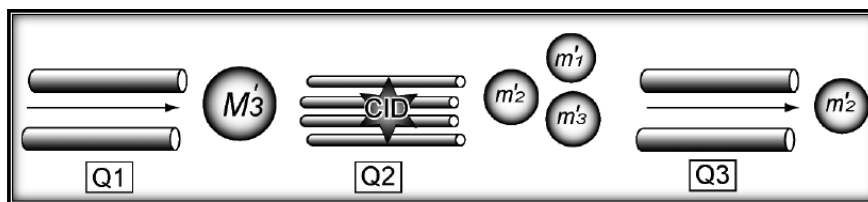


Figure 3.7. MRM scan mode.

In GC-QQQMS, we used helium as a carrier gas maintained at a constant column flow of 1.5 ml min^{-1} . The GC oven temperature program commenced at 303 K for 3 min, then the temperature was raised at 8 K min^{-1} to 373 K. After 2 min at this temperature, it was increased at 4 K min^{-1} to 553 K. We kept the temperature of injectors, ion sources and transfer lines at 523 K, 473 K and 373 K, respectively. The ionisation electron impact voltages were set at 70 eV. We identified eluted species by comparing their mass spectra with information from the NIST library. Most were validated by the injection of genuine standards.

For major brominated and non-brominated species, we developed an MRM method that eliminates the effect of noise (signal/noise ratio (S/N) = infinity) and identifies trace fractions of VOCs and SVOCs. MRM is one of the more powerful analytical tools available for the detection of target compounds in complex mixtures, even at trace levels. For quantification of VOCs and SVOCs, we used an MRM method based on the standard steps given in the flow diagram in Figure 3.8.

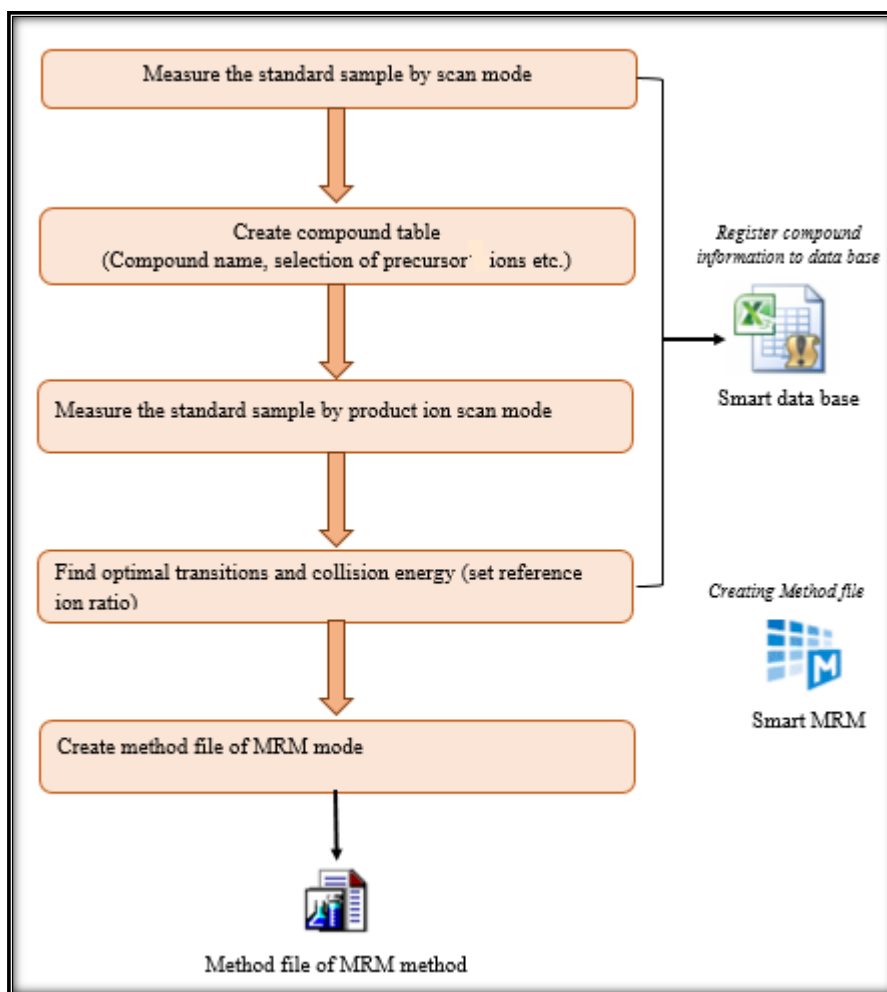


Figure 3.8. Steps for the creation of an MRM method.

The steps included: (i) identification of each compound's spectral peak based on genuine standard mass spectra, (ii) perform peak integration for all selected peaks having $S/N > 6$, (iii) set up qualitative table and create compound table (select two reference ions for each compound), (iv) create MS table using COAST option with the selection of product ion scan, and save the method, (v) use MRM optimisation tool to create a method batch with the selection of collision energy (CE) in the range of 3-54 V (with 3 V interval), (vi) analyse the sample for each value of CE, (vii) use MRM optimisation tool to select the best CE for each precursor ion of the selected species, and (viii) register MRM optimisation results with the smart database and create MRM method file.

Details of the MRM method for selected compounds are given in Table 3.4. To quantitate the major brominated and non-brominated compounds, we injected genuine standards and

CHAPTER 3 Research Methodology

prepared external calibration curves. The peak area for each compound was integrated from the chromatogram in MRM mode.

Table 3.4. MRM method details for the selected VOCs and SVOCs.

Compound Name	Start time (min)	End time (min)	Ch1 m/z	Ch1 CE	Ch2 m/z	Ch2 CE
phenol	6.79	9.04	94>66.1	9.0	94>55	18.0
1,3-dibromobenzene	9.04	12.31	236>155	21.0	236>157	21.0
1,2-dibromobenzene	9.04	12.31	234>154.9	21.0	236>155	18.0
4-bromophenol	12.31	13.85	172>65.1	24.0	174>65	24.0
2,4-dibromophenol	13.85	14.97	252>63.1	30.0	252>142.9	33.0
2,6-dibromophenol	14.97	16.03	252>63.1	27.0	252>143.1	24.0
1,3,5-tribromobenzene	16.03	19.65	314>234.8	27.0	316>234.8	24.0
2,4,6-tribromophenol	19.65	22.95	330>140.9	27.0	332>142.9	36.0
benzofuran	6.93	12.36	118>89.1	21.0	89.00>63.00	21.0
acenaphthylene	12.36	17.86	152>126	24.0	152.00>150.00	30.0
bromonaphthalene	17.86	18.84	208>127.1	21.0	206.00>127.10	21.0
dibenzofuran	18.84	21.60	168>139	24.0	139.00>89.10	21.0
3,5-dibromo-4-hydroxybenzaldehyde	21.60	28.37	355>73.2	12.0	355.00>266.80	18.0
2,2',5-tribromobiphenyl	28.37	34.28	230>151.1	18.0	311.00>231.90	18.0
bromobenzene	5.50	7.28	156>77.1	21.0	77>51	18.0
2-bromophenol	7.28	9.89	172>65.1	21.0	174>65	21.0
naphthalene	9.89	14.90	128>102	21.0	128>78	24.0

CHAPTER 3 Research Methodology

1,4-dibromobenzene	9.89	14.90	236>157	27.0	236>154	27.0
2,6-dibromo-4-methylphenol	14.90	21.45	185>77.1	15.0	187>77	18.0
2,6-dibromo-4-tertbutylphenol	21.45	30.16	295>214	15.0	293>219	12.0
bisphenol A	30.16	40.0	213>119	9.0	119>91.1	9.0

3.2. Computational methodology

In the current section, we outline the theoretical tools employed to investigate thermodynamic and kinetic properties and the mechanistic pathways of VOC and SVOC formation. Furthermore, we briefly illustrate the theories involved in the development of our computational tools. Estimates of molecular properties based on theoretical tools provide a close correlation between theoretical and experimental results.

3.2.1. Ab initio calculations

Ab initio quantum chemistry is an essential tool for describing the atomic and molecular properties of compounds, including complex systems. It is based solely on established laws of quantum mechanics. The theoretical foundations of ab initio method is the computational solution of an electronic, time-independent Schrödinger equation that describe the behaviour of electrons in the molecular system. This equation computes the stationary states of a quantum system such as atoms, molecules and electrons. The fundamental Schrödinger equation is written as:

$$\hat{H}\Psi = E\Psi \quad (1)$$

Where \hat{H} is the Hamiltonian operator, E is the total energy of the particle, and Ψ is the wave function. The wave function, Ψ , depends on the position of a molecular system's particle, and postulates the probabilistic details of an electron's behaviour. The wave

function should be continuous, normalised, single-valued and antisymmetric regarding the interchange of electrons [10-11].

The \hat{H} Hamiltonian operator is written as:

$$\hat{H} = -\sum_i^{particles} \left(\frac{\nabla^2}{2m_i} \right) + \sum_{i<j}^{particles} \sum \frac{q_i q_j}{r_{ij}} \quad (2)$$

Where m_i is the mass of particle i , q_i and q_j are the charges on particles (that include both electrons and nuclei) i and j , respectively, and r_{ij} is the distance between particles i and j .

The symbol ∇_i^2 denotes the Laplacian operator working on particle i , and is expressed as:

$$\nabla_i^2 = \frac{\partial^2}{\partial x_i^2} + \frac{\partial^2}{\partial y_i^2} + \frac{\partial^2}{\partial z_i^2} \quad (3)$$

3.2.2. Hartree-Fock method

The Hartree-Fock (HF) method is the fundamental of electronic structure theory. It constitutes the basis of the molecular orbital theory that relies on central field approximation [12-13]. The HF method affords the simplest method for the solution of an electronic Schrödinger equation. It incorporates the Coulombic repulsion term to account for the electron-electron repulsion [14]. It assumes that each electron experiences the presence of another electron explicitly through effective potential. The HF theory is based on the basic idea that the total electronic wave function expresses the motion of all electrons by taking the product of molecular or atomic wave function (i.e. orbitals), known as the Hartree product, and is depicted by an equation:

$$\Psi_{HP} (r_1, r_2, r_3, \dots, r_N) = \varphi_1(r_1) \varphi_2(r_2) \varphi_3(r_3) \dots \varphi_N \quad (4)$$

Where, φ is the notation of orbital number.

The above equation encounters one major drawback, i.e., it fails to satisfy the antisymmetric principle. That demands the wave function to be antisymmetric with regard

to an interchange of electron position. Therefore, later, equation 4 has been modified to accommodate the spin-orbital instead of orbital form and stated as:

$$\Psi_{\text{HP}}(r_1, r_2, r_3, \dots, r_N) = \chi_1(r_1) \chi_2(r_2) \chi_3(r_3) \dots \chi_N \quad (5)$$

Where, χ is the spin-orbital in equation 5. The spin orbital is modified in the form of wave function equation 6:

$$\Psi_{\text{HP}}(r_1, r_2, r_3, \dots, r_N) = -\Psi_1(r_2, r_2, r_3 \dots r_n) \quad (6)$$

Hence, the HF method describes the behaviour of an electron in the presence of a net field of all other electrons, based on each electron orbital and their wave function.

3.2.3. Density functional theory

Ab initio and HF methods share one common feature. Both compute the electronic properties of atoms and molecules based on the electronic wave function. When the wave function is known, other properties, including system energy, can be determined. However, the electronic wave function is not a simple measurable quantity. It relies on $3N$ spatial and one spin variable. N assumes the total number of electrons in the system. Therefore, this feature limits the use of HF and *ab initio* methods [15].

Density functional theory (DFT) [16] is a quantum chemical method that is based on a measurable quantity. DFT deploys “electron density” instead of the wave function to predict the properties of simple as well as complicated, larger systems. Owing to this characteristic, DFT has become one of the most frequently used computational methodologies today. The electron density is readily accessible via the experimental techniques such as electron diffraction or X-ray diffraction [17]. Electron density depends on three spatial coordinates (x, y, z), unlike *ab initio* and HF methods. Therefore, it demands much less computational time for the calculations. The theoretical background of DFT is based on the following theorems.

3.2.3.1. The Thomas-Fermi model

The background of DFT depends on the Thomas-Fermi (TF) model (1927) [18], which postulated the idea of “electron gas”, in which all molecular properties are expressed in terms of a measurable value of electron density (i.e. the number of electrons per unit volume). It constitutes the basis of modern DFT. The well-known TF kinetic energy functional equation is expressed as a function of local electron density.

$$T_{HF}[\rho] = C_F \int e^{\frac{5}{3}}(r) d^3r \quad (7)$$

Where, ρ is a 3-dimensional electron density, T_{HF} is the kinetic energy functional, and C_F is equal to the value of $3/10(3\pi^2)^{2/3}$. The TF model provides good predictions for the atoms. Unfortunately, it fails to describe the electronic features of complex systems or the systems involve chemical interactions. This is due to the fact that it does not incorporate the actual orbital structure of electrons.

3.2.3.2. The Hohenberg-Kohn theorem

Hohenberg-Kohn (HK) [19-20] introduces two theorems that constitute the basis of DFT as a practical computational approach. The first Hohenberg theorem (proposed in 1964) established the concept of electron density in a ground state that is measured by the electronic wave function. It measures the ground state electronic properties of molecules. Kohn theory states that electron distribution energy is generally expressed as a function of electronic density. The first theorem offers a drawback stated two different systems cannot have the same ground state density. The gap is filled by the Hohenberg – Kohn’s second theorem (1999), postulate that a true ground state charge density always minimises the value of total energy and originate as a true electron density. The HK energy is expressed in terms of the kinetic energy function (equation 8) of non-interacting particles, with U representing the electrostatic energy of Coulomb interactions. The most important parameter of the energy equation 8 is E_{xc} , the exchange and correlation energy functional that incorporates all system body interactions to the total energy.

The HK total energy equation is expressed as:

$$E[\rho] = T[\rho] + U[\rho] + E_{xc}[\rho] \quad (8)$$

Walter Kohn, a leading person in the development of DFT was awarded the Nobel Prize in Chemistry in 1998. He proposed the set of equations to compute quantum mechanical electronic structure that involve the electronic density (rather than the many-body wave function). Sadly, he passed away in the age of 93 on April 19, 2016.

3.2.3.3. Kohn-sham DFT

To accurately describe the properties of many particles interacting system, the Kohn-Sham theorem is used. Modern density functional theory (DFT)-based on molecular models, result from the Kohn-Sham theorem. It interprets the interacting system by means of an effective non-interacting particle system. The effective potential of non-interacting particle systems is completely estimated by means of the electron density of the interacting system (called as density functional).

The ideal energy (E) is determined as the sum of (i) electronic kinetic energy (E^T), (ii) potential energy of electron-nuclear attraction and nuclear-nuclear repulsion (E^V), (iii) exchange-correlation energy (E^{XC}), and (iv) electron-electron repulsion energy (E^J) along with the electron density Coulomb self-interaction. It is expressed as equation 9.

$$E = E^T + E^V + E^J + E^{CX} \quad (9)$$

The theorem reformulation is based on the single-particle orbitals that accurately support the development of initial approximation to electron density. All functional parameters in Equation 9, except E^V , are the functions of electron density.

The E^J and E^{XC} functionals are stated as:

$$E^J(\rho) = 1/2 \iint \frac{(\rho(r_1)\rho(r_2))}{r_{12}} dr_1 dr_2 \quad (10)$$

$$E^{XC}(\rho) = \int \varepsilon_{XC}^{KS}(r)\rho(r)dr \quad (11)$$

Where E^{XC} is the exchange-correlation energy functional. The KS differential equation is stated as:

$$\left(-\frac{1}{2}\nabla^2 + v_{ext}(r) + v_H(r) + v_{xc}(r)\right)\phi_i(r) = \epsilon_i\phi_i(r) \quad (12)$$

Where ϵ_i is the orbital energy of the corresponding KS orbital, ϕ_i , and r illustrates the position of ϕ_i , and v_{xc} is the exchange-correlation potential and expressed as:

$$v_{xc}(r) = \frac{\delta E^{XC}[\rho(r)]}{\delta[\rho(r)]} \quad (13)$$

It is the only unknown parameter in the KS-DFT method.

3.2.3.4. The exchange-correlation functional

In practice, to solve KS-DFT problems, the exchange-correlation functional must be known. Therefore, to acquire good values of exchange-correlation functionals, a number of approximations have been developed. The value E^{XC} is computed based on the values of electron spin densities and their gradients, as follows:

$$E^{XC} = \int f(\rho_\alpha(\vec{r}), \rho_{\beta\gamma}(\vec{r}), \nabla\rho_\alpha(\vec{r}), \nabla\rho_\beta(\vec{r}))d^3\vec{r} \quad (14)$$

The local functionals are based on the value of electron density (ρ), whereas gradient-corrected functionals depend on its gradient, $\nabla\rho(r)$. Perdew et al. [21] characterised the exchange functionals according to their level of complexity as rungs of a ‘‘Jacob’s ladder’’. The first rung is the local density approximation (LDA) method [22]. According to the LDA approach, the real inhomogeneous density is distributed into numerous small fragments, and electron density for each fragment is assumed to be constant. The LDA approach was effective, particularly for the slowly-changing density systems such as metals. Conversely, it predicts the higher values of cohesive energies for lattice constants of metals and insulators if compared with experimental values [23-25].

The LDA approach incorporates a shortcoming, for the molecules and materials that are expected to experience a rapid change in electron density. Since these systems entail the gradient of electron density $\nabla\rho(r)$. To overcome this shortcoming, another approach was developed, called generalised gradient approximation (GGA), also known as “semi-local” functionals. GGA functionals include both electron density and its gradient. Computations with GGA functionals provide more accurate estimates of the geometries and ground state energies of molecules and solids in comparison to LDA approximations [26]. The GGA approach works better for the systems with covalent and weak bonds. The most employed GGA functionals are the Becke-88 exchange functional (B88) [27], the Lee-Yang-Parr (LYP) [28], and Perdew-Wang exchange functional (PW91) [29].

One of the famous GGA functionals is meta-GGA, which uses the kinetic energy density or the Laplacian of the density for computations, and is dependent on orbitals [30-31]. Popular GGA functionals are M06-L [32], M11-L and TPSSLYP1W. The meta-hybrid GGA functionals include M06 [33] and M06-2X [33], used particularly for the applications such as kinetics, thermochemistry, electronic excitation energies and non-covalent interactions. The M06-2X functional affords the best performance for hydrogen-transfer barrier height computations. In the current DFT calculations, M06-2X is one of the highly recommended exchange-correlation functional for most of the computations [34-36].

3.2.3.5. Time dependent density functional theory (TDDFT)

Conventional DFT cannot be used to handle time-dependent and excited state problems. To overcome this shortcoming, another theory has been developed, called time-dependent density functional theory (TDDFT). The TDDFT approach handles electronic excited states and time-dependent phenomena very well. The Runge-Gross theorem [40] constitutes the mathematical foundation of the TDDFT approach and is a time-dependent generalisation of the Hohenberg-Kohn theorem [41] and the Kohn-Sham approach [42]. For any system with Hamiltonian can be written in the form:

$$H = T + W + V_{ext} \quad (15)$$

Where, T is kinetic energy operator, W is electron-electron interaction and V_{ext} is the external potential. In 1994, Casida et al., [43] elaborated an effective linear response (LR) formalism (-called random-phase approximation or Casida's equations) to determine the solution of TDDFT rapidly and efficiently. The implementation of TDDFT approach requires the selection of exchange-correlation functionals which focus on the approximation of the system. For the case of time-dependent systems, the Kohn-Sham electrons [41] follow the time-dependent Schrödinger equation:

$$i \frac{\partial}{\partial t} \phi_i(\mathbf{r}, t) = \left[-\frac{\nabla^2}{2} + v_{KS}(\mathbf{r}, t) \right] \phi_i(\mathbf{r}, t) \quad (16)$$

Where v_{KS} is the exchange-correlation potential. For the practical DFT calculations, a number of approximations have been developed. Therefore, in TDDFT, the most common approximation is the adiabatic approximation and is written as:

$$v_{KS}^{adia}[n](\mathbf{r}, t) = v_{KS}^{GS}[n_o](\mathbf{r})|_{n_o(\mathbf{r})=n(\mathbf{r},t)} \quad (17)$$

Here, the exchange potential at any time relies on the density parameters as a function of time. Adiabatic approximations provide the accurate results within TDDFT frame. Any ground state approximations (LDA and GGA) afford an adiabatic approximation (i.e., ALDA) in TDDFT. The applications of TDDFT enables it to compute vertical transition energies, excited state structures, emission wavelengths, measure the vibrationally resolved optical spectra, atomic charges, dipole moments and photochemical reactions.

In this thesis, we used DFT computations at *meta*-hybrid GGA (M06-2X) level to model reaction pathways. The M062X hybrid *meta* exchange correlation functional was designed to predict accurate thermochemical and kinetic parameters for general applications in organic reactions. However, the computations for the excited states involved the TDDFT method with adiabatic local exchange density functional approximation (ALDA) with the geometry optimisation performed using Dmol3 code at GGA-PW91 functional. The ALDA approximation can also be applied for many finite systems. GGA functional calculations reduce the absolute errors to about 3-5 kcal mol⁻¹.

3.2.4. Computational tools

3.2.4.1. Gaussian09

Gaussian09 [37] is the latest computational chemistry software used to optimise the molecular geometries and predict the energies, vibrational frequencies and molecular properties of various reactions by employing a number of DFT methods, as explained in Section 3.2.2. This software can be applied to both simple and complex stable species, as well as to the short-lived species appearing in the experimental measurements (i.e. intermediates and transition structures) in both gaseous and aqueous media. The difference in thermodynamic parameters for reactants, products and transition states are used to predict the thermodynamics and kinetics of the chemical reactions.

Gaussian09 efficiently investigates the reaction pathways by locating transition structures and verifying their minima of stationary points. The transition structure is a state along the reaction coordinate between a reactant and product, also called the intermediate adduct (transient species). During the course of a chemical reaction, the reactant is converted into product and corresponds a highest potential energy point along the reaction coordinates with regard to reactant and product. We located the transition structures for most of the pathway described in the thesis. One of the important features for Gaussian09 is the intrinsic reaction coordinates (IRC) [38] that helps to connect the reactants and products with their corresponding transition state. The IRC approach is based on the classical equation of motion that determines both the energy and geometry of the reaction system. The IRC calculations provide a unique path along the potential energy surface of the reacting system, from a transition state to the local minima value, with respect to the reactant and product. It not only measures the full reaction path but also depicts the reaction barrier along with the thermodynamic properties such as reaction dynamics and rate [39]. The barrier term in the thesis is defined as zero-point corrected electronic energy either at 0 K or 298.15 K.

Gaussian 09 is also used for the estimation of excited states of molecules in gaseous and aqueous media based on time-dependent density functional theory (TD-DFT).

3.2.4.2. Dmol³

Dmol³ is an accurate and reliable quantum mechanical software used in thermochemistry to compute the electronic properties of molecules and materials [44-46]. This method is applied to the molecules in the gas, liquid and solid states [47]. Dmol³ incorporates solvent effects by implementing the conductor-like screening model (COSMO) into a DFT program. To model the systems that encompass solvent effects, the solute is placed inside a cavity. The solvent is positioned outside the cavity in the form of a homogeneous dielectric medium. The solvent-induced surface charge on the solute surface is modelled in the form of electrostatic interactions. Dmol³ software computes the excited states of the molecules using TDDFT methods. It searches the transition states for reaction pathways using LST/QST/conjugate gradient approach. Dmol³ utilises the local (PWA, VWN) and GGA (PW91, BLYP, etc.) density theory functionals and Harris functional for the fast computations with a basic set of DN, DND, and DNP. Dmol³ serves to calculate the bond order, bond structure, electron work functions, Fukui indices, electrostatic moments, thermodynamic properties, charge analyses (Hirshfeld, Mulliken and EPS), UV-Vis spectra, excited states, polarizability and hyperpolarizability.

3.2.4.3. ChemRate

The ChemRate program [49] was developed to estimate Arrhenius parameters and reaction rates based on a database of unimolecular reactions and experimental results pertaining to molecular structures and transition states. It was also employed for the computation of molecular thermodynamic properties. In ChemRate, the master equation solver is based on Rice–Ramsperger–Kassel–Marcus theory (RRKM) [50-51] and also considers transition state theory (TST) [52] to compute the rate constants and thermal functions of energy transfer media and chemical activation processes in steady and non-steady conditions. It also helps in computing the temperature-dependent thermodynamic properties of chemical species and reactions.

3.2.4.4. KiSThelP

KiSThelP [53] is a kinetic and statistical thermodynamic package developed to estimate molecular and reaction properties based on the electronic structure data. It requires an input file in the form of electronic structure data from the output of three chemistry software packages (Gaussian, GAMESS and NWChem). KiSThelP performs statistical mechanics calculations using ab initio quantum chemistry data (described in Section 3.2.1) resulting in the computation of molecular thermodynamic properties, thermal equilibria and reaction rate constants [54-55]. It requires the mass, potential energy, electronic degeneracy, rotational symmetry number, vibrational frequencies and inertial moment data to accurately estimate reaction rate parameters.

KiSThelP software operates independently owing to its programming language, Java, which runs on many different operating systems. It uses TST, variational transition state theory (VTST) [54] and RRKM calculations to predict the reaction rate coefficients for gas phase elementary reactions. To improve the results, the program combines the features of vibrations and one-dimensional tunnelling treatment through Wigner correction or the Eckart potential energy barrier [56]. The first step of KiSThelP computation is the calculation of the partition function in the form of $Q_x(V,T)$. The electronic, translational and vibrational contributions are estimated based on the equation given in Table 3.5 [53].

Table 3.5. Partition functions contributing to the computation of thermodynamic and kinetic data.

Rotation					
	Translation	Vibration	Linear	Nonlinear	Electronic
$Q^{[a]}$	$Q_{\text{trans}} = \left(\frac{2\pi mk_b T}{h^2}\right)^{3/2} \frac{RT}{P}$	$Q_{\text{vib}}^{v=0} = \prod \frac{1}{1 - e^{-\theta_i/T}}$ $\theta_i = hv_i/k_b$	$Q_{\text{rot}} = \frac{T}{\sigma_r \theta_r}$ $\theta_r = \frac{h^2}{8\pi^2 I K_b}$	$Q_{\text{rot}} = \frac{\pi^{1/2}}{\sigma_r} \left(\frac{r^3}{\theta_a \theta_b \theta_c}\right)^{1/2}$	$Q_{\text{elec}} = g_{\text{elec}}^{\text{ground}}$
$U^{[b]}$	$U_{\text{trans}} = \frac{3}{2} RT$	$U_{\text{vib}}^{v=0} = R \sum_i \frac{\theta_i}{e^{\theta_i/T} - 1}$	$U_{\text{rot}} = RT$	$U_{\text{rot}} = \frac{3}{2} RT$	$U_{\text{elec}} = 0$
$S^{[c]}$	$S_{\text{trans}} = R \left(\ln Q_{\text{trans}} + \frac{5}{2}\right)$	$S_{\text{vib}} = R \ln Q_{\text{vib}}^{v=0} + \frac{U_{\text{vib}}^{v=0}}{T}$	$S_{\text{rot}} = R \ln Q_{\text{rot}} + \frac{U_{\text{rot}}}{T}$		$S_{\text{elec}} = R \ln g_{\text{elec}}^{\text{ground}}$
$C_v^{[d]}$	$C_{v,\text{trans}} = \frac{3}{2} R$	$C_{v,\text{vib}} = R \sum_i \frac{(\theta_i/T)^2 e^{\theta_i/T}}{(e^{\theta_i/T} - 1)^2}$	$C_{v,\text{rot}} = R$	$C_{v,\text{rot}} = \frac{3}{2} R$	$C_{v,\text{elec}} = 0$

Whereas, the total partition function of a molecule in a ground state is calculated as:

$$Q_{tot} = Q_{trans} \times Q_{vib} \times Q_{rot} \times Q_{elec} \quad (18)$$

All the relationships mentioned in Table 3.5 contribute considerably in predicting the thermodynamic properties of compounds.

References

- [1] Gomez, J., Bruneau, C., Soyer, N., Brault, A. Identification of thermal degradation products from diuron and iprodione. *J. Agric. Food Chem.* **1982**, 30, 180-182.
- [2] Rao, R.N., Khalid, S., Rajani, T., Husain, S. Gas chromatographic–mass spectrometric separation and identification of combustion products of organo-phosphorus and chlorine pesticides and evaluation of their impact on the environment. *J. Chromatogr. A.* **2002**, 954, 227-234.
- [3] Jie, G., Shun, L.Y., Xi, M.L. Product characterization of waste printed circuit board by pyrolysis. *J. Anal. Appl. Pyrolysis* **2008**, 83, 185-189.
- [4] Moltó, J., Font, R., Gálvez, A., Conesa, J.A. Pyrolysis and combustion of electronic wastes. *J. Anal. Appl. Pyrolysis* **2009**, 84, 68-78.
- [5] Evans, C.S., Dellinger, B. Mechanisms of dioxin formation from the high-temperature pyrolysis of 2-bromophenol. *Environ. Sci. Technol.* **2003**, 37, 5574-5580.
- [6] Moltó, J., Font, R., Conesa, J.A. Study of the organic compounds produced in the pyrolysis and combustion of used polyester fabrics. *Energy Fuels* **2006**, 20, 1951-1958.
- [7] Hou, S., Mackie, J.C., Kennedy, E.M., Dlugogorski, B.Z. Comparative study on the formation of toxic species from 4-chlorobiphenyl in fires: effect of catalytic surfaces. *Procedia Eng.* **2013**, 62, 350-358.
- [8] Egerton, A., Warren, D.R. Kinetics of the hydrogen/oxygen reaction. I. The explosion region in boric acid-coated vessels. *Proc. R. Soc. London, Ser. A* **1951**, 204, 465-476.
- [9] Zhou, C.R., Sendt, K., Haynes, B.S. Experimental and kinetic modelling study of H₂S oxidation. *Proc Combust Inst* **2013**, 34, 625-632.
- [10] Cramer, C.J. *Essentials of Computational Chemistry: Theories and Models.* **2013**, John Wiley & Sons.
- [11] Young, D. *Computational Chemistry: A Practical Guide for Applying Techniques to Real World Problems.* **2004**, John Wiley & Sons.
- [12] Lewars, E.G. *Computational Chemistry: Introduction to the Theory and Applications of Molecular and Quantum Mechanics.* **2010**, Netherlands: Springer.

- [13] Ramachandran, K.I., Deepa, G., Namboori, K. Computational Chemistry and Molecular Modeling: Principles and Applications. **2008**, Springer.
- [14] Hartree, D.R. The wave mechanics of an atom with a non-Coulomb central field. Part I. Theory and methods. *Proc. Cambridge Phil. Soc* **1928**, 24, 89-110.
- [15] Sholl, D., Steckel, J.A. Density Functional Theory: A Practical Introduction. **2011**, A John Wiley & Sons.
- [16] Becke, A.D. Density functional calculations of molecular bond energies. *J. Chem. Phys.* **1986**, 84, 4524-4529.
- [17] Drissi, M., Chouaih, A., Megrou, Y., Hamzaoui, F. Electron charge density distribution from x-ray diffraction study of the 4-methoxybenzenecarbothioamide compound. *J. Chem. Crystallogr.* **2013**, 1-7.
- [18] Koch, W., Holthausen, M.C. A Chemist's Guide to Density Functional Theory. **2011**, New York, Wiley-VCH.
- [19] Chong, D.P. Recent Advances in Density Functional Method. **1995**, World Scientific.
- [20] Kryachko, E.S. Hohenberg-Kohn theorem. *Int. J. Quantum Chem.* **1980**, 18, 1029-1035.
- [21] Perdew, J.P., Schmidt, K. Jacob's ladder of density functional approximations for the exchange-correlation energy. **2001**, Doren, VEV., Alseoy, K.V., Geerlings, P. (eds) Density Functional Theory and its Applications to Materials. American Institute of Physics, Melville, New York.
- [22] Andriotis, A.N. LDA exchange-energy functional. *Phys. Rev. B* **1998**, 58, 15300-15303.
- [23] Staroverov, V.N., Scuseria, G.E., Tao, J., Perdew, J.P. Tests of a ladder of density functionals for bulk solids and surfaces. *Phys. Rev. B* **2004**, 69, 1-11.
- [24] Csonka, G.I., Perdew, J.P., Ruzsinszky, A., Philipsen, P.H.T., Lebègue, S., Paier, J., Vydrov, O.A., Ángyán, J.G. Assessing the performance of recent density functionals for bulk solids. *Phys. Rev. B* **2009**, 79, 1-14.
- [25] Harl, J., Schimka, K., Kresse, G. Assessing the quality of the random phase approximation for lattice constants and atomization energies of solids. *Phys. Rev. B* **2010**, 81, 115126.
- [26] Gupta, V.P. Principles and Applications of Quantum Chemistry. **2016**, Elsevier, UK.

- [27] Becke, A.D. Density-functional exchange-energy approximation with correct asymptotic behaviour. *Phys. Rev. A* **1988**, 38, 3098-3100.
- [28] Lee, C., Yang, W., Parr, R.G. Development of the colle-salvetti correlation-energy formula into a functional of the electron density. *Phys. Rev. B* **1988**, 37, 785-789.
- [29] Perdew, J.P., Burke, K., Ernzerhof, M. Generalized gradient approximation made simple. *Phys. Rev. Lett.* **1996**, 77, 3865-3868.
- [30] Kohanoff, J. *Electronic Structure Calculations for Solids and Molecules: Theory and Computational Methods*. **2006**, Cambridge University Press.
- [31] Haq, Z.U., Madura, J.D. *Frontiers in Computational Chemistry: Computer Applications for Drug Design and Biomolecular Systems*. **2015**, Elsevier Science.
- [32] Zhao, Y., Truhlar, D.G. A new local density functional for main-group thermochemistry, transition metal bonding, thermochemical kinetics, and noncovalent interactions. *J. Chem. Phys.* **2006**, 125, 194101.
- [33] Zhao, Y., Truhlar, D.G. The M06 suite of density functionals for main group thermochemistry, thermochemical kinetics, noncovalent interactions, excited states, and transition elements: two new functionals and systematic testing of four M06-class functionals and 12 other functionals. *Theor. Chem. Acc* **2008**, 120, 215-241.
- [34] Walker, M., Harvey, A.J.A., Sen, A., Dessent, C.E.H. Performance of M06, M06-2X, and M06-HF density functionals for conformationally flexible anionic clusters: M06 functionals perform better than B3LYP for a model system with dispersion and ionic hydrogen-bonding interactions. *J. Phys. Chem. A* **2008**, 117, 12590–12600.
- [35] Bryantsev, V.S., Diallo, M.S., van Duin, A.C.T., Goddard, W.A. Evaluation of B3LYP, X3LYP, and M06-Class density functionals for predicting the binding energies of neutral, protonated, and deprotonated water clusters. *J. Chem. Theory Comput.* **2009**, 5, 1016–1026.
- [36] Hohenstein, E.G., Chill, S.T., Sherill, C.D. Assessment of the performance of the M05-2X and M06-2X exchange-correlation functionals for noncovalent interactions in biomolecules. *J. Chem. Theory Comput.* **2008**, 4, 1996–2000.
- [37] Frisch, M.J., Trucks, G.W., Schlegel, H.B., Scuseria, G.E., Robb, M.A., Cheeseman, J.R., Scalmani, G., Barone, V., Mennucci, B., Petersson, G.A.,

- Nakatsuji, H., Caricato, M., Li, X., Hratchian, H.P., Izmaylov, A.F., Bloino, J., Zheng, G., Sonnenberg, J.L., Hada, M., Ehara, M., Toyota, K., Fukuda, R., Hasegawa, J., Ishida, M., Nakajima, T., Honda, Y., Kitao, O., Nakai, H., Vreven, T., Montgomery, J.A., Peralta, J.E., Ogliaro, F., Bearpark, M., Heyd, J.J., Brothers, E., Kudin, K.N., Staroverov, V.N., Kobayashi, R., Normand, J., Raghavachari, K., Rendell, A., Burant, J.C., Iyengar, S.S., Tomasi, J., Cossi, M., Rega, N., Millam, N.J., Klene, M., Knox, J.E., Cross, J.B., Bakken, V., Adamo, C., Jaramillo, J., Gomperts, R., Stratmann, R.E., Yazyev, O., Austin, A.J., Cammi, R., Pomelli, C., Ochterski, J.W., Martin, R.L., Morokuma, K., Zakrzewski, V. G., Voth, G.A., Salvador, P., Dannenberg, J.J., Dapprich, S., Daniels, A.D., Farkas, O., Foresman, J.B., Ortiz, J.V., Cioslowski, J., Fox, D.J. **2009**, Gaussian09, Revision D.01; Gaussian Inc: Wallingford, CT.
- [38] Fukui, K. The path of chemical reactions-the IRC approach. *Accounts of chemical research. Acc. Chem. Res.* **1981**, 14, 363-368.
- [39] *The Reaction Path in Chemistry: Current Approaches and Perspectives*. Heidrich, D (ed.) **1995**, Netherlands: Springer.
- [40] Runge, E., Gross, E.K.U. Density-functional theory for time-dependent systems. *Phys. Rev. Lett.* **1984**, 52, 997.
- [41] Hohenberg, P., Kohn, W. Inhomogeneous electron gas. *Phys. Rev.* **1964**, 136, B864-B871.
- [42] Kohn, W., Sham, L.J. Self-consistent equations including exchange and correlation effects. *Phys. Rev.* **1965**, 140, A1133-A1138.
- [43] Casida, M.E. *Recent Advances in Density Functional Methods*. (Vol. 1) **1995**, 155–192, World Scientific: Singapore.
- [44] Delley, B. An all-electron numerical method for solving the local density functional for polyatomic molecules. *J. Chem. Phys* **1990**, 92, 508-517.
- [45] Delley, B. Time dependent density functional theory with DMol³. *J. Phys. Condens. Matter* **2010**, 22, 384208-34214.
- [46] Delley, B. From molecules to solids with the DMol³ approach. *J. Chem. Phys.* **2000**, 113, 7756-7764.
- [47] Andzelm, J., Kölmel, C., Klamt, A. Incorporation of solvent effects into density functional calculations of molecular energies and geometries. *J. Chem. Phys.* **1995**, 103, 9312-9320.

- [48] Mokrushin, V., Bedanov, V., Tsang, W., Zachariah, M., Knyazev, V., ChemRate, version 1.19. NIST: Gaithersburg, MD. **2002**.
- [49] Giacomo, F.D. A short account of RRKM theory of unimolecular reactions and of marcus theory of electron transfer in a historical perspective. *J. Chem. Educ.* **2015**, 92, 476-481.
- [50] Lindemann, F.A., Arrhenius, S., Langmuir, I., Dhar, N.R., Perrin, J., Lweis, W.C.M. Discussion on "the radiation theory of chemical action". *Trans. Faraday Soc.* **1922**, 17, 598-606.
- [51] Laidler, K.J., King, M.C. Development of transition-state theory. *J. Phys. Chem.* **1983**, 87, 2657-2664.
- [52] Canneaux, S., Bohr, F., Henon, E. KiSTheIP: A program to predict thermodynamic properties and rate constants from quantum chemistry results. *J. Comput. Chem* **2014**, 35, 82-93.
- [53] Fernandez-Ramos, A., Ellingson, B.A., Meana- Pañeda, R., Marques, J.M.C., Truhlar, D.G. Symmetry numbers and chemical reaction rates. *Theor. Chem. Acc.* **2007**, 118, 813-826.
- [54] Truhlar, D.G., Garrett, B.C., Klippenstein, S.J. Current status of transition-state theory. *J. Phys. Chem.* **1996**, 100, 12771-12800.
- [55] Eckart, C. The Penetration of a potential barrier by electrons. *Phys. Rev*, **1930**, 35, 1303-1309.

CHAPTER 4 THERMODYNAMIC PARAMETERS INCLUDING ACID DISSOCIATION CONSTANTS FOR BROMOCHLOROPHENOLS (BCPhs)

The following chapter is a modified version of the published paper:

Anam Saeed, Mohammednoor Altarawneh, Glenn Hefter, and Bogdan Z. Dlugogorski (2016) J. Chem. Eng. Data 61 (1), 160-172.

Table of Contents

Abstract	144
4.1. Introduction	145
4.2. Computational details	146
4.3. Results and discussion	147
4.3.1. Optimised geometries	147
4.3.2. Heat capacities and standard entropies	147
4.3.3. Standard enthalpy of formation of BCPhs and their radicals	155
4.3.4. Bond dissociation enthalpies	160
4.3.5. Gibbs energies of formation of BCPhs and their anions in gaseous and aqueous phases	162
4.3.6. Acid dissociation constants (pK_a)	163
4.4. Conclusions	168
Supporting information	168
References	169

Abstract

This chapter reports standard gas-phase enthalpies of formation ($\Delta_f H^\circ_{298}$), entropies (S°_{298}) and heat capacities ($C_p^\circ(T)$) for all plausible 64 bromochlorophenols (BCPhs) at the M062X meta hybrid level using polarised basis set of 6-311+G(d,p). Isodesmic work reactions served to calculate the standard enthalpies of formation for all bromochlorophenol molecules and several bromochlorophenoxy radicals. Standard entropies and heat capacity comprise correction terms due to the treatment of O-H bonds as hindered rotors. Values of dissociation enthalpies (BDHs) of O-H bonds, calculated for a selected series of bromochlorophenols, vary slightly with the change in the pattern and degree of halogenation of the phenyl ring. A thermodynamic cycle facilitated estimation of pK_a values, based on the calculated solvation and gas-phase deprotonation energies. We estimated the solvation energies of 19 out of 64 BCPhs and their respective anions based on the integral equation formalism polarisable continuum model using optimised structures in the aqueous phase. Values of pK_a decrease significantly from around 9 for monohalogenated to around 3 for pentahalogenated phenols.

4.1. Introduction

Phenols and their halogenated derivatives, such as chlorophenols (CPhs), bromophenols (BPhs) and bromochlorophenols (BCPhs) find frequent use in industrial and agricultural applications. BCPhs function as feedstocks and intermediates for many chemical products, most notably, herbicides, fungicides, wood preservatives and flame retardants [1-4]. As a result of their dispersive applications, BCPhs have been detected in marine ecosystems [5-7] and in industrial effluents [8-11]. BCPhs have properties typical of persistent organic pollutants (POPs). Furthermore, typical combustion processes and accidental fires generate complete homologue profiles of BCPhs [12-13]. BCPhs affect the thyroid hormone system [14-15]. Environmental as well as health impacts of BCPhs depend primarily on their physical and chemical properties.

Previous efforts have focused on elucidating reaction pathways [16-17], molecular structures and thermodynamic parameters [18-20] of halogenated homologue profiles of CPhs and BPhs. In comparison to CPhs and BPhs, corresponding data on BCPhs are rather scarce. In an analogy to the well-established role of CPhs and BPhs as precursors for the formation of polychlorinated dibenzo-*p*-dioxins and dibenzofurans (PCDD/Fs) and polybrominated dibenzo-*p*-dioxins and dibenzofurans (PBDD/Fs), BCPhs act as building blocks in the generation of mixed halogenated dibenzo-*p*-dioxins and dibenzofurans (PXDD/Fs, X=Br, Cl). PXDD/Fs appear to be common environmental pollutants, with known carcinogenicity and typical POP like properties [21-25]. Mixed halogenation at the lateral position of 2,3,7,8- induces PXDD/Fs to exhibit enhanced toxicity effects, if compared with their analogous PCDD/F and PBDD/F congeners [26-27]. PXDD/Fs have been identified in several environmental matrices such as air [28], soil and sediments [28-29] and in tissues of aquatic animals [30].

Consensus in the literature points to the formation of PXDD/Fs from CPhs and BPhs in thermal systems. Recent experimental studies have reported that, PXDD/Fs could also arise from the municipal waste incineration and industrial processes containing trace sources of brominated and chlorinated compounds [25, 31-34]. For example, Schwind et al. [35] detected formation of appreciable concentration of PXDD/Fs in fly ash of a typical municipal waste incinerator. Evans et al. [36-37] identified various congeners of

PXDD/Fs during the course of high temperature oxidation and pyrolysis of a mixture of CPhs and BPhs.

Overall, PXDD/Fs share similar chemical properties and formation mechanisms with their chlorinated and brominated analogues [38]. The yield and degree of halogenation of the PXDD/Fs depend strongly on available chlorine and bromine content and operational conditions, especially the ability of catalytic surfaces to induce halogenation and dehalogenation reactions [39-42]. Even trace quantities of bromine exert significant effect on the emission of products of incomplete combustion, such as PBDD/Fs and PXDD/Fs [41-43]. BPhs are more active precursors for the formation of PBDD/Fs [44-47] than CPhs for the generation of PCDD/Fs [47-49].

This chapter develops accurate thermochemical and structural parameters of the complete series of BCPhs and acid dissociation constants for selected species. Precise and detailed knowledge of physical and chemical properties of BCPhs constitute a prerequisite for gaining better understanding of environmental fate and transformation chemistry of BCPhs, including formation pathways of PXDD/Fs from BCPhs. Along the same line of inquiry, calculated thermochemical properties may shed light on the effect of thermodynamic stability on distribution of congeners in thermal or environmental reservoirs. To this end, the present chapter reports theoretically-derived thermochemical and structural properties of BCPhs congeners.

4.2. Computational details

Guassian09 program [50] provided a means to optimise chemical structures and to compute energies, at the M062X/6-311+G(d,p) [51] level of theory. M062X is a relatively new meta-hybrid density theory functional parameterised to yield accurate thermochemistry for general applications in organic compounds. Extended basis set of 6-311+G(3df,2p) facilitated the computations of single point energies. ChemRate [52] code aided the calculations of some thermochemical parameters, such as standard entropies, heat capacities and NASA polynomials. Finally, computation of acid/base behaviour of halogenated phenols demanded the estimation of solvation energies (ΔG^*_{solv}). We evaluated solvation energies of neutral and anionic species based on the integral equation

formalism polarisable continuum model (IEFPCM) developed by Tomasi and co-workers [53-54]. Section 4.3.6 presents the adopted computational approach for obtaining the acid dissociation constants (pK_a) for selected BCPh congeners.

4.3. Results and discussion

4.3.1. Optimised geometries

By analogy with the 2-chlorophenol molecule [55-56], the presence of the H atom in the OH group pointing toward a C(halogen) atom (*syn*) rather than toward a C(H) site (*anti*) is expected to produce slightly more stable isomers. Accordingly, we consider *syn* conformers in optimising all BCPh isomers. Figure 4.1 depicts optimised structures and geometrical features of selected congeners of BCPhs. Overall, variation in degree and pattern of halogenation induces rather minor changes in the geometries of BCPh congeners. For instance, calculated lengths of O-H and C-O bonds of all BCPhs vary in narrow ranges of 0.961-0.966 Å and 1.340-1.43 Å, respectively. Calculated geometries of BCPhs accord with theoretical predictions of corresponding BPhs [57] and CPhs [58]. For example, calculated bond distances in O-H and C-O in pentachlorophenol amount to 0.968 Å and 1.329 Å, correspondingly; i.e., they are in excellent agreement with relevant distances in BCPh congeners.

4.3.2. Heat capacities and standard entropies

Table 4.1 lists values of standard heat capacities ($C_p^\circ(T)$) and standard entropies (S°_{298}) of all 64 possible BCPh congeners, at selected temperatures; i.e., for BCPhs in a physical state of an ideal gas. Accurate determination of $C_p^\circ(T)$ and S°_{298} calls for treatment of the internal rotation of the H atom, in the hydroxyl group around the C-O bond, as hindered rotors (HR). The literature describes well the need and the procedure for such a treatment [59]. This treatment basically eliminates the vibrational frequency corresponding to the internal rotation and replaces it with the overall barrier of the rotor, its moment of inertia and its symmetry number, i.e., 2 in the considered BCPh systems. Figure 4.2 shows rotor

CHAPTER 4 Thermodynamic Parameters Including Acid Dissociation Constants for Bromochlorophenols (BCPhs)

potentials and Table 4.2 provides estimates of the HR corrections for $C_p^\circ(300\text{ K})$, $C_p^\circ(1000\text{ K})$ and S°_{298} .

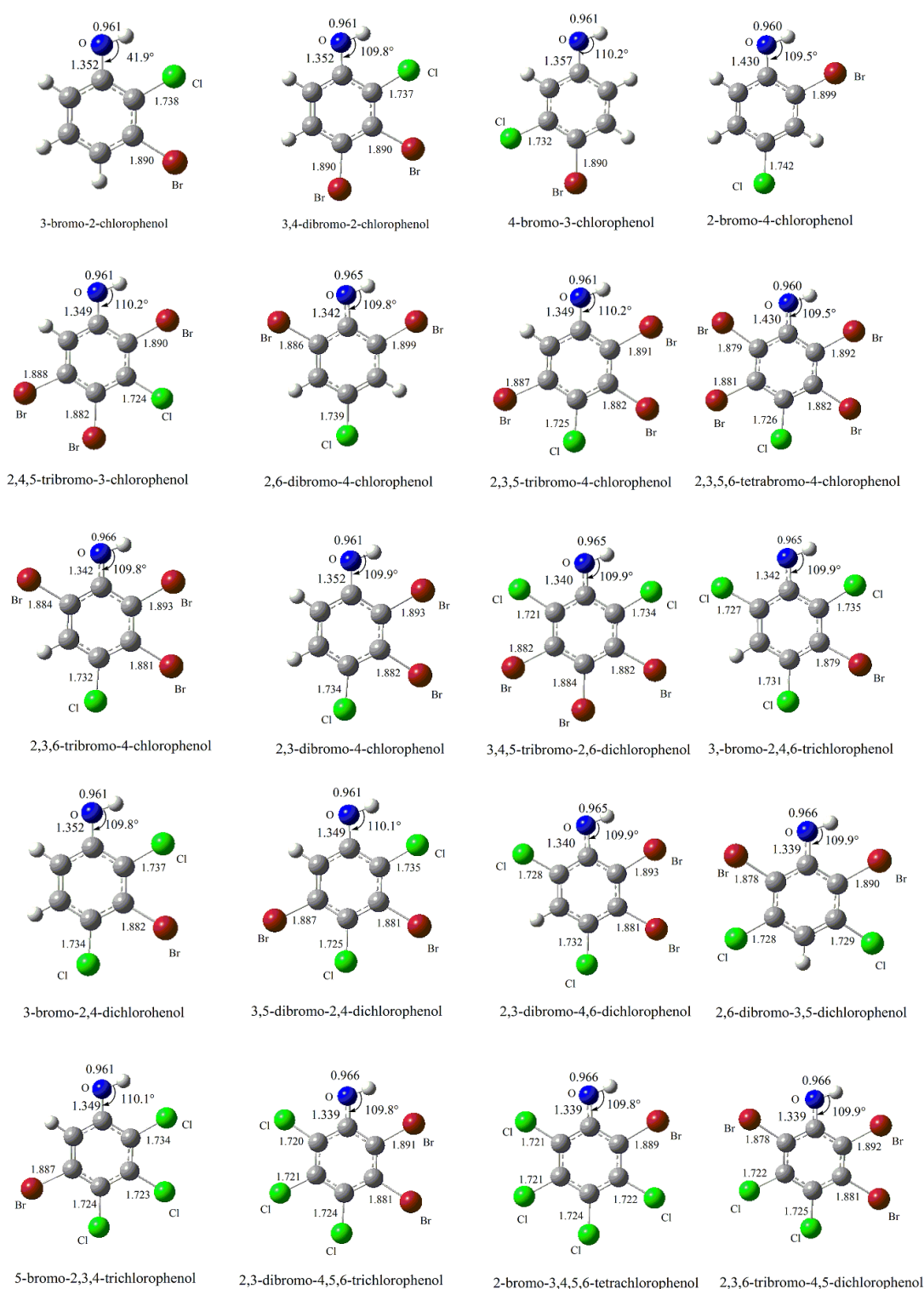


Figure 4.1. Optimised geometries of selected bromochlorophenol congeners with distances measured in Å and angles are in degrees.

CHAPTER 4 Thermodynamic Parameters Including Acid Dissociation Constants for Bromochlorophenols (BCPhs)

Table 4.1. S°_{298} and $C_p^{\circ}(T)$; both in $\text{J mol}^{-1} \text{K}^{-1}$.

Compound Name	S°_{298}	$C_p^{\circ}(T)$				
		300 K	500 K	800 K	1000 K	1500 K
3-bromo-2-chlorophenol	391.9	138.2	191.6	235.6	252.2	274.8
3-bromo-5-chlorophenol	396.4	139.7	192.5	234.7	250.5	273.1
3-bromo-4-chlorophenol	393.3	138.7	191.8	236.0	252.5	279.3
2-bromo-4-chlorophenol	392.9	138.2	191.5	235.6	252.1	274.8
2-bromo-5-chlorophenol	393.8	138.5	191.9	235.7	252.1	274.6
4-bromo-3-chlorophenol	395.2	139.5	192.2	234.3	250.3	272.9
2-bromo-3-chlorophenol	391.0	137.9	191.3	235.6	252.3	275.0
2-bromo-6-chlorophenol	392.4	137.8	191.2	235.2	251.6	274.2
3-bromo-6-chlorophenol	393.5	138.4	191.7	235.5	251.8	274.3
4-bromo-2-chlorophenol	393.6	138.4	191.6	235.4	251.7	272.3
3-bromo-2-chlorophenol	391.5	138.1	191.4	235.5	251.9	274.5
2-bromo-4,5-dichlorophenol	422.1	153.8	204.8	245.6	260.3	279.8
3-bromo-4,5-dichlorophenol	424.2	155.1	205.5	244.4	258.5	278.0
2-bromo-3,4-dichlorophenol	419.0	153.4	204.6	245.7	260.5	280.1
4-bromo-2,6-dichlorophenol	424.2	154.1	182.6	244.9	259.2	278.7
3-bromo-2,6-dichlorophenol	421.8	153.7	204.8	245.0	259.5	278.8
2-bromo-3,6-dichlorophenol	423.3	153.8	204.9	245.3	259.8	279.2
3-bromo-2,5-dichlorophenol	422.8	154.2	205.2	245.7	260.3	279.6
3-bromo-2,4-dichlorophenol	420.2	153.9	204.8	245.7	260.6	280.1
4-bromo-2,3-dichlorophenol	420.9	153.9	204.9	245.5	260.2	279.5
3-bromo-2,4,6-trichlorophenol	451.2	169.6	218.3	255.1	267.7	283.9
3-bromo-2,4,5-trichlorophenol	450.1	169.7	218.6	255.7	268.5	284.6
4-bromo-2,3,5-trichlorophenol	450.4	170.0	218.6	255.7	268.5	284.6
2-bromo-4,5,6-trichlorophenol	450.7	169.2	218.0	255.3	268.0	284.2
3-bromo-4,5,6-trichlorophenol	450.0	169.5	218.3	255.6	268.4	286.4
4-bromo-2,3,6-trichlorophenol	440.1	162.5	213.5	252.6	266.6	285.1
4-bromo-2,3,5,6-tetrachlorophenol	479.2	185.3	231.7	265.3	276.1	289.0
3-bromo-2,4,5,6-tetrachlorophenol	480.0	185.7	231.9	265.3	276.1	289.1

**CHAPTER 4 Thermodynamic Parameters Including Acid Dissociation Constants
for Bromochlorophenols (BCPhs)**

2-bromo-3,4,5,6-tetrachlorophenol	478.0	184.9	231.4	265.6	276.6	289.6
3,4-dibromo-6-chlorophenol	434.0	155.9	206.1	246.0	260.4	279.5
2,4-dibromo-6-chlorophenol	431.2	155.7	206.0	246.0	260.4	279.6
3,4-dibromo-5-chlorophenol	433.2	157.3	206.8	245.1	259.0	278.2
2,6-dibromo-4-chlorophenol	433.8	155.5	205.8	245.7	260.1	279.3
3,4-dibromo-2-chlorophenol	432.7	156.0	206.1	246.2	260.6	279.8
2,6-dibromo-3-chlorophenol	432.6	155.3	205.6	245.8	260.4	279.6
2,5-dibromo-3-chlorophenol	442.5	156.5	206.2	246.4	261.0	280.3
2,4-dibromo-3-chlorophenol	432.0	155.6	205.8	246.2	261.0	280.3
2,3-dibromo-4-chlorophenol	431.4	155.7	205.9	246.3	261.0	280.3
2,3-dibromo-5,6-dichlorophenol	461.5	170.9	219.0	256.0	268.7	284.8
2,3-dibromo-4,5-dichlorophenol	462.6	169.9	218.0	255.0	268.2	285.9
2,4-dibromo-3,6-dichlorophenol	462.6	171.1	217.5	256.0	268.7	284.7
2,6-dibromo-3,5-dichlorophenol	461.7	171.1	219.1	256.0	268.7	284.8
2,4-dibromo-3,5-dichlorophenol	460.9	171.5	219.4	256.4	269.2	285.7
2,6-dibromo-3,4-dichlorophenol	461.6	171.0	219.0	255.9	268.6	284.7
3,4-dibromo-2,6-dichlorophenol	462.3	171.3	219.2	255.6	268.1	284.1
2,3-dibromo-4,6-dichlorophenol	461.7	171.3	219.2	256.1	268.7	284.7
3,5-dibromo-4,6-dichlorophenol	461.2	171.5	219.6	256.2	268.8	284.7
2,6-dibromo-3,4,5-trichlorophenol	489.1	186.5	232.4	266.0	276.9	289.8
3,4-dibromo-2,5,6-trichlorophenol	489.6	187.2	232.9	265.9	276.6	289.3
2,4-dibromo-3,5,6-trichlorophenol	489.3	186.7	232.5	266.1	277.1	289.8
2,3-dibromo-4,5,6-trichlorophenol	489.0	186.7	232.5	266.1	277.0	289.8
2,3,4-tribromo-6-chlorophenol	470.9	173.0	220.1	256.5	269.1	284.9
2,3,4-tribromo-5-chlorophenol	471.8	173.4	220.5	257.0	269.7	285.6
2,3,6-tribromo-4-chlorophenol	472.8	172.9	220.0	256.7	269.5	285.5
2,3,5-tribromo-4-chlorophenol	471.6	173.1	220.4	256.9	269.7	285.6
2,4,6-tribromo-3-chlorophenol	473.6	172.8	220.0	256.4	268.9	284.8
2,4,5-tribromo-3-chlorophenol	465.2	170.9	218.9	256.1	269.0	285.1
2,3,4-tribromo-5,6-dichlorophenol	500.6	188.9	233.8	266.9	277.5	290.1
2,3,5-tribromo-4,6-dichlorophenol	499.7	190.5	234.8	267.4	277.9	290.3
2,5,6-tribromo-3,4-dichlorophenol	500.3	188.9	233.8	266.8	277.5	290.1

**CHAPTER 4 Thermodynamic Parameters Including Acid Dissociation Constants
for Bromochlorophenols (BCPhs)**

3,4,5-tribromo-2,6-dichlorophenol	500.9	189.2	234.1	266.5	277.0	289.5
2,3,4,5-tetrabromo-6-chlorophenol	511.2	190.9	235.0	267.4	277.9	290.3
2,3,4,6-tetrabromo-5-chlorophenol	493.3	190.5	234.7	267.3	277.9	290.3
2,3,5,6-tetrabromo-4-chlorophenol	510.6	190.5	234.8	267.4	277.9	290.3

CHAPTER 4 Thermodynamic Parameters Including Acid Dissociation Constants for Bromochlorophenols (BCPhs)

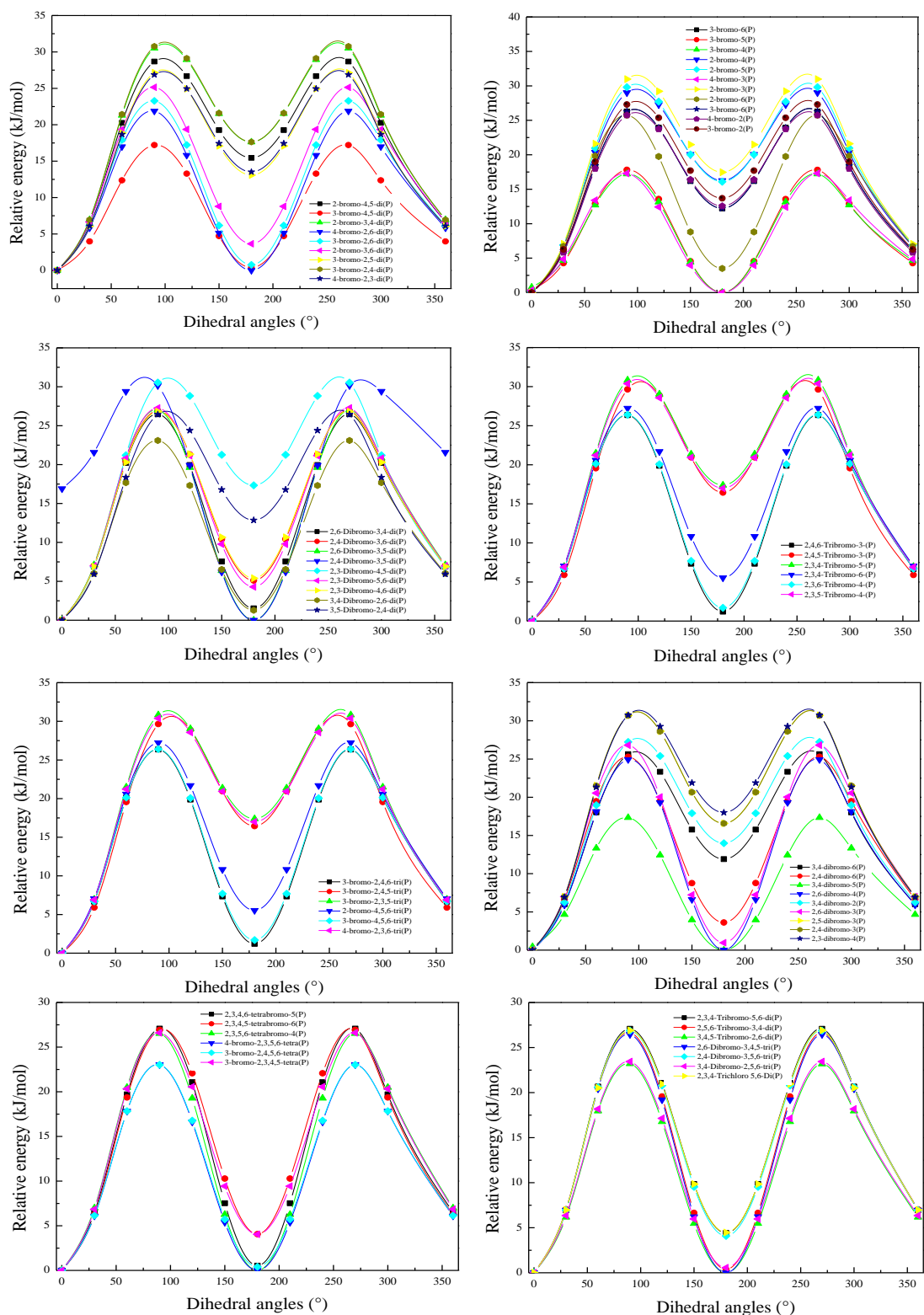


Figure 4.2. Potential energy profiles for internal rotations of H around C-O bond in BCPh congeners. (P) denotes chlorophenol.

CHAPTER 4 Thermodynamic Parameters Including Acid Dissociation Constants for Bromochlorophenols (BCPhs)

Table 4.2. Contribution from treatment of internal rotors as hindered rotors to the values of S°_{298} , $C_p^{\circ}(300\text{ K})$, and $C_p^{\circ}(1000\text{ K})$; both in $\text{J mol}^{-1}\text{ K}^{-1}$.

Compound Name	S°_{298}	$C_p^{\circ}(T)$	
		300 K	1000 K
3-bromo-2-chlorophenol	8.14	-2.30	-3.97
3-bromo-5-chlorophenol	-1.20	1.88	-0.84
3-bromo-4-chlorophenol	-2.58	1.30	1.21
2-bromo-4-chlorophenol	-1.72	1.71	1.09
2-bromo-5-chlorophenol	-2.17	33.0	16.9
4-bromo-3-chlorophenol	-0.89	1.96	-0.96
2-bromo-3-chlorophenol	-2.42	1.38	1.25
2-bromo-6-chlorophenol	-1.58	1.67	0.71
3-bromo-6-chlorophenol	-1.42	1.76	0.79
4-bromo-2-chlorophenol	-1.60	1.66	0.71
3-bromo-2-chlorophenol	-1.63	1.67	0.92
2-bromo-4,5-dichlorophenol	-2.10	1.50	1.00
3-bromo-4,5-dichlorophenol	-0.66	2.04	-1.00
2-bromo-3,4-dichlorophenol	-3.11	1.09	1.17
4-bromo-2,6-dichlorophenol	-0.69	2.01	0.08
3-bromo-2,6-dichlorophenol	-1.01	1.88	0.33
2-bromo-3,6-dichlorophenol	-1.38	1.71	0.63
3-bromo-2,5-dichlorophenol	-1.70	1.67	0.88
3-bromo-2,4-dichlorophenol	-2.20	1.46	1.21
4-bromo-2,3-dichlorophenol	-1.82	1.59	0.84
3-bromo-2,4,6-trichlorophenol	-0.74	2.01	0.29
3-bromo-2,4,5-trichlorophenol	-2.06	1.46	0.79
4-bromo-2,3,5-trichlorophenol	-1.40	1.76	0.84
2-bromo-4,5,6-trichlorophenol	-1.09	1.92	0.63
3-bromo-4,5,6-trichlorophenol	-1.84	1.55	0.75
4-bromo-2,3,6-trichlorophenol	-11.7	-4.85	-0.71
4-bromo-2,3,5,6-tetrachlorophenol	-0.63	2.09	0.33

CHAPTER 4 Thermodynamic Parameters Including Acid Dissociation Constants for Bromochlorophenols (BCPhs)

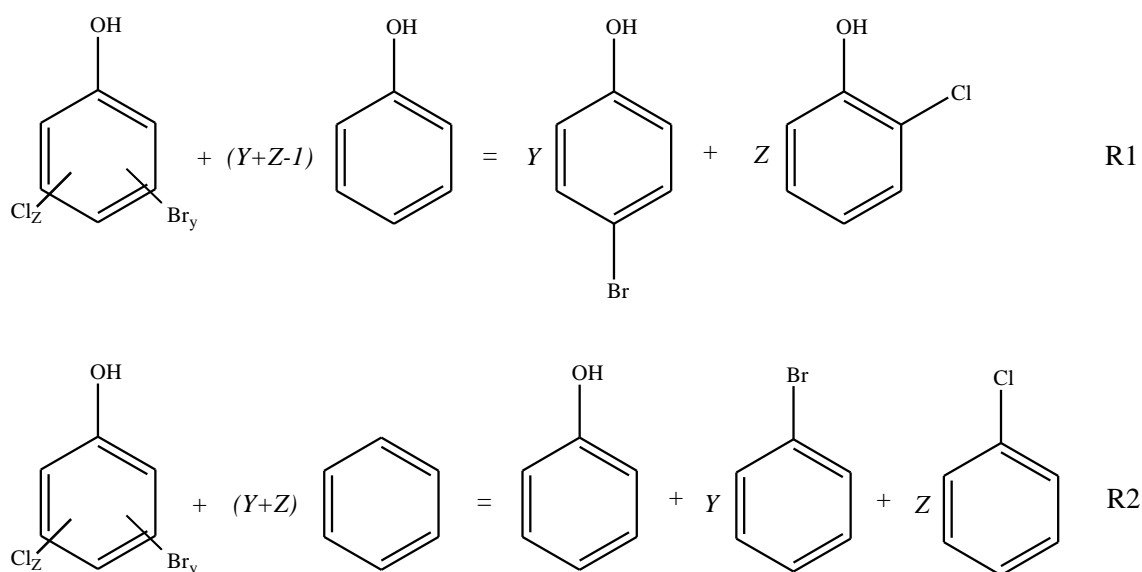
3-bromo-2,4,5,6-tetrachlorophenol	12.4	2.47	0.33
2-bromo-3,4,5,6-tetrachlorophenol	-1.63	1.67	0.84
3,4-dibromo-6-chlorophenol	-1.98	1.50	0.66
2,4-dibromo-6-chlorophenol	-6.0	1.67	0.67
3,4-dibromo-5-chlorophenol	-1.75	1.76	-0.96
2,6-dibromo-4-chlorophenol	-1.16	1.88	0.63
3,4-dibromo-2-chlorophenol	-1.43	1.80	0.92
2,6-dibromo-3-chlorophenol	-1.11	1.92	0.88
2,5-dibromo-3-chlorophenol	6.74	2.13	1.30
2,4-dibromo-3-chlorophenol	-2.15	1.30	1.21
2,3-dibromo-4-chlorophenol	-2.30	1.42	1.25
2,3-dibromo-5,6-dichlorophenol	-1.16	1.88	0.92
2,3-dibromo-4,5-dichlorophenol	-4.94	17.1	8.57
2,4-dibromo-3,6-dichlorophenol	-1.55	1.71	0.88
2,6-dibromo-3,5-dichlorophenol	-1.17	1.92	0.92
2,4-dibromo-3,5-dichlorophenol	-1.79	1.67	1.21
2,6-dibromo-3,4-dichlorophenol	-1.31	1.84	0.79
3,4-dibromo-2,6-dichlorophenol	-1.48	1.67	0.29
2,3-dibromo-4,6-dichlorophenol	-1.30	1.84	0.88
3,5-dibromo-4,6-dichlorophenol	-1.81	1.55	0.79
2,6-dibromo-3,4,5-trichlorophenol	-1.15	1.88	0.79
3,4-dibromo-2,5,6-trichlorophenol	-0.99	1.88	0.38
2,4-dibromo-3,5,6-trichlorophenol	-1.68	1.67	0.88
2,3-dibromo-4,5,6-trichlorophenol	-1.22	1.88	0.88
2,3,4-tribromo-6-chlorophenol	-7.5	1.84	0.92
2,3,4-tribromo-5-chlorophenol	-2.50	1.34	1.25
2,3,6-tribromo-4-chlorophenol	-2.22	1.50	1.25
2,3,5-tribromo-4-chlorophenol	-2.46	1.38	1.21
2,4,6-tribromo-3-chlorophenol	-1.54	1.71	0.88
2,4,5-tribromo-3-chlorophenol	-1.99	1.55	17.9
2,3,4-tribromo-5,6-dichlorophenol	-1.57	1.67	0.88
2,3,5-tribromo-4,6-dichlorophenol	-2.24	3.51	1.30

CHAPTER 4 Thermodynamic Parameters Including Acid Dissociation Constants for Bromochlorophenols (BCPhs)

2,5,6-tribromo-3,4-dichlorophenol	-1.47	1.71	0.84
3,4,5-tribromo-2,6-dichlorophenol	-0.69	2.05	0.33
2,3,4,5-tetrabromo-6-chlorophenol	-1.26	1.84	0.88
2,3,4,6-tetrabromo-5-chlorophenol	-8.8	1.84	0.92
2,3,5,6-tetrabromo-4-chlorophenol	-1.21	1.88	0.88

4.3.3. Standard enthalpy of formation of BCPhs and their radicals

Standard enthalpies of formation ($\Delta_f H^\circ_{298}$) for all congeners of BCPh are computed using two isodesmic reactions R1 and R2. Isodesmic reaction R1 employs the *para*-bromophenol and *ortho*-chlorophenol as resultant products. Taking into account the remaining isomers of chlorophenols and bromophenols in casting the isodesmic reactions, the calculated standard enthalpy of formation of BCPh congeners may change within 4.7 kJ mol⁻¹.



Scheme 1. Isodesmic reactions for obtaining the standard enthalpy of formation of BCPh.

These isodesmic reactions utilise experimental values of $\Delta_f H^\circ_{298}$ for phenol (-96.3 ± 0.59 kJ mol⁻¹) [60], *o*-chlorophenol (-131 kJ mol⁻¹) [61], *o*-bromophenol (-78 ± 1.9 kJ mol⁻¹)

CHAPTER 4 Thermodynamic Parameters Including Acid Dissociation Constants for Bromochlorophenols (BCPhs)

[62], *p*-chlorophenol (-145.5 ± 8.4 kJ mol⁻¹) [63], *p*-bromophenol (-69.3 ± 2.1 kJ mol⁻¹) [64], benzene (82.9 ± 0.9 kJ mol⁻¹) [64], bromobenzene (105.4 ± 4.20 kJ mol⁻¹) [65] and chlorobenzene (52.4 ± 0.42 kJ mol⁻¹) [66]. Table 4.3 provides calculated reaction enthalpies for R1 ($\Delta_{R1}H^{\circ}_{298}$) and R2 ($\Delta_{R2}H^{\circ}_{298}$) and $\Delta_f H^{\circ}_{298}$ of the target species.

Table 4.3. $\Delta_f H^{\circ}_{298}$ (kJ mol⁻¹) and $\Delta_{R}H^{\circ}_{298}$ (kJ) for all mixed brominated and chlorinated congeners of phenol.

Compound Name	$\Delta_{R1}H^{\circ}_{298}$	$\Delta_{R2}H^{\circ}_{298}$	$\Delta_{f1}H^{\circ}_{298}$	$\Delta_{f2}H^{\circ}_{298}$	$\Delta_{favg}H^{\circ}_{298}$
3-bromo-2-chlorophenol	-9.78	-1.1	-102.9	-102.9	-102.9
3-bromo-5-chlorophenol	-15.1	-6.5	-97.6	-97.6	-97.6
3-bromo-4-chlorophenol	-24.5	-15.9	-88.2	-88.2	-88.2
2-bromo-4-chlorophenol	-10.4	-1.8	-102.3	-102.3	-102.3
2-bromo-5-chlorophenol	-7.77	0.9	-104.9	-105.0	-104.9
4-bromo-3-chlorophenol	-23.7	-15.1	-89.0	-89.0	-89.0
2-bromo-3-chlorophenol	-15.4	-6.8	-97.3	-97.3	-97.3
2-bromo-6-chlorophenol	-15.7	-7.0	-97.0	-97.1	-97.1
3-bromo-6-chlorophenol	-9.79	-1.1	-102.9	-102.9	-102.9
4-bromo-2-chlorophenol	-11.5	-2.9	-101.2	-101.2	-101.2
3-bromo-2-chlorophenol	-17.3	-8.7	-95.4	-95.4	-95.4
2-bromo-4,5-dichlorophenol	-28.6	-16.4	-118.8	-95.5	-107.2
3-bromo-4,5-dichlorophenol	-43.5	-31.3	-103.9	-103.2	-103.6
2-bromo-3,4-dichlorophenol	-35.8	-23.6	-111.6	-110.8	-111.2
4-bromo-2,6-dichlorophenol	-30.3	-18.1	-117.1	-116.3	-116.7
3-bromo-2,6-dichlorophenol	-30.7	-18.5	-116.7	-115.9	-116.3
2-bromo-3,6-dichlorophenol	-29.2	-17.0	-118.2	-117.4	-117.8
3-bromo-2,5-dichlorophenol	-28.3	-16.1	-119.1	-118.3	-118.7
3-bromo-2,4-dichlorophenol	-37.9	-25.7	-109.5	-108.8	-109.1
4-bromo-2,3-dichlorophenol	-37.1	-24.9	-110.3	-109.6	-109.9
3-bromo-2,4,6-trichlorophenol	-58.3	-42.6	-123.8	-122.3	-123.0
3-bromo-2,4,5-trichlorophenol	-59.3	-43.6	-122.8	-121.3	-122.0
4-bromo-2,3,5-trichlorophenol	-58.8	-43.0	-123.3	-121.8	-122.6
2-bromo-4,5,6-trichlorophenol	-56.6	-40.8	-125.6	-124.0	-124.8

**CHAPTER 4 Thermodynamic Parameters Including Acid Dissociation Constants
for Bromochlorophenols (BCPhs)**

3-bromo-4,5,6-trichlorophenol	-59.1	-43.4	-123.0	-121.4	-122.2
4-bromo-2,3,6-trichlorophenol	-57.8	-42.0	-124.3	-122.8	-123.6
4-bromo-2,3,5,6-tetrachlorophenol	-89.1	-69.9	-127.7	-125.4	-126.5
3-bromo-2,4,5,6-tetrachlorophenol	-87.0	-67.7	-129.8	-127.5	-128.6
2-bromo-3,4,5,6-tetrachlorophenol	-87.0	-67.7	-129.8	-127.5	-128.6
3,4-dibromo-6-chlorophenol	-32.4	-18.7	-62.0	-62.8	-62.4
2,4-dibromo-6-chlorophenol	-30.2	-16.5	-64.2	-65.0	-64.6
3,4-dibromo-5-chlorophenol	-46.0	-32.3	-48.4	-49.2	-48.8
2,6-dibromo-4-chlorophenol	-29.7	-15.9	-64.7	-65.6	-65.1
3,4-dibromo-2-chlorophenol	-40.2	-26.4	-54.2	-55.1	-54.6
2,6-dibromo-3-chlorophenol	-33.8	-20.0	-60.6	-61.5	-61.0
2,5-dibromo-3-chlorophenol	-28.1	-14.4	-66.3	-67.1	-66.7
2,4-dibromo-3-chlorophenol	-37.3	-23.6	-57.1	-57.9	-57.5
2,3-dibromo-4-chlorophenol	-38.9	-25.2	-55.5	-56.3	-55.9
2,3-dibromo-5,6-dichlorophenol	-56.3	-39.0	-72.8	-72.9	-72.8
2,3-dibromo-4,5-dichlorophenol	-60.4	-43.1	-68.7	-68.7	-68.7
2,4-dibromo-3,6-dichlorophenol	-57.8	-40.5	-71.3	-71.3	-71.3
2,6-dibromo-3,5-dichlorophenol	-54.3	-37.0	-74.8	-74.9	-74.8
2,4-dibromo-3,5-dichlorophenol	-58.9	-41.6	-70.2	-70.2	-70.2
2,6-dibromo-3,4-dichlorophenol	-56.8	-39.5	-72.3	-72.4	-72.4
3,4-dibromo-2,6-dichlorophenol	-60.4	-43.1	-68.7	-68.7	-68.7
2,3-dibromo-4,6-dichlorophenol	-59.3	-42.0	-69.8	-69.9	-69.8
3,5-dibromo-4,6-dichlorophenol	-61.4	-44.1	-67.7	-67.8	-67.8
2,6-dibromo-3,4,5-trichlorophenol	-88.2	-67.4	-75.6	-74.9	-75.2
3,4-dibromo-2,5,6-trichlorophenol	-92.3	-71.5	-71.5	-70.8	-71.1
2,4-dibromo-3,5,6-trichlorophenol	-89.3	-68.4	-74.5	-73.8	-74.2
2,3-dibromo-4,5,6-trichlorophenol	-90.6	-69.7	-73.2	-72.5	-72.9
2,3,4-tribromo-6-chlorophenol	-61.7	-42.8	-14.4	-16.1	-15.2
2,3,4-tribromo-5-chlorophenol	-63.2	-44.4	-12.9	-14.5	-13.7
2,3,6-tribromo-4-chlorophenol	-59.6	-40.8	-16.5	-18.1	-17.3
2,3,5-tribromo-4-chlorophenol	-62.6	-43.7	-13.5	-15.2	-14.3
2,4,6-tribromo-3-chlorophenol	-58.1	-39.2	-18.0	-19.7	-18.9

CHAPTER 4 Thermodynamic Parameters Including Acid Dissociation Constants for Bromochlorophenols (BCPhs)

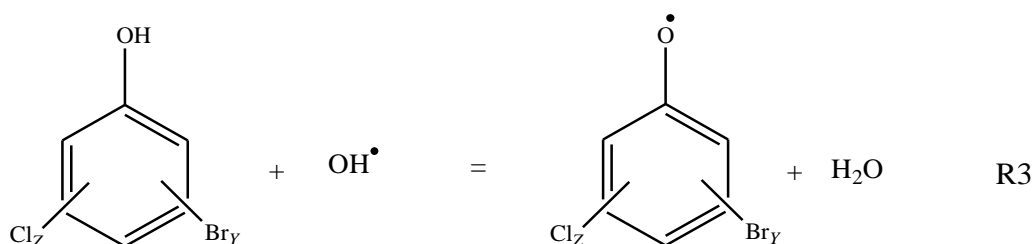
2,4,5-tribromo-3-chlorophenol	-61.9	-43.1	-20.5	-15.8	-18.2
2,3,4-tribromo-5,6-dichlorophenol	-93.5	-71.1	-17.3	-18.2	-17.8
2,3,5-tribromo-4,6-dichlorophenol	-93.1	-70.7	-17.7	-18.5	-18.1
2,5,6-tribromo-3,4-dichlorophenol	-91.1	-68.7	-19.7	-20.6	-20.1
3,4,5-tribromo-2,6-dichlorophenol	-96.2	-73.8	-14.6	-15.5	-15.1
2,3,4,5-tetrabromo-6-chlorophenol	-97.4	-73.4	39.6	37.1	38.3
2,3,4,6-tetrabromo-5-chlorophenol	-94.6	-70.7	36.9	34.4	35.7
2,3,5,6-tetrabromo-4-chlorophenol	-95.3	-71.3	37.5	35.0	36.3

The two isodesmic reactions yield close estimates of $\Delta_f H^\circ_{298}$, with the recommended $\Delta_f H^\circ_{298}$ corresponding to the average values. The uncertainty limit of the two isodesmic reactions (u_j) follows from the orthogonal addition of the uncertainty associated with each $\Delta_f H^\circ_{298}$ of the reference species; i.e., as $(\sum u_i^2)^{1/2}$. The overall uncertainty in enthalpy of formation is thus estimated as $1/2 * [\sum (u_j^2)]^{1/2}$ [67]. Table 4.4 presents typical overall uncertainty values for three BCPh congeners.

Table 4.4. Calculated uncertainty in $\Delta_f H^\circ_{298}$ of three congeners of bromochlorophenol in kJ mol^{-1} .

Compound Name	Reaction 1	Reaction 2	Overall uncertainty
	u_j	u_j	
3-bromo-2-chlorophenol	2.2	2.7	1.7
3,4-dibromo-2-chlorophenol	4.4	4.7	3.2
2,4,5-tribromo-3-chlorophenol	6.5	6.7	4.6

Values of $\Delta_f H^\circ_{298}$ for selected bromochlorophenoxy radicals are calculated based on Reaction R3:



CHAPTER 4 Thermodynamic Parameters Including Acid Dissociation Constants for Bromochlorophenols (BCPhs)

Scheme 2. An isodesmic reaction for obtaining the standard enthalpy of formation of BCPh radicals.

Reaction R3 deploys experimental values of $\Delta_f H^\circ_{298}$ for H₂O (-241.8 ± 0.040 kJ mol⁻¹) [68] and OH (37.3 ± 0.13 kJ mol⁻¹) [68] with calculated values of $\Delta_f H^\circ_{298}$ for BCPhs listed in Table 4.3. Table 4.5 presents calculated $\Delta_f H^\circ_{298}$ values for a series of 19 bromochlorophenoxy radicals. While we have considered isomers of all plausible BCPh molecules, we elect to choose representative isomers of radicals of BCPhs in each homologue group. As demonstrated in the upcoming discussion, the degree of halogenation has a minimal effect on the properties among the isomers in each homologue.

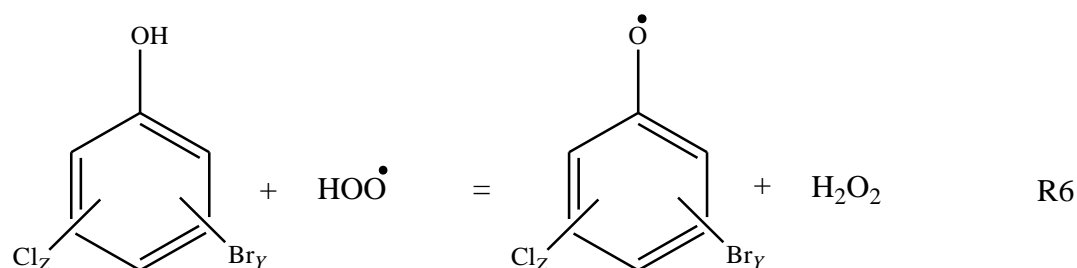
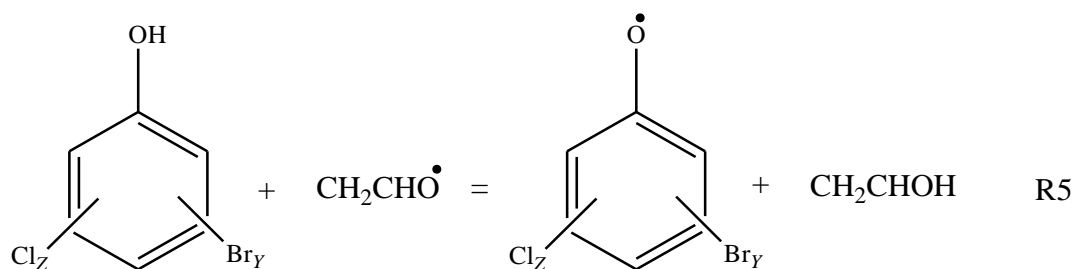
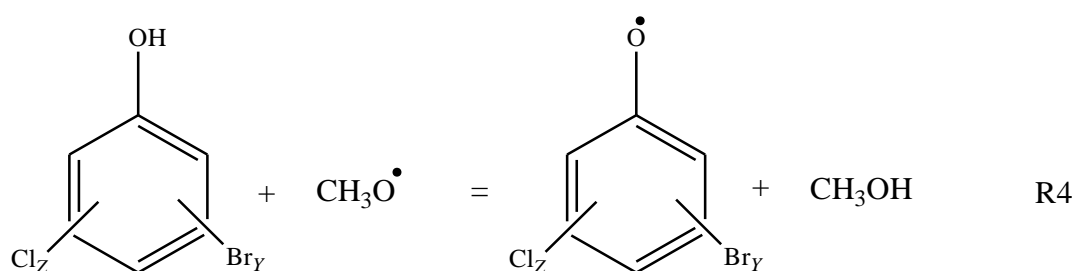
Table 4.5. $\Delta_{R3} H^\circ_{298}$ for R3 (kJ), $\Delta_f H^\circ_{298}$ (kJ mol⁻¹) of selected bromochlorophenoxy radicals and BDH of O-H bond in selected BCPh molecules (kJ mol⁻¹).

Compound Name	$\Delta_{R3} H^\circ_{298}$	$\Delta_f H^\circ_{298}$	BDH
3-bromo-2-chlorophenoxy radical	-106.6	77.1	390.4
4-bromo-3-chlorophenoxy radical	-115.0	75.2	382.0
2-bromo-4-chlorophenoxy radical	-112.6	64.5	384.4
3-bromo-2,4-dichlorophenoxy radical	-111.1	59.0	385.9
4-bromo-2,3,6-trichlorophenoxy radical	-116.4	38.7	380.6
3-bromo-4,5,6-trichloro-phenoxy radical	-107.6	48.5	389.4
2-bromo-3,4,5,6-tetrachlorophenoxy radical	-111.9	38.2	385.1
3,4-dibromo-2-chlorophenoxy radical	-109.9	115.0	387.0
2,6-dibromo-4-chlorophenoxy radical	-117.9	96.5	379.0
2,3-dibromo-4-chlorophenoxy radical	-109.7	114.3	387.3
3,5-dibromo-2,4-dichlorophenoxy radical	-107.4	104.0	389.6
2,3-dibromo-6,4-dichlorophenoxy radical	-116.0	93.3	381.0
2,3-dibromo-4,5,6-trichloro-phenoxy radical	-113.9	92.0	383.0
2,4,5-tribromo-3-chlorophenoxy radical	-104.7	194.9	392.2
2,3,5-tribromo-4-chlorophenoxy radical	-106.2	159.4	390.8
2,3,6-tribromo-4-chlorophenoxy radical	-115.3	147.3	381.7
3,4,5-tribromo-2,6-dichlorophenoxy radical	-113.9	150.6	383.1
2,5,6-tribromo-3,4-dichlorophenoxy radical	-113.0	146.4	384.0

2,3,5,6-tetrabromo-4-chlorophenoxy radical	-113.7	202.9	383.3
--	--------	-------	-------

4.3.4. Bond dissociation enthalpies

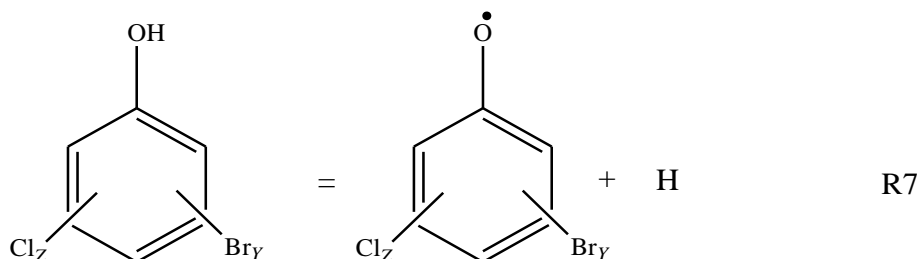
We estimate the bond dissociation enthalpies (BDH) of O-H bond in 19 BCPh congeners based on values of $\Delta_f H^\circ_{298}$ of BCPhs (Table 4.3) and bromochlorophenoxy radicals (Table 4.5) using three isodesmic reactions:



Scheme 3. Isodesmic reaction for estimating of O-H bond dissociation enthalpies (see text for explanation).

Reaction R7 signifies a direct fission of the O-H bond. In principle, values of BDHs of O-H bonds follows directly from R7. However, in order to improve accuracy of calculated results, we applied the isodesmic reactions R4-R6 to compute the BDH of the O-H bonds by applying equation (E1) [69]. This is due to the ability of R4-R6 isodesmic reactions to

maintain the same number and type of bonds on both sides of the reactions, to cause the cancellation of systematic errors in calculation of reaction enthalpies.



Scheme 4. Direct fission of the O-H bond in halogenated phenols.

Prior to taking averages, BDH for O-H bonds in BCPhs are calculated separately from each isodesmic reaction (R4 – R6). For example, Equation E1 presents a formula for obtaining the BDHs for Reaction R4:

$$\text{BDH (BCPh)} = \Delta_{\text{R4}}H^{\circ}_{298} + \Delta_{\text{f}}H^{\circ}_{298}(\text{H}) - \Delta_{\text{f}}H^{\circ}_{298}(\text{CH}_3\text{OH}) + \Delta_{\text{f}}H^{\circ}_{298}(\text{CH}_3\text{O}\cdot)$$

E1

Reactions R4-R6 deploy the experimental values of $\Delta_{\text{f}}H^{\circ}_{298}$ of $\text{CH}_3\text{O}\cdot$ ($18.57 \pm 2.9 \text{ kJ mol}^{-1}$) [70], CH_3OH ($-200.93 \pm 0.21 \text{ kJ mol}^{-1}$) [71], $\text{CH}_2\text{CHO}\cdot$ ($12.87 \pm 2.1 \text{ kJ mol}^{-1}$) [72], CH_2CHOH ($-125.31 \pm 2.1 \text{ kJ mol}^{-1}$) [73], $\text{HOO}\cdot$ ($13.37 \pm 2.09 \text{ kJ mol}^{-1}$) [74] and H_2O_2 ($-135.98 \pm 0.21 \text{ kJ mol}^{-1}$) [75]. The final BDHs correspond to averages based on Reactions R4-R6; see the right most column in Table 4.5 for numerical values of BDHs, for selected BCPh congeners.

Our calculated BDH values of O-H bond in BCPh congeners fall in the range of 379.0 to 392.4 kJ mol^{-1} . These values are in agreement with the analogue estimates of BDH reported in literature for O-H in phenol (370.0 to 374.4 kJ mol^{-1}) [69] and substituted phenols (356.1 to 383.6 kJ mol^{-1}) [76]. We remark that, patterns and degrees of halogenation induce a fairly slight variation in O-H BDHs.

4.3.5. Gibbs energies of formation of BCPhs and their anions in gaseous and aqueous phases

Table 4.6 lists the standard Gibbs energy of formation ($\Delta_f G^\circ_{298}$) for selected BCPhs congeners, based on computed $\Delta_f H^\circ_{298}$ and S°_{298} of BCPh molecules as presented in Equation E2:

$$\begin{aligned} \Delta_f G^\circ_{298(\text{gas})} = & \Delta_f H^\circ_{298} - TS^\circ_{298} \text{ (BCPh congeners)} \\ & + T \sum S^\circ_{298} \text{ (elements in their standard state)} \end{aligned} \quad \text{E2}$$

We extracted the values of S°_{298} for elements from reference [72]. Free energies of solvation (ΔG^*_{solv}) are estimated using an integral equation formalism polarisable continuum model based on the HF/6-31+G(d) optimised aqueous-phase geometries [52-53], whereas, the calculations of Gibbs free energy of formation in aqueous phase ($\Delta_f G^{\text{aq}}_{298}$) follow Equation E3:

$$\Delta_f G^{\text{aq}}_{298} = \Delta G^*_{\text{solv}} + \Delta_f G^\circ_{298} \quad \text{E3}$$

Table 4.6 presents values of ΔG^*_{solv} and $\Delta_f G^{\text{aq}}_{298}$. Calculated estimates of ΔG^*_{solv} indicate no discernible influence of the pattern and degree of halogenation on the phenol ring. This seems to be in contrast to results of previous theoretical predictions for chlorinated isomers of aniline and benzoic acid where ΔG^*_{solv} decrease with degree of chlorination [76-77].

Table 4.6. Standard Gibbs energies of formation in the gas phase $\Delta_f G^\circ_{298}$, Gibbs free energies of solvation ΔG^*_{solv} , and standard Gibbs free energies in aqueous phase $\Delta_f G^{\text{aq}}_{298}$ for selected mixed halogenated congeners of phenol. Note that, $\Delta_f G^\circ_{298}$ for the remaining BCPhs can be obtained directly from Equation E2. All values are in kJ mol^{-1} .

Compound Name	$\Delta_f G^\circ_{298}$	ΔG^*_{solv}	$\Delta_f G^{\text{aq}}_{298}$
Phenol	308.6	-26.9	281.7

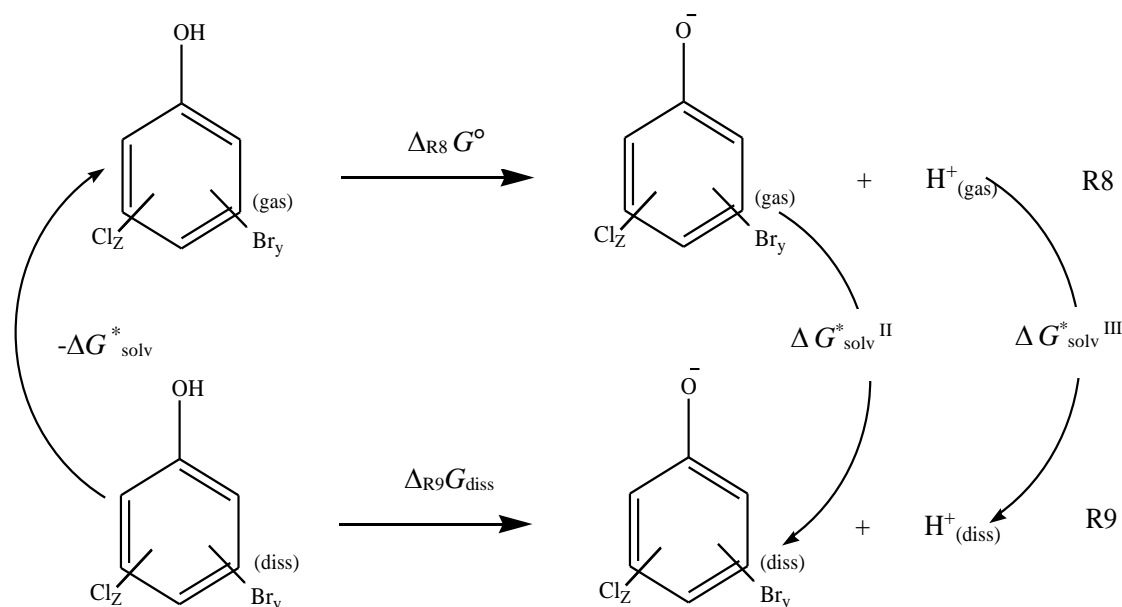
CHAPTER 4 Thermodynamic Parameters Including Acid Dissociation Constants for Bromochlorophenols (BCPhs)

<i>o</i> -chlorophenol	272.3	-20.1	252.2
<i>m</i> -chlorophenol	291.8	-27.7	264.2
<i>p</i> -chlorophenol	299.4	-28.0	271.4
<i>o</i> -bromophenol	367.2	-20.0	347.2
3-bromo-2-chlorophenol	356.7	-21.1	335.6
4-bromo-3-chlorophenol	362.1	-29.3	332.7
2-bromo-4-chlorophenol	349.7	-20.3	329.3
3-bromo-2,4-dichlorophenol	349.5	-22.3	327.2
4-bromo-2,3,6-trichlorophenol	343.6	-23.5	320.1
3-bromo-4,5,6-trichlorophenol	341.7	-21.8	319.8
3,4-dibromo-2-chlorophenol	403.6	-22.6	380.9
2,6-dibromo-4-chlorophenol	392.7	-28.3	364.4
2,3-dibromo-4-chlorophenol	403.1	-21.9	381.2
3,5-dibromo-4,6-dichlorophenol	396.6	-22.4	374.2
2,3-dibromo-4,6-dichlorophenol	394.3	-23.3	371.0
2,6-dibromo-3,5-dichlorophenol	389.3	-29.4	359.9
2,3-dibromo-4,5,6-trichlorophenol	397.8	-24.1	373.7
2,4,5-tribromo-3-chlorophenol	486.5	-22.1	464.4
2,3,5-tribromo-4-chlorophenol	450.6	-22.1	428.5
2,3,6-tribromo-4-chlorophenol	447.8	-23.5	423.8
3,4,5-tribromo-2,6-dichlorophenol	455.8	-31.7	424.1
2,5,6-tribromo-3,4-dichlorophenol	450.6	-30.9	419.9
2,3,5,6-tetrabromo-4-chlorophenol	507.9	-31.8	476.2

4.3.6. Acid dissociation constants (pK_a)

Biochemical and environmental applications require knowledge of pH dependence of deprotonation of substituted phenolic compounds. Theoretical determination of pK_a typically involves constructing a thermodynamic cycle that deploys values of gas-phase deprotonation energies, gas-phase Gibbs' energies of formation, as well as solvation energies of BCPhs and their corresponding anions. Computations of pK_a also comprise experimentally determined values of solvation and gas-phase energy for H^+ [78]. In

calculations of Scheme 8, we employed the derived value of $G_{\text{gas}}(\text{H}^+) = -26.3 \text{ kJ mol}^{-1}$ from the Sackur Tetrode equation [79] and the experimental measurement of $\Delta G_{\text{solv}}^* \text{ III} = 1107.1 \text{ kJ mol}^{-1}$ [80].



Scheme 5. Thermodynamic cycle for calculating pK_a .

Liptak et al. [81] applied the analogous thermodynamic cycle to derive accurate predictions of the absolute pK_a values for substituted phenols. In their cycle, they computed the gas-phase deprotonation energies ($\Delta_{\text{R8}}G^\circ$) using the CBS-QB3 composite method where R8 represents dissociation of halogenated phenols into their analogous phenolate anions and H^+ cations. Solvation energies were estimated based on the conductor-like polarisable continuum model (CPCM) and HF/6-31+G(d) optimised geometries for aqueous-phase. In the present study, we calculate $\Delta_{\text{R8}}G^\circ$ at the M06/6-311+(3df,2p)/M062X/6-311+g(d,p) level of theory and the solvation energies; i.e., ΔG_{solv}^* and $\Delta G_{\text{solv}}^{*\text{ II}}$, at the (UHF)IEFPCM/HF/6-31+G(d) level, based on optimised solvated phase geometries. The correction term $RT \ln(24.46)$ is added to the values of $\Delta_{\text{R8}}G^\circ$ to switch the reference state from the gas phase of 1 atm to the aqueous phase of 1 M; i.e., $\Delta_{\text{R8}}G^*$. Table 4.7 summarises the calculated values of pK_a based on Equation E5.

CHAPTER 4 Thermodynamic Parameters Including Acid Dissociation Constants for Bromochlorophenols (BCPhs)

$$\Delta_{R8}G^\circ = \Delta_f G^\circ(\text{halogenated phenolate}) + \Delta_f G^\circ(\text{H}^+) - \Delta_f G^\circ(\text{halogenated phenol}) \quad \text{E4}$$

$$pK_a = \frac{\Delta_{R8}G^* - \Delta G_{solv}^* + \Delta G_{solv}^{*II} + \Delta G_{solv}^{*III}}{2.303 RT} \quad \text{E5}$$

$$\text{where } \Delta_{R8}G^* = \Delta_{R8}G^\circ + RT \ln(24.46) \quad \text{E6}$$

Table 4.7. Calculated pK_a of phenol and selected halogenated phenols. Gibbs energy values are in kJ mol^{-1} .

Compound Name	$\Delta_{R8}G^\circ_g$	$\Delta G^*_{solv}^{II}$	$\Delta_{R9}G_{dis}$	calc	exptl	pK_a^{81}	Marvin
				pK_a	pK_a		pK_a^{95}
Phenol	1398.1	-268.7	56.1	9.83	9.98 ⁹⁴	9.88	10.02
<i>o</i> -chlorophenol	1385.3	-254.3	50.8	8.9	8.56 ⁹²	7.66	8.0
<i>m</i> -chlorophenol		-246.9	50.0	9.8	9.12 ⁹²	9.29	8.8
	1375.4						
<i>p</i> -chlorophenol	1369.0	-248.5	49.3	8.6	9.3 ⁹²	9.84	8.9
<i>o</i> -bromophenol	1380.4	-250.3	49.9	8.7	8.5 ⁹³		8.2
3-bromo-2-chlorophenol	1356.9	-237.6	40.3	7.1			7.3
4-bromo-3-chlorophenol	1349.8	-226.9	52.1	9.1			
2-bromo-4-chlorophenol	1355.0	-229.4	45.7	8.0			
3-bromo-2,4-dichlorophenol	1338.9	-222.5	38.5	6.7			
4-bromo-2,3,6-trichlorophenol	1306.7	-210.1	19.9	3.4			
3-bromo-4,5,6-trichlorophenol	1314.8	-208.3	28.1	4.9			
3,4-dibromo-2-chlorophenol	1335.4	-220.0	37.8	6.6			
2,6-dibromo-4-chlorophenol	1320.8	-215.9	33.0	5.7			
2,3-dibromo-4-chlorophenol	1336.8	-223.0	35.6	6.2			
3,5-dibromo-4,6-dichlorophenol	1313.9	-208.0	28.2	4.9			
2,3-dibromo-4,6-dichlorophenol	1307.4	-210.1	20.5	3.6			
2,6-dibromo-3,5-dichlorophenol	1301.4	-206.9	23.9				
				4.1			

CHAPTER 4 Thermodynamic Parameters Including Acid Dissociation Constants for Bromochlorophenols (BCPhs)

2,3-dibromo-4,5,6-trichlorophenol	1291.2	-201.8	13.4	2.3
2,4,5-tribromo-3-chlorophenol	1310.9	-205.0	27.8	4.8
2,3,5-tribromo-4-chlorophenol	1312.3	-206.1	28.2	4.9
2,3,6-tribromo-4-chlorophenol	1304.4	-207.6	20.2	3.5
3,4,5-tribromo-2,6-dichlorophenol	1289.8	-202.4	19.1	3.3
2,5,6-tribromo-3,4-dichlorophenol	1289.7	-200.3	20.2	3.5
2,3,5,6-tetrabromo-4-chlorophenol	1290.7	-200.3	22.0	3.8

To set a further benchmark for the accuracy of the calculated Gibbs energies of solvation, we compute herein gas-phase and aqueous-phase acidities for *m*- and *p*-chlorophenols with respect to phenol according to the general reaction $C_6H_5O^- + AH \rightarrow C_6H_5OH + A^-$ in which A signifies *m*-/*p*-chlorophenol. Values in the aqueous phase are based on optimised geometries in the aqueous medium. Contrasting values with analogous experimental estimates yield a satisfactory agreement. For example, our calculated gas and aqueous phase acidities for *m*-chlorophenol are $-25.5 \text{ kJ mol}^{-1}$ and -3.3 kJ mol^{-1} , respectively. These two values are in a reasonable agreement with analogous literature values of -29.7 [82]/ -33.1 [83] and -3.3 kJ mol^{-1} [82-83]; in that order. While deploying a thermodynamic cycle to predict pK_a values produces accurate results for carboxylic acids and phenol, some serious drawbacks were documented for certain classes of organic acids [84]. Substantial errors in predicting pK_a values may originate from the fundamental shortcoming of quantum chemical methods in evaluating solvation energies for ionic species that can induce the discrepancy of 7 or more units in estimated pK_a in comparison with experimentally measured values [85]. Other contributing factors include the significant difference in the experimental and/or theoretical values of proton solvation energies in the range between -1083.6 and $-1114.6 \text{ kJ mol}^{-1}$ [80, 85]. Nevertheless, the present method yields relatively accurate pK_a values for a wide variety of organic systems [86-88].

In case of mixed halogenated phenols, we find that pK_a values depend strongly on the degree of bromination and chlorination on phenol ring. From the results of the

calculations, we deduce that, the substitution of a large number of bromine and chlorine atoms on the phenol ring induces stronger acidity, with such compounds expected to dissociate more easily in aqueous media in comparison with less halogenated BCPh congeners as depicted in figure 4.3.

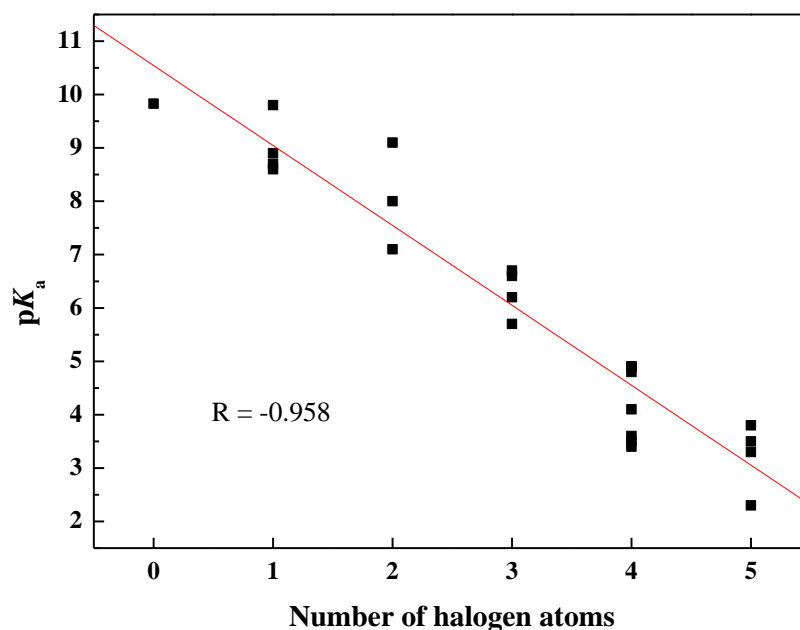


Figure 4.3. Correlation between the calculated acid dissociation constant (pK_a) and the number of halogen atoms attached to the aromatic ring.

Analogously, Li et al. [89] measured the pK_a values of polychlorinated congeners of phenols experimentally and point out to a decreasing trend for pK_a values as the number of chlorine atoms attached to the aromatic ring increase. To demonstrate the accuracy and reliability of our predictions of pK_a values, in Table 4.7 we compare the calculated values of pK_a for phenol, *o*-chlorophenol, *m*-chlorophenol, *p*-chlorophenol, and *o*-bromophenol with the measurements available in literature [80, 90-94]. As well as with estimates from the Marvin software [95] which deploys a neural network algorithm. For example, our calculated pK_a value for phenol is 9.83; in good agreement with another theoretical estimate of 9.88 offered by Liptak et al. [81]. While obtaining values of $\Delta_{R8}G^\circ$ based on the CBS-QB3 - as in the study by Liptak et al. [81] - might be computationally unfeasible for high-molecular-weight halogenated phenols, we have shown in this study a more computationally affordable approach for estimating pK_a .

4.4. Conclusions

The present chapter provides standard gas-phase enthalpies of formation, entropies and heat capacities for the complete series of bromochlorophenols, as well as standard aqueous-phase Gibbs energies of formation and pK_a for 19 selected congeners of bromochlorophenols. Overall, optimised structures exhibit minor changes in geometrical features. Although the calculated Gibbs energies of solvation of bromochlorophenols in water are highly exoergic, with the free energy of solvation increasing with the degree of substitution, the free energy change of the dissociation (Reaction R9) displays an opposite trend, mirrored by pK_a . This is because Reaction R9 includes other contributions, especially the gas-phase deprotonation energies that decrease with the increase in degree of halogen substitution. Thus, we conclude that, bromochlorophenols characterised by high degree of halogenation display stronger acidity and dissociate more easily in aqueous media (i.e., they are stronger acids than lower substituted phenols).

Supporting information

Cartesian coordinates for optimised structures and NASA polynomials for selected congeners. This material is available in appendix B (attached in CD). The authors declare no competing financial interest.

References

- [1] Balasundram, N., Sundram, K., Samman, S. Phenolic compounds in plants and agriindustrial by-products: Antioxidant activity, occurrence, and potential uses. *Food. Chem.* **2006**, *99*, 191-203.
- [2] Felton, L.C., McLaughlin, C.B. Some highly halogenated phenolic ethers as fungistatic compounds. *J. Org. Chem.* **1947**, *12*, 298-302.
- [3] Armenante, P.M. Anaerobic-aerobic treatment of halogenated phenolic compounds. *Water. Res.* **1999**, *33*, 681-692.
- [4] Swietoslowski, J., Silowiecki, A., Ratajczak, A., Nocon, B., Less, B.Z. Process for production of 4,4-isopropylidene-bis-2,6-dibromo/phenol. US4112242 A, **1987**.
- [5] Sim, W.J., Lee, S.H., Lee, I.S., Choi, S.D., Oh, J.E. Distribution and formation of chlorophenols and bromophenols in marine and riverine environments. *Chemosphere.* **2009**, *77*, 552-558.
- [6] Abrahamsson, K., Klick, S. Degradation of halogenated phenols in anoxic natural marine sediments. *Mar. Pollut. Bull.* **1991**, *22*, 227-233.
- [7] Rayne, S., Forest, K., Friesen, K.J. Mechanistic aspects regarding the direct aqueous environmental photochemistry of phenol and its simple halogenated derivatives. A review. *Environ. Int.* **2009**, *35*, 425-437.
- [8] Leuenberger, C., Giger, W., Coney, R., Graydon, J.W., Molnar, E.K. Persistent chemicals in pulp mill effluents: Occurrence and behaviour in an activated sludge treatment plant. *Water. Res.* **1985**, *19*, 885-894.
- [9] Gupta, V. K., Ali, I., Saini, V. K. Removal of chlorophenols from wastewater using red mud: An aluminum industry waste. *Environ. Sci. Technol.* **2004**, *38*, 4012-4018.
- [10] Schüler, D., Jager, J. Formation of chlorinated and brominated dioxins and other organohalogen compounds at the pilot incineration plant VERONA. *Chemosphere.* **2004**, *54*, 49-59.
- [11] Castillo, M., Puig, D., Barcelo, D. Determination of priority phenolic compounds in water and industrial effluents by polymeric liquid-solid extraction cartridges using automated sample preparation with extraction columns and liquid chromatography use of liquid-solid extraction cartridges for stabilization of phenols. *J. Chromatogr. A.* **1997**, *778*, 301-311.

- [12] Schaefer, W., Ballschmiter, K. Monobromo-polychloro-derivatives of benzene, biphenyl, dibenzofurane and dibenzodioxine formed in chemical-waste burning. *Chemosphere*. **1986**, 15, 755-763.
- [13] Heeb, N.V., Dolezal, I.S., Buhner, T., Mattrel, P., Wolfensberger, M. Distribution of halogenated phenols including mixed brominated and chlorinated phenols in municipal waste incineration flue gas. *Chemosphere*. **1995**, 31, 3033-3041.
- [14] Hovander, L., Malmberg, T., Athanasiadou, M., Athanassiadis, I., Rahm, S., Bergman, A., Wehler, E. K. Identification of hydroxylated PCB metabolites and other phenolic halogenated pollutants in human blood plasma. *Arch. Environ. Con. Tox.* **2002**, 42, 105-117.
- [15] Sandau, C.D. Analytical Chemistry of Hydroxylated Metabolites of PCBs and Other Halogenated Phenolic Compounds in Blood and Their Relationship to Thyroid Hormone and Retinol Homeostasis in Humans and Polar Bears. Thesis, Carleton University, Ottawa, Canada, **2000**.
- [16] Qu, X., W, Hui., Zhang, Q., Shi, X., Xu, F., Wang, W. Mechanistic and kinetic studies on the homogeneous gas-phase formation of PCDD/Fs from 2,4,5-trichlorophenol. *Environ. Sci. Technol.* **2009**, 43, 4068-4075.
- [17] Acero, J.L., Piriou, P., Gunten, V.U. Kinetics and mechanisms of formation of bromophenols during drinking water chlorination: Assessment of taste and odor development. *Water. Res.* **2005**, 39, 2979-2993.
- [18] Mahoney, L.R., DaRooge, M.A. Kinetic behavior and thermochemical properties of phenoxy radicals. *J. Am. Chem. Soc.* **1975**, 97, 4722-4731.
- [19] Han, J., Deming, R.L., Tao, F.M. Theoretical study of molecular structures and properties of the complete series of chlorophenols. *J. Phys. Chem. A.* **2004**, 108, 7736-7743.
- [20] Han, J., Lee, H., Tao, F.M. Molecular structures and properties of the complete series of bromophenols: Density functional theory calculations. *J. Phys. Chem. A.* **2005**, 109, 5186-5192.
- [21] Weber, L.W., Greim, H. The toxicity of brominated and mixed-halogenated dibenzo-*p*-dioxins and dibenzofurans: An overview. *J. Toxicol. Env. Health.* **1997**, 50, 195-215.

- [22] Behnisch, P.A., Hosoe, K., Sakai, S. Combinatorial bio/chemical analysis of dioxin and dioxin-like compounds in waste recycling, feed/food, humans/wildlife and the environment. *Environ. Int.* **2001**, 27, 495-519.
- [23] Poland, A., Knutson, J.C. 2,3,7,8-tetrachlorodibenzo-*p*-dioxin and related halogenated aromatic hydrocarbons: examination of the mechanism of toxicity. *Annu. Rev. Pharmacol. Toxicol.* **1982**, 22, 517-54.
- [24] Cormier, A.S., Lomnicki, S., Backes, W., Dellinger, B. Origin and health impacts of emissions of toxic by-products and fine particles from combustion and thermal treatment of hazardous wastes and materials. *Environ. Health. Perspect.* **2006**, 114(6), 810–817.
- [25] Xiezhi, Y., Markus, Z., Magnus, E., Anna, R., Maria, L., Hung, M.W., Roland, W. E-waste recycling heavily contaminates a Chinese city with chlorinated, brominated and mixed halogenated dioxins. *Organohalogen Compd.* **2008**, 70, 813-816.
- [26] Olsman, H., Engwall, M., Kammann, U., Klempt, M., Otte, J., Van Bavel, B., Hollert, H. Relative differences in aryl hydrocarbon receptor-mediated response for 18 polybrominated and mixed halogenated dibenzo-*p*-dioxins and furans in cell lines from four different species. *Environ. Toxicol. Chem.* **2007**, 26, 2448-2454.
- [27] Samara, F., Wyrzykowska, B., Tabor, D., Touati, D., Gullett, B.K. Toxicity comparison of chlorinated and brominated dibenzo-*p*-dioxins and dibenzofurans in industrial source samples by HRGC/HRMS and enzyme immunoassay. *Environ. Int.* **2010**, 36, 247-253.
- [28] Hayakawa, K., Takatsuki, H., Watanabe, I., Sakai, S. Polybrominated diphenyl ethers (PBDEs), polybrominated dibenzo-*p*-dioxins/dibenzofurans (PBDD/Fs) and monobromo-polychlorinated dibenzo-*p*-dioxins/dibenzofurans (MoBPXDD/Fs) in the atmosphere and bulk deposition in Kyoto, Japan. *Chemosphere.* **2004**, 57, 343–356.
- [29] Myers, L.A., Mabury, A.S., Reiner, J.E. Analysis of mixed halogenated dibenzo-*p*-dioxins and dibenzofurans (PXDD/PXDFs) in soil by gas chromatography tandem mass spectrometry (GC-MS/MS). *Chemosphere.* **2012**, 87(9):1063-1069.
- [30] Unger, M., Asplund, L., Haglund, P., Malmvarn, A., Arnoldsson, K., Gustafsson, O. Polybrominated and mixed brominated/chlorinated dibenzo-*p*-dioxins in

- sponge (*Ephydatia fluviatilis*) from the Baltic Sea. *Environ. Sci. Technol.* **2009**, 43, 8245–8250.
- [31] Huang, L.Q., Tong, H.Y., Donnelly, J.R. Characterization of dibromopolychlorodibenzo-*p*-dioxins and dibromopolychlorodibenzofurans in municipal waste incinerator fly ash using gas chromatography/mass spectrometry. *Anal. Chem.* **1992**, 64, 1034-1040.
- [32] Chatkittikunwong, W., Creaser, C.S. Bromo-, bromochloro- and chloro-dibenzo-*p*-dioxins and dibenzofurans in incinerator fly ash. *Chemosphere.* **1994**, 29, 559-566.
- [33] Du, B., Zheng, M., Huang, Y., Liu, A., Tian, H., Li, L., Li, N., Ba, T., Li, Y., Dong, S., Liu, W., Su, G. Mixed polybrominated/chlorinated dibenzo-*p*-dioxins and dibenzofurans in stack gas emissions from industrial thermal processes. *Environ. Sci. Technol.* **2010**, 44, 5818-5823.
- [34] Söderström, G., Marklund, S. Formation of PBCDD and PBCDF during flue gas cooling. *Environ. Sci. Technol.* **2004**, 38, 825-30.
- [35] Schwind, K.H., Hosseinpour, J., Thoma, H. Brominated/chlorinated dibenzo-*p*-dioxins and dibenzofurans: Part 1: brominated/chlorinated and brominated dibenzo-*p*-dioxins and dibenzofurans in fly ash from a municipal waste incinerator. *Chemosphere.* **1988**, 17, 1875-1884.
- [36] Evans, C.S., Dellinger, B. Formation of bromochlorodibenzo-*p*-dioxins and dibenzofurans from the high-temperature oxidation of a mixture of 2-chlorophenol and 2-bromophenol. *Environ. Sci. Technol.* **2006**, 40, 3036-3042.
- [37] Evans, C.S., Dellinger, B. Formation of bromochlorodibenzo-*p*-dioxins and furans from the high-temperature pyrolysis of a 2-chlorophenol/2-bromophenol mixture. *Environ. Sci. Technol.* **2005**, 39, 7940-7948.
- [38] Weber, R., Kuch, B. Relevance of BFRs and thermal conditions on the formation pathways of brominated and brominated–chlorinated dibenzodioxins and dibenzofurans. *Environ. Int.* **2003**, 29, 699-710.
- [39] Mosallanejad, S., Dlugogorski, B.Z., Kennedy, E.M., Stockenhuber, M., Altarawneh, M. Formation of dibenzo-*p*-dioxins and dibenzofurans in oxidation of 2-chlorophenol over iron oxide/silica surface. *Organohalogen Compd.* **2013**, 75, 919-923.

- [40] Mosallanejad, S., Dlugogorski, Z.B., Altarawneh, M., Kennedy, M.E., Yokota, M., Nakano, T., Stockenhuber, M. Decomposition of 2-chlorophenol on surfaces of neat alumina and alumina supported iron (iii) oxide catalysts. *Organohalogen Compd.* **2014**, 76, 396-399.
- [41] Lemieux, P.M., Stewart, E.S., Ryan, J.V. Pilot-scale studies on the effect of bromine addition on the emissions of chlorinated organic combustion by-products. *Waste. Manag.* **2002**, 22, 381-389.
- [42] Lemieux, P.M., Stewart, E.S. A pilot scale study of the precursors leading to the formation of mixed bromo-chloro dioxins and furans. *Environ. Eng. Sci.* **2004**, 21, 3-9.
- [43] Weber, R., Kuch, B., Ohno, T., Sakurai, T. De novo synthesis of mixed brominated-chlorinated PXDD/PXDF. *Organohalogen Compd.* **2002**, 56, 181-184.
- [44] Lemieux, P.M., Ryan, J.V. Enhanced formation of chlorinated PICs by the addition of bromine. *Combust. Sci. Technol.* **1998**, 134, 367-387.
- [45] Evans, C.S., Dellinger, B. Mechanisms of dioxin formation from the high temperature pyrolysis of 2-bromophenol. *Environ. Sci. Technol.* **2003**, 37, 5574-5580.
- [46] Howe, P.D., Dobson, S., Malcolm, H.M. 2,4,6-tribromophenol and other simple brominated phenols, Data Set for 2,4,6-tribromophenol. Concise International Chemical Assessment Document 66, World Health Organization, Geneva, **2005**.
- [47] Sidhu, S.S., Maqsd, L., Dellinger, B., Mascolo, G. The homogeneous gas-phase formation of chlorinated and brominated dibenzo-*p*-dioxin from 2,4,6-trichloro- and 2,4,6-tribromophenols. *Combust. Flame* **1995**, 100, 11-20.
- [48] Karasek, F.W., Dickson, L.C. Model studies of polychlorinated dibenzo-*p*-dioxin formation during municipal refuse incineration. *Science.* **1987**, 237, 754-756.
- [49] Milligan, M.S., Altwicker, E.R. Chlorophenol reactions on fly ash. 1. adsorption/desorption equilibria and conversion to polychlorinated dibenzo-*p*-dioxin. *Environ. Sci. Technol.* **1995**, 30, 225-229.
- [50] Frisch, M.J., Trucks, G.W., Schlegel, H.B., Scuseria, G.E., Robb, M.A., Cheeseman, J. R., Scalmani, G., Barone, V., Mennucci, B., Petersson, G.A., Nakatsuji, H., Caricato, M., Li, X., Hratchian, H.P., Izmaylov, A.F., Bloino, J., Zheng, G., Sonnenberg, J.L., Hada, M., Ehara, M., Toyota, K., Fukuda, R.,

- Hasegawa, J., Ishida, M., Nakajima, T., Honda, Y., Kitao, O., Nakai, H., Vreven, T., Montgomery, J.A., Jr., Peralta, J.E., Ogliaro, F., Bearpark, M., Heyd, J.J., Brothers, E., Kudin, K.N., Staroverov, V.N., Kobayashi, R., Normand, J., Raghavachari, K., Rendell, A., Burant, J.C., Iyengar, S. S., Tomasi, J., Cossi, M., Rega, N., Millam, N.J., Klene, M., Knox, J.E., Cross, J.B., Bakken, V., Adamo, C., Jaramillo, J., Gomperts, R., Stratmann, R.E., Yazyev, O., Austin, A.J., Cammi, R., Pomelli, C., Ochterski, J.W., Martin, R.L., Morokuma, K., Zakrzewski, V.G., Voth, G.A., Salvador, P., Dannenberg, J.J., Dapprich, S., Daniels, A.D., Farkas, Ö., Foresman, J.B., Ortiz, J.V., Cioslowski, J., Fox, D.J. Gaussian 09, Revision D.01, Gaussian, Inc., Wallingford, CT, 2009.
- [51] Zhao, Y., Truhlar, D. The M06 suite of density functionals for main group thermochemistry, thermochemical kinetics, noncovalent interactions, excited states, and transition elements: two new functionals and systematic testing of four M06-class functionals and 12 other functionals. *Theor. Chem. Acc.* **2008**, *120*, 215-241.
- [52] Mokrushin, V., Bedanov, V., Tsang, W., Zachariah, M., Knyazev, V. ChemRate, version 1.19. *NIST: Gaithersburg, MD* **2002**.
- [53] Cancès, E., Mennucci, B., Tomasi, J. A new integral equation formalism for the polarizable continuum model: Theoretical background and applications to isotropic and anisotropic dielectrics. *J. Chem. Phys.* **1997**, *107*, 3032-3041.
- [54] Mennucci, B., Cancès, E., Tomasi, J. Evaluation of solvent effects in isotropic and anisotropic dielectrics and in ionic solutions with a unified integral equation method: Theoretical bases, computational implementation, and numerical applications. *J. Phys. Chem. B*, **1997**, *101*, 10506–10517.
- [55] Carlson, G.L., Fateley, W.G., Manocha, A.S., Bentley, F.F. Torsional frequencies and enthalpies of intramolecular hydrogen bonds of *o*-halophenols. *J. Phys. Chem.* **1972**, *76*, 1553-1557.
- [56] Altarawneh, M., Dlugogorski, B.Z., Kennedy, E.M., Mackie, J.C. Quantum chemical and kinetic study of formation of 2-chlorophenoxy radical from 2-chlorophenol: Unimolecular decomposition and bimolecular reactions with H, OH, Cl, and O₂. *J. Phys. Chem. A*. **2008**, *112*, 3680–3692.

- [57] Zierkiewicz, W., Michalska, D., Zeegers, H.T. Molecular structures and infrared spectra of *p*-chlorophenol and *p*-bromophenol. Theoretical and experimental studies. *J. Phys. Chem. A*, **2000**, 104, 11685-11692.
- [58] Czarnik, M.B., Chandra, A.K., Tho, N.M., Zeegers, H.T. Theoretical and experimental (400–10000 cm⁻¹) study of the vibrational spectrum of pentachlorophenol. *J. Mol. Spectrosc.* **1999**, 195, 308-316.
- [59] Pfaendtner, J., Yu, X., Broadbelt, L. The 1 D hindered rotor approximation. *Theor. Chem. Acc.* **2007**, 118, 881-898.
- [60] Cox, J.D. The heats of combustion of phenol and the three cresols. *Pure Appl. Chem.* **1961**, 2, 125-128.
- [61] Zhu, L., Bozzellia, J.W. Thermochemical properties, $\Delta_f H^\circ$ (298.15 K), S° (298.15 K), and $C_p^\circ(T)$, of 1,4-dioxin, 2,3-benzodioxin, furan, 2,3-benzofuran, and twelve monochloro and dichloro dibenzo-*p*-dioxins and dibenzofurans. *J. Phys. Chem. Ref. Data.* **2003**, 32, 1713-1735.
- [62] Ribeiro da Silva, M.A.V., Lobo Ferreira, A.I.M.C. Gas phase enthalpies of formation of monobromophenols. *J. Chem. Thermodyn.* **2009**, 41 (10), 1104-1110.
- [63] Rappoport, Z. (editor) *The Chemistry of Phenol.* **2003**, 2, Wiley.
- [64] Roux, M.V., Temprado, M., Chickos, J.S., Nagano, Y. Critically evaluated thermochemical properties of polycyclic aromatic hydrocarbons. *J. Phys. Chem. Ref. Data.* **2008**, 37, 1855-1996.
- [65] Cox, J.D., Pilcher, G. Thermochemistry of organic and organometallic compounds. *Academic Press, London.* **1970**, 74, 727.
- [66] Cox, J.D., Wagman, D.D., Medvedev, V.A. CODATA key values for thermodynamics, Hemisphere Publishing Corp. *Hemisphere Publishing Corp., New York*, **1984**.
- [67] Simmie, J.M., Black, G., Curran, H.J., Hinde, J.P. Enthalpies of formation and bond dissociation energies of lower alkyl hydroperoxides and related hydroperoxy and alkoxy radicals. *J. Phys. Chem. A.* **2008**, 112, 5010-5016.
- [68] Ruscic, B., Pinzon, E.R., Morton, L.M., Srinivasan, K.N., Su, M., Sutherland, W.J., Michael, V.J. Active thermochemical tables: Accurate enthalpy of formation of hydroperoxyl radical, HO₂. *J. Phys. Chem. A* **2006**, 110 (21), 6592-6601.
- [69] Dasilva, G., Chen, C.C., Bozzelli, J.W. Bond dissociation energy of the phenol OH bond from ab initio calculations. *Chem. Phys. Lett.* **2006**, 424, 42-45.

- [70] Blanksby, S.J., Ellison, G.B. Bond dissociation energies of organic molecules. *Acc. Chem. Res.* **2003**, 36, 255-263.
- [71] Green, J.H.G. Revision of the values of the heats of formation of normal alcohols. *Chem. Ind. (London)* **1960**, 1215-1216.
- [72] da Silva, G., Kim, C.H., Bozzelli, J.W. Thermodynamic properties (enthalpy, bond energy, entropy, and heat capacity) and internal rotor potentials of vinyl alcohol, methyl vinyl ether, and their corresponding radicals. *J. Phys. Chem. A.* **2006**, 110, 7925-7934.
- [73] Holmes, J.L., Lossing, F.P. Heats of formation of the ionic and neutral enols of acetaldehyde and acetone. *J. Am. Chem. Soc.* **1982**, 104, 2648-2649.
- [74] Ramond, T.M., Blanksby, S.J., Kato, S., Bierbaum, V.M., Davico, G.E., Schwartz, R. L., Lineberger, W.C., Ellison, G.B. Heat of formation of the hydroperoxyl radical HOO via negative ion studies. *J. Phys. Chem. A.* **2002**, 106, 9641-9647.
- [75] Chase, M.W. NIST-JANAF Thermochemical Tables. *J. Phys. Chem. Ref. Monograph 9. J. Phys. Chem. Ref. Data.* **1998**, 1-1951.
- [76] Chandra, K.A., Uchimaru, T. The O-H bond dissociation energies of substituted phenols and proton affinities of substituted phenoxide ions: A DFT study. *Int. J. Mol. Sci.* **2002**, 3, 407-422.
- [77] Rayne, S., Forest, K. Accuracy of computational solvation free energies for neutral and ionic compounds: dependence on level of theory and solvent model. *Nature Precedings.* **2010**, DOI: 10.1038/npre.2010.4864.1.
- [78] Altarawneh, I., Altarawneh, K., Al-Muhtaseb, A.H., Alrawadieh, S., Altarawneh, M. Theoretical study of thermochemical and structural parameters of chlorinated isomers of aniline. *Comp. Theor. Chem.* **2012**, 985, 30-35.
- [79] McQuarrie, D.M. *Statistical Mechanics*, New York, Harper and Row, **1970**.
- [80] Tang, A., Wang, L., Zhou, R. Gibbs energies of formation of chlorinated benzoic acids and benzoates and application to their reductive dechlorination. *J. Mol. Struct.* **2010**, 960, 31-39.
- [81] Liptak, D.M., Gross, C.K., Seybold, G.P., Feldgus, S., Shields, C.G. Absolute pK_a determination for substituted phenols. *J. Am. Chem. Soc.* **2002**, 124, 6421-6427.

- [82] Fujio, M., McIver, R.T., Taft, W.R. Effects on the acidities of phenol from specific substituent-solvent interactions. Inherent substituent parameters from gas-phase acidities. *J. Am. Chem. Soc.* **1981**, 103, 4017-4029.
- [83] Arnett, E.M., Small, E.L., Oancea, D., Johnston, D. Heats of ionization of some phenols and benzoic acids in dimethyl sulfoxide. Heats of solvation of oxyanions in dimethyl sulfoxide and water. *J. Am. Chem. Soc.* **1976**, 98, 7346-7350.
- [84] Liptak, M.D., Shields, G.C. Experimentation with different thermodynamic cycles used for pK_a calculations on carboxylic acids using complete basis set and Gaussian models combined with CPCM continuum solvation methods. *Int. J. Quant. Chem.* **2001**, 85, 727-741.
- [85] Bryantsev, S.V., Diallo, S.M., Goddard, W.A. Calculation of solvation free energies of charged solutes using mixed cluster/continuum models. *J. Phys. Chem. B.* **2008**, 112, 9709-9719.
- [86] Ho, J., Coote, L.M. A universal approach for continuum solvent pK_a calculations: Are we there yet? *Theor. Chem. Acc.* **2010**, 125, 3-21.
- [87] Kelly, P.C., Cramer, J.C., Truhlar, G.D. Aqueous solvation free energies of ions and ion-water clusters based on an accurate value for the absolute aqueous solvation free energy of the proton. *J. Phys. Chem. B.* **2006**, 110, 16066-16081.
- [88] Kallies, B., Mitzner, R. pK_a values of amines in water from quantum mechanical calculations using a polarized dielectric continuum representation of the solvent. *J. Phys. Chem. B.* **1997**, 101, 2959-2967.
- [89] Li, S., Paleologou, M., Purdy, C.W. Determination of the acidity constants of chlorinated phenolic compounds by liquid chromatography. *J. Chromatogr. Sci.* **1991**, 29, 66-69.
- [90] Busch, M.S., Knapp, W.E. Accurate pK_a determination for a heterogeneous group of organic molecules. *Chem. Phys. Chem.* **2004**, 5, 1513 - 1522.
- [91] Pliego, R.J., Riveros, M.J. Theoretical calculation of pK_a using the cluster-continuum model. *J. Phys. Chem. A.* **2002**, 106, 7434-7439.
- [92] Jencks, W.P., Regenstein, J. Ionization constants for acids and bases. *In Handbook of Biochemistry and Molecular Biology.* Ed Fasman, G.D. 305-351.
- [93] *National Library of Medicine, HSDB Data Base*, 2-Bromophenol. *Hazardous substance Databank Number* 7648.

CHAPTER 4 Thermodynamic Parameters Including Acid Dissociation Constants for Bromochlorophenols (BCPhs)

- [94] Albert, A., Serjeant, E.P. Ionization constants of acids and bases. New York, John Willey & Sons Inc., **1962**, 1-41.
- [95] Szegezdi, J., Csizmadia, F. A method for calculating the pK_a values of small and large molecules. ChemAxon Ltd, Maramaros koz 3/a, 1037 Budapest, Hungary.

CHAPTER 5 PHOTODECOMPOSITION OF BROMOPHENOLS

The following is a modified version of the published paper:

Anam Saeed, Mohammednoor Altarawneh, Bogdan Z. Dlugogorski (2015), Chemosphere 150, 749-758

Table of Content

Abstract	180
5.1. Introduction	181
5.2. Computational details	182
5.3. Results and discussion	183
5.3.1. Optimised geometries for BPhs in ground and first excited states	183
5.3.2. Effect of degree and pattern of bromination on the photoreactivity	187
5.3.3. UV-Vis absorption	191
5.4. Conclusions	199
Acknowledgments	199
References	201

Abstract

Photodecomposition of bromophenols (BPhs) represents a potent channel of debromination and elimination of these species in the environment. From this perspective, the present contribution (chapter 5) reports geometrical parameters, electronic absorption spectra and excited states of the complete series of BPhs in their ground state (S_0), as well as their first singlet excited state (S_1). We calculate excitation energies for $S_0 \rightarrow S_1$ transition within the framework of the time-dependent density functional theory (TDDFT). We estimate and discuss charges on bromine atoms and HOMO-LUMO energy gaps (E^{H-L}) as molecular descriptors for the photo reactivity of BPhs and photo-induced debromination mechanism of BPhs. Spectral patterns reveal that, as the degree of bromination increases, peaks of absorption spectra red-shift toward wavelengths near 300 nm, for the pentabrominated phenol. Based on the analysis of optimised geometries and Hirshfeld's atomic charges, photodebromination of BPhs commences via the loss of an *ortho* Br atom. Overall, we demonstrate a linear correlation between numbers of bromine atoms in BPhs and excitation energies. This indicates that, higher brominated congeners of BPhs photodecompose more readily than lower brominated congeners.

5.1. Introduction

Bromophenols (BPhs) constitute principal components and intermediates in the production of a wide range of brominated flame retardants (BFRs). Structural entities of several BFRs such as tetrabromobisphenol A (TBBA) and polybrominated diphenyl ethers (PBDEs) incorporate moieties of BPhs. As a result, thermal decomposition of materials laden with BFRs often produce appreciable amounts of BPhs [1-5]. When non-bonded chemically to the polymeric matrix of treated objects, BFRs can leach out under ambient conditions [6-8]. Photodecomposition of desorbed BFRs into BPhs represents a chief route for diminishing the overall environmental burden of BPhs. For instance, de Wit et al. [9] found that, 2,4,6-tribromophenol evolves as a major product from exposure of TBBA to strong UV light. In addition to their well-established role as building blocks for the notorious polybrominated dibenzo-*p*-dioxin and polybrominated dibenzofuran (PBDD/F) pollutants [10-16], bromophenols exhibit strong toxicological effects [17-18], depending primarily on the pattern and degree of bromination [19].

Beside the oxidation of BPhs by atmospherically-persistent OH radicals [20], the photodecomposition process induced by sun radiation affords another potent elimination pathway of these chemicals in the environment [21]. Using theoretical and experimental approaches, great deal of research has revealed fundamental understanding pertinent to photodissociation of halogenated aromatics in aqueous media [22-28]. Depending on the type and position of halogens, fission of the halogen-carbon bond proceeds via multiple electronic states. A detailed dynamic analysis by the first principle calculations attributes the photodecomposition of aryl halides to non-adiabatic phenomena in which intersystem crossing occurs at 266 nm and involves a transition from singlet excited state to triplet excited state [29-32].

Studies on photodecomposition of brominated aromatics have mainly focused on PBDEs [25, 28] and bromobenzenes [23-24]. Relatively, few enquiries investigated photo-induced decomposition of monobromophenols by flash spectroscopy and photo fragment translational spectroscopy techniques [33-34]. These studies reported a monobromophenol molecule releasing a bromine atom from breaking the C-Br bond and a hydrogen atom originating from the fission of the hydroxyl O-H bond, under the UV

radiation. Joschek and Miller (1966) [33] suggested that, the photodecomposition of the C-Br bond in the monobromophenols proceeds via absorption of $472.7 \text{ kJ mol}^{-1}$. This considerable amount of energy engenders the excitation of the molecule and fission of the C-Br bond. During the photolysis process, fission of the C-Br bond in the ground state and the formation of the first lying singlet excited state require $343.0 \text{ kJ mol}^{-1}$ and $387.0 \text{ kJ mol}^{-1}$, respectively [24, 35]. Experimental [36-37] and theoretical [36, 38-39] studies reveal that, the dissociation of the C-Br bond in bromobenzene occurs via an intersystem crossing between (π, π^*) and (n, σ^*) states. Along the same line of enquiry, in our previous theoretical investigations, we have computed the Gibbs free energy of solvation and acid dissociation constant values for several substituted benzene [40-42].

To gain an atomic insight into the decomposition behaviour of BPhs under UV light, this contribution reports results of a time-dependent density functional theory (TDDFT) study into the electronic and geometrical properties for the complete series of BPhs. TDDFT provides detailed and accurate description for the excitation process of hydrocarbons [43-45]. We also elucidate the effect of the aqueous media on the photolytic reactivity of BPh molecules. We describe the effects of pattern and degree of bromination by calculating the partitioning of electronic density over all atoms in BP molecules, based on the Hirshfeld atomic-charge analysis [46-47]. We also investigate the lowest excitation energies for the singlet state and compute the oscillation strength to characterise the ability of BPh congeners to reach the excited state. The latter process initiates the C-Br bond cleavage. To this end, this study: (i) reports geometries of BPh congeners in the ground and first excited levels for both gas and aqueous phases, (ii) estimates the atomic charges on BPh molecules in both states, and (iii) links the thermal stability and photo reactivity of BPhs with prominent electronic descriptors.

5.2. Computational details

Structure optimisations for complete series of BPhs were performed using the DMol³ code [48] with the GGA-PW91 functional [49]. Our calculational methodology comprised a cut-off radius of 4.4 \AA and a double numerical basis set with d polarisation (DND) (1998). We obtained aqueous phase geometries by employing a conductor-like screening model (COSMO) [50-51]. Calculations of the excited states involved the TDDFT method with

adiabatic local exchange density functional approximation (ALDA). We set the tolerance for geometrical convergence to 10^{-6} Ha. Optical properties of molecules in ground and excited state entailed computations based on optimised ground state molecular structures. The TDDFT method afforded the computation of HUMO-LUMO energy gap of molecular orbitals, electronic excitation energies, oscillator strengths and UV-absorption spectra. Atomic charges for the most photoreactive bromine atom in BPh molecules followed from the Hirshfeld atomic population analysis [52]. Among the various computational formalisms that estimate atomic charges, Hirshfeld's analysis offers the most accurate methodology [47, 52].

5.3. Results and discussion

5.3.1. Optimised geometries for BPhs in ground and first excited states

The change in structure between ground state (S_0) and excited state (S_1) provides valuable information on the subsequent photodecomposition pathways. As conveyed in the introduction, the general consensus [26, 36, 39] indicates that, the aromatic carbon-halogen bond elongates when excited to the S_1 state. Theoretical studies on the photochemistry of the reductive debromination of PBDEs [26, 53] report significantly different geometries in the ground and excited states. These investigations discovered no elongation of the C-Br bond at the *para* position and distinct lengthening of the C-Br bond at the *ortho* position as function of the pattern of bromination.

Tables 5.1 and 5.2 enlist the calculated C-Br bond lengths for all BPh congeners in gaseous and aqueous media, respectively. We limit our discussion to the C-Br bonds as changes in all other geometries between S_0 and S_1 states, including the hydroxyl O-H bonds, remain negligible. Inspection of the extension of C-Br bonds in BPhs in the excited S_1 state, compared to bond lengths in the ground S_0 state, as listed in Tables 5.1, leads to the following findings:

- For lower brominated congeners ($n_{\text{Br}} \leq 2$), the most profound elongation of C-Br bond occurs at the *ortho* position. Corresponding distances at *meta* and *para* positions are either shortened or marginally lengthened. For example, C-Br bond in 2-MBPh

elongates by 12.4 % while analogous distances in 3-MBPh and 4-MBPh contract by 1.1 % and 1.6 %, respectively. In the 2,6-DBPh isomer, one of the two *ortho* C-Br bonds exhibits significant elongation of 10.5 % whereas the other C-Br bond stretches minimally by 2.5 %. Our finding, with regard to the minimal elongation of *para* C-Br bonds, accords with the relevant TDDFT results in the literature [26, 54-56] on PBDEs. These studies found that, bromine at *para* position resists photolytic elimination.

CHAPTER 5 Photodecomposition of Bromophenols (BPhs)

Table 5.1. Comparison of geometrical parameters for all 19 congeners of bromophenols in ground (S_0) and excited state (S_1) in gas phase. Bond lengths are in Å.

BPhs congener	Number of Br atoms	S_0	S_1
2-MBPh	1	1.934	2.174
3-MBPh	1	1.926	1.906
4-MBPh	1	1.926	1.896
2,3-DBPh	2(2,3)	1.922;1.916	2.082;2.014
2,4-DBPh	2(2,4)	1.930;1.923	2.126;1.959
2,5-DBPh	2(2,5)	1.929;1.922	2.088;1.932
2,6-DBPh	2(2,6)	1.933;1.916	2.135;1.963
3,4-DBPh	2(3,4)	1.915;1.914	2.069;1.998
3,5-DBPh	2(3,5)	1.922;1.922	2.019;2.030
2,3,4-TriBPh	3(2,3,4)	1.922;1.907;1.914	2.045;2.004;1.942
2,3,5-TriBPh	3(2,3,5)	1.919;1.913;1.919	2.030;2.036;1.929
2,3,6-TriBPh	3(2,3,6)	1.922;1.913;1.913	2.092;1.976;1.914
2,4,5-TriBPh	3(2,4,5)	1.926;1.912;1.912	2.027;1.985;1.969
2,4,6-TriBPh	3(2,4,6)	1.929;1.920;1.913	2.086;1.954;1.969
3,4,5-TriBPh	3(3,4,5)	1.915;1.905;1.915	2.015;1.967;2.004
2,3,4,5-TBPh	4(2,3,4,5)	1.920;1.907;1.906;1.913	1.996;2.006;1.944;1.942
2,3,4,6-TBPh	4(2,3,4,6)	1.922;1.905;1.913;1.911	2.051;1.971;1.948;1.919
2,3,5,6-TBPh	4(2,3,5,6)	1.920;1.911;1.911;1.904	2.043;1.972;1.948;1.920
2,3,4,5,6-PBPh	5(2,3,4,5,6)	1.921;1.906;1.907;1.906;1.905	1.997;1.966;1.948;1.948;1.925

Table 5.2. Comparison of geometrical parameters for all 19 congeners of bromophenols in ground (S_0) and excited state (S_1) in aqueous phase. Bond lengths are in Å.

BPhs congener	Number of Br atoms	S_0	S_1
2-MBPh	1	1.953	2.209
3-MBPh	1	1.952	2.232
4-MBPh	1	1.953	1.898
2,3-DBPh	2(2,3)	1.940;1.939	2.091;2.054
2,4-DBPh	2(2,4)	1.946;1.947	2.133;1.988
2,5-DBPh	2(2,5)	1.946;1.946	2.130;1.986
2,6-DBPh	2(2,6)	1.950;1.941	2.125;2.029
3,4-DBPh	2(3,4)	1.938;1.938	2.103;2.027
3,5-DBPh	2(3,5)	1.946;1.945	2.081;2.080
2,3,4-TriBPh	3(2,3,4)	1.939;1.928;1.937	2.039;2.039;1.963
2,3,5-TriBPh	3(2,3,5)	1.935;1.934;1.941	2.028;2.071;1.944
2,4,5-TriBPh	3(2,4,5)	1.941;1.934;1.934	1.977;2.029;2.022
2,4,6-TriBPh	3(2,4,6)	1.944;1.942;1.936	2.072;1.972;2.014
3,4,5-TriBPh	3(3,4,5)	1.937;1.927;1.937	2.031;1.992;2.030
2,3,4,5-TBPh	4(2,3,4,5)	1.935;1.927;1.927;1.934	1.980; 2.030;1.969;1.960
2,3,4,6-TBPh	4(2,3,4,6)	1.937;1.924;1.933;1.932	2.047;1.996;1.966;1.930
2,3,5,6-TBPh	4(2,3,5,6)	1.934;1.930;1.931;1.926	2.022;1.986;1.977;1.953
2,3,4,5,6-PBPh	5(2,3,4,5,6)	1.934;1.925;1.928;1.926;1.926	1.978;1.978;1.966;1.971;1.943

- In all BPh congeners, the degree of elongation of C-Br bonds between the S_0 and S_1 states generally follows the sequence of *ortho* > *meta* > *para* position, i.e., stretching of C-Br bonds is sensitive to the position of bromine atoms. Based on the geometries in Table 5.1, photodegradation of BPhs commences via the loss of an *ortho* Br atom. The presence of an *ortho* Br decreases bond extension at *meta* and *para* sites in reference to non-*ortho* BPh congeners. This observation follows from contrasting C-Br distances in the S_1 state in the 2,4-DBPh isomer against analogous distances in the 3,4-DBPh and 3,5-DBPh molecules.

- Apart from minimal differences, we cannot deduce a relationship between the susceptibility of BPh congeners toward photo-induced debromination (as expressed in terms of the maximum C-Br elongation in the S_1 states as compared to the relevant S_0 states) and the degree of bromination. In other words, lengthening of the *ortho* C-Br bond among tri-pentaBPh congeners displays inconsistent variation with respect to the number of substituted bromine atoms.

Next, we turn our attention to illustrate the effect of deploying water solvent on the elongation of the C-Br bonds. As disclosed in Table 5.2, extension of the C-Br bonds in excited-state BPhs in aqueous solutions slightly overshoots the corresponding separations in gaseous-phase BPhs. The minor differences in the elongation of the C-Br bonds in the S_1 state of BPhs in the gaseous and aqueous phases do not enable drawing a concluding remark with regard to the relative photodegradation reactivity in the two media.

5.3.2. Effect of degree and pattern of bromination on the photoreactivity

5.3.2.1. HOMO-LUMO energy gap (E^{H-L})

The difference in energy between frontier molecular orbitals, the highest occupied molecular orbital (HOMO) and the lowest unoccupied molecular orbital (LUMO), E^{H-L} , often serves as a molecular descriptor of macro scale properties of molecules and materials alike [57-58]. In the current context, the photolytic reactivity of PBDEs in various solvents correlates inversely with values of E^{H-L} [26]. This is intuitively appealing as the difference in energy between HOMO and LUMO dominates the electronic excitation energy from a S_0 state to the relevant S_1 state [25, 58-59].

Figure 5.1a assembles E^{H-L} values for all congeners of BPhs. These values decrease linearly as function of the increasing number of bromine substituents. A similar remark applies to PBDE congeners [26]. Values of E^{H-L} for all isomers reside in the relatively narrow range of 2.0 eV to 4.29 eV. As the $S_0 \rightarrow S_1$ transition mainly involves HOMO and LUMO orbitals, higher brominated congeners of BPhs are more liable to undergo excitation and display elevated susceptibility to photodecomposition.

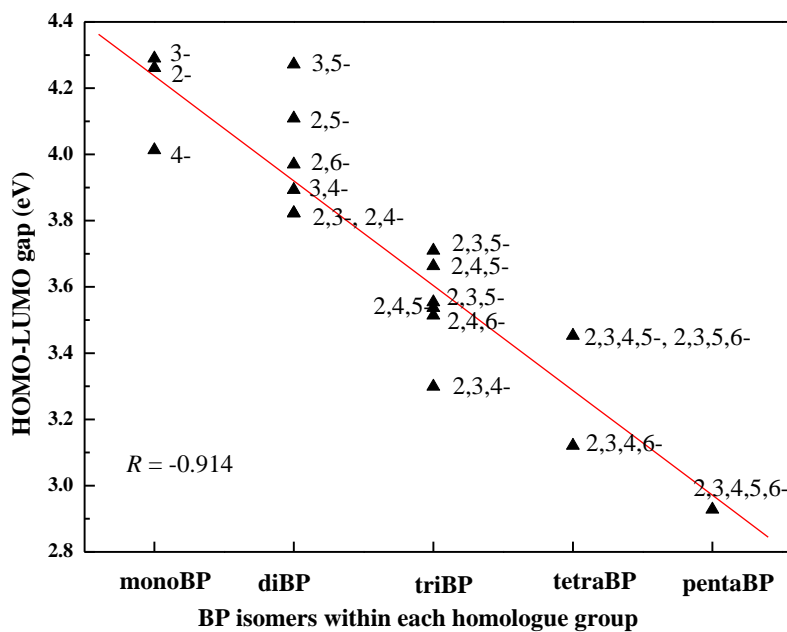


Figure 5.1a. Correlation between the frontier molecular orbitals energy E^{H-L} gap versus bromine substitution pattern.

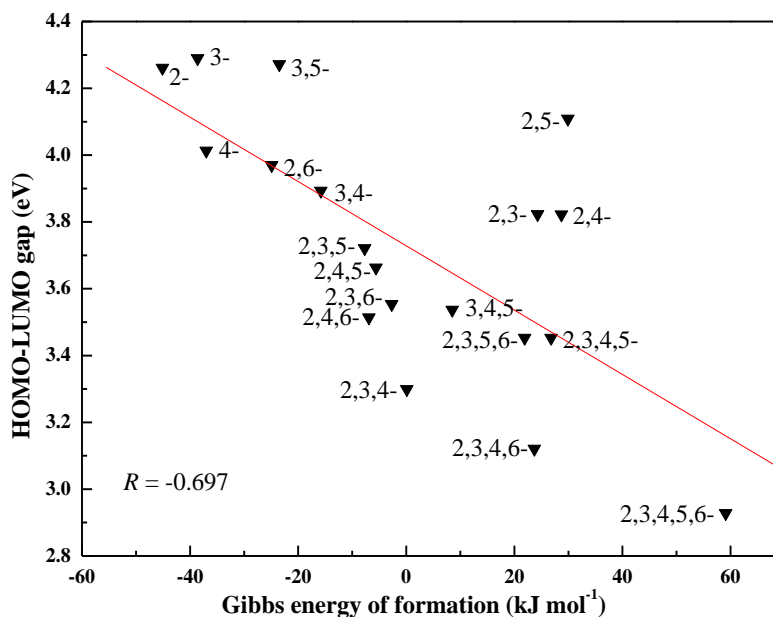


Figure 5.1b. Correlation between the frontier molecular orbitals energy E^{H-L} gap and the Gibbs free energy of formation for BPh isomers.

We now turn our attention to elucidating the effect of the degree and pattern of bromination on the photoreactivity of BPh congeners, such as linking the thermal stability

of BPhs in their ground states with their calculated $E^{\text{H-L}}$ values. Higher values of $E^{\text{H-L}}$ imply more thermodynamic stability, and hence lower $\Delta_f G^{\circ}_{298}$ values. Figure 5.1b correlates values of $E^{\text{H-L}}$ with the standard Gibbs free energies of formation ($\Delta_f G^{\circ}_{298}$) as reported in the literature [60] for all BPh congeners. As seen in the figure, 2,3,4,5,6-PBPh is the least stable congener as it displays the lowest $E^{\text{H-L}}$ energy gap and the highest $\Delta_f G^{\circ}_{298}$ value among all BPh, whereas 3-MBPh constitutes the most stable congener as it exhibits the highest $E^{\text{H-L}}$ energy gap. Positive correlation arises among homologue groups rather than among isomers within the same homologue group. Overall, a thermodynamic control on the homologue distribution of halogenated aromatics remains a matter of debate [15-16].

5.3.2.2. Atomic charges

Figure 5.2 documents atomic charges on selected atoms in all BPh congeners. Charges on bromine atoms (q_{Br}) determine to some extent their photoreactivity. The larger q_{Br} value, the easier is for the atom to depart its molecule [26-27]. Figure 5.3 reveals a positive linear correlation between the values of q_{Br} on the most photoreactive Br atoms (based on geometries in Table 5.1) and the degree of bromination. As can be deduced from Figure 5.2, net positive charges accompany all photoreactive Br atoms. The trend in q_{Br} (Figure 5.3) mirrors the decrease of $E^{\text{H-L}}$ with respect to increasing numbers of bromine atoms (Figure 5.1a). Our analysis herein coincides with other theoretical predictions on photodecomposition of C-Br bonds [26, 61]. Upon excitation, Br atoms associated with elongated bonds become more positively charged. Figure 5.3 also illustrates a linear correlation between q_{Br} in the excited S_1 state and the degree of bromination.

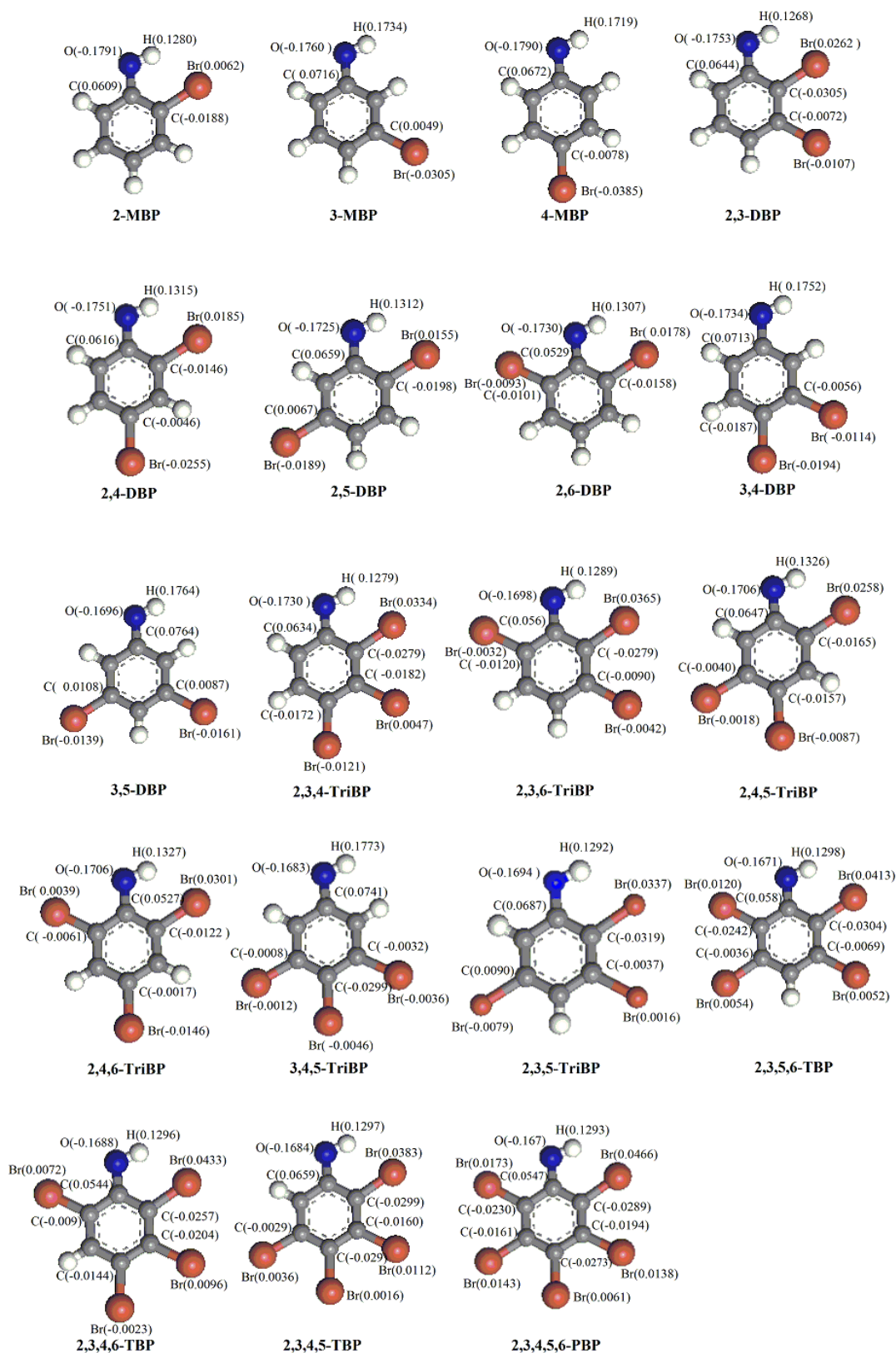


Figure 5.2. Optimised geometries of BPhs with net atomic charge presented on selected atoms.

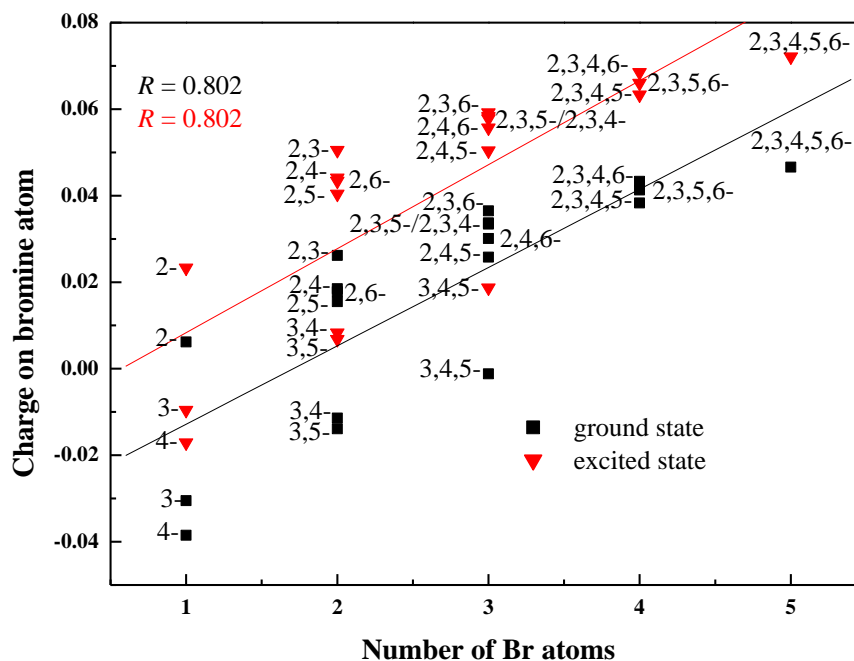


Figure 5.3. Correlation between the calculated bromine atomic charge (q_{Br}) in the S_0 and S_1 states and the number of bromine atoms.

5.3.3. UV-Vis absorption

During a photochemical process, molecules absorb energy in the form of photons to become photoexcited. The energy of photons triggers photochemical reactions that generate transient excited state. This process accelerates the photochemical reactions, readily transforming excited molecules into product species [62]. In principle, in the presence of a photocatalyst, the visible light functions as an effective environmental remediation agent that degrades the toxic organic pollutants [39, 63-65]. However, in the absence of a photocatalysts, nearly all halogenated aromatics absorb light in the UV region [66-67], away from the visible light.

Tables 5.3 and 5.4 list computed electronic excitation energies and oscillator strength values for the five lowest excited states of singlets of BPhs in gas and aqueous phase, respectively. Oscillator strength presents the probability of molecules to absorb radiations in between energy level transitions. In the aqueous phase, the oscillator strength assumes very negligible values for the five lowest excited states of singlets BPh congeners. Comparison of calculated oscillator strengths for gas (Table 5.3) and aqueous (Table 5.4) phases, illustrate that that potential for photodecomposition in water is reduced when

contrasted with the gaseous photolysis. Furthermore as Figure 5.5b indicates, excitation energies for the five lowest excited states of singlets BPh congeners in the aqueous phase entail noticeably lower values if compared with analogous gas phase values.

Table 5.3. The calculated excitation energies of molecules as photon absorption energy E (in eV) and the oscillator strength (f) of the five lowest excited states of singlets of BPh congeners in the gas phase.

	E (eV)	f	E (eV)	f	E (eV)	f
	2-MBPh		3-MBPh		4-MBPh	
S1	4.57	0.000399	4.71	0.029832	4.43	0.026043
S2	4.72	0.036871	4.87	0.000072	4.85	0.000357
S3	5.23	0.000456	5.37	0.049925	5.31	0.000102
S4	5.49	0.028575	5.45	0.000408	5.36	0.190751
S5	5.99	0.137404	5.49	0.000069	6.33	0.065168
	2,3-DBPh		2,4-DBPh		2,5-DBPh	
S1	3.96	0.000026	4.05	0.000017	4.51	0.000248
S2	4.42	0.000620	4.35	0.037232	4.52	0.045146
S3	4.62	0.023931	4.98	0.000114	4.89	0.000000
S4	5.14	0.005823	5.23	0.095048	5.01	0.000446
S5	5.24	0.029601	5.25	0.000595	5.15	0.108445
	2,6-DBPh		3,4-DBPh		3,5-DBPh	
S1	4.17	0.000348	4.11	0.000301	4.49	0.000073
S2	4.56	0.034470	4.36	0.031425	4.60	0.013772
S3	4.59	0.000169	4.82	0.000144	4.72	0.000000
S4	5.15	0.035919	4.92	0.000004	5.15	0.050797
S5	5.27	0.001742	5.14	0.024793	5.51	0.199267
	2,3,4-TriBPh		2,3,6-TriBPh		2,4,5-TriBPh	
S1	3.43	0.000006	3.69	0.000006	3.89	0.000017
S2	4.10	0.000324	4.20	0.000387	4.24	0.047110
S3	4.29	0.033757	4.40	0.037442	4.43	0.000001
S4	4.38	0.000534	4.83	0.000203	4.60	0.000550
S5	5.06	0.005647	4.96	0.100892	4.99	0.041151
	2,4,6-TriBPh		3,4,5-TriBPh		2,3,5-TriBPh	

CHAPTER 5 Photodecomposition of Bromophenols (BPhs)

S1	3.70	0.000055	3.70	0.000232	3.88	0.000058
S2	4.26	0.039287	4.13	0.000001	4.01	0.000100
S3	4.30	0.000005	4.30	0.026789	4.13	0.022173
S4	5.02	0.014778	4.40	0.000116	4.35	0.005536
S5	5.11	0.001843	4.99	0.000705	4.45	0.073409
2,3,5,6-TBPh			2,3,4,6-TBPh		2,3,4,5-TBPh	
S1	3.58	0.000017	3.24	0.000002	3.28	0.000015
S2	3.76	0.000057	3.75	0.000090	3.69	0.000071
S3	4.30	0.010963	4.17	0.039643	3.92	0.035701
S4	4.34	0.004198	4.21	0.003770	4.20	0.000001
S5	4.79	0.085102	4.52	0.001896	4.47	0.000115
2,3,4,5,6-PBPh						
S1	3.03	0.000002				
S2	3.32	0.000004				
S3	3.48	0.000009				
S4	4.11	0.027390				
S5	4.15	0.003811				

Table 5.4. The calculated excitation energies of molecules as photon absorption energy E (in eV) and the oscillator strength (f) of the five lowest excited states of singlets of BPh congeners in the aqueous phase.

	E (eV)	f	E (eV)	f	E (eV)	f
	2-MBPh		3-MBPh		4-MBPh	
S1	4.12	0.000000	4.10	0.000000	3.88	0.000000
S2	4.23	0.000000	4.24	0.000000	4.13	0.000000
S3	4.39	0.000000	4.51	0.000000	4.42	0.000000
S4	4.54	0.000000	4.60	0.000000	4.58	0.025455
S5	4.61	0.000343	4.73	0.000049	4.69	0.000000
	2,3-DBPh		2,4-DBPh		2,5-DBPh	
S1	3.83	0.000000	3.83	0.000000	3.99	0.000000
S2	3.94	0.000027	3.91	0.000000	4.14	0.000000
S3	4.05	0.000000	4.05	0.000000	4.33	0.000000

CHAPTER 5 Photodecomposition of Bromophenols (BPhs)

S4	4.12	0.000000	4.12	0.000005	4.36	0.000000
S5	4.14	0.000000	4.46	0.000000	4.59	0.000121
2,6-DBPh		3,4-DBPh		3,5-DBPh		
S1	4.02	0.000000	3.80	0.000000	4.09	0.000000
S2	4.06	0.000000	3.86	0.000000	4.13	0.000000
S3	4.13	0.000000	4.00	0.000264	4.24	0.000000
S4	4.21	0.000385	4.06	0.000000	4.33	0.000046
S5	4.33	0.000000	4.42	0.000000	4.43	0.000000
2,3,4-TriBPh		2,3,6-TriBPh		2,4,5-TriBPh		
S1	3.28	0.000000	3.64	0.000000	3.67	0.000000
S2	3.43	0.000008	3.77	0.000019	3.78	0.000000
S3	3.80	0.000074	3.90	0.000000	3.88	0.000057
S4	3.83	0.000000	3.93	0.000000	3.97	0.000002
S5	4.07	0.000270	4.07	0.000000	4.27	0.000000
2,4,6-TriBPh		3,4,5-TriBPh		2,3,5-TriBPh		
S1	3.56	0.000000	3.41	0.000000	3.73	0.000000
S2	3.74	0.000045	3.57	0.000199	3.88	0.000035
S3	3.78	0.000000	3.84	0.000000	4.04	0.000000
S4	3.96	0.000000	3.86	0.000000	4.04	0.000000
S5	4.11	0.000000	4.03	0.000000	4.19	0.000000
2,3,5,6-TBPh		2,3,4,6-TBPh		2,3,4,5-TBPh		
S1	3.50	0.000000	3.14	0.000000	3.11	0.000000
S2	3.58	0.000000	3.29	0.000001	3.26	0.000024
S3	3.62	0.000037	3.57	0.000000	3.50	0.000000
S4	3.79	0.000011	3.72	0.000000	3.67	0.000056
S5	3.85	0.000000	3.75	0.000077	3.78	0.000002
2,3,4,5,6-PBPh						
S1	2.88	0.000000				
S2	3.03	0.000003				
S3	3.15	0.000000				
S4	3.32	0.000001				
S5	3.39	0.000001				

All congeners entail very weak S_1 oscillators in the deep UV region (200-300 nm) for both gas and aqueous phase. This indicates that, BPhs could not decompose photochemically in the ambient environment. Nonetheless, UV light could be used to activate the photodecomposition process. Figure 5.4 presents the UV spectra of selected congeners of BPhs in gaseous (a) and aqueous media (b), respectively. It can be seen from Figure 5.4 that spectra in the two phases share very similar shape. Spectra of mono-triBPh congeners resolve into two intensive bands separated by a region of low absorption with an oscillator strength of less than 0.10.

CHAPTER 5 Photodecomposition of Bromophenols (BPhs)

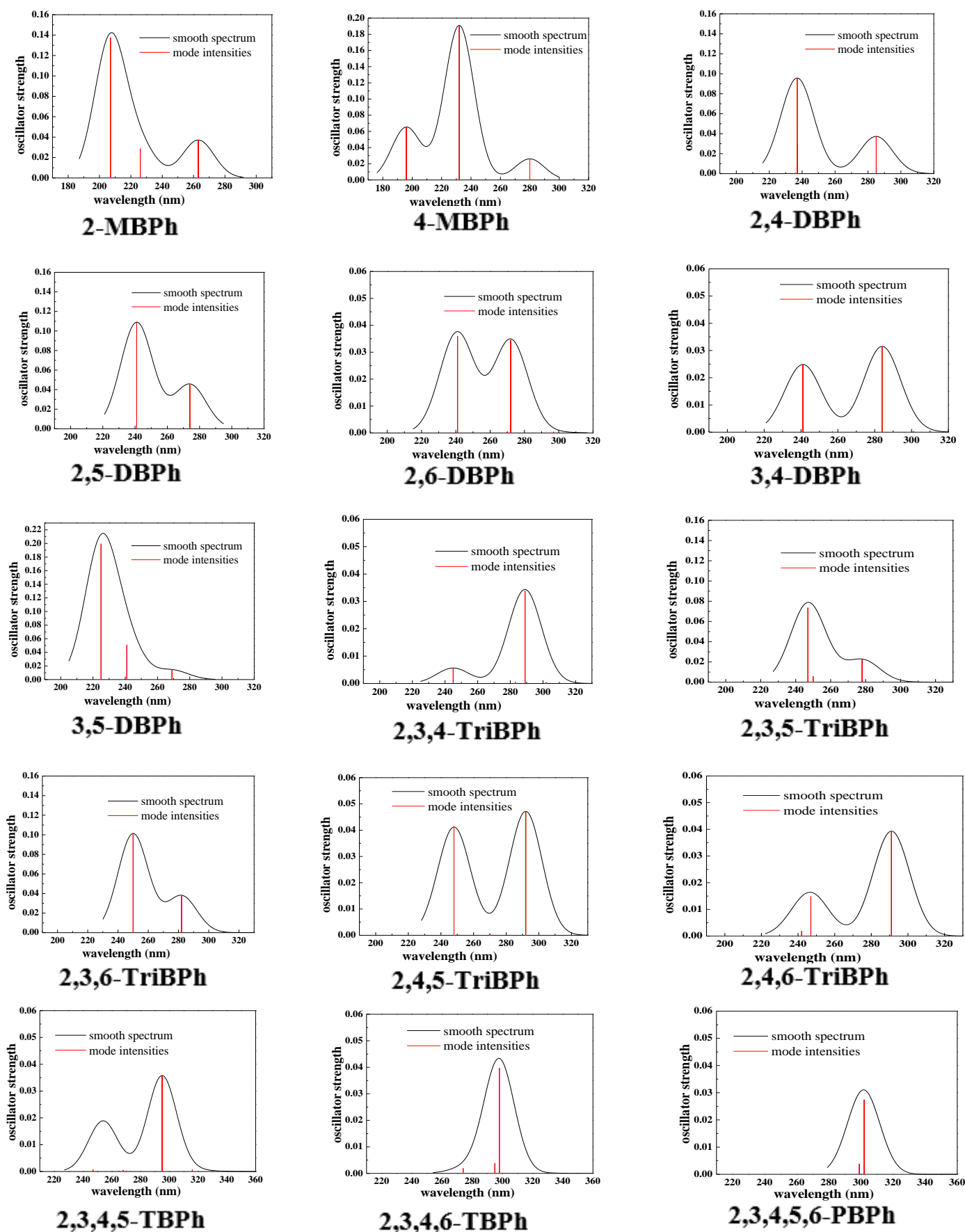


Figure 5.4a. The calculated gas-phase UV absorption spectra of selected bromophenols.

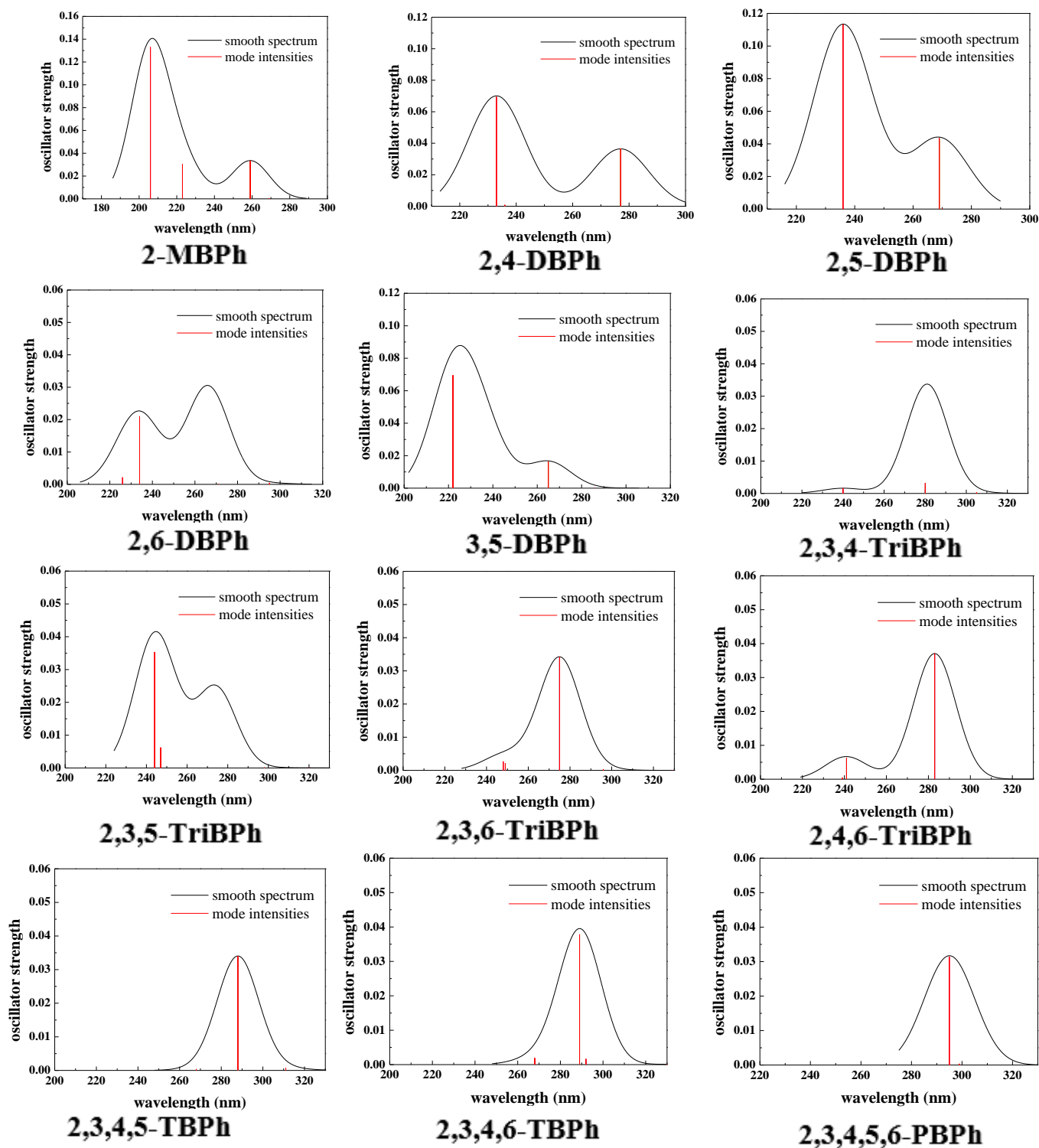
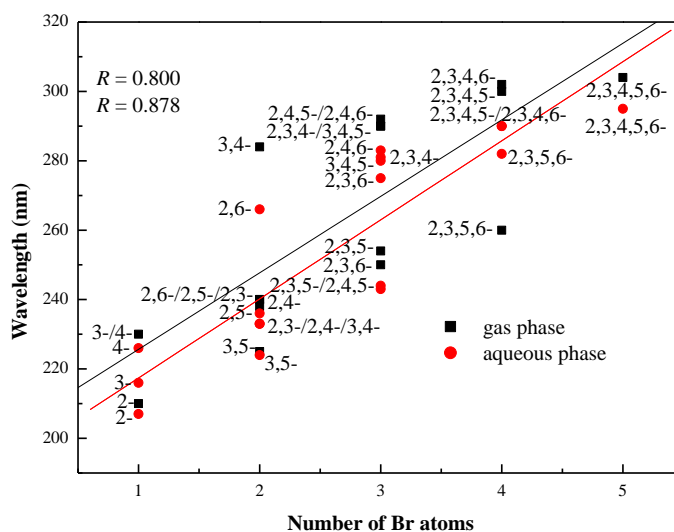


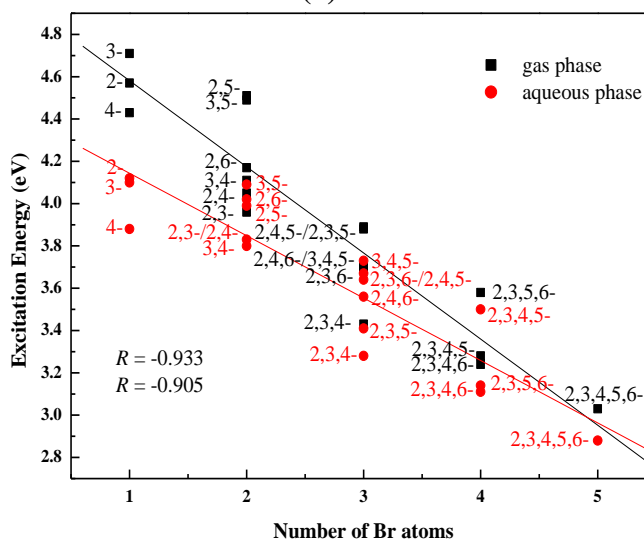
Figure 5.4b. The calculated aqueous-phase UV absorption spectra of selected bromophenols.

Absorption regions of mono and dibrominated congeners occur in a narrow wavelength region of 200 nm – 280 nm. This finding agrees well with the UV absorption spectrum

of 4-MBPh recorded experimentally [66]. Spectra of higher brominated congeners, especially tetrabromophenols and the pentabromophenol, display one intensive absorption band in the wavelength range of between 280 nm and 320 nm. Figure 5.5a discloses that, as the degree of bromination increases in gaseous and aqueous phases, the absorption bands shift towards longer wavelength. Consistently, higher brominated congeners entail lower values of the excitation energy. Figure 5.5b portrays a linear correlation between the number of bromine atoms and the excitation energy in the two phases, i.e. in agreement with the trend reported in Figure 5.1a between $E^{\text{H-L}}$ and the number bromine atoms.



(a)



(b)

Figure 5.5. Correlation between (a) the calculated wavelength (nm) at maximum UV absorption and the number of bromine atoms (b) calculated lowest excitation energy values (eV) and the number of bromine atoms.

The comparison of gas phase spectra with an aqueous phase spectra in Figure 5.5a reveal that the gas phase strongest absorption band for most of the BPh congeners exhibit a blue shift (shift towards a longer wavelength) when the process occurs in the aqueous phase. For example, the strongest absorption band for a gas phase 3,4,5,6-TBPh molecule reduces by nearly 10 nm in comparison with an aqueous phase molecule. However, other molecules such as 2,6-DBPh display an opposite trend i.e., longer wavelength for the strongest absorption band in the aqueous phase.

Having established general trends for the photo reactivity of BPhs, we make a parting remark that, it will be insightful in a future publication to address the mechanism of bromine loss from excited BPhs by mapping out corresponding potential energy surfaces.

5.4. Conclusions

With the aim to acquire an insight into the phototransformations of BPhs in the environment, this chapter investigated geometrical and electronic properties of the complete series of BPhs, both in the gaseous and aqueous media. In agreement with the analogous work on PBDEs, we found that the photoreactivity of bromine atoms in BPhs follows the sequence of *ortho* > *meta* > *para*. We clarify the effect of the degree and pattern of bromination on the photodebromination of BPhs based on several molecular descriptors; namely, geometries of the excited S_1 state, values of the HOMO-LUMO gap E^{H-L} and atomic charges q_{Br} . It is inferred that excitation of BPh congeners in the aqueous phase requires less photon absorption energies than in the gas phase. However, based on the oscillator strengths values, tendency for photodecomposition prevail in the gas phase in comparison to that in the aqueous phase. The photoreactivity of BPhs rises with the degree of bromination. Overall, in the absence of photocatalysts, isomers of BPhs are unlikely to absorb a photon in the visible or near UV regions. Photodegradation of BPhs requires a deep UV environment.

Acknowledgments

This study has been supported by the Australian Research Council (ARC), and grants of computing time from the National Computational Infrastructure (NCI), Australia as well

CHAPTER 5 Photodecomposition of Bromophenols (BPhs)

as the Pawsey Supercomputing Centre. A.S. thanks Murdoch University, Australia, for the award of postgraduate research scholarship.

References

- [1] Weber, R., Kuch, B. Relevance of BFRs and thermal conditions on the formation pathways of brominated and brominated–chlorinated dibenzodioxins and dibenzofurans. *Environ. Int.* **2003**, 29, 699-710.
- [2] Barontini, F., Cozzani, V., Marsanich, K., Raffa, V., Petarca, L. An experimental investigation of tetrabromobisphenol A decomposition pathways. *J. Anal. Appl. Pyrol.* **2004**, 72, 41-53.
- [3] Barontini, F., Cozzani, V. Formation of hydrogen bromide and organobrominated compounds in the thermal degradation of electronic boards. *J. Anal. Appl. Pyrol.* **2006**, 77, 41-55.
- [4] Grause, G., Furusawa, M., Okuwaki, A., Yoshioka, T. Pyrolysis of tetrabromobisphenol-A containing paper laminated printed circuit boards. *Chemosphere* **2008**, 71, 872-878.
- [5] Terakado, O., Ohhashi, R., Hirasawa, M. Thermal degradation study of tetrabromobisphenol A under the presence metal oxide: Comparison of bromine fixation ability. *J. Anal. Appl. Pyrol.* **2011**, 91, 303-309.
- [6] Kim, Y.J., Osako, M., Sakai, S. Leaching characteristics of polybrominated diphenyl ethers (PBDEs) from flame-retardant plastics. *Chemosphere* **2006**, 65, 506-513.
- [7] Choi, K.I., Lee, S.H., Osako, M. Leaching of brominated flame retardants from TV housing plastics in the presence of dissolved humic matter. *Chemosphere* **2009**, 74, 460-466.
- [8] Zhou, X., Guo, J., Lin, K., Huang, K., Deng, J. Leaching characteristics of heavy metals and brominated flame retardants from waste printed circuit boards. *J. Hazard. Mater.* **2013**, 246-247, 96-102.
- [9] de Wit, C.A. *Brominated Flame Retardants*, Swedish Environmental Protection Agency, Report 5065, **2000**, Stockholm, Sweden.
- [10] Evans, C.S., Dellinger, B. Mechanisms of dioxin formation from the high-temperature pyrolysis of 2-bromophenol. *Environ. Sci. Technol.* **2003**, 37, 5574-5580.

- [11] Evans, C.S., Dellinger, B. Mechanisms of dioxin formation from the high-temperature oxidation of 2-bromophenol. *Environ. Sci. Technol.* **2005**, 39, 2128-2134.
- [12] Schöler, D., Jäger, J. Formation of chlorinated and brominated dioxins and other organohalogen compounds at the pilot incineration plant VERONA. *Chemosphere* **2004**, 54, 49-59.
- [13] Arnoldsson, K., Andersson, P.L., Haglund, P. Formation of environmentally relevant brominated dioxins from 2,4,6-tribromophenol via bromoperoxidase-catalyzed dimerization. *Environ. Sci. Technol.* **2012**, 46, 7239-7244.
- [14] Altarawneh, M., Dlugogorski, B.Z. A Mechanistic and kinetic study on the formation of PBDD/Fs from PBDEs. *Environ. Sci. Technol.* **2013**, 47, 5118-5127.
- [15] Altarawneh, M., Dlugogorski, B.Z., Kennedy, E.M., Mackie, J.C. Mechanisms for formation, chlorination, dechlorination and destruction of polychlorinated dibenzo-*p*-dioxins and dibenzofurans (PCDD/Fs). *Prog. Energy Combust. Sci.* **2009**, 35, 245-274.
- [16] Altarawneh, M., Carrizo, D., Ziolkowski, A., Kennedy, E.M., Dlugogorski, B.Z., Mackie, J.C. 2009. Pyrolysis of permethrin and formation of precursors of polychlorinated dibenzo-*p*-dioxins and dibenzofurans (PCDD/F) under non-oxidative conditions. *Chemosphere* **2009**, 74, 1435-1443.
- [17] Lau, S.S., Monks, T.J., Greene, K.E., Gillette, J.R. The role of ortho-bromophenol in the nephrotoxicity of bromobenzene in rats. *Toxicol. Appl. Pharmacol.* **1984**, 72, 539-549.
- [18] Olsen, C.M., Meussen-Elholm E.T., Holme, J.A., Hongslo, J.K. Brominated phenols: characterization of estrogen-like activity in the human breast cancer cell-line MCF-7. *Toxicol. Lett.* **2002**, 129, 55-63.
- [19] Eljarrat, E., Barceló, D. *Brominated Flame Retardants. The Handbook of Environmental Chemistry*, **2011**, Springer.
- [20] Evans, C.S., Dellinger, B. Formation of bromochlorodibenzo-*p*-dioxins and dibenzofurans from the high-temperature oxidation of a mixture of 2-chlorophenol and 2-bromophenol. *Environ. Sci. Technol.* **2006**, 40, 3036-3042.
- [21] Komiya, T., Kawakishi, S., Namiki, M. Decomposition pathways of *p*-bromophenol on γ -irradiation in aqueous systems. *Agric. Biol. Chem.* **1974**, 38, 1589-1595.

- [22] Chen, S.F., Liu, F.Y., Liu, Y.J. An ab initio investigation of the mechanisms of photodissociation in bromobenzene and iodobenzene. *J. Chem. Phys.* **2009**, 131, 124304 (1-7).
- [23] Loeff, I., Lutz, H., Lindqvist, L. Transient species in the laser photolysis at 265 M μ of the halogenobenzenes in solution. *Isr. J. Chem.* **1970**, 8, 141-146.
- [24] Tang, B., Zhu, R., Tang, Y., Ji, L., Zhang, B. Photodissociation of bromobenzene at 267 and 234 nm: experimental and theoretical investigation of the photodissociation mechanism. *Chem. Phys. Lett.* **2003**, 381, 617-622.
- [25] Fang, L., Huang, J., Yu, G., Wang, L. Photochemical degradation of six polybrominated diphenyl ether congeners under ultraviolet irradiation in hexane. *Chemosphere* **2008**, 71, 258-267.
- [26] Wang, S., Hao, C., Gao, Z., Chen, J., Qiu, J. Effects of excited-state structures and properties on photochemical degradation of polybrominated diphenyl ethers: A TDDFT study. *Chemosphere* **2012**, 88, 33-38.
- [27] Xie, Q., Chen, J., Shao, J., Chen, C., Zhao, H., Hao, C. Important role of reaction field in photodegradation of deca-bromodiphenyl ether: theoretical and experimental investigations of solvent effects. *Chemosphere* **2009**, 76, 1486-1490.
- [28] Zeng, X., Massey Simonich, S.L., Robrock, K.R., Korytár, P., Alvarez-Cohen, L., Barofsky, D.F. Development and validation of a congener-specific photodegradation model for polybrominated diphenyl ethers. *Environ. Toxicol. Chem.* **2008**, 27, 2427-2435.
- [29] Freedman, A., Yang, S.C., Kawasaki, M., Bersohn, R. Photodissociation of aryl and aryl-alkyl halides at 193 nm: Fragment translational energy distributions. *J. Chem. Phys.* **1980**, 72, 1028-1033.
- [30] Gu, X.B., Wang, G.J., Huang, J.H., Han, K.L., He, G.Z., Lou, N.Q. Photofragment translational spectroscopy of 1-bromo-3-fluorobenzene and 1-bromo-4-fluorobenzene at 266 nm. *J. Phys. Chem.* **2001**, 105, 354-362.
- [31] Borg, O.A., Liu, Y.J., Persson, P., Lunell, S., Karlsson, D., Kadi, M., Davidsson, J. Photochemistry of bromofluorobenzenes. *J. Phys. Chem. A.* **2006**, 110, 7045-7056.
- [32] Han, K.L., He, G.Z. Photochemistry of aryl halides: Photodissociation dynamics. *J. Photochem. Photobiol. C: Photochem. Rev.* **2007**, 8, 55-66.
- [33] Joschek, H.I., Miller, S.I. Photocleavage of phenoxyphenols and bromophenols. *J. Am. Chem. Soc.* **1966**, 88, 3269-3272.

- [34] Lipczynska-Kochany, E. Direct photolysis of 4-bromophenol and 3-bromophenol as studied by a flash photolysis/HPLC technique. *Chemosphere* **1992**, 24, 911-918.
- [35] Grünewald, H. *Handbook of Chemistry and Physics*. By R. C. Weast. Angew. Chem. Int. Ed. Engl. **1972**, 11, 445-449. doi: 10.1002/anie.197204492.
- [36] Zhang, H., Zhu, R.S., Wang, G.J., Han, K.L., He, G.Z., Lou, N.Q. Photodissociation of bromobenzene at 266 nm. *J. Chem. Phys.* **1999**, 110, 2922-2927.
- [37] Park, M.S., Lee, K.W., Jung, K.H. Br(²P_j) and Cl(²P_j) atom formation dynamics of allyl bromide and chloride at 234 nm. *J. Chem. Phys.* **2001**, 114, 10368-10374.
- [38] Rasmusson, M., Lindh, R., Lascoux, N., Tarnovsky, A.N., Kadi, M., Kühn, O., Sundström, V., Åkesson, E. Photodissociation of bromobenzene in solution. *Chem. Phys. Lett.* **2003**, 367, 759-766.
- [39] Liu, Y.J., Persson, P., Karlsson, H.O., Lunell, S., Kadi, M., Karlsson, D., Davidsson, J. Photodissociation of bromobenzene, dibromobenzene, and 1,3,5-tribromobenzene. *J. Chem. Phys.* **2004**, 120, 6502-6509.
- [40] Zanganeh, J., Altarawneh, M., Saraireh, I., Namazi, S., Zanganeh, J. Theoretical study on thermochemical parameters and pK_a values for fluorinated isomers of toluene. *Comp. Theor. Chem.* **2013**, 1011, 21-29.
- [41] Altarawneh, I., Altarawneh, L., Al-Muhtaseb, H.A., Alrawadieh, S., Altarawneh, M. Theoretical study of thermochemical and structural parameters of chlorinated isomers of aniline. *Comp. Theor. Chem.* **2012**, 985, 30-35.
- [42] Altarawneh, I., Altarawneh, M., Rawadieh, S. Theoretical study on thermochemical parameters and IR spectra of chlorinated isomers of nitrobenzene. *Can. J. Chem.* **2013**, 91, 999 -1008.
- [43] Casida, M.E. Time-dependent density-functional theory for molecules and molecular solids. *J. Mol. Struct.* **2009**, 914, 3-18.
- [44] Isborn, C.M., Luehr, N., Ufimtsev, I.S., Martínez, T.J. Excited-state electronic structure with configuration interaction singles and tamm–dancoff time-dependent density functional theory on graphical processing units. *J. Chem. Theory Comput.* **2011**, 7, 1814-1823.
- [45] Han, L.H., Zhang, C.R., Zhe, J.W., Jin, N.Z., Shen, Y.L., Wang, W., Gong, J.J., Chen, Y.H., Liu, Z.J. Understanding the electronic structures and absorption properties of porphyrin sensitizers YD2 and YD2-o-C8 for dye-sensitized solar cells. *Int J Mol Sci.* **2013**, 14, 20171-20188.

- [46] De Proft, F., Van Alsenoy, C., Peeters, A., Langenaeker, W., Geerlings, P. Atomic charges, dipole moments, and Fukui functions using the Hirshfeld partitioning of the electron density. *J. Comput. Chem.* **2002**, 23, 1198-1209.
- [47] Fonseca G.C., Handgraaf, J.W., Baerends, E.J., Bickelhaupt, F.M. Voronoi deformation density (VDD) charges: Assessment of the Mulliken, Bader, Hirshfeld, Weinhold, and VDD methods for charge analysis. *J. Comput. Chem.* **2004**, 25, 189-210.
- [48] Delley, B. From molecules to solids with Dmol³ approach. *J. Chem. Phys.* **2000**, 113, 7756-7764.
- [49] Perdew, J.P., Wang, Y. Accurate and simple analytic representation of the electron-gas correlation energy. *Phys. Rev. B*, **1992**, 45, 13244-13249.
- [50] Klamt, A. Conductor-like screening model for real solvents: a new approach to the quantitative calculation of solvation phenomena. *J. Phys. Chem.* **1995**, 99, 2224-2235.
- [51] Klamt, A., Schüürmann, G. COSMO: A new approach to dielectric screening in solvents with explicit expressions for the screening energy and its gradient. *J. Chem. Soc. Perkin Trans.* **1993**, 2, 799-805.
- [52] Delley, B. An all-electron numerical method for solving the local density functional for polyatomic molecules. *J. Chem. Phys.* **1990**, 92, 508-517.
- [53] Luo, J., Hu, J., Wei, X., Li, L., Huang, X. Excited states and photodebromination of selected polybrominated diphenyl ethers: computational and quantitative structure—property relationship studies. *Int. J. Mol. Sci.* **2015**, 16, 1160-1178.
- [54] Li, A., Tai, C., Zhao, Z., Wang, Y., Zhang, Q., Jiang, G., Hu, J. Debromination of decabrominated diphenyl ether by resin-bound iron nanoparticles. *Environ. Sci. Technol.* **2007**, 41, 6841-6846.
- [55] Li, J., Ma, W., Huang, Y., Tao, X., Zhao, J., Xu, Y. Oxidative degradation of organic pollutants utilizing molecular oxygen and visible light over a supported catalyst of Fe(bpy)₃²⁺ in water. *Appl. Catal., B: Environmental.* **2004**, 48, 17-24.
- [56] Wang, J.Z., Hou, Y., Zhang, J., Zhu, J., Feng, Y.L. Transformation of 2,2',4,4'-tetrabromodiphenyl ether under UV irradiation: Potential sources of the secondary pollutants. *J. Hazard. Mater.* **2013**, 263, 778-783.
- [57] Pearson, R.G. Absolute electronegativity and hardness correlated with molecular orbital theory. *Proc. Natl. Acad. Sci. USA.* **1986**, 83, 8440-8441.

- [58] Zhao, G.J., Han, K.L. Excited state electronic structures and photochemistry of heterocyclic annulated perylene (HAP) materials tuned by heteroatoms: S, Se, N, O, C, Si, and B. *J. Phys. Chem. A.* **2009**, 113, 4788-4794
- [59] Zhao, G.J., Han, K.L. pH-controlled twisted intramolecular charge transfer (TICT) excited state via changing the charge transfer direction. *Phys. Chem. Chem. Phys.* **2010**, 12, 8914-8918.
- [60] Dolfing, J., Novak, I. The Gibbs free energy of formation of halogenated benzenes, benzoates and phenols and their potential role as electron acceptors in anaerobic environments. *Biodegradation* **2015**, 26, 15-27.
- [61] Eriksson, J., Green, N., Marsh, G., Bergman, A. Photochemical decomposition of 15 polybrominated diphenyl ether congeners in methanol/water. *Environ. Sci. Technol.* **2004**, 38, 3119-3125.
- [62] Pulgarin, C., Kiwi, J. Overview on photocatalytic and electrocatalytic pretreatment of industrial non-biodegradable pollutants and pesticides. *CHIMIA* **1996**, 50, 50-55.
- [63] Zhao, J., Chen, C., Ma, W. Photocatalytic degradation of organic pollutants under visible light irradiation. *Top. Catal.* **2005**, 35, 269-278.
- [64] Zhao, W., Ma, W., Chen, C., Zhao, J., Shuai, Z. Efficient degradation of toxic organic pollutants with $\text{Ni}_2\text{O}_3/\text{TiO}_{(2-x)}\text{B}_x$ under visible irradiation. *J. Am. Chem. Soc.* **2004**, 126, 4782-4783.
- [65] Chatterjee, D., Dasgupta, S. Visible light induced photocatalytic degradation of organic pollutants. *J. Photochem. Photobiol. C: Photochem. Rev.* **2005**, 6, 186-205.
- [66] Pandiyan, T., Martínez Rivas, O., Orozco Martínez, J., Burillo Amezcua, G., Martínez-Carrillo, M.A. Comparison of methods for the photochemical degradation of chlorophenols. *J. Photochem. Photobiol. A.* **2002**, 146, 149-155.
- [67] Sun, C. Degradation of polybrominated diphenyl ethers. *Rev. Adv. Sci. Eng.* **2014**, 3, 28-47.
- [68] Devine, A.L., Nix, M.G., Cronin, B., Ashfold, M.N. Near-UV photolysis of substituted phenols, I: 4-fluoro-, 4-chloro- and 4-bromophenol. *Phys. Chem. Chem. Phys.* **2007**, 9, 3749-3762.

CHAPTER 6 PROPERTIES OF BROMINATED FLAME RETARDANTS (BFRs) ON THE VERGE OF THEIR PHOTODECOMPOSITION

Table of Contents

Abstract	208
6.1. Introduction	209
6.2. Computational details	211
6.3. Results and discussion	213
6.3.1. Optimised structures in ground and excited states for selected BFRs	213
6.3.2. Frontier molecular orbitals; the HUMO-LUMO energy gap	217
6.3.3. Charge distribution	219
6.3.4. Optical properties including UV-Vis absorption spectra, excitation energies and oscillation strengths	221
6.4. Conclusion	230
Acknowledgments	230
References	231

Abstract

This chapter investigates the geometric and electronic properties of selected BFRs in ground (S_0) and first singlet excited states (S_1) using density functional theory (DFT) and time-dependent density functional theory (TDDFT) methods. We estimate C-Br bond elongations upon the $S_0 \rightarrow S_1$ transition, identify involved frontier molecular orbitals in the excitation process and compute partial atomic charges for the most photoreactive bromine atoms. The bromine atom attached to an *ortho* position in 2,3,4,5-TBP, TBBA (with respect to the hydroxyl group) and BTBPE (in reference to C-O linkage) bears the highest positive atomic charge. This suggests that these positions undergo reductive debromination reactions to produce lower brominated molecules. Analysis of the frontier molecular orbitals indicates that the excited title BFRs proceed via either $\pi\pi^*$ or $\pi\sigma^*/n\sigma^*$ electronic transitions. The value of the HOMO-LUMO gap (E^{H-L}) is lower (3.2 – 4.0 eV) for all investigated bromine-substituted aromatic molecules compared with their non-brominated analogous compounds (3.4 – 8.1 eV), in both aqueous and gaseous media. Excitation energies display a positive correlation with E^{H-L} values. Spectral analysis in the gas phase reveals that the studied brominated aromatics endure lower excitation energies and exhibit red shifts of their absorption bands (repositioning towards longer wavelengths near 300 nm) in contrast to non-brominated moieties. In summary, this study further confirms that halogenated aromatics only absorb light in the UV spectrum, and that photodegradation of these pollutants requires the existence of photocatalysts.

6.1. Introduction

Brominated flame retardants (BFRs) are bromine-bearing hydrocarbons commonly added to polymeric constituents in consumer products to enhance their fire retardancy. In light of their substantial deployments over the last few decades, BFRs have accumulated in various environmental compartments such as sewage sludge, sediments [1-2] the air and water bodies [3-5]. While the presence of historically-deployed BFRs in the environment is common, elevated concentrations of so-called novel BFRs have also been detected at alarming loads [6-11].

The bioaccumulative and persistent nature of BFRs has rendered them as a main topic of research among environmental chemists. High concentrations of certain BFRs can provoke toxic effects in humans and wildlife [12-13]. While BFRs can be toxic in their own right, their major environmental burden lies in their structural functionality as direct building blocks for the notorious polybrominated dibenzo-*p*-dioxins and dibenzofurans (PBDD/Fs) [14-17]. As thermal treatment is a mainstream strategy for the recovery and disposal of materials laden with BFRs (i.e., plastics and electronic wastes), several studies have elucidated scenarios and pathways underpinning the transformation of BFRs into PBDD/Fs at the temperatures applicable to waste energy applications [18-21]. In addition to PBDD/Fs, the thermal decompositions of BFRs generates a wide array of small brominated C₁-C₄ species, as well as large macromolecules [22-27].

BFRs can be released into the environment via several routes, most notably through direct diffusion from treated objects at room temperatures [28-29] and open burning and/or dumping of BFR-containing materials [30-32]. Thus, it is of great importance to trace the chemical transformation pathways of BFRs in the environment. While thermal processes decontaminate BFRs by destroying their structures, the transformation pathways that prevail in the environment are fundamentally distinct.

Photolysis and photochemical decomposition are the primary routes of chemical transformation of BFRs in the environment. Most relevant experimental investigations have focused on the photo-induced decay of polybrominated diphenyl ethers (PBDEs). Söderström et al. (2004) investigated the photolysis of Deca-BDE in different

CHAPTER 6 Properties of Brominated Flame Retardants (BFRs) on the Verge of their Photodecomposition

environmental matrices [33]. Lower brominated congeners of diphenylethers were observed under different sunlight conditions. The reaction medium (i.e., solid, sediment or sand) has little influence on the debromination process; however, it significantly affects the temporal scale of the reaction. In addition to the lower isomers of PBDEs, several isomers of PBDFs were also detected. The occurrence of debromination during PBDE photolysis has been consistently reported [34-36]. Eriksson et al. (2004) illustrated that different isomers of PBDEs exhibit distinct photolytic decay rates [34]. Similarly, experiments by Otha et al. (2001) established that different sources of light (sunlight versus UV-lamps) produce different patterns of debrominated products [37].

The study of excited state properties of organic compounds is of significant importance from a photolytic point of view. Theoretically, calculations based on the time-dependent density functional theory (TDDFT) formalism have elucidated the structures and electronic properties of various BFRs in their first excited states, relevant to their photoreactivity [38-41]. These investigations assessed (i) the transformation of brominated moieties in their singlet or triplet excited states, and (ii) the effect of the degree and pattern of bromination on the photodecomposition process. Likewise, in chapter 5, we computed properties of the complete series of bromophenols (BPhs) in their ground and first excited state [42]. Our results suggest that, when brominated compounds become photoexcited, debromination follows a sequence of *ortho* > *meta* > *para* positions. Furthermore, congeners entailing a high degree of bromination (demanding lower excitation energies) photodecompose more readily than the lower brominated isomers. Thus, it is inferred from these theoretical studies that reductive debromination depends on the pattern and degree of bromine substituents on the aromatic ring.

Brominated aromatic compounds, in general, absorb light in the UV region. If a sufficient amount of energy is absorbed, it triggers a facile homolytic fission of the C-Br bond and provokes possible rearrangements and ether bond cleavage. Mechanistically, the UV radiation absorbed by a molecule is consumed in two ways (i) a large fraction of energy is used to remove electrons or derive electron transitions between $\pi\pi^*$ and n,σ^* orbitals, (ii) the remainder is utilised to rupture C-Br bonds [43]. In a nutshell, photoexcited BFRs undergo singlet or triplet excited state transitions in which aromatic C-Br bonds are substantially weakened.

While the photodecomposition of neat BFRs is not possible in daylight, certain species can act as photocatalysts in an aqueous medium. A pioneering study by Sun et al. demonstrated a visible-light reductive debromination process of PBDEs in which carboxylate anions act as a mediator [39]. The coexistence of BFRs with other organic acids in the environment might be a common scenario. For example, the hydrophobic nature of BFRs facilitates their adsorption in the waxy outer surfaces of plants and even human skin [44-45].

The reported reductive debromination of BFRs in the ambient environment has motivated us to study the properties of selected BFRs on the verge of their photodecomposition. To this end, the current chapter investigates DFT and TDDFT with the purpose of evaluating the photodecomposition behaviour of the most commonly-deployed BFRs, namely, 4,4'-dibromobiphenyl (4,4'-diBB), 4,4'-dibromodiphenylether (4,4'-diBDE), hexabromocyclododecane (HBCD) and tetrabromobisphenol A (TBBA); 2,3,4,5-tetrabrominated phenol (2,3,4,5-TBP), and 1,2-bis(2,4,6-tribromophenoxy)ethane (BTBPE). The effect of bromine loadings on electronic and structural properties was observed by contrasting analogous results from brominated and non-brominated molecules. Investigated properties include singlet state lowest excitation energies, oscillator strength, partial atomic charges, and UV-Vis absorption spectra. We tackle different aspects in this paper. For instance, the visible light irradiation of PBDEs by carboxylate anions was carried out in an aqueous medium. Thus, it is of a practical significance to report the properties of the first excited states of titled BFRs in water. We have also attempted to elucidate a relationship between the thermal stability and photoreactivity of selected molecules with reference to prominent molecular descriptors that are the difference in energy between frontier molecular orbitals and the electronic charges.

6.2. Computational details

Electronic structure calculations for selected brominated and non-brominated molecules of the flame retardant, in ground and excited states, were executed using the Accelrys' Dmol³ program [46]. Geometry optimisation for all structures was performed using the

DFT functional of GGA-PW91 [47]. The theoretical approach encompasses a double numerical basis set with a d polarisation function (DND) (1998) with an orbital cut-off radius of 4.4 Å for numerical integration. The size of our numerical basis set is comparable to the Gaussian basis set of 6-31G*. Owing to numerical optimisation, the DND basis set is much more accurate and holds smaller superposition errors than the Gaussian basis set of the same size [48].

We deployed a conductor-like screening model (COSMO) to induce the solvation effects in geometry optimisation [49-50]. All aqueous phase calculations were performed using a dielectric constant value of 78.5, corresponding to water. We studied the excited states of considered molecules by implementing the TDDFT approach (geometric convergence set to 10^{-6} Ha) along with the adiabatic local exchange density functional approximation (ALDA) [51]. The UV-Vis absorption spectra were simulated using TDDFT calculations for ground and excited states in both gaseous and aqueous media [52]. The electronic transition from initial (i) to final (f) state in the absorption process is illustrated by Equation [1] [53-55]:

$$W_{i \rightarrow f}(\omega) = \frac{2\pi}{\hbar^2} |\mu_{fi} \cdot E_0(\omega)|^2 \sum_v \sum_{v'} P_{iv} |(\theta_{fv'} | \theta_{iv})|^2 D(\omega_{fv',iv} - \omega, \gamma_{fv',iv}) \quad [1]$$

Whereas the UV-Vis absorption spectrum is expressed by Equation [2]:

$$\alpha(\omega) = \frac{4\pi^2\omega}{3\hbar c a} |\mu_{fi}|^2 \sum_v \sum_{v'} P_{iv} |(\theta_{fv'} | \theta_{iv})|^2 D(\omega_{fv',iv} - \omega, \gamma_{fv',iv}) \quad [2]$$

In equations [1] and [2], μ_{fi} signifies the electronic transition dipole moment between the f and i states. E_0 denotes the amplitude of the vector for the incident sinusoidal electric field. P_{iv} stands for the Boltzmann distribution factor. $|(\theta_{fv'} | \theta_{iv})|$ characterises the Frank-Condon factor. $D(\omega_{fv',iv} - \omega, \gamma_{fv',iv})$ is the Lorentzian shape function with a damping factor (γ), v and v' are the vibrational quantum numbers corresponding to electronic states f and i . c corresponds to the speed of light, and a expresses the solvation effect.

We examined the atomic charges for the most photoreactive bromine atoms in BFR compounds based on the Hirshfeld population analysis [48]. According to Fonseca et al. hirshfeld methods are among the most accurate computational formalism for the determination of atomic charges [56]. Optical property calculations for both gas and aqueous phases, in ground and excited states, were carried out based on optimised ground state molecular structures [57].

6.3. Results and discussion

6.3.1. Optimised structures in ground and excited states for selected BFRs

Figure 6.1 presents the optimised geometries of the six considered BFRs and their non-brominated counterparts in their gas phase at ground state (S_0), along with illustrating atomic numberings and C-Br bond lengths (in Å). While HBCDs assume various energy-degenerate structural configurations, we elected to study properties of the δ isomer [58]. Table 6.1 lists prominent interatomic distances for C-Br bonds in the gaseous and aqueous configurations (at the S_0 and S_1 states). Analysing these geometries and contrasting geometrical features in the S_0 and S_1 states should provide valuable insight into the trends governing the photodecomposition process, as well as the effect of the degree of bromination on the photoreactivity of the title BFRs.

CHAPTER 6 Properties of Brominated Flame Retardants (BFRs) on the Verge of their Photodecomposition

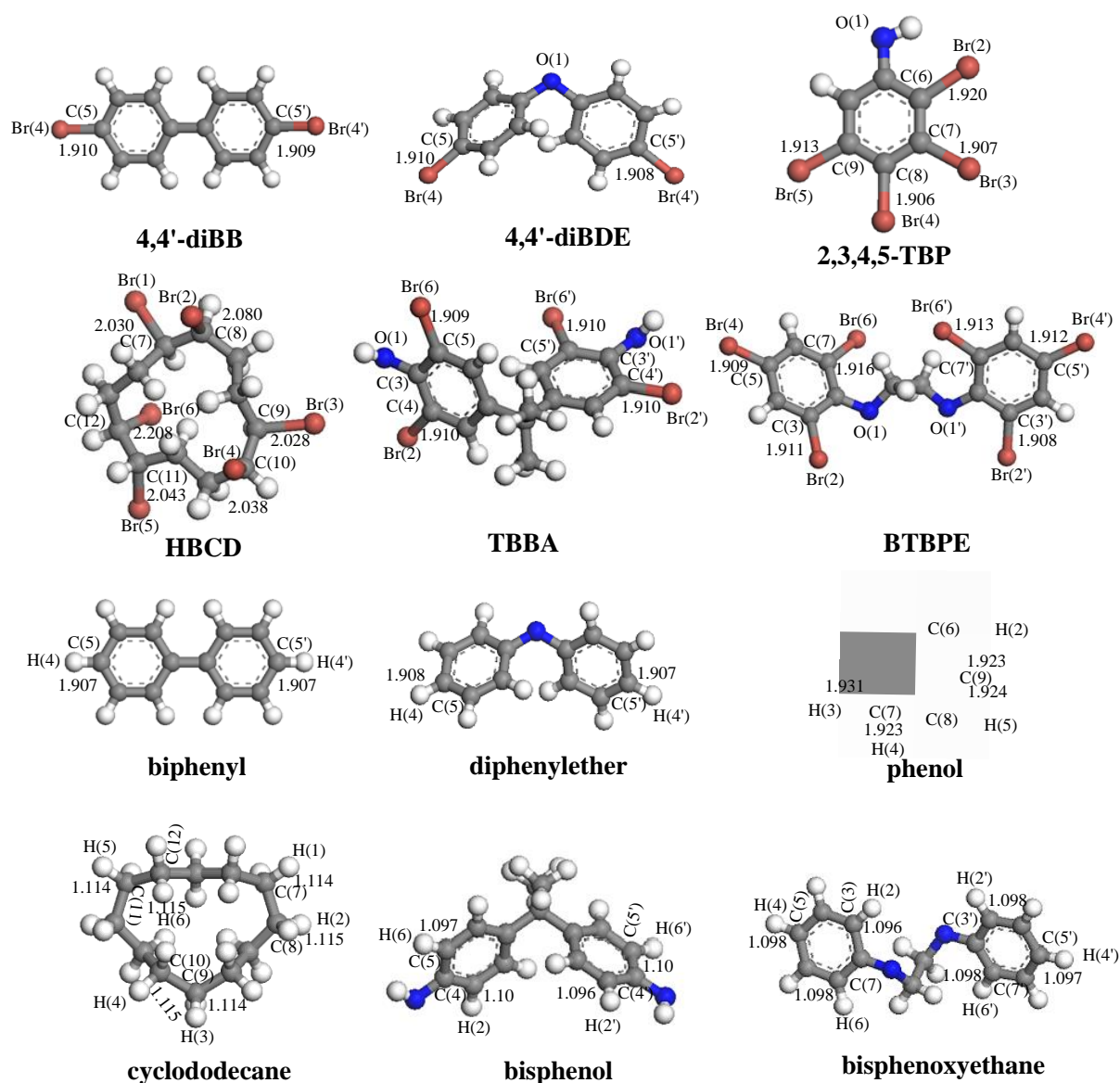


Figure 6.1. Optimised geometries of selected BFRs and their non-brominated isomers with C-Br bond distance (in Å) measured in the gaseous S_0 state. Bromine and oxygen atoms are denoted by red and blue spheres, respectively.

The structural parameters (particularly carbon-halogen bond lengths) for brominated compounds in the S_0 state are distinguished from those in the S_1 state, both in gaseous and aqueous phases. For example, for TBBA and 4,4'-diBDE, our calculated C-Br bond distances in ground state ranged between 1.908 – 1.910 Å, which matched the analogous theoretically- and experimentally-measured geometries very well [41, 59-60]. The striking feature inferred from the values in Table 6.1 is a significant elongation of C-Br

bond lengths upon the $S_0 \rightarrow S_1$ transition. In summary, the following conclusions can be made:

- (i) Upon excitation from the S_0 to S_1 state, the elongation in C-Br bonds mainly occurs at the *ortho* position [61-62]. Consequently, we observed a nominal increase in bond lengths of 5.2 % and 5.4 % for 4,4'-diBB and 4,4'-diBDE, respectively (both BFRs hold bromine substitution at the *para* position with respect to the C-C and O-C bridges). Analogous values in water were 3.5 % and 3.6 %, respectively.
- (ii) The presence of *ortho* bromine substitutions in TBBA (with respect to the hydroxyl group) and in BTBPE (with respect to the C-O linkage) results in significant C-Br bond elongations of 12.1 % and 7.8 %, correspondingly in the gas phase.
- (iii) C-Br bond distances in the aqueous ground state slightly exceed their analogous effective values in the gas phase. For instance, the C-Br bonds in gaseous TBBA are marginally reduced (by 2.3 %) compared with aqueous TBBA.
- (iv) The extent of elongation (as a percentage and an absolute value) is generally more profound in the $S_0 \rightarrow S_1$ gas phase than in the water-based medium. For example, the *para* C-Br (with respect to C-C linkage) in 4,4'-diBB in the gas phase elongates by 0.100 Å (5.2 %) in comparison with 0.068 Å (3.5 %) in an aqueous medium.
- (v) No significant variation in geometries can be observed when non-brominated moieties are excited from the S_0 to S_1 state in either medium. This finding is consistent with the general consensus that brominated compounds are more susceptible to photodecomposition than their non-substituted counterparts [41, 63-64]. Additionally, it can be deduced from Table 6.1 that the presence of any media- like water does not induce any effect on the geometrical parameters of non-halogenated compounds.

CHAPTER 6 Properties of Brominated Flame Retardants (BFRs) on the Verge of their Photodecomposition

- (vi) The non-aromatic C-Br bonds (in HBCD) experience the highest $S_0 \rightarrow S_1$ stretching (by 0.18 Å in gas and 0.17 Å in water). Our computed C-Br bond lengths in the gaseous S_0 state ranged between 2.023 – 2.043 Å, and were in reasonable agreement with other analogous theoretically computed C-Br bond lengths for gaseous HBCDs (i.e., 1.991 – 2.020 Å) [65].

Table 6.1. Comparison of bond lengths (C-Br, in Å) for title BFRs and their non-brominated counterparts in ground (S_0) and excited (S_1) states in both gaseous and aqueous media. Atomic positions are shown in Figure 6.1.

Compound	Gaseous phase		
	Position of C-Br bonds	C-Br bond lengths in S_0 state	C-Br bond lengths in S_1 state
4,4'-diBB	5-4; 5'-4'	1.910; 1.909	2.009; 2.009
4,4'-diBDE	5-4; 5'-4'	1.910; 1.908	2.013; 2.012
2,3,4,5-TBP	6-2; 7-3; 8-4; 9-5	1.907; 1.920; 1.906; 1.913	2.006; 1.996; 1.944; 1.942
HBCD	7-1; 8-2; 9-3; 10-4; 11-5; 12-6	2.03; 2.08; 2.028; 2.038; 2.043; 2.028	2.197; 2.104; 2.104; 2.098; 2.118; 2.208
TBBA	4-2; 5-6; 5'-2'; 4'-6'	1.910; 1.909; 1.910; 1.910	2.069; 2.08; 2.141; 2.040
BTBPE	3-2; 5-4; 7-6; 3'-2'; 5'-4'; 7'-6'	1.911; 1.909; 1.916; 1.908; 1.912; 1.913	2.046; 2.032; 2.039; 2.057; 2.026; 2.048
	Position of C-H atoms	C-H bond lengths in S_0 state	C-H bond lengths in S_1 state
biphenyl	5-4; 5'-4'	1.097; 1.097	1.097; 1.097
diphenylether	5-4; 5-4'	1.098; 1.097	1.098; 1.097
phenol	6-2; 7-3; 8-4; 9-5	1.10; 1.098; 1.098; 1.098	1.10; 1.098; 1.098; 1.098; 1.097
cyclododecane	7-1; 8-2; 9-3; 10-4; 11-5; 12-6	1.114; 1.115; 1.114; 1.115; 1.114; 1.115	1.117; 1.115; 1.114; 1.115; 1.114; 1.115
bisphenol A	4-2; 5-6; 4'-2'; 5'-6'	1.10; 1.097; 1.096; 1.10	1.10; 1.097; 1.10; 1.096
bisphenoxyethane	3-2; 5-4; 7-6; 2'-3'; 5'-4'; 7'-6'	1.096; 1.098; 1.098; 1.098; 1.097; 1.097; 1.098	1.097; 1.097; 1.095; 1.097; 1.095; 1.094
Aqueous phase			
	Position of C-Br atoms	C-Br bond lengths in S_0 state	C-Br bond lengths in S_1 state
4,4'-diBB	5-4; 5'-4'	1.939; 1.939	2.007; 2.007
4,4'-diBDE	5-4; 5'-4'	1.942; 1.941	2.011; 2.010
2,3,4,5-TBP	6-2; 7-3; 8-4; 9-5	1.923; 1.924; 1.923; 1.931	1.980; 2.030; 1.969; 1.960

CHAPTER 6 Properties of Brominated Flame Retardants (BFRs) on the Verge of their Photodecomposition

HBCD	7-1; 8-2; 9-3; 10-4; 11-5; 12-6	2.028; 2.031; 2.028; 2.043; 2.038; 2.028	2.196; 2.100; 2.104; 2.009; 2.119; 2.207
TBBA	4-2; 5-6; 5'-2'; 4'-6'	1.934; 1.953; 1.933; 1.954	2.010; 2.006; 2.104; 2.057
BTBPE	3-2; 5-4; 7-6; 3'-2'; 5'-4'; 7'-6'	1.935; 1.937; 1.931; 1.935; 1.937; 1.931	2.020; 2.005; 2.013; 2.042; 2.033; 2.047
	Position of C-H atoms	C-H bond lengths in S₀ state	C-H bond lengths in S₁ state
biphenyl	5-4; 5'-4'	1.097; 1.097	1.097; 1.097
diphenylether	5-4; 5'-4'	1.098; 1.097	1.098; 1.097
phenol	6-2; 7-3; 8-4; 9-5	1.10; 1.098; 1.098; 1.098	1.10; 1.098; 1.098; 1.099
cyclododecane	7-1; 8-2; 9-3; 10-4; 11-5; 12-6	1.114; 1.115; 1.114; 1.115; 1.114; 1.115	1.114; 1.115; 1.114; 1.115; 1.114; 1.115
bisphenol A	4-2; 5-6; 4'-2'; 5'-6'	1.10; 1.097; 1.096; 1.10	1.10; 1.098; 1.097; 1.10
bisphenoxyethane	3-2; 5-4; 7-6; 2'-3'; 5'-4'; 7'-6'	1.096; 1.098; 1.098; 1.098; 1.097; 1.098	1.099; 1.098; 1.101; 1.100; 1.098; 1.098

Overall, the values in Table 6.1 clearly establish the anticipated C-Br bond elongation induced by the $S_0 \rightarrow S_1$ transition, which is the rate-determining step in the photodecomposition process of BFRs [66]. The removal of the weakened Br atom (i.e., the atom associated with the highest photoreactivity) upon photodecomposition paves the way for subsequent hydrogenation (formation of lower brominated congeners), which has been observed experimentally [67-69].

6.3.2. Frontier molecular orbitals; the HUMO-LUMO energy gap

Analysis of frontier molecular orbitals, in terms of the energy difference between the highest occupied molecular orbital (HOMO) and the lowest unoccupied molecular orbital (LUMO), expressed by E^{H-L} values, serves as an informative molecular descriptor pertinent to the photoreactivity of molecules [57, 70]. Movement of an electron from HOMO to LUMO during the $S_0 \rightarrow S_1$ shift is determined by E^{H-L} values [57, 67]. Fang et al. (2009) established a negative correlation between E^{H-L} values and the photolytic reactivity $\log k$ for isomers of PBDEs in various media, including gas phase and hexane. With decreasing E^{H-L} , photoreactivity increases linearly to some extent [71].

Figures 6.S1 and 6.S2 in the supplementary information depict the HOMO and LUMO orbitals for all considered molecules, in both gaseous and aqueous media. Inspection of

Figure 6.S1 reveals the molecular fragments involved in the excitation process. We find that the transition from HOMO-LUMO is generally of either a $\pi \rightarrow \pi^*$ or $\pi \rightarrow \sigma^*$ character. The HOMOs (the departure state) were observed to be of π character, with the charge density distributed mainly over the aromatic rings (except for HBCD i.e., of n nature). Conversely, the LUMOs (the arrival state) features either π^* or σ^* characters. In molecules of 4,4'-diBB, 4,4'-diBDE, phenol, bisphenol, biphenyl and diphenylether molecules, it is of $\pi\pi^*$ character, in which LUMOs are distributed over the entire aromatic rings.

As Figure 6.S1 shows, transitions from HOMO-LUMO for 2,3,4,5-TBP, TBBA, BTBPE and cyclododecane molecules are of $\pi \rightarrow \sigma^*$ character, and for HBCD ($n \rightarrow \sigma^*$) nature, LUMO is mainly located on either the entire molecule (2,3,4,5-TBP and cyclododecane), on one phenyl group (TBBA and BTBPE), or on part of a molecule (HBCD). Our calculated HOMO-LUMO orbital transition, in terms of the involved molecular fragments for the 4,4'-diBDE congener, is in accord with other TDDFT studies [41, 72-73].

Figure 6.2 presents E^{H-L} values for the considered BFRs and their non-brominated isomers, in both gaseous and aqueous media. Calculated E^{H-L} values fall in a range of 3.2 – 5.1 eV for gaseous and aqueous configurations, except for cyclododecane which reaches around 8.0 eV. The noticeable difference in the E^{H-L} value of cyclododecane in reference to other non-brominated molecules could be rationalised based on its non-aromatic structure [74-75]. Bromine substitution in HBCD significantly reduces the E^{H-L} values to 5.016 eV and 5.093 eV in gas and water media, respectively, in reference to non-brominated cyclododecane (i.e., 8.065 eV and 8.087 eV, respectively). It is well-known that the E^{H-L} value correlates inversely with the degree of bromination [41-42]. It follows that two factors contribute to the high E^{H-L} value for cyclododecane: its non-aromatic structure and the absence of bromine substituents.

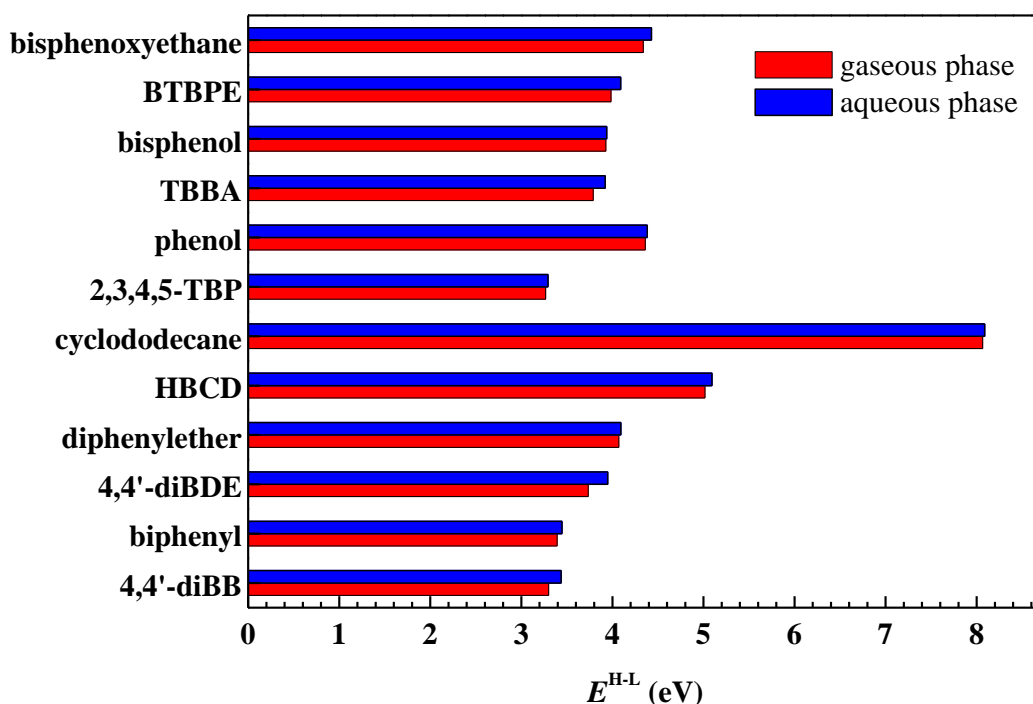


Figure 6.2. Correlation between calculated molecular orbital energy E^{H-L} (in eV) and selected BFRs and their non-brominated isomers in gaseous and aqueous media.

The E^{H-L} values for aromatic BFRs substituted with two to four bromine atoms reside in the narrow range of 3.2 - 3.7 eV. The values of the E^{H-L} energy gap are lower for all brominated substituents than for their non-brominated homologues, in both media. The lowest values of E^{H-L} are reported for 2,3,4,5-TBP, at 3.267 eV and 3.293 eV in gas and water media, respectively. These values are significantly lower than for non-halogenated phenol (4.361 eV in gas, 4.382 eV in water). This finding is in line with the general consensus in the literature, that photoreactivity is positively correlated with the degree of bromination. Our E^{H-L} energy analysis coincides with the theoretical predictions of E^{H-L} for PBDE congeners [38, 41]. Overall, the medium (gas phase versus water solvent) induces a minor influence on the E^{H-L} energies, which is in accordance with previous theoretical findings on HBCDs [65] and PBDEs [41].

6.3.3. Charge distribution

We computed the partitioning of electronic density in the considered brominated and non-brominated compounds based on the Hirshfeld partitioning scheme [76-77].

CHAPTER 6 Properties of Brominated Flame Retardants (BFRs) on the Verge of their Photodecomposition

Table 6.2. Atomic charges on selected BFRs. Note that n denotes the position of oxygen (O), bromine (Br) and carbon (C) atoms with values of net atomic charge presented in the ground state (S_0) in the gas phase. Atomic positions are depicted in Figure 6.1.

Compound	n	Gas phase (atomic charges)
		S_0
4,4'-diBB	Br(4); Br(4'); C(5); C(5')	-0.0116; -0.0116; -0.0048; -0.0048
4,4'-diBDE	O(1); Br(4); Br(4'); C(5); C(5')	-0.1001; -0.0173; -0.0167; -0.0118; -0.0118
2,3,4,5-TBP	O(1); Br(2); Br(3); Br(4); Br(5); C(6); C(7); C(8); C(9)	-0.1684; 0.0383; 0.0112; 0.0016; 0.0036; -0.0299; -0.0160; -0.029; - 0.0029
HBCD	Br(1); Br(2); Br(3); Br(4); Br(5); Br(6); C(7); C(8); C(9); C(10); C(11); C(12)	0.0366; 0.0250; 0.0416; 0.0276; 0.0298; 0.0372; -0.0271; -0.0282; - 0.0280; -0.0343; -0.0289; -0.0312
TBBA	O(1); O(1'); Br(2); Br(2'); C(3); C(3'); C(4); C(4'); C(5); C(5'); Br(6); Br(6')	-0.1722; -0.1721; 0.0065; 0.0314; 0.0433; 0.0432; -0.018; -0.0233; - 0.0204; -0.0204; 0.0270; 0.0036
BTBPE	O(1); O(1'); Br(2); Br(2'); C(3); C(3'); Br(4); Br(4'); C(5); C(5'); Br(6); Br(6'); C(7); C(7')	-0.1324; -0.1326; 0.0341; 0.0349; - 0.0085; -0.0086; 0.0052; 0.0051; - 0.0028; -0.0027; 0.0239; 0.0341; - 0.0090; -0.0027

Hirshfeld charge formalism provides a robust methodology for estimating atomic charges that is insensitive to the deployed basis set, compared with the commonly-deployed Mulliken population analysis [78-79]. Table 6.2 depicts atomic charges on selected positions of all title compounds for the S_0 gaseous state, while Figure 6.S3 draws atomic charge contours. Charges on the bromine atoms (q_{Br}) substituted at different positions of the molecule provide a measure for the extent of photoreactivity at *-ortho/-meta* and *-para* sites, with regard to C-C/C-O linkages and OH groups. The higher the charge on a bromine atom (q_{Br}), the greater the propensity for the Br atom to depart the molecule via photodecomposition [41, 71, 80]. The most photoreactive bromine atom holds the most positive charge in the gaseous ground state. Our estimated charge analysis results are

consistent with earlier theoretical studies [34, 41]. The carbon atoms attached to bromine atoms are richer in electrons and therefore carry a negative charge.

As Figure 6.3 infers, we observe a positive correlation between the atomic charges of Br atoms in the S_0 state, and elongation in C-Br bond lengths in the S_1 state, for TBBA and BTBPE, in both media. We find that the bromine atom with the highest positive charge in the ground state experiences the maximum elongation in C-Br bond length upon excitation ($S_0 \rightarrow S_1$ transition). For example, in S_0 BTBPE and 2,3,4,5-TBP molecules, the bromine atoms at *ortho* positions (with respect to C-O linkages and the hydroxyl groups, respectively) endure the highest positive atomic charge values ($0.0349e$ and $0.0383e$, correspondingly; refer to values in Table 6.2) and hence, the longest C-Br elongation upon excitation (in the S_1 state). Similarly, in TBBA and BTBPE ground state molecules, bromine atoms substituted at *ortho*-C(Br) positions (with respect to hydroxyl groups and C-C linkages, respectively) bear the highest positive atomic charges of $0.0314e$ and $0.0349e$ (most photoreactive Br atoms) and encounter the maximum elongation of C-Br bonds (12.1 % and 7.8 %, respectively) in the first excited state.

6.3.4. Optical properties including UV-Vis absorption spectra, excitation energies and oscillation strengths

Molecules absorb light as a discrete bundle of electromagnetic radiation (e.g., sunlight) in the form of photons. Thus, the energy of photons in the form of visible or ultraviolet light is adequate to disrupt/rearrange covalent bonds, accelerating the photochemical process and generating the transient excited states that allow transformation into a distinctive product [81-82]. As discussed in the introduction, most organohalogen compounds absorb light in the UV-vis spectrum window. However, the presence of photocatalysts shifts the absorption of light from the UV region to the visible light region, allowing more photons to be absorbed which prompts photochemical reactions. Therefore, we computed photochemical properties such as excitation energies, oscillation strengths and UV-Vis absorption spectra of the selected BFRs and their non-brominated counterparts.

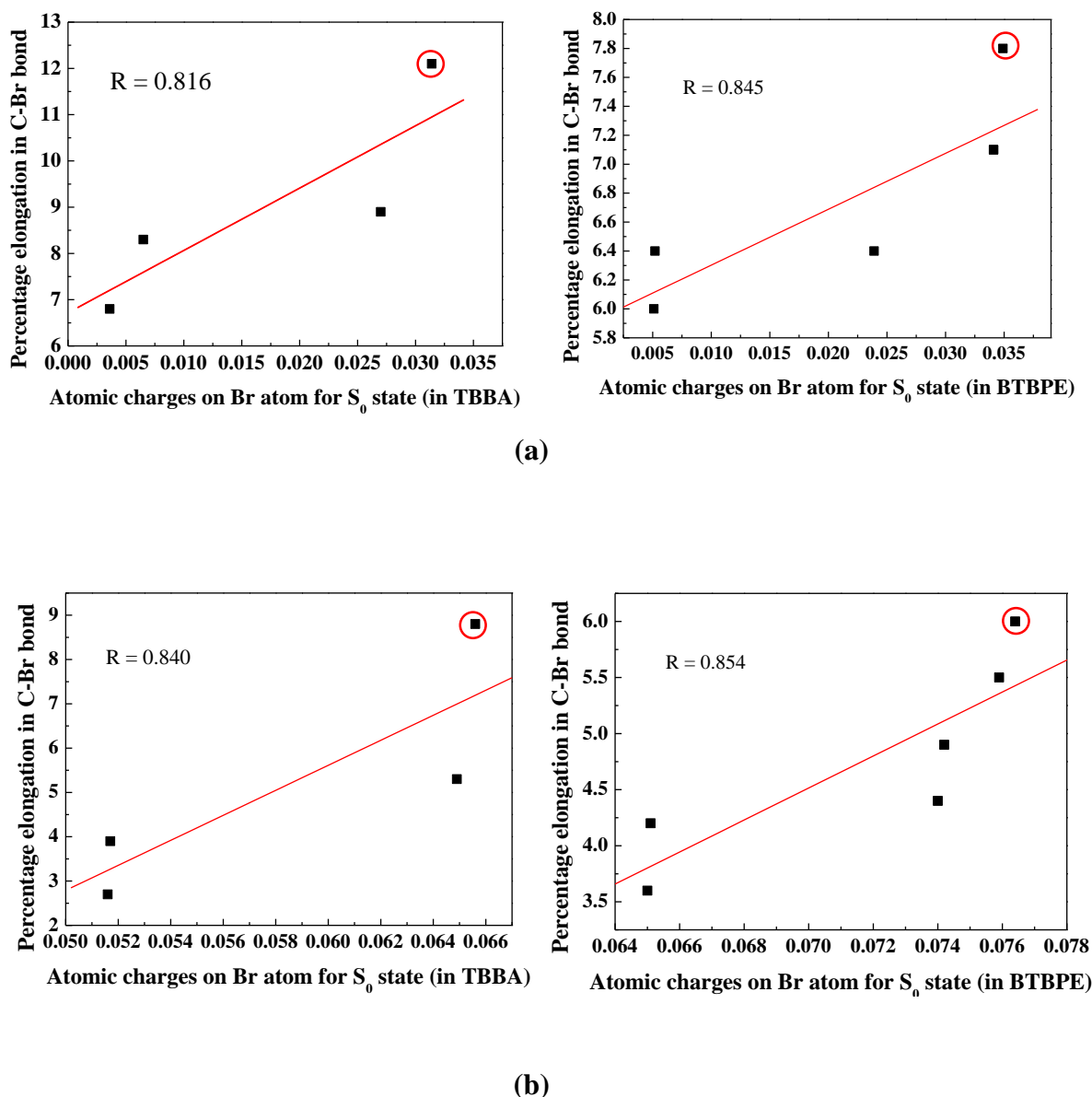


Figure 6.3. Correlation between the calculated bromine atomic charge (q_{Br}) in the S₀ state and the percentage elongation of C-Br bonds upon the S₀ → S₁ transition, for TBBA and BTBPE in (a) gas, and (b) aqueous media. The bromine atom attached at an *ortho* position with regard to the hydroxyl group (in TBBA) and C-O linkage (in BTBPE) has the highest positive charge (shown in red circles). The correlation coefficient of the trend lines is given by the R (depict the reliability of values).

Tables 6.3 and 6.4 present the results of calculated excitation energies (in eV) and oscillator strengths (f) for the five lowest excited states of selected brominated and non-brominated molecules in gaseous and aqueous phases. Oscillator strength is interpreted

as the probability that a moiety absorbs or emits electromagnetic radiation that triggers electron transition between energy levels. Our results illustrate that in the gas phase, all molecules assume lower excitation energies (in eV) in reference to excitation energies in the aqueous phase. However, the oscillator strength for the five lowest excited states of aqueous phase molecules entails slightly higher values when compared to analogous gas phase values. The electron transition probability from the $S_0 \rightarrow S_3$ energy level for 4,4'-diBB, 4,4'-diBDE, 2,3,4,5-TBP and bisphenol is much higher in comparison to the other energy level transitions. Similarly, based on the values of excitation energies, $S_0 \rightarrow S_2$, $S_0 \rightarrow S_4$ and $S_0 \rightarrow S_1$ represent the most accessible transitions in HBCD, TBBA and BTBPE molecules, respectively. Figure 6.4 shows that excitation energy increases with E^{H-L} values.

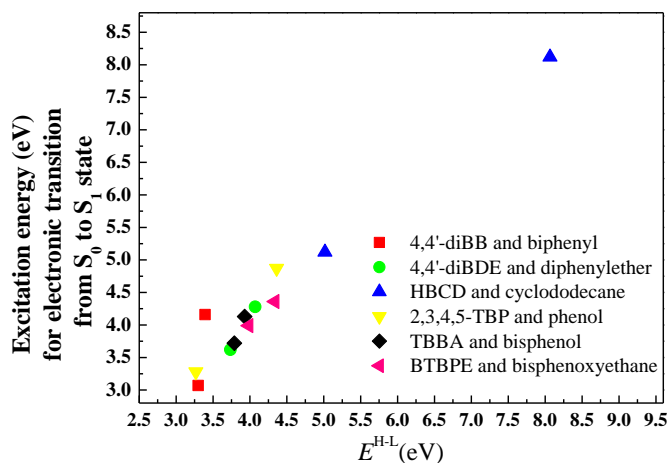


Figure 6.4. Correlation between E^{H-L} (in eV) and excitation energy (in eV) for the $S_0 \rightarrow S_1$ transition for brominated and non-brominated compounds. The lowest point of each series represents the brominated isomer and the upper point represents its non-brominated isomer

Table 6.3. Calculated molecular excitation energies expressed as photon absorption energy (in eV) and oscillator strength (f) of the five lowest excited states of selected BFRs and their non-brominated analogous molecules in the gaseous phase.

E (in eV)	<i>f</i>	E (in eV)	<i>f</i>	E (in eV)	<i>f</i>
4,4'-diBB		4,4'-diBDE		2,3,4,5-TBP	

CHAPTER 6 Properties of Brominated Flame Retardants (BFRs) on the Verge of their Photodecomposition

S1	3.07	0.000000	3.62	0.000000	3.28	0.000015
S2	3.68	0.000000	3.76	0.000000	3.69	0.000071
S3	3.95	0.752908	3.93	0.009209	3.92	0.035701
S4	4.00	0.000000	3.94	0.000000	4.20	0.000001
S5	4.11	0.000000	4.08	0.000000	4.47	0.000115
HBCD		TBBA		BTBPE		
S1	5.12	0.000916	3.72	0.000000	3.99	0.000182
S2	5.20	0.002731	3.75	0.000000	3.99	0.000143
S3	5.25	0.000112	3.79	0.000000	4.10	0.000028
S4	5.26	0.000093	3.84	0.005748	4.10	0.000068
S5	5.28	0.000718	3.86	0.002312	4.19	0.000001
biphenyl		diphenylether		phenol		
S1	4.16	0.000000	4.28	0.157267	4.87	0.021008
S2	4.27	0.528043	4.55	0.167366	5.79	0.038655
S3	4.44	0.005237	4.59	0.168861	6.11	0.000321
S4	4.82	0.000001	4.82	0.177248	6.63	0.211280
S5	5.09	0.045887	5.01	0.184148	6.77	0.000938
cyclododecane		bisphenol A		bisphenoxyethane		
S1	8.12	0.023689	4.13	0.026168	4.36	0.001883
S2	8.15	0.000128	4.22	0.000329	4.51	0.003150
S3	8.34	0.003114	4.52	0.049700	4.55	0.003084
S4	8.37	0.000475	4.58	0.001626	4.83	0.005917
S5	8.40	0.009544	4.74	0.010612	4.85	0.013199

Table 6.4. Calculated molecular excitation energies expressed as photon absorption energy E (in eV) and oscillator strength (f) of the five lowest excited states of selected BFRs and their non-brominated analogous molecules in the aqueous phase.

	E	f	E	f	E	f
	(in eV)		(in eV)		(in eV)	
	4,4'-diBB		4,4'-diBDE		2,3,4,5-TBP	
S1	4.13	0.756427	4.16	0.009224	3.39	0.000043

CHAPTER 6 Properties of Brominated Flame Retardants (BFRs) on the Verge of their Photodecomposition

S2	4.14	0.000000	4.41	0.001709	3.77	0.000086
S3	4.56	0.000051	4.49	0.254724	4.43	0.000780
S4	4.68	0.000004	4.65	0.001598	4.51	0.028090
S5	4.80	0.000010	4.71	0.000346	4.76	0.000270
HBCD		TBBA		BTBPE		
S1	5.21	0.001312	3.98	0.010096	4.10	0.000189
S2	5.29	0.003102	3.98	0.000495	4.10	0.000184
S3	5.31	0.000350	4.23	0.038002	4.21	0.000027
S4	5.34	0.000386	4.27	0.001046	4.21	0.000040
S5	5.36	0.005062	4.29	0.001159	4.26	0.000001
biphenyl		diphenylether		phenol		
S1	4.17	0.000000	4.30	0.009881	4.89	0.020545
S2	4.28	0.527685	4.58	0.002512	5.80	0.039108
S3	4.45	0.005736	4.61	0.162617	6.64	0.215791
S4	4.83	0.000001	4.84	0.001251	6.68	0.000634
S5	5.10	0.041462	5.02	0.002377	6.84	0.538288
cyclododecane		bisphenol A		bisphenoxyethane		
S1	8.14	0.023283	4.14	0.025994	4.37	0.001973
S2	8.17	0.000113	4.23	0.000373	4.52	0.003131
S3	8.35	0.003426	4.53	0.051397	4.56	0.003101
S4	8.38	0.000767	4.60	0.001396	4.84	0.005482
S5	8.42	0.009694	4.75	0.010763	4.86	0.014184

For example, in the case of biphenyl, the excitation energy is 4.27 eV (against $E^{\text{H-L}}$ 3.39 eV) which is higher in comparison to 4,4'-diBB substituted with two bromine atoms, i.e., 3.95 eV (against $E^{\text{H-L}}$ 3.29 eV). Additionally, for 2,3,4,5-TBP, the required excitation energy is 3.92 eV versus 3.26 eV $E^{\text{H-L}}$, which is lower in contrast to phenol, which necessitates 6.63 eV of excitation energy versus $E^{\text{H-L}}$ 4.36 eV. Thus, we can say that with an increasing number of bromine substituents, excitation energy decreases along with the $E^{\text{H-L}}$ energy gap. In a similar manner, our recent theoretical investigation (chapter 5) on bromophenols [42], predicted that bromophenol congeners with the lowest excitation energies are those with the minimum $E^{\text{H-L}}$ values within each homologue group.

Figure 6.5 shows the UV-Vis absorption spectra for all selected brominated and non-brominated compounds in the two media. Our calculated UV absorbance spectra of 4,4'-diBDE is in very good agreement with the analogous experimental spectrum [71, 83]. Oscillator strength for all brominated and non-brominated molecules falls within the UV region, i.e., 130 – 340 nm wavelength for both gas and solution media. The optical spectra exhibited similar shapes in both gaseous and aqueous media for most compounds, excepting 4,4'-diBB, 4,4'-diBDE and BTBPE. These three compounds displayed two intensive absorbance bands in the aqueous phase, but only one intensive band in the gaseous phase. For example, in 4,4'-diBB, we observed one intense peak at a wavelength near 315 nm in the gas phase that transformed into two peaks with high absorption bands at wavelengths of 240 nm and 300 nm in the aqueous medium. Nevertheless, for brominated compounds in the aqueous phase, the absorption band exhibited a relevant blue shift (shifts towards shorter wavelengths) in contrast to brominated compounds in the gas phase. Consistently, investigated brominated compounds had lower excitation energies in the gas phase than the aqueous phase, and displayed a red shift (shift towards longer wavelengths) in comparison to brominated molecules in the liquid phase. In summary, brominated compounds had lower excitation energies than non-brominated ones, and absorbed light in the region of longer wavelengths.

Now we turn our attention to explain the effect of bromination degree on the photolytic properties of the studied molecules. For instance, HBCD (with six bromine atoms) exhibits an intense absorption peak at a wavelength of 234 nm that shifts towards shorter wavelengths by 83 nm for cyclododecane molecules (no bromine atom) in the gaseous phase. Likewise, for 4,4'-diBDE (bearing two bromine atoms), the highest absorption band occurs at a wavelength of 288 nm and is reduced by nearly 18 nm for diphenylether in the gas phase. Accordingly, we can draw the conclusion that the number of bromine atoms attached to the molecule plays a potent role in altering its photoreactivity by inducing a red shift in UV light absorbance. Analogously, six bromine atoms attached to a molecule (HBCD and BTBPE) induced red shifts of 83 nm and 68 nm, respectively, while molecules with two bromine atoms attached (4,4'-diBB and 4,4'-diBDE) stimulate red shifts of 24 nm and 18 nm in gas phase (illustrated in Figures 6.5a and 6.5b). We detected a similar correlation for absorption spectra red shift and number of bromine

CHAPTER 6 Properties of Brominated Flame Retardants (BFRs) on the Verge of their Photodecomposition

substituents in the aqueous phase as well. However, the degree of red shift is more profound for gaseous molecules. The number of bromine substituents is positively correlated with the computed wavelength of maximum absorbance. This observation is in line with experimental studies on the photodecomposition of PBDEs [34].

The careful examination of absorption spectra for non-brominated compounds in both gas and water media indicates that when there is an absence of halogen atoms in aromatic compounds, the absorption bands do not exhibit any shift on going from gas to water. For example, the biphenyl molecule shows three absorption peaks, with maximum intensities at 191 nm, 242 nm and 290 nm, in both water and gas mediums.

CHAPTER 6 Properties of Brominated Flame Retardants (BFRs) on the Verge of their Photodecomposition

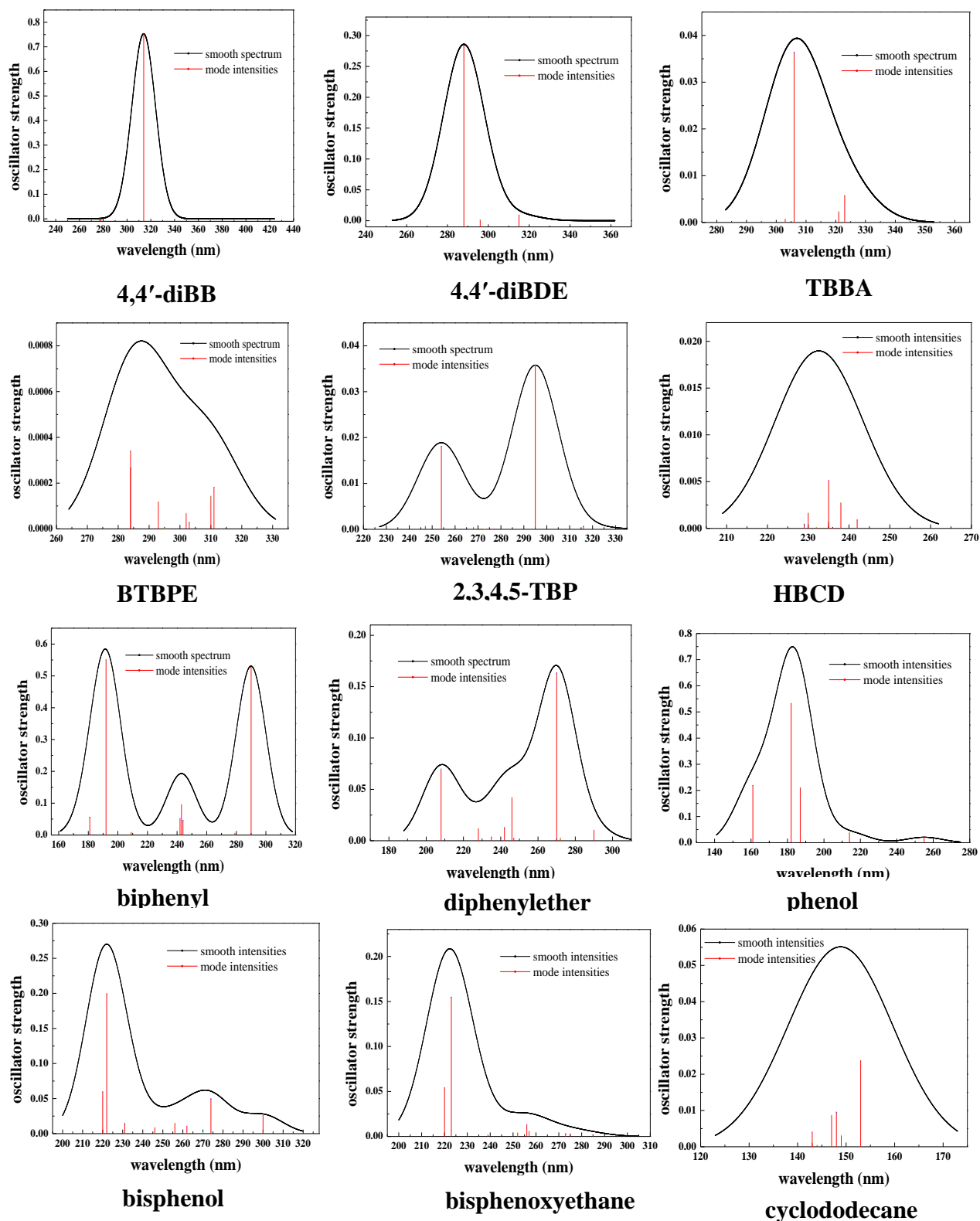


Figure 6.5a. Calculated gaseous-phase UV absorption spectra of studied BFRs and their non-brominated molecules.

CHAPTER 6 Properties of Brominated Flame Retardants (BFRs) on the Verge of their Photodecomposition

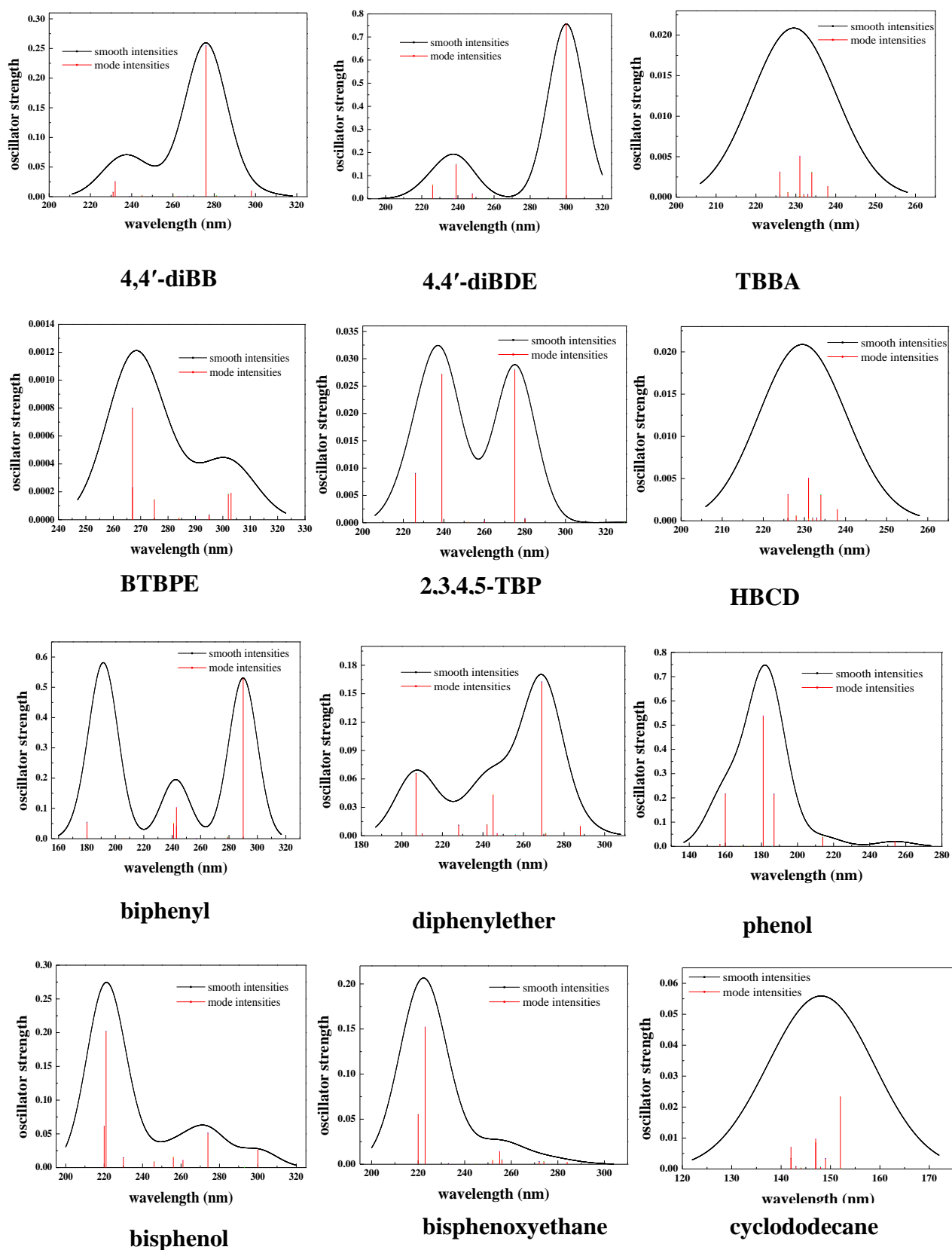


Figure 6.5b. Calculated aqueous-phase UV absorption spectra of studied BFRs and their non-brominated molecules.

6.4. Conclusion

The current chapter illustrates that geometric and electronic properties are correlated, and are equally important in determining the photoreactive nature of halogenated aromatic molecules. Compounds with the highest degree of bromination entail lower $E^{\text{H-L}}$ values and, hence, require lower excitation energies for excited state transitions. They exhibit a red shift of their maximum absorbance peaks in the UV-Vis spectrum. Br atoms attached to *ortho*-C (with respect to C-C and C-O linkages or the hydroxyl groups) hold the highest positive atomic charges and thus experience the highest lengthening in C-Br in their first excited state, in both mediums, prompting their reductive debromination. On the other hand, the analogous non-brominated aromatic hydrocarbons display higher $E^{\text{H-L}}$ excitation energies and absorption peaks at shorter wavelengths, indicating their relative stability against photodecomposition in both media. The computed $E^{\text{H-L}}$ values for selected BFRs and their non-brominated molecules infer that the number of bromine substituents and the nature of structure (aromatic/non-aromatic) contribute significantly towards the photoreactivity of molecules.

Acknowledgments

This study has been supported by the Australian Research Council (ARC), and grants of computing time from the National Computational Infrastructure (NCI), Australia as well as the Pawsey Supercomputing Centre. A.S. thanks Murdoch University, Australia, for a postgraduate research scholarship.

Supporting information

The frontier molecular orbitals and optimised structures of brominated and non-brominated molecules along with the net atomic charges are available in appendix C.

References

- [1] Sellström, U., Kierkegaard, A., Alsberg, T., Jonsson, P., Wahlberg, C., De Wit, C. Brominated flame retardants in sediments from European estuaries, the Baltic Sea and in sewage sludge. *Organohalogen Compd.* **1999**, 40, 383-386.
- [2] Morris, S., Allchin, C.R., Zegers, B.N., Haftka, J.J.H., Boon, J.P., Belpaire, C., Leonards, P.E.G., van Leeuwen, S.P.J., de Boer, J. Distribution and fate of HBCD and TBBPA brominated flame retardants in North Sea estuaries and aquatic food webs. *Environ. Sci. Technol.* **2004**, 38, 5497-5504.
- [3] Covaci, A., Voorspoels, S., de Boer, J. Determination of brominated flame retardants, with emphasis on polybrominated diphenyl ethers (PBDEs) in environmental and human samples—a review. *Environ. Int.* **2003**, 29, 735-756.
- [4] Eljarrat, E., de la Cal, A., Raldua, D., Duran, C., Barcelo, D. Brominated flame retardants in Alburnus from Cinca River Basin (Spain). *Environ. Pollut.* **2005**, 133, 501-508.
- [5] Möller, A., Xie, Z., Sturm, R., Ebinghaus, R. Polybrominated diphenyl ethers (PBDEs) and alternative brominated flame retardants in air and seawater of the European Arctic. *Environ. Pollut.* **2011**, 159, 1577-1583.
- [6] Ali, N., Harrad, S., Goosey, E., Neels, H., Covaci, A. “Novel” brominated flame retardants in Belgian and UK indoor dust: Implications for human exposure. *Chemosphere* **2011a**, 83, 1360-1365.
- [7] Ali, N., Harrad, S., Muenhor, D., Neels, H., Covaci, A. Analytical characteristics and determination of major novel brominated flame retardants (NBFRs) in indoor dust. *Anal. Bioanal. Chem.* **2011b**, 400, 3073-3083.
- [8] Covaci, A., Harrad, S., Abdullah, M. A.E., Ali, N., Law, J. R., Herzke, D., de Wit, C. A. Novel brominated flame retardants: A review of their analysis, environmental fate and behaviour. *Environ. Int.* **2011**, 37, 532-556.
- [9] de Wit, C.A. An overview of brominated flame retardants in the environment. *Chemosphere* **2002**, 46, 583-624.
- [10] Eriksson, P., Jakobsson, E., Fredriksson, A. Brominated flame retardants: a novel class of developmental neurotoxicants in our environment? *Environ Health Perspect.* **2001**, 109, 903-908.

- [11] Fromme, H., Hilger, B., Kopp, M., Völkel, W.M. Polybrominated diphenyl ethers (PBDEs), hexabromocyclododecane (HBCD) and “novel” brominated flame retardants in house dust in Germany. *Environ. Int.* **2014**, 64, 61-68.
- [12] Darnerud, P.O. Toxic effects of brominated flame retardants in man and in wildlife. *Environ. Int.* **2003**, 29, 841-853.
- [13] Watanabe, I., Sakai, S.I. Environmental release and behavior of brominated flame retardants. *Environ. Int.* **2003**, 29, 665-682.
- [14] Buser, H.R. Polybrominated dibenzofurans and dibenzo-*p*-dioxins: thermal reaction products of polybrominated diphenyl ether flame retardants. *Environ. Sci. Technol.* **1986**, 20, 404-408.
- [15] Luijk, R., Govers, H.A.J. The formation of polybrominated dibenzo-*p*-dioxins (PBDDs) and dibenzofurans (PBDFs) during pyrolysis of polymer blends containing brominated flame retardants. *Chemosphere* **1992**, 25, 361-374.
- [16] Sakai, S., Watanabe, J., Honda, Y., Takatsuki, H., Aoki, I., Futamatsu, M., Shiozaki, K. Combustion of brominated flame retardants and behavior of its byproducts. *Chemosphere* **2001**, 42, 519-531.
- [17] Weber, R., Kuch, B. Relevance of BFRs and thermal conditions on the formation pathways of brominated and brominated–chlorinated dibenzodioxins and dibenzofurans. *Environ. Int.* **2003**, 29, 699-710.
- [18] Altarawneh, M., Dlugogorski, B.Z. A mechanistic and kinetic study on the formation of PBDD/Fs from PBDEs. *Environ. Sci. Technol.* **2013**, 47, 5118-5127.
- [19] Altarawneh, M., Dlugogorski, B.Z. Thermal decomposition of 1,2-bis(2,4,6-tribromophenoxy)ethane (BTBPE), a novel brominated flame retardant. *Environ. Sci. Technol.* **2014a**, 48, 14335-14343.
- [20] Altarawneh, M., Dlugogorski, B.Z. Mechanism of thermal decomposition of tetrabromobisphenol A (TBBA). *J. Phys. Chem. A.* **2014b**, 118, 9338-9346.
- [21] Altarawneh, M., Dlugogorski, B.Z. Formation of polybrominated dibenzofurans from polybrominated biphenyls. *Chemosphere* **2015**, 119, 1048-1053.
- [22] Barontini, F., Cozzani, V., Marsanich, K., Raffa, V., Petarca, L. An experimental investigation of tetrabromobisphenol A decomposition pathways. *J. Anal. Appl. Pyrolysis.* **2004**, 72, 41-53.

- [23] Barontini, F., Cozzani, V. Formation of hydrogen bromide and organobrominated compounds in the thermal degradation of electronic boards. *J. Anal. Appl. Pyrolysis*. **2006**, 77, 41-55.
- [24] Luda, M.P., Balabanovich, A.I., Camino, G. Thermal decomposition of fire retardant brominated epoxy resins. *J. Anal. Appl. Pyrolysis*. **2002**, 65, 25-40.
- [25] Ortuño, N., Moltó, J., Conesa, J. A., Font, R. Formation of brominated pollutants during the pyrolysis and combustion of tetrabromobisphenol A at different temperatures. *Environ. Pollut.* **2014**, 191, 31-37.
- [26] Saeed, A, Dlugogorski, B.Z., Altarawneh M. Formation of brominated and non-brominated species from gas-phase thermal decomposition of pure TBBA. 14th International Congress on Combustion By-Products and Their Health Effects, **2015**, Umeå, Sweden.
- [27] Saeed A., Altarawneh, M., Dlugogorski BZ. Formation of PBDD/F precursors in gas-phase decomposition of tetrabromobisphenol a (TBBA). *Organohalogen Compd.* **2016**, *Submitted*.
- [28] Choi, K.I., Lee, S.H., Osako, M. Leaching of brominated flame retardants from TV housing plastics in the presence of dissolved humic matter. *Chemosphere* **2009**, 74, 460-466.
- [29] Stapleton, H.M., Klosterhaus, S., Keller, A., Ferguson, P.L., Bergen, S.V., Coopert, E., Webster, T.F., Blum, A. Identification of flame retardants in polyurethane foam collected from baby products. *Environ. Sci. Technol.* **2011**, 45, 5323-5331.
- [30] Gullett, B.K., Linak, W.P., Touati, A., Wasson, S.J., Gatica, S., King. C.J. Characterization of air emissions and residual ash from open burning of electronic wastes during simulated rudimentary recycling operations. *J. Mater. Cycles Waste Manage.* **2007**, 9, 69-79.
- [31] Eguchia, A., Isobea, T., Ramua, K., Tuea, N.M., Sudaryantoa, A., Devanathana, G., Vietd, P.H., Tanae, R.S., Takahashia, S., Subramaniana, A., Tanabea, S. Soil contamination by brominated flame retardants in open waste dumping sites in Asian developing countries. *Chemosphere* **2013**, 90, 2365-2371.
- [32] Tian, M., Chen, S.J., Wang, J., Zheng, X.B., Luo, X.J., Mai, B,X. Brominated flame retardants in the atmosphere of e-waste and rural sites in southern china:

- seasonal variation, temperature dependence, and gas-particle partitioning. *Environ. Sci. Technol.* **2011**, 45, 8819-8825.
- [33] Söderström, G., Sellström, U., de Wit, C.A., Tysklind, M. Photolytic debromination of decabromodiphenyl ether (BDE 209). *Environ. Sci. Technol.* **2004**, 38, 127-132.
- [34] Eriksson, J., Green, N., Marsh, G., Bergman, Å. Photochemical decomposition of 15 polybrominated diphenyl ether congeners in methanol/water. *Environ. Sci. Technol.* **2004**, 38, 3119-3125.
- [35] Watanabe, I., Tatsukawa, R. Formation of brominated dibenzofurans from the photolysis of flame retardant decabromobiphenyl ether in hexane solution by UV and sun light. *Bull. Environ. Contam. and Toxicol.* **2008**, 39, 953-959.
- [36] Norris, J.M., Ehrmantraut, J.W., Gibbons, C.L., Kociba, R.J., Schwetz, B.A., Rose, J.Q., Humiston, C.G., Jewett, G.L., Crummett, W.B., Gehring, P.J., Tirsell, J.B., Brosier, J.S. Toxicological and environmental factors involved in the selection of decabromodiphenyl oxide as a fire retardant chemical. *Appl. Polym. Symp.* **1973**, 22, 195-219.
- [37] Otha, S., Nishimura, H., Nakao, T., Aozasa, O., Miyata, H. Characterization of the photolysis of Decabromodiphenyl ether and the levels of PBDEs as its photoproducts in atmospheric air of Japan. *Organohalogen Compd.* **2001**, 52, 321-324.
- [38] Luo, J., Hu, J., Wei, X., Li, L., Huang, X. Excited states and photodebromination of selected polybrominated diphenyl ethers: computational and quantitative structure–property relationship studies. *Int. J. Mol. Sci.* **2015**, 16, 1160.
- [39] Sun, C., Chang, W., Ma, W., Chen, C., Zhao, J. Photoreductive debromination of decabromodiphenyl ethers in the presence of carboxylates under visible light irradiation. *Environ. Sci. Technol.* **2013**, 47, 2370–2377.
- [40] Suh, Y.W., Buettner, G.R., Venkataraman, S., Treimer, S.E., Robertson, L.W., Ludewig, G. UVA/B-induced formation of free radicals from decabromodiphenyl ether. *Environ. Sci. Technol.* **2009**, 43, 2581–2588.
- [41] Wang, S., Hao, C., Gao, Z., Chen, J., Qiu, J. Effects of excited-state structures and properties on photochemical degradation of polybrominated diphenyl ethers: A TDDFT study. *Chemosphere* **2012**, 88, 33-38.

- [42] Saeed, A., Altarawneh, M., Dlugogorski, B.Z. Photodecomposition of bromophenols. *Chemosphere* **2016**, 150, 749-758.
- [43] Joschek, H.I., Miller, S.I. Photocleavage of phenoxyphenols and bromophenols. *J. Am. Chem. Soc.* **1966**, 88, 3269-3272.
- [44] Jaward, F.M., Farrar, N.J., Harner, T., Sweetman, A.J., Jones, K.C. Passive air sampling of PCBs, PBDEs, and organochlorine pesticides across Europe. *Environ. Sci. Technol.* **2004**, 38, 34-41.
- [45] Mimmoa, T., Hannb, S., Jaitzb, L., Cescoa, S., Gessac, C.E., Puschenreiterd, M. Time and substrate dependent exudation of carboxylates by *Lupinus albus* L. and *Brassica napus* L. *Plant Physiol. Biochem.* **2011**, 49, 1272-1278.
- [46] Delley, B. From molecules to solids with the DMol³ approach. *J. Chem. Phys.* **2000**, 113, 7756-7764.
- [47] Perdew, J.P., Chevary, J.A., Vosko, S.H., Jackson, K.A., Pederson, M.R., Singh, D.J., Fiolhais, C. Atoms, molecules, solids, and surfaces: Applications of the generalized gradient approximation for exchange and correlation. *Phys. Rev. B.* **1992**, 46, 6671-6687.
- [48] Delley, B. An all-electron numerical method for solving the local density functional for polyatomic molecules. *J. Chem. Phys.* **1990**, 92, 508-517.
- [49] Klamt, A., Schüürmann, G. COSMO: a new approach to dielectric screening in solvents with explicit expressions for the screening energy and its gradient. *J. Chem. Soc. Perkin. Trans.* **1993**, 2, 799-805.
- [50] Klamt, A. Conductor-like screening model for real solvents: A new approach to the quantitative calculation of solvation phenomena. *J. Phys. Chem.* **1995**, 99, 2224-2235.
- [51] Zangwill, A., Soven, P. Density-functional approach to local-field effects in finite systems: Photoabsorption in the rare gases. *Phys. Rev. A* **1980**, 21, 1561-1572.
- [52] Delley, B. Time dependent density functional theory with DMol³. *J. Phys.: Condens. Matter.* **2010**, 22, 384208.
- [53] Yao, L., Lin, S.H. The anharmonic effect study of coupled morse oscillators for the unimolecular reaction. *Sci. China, Ser. B, Chem.* **2008**, 51, 1146-1152.
- [54] Zhu, C., Liang, K.K., Hayashi, M., Lin, S.H. Theoretical treatment of anharmonic effect on molecular absorption, fluorescence spectra, and electron transfer. *J. Chem. Phys.* **2009**, 130, 137-146.

- [55] Wang, H., Zhu, C., Yu, J.G., Lin, S.H. Anharmonic Franck–Condon simulation of the absorption and fluorescence spectra for the low-lying S_1 and S_2 excited states of pyridine. *J. Phys. Chem. A* **2009**, 113, 14407-14414.
- [56] Fonseca, C. G., Handgraaf, J.W., Baerends, E.J., Bickelhaupt, F.M. Voronoi deformation density (VDD) charges: Assessment of the Mulliken, Bader, Hirshfeld, Weinhold, and VDD methods for charge analysis. *J. Comput. Chem* **2003**, 25, 189-210.
- [57] Zhao, G.J., Han, K.L. Excited state electronic structures and photochemistry of heterocyclic annulated perylene (HAP) materials tuned by heteroatoms: S, Se, N, O, C, Si, and B. *J. Phys. Chem. A*, **2009**, 113, 4788-4794.
- [58] Heeb, N.V., Schweizer, W.B., Kohler, M., Gerecke, A.C. Structure elucidation of hexabromocyclododecanes –a class of compounds with a complex stereochemistry. *Chemosphere* **2005**, 61, 65-73.
- [59] Eriksson, J., Eriksson, L. 2,2',6,6'-Tetrachloro-4,4'-propane-2,2-diyldiphenol, 2,2',6-tribromo-4,4'-propane-2,2-diyldiphenol and 2,2',6,6'-tetrabromo-4,4'-propane-2,2-diyldiphenol. *Acta Crystallogr. Sect. C* **2001**, 57, 1308-1312.
- [60] Qiu, S., Wei, J., Pan, F., Liu, J., Zhang, A. Vibrational, NMR spectrum and orbital analysis of 3,3',5,5'-tetrabromobisphenol A: A combined experimental and computational study. *Spectrochim. Acta Mol. Biomol. Spectrosc.* **2013**, 105, 38-44.
- [61] Alaei, M., Arias, P., Sjödin, A., Bergman, Å. An overview of commercially used brominated flame retardants, their applications, their use patterns in different countries/regions and possible modes of release. *Environ. Int.* **2003**, 29, 683-689.
- [62] Li, A., Tai, C., Zhao, Z., Wang, Y., Zhang, Q., Jiang, G., Hu, J. Debromination of decabrominated diphenyl ether by resin-bound iron nanoparticles. *Environ. Sci. Technol.* **2007**, 41, 6841-6846.
- [63] Cruz, J.B., Jafvert, C. T., Hua, I. Solar photodecomposition of decabromodiphenyl ether: products and quantum yield. *Environ. Sci. Technol.* **2004**, 38, 4149-4156.
- [64] Eriksson, J., Jakobsson, E., Marsh, G., Bergman, A. Photodecomposition of brominated diphenylethers in methanol/water [Abstract]. Presented at the Second International Workshop on Brominated Flame Retardants, 14–16 May, **2001a** Stockholm, Sweden.

- [65] Zhao, Y.Y., Zhang, X.H., Sojnu, O.S.S. Thermodynamics and photochemical properties of a, b, and c-hexabromocyclododecanes: A theoretical study. *Chemosphere* **2010**, 80, 150-156.
- [66] Zeng, X. Development, Validation and the Application of a Congener Specific Photodegradation Model for PBDEs. **2007**, Oregon State University
- [67] Fang, L., Huang, J., Yu, G., Wang, L. Photochemical degradation of six polybrominated diphenyl ether congeners under ultraviolet irradiation in hexane. *Chemosphere* **2008**, 71, 258-267.
- [68] Christiansson, A., Eriksson, J., Teclechiel, D., Bergman, Å. Identification and quantification of products formed via photolysis of decabromodiphenyl ether. *Environ. Sci. Pollut. Res.* **2009**, 16, 312-321.
- [69] Mas, S., Juan, A. d., Lacorte, S., Tauler, R. Photodegradation study of decabromodiphenyl ether by UV spectrophotometry and a hybrid hard- and soft-modelling approach. *Anal. Chim. Acta.* **2008**, 618, 18-28.
- [70] Petr Klán, J.W. Photochemistry of Organic Compounds. **2009**, John Wiley & Sons.
- [71] Fang, L., Huang, J., Yu, G., Li, X. Quantitative structure–property relationship studies for direct photolysis rate constants and quantum yields of polybrominated diphenyl ethers in hexane and methanol. *Ecotoxicol. Environ. Saf.* **2009**, 72, 1587-1593.
- [72] Zhao, Y.Y., Tao, F.M., Zeng, E.Y. Theoretical study on the chemical properties of polybrominated diphenyl ethers. *Chemosphere* **2008**, 70, 901-907.
- [73] Pan, L., Bian, W. Theoretical study on the photodegradation mechanism of nona-BDEs in methanol. *ChemPhysChem* **2013**, 14, 1264-1271.
- [74] Rai, D., Joshi, H., Kulkarni, A.D., Gejji, S.P., Pathak, R.K. Electric field effects on aromatic and aliphatic hydrocarbons: a density-functional study. *J. Phys. Chem. A.* **2007**, 111, 9111-9121.
- [75] Kornilovich, P., Bratkovski, A.M., Chang, S.C., Williams, R.S. Low-forward-voltage molecular rectifier. Google Patent, **2003**, US 6670631 B2.
- [76] Hirshfeld, F.L. Bonded-atom fragments for describing molecular charge densities. *Theoretica chimica acta* **1977**, 44, 129-138.
- [77] Wiberg, K.B., Rablen, P.R. Comparison of atomic charges derived via different procedures. *J. Comput. Chem.* **1993**, 14, 1504-1518.

- [78] Guerra, F.C., Handgraaf, J.W., Baerends, E.J., Bickelhaupt, F.M. Voronoi deformation density (VDD) charges: assessment of the mulliken, bader, hirshfeld, weinhold, and VDD methods for charge analysis. *J. Comput. Chem.* **2004**, 25, 189-210.
- [79] Davidson, E.R., Chakravorty, S. A test of the Hirshfeld definition of atomic charges and moments. *Anal. Chim. Acta.* **1992**, 83, 319-330.
- [80] Xie, Q., Chen, J., Shao, J., Chen, C.e., Zhao, H., Hao, C. Important role of reaction field in photodegradation of deca-bromodiphenyl ether: Theoretical and experimental investigations of solvent effects. *Chemosphere* **2009**, 76, 1486-1490.
- [81] Becker, R.S. Photochemical process. **1971**, Google Patent.
- [82] Jackson, D.P. Dense phase gas photochemical process for substrate treatment. **1991**, Google Patent.
- [83] Marsh, G., Hu, J., Jakobsson, E., Rahm, S., Bergman, Å. Synthesis and characterization of 32 polybrominated diphenyl ethers. *Environ. Sci. Technol.* **1999**, 33, 3033-3037.

CHAPTER 7 THERMAL DECOMPOSITION OF TETRABROMOBISPHENOL A (TBBA)

Table of Content

Abstract	240
7.1. Introduction	241
7.2. Experimental	244
7.2.1. Materials	244
7.2.2. Experimental setup and procedure	245
7.2.2.1 Blanks and replicates	248
7.2.3. Computational methodology	249
7.3. Results and discussion	249
7.3.1. TBBA decomposition	249
7.3.2. Formation of brominated bisphenols and HBr	251
7.3.3. Formation of brominated phenols, brominated alkylated phenols, brominated benzenes and brominated alkylated benzenes	253
7.3.4. Formation of polyaromatic hydrocarbons (PAHs)	257
Supporting information	261
Acknowledgement.....	261
References	262

Abstract

This contribution reports detailed experimental measurements and quantum chemical calculations of the pollutants formed in the gas-phase decomposition of the most common brominated flame retardant, tetrabromobisphenol A (TBBA), and develops a comprehensive reaction mechanism that operates over a temperature range of 673 K to 1123 K. The objective is to decouple the gas-phase reactions from the overall decomposition of TBBA that blurs the relative importance of the condensed and gas-phase pathways, limiting the range of application of the existing models. The identification and quantification of product species involved the use of gas chromatograph - triple quadrupole mass spectrometer (GC-QQQMS) instrument functioning in multiple reaction monitoring (MRM) and total ion current (TIC) modes. The product analysis revealed that, the thermal degradation of TBBA commences at 723 K. The experimental measurements suggest the generation of HBr, mono-tribrominated bisphenols, benzene, phenol, mono-tribrominated congeners of phenol and benzene, brominated and non-brominated congeners of alkylated benzene, PAHs substituted with bromine, benzofuran, bromobenzofuran, dibenzofuran, 3,5-dibromo-4-hydroxybenzaldehyde, biphenyl and biphenylene. Gas phase decomposition of TBBA initiates with the abstraction of bromine in the form of HBr, the subsequent formation of di-tribromobisphenols A, and the cleavage of isopropylidene linkage in TBBA that generates appreciable amounts of di-tribrominated phenols and alkylated bromophenols. The yields of di-tribrominated benzenes concur with the concentrations of their phenolic counterparts and indicate the occurrence of an *ipso*-hydrogen addition resulting in the displacement of the hydroxyl group in bromophenols. The present results resolve the formation of toxic brominated products in the homogenous gas-phase decomposition of TBBA.

7.1. Introduction

4,4'-Isopropylidene-bis-2,6-dibromophenol commonly known as tetrabromobisphenol A (TBBA), accounts for more than half of the world's total production and usage of brominated flame retardants (BFRs). TBBA also serves as an intermediate for the manufacturing of other commercial BFRs and production of phenolic, epoxy and polycarbonate resins [1-4]. The extensive use of TBBA as an additive and reactive BFR has led to its widespread occurrence in various environmental matrices [5-6]. Thermal recycling of materials laden with BFRs constitutes the mainstream strategy of metal recovery and waste-to-energy conversion of the remaining (fuel) fraction of the materials. Unfortunately, detailed decomposition pathways remain unelucidated, preventing one from predicting, from the first principles, the pollutants formed in the thermal recycling of BFRs. One of the outstanding questions is the decomposition of TBBA in unimolecular and bimolecular gas-phase reactions.

Previous investigations have made significant progress in gaining understanding of the thermal decomposition behaviour of pure TBBA and polymeric materials laden with TBBA, under both inert and oxidative atmospheres, over a wide temperature window of 453 – 1073 K [7-23], but without decoupling the gas and solid-phase processes. For example, the thermogravimetric (TG) measurements of Luda et al., [13] performed at a heating rate of 10 K min⁻¹ in nitrogen atmosphere revealed that, the mass loss of TBBA proceeds in two stages of 473 – 563 K and 563 – 773 K. The first stage consumes nearly 60 % of the initial mass of TBBA. Subsequently, Barontini et al., [8] using similar operating conditions, suggested to extend the onset of the second stage to nearly 623 K. In both studies, about 20 % of the initial mass of TBBA remained as residue at temperatures above 723 K. In contrast to TBBA, mass loss of (unbrominated) bisphenol A, occurs in one step interval (473 – 543 K) without leaving any residue [13]. The TG studies afforded the identification of evaporation and solid-phase decomposition as two mechanisms governing the pyrolytic mass loss of TBBA. The investigations involving the differential scanning calorimeter (DSC) differentiated the decomposition pathways due to melting of TBBA and its evaporation [8-10, 13], confirming the melting temperature of TBBA as 456 K, but without reporting the enthalpy of melting. The evaporation channel predominates the overall decay of TBBA up to around 513 K, contributing about 15 % at 543 K [7, 11]. As it will become evident from the results of

the present study, at this low temperature of decomposition, no gas-phase reaction takes place and the entire degradation of TBBA occurs only via the solid-phase reactions.

The situation is however quite different for experiments performed above 673 K, where both the gas and solid phase decomposition reactions operate simultaneously. Flow-reactor studies on thermal degradation of TBBA yielded qualitative and semi-quantitative data on the decomposition products [14-17]. The consensus of opinions in literature indicates that, primary degradation products from pyrolysis of TBBA encompass HBr (both from solid and gas-phase reactions), brominated phenols, brominated derivatives of bisphenol A, in addition to the solid residue (char). The recent study of Ortuño et al., [14] that employed a tubular reactor operated at 873 K and 1123 K, perhaps represents the only contribution that provides quantitative and semi-quantitative measurements of all TBBA decomposition products. Although of significant importance in their own right, these studies could not differentiate between decomposition of TBBA via solid and gas-phase reactions, and did not set apart the gas-phase breakdown of non-TBBA species formed in the solid-phase reactions from that of the gas-phased decomposition of the evaporated TBBA itself. In fact, both the residence time and the temperature history of the reacting gases have often remained poorly defined [14].

Available kinetic models on the decomposition of TBBA comprise single-step global apparent kinetics, a detailed model of Marongiu et al., as well as correlational and simplified mechanistic model of Font et al. [24]. The comprehensive model of Marongiu et al. [23] incorporates about 60 components (real and lumped molecules/radicals) and 900 reactions. Validating this model, against experimental data obtained under isothermal and dynamic TGA runs, satisfactorily reproduces many aspects of the degradation and vaporisation of TBBA. It includes overall decay of TBBA, relative yields of HBr and carbonaceous residue, evaporation rates of TBBA and relative distribution of gaseous products (bromophenols A and HBr). Marongiu et al. overestimated the gaseous formation of HBr in reference to the experimental results of Barontini et al. [9]. Marongiu et al. transposed the kinetic parameters from the analogous gas-phase reactions [25] to develop a comprehensive condensed-phase kinetic model. Addressing the emissions of volatile compounds from condensed phase TBBA also requires assessing the effect of surface area, mass diffusion across the surface interface and heat transfer. This, and lack

of accounting for the contribution of the gas phase decomposition of TBBA, constitute a fundamental shortcoming of Marongiu et al.'s approach. In summary, the available models formulated the kinetics of condensed-phase reactions that are fundamentally different from the kinetics of gas-phase reactions [26].

From the results of previous studies, we now know that the decomposition of TBBA occurs in three phases, in the gas phase ($T \geq 623$ K), in the condensed phase upon melting of TBBA ($513 \text{ K} \leq T \leq 623 \text{ K}$), and during further charring of residue if longer residence time permits. Prominent decomposition reactions in the condensed media are primarily different from the corresponding reactions prevailing in the gas phase. In the latter, unimolecularly-derived pathways dominate the decomposition of TBBA, whereas bimolecular reactions govern the breakdown of TBBA in the solid phase. Based on the evaporation rates reported by Marsanich et al. [11] and the IR spectra measured by Luda et al. [13] TBBA starts to evaporate just above its melting point of 453 K. Thus, products reported at temperatures below 453 K represent only the decomposition of the evaporated TBBA, and feed impurities.

The aforementioned studies investigated the thermal breakdown of TBBA and TBBA-linked polymers in a condensed (solid or liquid) phase, even in light of significant evaporation of TBBA. In our recent theoretical study [26], we have constructed a mechanism of the thermal decomposition of TBBA in the gas phase. Investigated reactions included unimolecular decomposition of TBBA and its bimolecular reactions with important radicals that arise in the pyrolytic medium, namely, H, CH₃ and Br. The theoretically-established pathways of Reference 26 represent the only contribution towards elucidating the gas-phase reactions of TBBA. Literature offers no experimental account of gas-phase decomposition of TBBA. Thus, the objective of the current work is to determine the gas-phase thermal degradation process of TBBA, via combined experimental and theoretical techniques. We develop temperature profiles for the emission of a large number of species and construct reaction networks that connect the decomposition products with the parent TBBA. The present gas-phase account of the pyrolysis of TBBA assesses the formation of toxic brominated products, most notably the direct building blocks [27-32] for the synthesis of the notorious polybrominated dibenzo-*p*-dioxins and furans (PBDD/Fs) and other brominated polyaromatic hydrocarbons.

7.2. Methodology

7.2.1. Materials

We purchased a sample of tetrabromobisphenol A (> 97 %), a white solid powder, from Sigma-Aldrich (Australia). Figures 7.S1 and 7.S2 of Supporting Information (SI) plot the total ion currents of the neat TBBA and its impurities, respectively. Although, we did not quantitate the contaminants (cyclohexene oxide, *o*-xylene, styrene, 2-cyclohexenone, mesitylene, undecane and traces of other hydrocarbons), the purity of TBBA appears to exceed significantly 97 % specified by Sigma-Aldrich. To examine the impurities present in TBBA sample, initially, we dissolved TBBA in dichloromethane (DCM) solvent and analysed the solution in the gas chromatograph - triple quadrupole mass spectrometer (GC-QQQMS) detecting no impurities. We then performed an experiment, in which we placed TBBA in a sample-holder tube installed in an oven operated at 450 K. The experiment proceeded for 3 h with impurities captured in dichloromethane (DCM) solvent trap, cooled by sodium-chloride/ice bath and positioned after the oven. The product solution from the solvent trap was concentrated to a final volume of 1 mL in a rotary evaporator and injected into the GC-QQQMS for analysis (results presented in Figure 7.S2).

The nitrogen generator installed in our laboratory (Peak Scientific Australia) generated a stream of 99.998 % pure N₂, at outlet pressure of 80 psi. BOC Australia supplied 99.999 % helium used as a carrier gas in GC-QQQMS (GC: 2010 Plus, QQQMS: TQ8040 series, Shimadzu, Japan). Chem Supply and Merck Millipore (*Australia*) provided the GC grade of DCM (purity > 99.9 %) for the trace analysis.

Finally, we purchased from Sigma-Aldrich the standards of phenol, isomers of mono-tribromophenols, benzene, and isomers of mono-tribromobenzene to prepare calibration solutions. Deuterated biphenyl-D10 and benzene-13C, also from Sigma-Aldrich, acted as internal and surrogate standards. The remaining brominated and non-brominated standards used for quantitation of species listed in Table 7.S8 of SI were obtained from

Novachem (representative of Cambridge Isotope Laboratories, LGC, AccuStandard and Cerilliant) and Wellington Laboratories.

7.2.2. Experimental setup and procedure

Figure 7.1 illustrates the experimental apparatus developed for the present study. The setup comprises a TBBA vaporiser and an isothermal tubular reactor (12.7 mm o.d., 10.0 mm i.d., 960 mm length) connected to a sampling train to capture a large variety of decomposition products. The reactor tube, sourced from H. Baumbach & Co. Ltd., USA, was made from high purity quartz (99.995 %, see Table 7.S1 in SI) and coated in our laboratory with a solution of boric acid in ethanol [33-35]. Once baked at 773 K for 3 h, a transparent layer of B_2O_3 formed on the inside surface of the quartz tube. The layer eliminates the effect of catalytic reactions induced by (i) the conversion of triplet oxygen to singlet oxygen ($^1\Delta_g O_2$) on surfaces of reactor walls [33] and (ii) the presence of around 20 ppm of metal impurities in the quartz.

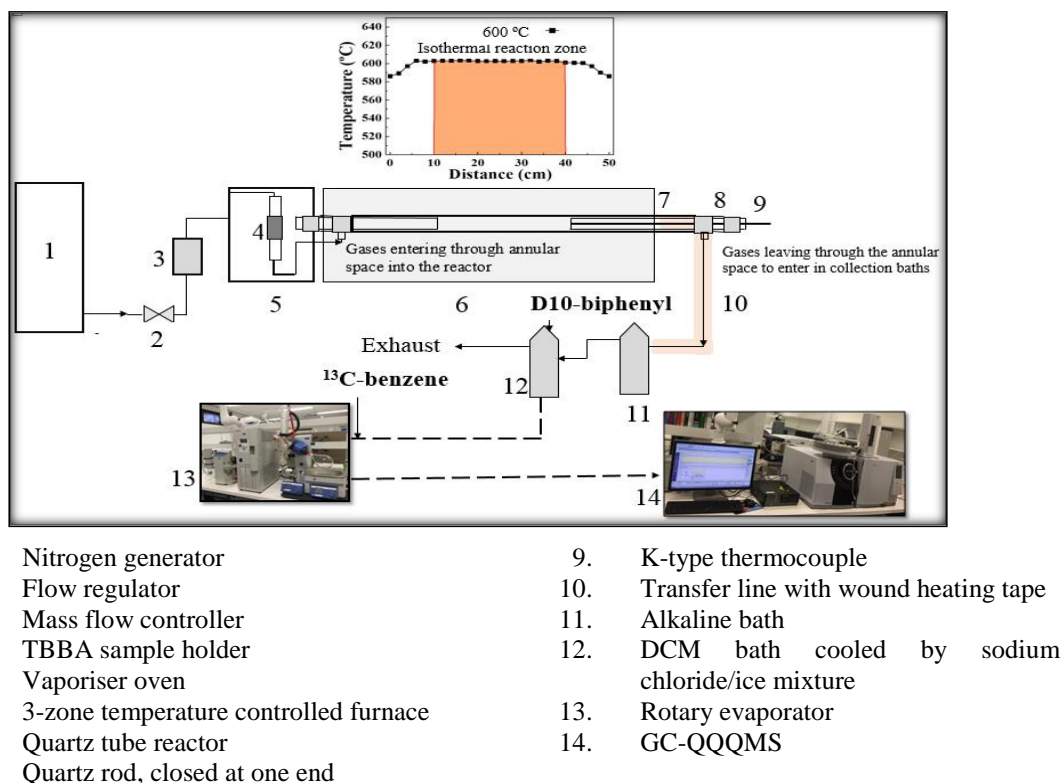


Figure 7.1. Schematic diagram for the experimental setup; biphenyl-D10 was added prior to experiments and benzene- ^{13}C prior to recovery.

As illustrated in the inset to Figure 7.1 tubular reactor (235.0 mm³ in volume) is placed along the centre line of an electrically-heated horizontal 3-zone laboratory furnace (Lebec, Australia 40 mm i.d., 500 mm heated length). Intelligent temperature controllers (UDIEN 708, measuring accuracy 0.2 %, Australia) can independently set the temperature of each zone, although in practice only the middle zone required the temperature adjustment. We located the constant temperature zone in the reactor (up to 1123 K) with an external thermocouple (supplied by OMEGA Engineering, USA) inserted and moved horizontally inside the reactor. The reactor encompasses about 30 cm of the tube, as portrayed in the inset to Figure 7.1 for a reaction temperature of 873 K.

Two high purity quartz cylinders (9.5 mm o.d.), with one end closed inserted from the opposite ends into the reactor tube, serve three functions (i) to afford insertion of a thermocouple to monitor accurately the reactor-zone temperature, (ii) to modify the reactor volume by varying the length of reaction zone to maintain the residence time constant at different levels of temperature, and (iii) to ensure the rapid transport of reactants and products that enter and leave the reactor through the annular space, reducing the possibility of reactions taking place in low-temperature regions. We connected the tail ends of the reactor to the feed preparation and product collection systems, respectively. The heating tape (HTC-030), wrapped around the product connection line to hold its temperature constant at 433 K to avoid the condensation of products in the transfer line.

The vaporiser consisted of a vertical quartz tube loaded with a sample of TBBA of about 60 mg in mass and placed inside an oven (*S.E.M.* Pty Ltd), with its temperature set accurately to 450 K. A stream of nitrogen flowed through the vaporiser at a rate of 705 cm³ min⁻¹, as metered at STP, to entrain TBBA evaporating at 0.06 mg min⁻¹ maintained the concentration of TBBA (0.085 ppm) in the reactor. The sampling of reactant, intermediates and products from the reaction system started immediately after commencement of each experiment and continued for about 5 h, consuming about 18 mg of TBBA per run. Pyrolysis experiments were conducted over a wide range of temperature (673 – 1123 K), at atmospheric pressure and a residence time of 2 s. We selected this residence time and this temperature range as no gas-phase reactions occur below 673 K and the EU Directive 2000/76/EC sets [36] the minimum residence time of 2 at 1123 K for the post-combustion zone in an incinerator. The connection tubes, made solely of

polytetrafluoroethylene (PTFE) (Plasmatech, USA), and the quartz reactor were rinsed with DCM to recover adsorbed compounds and to avoid contamination of successive runs.

In each run, the evolved product gaseous stream escaping the reactor passed through two consecutive impingers: (i) an alkaline bath loaded with a solution of 0.1 N sodium hydroxide captured the released HBr and (ii) a solvent trap, filled with DCM and cooled by a sodium chloride/ice bath, condensed all volatile (VOCs) and semi-volatile (SVOCs) organic compounds produced in the reactor. After each run, we titrated the NaOH solution against 0.1 N HCl to estimate its HBr contents. The DCM solvent from the cold trap was concentrated to a volume of 1 mL in a rotary evaporator prior to analysis.

GC-QQQMS functioned in the positive electron impact (EI) mode at an ionisation energy of 70 eV, to produce the multiple reaction monitoring (MRM) and the total ion current (TIC) chromatograms, for the accurate identification and quantification of VOCs and SVOCs. GC oven housed a short Rxi-5Sil MS equivalent to DB-5MS column (15 m length \times 0.25 mm i.d. \times 0.25 μ m thickness, from Restek) required for the analysis of low boiling-point brominated species. In addition, we analysed the solvent collected from washing the reactor and transfer line. Helium streamed through the column at a rate of 1.5 mL min⁻¹ maintained by the GC flow control. The injection volume corresponded to 1 mm³ operated in splitless mode for one min then at a split ratio of 1:10, with an injector, interface and ion source temperatures set to 523 K, 573 K and 473 K, respectively. The oven temperature program commenced at 303 K, retained for a period of 3 min, ramped to a temperature of 373 K at a heating rate of 8 K min⁻¹, kept for 2 min, followed by a subsequent temperature ramp of 4 K min⁻¹ to reach 563 K that was held for 2 min.

MRM represents a highly sensitive MS method [37] that optimises the formation of a daughter ion for each species, as a function of collision energy (Figures 7.S3-7.S5 in Section S3 of SI provide details of our MRM method and examples of MRM chromatograms). The approach maximises the signal to noise ratio and affords low limits of detection. We developed an MRM method for the precise quantitation of each target species listed in Table 7.S2-7.S4 of SI. The quantitation process involved the preparation of calibration curves at 7 levels of concentration using external standards. Thermal decomposition of TBBA releases a number of products. Table 7.S8 lists all species

identified and quantitated by external standards. It was not practical to do this for all products. Compounds listed in Table 7.S9 were identified by comparing their spectra with those in the NIST library [38] or in the literature [7]. Table 7.S9 lists the identities, retention time and the peak areas of selected molecular species that correspond to their relative amounts.

To estimate the percentage recovery for each product, we dissolved deuterated biphenyl (D10) as a pre-sampling (surrogate) standard (2 ppm) in the solvent bath, prior to each experiment. Likewise, to ascertain the recovery of light VOCs, we spiked the solvent solution in the bath with benzene-13C in a concentration of 2 ppm, before sample preparation. Table 7.S5 of SI assembles the percentage recoveries for both biphenyl-D10 (typical variation of 73 – 94 %) and benzene-13C (97 – 99 %) in the temperature range of 673 – 1123 K.

For the measurement of benzene-13C, we executed the GC-QQQ analysis employing a Rxi-5Sil (30 m × 0.25 mm i.d. × 0.25 μm) column (Restek, USA). This amendment allowed us to measure the peak area of benzene-13C (which on 15 m Rxi-5Sil MS column partially co-eluted with DCM), whereas for the remaining brominated and non-brominated species we used the Rxi-5Sil MS column (as explained above). Figure 7.S6 depicts a full scan chromatogram (for an experiment performed at 973 K) of the VOCs and SVOCs identified in this work.

7.2.2.1 Blanks and replicates

A blank run, performed at 773 K, involved no injection of TBBA into the system. We detected negligible amounts of impurities, as depicted in Table 7.S6 of SI, probably representing the contamination from previous runs. Another blank run included the injection of phenol as a reactant, with the reactor temperature set to 323 K, to estimate its capture efficiency (typical efficiency ~ 98 %). In two additional blank experiments, we spiked the DCM bath with benzene and phenol, obtaining 63.9 % and 79.0 % recoveries of these species, respectively.

The thermal decomposition of TBBA in the gas phase released VOCs and SVOCs in the highest yield between 873 K and 973 K. Therefore, we repeated our experimental

measurements (as shown in Table 7.S7) at temperatures of 873 K, 923 K and 973 K, in order to verify the reproducibility of our results in the critical temperature window. The results from replicate experiments suggest reasonable reproducibility, with variation of less than 20 %.

7.2.3. Computational methodology

The Gaussian 09 [39] suit of programs afforded all structural optimisation and energy calculations for chemical reactants, products and intermediates. We have investigated the reaction corridors using the density functional theory (DFT) with the *meta*-hybrid exchange-correlation functional of M06-2X [40], in combination with a basis set of 6-311+G(d,p) [41]. M06-2X displays outstanding performance for the reaction kinetics and thermochemistry of gas phase systems [40, 42]. The transition structures (TS), verified through the analysis of their harmonic vibrational frequencies, contained only one imaginary frequency along the reaction coordinate. Computation of the intrinsic reaction coordinate (IRC) [43] confirmed the reaction pathways and ensured that each TS corresponded to its reactants and products.

7.3. Results and discussion

In the discussion that follows, we explore the temperature-dependent gas phase decomposition of pure TBBA and estimate the yields of a number of brominated and non-brominated compounds. The GC-MS product analysis unveiled the generation of more than 50 product species along with the formation of carbonaceous material (char) that arise by the thermal breakdown of the parent TBBA in the pyrolytic environment. We quantitated the yields (defined as the ratio of mass of species *i* produced divided by the mass of TBBA introduced into the reactor) of the most important products based on MRM analyses (Table 7.S8 of SI) in μg of product per g of the TBBA introduced into the reactor. The remaining products were estimated based on their peak areas (Table 7.S9 of SI). Tables 7.S8 list all quantitated products along with their structures and retention times.

7.3.1. TBBA decomposition

Figure 7.2 portrays the conversion of TBBA versus temperature, indicating the conversion of 25 %, 33 %, 48 % and 86 % at temperatures of 773 K, 873 K, 973 K and 1073 K, respectively. TBBA commences to disintegrate at 723 K, with the conversion gradually increasing from 773 K to 973 K, followed by a steep increase at 1123 K to reach ~ 92.0 %.

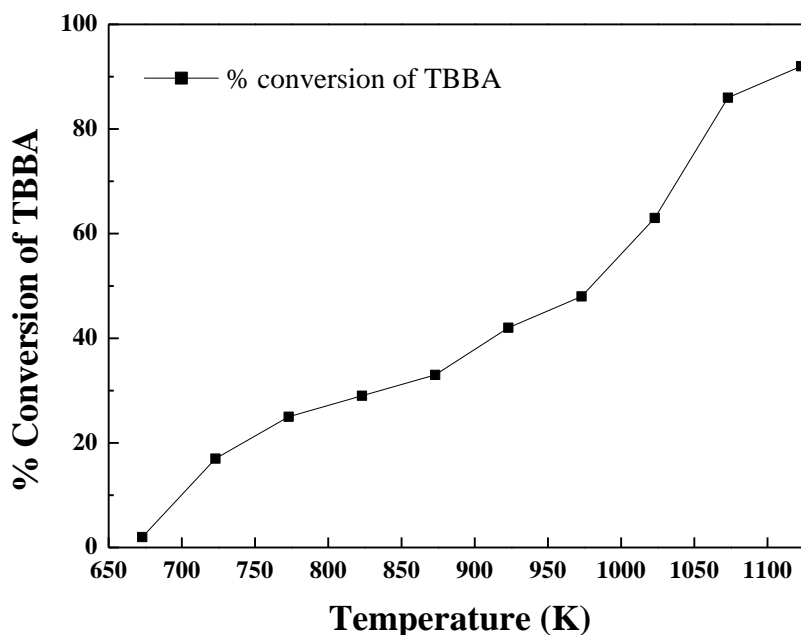


Figure 7.2. Percentage conversion of TBBA in the reactor for a temperature range of 673 – 1123 K at a residence time of 2 s.

Although the conversion of TBBA amounted to around 17% at 723 K, only trivial amounts of brominated phenols and benzenes formed at that temperature (Table 7.S8), indicating that the isopropylidene linkage remained largely intact at this temperature. The initial decomposition products appearing at 723 K (Table 7.S9, rows 32-37) comprised mainly 4-[1-(3-bromophenyl)ethyl]phenol, 1-bromo-3-(1-phenylethyl)benzene, 1,3-dibromo-5-[2-(3-bromophenyl)propan-2-yl]benzene, 2-bromo-4-[1-(3-bromo-4-hydroxyphenyl)ethyl]phenol and dibromobisphenol A. These species indicate that the initial decomposition channels that operate at 723 K include debromination and expulsion of methyl radicals. Only trace quantities of species composed of single benzene rings appear at this temperature, such as 2,6-dibromophenol, 2,4,6-tribromophenol, 2,6-dibromo-4-methylphenol, 2,6-dibromo-4-tertbutylphenol and 3,5-dibromo-4-hydroxybenzaldehyde (see Table 7.S8). In our recent theoretical study on thermal decomposition of TBBA [26], we have mapped out potential energy surfaces for the

unimolecular degradation of TBBA as well its bimolecular reactions with prominent radicals. Figures 7.3 and 7.4 expand on the results from that study [26], providing the numerical values of reaction and activation enthalpies at 298.15 K.

7.3.2. Formation of brominated bisphenols and HBr

The thermal breakdown of TBBA is initiated by the cleavage of relatively weak aromatic C-Br bonds and/or Br abstraction by H atoms from the parent TBBA, and produces tribrominated bisphenol A, as shown in Figure 7.3.

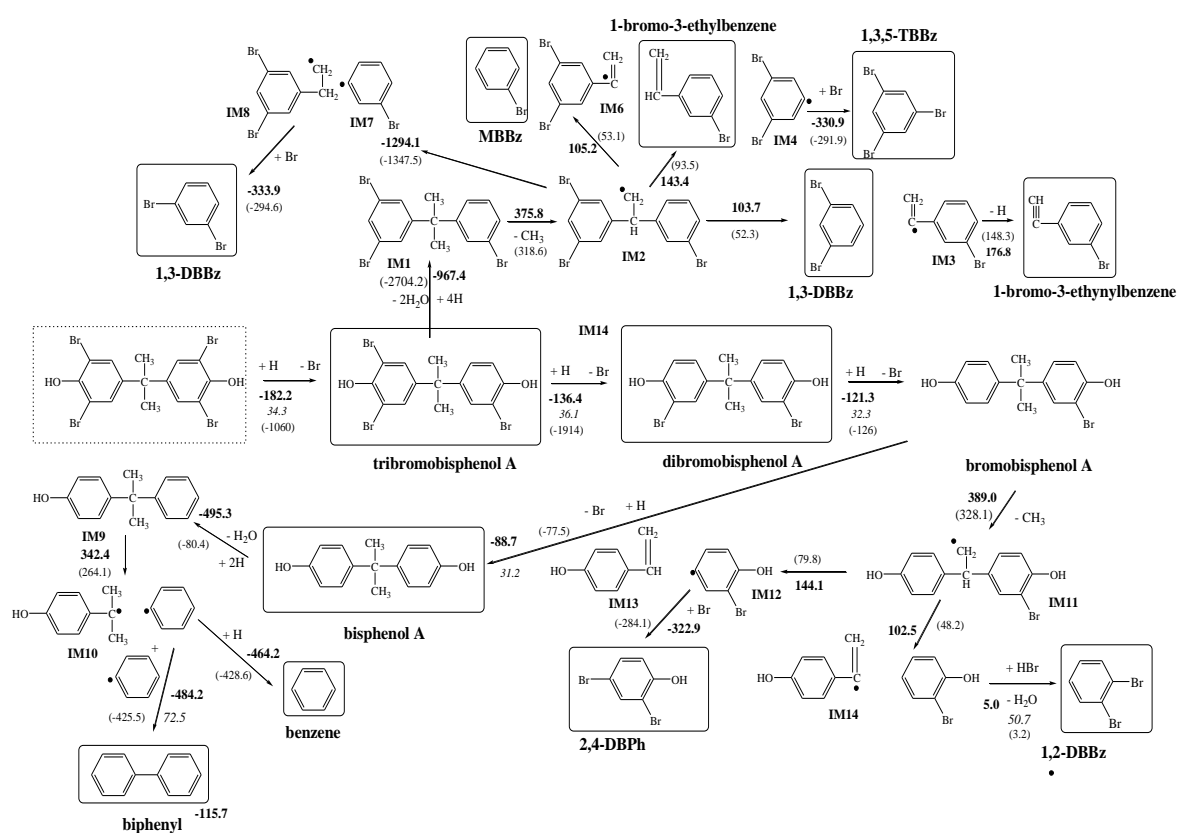


Figure 7.3. Pathways for the formation of major VOCs and SVOCs from the decomposition of TBBA, initiated by the abstraction of Br and OH and cleavage of isopropylidene linkages. Values in bold and italic denote reaction and activation enthalpies (in kJ mol⁻¹), respectively. Values in brackets represent the Gibbs free energy change of reaction (in kJ mol⁻¹). All values are reported at 298.15 K.

The successive debromination and H-induced displacement of Br produce mono-tribrominated bisphenols along with HBr as the primary decomposition products of exothermic reactions. The exothermicity of these reaction amounts to between 121.3 – 136.4 kJ mol⁻¹, with the corresponding enthalpic barriers of 36.1 – 31.2 kJ mol⁻¹. The Gibbs free energy changes ($\Delta_r G_{298}^\circ$) for H-induced displacement reactions are exoergic and lie in the range of 1914.0 – 126.0 kJ mol⁻¹. The conversion of tribromobisphenol A into dibromobisphenol A is considered to be the most spontaneous reaction, and releases a significant amount of energy (-1914.0 kJ mol⁻¹). Consequently, the generation of lower brominated bisphenol congeners represents the highly preferred corridors, both thermodynamically and kinetically.

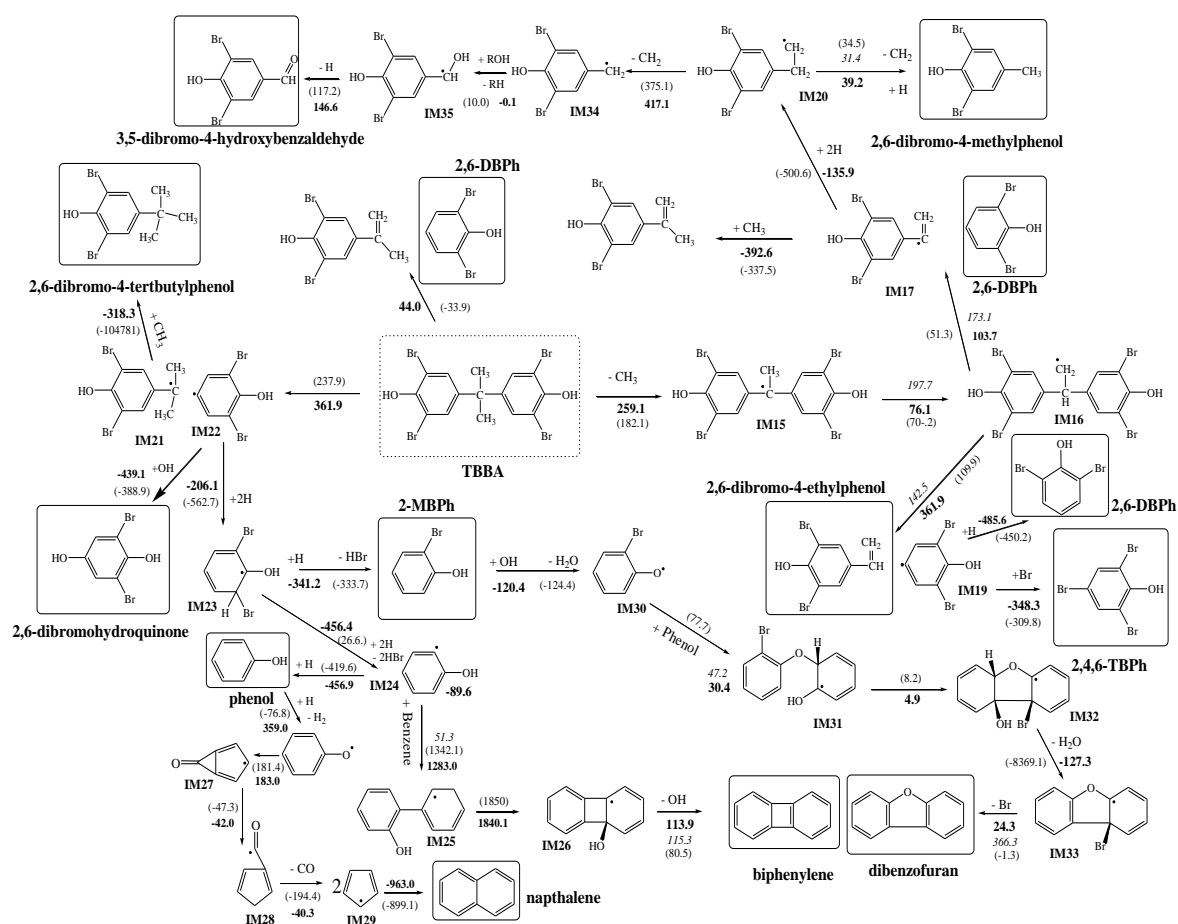


Figure 7.4. Pathways initiated by the fission of CH₃ groups and cleavage of isopropylidene linkages to form major VOCs and SVOCs. Values in bold and italic denote reaction and activation enthalpies (in kJ mol⁻¹), respectively. Values in brackets

represent the Gibbs free energy change of reaction (in kJ mol^{-1}). All values are reported at 298.15 K.

Therefore, our experimental measurements confirm the formation of HBr and brominated bisphenols as first products of pyrolysis at 723 K (cf. Table S9 in SI). We confirmed the identity of brominated bisphenols by comparing their mass spectra with the analogous mass spectra published in the literature [7]. Our analysis of the alkaline solution shows a concentration of HBr corresponding to a yield of 4.7 %. The yield of HBr increases to 47 % at 1073 K. This is in line with previous FTIR results, where HBr accounted for 52 – 59 % of the bromine initially present in TBBA samples [44].

7.3.3. Formation of brominated phenols, brominated alkylated phenols, brominated benzenes and brominated alkylated benzenes

The rupture of isopropylidene linkages in di-tetrabrominated bisphenols opens up an exit channel for isomers of phenols (BPhs) brominated at positions 2, 4 and 6. A number of studies have suggested that brominated phenols synthesise PBDD/Fs [45-48]. This underpins the importance of PBPhs formation during the decomposition of TBBA in thermal systems. As mentioned above, we observed the production of 2,6- and 2,4,6-brominated congeners of phenols in trivial quantities at an initial decomposition temperature of 723 K. The other isomers of brominated phenols (BPhs) appeared at 773 K and reached their maximum yields at around 923 K (cf. Figure 7.5). At all reaction temperatures, 2,6-dibromophenol (2,6-DBPh) and 2,4,6-tribromophenol (2,4,6-TBPh) predominated in the product profile of brominated species, which is in agreement with previous studies on TBBA pyrolysis [7, 11, 14] and with our proposed mechanism. The rupture of isopropylidene linkages to phenolic radical adducts is endoergic in nature, demanding $51.3 - 237.9 \text{ kJ mol}^{-1}$ of $\Delta_r G_{298}^\circ$ to ensue, except the corridor that involves the fission of TBBA into stable adducts (i.e., $\text{TBBA} \rightarrow 2,6\text{-DBPh} + 2,6\text{-dibromo-4-methylethylphenol}$) is exoergic by 33.9 kJ mol^{-1} . The fission of isopropylidene linkages generates phenolic radical species (IM22, IM14, IM19 and IM21) that transform readily into stable products through spontaneous reactions with H, Br and CH_3 radicals.

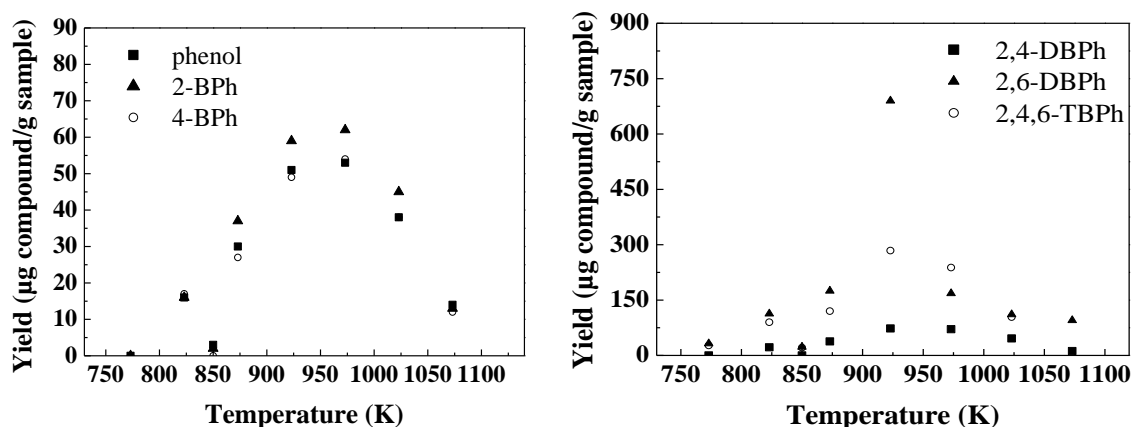


Figure 7.5. Yields of phenol, mono-triBPhs obtained from the gas phase pyrolysis of TBBA at different temperatures.

The experimentally comparable yields of 2,6-DBPh and 2,4,6-TBPh obtained at most temperatures suggest that both molecules stem from similar pathways. Hydrogen and bromine addition at the *para* vacant site of IM19 produce 2,6-DBPh and 2,4,6-TBPh, respectively (the right part of Figure 7.4). The addition of H and Br atoms at *para* vacant sites of phenolic species (i.e., IM19) proceeds through spontaneous corridors characterised by exoergicities of $309.8 \text{ kJ mol}^{-1}$ and 450 kJ mol^{-1} , correspondingly. Experimentally, phenol and monobromophenols (MBPhs) appear in lower concentrations in comparison to other BPh congeners. The significantly lower concentrations of phenol and MBPhs (Figure 7.5), in reference to di-triBPhs, reveals that these species form upon debromination of the latter, either via direct scission of aromatic-Br bonds or through bimolecular-derived reactions.

Furthermore, Figures 7.3 and 7.4, as well as Table S9 of the SI, document the by-products of BPhs. We established the product profile for 3,5-dibromo-4-hydroxybenzaldehyde, 2,6-dibromo-4-methylphenol and 2,6-dibromo-4-tertbutylphenol (as plotted in Figure 7.6) based on experimental measurements. These moieties achieve their highest abundance at a temperature of 873 K. At the same time, the two isomers of 3,5-dibromo-4-hydroxybenzaldehyde appear in the temperature range of 723 – 1073 K. 3,5-dibromo-4-hydroxybenzaldehyde exhibits a significant increase in concentration ($\sim 1200 \text{ µg g}^{-1}$) at 873 K.

Now we turn our attention to illustrating the pathways of brominated alkylated phenol formation (as illustrated in Figure 4). For example, the direct fission of isopropylidene bonds prompts the appearance of intermediates IM21 (pre-2,6-dibromo-4-tertbutylphenol) and IM22 (pre-structure of 2,6-dibromohydroquinone), and an intramolecular H transfer generates 2,6-dibromo-4-methylethylphenol (refer to the middle part in Figure 7.4).

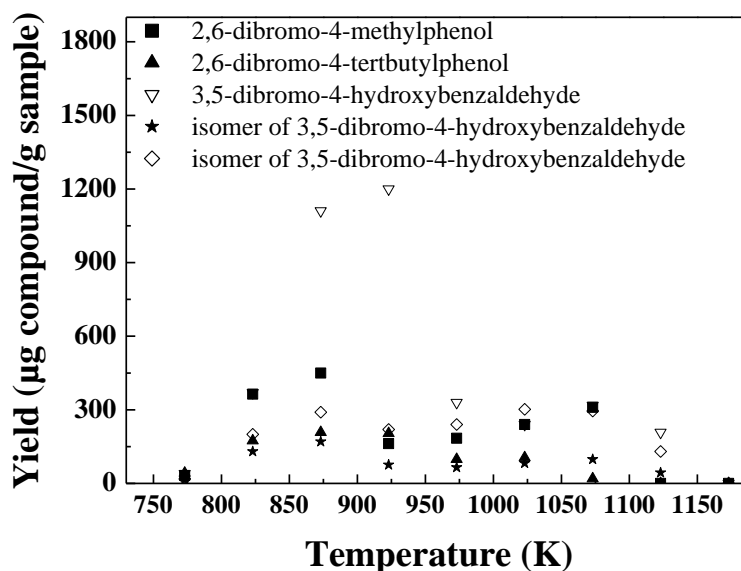


Figure 7.6. Yields of 2,6-dibromo-4-methylphenol, 2,6-dibromo-4-tertbutylphenol and isomers of 3,5-dibromo-4-hydroxybenzaldehyde from the gas phase pyrolysis of TBBA at different temperatures.

As indicated in Figure 7.4, a 1,2-H shift via the activation enthalpic barrier of $197.7 \text{ kJ mol}^{-1}$, followed by the fission of C-C linkages in the intermediate IM16 through transition states overcoming enthalpic barriers of 173.1 and $142.5 \text{ kJ mol}^{-1}$, respectively, produces a direct precursor for the formation of the experimentally-detected BPhs (Figure 7.5) and alkylated BPhs (Figure 7.6). The intramolecular rearrangement, and plausible bimolecular reactions of the precursor intermediate species with CH_3 radicals, transforms them into stable alkylated BPhs via vast exoergic reactions ($\text{IM17} + \text{CH}_3 \rightarrow 2,6\text{-dibromo-4-methylethylphenol}$; $\text{IM21} + \text{CH}_3 \rightarrow 2,6\text{-dibromo-4-tertbutylphenol}$). Although 3,5-dibromo-4-hydroxybenzaldehyde appears in comparatively high yields, we were unable to find a direct pathway that generates this compound from TBBA pyrolysis. In the uppermost pathway of Figure 7.4, we postulate that 3,5-dibromo-4-hydroxybenzaldehyde

may form via abstraction of the hydroxyl group by the intermediate IM20 through a series of endoergic reactions.

The GC-QQQMS analysis of product condensate identified mono-tribrominated congeners of benzene and alkylated benzenes. Figure 7.7 compares the yields of mono-tribrominated benzenes. The yields of all brominated congeners of benzene increase with reaction temperature up to a maximum at 973 K, then yields decrease to zero at 1123 K. Formation of brominated benzenes, initiated by the abstraction of OH groups by H radicals in TBBA, tri-monobromobisphenol A, and bisphenol A molecules, is followed by the cleavage of isopropylidene bonds. Based on $\Delta_r G_{298}^\circ$ values, we predict the abstraction of OH by an H radical (i.e., $\text{TBBA} + 4 \text{H} \rightarrow \text{IM1} + 2 \text{H}_2\text{O}$) to be vastly spontaneous, evolving $-2704.2 \text{ kJ mol}^{-1}$ of Gibbs free energy. Therefore, we experimentally observed the high relative peak areas of brominated and non-brominated alkylated benzene (Table 7.S9).

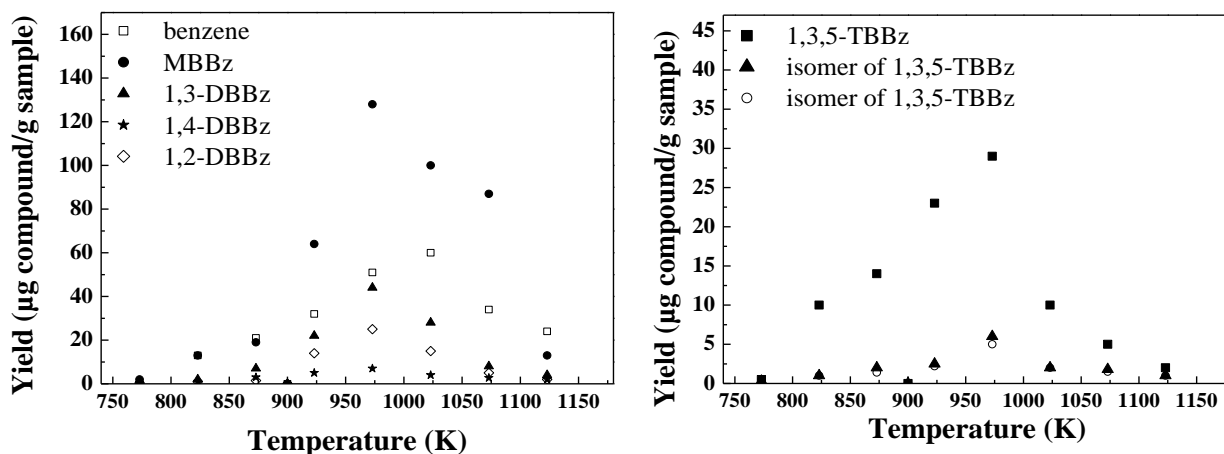


Figure 7.7. Yields of mono- tribrominated congeners of benzene from the gas phase pyrolysis of TBBA at different temperatures.

Figure 7.3 shows the mechanistic pathways for the formation of benzene, monobromobenzene (MBBz), 1,3/1,2-dibromobenzene (1,3/1,2-DBBz) and 1,3,5-tribromobenzene (1,3,5-TBBz) from bisphenol, IM2, IM11 and IM4 molecules. Displacement of the hydroxyl group from BPh isomers by H atoms results in the noticeable consistencies between BBz congeners (Figure 7.7) and their analogous BPH isomers (Figure 7.5). For instance, the most abundant 1,3,5-TBBz forms by an *ipso*-

hydrogen addition to 2,4,6-TBPh, followed by elimination of the OH group. Although the experimental yield of MBBz in comparison to other BBz congeners is unexpectedly high, it is most likely due to the scission of the weak C-Br bonds in all BBz isomers in exoergic reactions.

The other by-products that evolve by the cleavage of isopropylidene linkages, followed by H, Br and CH₃ substitution in bisphenol and di-tetrabromobisphenol A, include 1-bromo-4-ethynylbenzene, benzene(bromoethynyl), 2,4-dibromo-6-(bromomethyl)phenol, 1,3-dibromo-2-methylbenzene and 3,5-dimethyl-2,4,6-tribromophenol. The cleavage of isopropylidene linkages suggests a reversible thermodynamic corridor. The high reaction temperatures allow the formation of non-brominated and non-phenolic products such as phenylethyne, benzene, 1-ethynyl-2-methyl and 1,4-diethynylbenzene (details are given in Table 7.S9 of the SI), owing to the ability of Br and OH atoms to abstract in highly spontaneous reactions.

7.3.4. Formation of polyaromatic hydrocarbons (PAHs)

Now we turn our attention to describing the formation of polyaromatic hydrocarbons (PAHs). We have detected PAH products from TBBA pyrolysis, including naphthalene, congeners of monobromonaphthalene, methylnaphthalene, biphenyl, mono- and tetra-brominated congeners of biphenyl, biphenylene, acenaphthylene and its monobrominated isomers, anthanthrene, phenanthrene, phenalenone, acenapthenone, dibromoacenapthenone and pyrene, mainly observed above 873 K (Table 7.S9).

Figure 7.8a reports yields as function of temperature for naphthalene, acenaphthylene and 2-bromonaphthalene. Naphthalene and bromonaphthalene commence to form at approximately 773 K and increase rapidly to a peak value at 1023 K. The decomposition reactions of phenoxy or bromophenoxy radicals, along with the ring contraction/CO elimination mechanism, produce cyclopentadienyl or brominated cyclopentadienyl radicals, which serve as potent precursors for the formation of naphthalene and bromonaphthalene [49-51]. All the mechanistic pathways involved in the generation of naphthalene and its brominated congeners are highly exoergic (spontaneous) except the

ring contraction reaction, which is reversible to a small extent, and demands $181.4 \text{ kJ mol}^{-1}$ of energy to occur (depicted in lowermost part of Figure 7.4).

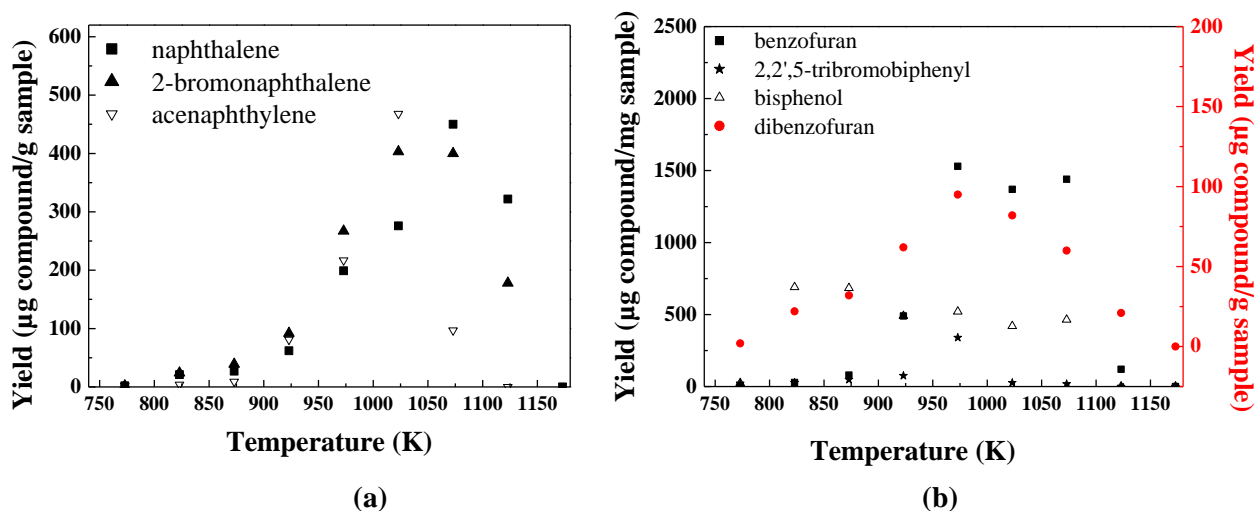


Figure 7.8. Yields for naphthalene, bromonaphthalene and acenaphthylene (a) and benzofuran, dibenzofuran, 2,2',5-tribromobiphenyl and bisphenol A (b) from the gas phase pyrolysis of TBBA at different temperatures.

With respect to benzofuran and dibenzofuran (DF), Figure 7.8b summarises their yields at temperatures of 723 – 1023 K. Table 7.S9 demonstrates that 5-bromobenzofuran formation commences at a temperature of 873 K. Evidently, the concentration of these compounds increases considerably above 898 K, benzofuran and 5-bromobenzofuran become the dominant products at 973 K. The formation of benzofuran and DF products can be explained by the direct condensation reaction of bromophenoxy radicals with themselves or with phenol. As the lowermost part of Figure 7.4 shows, a plausible route for the formation of DF arises from the bimolecular reaction of a 2-BPhxy radical and a phenol molecule. Subsequent steps involve a ring cyclisation reaction from IM31 to IM32 (entailing a trivial amount of endoergicity, i.e., 4.9 kJ mol^{-1}) followed by unimolecular elimination of a water molecule that proceeds through the release of excessive energy. Finally, the facile abstraction of out-of-plane Br atoms from C-C linkages produces DF molecules in a less spontaneous reaction. Similarly, biphenylene may develop from the addition of an *ortho*-OH phenyl radical (IM24) to a benzene molecule, following subsequent stepwise ring cyclisation and OH abstraction via highly endoergic reactions,

which are believed to be the least preferred corridors. The requirement of high reaction energy makes this pathway unlikely to occur.

Finally, Figure 7.8b shows yield versus temperature for 2,2',5-tribromobiphenyl and bisphenol A. Thermal breakdown of TBBA generates isomers of 2,2,5'-tribromobiphenyl (773 – 1023 K) and di-tribromo bisphenol A over a temperature range of 723 – 1023 K. Peak profiles establish that, above 973 K, mono-tribrominated congeners of bisphenols disappear, as higher temperatures cause debromination reactions to prevail. Whereas, a maximum formation of bisphenol A occurs at 823 K, the formation process exhibits a gradual decrease in concentration up to 1123 K. This can be explained by the formation of brominated biphenyls that proceeds by the coupling of brominated phenyl radicals that are abundant in the pyrolytic environment. The generation of biphenyl moieties is preferred thermodynamically via the elevated spontaneous reaction that liberates $425.5 \text{ kJ mol}^{-1}$ of free energy from the reaction. Because of the free energy change of this reaction, the generation of bisphenol A implies the debromination of TBBA through a series of exoergic reactions.

Species that emerge in large concentrations in the temperature range of 723 – 923 K include di-tribromobisphenol A, 2-bromo-4-[1-(3-bromo-4-hydroxyphenyl)ethyl]phenol, 1,3-dibromo-5-[2-(3-bromophenyl)propan-2-yl]benzene and 1-bromo-3-(1-phenylethyl)benzene. The remaining species comprise substituted mono-aromatic compounds such as 1,4-diethynylbenzene, phenylethyne and 1-bromo-3-ethynylbenzene that usually appear at higher temperatures. PAHs that encompass more than one aromatic ring include methyl naphthalene, 2-bromonaphthol, benzophenone, bromo acenaphthylene, 2,3',5-tribromobiphenyl, 2,4,6-tribromobiphenyl, 4,4'-dimethoxy-3,3',5,5'-tetrabromobiphenyl and phenalene. The non-brominated species and PAHs emerge in higher quantities at elevated temperatures. For example, above 1023 K, most of the brominated isomers of ethylmethylbenzene start to transform into non-brominated isomers of ethylmethylbenzene.

Finally, we note that the yields of decomposition products appearing from the gas phase degradation of TBBA are slightly different from those obtained by Ortuño et al. [14] from the break-down of powdered TBBA under very similar operational conditions. The yields of brominated congeners of phenol are more than 10 times lower than those from

powdered TBBA. In the case of gas phase thermal decomposition, we observed the presence of all mono- and tri-brominated congeners of benzene, which is attributed to the replacement of the hydroxyl group in BPhs. Likewise, the yield of naphthalene is considerably lower when compared with the results of Ortuño et al., whereas the yields of the mono- and di-brominated naphthalenes in our study exceed those reported by Ortuño et al [14].

In contrast to Ortuño et al. [14], our yield of benzofuran surpassed that observed in gas-phase decomposition of TBBA by approximately 55-fold. Pyrolysis reactions of TBBA in condensed media did not produce any of the brominated and monobrominated congeners of biphenyl and biphenylene, compared with gas phase TBBA decomposition reactions. The difference in the product profiles between gaseous and powdered TBBA could be rationalised in view of the distinct mechanisms operating in the two systems. In the condensed medium, the decomposition process seems to be dominated by successive bimolecular cross-linkage reactions that lead to the elimination of HBr [23].

The literature consistently reports the appearance of PBDD/F congeners from TBBA decomposition. Combustion of TBBA generally yields more PBDD/Fs in reference to pyrolytic conditions. This is evident from the measurements of Ortuño et al. [14] and Thoma et al. [22], who reported total PBDD/F yields of around 20 ppm and 25 ppb at 800 °C under oxidative and pyrolytic conditions, respectively. During the condensed-phase decomposition of TBBA, bromine-deficient char may also promote the de novo formation of PBDD/F. Herein, we limit our analysis to major VOCs and SVOCs. We expect the formation of BPhs and BBz in appreciable concentrations to result in the emission of PBDD/Fs. Detection of PBDD/Fs from the gas phase decomposition of TBBA will be investigated in due course.

In conclusion, we investigated the thermal decomposition of gaseous TBBA under an inert atmosphere, using a laboratory-scale reactor and sampling train to trap a wide range of VOCs and SVOCs. The results presented herein conclude that TBBA undergoes complete pyrolysis and generates a variety of by-products. Product analysis confirms the generation of several important toxic species, including PAHs, benzofurans and dibenzofurans, brominated biphenyls and bisphenols, bromine methylated phenol, brominated

tertbutylphenols, and precursors to PBDD/Fs such as mono-tribrominated congeners of phenols and benzenes. We quantitated the yields of numerous species under various temperatures to illustrate the dependence of their formation on temperature. Particularly, most of the decomposition products arose in trivial concentrations at a temperature of 773 K, and peaked at around 923 – 973 K. Generally, higher temperatures favoured the formation of non-brominated species. Based on our current measurements, we developed reaction pathways for the formation of decomposition products arising during the gas phase degradation of pure TBBA. We found that the removal of Br and OH atoms from the parent molecules are the most favourable reaction corridors, both thermodynamically and kinetically leading to the formation of brominated bisphenols and brominated isopropylidenedibenzene adducts. The fission of isopropylidene linkages produces several precursor species requiring moderate amounts of energy. This can be supplied by the complex exoergic reactions occurring in the thermal systems. The precursor species transform into stable brominated and non-brominated alkylated benzenes, biphenyls and PAH through spontaneous reactions.

Supporting information

Supporting information appendix D compiles the details for the analysis of neat TBBA, percentage recoveries of benzene-13C and biphenyl-D10; MRM chromatograms, details of the MRM method, yields (for quantitated species) and TIC (for non-quantitated species) values VOCs and SVOCs, results of blank and replicated experiments.

Cartesian coordinates and standard thermodynamic values for all structures available in (appendix D) attached CD.

Acknowledgements

This study has been supported by the Australian Research Council (ARC), and grants of computing time from the National Computational Infrastructure (NCI), Australia as well as the Pawsey Supercomputing Centre. A.S. thanks Murdoch University, Australia, for a postgraduate research scholarship. We thank Dr Juita for her useful comments about experimental measurements.

References

- [1] Levchik, V.S., Weil, E.D. Thermal decomposition, combustion and flame-retardancy of epoxy resins - a review of the recent literature. *Polym. Int.* **2004**, 53, 1901-1929.
- [2] Beck, H.N. Mixtures of tetrabromobisphenol-A polycarbonate and bis (2-ethoxyethyl) ether: Examples of a lower critical solution temperature. *J. Appl. Polym. Sci* **1993**, 48, 21-23.
- [3] Bozi, J., Czégény, Z., Mészáros, E., Blazsó, M. Thermal decomposition of flame retarded polycarbonates. *J. Anal. Appl. Pyrolysis* **2007**, 79, 337-345.
- [4] Knop, A., Pilato, L.A. *Phenolic Resins: Chemistry, Applications and Performance*. **1985**, Berlin Heidelberg GmbH: Springer-Verlag.
- [5] Hedemalm, P., Eklund, A., Bloom, R., Haggstrom, J. Brominated flame retardants - an overview of toxicology and industrial aspects. *Electronics and the Environment. ISEE 2000. Proceedings of the 2000 IEEE International Symposium on.* **2000**, 203-208.
- [6] Kesner, M., de Vos, W. Teaching about flame retardants. A joint Israeli-Dutch project. *J. Chem. Educ.* **2001**, 78, 41-45.
- [7] Barontini, F., Cozzani, V., Marsanich, K., Raffa, V., Petarca, L. An experimental investigation of tetrabromobisphenol A decomposition pathways. *J. Anal. Appl. Pyrolysis* **2004**, 72, 41-53.
- [8] Barontini, F., Marsanich, K., Petarca, L., Cozzani, V. The thermal degradation process of tetrabromobisphenol A. *Ind. Eng. Chem. Res.* **2004**, 43, 1952-1961.
- [9] Barontini, F., Cozzani, V. Formation of hydrogen bromide and organobrominated compounds in the thermal degradation of electronic boards. *J. Anal. Appl. Pyrolysis* **2006**, 77, 41-55.
- [10] Barontini, F., Marsanich, K., Petarca, L., Cozzani, V. Thermal degradation and decomposition products of electronic boards containing BFRs. *Ind. Eng. Chem. Res.* **2005**, 44, 4186-4199.
- [11] Marsanich, K., Zanelli, S., Barontini, F., Cozzani, V. Evaporation and thermal degradation of tetrabromobisphenol A above the melting point. *Thermochim. Acta* **2004**, 421, 95-103.

- [12] Grause, G., Furusawa, M., Okuwaki, A., Yoshioka, T. Pyrolysis of tetrabromobisphenol-A containing paper laminated printed circuit boards. *Chemosphere* **2008**, 71, 872-878.
- [13] Luda, M.P., Balabanovich, A.I., Hornung, A., Camino, G. Thermal degradation of a brominated bisphenol A derivative. *Polym. Adv. Technol.* **2003**, 14, 741-748.
- [14] Ortuño, N., Moltó, J., Consea, A.J., Font, R. Formation of brominated pollutants during the pyrolysis and combustion of tetrabromobisphenol A at different temperatures. *Environ. Pollut.* **2014**, 191, 31-37.
- [15] Wichmann, H., Dettmer, F.T., Bahadir, M. Thermal formation of PBDD/F from tetrabromobisphenol A - a comparison of polymer linked TBBP A with its additive incorporation in thermoplastics. *Chemosphere* **2002**, 47, 349-355.
- [16] Luijk, R., Govers, H.A.J. The formation of polybrominated dibenzo-*p*-dioxins (PBDDs) and dibenzofurans (PBDFs) during pyrolysis of polymer blends containing brominated flame retardants. *Chemosphere* **1992**, 25, 361-374.
- [17] Söderström, G., Marklund, S. PBCDD and PBCDF from incineration of waste-containing brominated flame retardants. *Environ. Sci. Technol.* **2002**, 36, 1959-1964.
- [18] Quan, C., Li, A., Gao, N. Research on pyrolysis of PCB waste with TG-FTIR and Py-GC/MS. *J. Therm. Anal. Calorim.* **2012**, 110, 1463-1470.
- [19] Borojovich, E.J.C., Aizenshtat, Z. Thermal behavior of brominated and polybrominated compounds II: Pyroproducts of brominated phenols as mechanistic tools. *J. Anal. Appl. Pyrolysis* **2002**, 63, 129-145.
- [20] Dettmer, F.T. Brominated Flame Retardants Analytical requirements and Thermal Formation of Polybrominated Dibenzo-*p*-dioxins and Dibenzofurans. **2001**, University of Braunschweig: Germany.
- [21] Dumler, R., Thoma, H., Lenoir, D., Hutzinger, O. PBDF and PBDD from the combustion of bromine containing flame retarded polymers: A survey. *Chemosphere* **1989**, 19, 2023-2031.
- [22] Thoma, H., Rist, S., Hutzinger, O.H. Polybrominated dibenzodioxins and -furans from the pyrolysis of some flame retardants. *Chemosphere* **1986**, 15, 649-652.
- [23] Marongiu, A., Bozzano, G., Ranzi, E.D., Faravelli, T. Detailed kinetic modeling of pyrolysis of tetrabromobisphenol A. *J. Anal. Appl. Pyrolysis* **2007**, 80, 325-345.

- [24] Font, R., Moltó, J., Ortuño, N. Kinetics of tetrabromobisphenol A pyrolysis. Comparison between correlation and mechanistic models. *J. Anal. Appl. Pyrolysis* **2012**, 94, 53-62.
- [25] Khachatryan, L., Burcat, A., Dellinger, B. An elementary reaction-kinetic model for the gas-phase formation of 1,3,6,8- and 1,3,7,9-tetrachlorinated dibenzo-*p*-dioxins from 2,4,6-trichlorophenol. *Combust. Flame* **2003**, 132, 406-421.
- [26] Altarawneh, M., Dlugogorski, B.Z. Mechanism of thermal decomposition of tetrabromobisphenol A (TBBA). *J. Phys. Chem. A* **2014**, 118, 9338-9346.
- [27] Altarawneh, M., Dlugogorski, B.Z. A Mechanistic and kinetic study on the formation of PBDD/Fs from PBDEs. *Environ. Sci. Technol.* **2013**, 47, 5118-5127.
- [28] Saeed, A., Altarawneh, M., Dlugogorski, B.Z. Formation of mixed halogenated dibenzo-*p*-dioxins and dibenzofurans (PXDD/Fs). *Chemosphere* **2015**, 137, 149-156.
- [29] Saeed, A., Altarawneh, M., Dlugogorski, B.Z. Reactions of 2-chlorophenol and 2-bromophenol: Mechanisms of formation of mixed halogenated dioxins and furans (PXDD/Fs). *Organohalogen Compd.* **2014**, 76, 345-348.
- [30] Saeed, A., Altarawneh, M., Dlugogorski, B.Z. Formation of PBDFs and PBBs from bromobenzenes. *Organohalogen Compd.* **2015**, 77, 606-609.
- [31] Saeed, A., Altarawneh, M., Dlugogorski, B.Z. Photodecomposition of bromophenols. *Chemosphere* **2016**, 150, 749-758.
- [32] Altarawneh, M., Dlugogorski, B.Z. Thermal decomposition of 1,2-bis(2,4,6-tribromophenoxy)ethane (BTBPE), a novel brominated flame retardant. *Environ. Sci. Technol.* **2014**, 48(24), 14335-14343.
- [33] Hou, S., Mackie, J.C., Kennedy, E.M., Dlugogorski, B.Z. Comparative study on the formation of toxic species from 4-chlorobiphenyl in fires: effect of catalytic surfaces. *Procedia Eng.* **2013**, 62, 350-358.
- [34] Egerton, A., Warren, D.R. Kinetics of the hydrogen/oxygen reaction. I. The explosion region in boric acid-coated vessels. *P. Roy. Soc. Lond. A Mat.* **1951**, 204, 465-476.
- [35] Zhou, C., Sendt, K., Haynes, B.S. Experimental and kinetic modelling study of H₂S oxidation. *Proc Combust Inst.* **2013**, 34, 625-632.

- [36] Directive 2000/76/EC of the European Parliament and of the Council of 4 December 2000 on the incineration of waste Official Journal L 332 , 28/12/2000 P. 0091 – 0111.
- [37] Yates, J.R., Ruse, C.I., Nakorchevsky, A. Proteomics by mass spectrometry: approaches, advances, and applications. *Annu Rev Biomed Eng.* **2009**, 11, 49-79.
- [38] Linstrom, P.J., Mallard, W.G. *NIST Chemistry WebBook, NIST Standard Reference Database Number 69*, National Institute of Standards and Technology, Gaithersburg, MD, June 2005, <http://webbook.nist.gov/chemistry>.
- [39] Frisch, M.J., Trucks, G.W., Schlegel, H.B., Scuseria, G.E., Robb, M.A., Cheeseman, J. R., Scalmani, G., Barone, V., Mennucci, B., Petersson, G.A., Nakatsuji, H., Caricato, M., Li, X., Hratchian, H.P., Izmaylov, A.F., Bloino, J., Zheng, G., Sonnenberg, J.L., Hada, M., Ehara, M., Toyota, K., Fukuda, R., Hasegawa, J., Ishida, M., Nakajima, T., Honda, Y., Kitao, O., Nakai, H., Vreven, T., Montgomery, J.A., Jr., Peralta, J.E., Ogliaro, F., Bearpark, M., Heyd, J.J., Brothers, E., Kudin, K.N., Staroverov, V.N., Kobayashi, R., Normand, J., Raghavachari, K., Rendell, A., Burant, J.C., Iyengar, S.S., Tomasi, J., Cossi, M., Rega, N., Millam, J.M., Klene, M., Knox, J.E., Cross, J.B., Bakken, V., Adamo, C., Jaramillo, J., Gomperts, R., Stratmann, R.E., Yazyev, O., Austin, A.J., Cammi, R., Pomelli, C., Ochterski, J.W., Martin, R.L., Morokuma, K., Zakrzewski, V.G., Voth, G. A., Salvador, P., Dannenberg, J.J., Dapprich, S., Daniels, A.D., Farkas, O., Foresman, J. B., Ortiz, J.V., Cioslowski, J., Fox, D.J. Gaussian 09, revision A.1; Gaussian, Inc.: Wallingford, CT, **2009**.
- [40] Zhao, Y., Truhlar, D.G. The M06 suite of density functionals for main group thermochemistry, thermochemical kinetics, noncovalent interactions, excited states, and transition elements: two new functionals and systematic testing of four M06-class functionals and 12 other functionals. *Theor. Chem. Acc.* **2008**, 120, 215-241.
- [41] Montgomery, J.A., Ochterski, J.W., Petersson, G.A. A complete basis set model chemistry. IV. An improved atomic pair natural orbital method. *J. Chem. Phys.* **1994**, 101, 5900-5909.
- [42] Mardirossian, N., Head-Gordon, M. ω B97X-V: A 10-parameter, range-separated hybrid, generalized gradient approximation density functional with nonlocal correlation, designed by a survival-of-the-fittest strategy. *Phys. Chem. Chem. Phys.* **2014**, 16, 9904-9924.

- [43] Fukui, K. The path of chemical reactions - the IRC approach. *Acc. Chem. Res.* **1981**, 14, 363-368.
- [44] Barontini, F., Marsanich, K., Cozzani, V. The use of TG-FTIR technique for the assessment of hydrogen bromide emissions in the combustion of BFRs. *J. Therm. Anal. Calorim.* **2004**, 78, 599-619.
- [45] Yu, W., Hu, J., Xu, F., Sun, X., Gao, R., Zhang, Q., Wang, W. Mechanism and direct kinetics study on the homogeneous gas-phase formation of PBDD/Fs from 2-BP, 2,4-DBP, and 2,4,6-TBP as precursors. *Environ. Sci. Technol.* **2011**, 45, 1917-1925.
- [46] Schüler, D., Jager, J. Formation of chlorinated and brominated dioxins and other organohalogen compounds at the pilot incineration plant VERONA. *Chemosphere* **2004**, 54, 49-59.
- [47] Evans, C.S., Dellinger, B. Mechanisms of dioxin formation from the high-temperature pyrolysis of 2-bromophenol. *Environ. Sci. Technol.* **2003**, 37, 5574-5580.
- [48] Evans, C.S., Dellinger, B. Surface-mediated formation of PBDD/Fs from the high-temperature oxidation of 2-bromophenol on a CuO/silica surface. *Chemosphere* **2006**, 63, 1291-1299.
- [49] Lu, M., Mulholland, J.A. Aromatic hydrocarbon growth from indene. *Chemosphere* **2001**, 42, 625-633.
- [50] Kim, D.H., Mulholland, J.A., Ryu, J.Y. Formation of polychlorinated naphthalenes from chlorophenols. *Proc. Combust. Inst.* **2005**, 30, 1245-1253.
- [51] Wang, D., Violi, A. Formation of naphthalene, indene, and benzene from cyclopentadiene pyrolysis: A DFT Study. *J. Phys. Chem. A* **2006**, 110, 4719-4725.

CHAPTER 8 FORMATION OF MIXED HALOGENATED DIBENZO-*P*-DIOXINS AND DIBENZO FURANS (PXDD/Fs)

The following is a modified version of the published paper:

*Anam Saeed, Mohammednoor Altarawneh, Bogdan Z. Dlugogorski (2015), Chemosphere
150, 749-758*

Table of Contents

Abstract	268
8.1. Introduction	269
8.2. Computational details	271
8.3. Results and discussion	271
8.3.1. Formation of 2-chlorophenoxy and 2-bromophenoxy radicals	272
8.3.2. Reactions of 2-chlorophenoxy and 2-bromophenoxy radicals	272
8.3.3. Formation of DD, 1-MBDD, 1-MCDD, 1-B,6-CDD and 1-B,9-CDD	273
8.3.4. Formation of 4-MCDF, 4-MBDF and 4-B,6-CDF	276
8.3.5. Reaction rate constant calculations	277
8.4. Conclusion	282
Supporting information	283
Acknowledgments	283
References	284

Abstract

This contribution investigates mechanistic and kinetic parameters pertinent to formation of mixed dibenzo-*p*-dioxins and dibenzofurans (PXDD/Fs) from the condensation reactions involving 2-chlorophenoxy (2-CPhxy) and 2-bromophenoxy (2-BPhxy) radicals. Keto-ether structures act as direct intermediates for the formation of DD, 1-MCDD, 1-MBDD, 1-B,6-CDD and 1-B,9-CDD molecules. Likewise, diketo adducts initiate the formation of 4-MCDF, 4-MBDF and 4-B,6-CDF compounds through interconversion and rearrangement reactions. As formation mechanisms of halogenated dibenzo-*p*-dioxins and dibenzofurans from precursors of brominated and chlorinated phenols are insensitive to substitution at *meta* and *para* sites, our mechanistic and kinetic analysis of reactions involving 2-BPhxy and 2-CPhxy should also apply to higher halogenated phenoxy radicals.

8.1. Introduction

Brominated flame retardants (BFRs) signify a group of brominated hydrocarbons added frequently to polymeric materials to delay ignition and to improve the fire resistance traits of treated materials. Based on their combustion chemistry, these compounds display tendency to transform into incomplete combustion products (ICPs), most notably, polybrominated dibenzo-*p*-dioxins and dibenzofurans (PBDD/Fs) [1-3]. PBDD/Fs along with their chlorinated counterparts, polychlorinated dibenzo-*p*-dioxins and dibenzofuran (PCDD/Fs) discharge into the environment from nearly all thermal processes, including uncontrolled fires, recycling facilities, municipal waste incinerators, smouldering and other combustion systems [4-8].

Both gas-phase homogeneous and surface-mediated routes operate in the formation of PCDD/Fs and PBDD/Fs. Heterogeneous pathways, especially, via the so-called *de novo* synthesis, appear to bear more importance than pure gas-phase corridors in the formation of PCDD/Fs and PBDD/Fs alike [9-10]. However, the presence of potent gas phase precursors greatly enhances the contribution of the gaseous corridor [11-13]. Chlorophenols (CPhs) [11, 14-15] and bromophenols (BPhs) [16-18] comprise the most-discussed precursors for the formation of PCDD/Fs and PBDD/Fs, respectively. In addition, CPhs and BPhs function commonly as feed stocks and intermediates in manufacturing of halogenated flame retardant chemicals.

Along the same line of enquiry, the co-combustion of bromine and chlorine-bearing materials, as in fire involving BFRs and polyvinyl chloride (PVC), leads the formation of mixed halogenated dibenzo-*p*-dioxins and dibenzofurans (PXDD/Fs) [2, 19-20]. Stieglitz et al. [22] reported the formation of PXDD/Fs from carbonaceous particulate matter and inorganic chloride in the presence of bromine. Söderström and Marklund [22] observed the generation of complex mixture of PXDD/Fs from incineration of artificial municipal wastes containing both chlorine and bromine input sources. Open burning of municipal waste and the thermal recycling of discarded electrical and electronic equipment constitute major sources for emission of PXDD/Fs [2, 23-26]. Once emitted into air and water bodies, these pollutants can easily undergo long-range transport to remote areas.

Isomers of PXDD/Fs have been detected in various environmental matrices such as sewage sludge [27], air and bulk deposition [19], soil and sediments [28-29], fly ash [30-33], and industrial emissions [35]. In total, there exist 4600 distinct congeners of PXDD/Fs [35]. The toxicity of each congener depends on the degree, position and type of halogenated substituents on the aromatic ring. Therefore, close to one thousand congeners of PXDD/Fs are reported to induce toxic effects as a consequence of halogenation at the lateral 2,3,7 and 8 positions [35-37].

Quantum chemical and experimental studies have revealed detailed reaction mechanisms and kinetic parameters for the formation of PCDD/Fs and PBDD/Fs, whereas, the available literature on the reaction pathways controlling emission of PXDD/Fs remains rather scarce. Dillinger's group examined experimentally, the potential of a mixture of 2-CPh and 2-BPh to produce congeners of PXDD/Fs in inert and oxidising environments [38-39]. Few studies addressed the effect of temperature and residence time on the degree of halogenation of PXDD/Fs [44-45]. These authors demonstrated that, formation of PXDD/Fs follows the same operating mechanism as that for PCDD/Fs and PBDD/Fs. However, distinct halogenation patterns appear for PXDD/Fs, in reference to those of PCDD/Fs and PBDD/Fs. Reduction in temperature and longer residence time increase the chlorine to bromine ratio in PXDD/Fs. Yields of PXDD/Fs and their homologue distributions depend on bromine and chlorine content in input feed stream [46-47].

Based on an analogy to the controlling mechanisms that underpin the production of PCDD/Fs and PBDD/Fs in the combustion systems, PXDD/Fs arise in mixtures of CPhs and BPhs through condensation modes incorporating molecule/molecule, molecule/radical and radical/radical reactions followed by intermolecular rearrangements of initially formed intermediates. Among these condensation modes, radical/radical dimerisation reactions represent the most accessible corridors in the formation of PCDD/Fs and PBDD/Fs, in comparison to molecule/molecule coupling reactions that demand high activation barriers [13, 48]. Halogenated phenoxy radicals form either via direct fission of their hydroxyl OH bonds or through bimolecular reactions with OH, H, Br and Cl [49-51]. Furthermore, enzyme-catalysed reactions readily degrade CPhs into smaller, yet toxic constituents [52-53].

To this end, the current study elucidates gas phase mechanistic pathways leading to the formation of PXDD/Fs from bimolecular reactions of 2-CPh and 2-BPh molecules and their derived phenoxy radicals. The objective is twofold, firstly to assess the energy requirements for all routes participating in the formation of PXDD/Fs, and secondly to deduce reaction rate constants of key elementary unimolecular and bimolecular reactions. The chapters investigate thoroughly the relative importance of the competing pathways, providing the first mechanistic interpretation for the experimental trends reported in literature.

8.2. Computational details

The Gaussian09 [54] programme executes all structure optimisations and energy calculations. All calculations have been performed at the meta hybrid density theory functional (DFT) level of M062X [55], together with the polarised basis set of 6-311+G(d,p). The M062X hybrid *meta* exchange correlation functional was designed to predict accurate thermochemical and kinetic parameters for general applications in organic reactions. Single-point energy calculations, with the extended basis set of 6-311+G(3df,2p) for selected reaction, have modified the computed reaction (in kJ) and activation enthalpies (in kJ mol⁻¹) only marginally, in the range of 0.2 – 1.5 units. This finding agrees with our analogous result from recent studies on formation of PCDD/Fs and PBDD/Fs from chlorinated and brominated diphenyl ethers, respectively [14, 57]. We have shown that deploying higher basis sets alters marginally the energies calculated by M05 and M06 functionals. Intrinsic reaction coordinate (IRC) [58-59] calculations serve to link the transition states with their reactants and products. The kinetic and statistical-thermodynamic (KiSTheP) program [60] computes all reaction rate constants based on the conventional transition state theory (TST). A one-dimensional Eckart functional accounts for the plausible contributions from quantum tunnelling effects [61]. We fit reaction rate constants to the Arrhenius formula, $k(T)=Ae^{-(E_a/RT)}$, over the temperature range of 300 – 1200 K.

8.3. Results and discussion

8.3.1. Formation of 2-chlorophenoxy and 2-bromophenoxy radicals

Self-dimerisation reactions of chlorophenoxy [9, 43] and bromophenoxy [13, 17-18] radicals initiate all proposed formation mechanisms of PCDD/Fs and PBDD/Fs, respectively. Decomposition of halogenated phenols into halogenated phenoxy radicals proceeds via a unimolecular cleavage of the O-H bond and/or through bimolecular reactions involving active radical pool of H, OH, Cl and Br. 2-CPh and 2-BPh molecules exhibit comparable O-H bond dissociation energies; i.e., 359.4 kJ mol⁻¹ and 361.2 kJ mol⁻¹. This implies that both 2-chlorophenoxy (2-CPhxy) and 2-bromophenoxy (2-BPhxy) radicals arise in the same temperature window.

8.3.2. Reactions of 2-chlorophenoxy and 2-bromophenoxy radicals

Owing to their resonance delocalised electronic system, 2-CPhxy and 2-BPhxy radicals comprise four active radical sites. Their radical character appears at the phenolic oxygen, the *ortho* carbon bearing hydrogen or halogen atom and *para* carbon bonded to a hydrogen atom. Recently, we have reported energetic requirements for the formation of direct pre-intermediates of PXDD/Fs [63]. Figure 8.1 summarises pre-PXDD/Fs products that evolve through bimolecular reactions of 2-CPhxy and 2-BPhxy radicals. The two phenyl rings of pre-PXDDs and pre-PXDFs structures rotate about their corresponding C-C/C-O linkages. Thus, we have considered the most stable conformers for each pre-PXDDs and pre-PXDFs intermediate. Prestructures of PXDDs appear through the additions of a phenoxy O at *ortho* C(H), C(Cl) and C(Br) sites, whereas, pre-PXDFs structures evolve via *ortho* C-C bridgings. Structures I1 - I4 serve as direct intermediates of PXDDs, whereas, I5 - I7 adducts function as direct prestructures of PXDFs.

Formation of all pre-PXDD and pre-PXDF structures occurs without encountering an intrinsic reaction barrier, presumably due to large electron densities accumulated at phenoxy O and *ortho* C positions. Profound exothermicity accompanies the formation of pre-PXDFs and pre-PXDDs structures, in the range of 92.6 kJ – 106.3 kJ and 129.4 kJ – 135.5 kJ, in that order.

CHAPTER 8 Formation of Mixed Halogenated Dibenzo-*p*-dioxins and Dibenzofurans (PXDD/Fs)

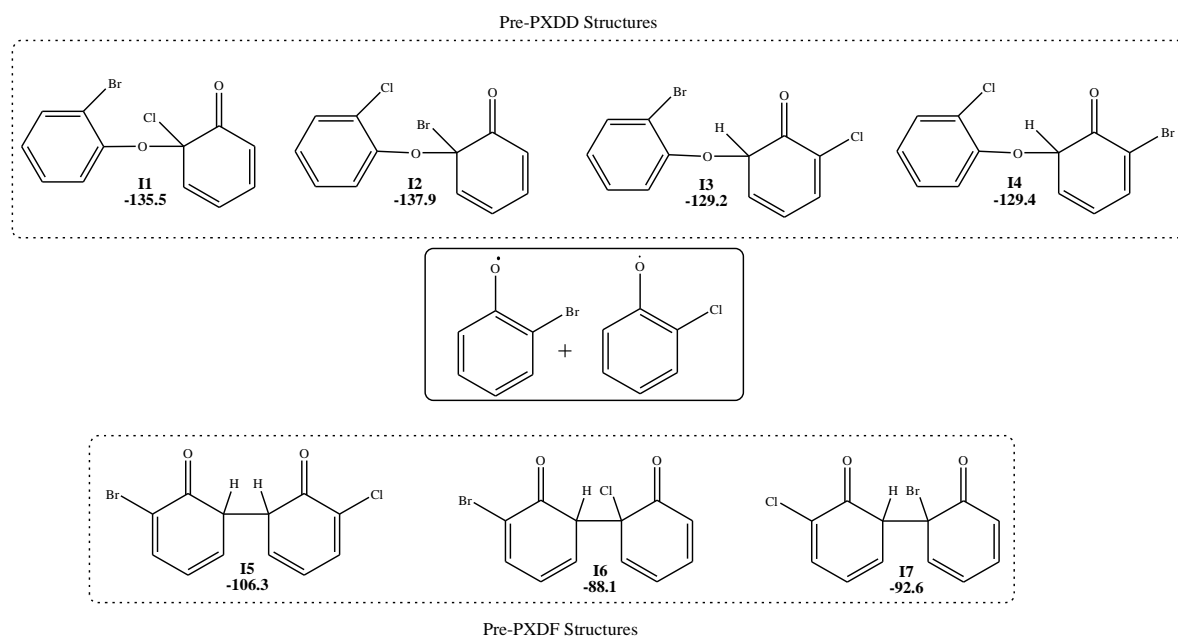


Figure 8.1. Formation of Pre-PXDD/Fs from the reaction of 2-bromophenoxy and 2-chlorophenoxy radicals. Values in bold are reaction enthalpies at 298.15 K (kJ) [64].

8.3.3. Formation of DD, 1-MBDD, 1-MCDD, 1-B,6-CDD and 1-B,9-CDD

Rearrangements and interconversion of pre-dioxin moieties influence the resultant homologue profiles. Figure 8.2 illustrates mechanistic pathways for the formation of dibenzo-*p*-dioxin (DD), 1-monobromodibenzo-*p*-dioxin (1-MBDD), 1-monochlorodibenzo-*p*-dioxin (1-MCDD), 1-bromo-6-chlorodibenzo-*p*-dioxin (1-B,6-CDD) and 1-bromo-9-chlorodibenzo-*p*-dioxin (1-B,9-CDD). This figure presents calculated reaction and activation enthalpies of individual steps.

Intermediate I1 acts as a direct building block for the production of DD and 1-MBDD. Likewise, the I2 structure constitutes a pre-structure for the formation of DD and 1-MCDD. Intermediate I3 morphs into 1-MCDD, 1-B,6-CDD and 1-B,9-CDD molecules. 1-MBDD, 1-B,6-CDD, and 1-B,9-CDD molecules could also be sourced from the I4 structure. Abstraction of H, Cl and Br atoms bound to the pivot carbon atom of the ether bridge represents the first step in the formation of dioxin structures from their corresponding ether-type intermediates (I1, I2, I3 and I4). Loss of a Cl atom from I1 by H and OH radicals demands activation enthalpies of 34.5 kJ mol^{-1} (TS1) and 57.1 kJ mol^{-1}

¹ (TS2), respectively. Similarly, abstraction of a Br atom from the I2 intermediate by H and OH radicals requires activation enthalpies of 19.6 kJ mol⁻¹ (TS6) and 21.7 kJ mol⁻¹ (TS7), correspondingly. Lower activation enthalpy, pertinent to abstraction of Br in reference to Cl, is attributed to the nature of Br atom as a good leaving group. In other words, Br atom connects rather weakly to the pivot carbon, as signified by elongation of the C-Br bond in the I2 structure to 2.03 Å, 7.4 % longer in reference to the aromatic-Br bond. Removal of an H atom from the ether bridge in the I3 and I4 structures by H radicals takes place through trivial activation enthalpies of 12.9 kJ mol⁻¹ (TS11) and 12.8 kJ mol⁻¹ (TS20). Despite of our best efforts, we were unable to locate transition structures for H abstractions from the I3 and I4 structures by OH radicals. The formation of the ether-type structures I8, I10, I12 and I17 via H/OH bimolecular-derived reactions are highly exothermic.

In pathways, 1, 3, 5 and 9, formation of DD, 1-MCDD and 1-MBDD proceed through a one- step process involving ring closure accompanied with an intramolecular displacement of a halogen atom from intermediate moieties of I8, I10, I12 and I17, correspondingly. These cyclisation reactions necessitate activation enthalpies in the narrow range of 113.0 kJ mol⁻¹ – 115.5 kJ mol⁻¹. Alternatively, I8, I10, I12 and I17 adducts undergo a two-step process to yield 1-MBDD and 1-MCDD and 1-B,6-CDD molecules, accordingly. The first step characterises a cyclisation of the phenoxy O atom toward an *ortho* C(H) position of the other phenyl ring, with the second step involving a self-ejection of an out-of-plane H atom. Activation enthalpies for the ring-closure reactions along 2, 4, 6, and 10 corridors fall within 106.7 kJ mol⁻¹ – 108.6 kJ mol⁻¹ window, demanding slightly lesser activation enthalpies than phenoxy O attachment to an *ortho* halogen bearing site. The out-of-plane H atom departs I9, I13 and I18 while experiencing similar enthalpic barriers of 120.9 kJ mol⁻¹ – 122.1 kJ mol⁻¹.

Surprisingly, pathways leading to intramolecular elimination of Cl (corridors 3, 9 and 12) hold comparable activation enthalpies to corresponding pathways entailing displacement of Br atoms (corridors 1, 5 and 8). Smiles rearrangements transform I12 and I17 adducts into I14 and I19 moieties, through moderate activation enthalpies of 104.3 kJ mol⁻¹ (TS15) and 102.0 kJ mol⁻¹ (TS24), respectively. As shown in Figure 8.2, further unimolecular

CHAPTER 8 Formation of Mixed Halogenated Dibenzo-*p*-dioxins and Dibenzofurans (PXDD/Fs)

arrangements of I14 and I19 produce 1-B,9-CDD (corridor 7 and 11), 1-MCDD (corridor 8) and 1-MBDD (corridor 12).

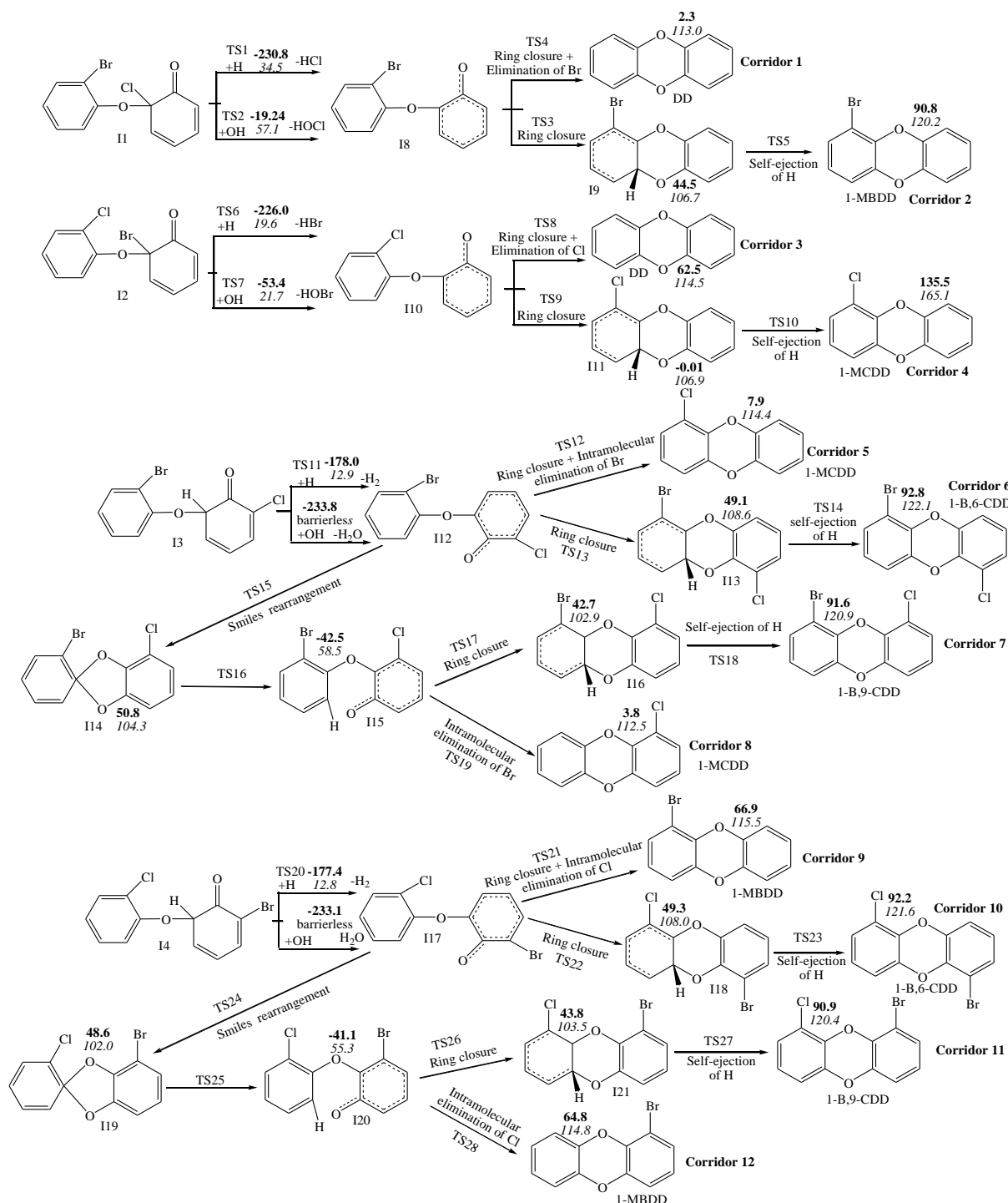


Figure 8.2. Formation of DD and PXDDs (X=Cl, Br) from the reaction of 2-chlorophenoxy and 2-bromophenoxy radicals. Values in bold and italic are the reaction (in kJ) and activation enthalpies (in kJ mol^{-1}) respectively in reference to the reactants in each reaction at 298.15 K.

8.3.4. Formation of 4-MCDF, 4-MBDF and 4-B,6-CDF

Figure 8.3 presents mechanistic pathways for the formation of 4-bromo-6-chlorodibenzofuran (4-B,6-CDF), 4-monobromodibenzofuran (4-MBDF), and 4-monochlorodibenzofuran (4-MCDF) from the I5, I6 and I7 di-keto adducts, accordingly. Among these, corridor 13 demonstrates an open-shell pathway for the formation of 4-B,6-CDF. The first step characterises a facile abstraction of an H atom from the C-C linkage by H and OH radicals. The following steps involve a tautomerisation process from the keto-keto I22 structure to the keto-enol structure of I23. This step requires an activation barrier of 80.6 kJ mol⁻¹ (TS30). The ring closure reaction along TS31 constitutes a bottleneck for the overall transformation of I5 intermediate into 4-B,6-CDF as this step demands a sizable activation enthalpy of 129.3 kJ mol⁻¹. Finally, an OH moiety leaves the I24 radical affording the 4-B,6-CDF molecule while requiring an activation enthalpy of 87.4 kJ mol⁻¹ (TS32). Formation of 4-MBDF and 4-MCDF from I6 and I7 intermediates (corridors 14 and 15) exhibits very similar mechanistic steps and energy requirements to these described above for the production of 4-B,6-CDF (corridor 13). Figure 8.1S in the supporting information depicts optimised geometries of selected transition structures covered in mechanisms of Figure 8.2 and 8.3.

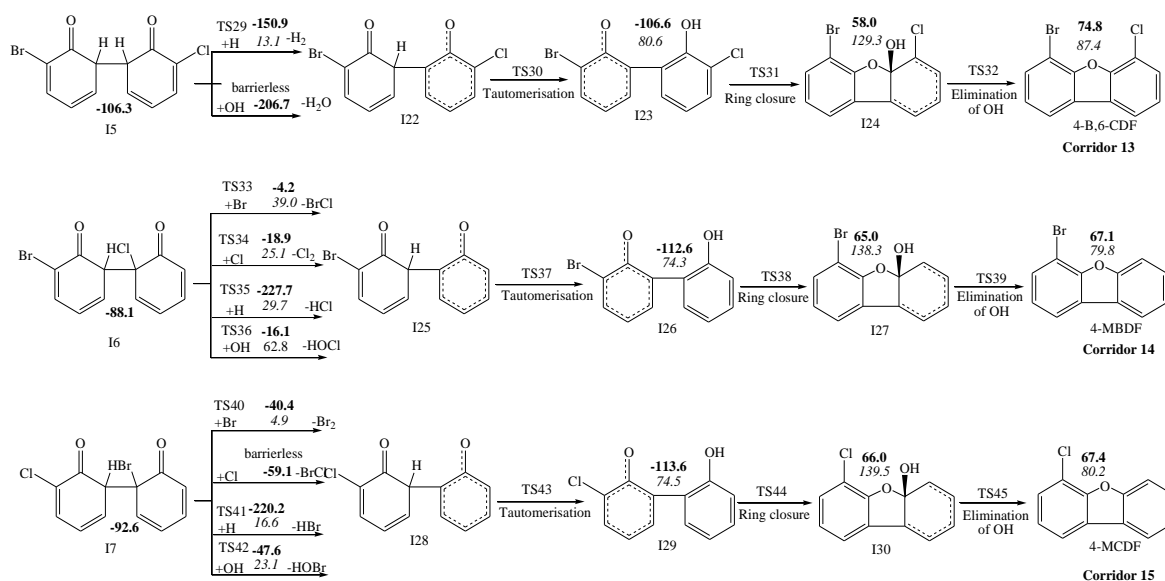


Figure 8.3. Formation of PXDFs (X=Cl, Br) from the reaction of 2-chlorophenoxy and 2-bromophenoxy radicals. Values in bold and italic are the reaction (in kJ) and activation enthalpies (in kJ mol⁻¹) respectively in reference to the reactants in each reaction at 298.15 K.

8.3.5. Reaction rate constant calculations

Tables 8.1 and 8.2 enlist the reaction rate constants in terms of the modified Arrhenius parameters for all considered reactions over the wide temperature range of 300 K to 1200 K.

Table 8.1. Arrhenius rate parameters for bimolecular/unimolecular reactions involved in the formation pathways of PXDDs from reaction of 2-chlorophenoxy and 2-bromophenoxy radicals fitted in the temperature range of 300 K – 1200 K. Values of Arrhenius parameter (*A*) are in cm³ s⁻¹ molecule⁻¹ and values of activation enthalpies (*E_a*) are in kJ mol⁻¹.

Reactions	<i>A</i>	<i>n</i>	<i>E_a</i>
I1 + H → I8 + HCl	1.57 × 10 ⁻¹⁰	0.00	39.1
I1 + OH → I8 + OHCl	6.51 × 10 ⁻¹¹	0.00	69.2
I8 → DD + Br	2.74 × 10 ¹¹	0.00	111.3
I8 → I9	6.27 × 10 ¹¹	0.00	105.6
I9 → 1-MBDD + H	5.92 × 10 ¹³	0.00	102.5
I2 + H → I10 + HBr	2.01 × 10 ⁻¹⁰	0.00	25.2
I2 + OH → I10 + OHBr	2.07 × 10 ⁻¹¹	0.00	35.6
I10 → DD + Cl	5.37 × 10 ¹³	-0.67	116.1
I10 → I11	3.09 × 10 ¹⁴	-0.94	105.7
I11 → 1-MCDD + H	7.70 × 10 ¹¹	0.00	148.2
I3 + H → I12 + H ₂	6.49 × 10 ⁻¹¹	0.00	9.68
I12 → 1-MCDD + Br	1.18 × 10 ¹³	-0.54	114.0
I12 → I13	6.99 × 10 ¹¹	0.00	109.9
I13 → 1-B,6-CDD + H	5.28 × 10 ¹³	0.00	106.5
I12 → I14	2.09 × 10 ¹²	-0.06	100.6

CHAPTER 8 Formation of Mixed Halogenated Dibenzo-*p*-dioxins and Dibenzofurans (PXDD/Fs)

I14 → I15	2.86×10^{12}	0.34	55.1
I15 → I16	5.33×10^{11}	0.00	102.6
I16 → 1-B,9-CDD + H	5.71×10^{13}	0.00	104.8
I15 → 1-MCDD + Br	2.73×10^{13}	-0.68	109.2
I4 + H → I18 + H ₂	5.51×10^{-11}	0.00	9.7
I17 → 1-MBDD + Cl	2.7×10^{11}	0.00	114.5
I17 → I18	5.17×10^{11}	0.00	107.6
I18 → 1-B,6-CDD + H	6.32×10^{13}	0.00	105.9
I18 → I19	1.97×10^{12}	-0.08	99.7
I20 → I21	6.37×10^{11}	0.00	103.2
I21 → 1-B,9-CDD + H	5.20×10^{13}	0.00	104.6
I20 → 1-MBDD + Cl	3.80×10^{11}	0.00	108.3

Table 8.2. Arrhenius rate parameters for bimolecular/unimolecular reactions involved in the formation pathways of PXDFs from reaction of 2-chlorophenoxy and 2-bromophenoxy fitted in the temperature range of 300 K – 1200 K. Values of Arrhenius parameter (*A*) are in cm³ s⁻¹ molecule⁻¹ and values of activation enthalpies (*E_a*) are in kJ mol⁻¹.

Reactions	<i>A</i>	<i>n</i>	<i>E_a</i>
I5 + H → I22 + H ₂	1.10×10^{-10}	0.00	9.41
I22 → I23	3.89×10^{11}	0.00	50.5
I23 → I24	1.81×10^{11}	0.51	122.1
I24 → 4-B,6-CDF + OH	9.04×10^{13}	0.00	85.6
I6 + Cl → I25 + Cl ₂	2.19×10^{-11}	0.00	29.9
I6 + H → I25 + HCl	9.41×10^{-11}	0.00	34.3
I6 + OH → I25 + OHCl	4.19×10^{-12}	0.00	74.7
I25 → I26	5.63×10^{11}	0.00	49.1
I26 → I27	1.77×10^{11}	0.47	130.6
I27 → 4-MBDF + OH	1.18×10^{14}	0.00	78.2
I7 + Br → I28 + Br ₂	2.08×10^{-11}	0.00	9.9
I7 + H → I28 + HBr	3.48×10^{-10}	0.00	22.1
I7 + OH → I28 + OHBr	6.58×10^{-12}	0.00	36.1

CHAPTER 8 Formation of Mixed Halogenated Dibenzo-*p*-dioxins and Dibenzofurans (PXDD/Fs)

I28 → I29	1.09×10^{12}	0.00	54.0
I29 → I30	1.70×10^{11}	0.47	131.8
I30 → 4-MCDF + OH	9.15×10^{14}	-0.36	79.1

As demonstrated in the two preceding sections, several intermediates branch into two competing channels. Figures 8.4 and 8.5 depict branching ratios as a function of temperature for the two exit channels available for I8, I10, I15 and I20 intermediates, respectively. These figures reveal that, cyclisation of the phenoxy O toward a C(H) position predominate consistently over corresponding ring closures toward a carbon atom bearing a halogen atom throughout the considered temperature window. It follows that formation of 1-MBDD (corridor 2) and 1-MCDD (corridor 4) holds more importance than competing pathways that generate DD (corridors 1 and 3). Our interpretation here clearly contrasts with the experimental results of Dellinger's group [38-39]. Under pyrolytic and oxidative conditions, yields of DD were significantly higher than those of 1-MCDD and 1-MBDD; i.e., by factors in the range of 250 – 400. The net yield of PCDD/Fs and PBDD/Fs represents a superposition or a balance between formation and decomposition pathways [9].

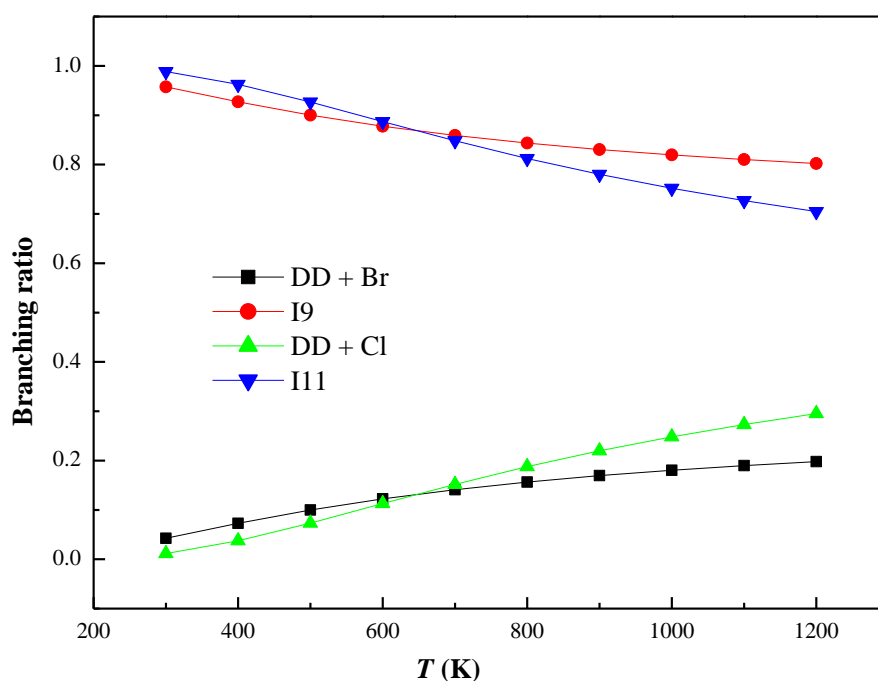


Figure 8.4. Branching ratios for the reactions (I8 → DD + Br, I8 → I9) and (I10 → DD + Cl, I10 → I11) as a function of temperature in the range of 300 K – 1200 K.

The experimentally-measured high yield of DD in comparison to that of 1-MCDD and 1-MBDD could partially be attributed to that fact that, 1-MCDD and 1-MBDD decompose at a faster rate than DD, owing to a significantly weaker C-Cl ($\sim 406.1 \text{ kJ mol}^{-1}$) and aromatic-Br ($\sim 345.5 \text{ kJ mol}^{-1}$) bonds when compared with that of aromatic-H bond ($\sim 460.0 \text{ kJ mol}^{-1}$). By adopting kinetic data from analogous systems of benzene, chlorobenzene and bromobenzene [40], at 1000 K, fission of C-H, C-Cl and C-Br bonds occur at rates of $1.87 \times 10^{-7} \text{ s}^{-1}$, $3.82 \times 10^{-5} \text{ s}^{-1}$ and $3.82 \times 10^{-3} \text{ s}^{-1}$, respectively.

Upon fission of C-Cl or C-Br bond, reaction of the formed phenyl-type radical with oxygen molecules proceeds rapidly and results in the oxidative decomposition of 1-MCDD and 1-MBDD, in an analogy to the oxidation of substituted DD [41]. The abundant H atom in pyrolysis media could readily abstract and/or displace a halogen atom from the aromatic ring, the process that ultimately converts 1-MCDD/1-MBDD into DD [42]. We calculate displacements of Cl and Br atoms in 1-MCDD and 1-MBDD by a hydrogen atom to be exothermic by -73.5 kJ and -133.0 kJ , respectively. The surface assisted reactions could account for the observed fast decomposition rate of 2-CPh and 2-BPh molecules at lower temperatures. For example, at pure pyrolytic conditions, the onset temperatures for the decomposition of 2-CPh [43] and 2-BPh [17] molecules correspond to 593 K and 573 K, correspondingly. These relatively low temperatures do not coincide with the onset temperature for the homogenous reactions for the formation of PCDD/Fs and PBDD/Fs, i.e. 673 K [12]. Within this context, 1-MCDD and 1-MBDD appear more prone to surface-mediated destruction reactions than DD. Figure 8.5 predict the formation of 1-B,9-CDD (corridor 7) and 1-B,9-CDD (corridor 11) to be more kinetically accessible than generation of 1-MCDD (corridor 8) and 1-MBDD (corridor 12), respectively. However, no experiments detected PXDDs, presumably because their concentrations remained below the detection limit.

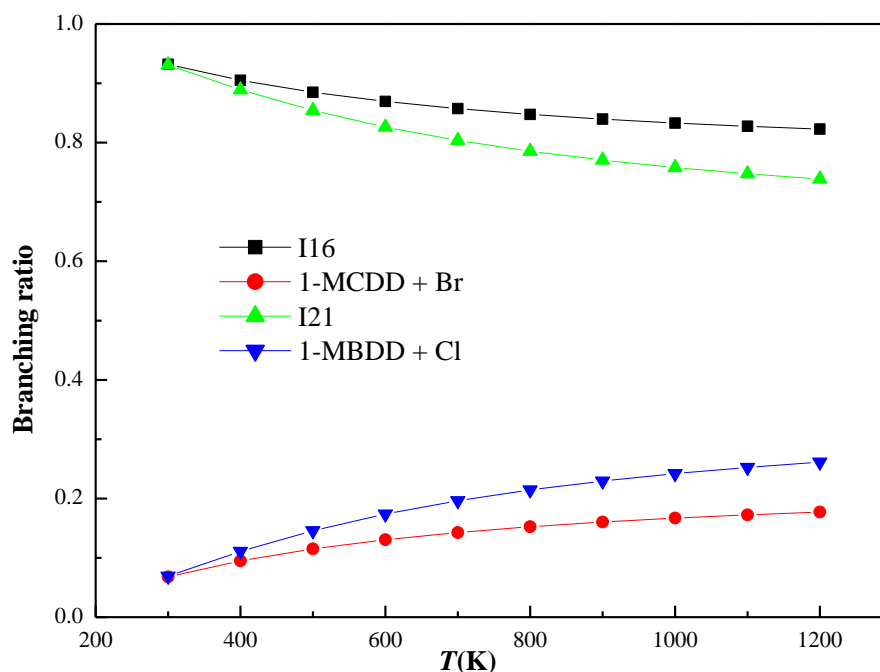


Figure 8.5. Branching ratios for the reactions ($I15 \rightarrow I16$, $I15 \rightarrow 1\text{-MCDD} + \text{Br}$) and ($I20 \rightarrow I21$, $I20 \rightarrow 1\text{-MBDD} + \text{Cl}$) as a function of temperature in the range of 300 K to 1200 K.

Conservatively, our estimated DD/1-MCDD ratios are in a qualitative agreement with the corresponding trends observed experimentally in pyrolysis [43] and oxidation [62] of 2-chlorophenols. For example, in the course of oxidation of 2-chlorophenol, the yield of 1-MCDD exceeds that of DD by a factor of 1.8 at a temperature of ~ 973 K. Under pyrolytic conditions at the same temperature, the concentration of 1-MCDD overshoots that of DD by a factor of 6.2. For the 2-bromophenol system, the corresponding yield of DD surpasses that of 1-MBDD by factors as high as 32.0 (oxidation) [18] and 133.5 (pyrolysis) [17]. The relatively comparable production of DD versus that of 1-MCDD, in systems of 2-chlorophenols [43, 62], and the dominance of DD over 1-MBDD, in systems of 2-bromophenols [17-18], concur with our aforementioned interpretation. That is, the destruction of 1-MBDD proceeds at a rate significantly faster than that of DD, as the C-Br bond is considerably weaker than that of C-H.

To the best of our knowledge, available literature offers no experimental measurement of rate constants for the pathways leading to the formation of PXDD/Fs. Therefore, an

alternative method to verify the consistency of our computed rate constants is to compare calculated pre-exponential factors (A) with those of structurally similar reactions relevant to the formation of PBDD/Fs [13]. For example, we estimate the A factor for the one-step ring closure and intramolecular elimination reaction of Br (I8 \rightarrow DD + Br) as $3.58 \times 10^{11} \text{ s}^{-1}$ in the temperature range of 600 K - 1200 K. This estimation concurs with that for an analogous reaction in a 2-BPh system [13]. By the same manner, our estimated A factor for the ring closure reaction (I29 \rightarrow I30) falls in a reasonable agreement with the analogous reaction for the formation of PCDD/Fs from 2-CPh, i.e., $5.52 \times 10^{12} \text{ s}^{-1}$ versus $2.04 \times 10^{12} \text{ s}^{-1}$, in the same temperature window [64].

Herein, we have explored pathways for the formation of PXDD/Fs from two halogenated phenoxy radicals, each with a different *ortho*-halogen substituent. Generation of PXDD/Fs from mixed polyhalogenated phenoxy radicals warrants further investigation. Mechanisms of formation of PXDD/Fs from halogenated phenoxy radicals are largely insensitive to patterns and degrees of halogenation on *meta* and *para* sites. It follows that, a limiting-case scenario involving mixed halogenation at the two *ortho* sites (e.g., self-condensation of two 2-bromo-6-chlorophenoxy radicals) may necessitate re-investigating the corridors in Figure 8.2 to obtain further insights into the generation of PXDD/Fs from mixed polyhalogenated phenoxy radicals.

8.4. Conclusion

In this chapter, we have examined reaction pathways involving 2-CPhxy and 2-BPhxy radicals. Formation of PXDD/Fs congeners follows the well-established analogous mechanisms for the formation of PCDD/Fs and PBDD/Fs. Reaction rate constants for unimolecular/bimolecular reactions were estimated using transition state theory over a temperature range of 300 K – 1200 K. Results presented herein show that, our estimated A factors reasonably agree with the recent theoretically-predicted values for the analogous systems of PCDD/Fs and PBDD/Fs. Herein, we have explored pathways for the formation of PXDD/Fs from two halogenated phenoxy radicals, each with a different *ortho*-halogen substituent. Formation of PXDD/Fs from mixed polyhalogenated phenoxy radicals warrants further investigation. Mechanisms of formations from halogenated phenoxy radicals are largely insensitive to patterns and degrees of halogenation on *meta* and *para*

sites. It follows that a limiting case scenario to underpin PXDD/Fs formation mechanisms from mixed polyhalogenated phenoxy radicals necessitates re-investigating of corridors in Figure 8.2 while considering self-condensation of two 2-bromo,6-chloro-phenoxy radicals; i.e. mixed halogenation at the two *ortho* sites.

Supporting information

Cartesian coordinates, total energies and standard thermodynamic values for all structures (available in appendix E in CD).

Acknowledgments

This study has been supported by the Australian Research Council (ARC), and grants of computing time from the National Computational Infrastructure (NCI), Australia as well as the Pawsey Supercomputing Centre. A.S. thanks Murdoch University, Australia, for a postgraduate research scholarship.

References

- [1] Ebert, J., Bahadir, M. Formation of PBDD/F from flame-retarded plastic materials under thermal stress. *Environ. Int.* **2003**, 29, 711-716.
- [2] Weber, R., Kuch, B. Relevance of BFRs and thermal conditions on the formation pathways of brominated and brominated–chlorinated dibenzodioxins and dibenzofurans. *Environ. Int.* **2003**, 29, 699-710.
- [3] Birnbaum, L.S., Staskal, D.F. Brominated flame retardants: cause for concern? . *Environ. Health. Perspect.* **2004**, 112, 9–17.
- [4] Tame, N.W., Dlugogorski, B.Z., Kennedy, E.M. Formation of dioxins and furans during combustion of treated wood. *Prog. Energ. Combust.* **2007**, 34, 384–408.
- [5] Tame, N.W., Dlugogorski, B.Z., Kennedy, E.M. Increased PCDD/F formation in the bottom ash from Fires of CCA-treated Wood. *Chemosphere* **2003**, 50, 1261–1263.
- [6] Wang, L.C., Wang, Y.F., Hsi, H.C., Chang-Chien, G.P. Characterizing the emissions of polybrominated diphenylethers (PBDEs) and polybrominated dibenzo-*p*-dioxins and dibenzofurans (PBDD/Fs) from metallurgical processes. *Environ. Sci. Technol.* **2010**, 44, 1240-1246.
- [7] Wanga, M.S., Chena, S.J., Huang, K.L., Lai, Y.C., Chang-Chien, P.G., Tsai, J.H., Lind, W.Y., Changa, K.C., Lee, J.T. Determination of levels of persistent organic pollutants (PCDD/Fs, PBDD/Fs, PBDES, PCBs, and PBBs) in atmosphere near a municipal solid waste incinerator. *Chemosphere* **2010**, 80, 1220–1226.
- [8] Duan, H., Li, J. Characterization and inventory of PCDD/Fs and PBDD/Fs emissions from the incineration of waste printed circuit board. *Environ. Sci. Technol.* **2011**, 45, 6322–6328.
- [9] Tuppurainen, K., Asikainen, A., Ruokojarvi, P., Ruuskanen, J. Perspectives on the formation of polychlorinated dibenzo-*p*-dioxins and dibenzofurans during municipal solid waste (MSW) incineration and other combustion processes. *Acct. Chem. Res.* **2003**, 36, 652-658.
- [10] Ortuno, N., Conesa, J.A., Molto, J., Font, R. De novo synthesis of brominated dioxins and furans. *Environ. Sci. Technol.* **2014**, 48, 7959–7965.

- [11] Dickson, L.C., Lenolr, D., Hutzinger, O. Quantitative comparison of de novo and precursor formation of polychlorinated dibenzo-*p*-dioxins under simulated municipal solid waste incinerator post combustion conditions. *Environ. Sci. Technol.* **1992**, 26, 1822-1828.
- [12] Altarawneh, M., Dlugogorski, B.Z., Kennedy, E.M., Mackie, J.C. Mechanisms for formation, chlorination, dechlorination and destruction of polychlorinated dibenzo-*p*-dioxins and dibenzofurans (PCDD/Fs). *Prog. Energ. Combust* **2009**, 35, 245–274.
- [13] Yu, W., Hu, J., Xu, F., Sun, X., Gao, R., Zhang, Q., Wang, W. Mechanism and direct kinetics study on the homogeneous gas-phase formation of PBDD/Fs from 2-BP, 2,4-DBP, and 2,4,6-TBP as precursors. *Environ. Sci. Technol.* **2011**, 45, 1917–1925.
- [14] Karasek, F.W., Dickson, L.C. Model studies of polychlorinated dibenzo-*p*-dioxin formation during municipal refuse incineration. *Science* **1987**, 237, 754-756.
- [15] Kari, A., Tuppurainen, P.H., Ruokojarvi, A.H., Aatamila, M.A., Ruuskanen, J. Chlorophenols as precursors of PCDD/Fs in incineration processes: correlations, PLS modelling, and reaction mechanisms. *Environ. Sci. Technol.* **2000**, 34, 4958-4962.
- [16] Dumler, R., Thoma, H., Lenoir, D., Hutzinger, O. thermal formation of polybrominated dibenzodioxins (PBDD) and dibenzofurans (PBDF) from bromine containing flame retardants. *Chemosphere* **1989**, 19, 305-308
- [17] Evans, C.S., Dellinger, B. Mechanisms of dioxin formation from the high-temperature pyrolysis of 2-bromophenol. *Environ. Sci. Technol.* **2003a**, 37, 5574-5580.
- [18] Evans, C.S., Dellinger, B. Mechanisms of dioxin formation from the high-temperature oxidation of 2-bromophenol. *Environ. Sci. Technol.* **2005b**, 39, 2128-2134.
- [19] Hayakawa, K., Takatsuki, H., Watanabe, I., Sakai, S.I. Polybrominated diphenyl ethers (PBDEs), polybrominated dibenzo-*p*-dioxins/dibenzofurans (PBDD/Fs) and monobromo-polychlorinated dibenzo-*p*-dioxins/dibenzofurans (MoBPXDD/Fs) in the atmosphere and bulk deposition in Kyoto, Japan. *Chemosphere* **2004**, 57, 343–356.

- [20] Schuler, D., Jager, J. Formation of chlorinated and brominated dioxins and other organohalogen compounds at the pilot incineration plant VERONA. *Chemosphere* **2004**, 54, 49–59.
- [21] Stieglitz, L., Zwick, G., Beck, J., Bautz, H., Roth, W. Carbonaceous particles in fly ash - a source for the de novo synthesis of organochloro compounds. *Chemosphere* **1989**, 19, 283–290.
- [22] Söderström, G., Marklund, S. PBCDD and PBCDF from incineration of waste-containing brominated flame retardants. *Environ. Sci. Technol.* **2002**, 36, 1959–1964.
- [23] Buser, H.R. Brominated and Brominated/chlorinated dibenzodioxins and dibenzofurans: potential environmental contaminants. *Chemosphere* **1987**, 16, 713–732.
- [24] Vehlow, J., Bergfeldt, B., Jay, K., Seifert, H., Wanke, T., Mark, F.E. Thermal treatment of electrical and electronic waste plastics. *Waste Manage Res.* **2000**, 18, 131–140.
- [25] Lemieux, P.M., Stewart, E.S., Ryan, J.V. Pilot-scale studies on the effect of bromine addition on the emissions of chlorinated organic combustion by-products. *Waste Manage.* **2002**, 22, 381–389.
- [26] Xiezh, Y., Markus, Z., Magnus, E., Anna, R., Maria, L., Hung, W.M., Roland, W. E-waste recycling heavily contaminates a chinese city with chlorinated, brominated and mixed halogenated dioxins. *Organohalogen Compd.* **2008**, 70, 813–816.
- [27] Hagenmaier, H., She, J., Benz, T., Dawidowsky, N., Dusterhoft, L., Lindig, C. Analysis of sewage sludge for polyhalogenated dibenzo-*p*-dioxins, dibenzofurans, and diphenylethers. *Chemosphere* **1992**, 25, 1457–1462.
- [28] Kannan, K., Watanabe, I., Giesy, J. Congener profile of polychlorinated/brominated dibenzo-*p*-dioxins and dibenzofurans in soil and sediments collected at a former chlor-alkali plant. *Toxicol. Environ. Chem.* **1998**, 67, 135–146.
- [29] Myers, A.L., Mabury, S.A., Reiner, E.J. Analysis of mixed halogenated dibenzo-*p*-dioxins and dibenzofurans (PXDD/PXDFs) in soil by gas chromatography tandem mass spectrometry (GC–MS/MS). *Chemosphere* **2012**, 87, 1063–1069.

- [30] Schafer, W., Ballschmiter, K. Monobromo-polychloro-derivatives of benzene, biphenyl, dibenzofurane and dibenzodioxine formed in chemical-waste burning. *Chemosphere* **1986**, 15, 755–763.
- [31] Harless, R., Lewis, R. Identification of bromo/chloro dibenzo-*p*-dioxins and dibenzofurans in ash samples. *Chemosphere* **1989**, 18, 201–208.
- [32] Schwind, K.H., Hosseinpour, J., Thoma, H. Brominated/chlorinated dibenzo-*p*-dioxins and dibenzofurans: part 1: brominated/chlorinated and brominated dibenzo-*p*-dioxins and dibenzofurans in fly ash from a municipal waste incinerator. *Chemosphere* **1998**, 17, 1875-1884.
- [33] Nakao, T., Ohta, S., Aozasa, O., Miyata, H. Investigation of PCDD/DF, PXDD/DF, PBDD/DF, and nitro-PAH detected on flue gas from waste incinerator. *Organohalogen Compd.* **2002**, 56, 349-352.
- [34] Du, B., Zheng, M., Huang, Y., Liu, A., Tian, H., Li, L., Li, N., Ba, T., Li, Y., Dong, S., Liu, W., Su, G. Mixed polybrominated/chlorinated dibenzo-*p*-dioxins and dibenzofurans in stack gas emissions from industrial thermal processes. *Environ. Sci. Technol.* **2010**, 44, 5818–5823.
- [35] Brigden, K., Labunska, I. Mixed Halogenated Dioxins and Furans: A Technical Background Document. Greenpeace Research Laboratories Technical Note. **2009**.
- [36] Mason, G., Denomme, M.A., Safe, L., Safe, S. Polybrominated and chlorinated dibenzo-*p*-dioxins: synthesis biologic and toxic effects and structure-activity relationship. *Chemosphere* **1987**, 16, 1729-1731.
- [37] Behnisch, P.A., Hosoe, K., Sakai, S. Combinatorial bio/chemical analysis of dioxins and dioxins like compounds in waste recycling, feed/food. humans/wildlife and the environment. *Environ. Int.* **2001**, 27, 495-519.
- [38] Evans, C.S., Dellinger, B. Formation of bromochlorodibenzo-*p*-dioxins and furans from the high temperature oxidation of a 2-chlorophenol/2-bromophenol mixture. *Environ. Sci. Technol.* **2006**, 40, 3036-3042.
- [39] Evans, C.S., Dellinger, B. Formation of bromochlorodibenzo-*p*-dioxins and furans from high temperature pyrolysis of a 2-chlorophenol/2-bromophenol mixture. *Environ. Sci. Technol.* **2005a**, 39, 7940–7948.
- [40] Manion, J.A., Huie, R.E., Levin, R.D., Burgess Jr, D.R., Orkin, V.L., Tsang, W., McGivern, W.S., Hudgens, J.W., Knyazev, V.D., Atkinson, D.B., Chai, E., Tereza, A.M., Lin, C.Y., Allison, T.C., Mallard, W.G., Westley, F., Herron, J.T., Hampson,

- R.F., Frizzell, D.H. NIST Chemical Kinetics Database, NIST Standard Reference Database 17. National Institute of Standards and Technology, Gaithersburg, Maryland. **2013**, 20899-28320.
- [41] Summoogum, S.L., Altarawneh, M., Mackie, J.C., Kennedy, E.M., Dlugogorski, B.Z. Oxidation of dibenzo-*p*-dioxin: formation of initial products, 2-methylbenzofuran and 3-hydro-2-methylenebenzofuran. *Combust. Flame* **2012**, 159, 3056-3065.
- [42] Altarawneh, M., Dlugogorski, B.Z. A Mechanistic and kinetic study on the formation of PBDD/Fs from PBDEs. *Environ. Sci. Technol.* **2013**, 47, 5118-5127.
- [43] Evans, C.S., Dellinger, B. Mechanisms of dioxin formation from the high-temperature pyrolysis of 2-chlorophenol. *Environ. Sci. Technol.* **2003b**, 37, 1325-1330.
- [44] Söderström, G., Marklund, S. Formation of PBCDD and PBCDF during flue gas cooling. *Environ. Sci. Technol.* **2004**, 38, 825-830.
- [45] Söderström, G., Marklund, S. PXDD and PXDF from combustion of bromoflame retardant containing MSW. *Organohalogen Compd.* **2000**, 47, 225-228.
- [46] Funcke, W., Hemminghaus, H.J., Mark, F.E., Vehlow, J. PXDF/D in flue gas from an incinerator charging wastes containing cl and br and a statistical description of the resulting PXDF/D combustion profiles. *Organohalogen Compd.* **1997**, 31, 93-98.
- [47] Kawamoto, K., Ishikawa, N. Experimental evidence for de novo synthesis of PBDD/PBDF and PXDD/PXDF as well as dioxins in the thermal processes of ash samples. *Organohalogen Compd.* **2005**, 67, 2219-2221.
- [48] Altarawneh, M., Dlugogorski, B.Z., Kennedy, E.M., Mackie, J.C. quantum chemical investigation of formation of polychlorodibenzo-*p*-dioxins and dibenzofurans from oxidation and pyrolysis of 2-chlorophenol. *J. Phys. Chem. A* **2007**, 111, 2563-2573.
- [49] Altarawneh, M., Dlugogorski, B.Z., Kennedy, E.M., Mackie, J.C. Quantum chemical and kinetic study of formation of 2-chlorophenoxy radical from 2-chlorophenol: unimolecular decomposition and bimolecular reactions with H, OH, Cl, and O₂. *J. Phys. Chem. A* **2008**, 112, 3680-3692.

- [50] Xu, F., Wang, H., Zhang, Q., Zhang, R., Qu, X., Wang, W. Kinetic properties for the complete series reactions of chlorophenols with OH radicals-relevance for dioxin formation. *Environ. Sci. Technol.* **2010**, 44, 1399–1404.
- [51] Gao, R., Xu, F., Li, S., Hu, J., Zhang, Q., Wang, W. formation of bromophenoxy radicals from complete series reactions of bromophenols with H and OH radicals. *Chemosphere* **2013**, 92, 382-390.
- [52] Öberg, G.L., Glas, B., Swanson, S. E., Rappe, C., Paul, K. G. Peroxidase-catalyzed oxidation of chlorophenols to polychlorinated dibenzo-*p*-dioxins and dibenzofurans. *Arch. Environ. Contam. Toxicol.* **1990**, 19, 930-938.
- [53] Li, Y., Zhang, R., Du, L., Zhang, Q., Wang, W. Insights into the catalytic mechanism of chlorophenol 4-monooxygenase: a quantum mechanics/molecular mechanics study. *RSC Adv.* **2015**, 5, 13871-13877.
- [54] Frisch, M.J., Trucks, G.W., Schlegel, H.B., Scuseria, G.E., Robb, M.A., Cheeseman, J.R., Scalmani, G., Barone, V., Mennucci, B., Petersson, G.A., Nakatsuji, H., Caricato, M., Li, X., Hratchian, H.P., Izmaylov, A.F., Bloino, J., Zheng, G., Sonnenberg, J.L., Hada, M., Ehara, M., Toyota, K., Fukuda, R., Hasegawa, J., Ishida, M., Nakajima, T., Honda, Y., Kitao, O., Nakai, H., Vreven, T., Montgomery, J., Jr, A., Peralta, J.E., Ogliaro, F., Bearpark, M., Heyd, J.J., Brothers, E., Kudin, K.N., Staroverov, V.N., Kobayashi, R., Normand, J., Raghavachari, K., Rendell, A., Burant, J.C., Iyengar, S.S., Tomasi, J., Cossi, M., Rega, N., Millam, N.J., Klene, M., Knox, J.E., Cross, J.B., Bakken, V., Adamo, C., Jaramillo, J., Gomperts, R., Stratmann, R.E., Yazyev, O., Austin, A.J., Cammi, R., Pomelli, C., Ochterski, J.W., Martin, R.L., Morokuma, K., Zakrzewski, V.G., Voth, G.A., Salvador, P., Dannenberg, J.J., Dapprich, S., Daniels, A.D., Farkas, O., Foresman, J.B., Ortiz, J.V., Cioslowski, J., Fox, D.J., **2009**. Gaussian 09, Revision D.01; Gaussian, Inc.: Wallingford, CT.
- [55] Zhao, Y., Truhlar, D.G. The M06 suite of density functionals for main group thermochemistry, thermochemical kinetics, noncovalent interactions, excited states, and transition elements: two new functionals and systematic testing of four m06-class functionals and 12 other functionals. *Theor. Chem. Acc.* **2008**, 120, 215-241.
- [56] Montgomery, J.A., Ochterski, J.W., Petersson, G.A. A Complete Basis Set Model Chemistry. IV. An Improved Atomic Pair Natural Orbital Method. *J. Chem. Phys.* **1994**, 101, 5900-5909.

- [57] Altarawneh, M., Dlugogorski, B. Mechanisms of transformation of polychlorinated diphenyl ethers into polychlorinated dibenzo-*p*-dioxins and dibenzofurans. *Chemosphere* **2014**, 114, 129-135.
- [58] Fukui, K. The Path of Chemical-Reactions - The IRC Approach. *Acc. Chem. Res.* **1981**, 14, 363-368.
- [59] Hrant, P., Hratchian, H., Bernhard, S. Finding Minima, Transition States, and Following Reaction Pathways on Ab Initio Potential Energy Surfaces. in: Dykstra, C.E., Frenking, G., Kim, K. S., Scuseria, G., (Ed.). *Theory and Applications of Computational Chemistry*. Elsevier, Amsterdam, **2005**, 195-249.
- [60] Canneaux, S., Bohr, F., Henon, E. KiSThelp: A program to predict thermodynamic properties and rate constants from quantum chemistry results. *J. Comput. Chem.* **2004**, 35, 82-93.
- [61] Eckart, C. The Penetration of a Potential Barrier by Electrons. *Physical Review*. **1930**, 35, 1303-1309.
- [62] Evans, C.S., Dellinger, B. Mechanisms of dioxin formation from the high-temperature oxidation of 2-chlorophenol. *Environ. Sci. Technol.* **2005c**, 39, 122-127.
- [63] Saeed, A., Altarawneh, M., Dlugogorski, B.Z. reactions of 2-chlorophenol and 2-bromophenol: mechanisms of the formation of mixed halogenated dioxins and furans (PXDD/Fs). *Organohalogen Compd.* **2014**, 76, 345-348.
- [64] Zhang, Q., Li, S., Qu, X., Shi, X., Wang, W. A quantum mechanical study on the formation of PCDD/Fs from 2-chlorophenol as precursor. *Environ. Sci. Technol.* **2008**, 42, 7301-7308.

CHAPTER 9 FORMATION OF POLYBROMINATED DIBENZOFURANS (PBDFs) AND POLYBROMINATED DIPHENYL ETHERS (PBDEs) FROM OXIDATION OF BROMINATED FLAME RETARDANTS (BFRs)

The following is a modified version of the paper under review:

Anam Saeed, Mohammednoor Altarawneh, Stina Jansson, Bogdan Z. Dlugogorski (2016), Environ. Sci. Technol.

Table of Contents

Abstract	292
9.1. Introduction	293
9.2. Computational details	295
9.3. Results and discussion	296
9.3.1. Formation of pre-PBDFs and pre-PBDEs	296
9.3.2. Formation of PBDFs and DBDEs	298
9.3.3. Reaction rate constants	303
9.4. Conclusions	307
Acknowledgments	307
Supplementary material	308
References	309

Abstract

Brominated aromatic rings constitute main structural entities in virtually all commercially deployed brominated flame retardants (BFRs). Oxidative decomposition of BFRs liberates appreciable quantities of bromobenzenes (BBzs). This contribution maps out reaction pathways and reports kinetic parameters for the build-up of notorious polybrominated dibenzofurans (PBDFs) and polybrominated diphenyl ethers (PBDEs) from a monobromobenzene (MBBz) molecule and its derived *ortho*-bromophenoxy (*o*-BPhxy) radical. Bimolecular reactions of MBBz and *o*-BPhxy result in the generation of twelve pre-PBDF intermediates, of which four can also serve as building blocks for the synthesis of PBDEs. These four intermediates are denoted as pre-PBDE/pre-PBDF, with the remaining eight symbolised as pre-PBDF. The resonance-stabilised structure of the *o*-BPhxy radical accumulates more spin density character on its phenoxy O atom (30.9 %) in reference to *ortho*-C and *para*-C sites. Thus, the formation of the pre-PBDE/pre-PBDF structures via O/*o*-C couplings advances faster as it requires lower activation enthalpies (79.2 – 84.9 kJ mol⁻¹) than the pre-PBDF moieties, which arise via pairing reactions involving *o*-C(H or Br)/*o*-C(H or Br) sites (97.2 – 180.2 kJ mol⁻¹). Kinetic analysis indicates that, the O/*o*-C pre-PBDE/pre-PBDF adducts self-eject the out-of-plane H atoms to produce PBDEs, rather than undergo a three-step mechanism forming PBDFs. Since formation mechanisms of PBDFs and polybrominated dibenzo-*p*-dioxins (PBDDs) are typically only sensitive to the bromination at *ortho* positions, the results reported herein apply also to higher brominated isomers of BBzs. Hence, we demonstrate that, the oxidation of PBBz preferentially yields PBDEs, rather than PBDFs. PBDFs arise in subsequent oxidation of PBDEs.

9.1. Introduction

Halogenated benzenes and phenols represent the most important direct building blocks in the homogenous gas-phase formation of halogenated dioxins and furans, namely polychlorinated dibenzo-*p*-dioxins and polychlorinated dibenzofurans (PCDD/Fs) [1-4] and their analogous brominated counterparts, i.e., polybrominated dibenzo-*p*-dioxins and polybrominated dibenzofurans (PBDD/Fs) [5-7]. The gas-phase route holds more importance in the formation of PBDD/Fs than for PCDD/Fs. This is because, the heterogeneous pathways dominate the generation of PCDD/Fs, namely, the de novo route [8-9] and the catalytically-assisted coupling of the precursors [10-11].

By comparing isomer profiles of PCDD/Fs across various emission sources including municipal waste incinerators, accidental fires/open burnings at domestic and industrial scale and forest fires dominated by the de novo mechanism, one notes two interesting remarks: the total yield of PCDFs significantly exceeds that of PCDDs, and the isomers in each homologue group of PCDD/Fs display very comparable abundance [2, 12-13]. Clearly, this indicates that, a governing formation mechanism of PCDD/Fs must be insensitive to the chlorination pattern of gaseous chlorinated benzenes and phenols. Nonetheless, conflicting views in the literature assign a contribution of the homogenous precursor route as high as 30 % of the total yield of PCDD/Fs [10]. On the contrary, profiles of PBDD/Fs exhibit considerable variations among different thermal processes. Another prominent difference is that, chlorine in PCDD/Fs stems from inorganic sources (i.e., metal chlorides) [14], whereas bromine in PBDD/Fs is of an organic origin [15]. However, the source of chlorine (either organic or inorganic) does not provoke any significant difference on the congener pattern of PCDD/Fs formed during combustion processes [16].

Thermal decomposition of brominated flame retardants (BFRs) [17-18] constitutes the main source for the emission of PBDD/Fs and their potent precursors such as brominated benzenes (BBzs) and brominated phenols (BPhs). PBDD/Fs arise directly from the structural arrangements of certain BFRs. We have shown recently that, the ring closure of polybrominated diphenyl ethers (PBDEs) – after the loss of an *ortho*-H/Br atom leads

CHAPTER 9 Formation of Polybrominated Dibenzofurans (PBDFs) and Polybrominated Diphenyl Ethers (PBDEs) from Oxidation of Brominated Flame Retardants (BFRs)

to the formation of PBDFs, whereas, addition of an oxygen molecule at an *ortho* site in PBDEs or brominated biphenyls prompts a complex exothermic mechanism that forms PBDDs [19-20]. Decomposition of BFRs containing aromatic rings, such as tetrabromobisphenol A (TBBA) [21], PBDEs [22-23] and 1,2-bis(tribromophenoxy) ethane (BTBPE) [6] results in emission of appreciable amounts of BBzs and BPhs. For example, the thermolysis of TBBA yields a substantial quantity of BPhs (up to 79.6 mg (kg TBBA)⁻¹) and BBzs (up to 172 mg (kg TBBA)⁻¹) [24]. In our recent experimental study on the self-decomposition of gaseous TBBA [25], we have detected elevated concentrations of several isomers of BBzs and BPhs, commencing at 723 K and peaking around 973 K. These two groups of compounds may also appear from the combination of small brominated hydrocarbons, upon the full destruction of BFR bearing materials in the post-combustion zone of a typical municipal solid waste incinerator [5].

Previous experimental [26-27] and theoretical [7] accounts have aimed to address the emission of PBDD/Fs from BPhs under a wide range of operating conditions. Yu et al. [7] have shown the homogenous gas phase formation mechanism of PBDD/Fs from the dimerisation reactions of bromophenoxy (BPhxy) radicals that evolve directly from BPhs by the loss of phenoxy-hydrogen in unimolecular or bimolecular reactions. Oxidative and pyrolytic decomposition of 2-monobromophenol (2-MBPh) leads to the formation of few monodibrominated congeners of DD/Fs. However, studies on the production of PBDD/Fs from oxidation and pyrolysis of BBzs are rather scarce. In general, the formation of halogenated furan compounds from halogenated benzenes have received considerably less attention if compared with analogous formation from halogenated phenols. PCDD/Fs arise as by-products during the production of chlorobenzenes [28]. Oxidation reactions of chlorobenzene produce PCDFs in substantial yields that includes monochlorodibenzofuran (MCDF), dichlorodibenzofuran (DCDF), trichlorodibenzofuran (TriCDF) and tetrachlorodibenzofuran (TCDF) at a temperature above 573 K [29-31].

In a previous theoretical study, we have illustrated prominent reactions leading to the formation of PCDFs from the oxidation of monochlorobenzene [32]. Suggested pathways encompass: (i) abstraction of a hydrogen or a chlorine atom from the parent chlorobenzene molecule, (ii) formation of chlorophenyl peroxy moieties via the addition of oxygen

CHAPTER 9 Formation of Polybrominated Dibenzofurans (PBDFs) and Polybrominated Diphenyl Ethers (PBDEs) from Oxidation of Brominated Flame Retardants (BFRs)

molecule at the vacant radical site in chlorophenyls, (iii) fission of the O-O bond in peroxy adducts and (iv) bimolecular reaction of chlorophenoxy radicals with a chlorobenzene molecule followed by a ring closure step. Subsequent electrophilic chlorination reactions play a role in the development of the product distribution patterns of PCDF congeners [33-35]. Chlorination reactions of chlorophenoxy radicals and/or the pre-PCDF intermediates lead to the formation of higher chlorinated congeners of PCDF [31]. Nonetheless, the exact chlorination mechanism and the plausible occurrence of electrophilic substitution mediated by the metal oxychlorides remain largely speculative [36-38].

To the best of our knowledge, literature presents no experimental or theoretical study on the oxidation of BBz congeners, arising in partial oxidation of BFRs, and the subsequent formation of PBDFs and PBDEs, in spite of significant importance of these pollutants. To this end, the current investigation determines the mechanistic pathways and kinetic parameters encountered in the formation of PBDFs and PBDEs from the oxidative decomposition of MBBz.

9.2. Computational details

Structure optimisation and frequency calculations were executed at the meta-hybrid density functional theory (DFT) level of M062X along with the polarised basis set of 6-311+G(d,p) [39] as implemented in the Gaussian 09 [40] suite of programs. The M062X performs well in predicting thermochemistry and kinetics in general applications to organic chemistry [41]. Our recent studies on the formation of PBDD/Fs from the decomposition of several BFRs [42-45] have established thermal and kinetic accuracy benchmarks for the performance of the adopted methodology in describing systems of brominated aromatic compounds.

In the results of our computations, each transition state held one and only one imaginary frequency along the specified reaction coordinates. Intrinsic reaction coordinate (IRC) calculations [46] confirmed reaction pathways via connecting transition states with their reactants and products, except for the elimination of HBr in three reactions, as described at the end of the section on formation of PBDFs and DBDEs. We report all reaction and

CHAPTER 9 Formation of Polybrominated Dibenzofurans (PBDFs) and Polybrominated Diphenyl Ethers (PBDEs) from Oxidation of Brominated Flame Retardants (BFRs)

activation enthalpies at 298 K. Reaction rate constants in terms of activation energy (E_a) and pre-exponential factor (A), fit to the Arrhenius $k(T) = Ae^{-(E_a/RT)}$ formula, have been estimated with the aid of kinetic and statistical-thermodynamic program, KiSThelP [47]. KiSThelP derives reaction rate constants based on the conventional transition state (TST) along with the inclusion of a one-dimensional Eckart barrier [48] to account for quantum tunnelling effects on the computed reaction rate coefficients. Finally, the ChemRate programme [49] has served to estimate the Gibbs free energies (ΔG_r) for selected reactions at 800 K.

9.3. Results and discussion

9.3.1. Formation of pre-PBDFs and pre-PBDEs

This chapter complements our recent contribution [50], in which we describe reaction channels for the oxidative conversion of MBBz into the three isomers of monobromophenoxy (MBPhxy) radical. While the aromatic C-Br bond is significantly weaker than the corresponding C-H bond ($347.3 \text{ kJ mol}^{-1}$ versus $469.8 \text{ kJ mol}^{-1}$) [51], H/Br radicals could readily abstract a hydrogen atom from the three distinct sites in the MBBz molecule [19]. Subsequent addition of an oxygen molecule to the vacant radical site of monobromophenyl results in the formation of *m*-, *p*- and *o*-BPhxy radicals. Herein, we limit the analysis to the *o*-BPhxy radical, but the results apply to other BPhxy radicals, as the condensation reactions forming PBDDs/Fs are only sensitive to substituents at the *ortho* position, i.e., H and Br. We elaborate on this point further in the section titled “Reaction rate constants”.

As a resonance stabilised structure, we find that, the spin density in the *o*-BPhxy radical accumulates on the phenoxy O atom (30.9%) as well as *o*-C(H) (14.2%), *o*-C(Br) (16.8%) and *p*-C(H) (21.8%) sites. Accordingly, addition of a MBBz molecule to the three radical centres in the *o*-BPhxy moiety produces sixteen different structures. Figure 9.1 portrays structures and energies of twelve of these intermediates. The couplings involving the *p*-C(H) site in the BPhxy radical leads to the formation of adducts that do not act as building blocks for either PBDFs or PBDEs; hence, they are not discussed here.

CHAPTER 9 Formation of Polybrominated Dibenzofurans (PBDFs) and Polybrominated Diphenyl Ethers (PBDEs) from Oxidation of Brominated Flame Retardants (BFRs)

The phenoxy oxygen exists in an *ortho* position relative to the C-C bridge in only eight of these structures, IP1 – IP8 (*o*-C/*o*-C couplings). For that reason, these structures (denoted as pre-PBDFs) act as intermediates for the generation of dibenzofuran (DF) and monobromodibenzofuran (MBDF) isomers. (For convenience, in this article, the terms PBDFs and PBDEs also include the non-brominated and monobrominated congeners).

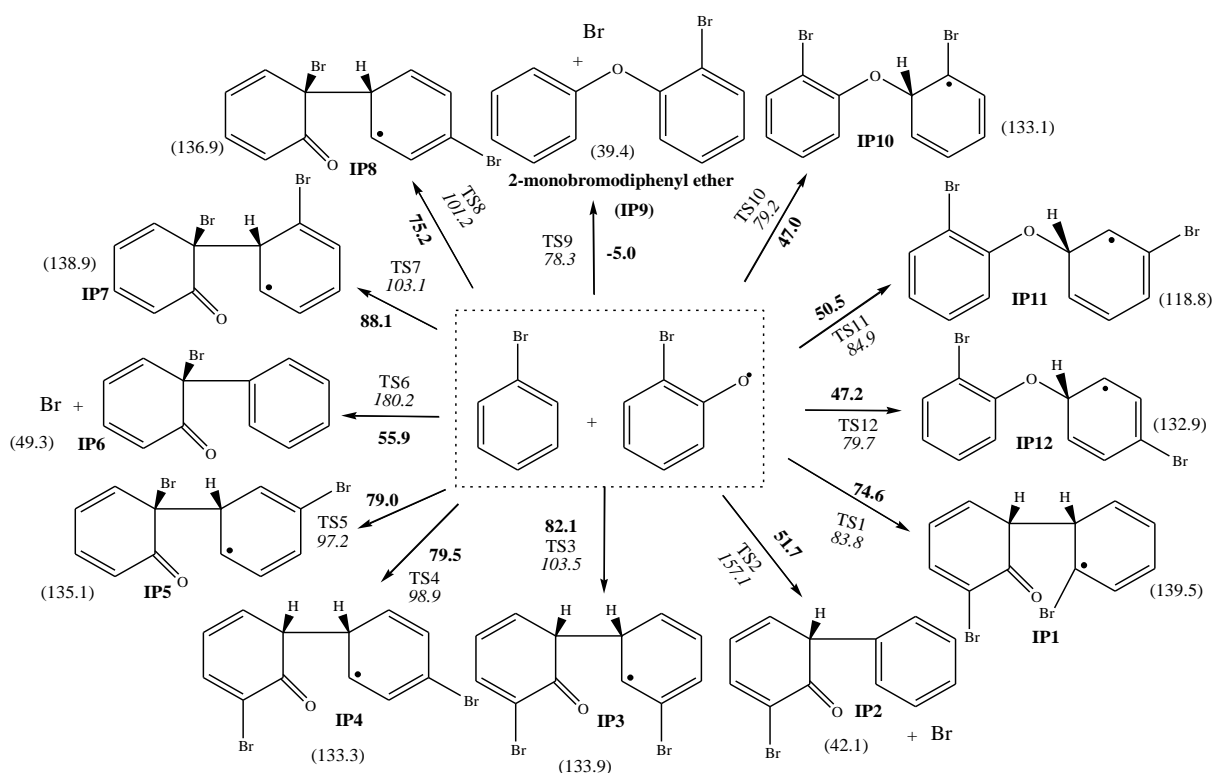


Figure 9.1. Initial products obtained from couplings of MBBz molecule and BPhxy radical [50]. Values in bold and italic denote reaction and activation enthalpies in kJ mol⁻¹, respectively at 298 K. Values in bracket represent Gibbs free energy change of reaction at 800 K (in kJ mol⁻¹).

Production of IP2 and IP6 intermediates, accompanied with the expulsion of the bromine atom from the MBBz molecule, represents the kinetically least preferred channels among the *o*-C/*o*-C intermediates, as their formation requires overcoming sizeable activation enthalpy barriers of 157.1 kJ mol⁻¹ and 180.2 kJ mol⁻¹, respectively. On the other hand, the formation of IP1, IP3-IP5 and IP7-IP8 necessitates modest reaction barriers in the

CHAPTER 9 Formation of Polybrominated Dibenzofurans (PBDFs) and Polybrominated Diphenyl Ethers (PBDEs) from Oxidation of Brominated Flame Retardants (BFRs)

range of 97.2 – 103.5 kJ mol⁻¹. Similarly, the addition of phenoxy O atom in the *o*-BPhxy radical at the -C(Br) position in the MBBz molecule expels the Br atom from the MBBz molecule and affords 2-monobromodiphenyl ether (2-MBDE), IP9, via a slightly exothermic reaction with an activation enthalpy of 78.3 kJ mol⁻¹.

Intermediates IP10 – IP12 and 2-monobromodiphenyl ether (IP9) form upon bimolecular coupling of the phenoxy O atom in the *o*-BPhxy radical at the three C(H) sites in the MBBz molecule (O/-C(H) pairings). The appearance of the IP10-IP12 radicals entails somewhat accessible activation enthalpies in the range of 79.2 – 84.9 kJ mol⁻¹. These radicals serve as direct pre-structures for the generation of mono to dibrominated diphenyl ether via loss of an *ortho* H atom, and for the production of mono-dibrominated DFs via subsequent ring closure reactions. Because of the potential of IP9-IP12 intermediates to form both PBDEs and PBDFs, in the remaining part of this article, we denote IP9-IP12 as pre-PBDEs/pre-PBDFs.

9.3.2. Formation of PBDFs and DBDEs

Figure 9.2 depicts pathways for the formation of DF, isomers of MBDF (i.e., 1-MBDF, 2-MBDF, 3-MBDF and 4-MBDF) and dibromodibenzofuran (i.e., 4,6-DBDF and 3,6-DBDF) from ring closures of their respective intermediate pre-PBDFs (IP1-IP8) presented in Figure 9.1. All channels leading to the formation of mono- and dibrominated DFs involve two principal steps: (i) ring cyclisation of phenoxy oxygen towards an *ortho* carbon; and, (ii) unimolecular elimination of a hydrogen molecule or hydrogen bromide molecule and H/Br atom from the formed C-C bridge or ether type linkage. Out-of-plane C-H and C-Br bonds in all intermediates are significantly weaker than the aromatic C-H and C-Br bonds entailing relatively facile unimolecular eliminations of H₂ or HBr across pathways depicted in Figure 9.2.

The uppermost route in Figure 9.2 (Pathway 1) characterises a corridor for the synthesis of 4-MBDF in a three-step mechanism. In the first reaction, the phenoxy O atom attacks an *ortho* C-Br site on the neighbouring ring via the transition state TS13 overcoming a modest enthalpic barrier of 92.7 kJ mol⁻¹. Formation of the three-membered ring structure

CHAPTER 9 Formation of Polybrominated Dibenzofurans (PBDFs) and Polybrominated Diphenyl Ethers (PBDEs) from Oxidation of Brominated Flame Retardants (BFRs)

IM1 is endothermic by 18.5 kJ mol^{-1} . A self-expulsion of HBr molecule from IM1 requires an activation enthalpy of 92.2 kJ mol^{-1} via TS14 and results in the production of a pre-PBDF structure of IM2 in a highly exothermic process ($-61.9 \text{ kJ mol}^{-1}$). Finally, an H atom departs the IM2 structure with an intrinsic reaction barrier of 84.2 kJ mol^{-1} . In the latter step, the formation of 4-MBDF from IM2 generates 48.0 kJ mol^{-1} of excess enthalpy.

CHAPTER 9 Formation of Polybrominated Dibenzofurans (PBDFs) and Polybrominated Diphenyl Ethers (PBDEs) from Oxidation of Brominated Flame Retardants (BFRs)

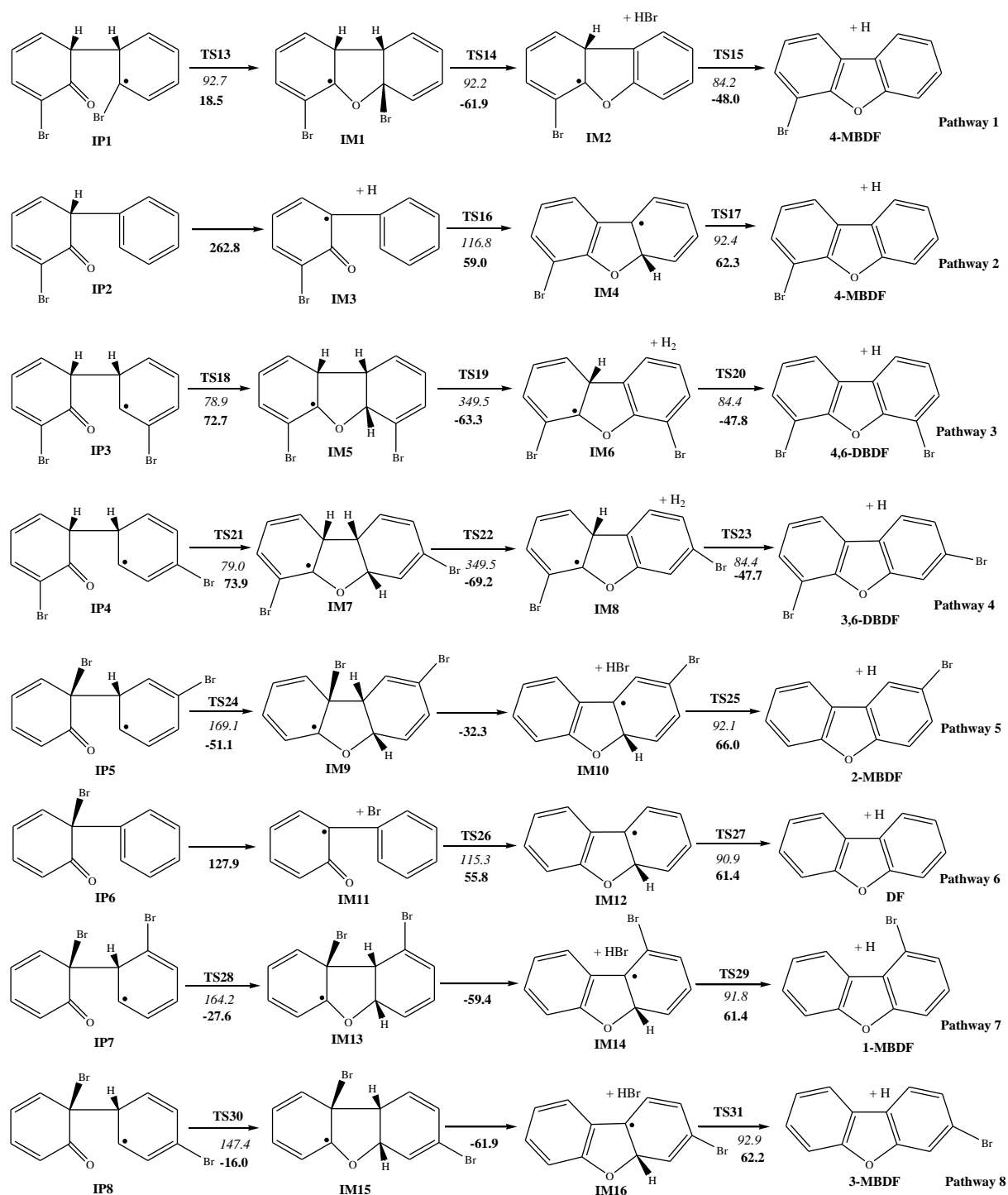


Figure 9.2. Pathways for the formation of DF, isomers of MBDF and DBDF from structural arrangements of IP1–IP8 intermediates. Values in bold and italic signify reaction and activation enthalpies in kJ mol^{-1} , respectively (at 298 K).

CHAPTER 9 Formation of Polybrominated Dibenzofurans (PBDFs) and Polybrominated Diphenyl Ethers (PBDEs) from Oxidation of Brominated Flame Retardants (BFRs)

In the second pathway, an H atom leaves the intermediate IP2 in a barrierless endothermic reaction ($262.8 \text{ kJ mol}^{-1}$) and forms the IM3 radical. The ring cyclisation reaction across TS16 proceeds via an activation enthalpy of $116.8 \text{ kJ mol}^{-1}$. The IM4 ejects the out-of-plane H atom climbing a barrier of 92.4 kJ mol^{-1} and affords the 4-MBDF molecule. However, the excessively high enthalpic barrier for the first step makes this pathway unlikely to occur. The same steps also conclude Pathways 5-8 and results in the production of 2-MBDF, DF, 1-MBDF and 3-MBDF molecules, respectively.

In Pathways 3 and 4, the addition of phenoxy O at *ortho* C-H position of the other ring assumes slightly lower activation enthalpies through transition states TS18 (78.9 kJ mol^{-1}) and TS21 (79.0 kJ mol^{-1}), correspondingly, if contrasted with the activation enthalpy of the opening step in Pathway 1 (i.e., 92.7 kJ mol^{-1} via TS13). Self-elimination of a hydrogen molecule in the second step in Pathways 3 and 4 occur via enthalpic barriers of $349.5 \text{ kJ mol}^{-1}$ (TS19 and TS22) with corresponding exothermicity of 63.3 kJ mol^{-1} and 69.2 kJ mol^{-1} , respectively. In the final step, 4,6-DBDF and 3,6-DBDF molecules are formed following a unimolecular loss of an H atom from IM6 and IM8 intermediates in Pathways 3 and 4, in that order. The extremely high enthalpic barriers rule out these pathways in practical systems.

Synthesis of MBDF isomers and DF through Pathways 5-8 share very similar kinetic and mechanistic features with the aforementioned steps in Pathways 1-4. The ejection of Br atom from IP6 (Pathway 6) ensues without encountering an intrinsic reaction barrier. Albeit, fission of C-Br bond and elimination of HBr molecule (i.e, from the IM1 intermediate in Pathway 1) necessitate a significantly lower activation enthalpy (92.2 kJ mol^{-1}) if compared with the analogous process leading to the elimination of a hydrogen molecule ($349.5 \text{ kJ mol}^{-1}$) as depicted in Pathways 3 and 4. Considering reaction and activation enthalpies, Pathways 5-8 appear less likely to operate than Pathway 1 but more likely than Pathways 3-4. This seems to indicate that, in a practical system, 4-MBDF constitutes the only viable product of Pathways 1-8.

Figure 9.3 presents transformation pathways of pre-PBDEs/pre-PBDFs (IP10-IP12) intermediates. Two competing exit channels control the fate of these adducts, namely,

CHAPTER 9 Formation of Polybrominated Dibenzofurans (PBDFs) and Polybrominated Diphenyl Ethers (PBDEs) from Oxidation of Brominated Flame Retardants (BFRs)

loss of an H atom from the ether linkage leading to the formation of DBDE isomers and a three-step mechanism towards the formation MBDF and DF species. The unimolecular loss of an H atom from IP10, IP11 and IP12 structures exhibit very comparable activation enthalpies (106.3 – 124.1 kJ mol⁻¹) through transition states TS32, TS34 and TS37 and afford 2,2'-dibromodiphenyl ether (2,2'-DBDE), 2,3'-dibromodiphenyl ether (2,3'-DBDE) and 2,4'-dibromodiphenyl ether (2,4'-DBDE) molecules, in that order.

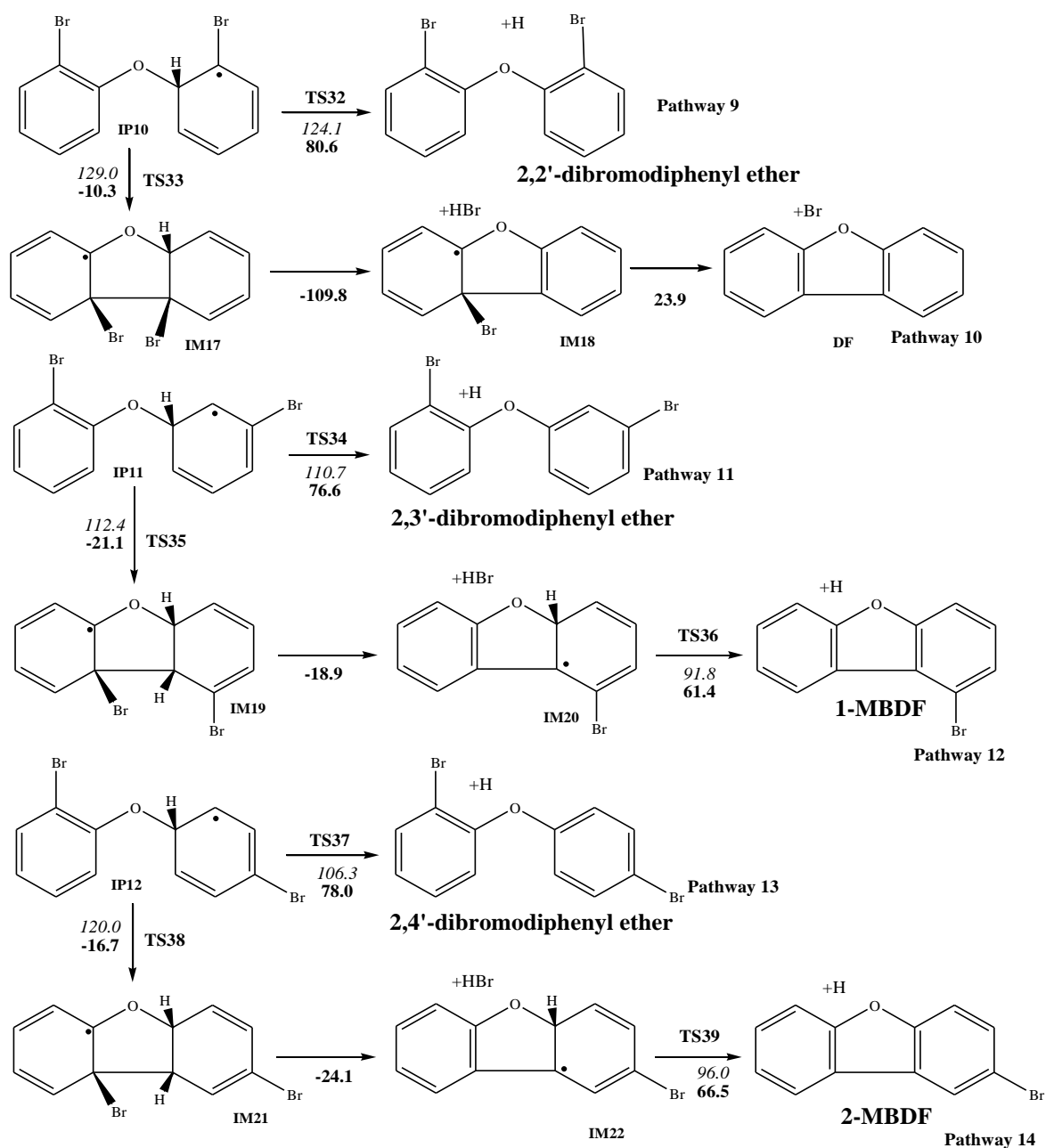


Figure 9.3. Formation of DF, MBDFs and dibrominated congeners of diphenyl ether

CHAPTER 9 Formation of Polybrominated Dibenzofurans (PBDFs) and Polybrominated Diphenyl Ethers (PBDEs) from Oxidation of Brominated Flame Retardants (BFRs)

from intermediates IP10-IP12. Values in bold and italic are reaction and activation enthalpies in kJ mol^{-1} , respectively. All values are reported at 298 K.

In the competing process, a C-C bond closure initiates the formation of MBDF and DF molecules. This step requires activation enthalpies in the narrow window of 112.4 – 129.0 kJ mol^{-1} (TS33, TS35 and TS38). Despite our best efforts, we were unable to locate transition states for the elimination of HBr. Consecutive cleavages of H and Br atoms might be also occurring, rather than the direct elimination of HBr. In the last step, activation enthalpies for the self-ejection of H atoms match values pertinent to the corresponding reactions in Figure 9.2.

9.3.3. Reaction rate constants

Tables 9.1 and 9.2 list modified Arrhenius parameters fitted over a temperature range of 300 – 1200 K. To the best of our knowledge, no analogous experimental and theoretical kinetic data that describe the generation of PBDFs from BBzs exist in the literature. Computed coefficients in Tables 9.1 and 9.2 serve to assess the relative importance of the competing reaction channels.

Table 9.1. Arrhenius rate parameters for the bimolecular/unimolecular reactions depicted in Figures 9.1 and 9.3, fitted over a temperature range of 300 – 1200 K. Values of pre-exponential A factor are in s^{-1} or $\text{cm}^3 \text{s}^{-1} \text{molecule}^{-1}$ and values of activation energies (E_a) are in kJ mol^{-1} .

Reactions	A	n	E_a
BB + BPhenoxy \rightarrow IP1	4.71×10^{-15}	0	94.9
BB + BPhenoxy \rightarrow IP2 + Br	4.53×10^{-14}	-0.08	161.3
BB + BPhenoxy \rightarrow IP3	1.13×10^{-14}	0	114.6
BB + BPhenoxy \rightarrow IP4	4.90×10^{-15}	0	90.1
BB + BPhenoxy \rightarrow IP5	3.35×10^{-15}	0	108.1
BB + BPhenoxy \rightarrow IP6 + Br	1.48×10^{-16}	0	188.6
BB + BPhenoxy \rightarrow IP7	2.42×10^{-15}	0	113.7
BB + BPhenoxy \rightarrow IP8	3.88×10^{-15}	0	111.8

CHAPTER 9 Formation of Polybrominated Dibenzofurans (PBDFs) and Polybrominated Diphenyl Ethers (PBDEs) from Oxidation of Brominated Flame Retardants (BFRs)

BB + BPhenoxy → IP9 + Br	1.66×10^{-15}	0	85.5
BB + BPhenoxy → IP10	1.22×10^{-14}	0	89.5
BB + BPhenoxy → IP11	4.37×10^{-15}	0	93.4
BB + BPhenoxy → IP12	4.45×10^{-15}	0	89.1
IP10 → 2,2'-DBDE + H	3.43×10^{13}	0	114.9
IP10 → IM17	4.15×10^{11}	0	124.9
IM18 → DF + H	2.15×10^{13}	0	74.3
IP11 → 2,3'-DBDE + H	1.41×10^{13}	0	92.1
IP11 → IM19	1.23×10^{12}	0	109.9
IM20 → 1-MBDF + H	2.24×10^{13}	0	74.5
IP12 → 2,4'-DBDE + H	1.11×10^{13}	0	87.9
IP12 → IM21	1.12×10^{12}	0	118.3
IM22 → 2-MBDF + H	2.20×10^{13}	0	78.9

In accord with the enthalpic values reported in Figure 9.3, we find that the loss of an H atom leading to the formation of DBDE isomers consistently predominates over the C-C ring closure reactions affording MBDFs and DF. For example, at 800 K, the reaction rate constant for pathway IP10 → 2,2'-DBDE + H ($1.08 \times 10^6 \text{ s}^{-1}$) exceeds that of the parallel IP10 → IM17 (i.e., $2.90 \times 10^3 \text{ s}^{-1}$) corridor. Similarly, the C-C ring closure reaction (IP12 → IM21) assumes a negligible importance ($2.21 \times 10^4 \text{ s}^{-1}$ at 800 K) when compared with the competing channel forming 2,4-DBDE (IP12 → 2,4-DBDE + H) that proceeds at a rate constant of $2.02 \times 10^7 \text{ s}^{-1}$ at 800 K. On the first glance, considering barriers of the backward reactions for the two competing channels IP10 → 2,2'-DBDE + H and IP10 → IM17 (43.5 kJ mol^{-1} versus $139.3 \text{ kJ mol}^{-1}$), the former channel experiences significant reversibility if compared with the latter. However, any species present in the reaction system instantaneously consume the reactive H atoms produced in the IP10 → 2,2'-DBDE + H corridor. This minimises the backward formation of IP10 from 2,2'-DBDE + H.

Table 9.2. Arrhenius rate parameters for the unimolecular reactions depicted in Figure 9.2, fitted over a temperature range of 300 – 1200 K. Values of pre-exponential A factor are in s^{-1} and values of activation energies (E_a) are in kJ mol^{-1} .

Reactions	A	n	E_a
-----------	---	---	-------

CHAPTER 9 Formation of Polybrominated Dibenzofurans (PBDFs) and Polybrominated Diphenyl Ethers (PBDEs) from Oxidation of Brominated Flame Retardants (BFRs)

IP1 → IM1	4.83×10^{12}	-0.20	89.9
IM1 → IM2 + HBr	3.23×10^{13}	0.00	81.9
IM2 → 4-MBDF + H	2.01×10^{13}	0.00	66.9
IM3 → IM4	2.27×10^{12}	0.00	115.8
IM4 → 4-MBDF + H	2.07×10^{13}	0.00	75.5
IP3 → IM5	4.97×10^{12}	-0.17	80.3
IM5 → IM6 + H ₂	3.01×10^8	0.00	357.0
IM6 → 4,6-DBDF + H	1.57×10^{13}	0.00	66.4
IP4 → IM7	2.86×10^{11}	0.13	79.0
IM7 → IM8 + H ₂	1.22×10^{14}	0.00	321.4
IM8 → 3,6-DBDF + H	2.99×10^{13}	0.00	68.4
IP5 → IM9	5.03×10^{13}	-0.45	163.8
IM10 → 2-MBDF + H	2.10×10^{13}	0.00	76.1
IM11 → IM12	1.56×10^{12}	0.00	113.8
IM12 → DF + H	2.16×10^{13}	0.00	74.9
IP7 → IM13	2.95×10^{13}	-0.39	158.6
IM14 → 1-MBDF + H	2.24×10^{13}	0.00	75.9
IP8 → IM15	7.96×10^{11}	0.11	149.6
IM16 → 3-MBDF + H	2.11×10^{13}	0.00	76.9

Now, we turn our attention to comment on the relative preference of the first cyclisation step in Figure 9.2, either toward C(H) or C(Br) sites. At 800 K, the coupling of phenoxy O at C(H) site of neighbouring ring (IP3 → IM5) proceeds at a rate constant of 1.0×10^7 s⁻¹ in comparison to the pairing of phenoxy towards C(Br) position (IP1 → IM1), which occurs at a rate constant of 1.7×10^6 s⁻¹. The ring cyclisation of phenoxy proceeds faster towards *ortho* C(H) site in comparison to the C(Br) and C(Cl) positions. In an analogy to this finding, our recent theoretical account [44], on formation of hydroxylated dibenzo-*p*-dioxin from catechol (C₆H₄(OH)₂), assesses the relative kinetic preference of ring closure channels towards C(Cl), C(Br), C(OH) and C(H) sites from diphenyl ether-like moieties. Our calculations predict variations in the rate of the O-C cyclisation step in respect to the functional group substituted at the *ortho* position and follow the order OH>H>Br>Cl. The preference of ring closure towards a C(H) site may affect the observed bromination

CHAPTER 9 Formation of Polybrominated Dibenzofurans (PBDFs) and Polybrominated Diphenyl Ethers (PBDEs) from Oxidation of Brominated Flame Retardants (BFRs)

pattern. However, the unfavoured thermodynamics or kinetics of the remaining steps in Pathways 2-8 make these pathways unlikely to occur. Clearly, the quantum chemical calculations presented in this article provide important mechanistic insights that one cannot obtain from experiments. This is because, experiments cannot distinguish the direct formation of PBDFs in Pathways 1-8 from that involving the oxidation of PBDEs that also form in the process (*vide infra*).

Let us now compare the corridors generating the pre-PBDF structures (IP1-IP8) (refer to Figure 9.1) with those affording the pre-PBDE/pre-PBDF species (IP9-IP12). Higher reaction enthalpies accompany the formation of pre-PBDF structures of IP1-IP8 when compared with the formation of pre-PBDE/pre-PBDF species (51.7 – 88.1 kJ mol⁻¹ versus 47.0 - 50.5 kJ mol⁻¹). However, it is more intuitively appealing to discuss the thermodynamic trends for reactions in Figure 9.1 at temperatures relevant to the homogenous corridor for the formation of halogenated dioxins (700 – 1000 K), rather than at 298 K. For this reason, we have computed the Gibbs free energy changes (ΔG_r) for reactions (BBz + BPhxy \rightarrow IP1-IP12) to assess the thermodynamic feasibility of these reactions at 800 K. In accordance with the reaction enthalpies computed at 298 K, ΔG_r values at 800 K, for the generation of pre-PBDE/pre-PBDF moieties of IP10-IP12, fall below the analogous estimates for the corridors affording pre-PBDF (IP1, IP3-IP5, IP7-IP8) structures (118.8 – 133.1 kJ mol⁻¹ versus 133.3 – 139.5 kJ mol⁻¹). The formation of IP2 (42.1 kJ mol⁻¹) and IP6 (49.3 kJ mol⁻¹), which involves the exclusion of Br atom, displays higher barrier than that of IP9 (39.4 kJ mol⁻¹). These considerations render the formation of pre-PBDF structures more reversible (i.e., less spontaneous) thermodynamically, when compared with analogues channels forming the pre-PBDE/pre-PBDF intermediates. Now, we turn our attention to compare the kinetics of these reactions (pre-PBDF versus pre-PBDE/pre-PBDF formation) at 800 K. We found that, the production of pre-PBDEs/pre-PBDFs proceeds with reaction rate constants of 6.8×10^{-21} to 1.7×10^{-20} cm³ s⁻¹ molecule⁻¹, significantly faster than the parallel reactions generating pre-PBDFs of 7.4×10^{-29} – 6.2×10^{-21} cm³ s⁻¹ molecule⁻¹. Thus, bimolecular MBBz + BPhxy reactions most likely result in the formation of pre-PBDEs/pre-PBDFs as the major oxidation products of MBBz on the thermodynamic and kinetic grounds.

CHAPTER 9 Formation of Polybrominated Dibenzofurans (PBDFs) and Polybrominated Diphenyl Ethers (PBDEs) from Oxidation of Brominated Flame Retardants (BFRs)

The above discussion demonstrates that, the oxidation of MBBz preferably leads to PBDE rather than PBDF, except for 4-MBDF arising in Pathway 1 (Figure 9.2). However, PBDFs (and PBDDs) also arise from the oxidative decomposition of PBDEs. In accord with the experimental findings [22, 52-55] pertinent to the high yield of PBDFs from oxidation of PBDEs, in our recent theoretical study [19], we illustrated a low-energy mechanism for the transformation of PBDEs into PBDFs and PBDDs. A key to this mechanism is the addition of an oxygen molecule at an *ortho* site (with respect to the ether linkage) in PBDEs followed by complex unimolecular re-arrangements.

9.4. Conclusions

In conclusion, the initial bimolecular reactions of a MBBz molecule and a BPhxy radical produce pre-structures of PBDFs and PBDEs that require enthalpic barriers in the range of 79.2 – 180.2 kJ mol⁻¹. These pre-structures form either via *O/o-C* or *o-C/o-C* coupling. Our kinetic analysis indicates that *O/o-C* coupling MBBz + BPhxy reactions lead to the formation of PBDE rather than PBDF. On the other hand, cyclisation of pre-PBDF *o-C/o-C*(H) intermediates to PBDF appears faster than that of *o-C/o-C*(Br) intermediates. However, except for the formation of 4-MBDF, the *o-C/o-C* pathways require high reaction and activation enthalpies, limiting their practical importance. Consequently, in a real thermal system, 4-MBDF evolve as the only viable product of pathways 1-8. This means that PBDFs arising in oxidation of PBBzs appear in a two-step process that involves the initial synthesis of PBDEs and their subsequent transformation to PBDFs. The mechanisms and the kinetic parameters presented in this chapter explain the formation of PBDEs and PBDFs from the oxidation of BBz molecules, and should facilitate constructing the kinetic models.

Acknowledgments

This study has been supported by the Australian Research Council (ARC), and grants of computing time from the National Computational Infrastructure (NCI), Australia as well as the Pawsey Supercomputing Centre. A.S. thanks Murdoch University, Australia, for a postgraduate research scholarship.

Supplementary material

Supplementary material (Appendix F in attached CD) lists the cartesian coordinates, vibrational frequencies and rotational constants for the species involve in the formation of PBDFs and PBDEs from the coupling of MBBz and BPhxy radical.

References

- [1] Buser, H.R., Bosshardt, H.P., Rappe, C. Formation of polychlorinated dibenzofurans (PCDFs) from the pyrolysis of PCBs. *Chemosphere* **1978**, 7, 109-119.
- [2] Buser, H.R. Formation of polychlorinated dibenzofurans (PCDFs) and dibenzo-*p*-dioxins (PCDDs) from the pyrolysis of chlorobenzenes. *Chemosphere* **1979**, 8, 415-424.
- [3] Lindahl, R., Rappe, C., Buser, H.R. Formation of polychlorinated dibenzofurans (PCDFs) and polychlorinated dibenzo-*p*-dioxins (PCDDs) from the pyrolysis of polychlorinated diphenyl ethers. *Chemosphere* **1980**, 9, 351-361.
- [4] Rappe, C., Garå, A., Buser, H.R. Identification of polychlorinated dibenzofurans (PCDFs) in commercial chlorophenol formulations. *Chemosphere* **1978**, 7, 981-991.
- [5] Schüler, D., Jager, J. Formation of chlorinated and brominated dioxins and other organohalogen compounds at the pilot incineration plant VERONA. *Chemosphere* **2004**, 54, 49-59.
- [6] Striebich, R.C., Rubey, W.A., Tirey, D.A., Dellinger, B. High temperature degradation of polybrominated flame retardant materials. *Chemosphere* **1991**, 23, 1197-1204.
- [7] Yu, W., Hu, J., Xu, F., Sun, X., Gao, R., Zhang, Q., Wang, W. Mechanism and direct kinetics study on the homogeneous gas-phase formation of PBDD/Fs from 2-BP, 2,4-DBP, and 2,4,6-TBP as precursors. *Environ. Sci. Technol.* **2011**, 45, 1917-1925.
- [8] Huang, H., Buekens, A. De novo synthesis of polychlorinated dibenzo-*p*-dioxins and dibenzofurans proposal of a mechanistic scheme. *Sci. Total Environ.* **1996**, 193, 121-141.
- [9] Iino, F., Imagawa, T., Takeuchi, M., Sadakata, M. De novo synthesis mechanism of polychlorinated dibenzofurans from polycyclic aromatic hydrocarbons and the characteristic isomers of polychlorinated naphthalenes. *Environ. Sci. Technol.* **1999**, 33, 1038-1043.

CHAPTER 9 Formation of Polybrominated Dibenzofurans (PBDFs) and Polybrominated Diphenyl Ethers (PBDEs) from Oxidation of Brominated Flame Retardants (BFRs)

- [10] Altarawneh, M., Dlugogorski, B.Z., Kennedy, E.M., Mackie, J.C. Mechanisms for formation, chlorination, dechlorination and destruction of polychlorinated dibenzo-*p*-dioxins and dibenzofurans (PCDD/Fs). *Prog. Energy Combust. Sci.* **2009**, 35, 245-274.
- [11] Tuppurainen, K.A., Ruokojärvi, P.H., Asikainen, A.H., Aatamila, M., Ruuskanen, J. Chlorophenols as precursors of PCDD/Fs in incineration processes: correlations, PLS modeling, and reaction mechanisms. *Environ. Sci. Technol.* **2000**, 34, 4958-4962.
- [12] Focant, J.F., Eppe, G., Pirard, C., Massart, A.C., André, J.E., De Pauw, E. Levels and congener distributions of PCDDs, PCDFs and non-*ortho* PCBs in Belgian foodstuffs: Assessment of dietary intake. *Chemosphere* **2002**, 48, 167-179.
- [13] Stieglitz, L., Vogg, H. On formation conditions of PCDD/PCDF in fly ash from municipal waste incinerators. *Chemosphere* **1987**, 16, 1917-1922.
- [14] Lu, S.Y., Yan, J.H., Li, X.D., Ni, M.J., Cen, K.F., Dai, H.F. Effects of inorganic chlorine source on dioxin formation using fly ash from a fluidized bed incinerator. *J. Environ. Sci.* **2007**, 19, 756-761.
- [15] Wang, L.C., Chang-Chien, G.P. Characterizing the emissions of polybrominated dibenzo-*p*-dioxins and dibenzofurans from municipal and industrial waste incinerators. *Environ. Sci. Technol.* **2007**, 41, 1159–1165.
- [16] Wikström, E.; Marklund, S. The influence of level and chlorine source on the formation of mono- to octa-chlorinated dibenzo-*p*-dioxins, dibenzofurans and coplanar polychlorinated biphenyls during combustion of an artificial municipal waste. *Chemosphere* **2001**, 43, 227-234.
- [17] Gouteux, B., Alae, M., Mabury, S.A., Pacepavicius, G., Muir, D.C.G. Polymeric brominated flame retardants: Are they a relevant source of emerging brominated aromatic compounds in the environment? *Environ. Sci. Technol.* **2008**, 42, 9039-9044.
- [18] Tian, M., Chen, S.J., Wang, J., Shi, T., Luo, X.J., Mai, B.X. Atmospheric deposition of halogenated flame retardants at urban, e-waste, and rural locations in southern China. *Environ. Sci. Technol.* **2011**, 45, 4696-4701.
- [19] Altarawneh, M., Dlugogorski, B.Z. A mechanistic and kinetic study on the formation of PBDD/Fs from PBDEs. *Environ. Sci. Technol.* **2013**, 47, 5118-5127.

CHAPTER 9 Formation of Polybrominated Dibenzofurans (PBDFs) and Polybrominated Diphenyl Ethers (PBDEs) from Oxidation of Brominated Flame Retardants (BFRs)

- [20] Altarawneh, M., Dlugogorski, B.Z. Formation of polybrominated dibenzofurans from polybrominated biphenyls. *Chemosphere* **2015**, 119, 1048-1053.
- [21] Wichmann, H., Dettmer, F.T., Bahadir, M. Thermal formation of PBDD/F from tetrabromobisphenol A - a comparison of polymer linked TBBP A with its additive incorporation in thermoplastics. *Chemosphere* **2002**, 47, 349-355.
- [22] Buser, H.R. Polybrominated dibenzofurans and dibenzo-*p*-dioxins: Thermal reaction products of polybrominated diphenyl ether flame retardants. *Environ. Sci. Technol.* **1986**, 20, 404-408.
- [23] Pijnenburg, A.M.C.M., Everts, J.W., de Boer, J., Boon, J.P. Polybrominated biphenyl and diphenylether flame retardants: analysis, toxicity, and environmental occurrence: In *Rev. Environ. Contam. Toxicol.*, Ware, G.W., Gunther, F.A., Eds.; Springer: New York **1995**; pp 1-26.
- [24] Dettmer, F.T. Bromorganische flammenschutzmittel analytische anforderungen und thermische bildung von polybromierten dibenzo-*p*-dioxinen und dibenzofuranen. Ph.D. Dissertation, University of Braunschweig, Germany, **2001**.
- [25] Saeed, A., Dlugogorski, B.Z., Altarawneh, M. Formation of brominated and non-brominated species from gas-phase thermal decomposition of pure TBBA. *14th International Congress on Combustion By-Products and Their Health Effects*, Umeå, Sweden, **2015**.
- [26] Evans, C.S., Dellinger, B. Mechanisms of dioxin formation from the high-temperature pyrolysis of 2-bromophenol. *Environ. Sci. Technol.* **2003**, 37, 5574-5580.
- [27] Evans, C.S., Dellinger, B. Mechanisms of dioxin formation from the high-temperature oxidation of 2-bromophenol. *Environ. Sci. Technol.* **2005**, 39, 2128-2134.
- [28] Liu, W., Zheng, M., Wang, D., Xing, Y., Zhao, X., Ma, X., Qian, Y. Formation of PCDD/Fs and PCBs in the process of production of 1,4-dichlorobenzene. *Chemosphere* **2004**, 57, 1317-1323.
- [29] Fadli, A., Briois, C., Baillet, C., Sawerysyn, J.P. Experimental study on the thermal oxidation of chlorobenzene at 575–825 °C. *Chemosphere* **1999**, 38, 2835-2848.
- [30] Higgins, B., Thomson, M.J., Lucas, D., Koshland, C.P., Sawyer, R.F. An experimental and numerical study of the thermal oxidation of chlorobenzene. *Chemosphere* **2001**, 42, 703-717.

CHAPTER 9 Formation of Polybrominated Dibenzofurans (PBDFs) and Polybrominated Diphenyl Ethers (PBDEs) from Oxidation of Brominated Flame Retardants (BFRs)

- [31] Sommeling, P.M., Mulder, P., Louw, R. Formation of PCDFs during chlorination and oxidation of chlorobenzene in chlorine/oxygen mixtures around 340 °C. *Chemosphere* **1994**, 29, 2015-2018.
- [32] Altarawneh, M., Mackie, J.C., Kenndy, E.M., Dlugogorski, B.Z. Mechanism for PCDF and PCB formation from fires: Pathways from oxidation of chlorobenzene. *Proc. 7th Asia-Oceania Symposium on Fire Science and Technology*. **2007**, 1-12.
- [33] Jansson, S., Andersson, P.L. Relationships between congener distribution patterns of PCDDs, PCDFs, PCNs, PCBs, PCBzs and PCPhs formed during flue gas cooling. *Sci. Total Environ.* **2012**, 416, 269-275.
- [34] Jansson, S., Fick, J., Tysklind, M., Marklund, S. Post-combustion formation of PCDD, PCDF, PCBz, and PCPh in a laboratory-scale reactor: Influence of dibenzo-*p*-dioxin injection. *Chemosphere* **2009**, 76, 818-825.
- [35] Altarawneh, M., Dlugogorski, B.Z. Formation and chlorination of carbazole, phenoxazine, and phenazine. *Environ. Sci. Technol.* **2015**, 49, 2215-2221.
- [36] Hoffman, R.V., Eiceman, G.A., Long, Y.T., Collins, M.C., Lu, Q.M. Mechanism of chlorination of aromatic compounds adsorbed on the surface of fly ash from municipal incinerators. *Environ. Sci. Technol.* **1990**, 24, 1635-1641.
- [37] Olie, K., Addink, R., Schoonenboom, M. Metals as catalysts during the formation and decomposition of chlorinated dioxins and furans in incineration processes. *J. Air Waste Manag. Assoc.* **1998**, 48, 101-105.
- [38] Wikström, E., Marklund, S. Secondary formation of chlorinated dibenzo-*p*-dioxins, dibenzofurans, biphenyls, benzenes, and phenols during MSW combustion. *Environ. Sci. Technol.* **2000**, 34, 604-609.
- [39] Montgomery, J.A., Ochterski, J.W., Petersson, G.A. A complete basis set model chemistry. IV. an improved atomic pair natural orbital method. *J. Chem. Phys.* **1994**, 101, 5900-5909.
- [40] Frisch, M.J., Trucks, G.W., Schlegel, H.B., Scuseria, G.E., Robb, M.A., Cheeseman, J.R., Scalmani, G., Barone, V., Mennucci, B., Petersson, G.A., Nakatsuji, H., Caricato, M., Li, X., Hratchian, H.P., Izmaylov, A.F., Bloino, J., Zheng, G., Sonnenberg, J.L., Hada, M., Ehara, M., Toyota, K., Fukuda, R., Hasegawa, J., Ishida, M., Nakajima, T., Honda, Y., Kitao, O., Nakai, H., Vreven, T., Montgomery, J.A., Peralta, J.E., Ogliaro, F., Bearpark, M., Heyd, J.J., Brothers, E., Kudin, K.N.,

CHAPTER 9 Formation of Polybrominated Dibenzofurans (PBDFs) and Polybrominated Diphenyl Ethers (PBDEs) from Oxidation of Brominated Flame Retardants (BFRs)

- Staroverov, V.N., Kobayashi, R., Normand, J., Raghavachari, K., Rendell, A., Burant, J.C., Iyengar, S.S., Tomasi, J., Cossi, M., Rega, N., Millam, N.J., Klene, M., Knox, J. E., Cross, J.B., Bakken, V., Adamo, C., Jaramillo, J., Gomperts, R., Stratmann, R.E., Yazyev, O., Austin, A.J., Cammi, R., Pomelli, C., Ochterski, J.W., Martin, R.L., Morokuma, K., Zakrzewski, V.G., Voth, G.A., Salvador, P., Dannenberg, J.J., Dapprich, S., Daniels, A.D., Farkas, O., Foresman, J. B., Ortiz, J. V., Cioslowski, J., Fox, D.J. **2009**, Gaussian09, Revision D.01; Gaussian Inc: Wallingford, CT.
- [41] Zhao, Y., Truhlar, D.G. The M06 suite of density functionals for main group thermochemistry, thermochemical kinetics, noncovalent interactions, excited states, and transition elements: Two new functionals and systematic testing of four M06-class functionals and 12 other functionals. *Theor. Chem. Acc.* **2008**, 120, 215-241.
- [42] Altarawneh, M., Dlugogorski, B.Z. Thermal decomposition of 1,2-bis(2,4,6-tribromophenoxy)ethane (BTBPE), a novel brominated flame retardant. *Environ. Sci. Technol.* **2014**, 48, 14335-14343.
- [43] Altarawneh, M., Dlugogorski, B.Z. Mechanism of thermal decomposition of tetrabromobisphenol A (TBBA). *J. Phys. Chem. A.* **2014**, 118, 9338-9346.
- [44] Altarawneh, M., Dlugogorski, B.Z. Formation of dibenzofuran, dibenzo-*p*-dioxin and their hydroxylated derivatives from catechol. *Phys. Chem. Chem. Phys.* **2015**, 17, 1822-1830.
- [45] Saeed, A., Altarawneh, M., Dlugogorski, B.Z. Formation of mixed halogenated dibenzo-*p*-dioxins and dibenzofurans (PXDD/Fs). *Chemosphere* **2015**, 137, 149-156.
- [46] Hratchian, H.P., Schlegel, H.B. Finding minima, transition states, and following reaction pathways on ab initio potential energy surfaces. In *Theory and Applications of Computational Chemistry: The First Forty Years*; Dykstra, E. C., Frenking, G., Kim, S. K., Scuseria, E. G., Eds.; Elsevier: Amsterdam 2005; pp 195-243.
- [47] Canneaux, S., Bohr, F., Henon, E. KiSThelp: A program to predict thermodynamic properties and rate constants from quantum chemistry results. *J. Comput. Chem.* **2014**, 35, 82-93.
- [48] Eckart, C. The penetration of a potential barrier by electrons. *Phys. Rev.* **1930**, 35, 1303-1309.
- [49] Mokrushin, V.B., Bedanov, V., Tsang, W., Zachariah, M., Knyazev, V. ChemRate, V.1.19; NIST: Gaithersburg, MD, 2002.

CHAPTER 9 Formation of Polybrominated Dibenzofurans (PBDFs) and Polybrominated Diphenyl Ethers (PBDEs) from Oxidation of Brominated Flame Retardants (BFRs)

- [50] Saeed, A., Altarawneh, M., Dlugogorski B.Z. Formation of PBDFs and PBBs from bromobenzenes. *Organohalogen Compd.* **2015**, 77, 606-609.
- [51] Luo, R. Y. *Handbook of Bond Dissociation Energies in Organic Compounds*; CRC Press: New York, 2003.
- [52] Dumler, R., Thoma, H., Lenoir, D., Hutzinger, O. Thermal formation of polybrominated dibenzodioxins (PBDD) and dibenzofurans (PBDF) from bromine containing flame retardants. *Chemosphere* **1989a**, 19, 305-308.
- [53] Dumler, R., Thoma, H., Lenoir, D., Hutzinger, O. PBDF and PBDD from the combustion of bromine containing flame retarded polymers: A survey. *Chemosphere* **1989b**, 19, 2023-2031.
- [54] Sakai, S., Watanabe, J., Honda, Y., Takatsuki, H., Aoki, I., Futamatsu, M., Shiozaki, K. Combustion of brominated flame retardants and behavior of its byproducts. *Chemosphere* **2001**, 42, 519-531.
- [55] Weber, R., Kuch, B. Relevance of BFRs and thermal conditions on the formation pathways of brominated and brominated–chlorinated dibenzodioxins and dibenzofurans. *Environ. Int.* **2003**, 29, 699-710.

CHAPTER 10 CONCLUSION AND RECOMMENDATIONS

Table of Contents

10.1. Conclusion	316
10.2. Recommendations for future work.....	320

10.1. Conclusion

This thesis aimed to investigate the decomposition behaviour of selected BFRs. The main findings comprise: (i) determination of the thermodynamic parameters of BCPhs, (ii) estimation of the photodecomposition properties of major BFRs and BPhs, (iii) identification and quantitation of a number of brominated and non-brominated toxic compounds produced from the thermal breakdown of TBBA, and (v) construction of comprehensive mechanistic corridors for the generation of PXDD/Fs from the coupling reactions of BPhs and CPhs, and for the production of PBDFs and PBDEs from BBz oxidation.

A literature review (Chapter 2) provided a summary of studies on the thermal destruction of BFRs and the subsequent formation of toxic products, most notably PBDD/Fs. It was reported that the degradation of BFRs is controlled by physical processes and chemical reactions. Evaporation contributes significantly to the weight loss of BFRs and their further decomposition. This phenomenon should be taken into account when designing safer operational conditions for recycling BFR-laden materials. The majority of experimental studies of BFR thermal decomposition have focused on two aspects: thermal stability behaviour and qualitative detection of products. Very few studies reported a complete profile of decomposition products under rather limited conditions. The presence of BFRs in polymeric materials significantly impairs their thermodynamic stability. On the other hand, hydrogen and hydrocarbon entities promote BFR decomposition at relatively low temperature (643 – 673 K). Functional groups of specific polymeric resins participate in BFR decomposition; mainly via their reactions with Br atoms, thereby shifting homologue patterns toward lower brominated congeners. The functional groups may act as nucleophilic attacking agents, thus causing a rapid decomposition of brominated epoxy resins. Pyrolysis or incineration of BFR-bearing materials establishes a molecular bromine-rich environment, as evident from pilot-scale plant experiments and thermodynamic models. This partially explains the formation of higher brominated PBDD/Fs in comparison with lower chlorinated PCDD/Fs in thermal systems. In industrial thermal processes, congener distributions of PCDD/Fs are highly consistent among different emission end-points. This is in contrast to PBDD/F profiles which exhibit significant discrepancies. Incomplete combustion, often encountered during uncontrolled incineration of BFRs, promotes formation of PBDD/Fs via a precursor pathway in which

structural moieties of several BFRs and BPhs serve as building blocks. Formation of PBDD/Fs from complete destruction of BFRs follows a *de novo* pathway. In both homogenous and heterogeneous pathways, the source of bromine in PBDD/Fs is chiefly of an organic nature. It follows that heterogeneous bromination pathways are less prevalent than the dominant Deacon reactions and direct-surface chlorination pathways. Nonetheless, the high metallic content in e-waste plays a potent catalysing role in the *de novo* formation of PBDD/Fs.

Chapter 4 investigated the thermochemical parameters of the complete series of halogenated phenols, i.e., BCPs. We found the presence of H atoms in the OH group of BCP molecules oriented towards a C(halogen) atom (*syn*) rather than toward a C(H) site (*anti*) affords slightly more stable isomers. Our calculated O–H and C–O bond lengths of all BCPs varied from 0.961 – 0.966 Å and 1.340 – 1.410 Å, respectively, which are in good agreement with theoretical predictions for corresponding BPhs and CPhs. The degree of halogenation induces a minimal effect on the thermodynamic properties among the isomers in each homologue group. However, the patterns and degrees of halogenation provoke a fairly slight variation in O–H BDHs. Values of pK_a strongly depend on the degree of bromination and chlorination on the phenol ring (i.e., large numbers of halogen substituents on a phenol ring induces stronger acidity).

In Chapter 5, we presented photodecomposition characteristics for all brominated congeners of phenols. Our computed bond lengths, in S_0 and S_1 states, demonstrate that, the extent of elongation of C–Br bonds in brominated aromatics is sensitive to position, and follows a sequence of *ortho* > *meta* > *para* sites. The E^{H-L} value decreases linearly with increasing numbers of bromine substituents, and higher brominated congeners are more liable to undergo excitation processes. Higher values of E^{H-L} imply greater thermodynamic stability and, hence, lower $\Delta_f G_{298}^0$ values. The values of q_{Br} on the most photoreactive Br atoms increase with the degree of bromination. Spectral patterns reveal that as the degree of bromination increases, peaks of absorption spectra are red-shifted toward wavelengths near 300 nm (for pentabrominated phenol). The photoreactivity of BPhs rises with the degree of bromination. Overall, in the absence of photocatalysts, BPh isomers are unlikely to absorb a photon in the visible or near-UV wavelengths. Photodegradation of BPhs requires a deep UV environment.

Chapter 6 reported the geometric/electronic properties of major BFRs with regard to photolysis. We estimated C-Br bond elongations upon the $S_0 \rightarrow S_1$ transition. The bromine atom attached to an *ortho* position in 2,3,4,5-TBP, TBBA (with respect to the hydroxyl group) and BTBPE (in reference to C-O linkage) bears the highest positive atomic charge. This suggests that these positions undergo reductive debromination reactions to produce lower brominated molecules. Compounds with the highest degree of bromination entail lower values of E^{H-L} and, hence, necessitate lower excitation energies for excited state transitions. They exhibit a red shift of their maximum absorbance peaks in the UV-Vis spectrum. Analysis of the frontier molecular orbitals indicates that the excited title BFRs proceed via either $\pi\pi^*$ or $\pi\sigma^*/n\sigma^*$ electronic transitions. We did not observe any significant variation in geometrical properties for non-brominated aromatic compounds. Furthermore, the non-brominated aromatic hydrocarbons displayed higher E^{H-L} excitation energies and maximum absorption peaks at shorter wavelengths, indicating their relative stability against photodecomposition in both gaseous and aqueous media.

The investigation of the thermal decomposition of TBBA in the gas phase (Chapter 7) identified major species formed in a quartz reactor at temperatures of 673 – 1123 K with a residence time of 2 s. Results concluded that the thermal breakdown of gaseous TBBA initiates at 723 K and undergoes complete pyrolysis, generating various by-products. HBr, mono-tribromobisphenols, benzene, phenol, mono-tribrominated congeners of phenol and benzene, brominated and non-brominated congeners of alkylated benzene, brominated and non-brominated PAHs, benzofuran, bromobenzofuran, dibenzofuran, 3,5-dibromo-4-hydroxybenzaldehyde, biphenyl and biphenylene appeared as decomposition products. Quantum chemical calculations suggest that, the degradation of TBBA commences with the abstraction of bromine (in the form of HBr) producing di-tribromobisphenol A. The fission of isopropylidene linkages in TBBA generates appreciable quantities of di-tribromophenols and alkylated bromophenols. The occurrence of an *ipso*-hydrogen addition results in the facile displacement of OH groups in phenolic moieties and yields brominated and alkylated benzenes. At high temperatures, most of the brominated species transform into non-brominated moieties.

In Chapter 8, we established a comprehensive mechanism for the formation of PXDD/Fs from the reactions of 2-BPhxy and 2-CPhxy radicals. As 2-BPh and 2-CPh molecules exhibit very similar O-H bond dissociation enthalpies (i.e., 361.2 kJ mol⁻¹ and 359.4 kJ

mol⁻¹), it was predicted that their corresponding radicals (2-BPhxy and 2-CPhxy) would appear in the same temperature window via unimolecular or bimolecular reactions. The coupling of 2-BPhxy and 2-CPhxy radicals produced pre-intermediates of PXDD/Fs without encountering an intrinsic reaction barrier, owing to the large electron density accumulated at phenoxy O and *ortho* C sites. Formation of pre-PXDD and pre-PBDF structures evolved 129.0 – 135.5 kJ and 92.6 – 106.3 kJ reaction enthalpies, respectively. The dioxin-type species arise either (i) in a one-step process (ring closure accompanied by an intramolecular displacement of a halogen atom) generating DD, 1-MCDD and 1-MBDD, or (ii) in a two-step process (cyclisation of phenoxy oxygen atom towards an *ortho* C(H) position of the other phenyl ring, then self-ejection of out-of-plane H atoms from the intermediate structure) yielding 1-MBDD, 1-MCDD and 1-B,6-CDD. The formation of furan adducts follows the subsequent reactions: (i) facile abstraction of an H atom from the C-C linkage by an H or OH radical, (ii) a tautomerisation process from keto-keto to keto-enol structures, (iii) a ring closure reaction of intermediate species, and (iv) removal of OH moieties for pre-PXDF intermediates.

Finally, Chapter 9 discussed condensation reactions of MBBz and BPhxy radicals that produce pre-intermediate structures of PBDFs and PBDEs. In our study, we first analysed the formation of BPhxy radicals from MBBz molecules. We observed that production of BPhxy radicals proceeds by the abstraction of H atoms from *ortho*, *meta* and *para* sites of MBBz, with Br atoms generating bromophenyl adducts. The bromophenyl structures transform into bromophenylperoxy radicals by the addition of oxygen to the vacant radical site of bromophenyl. Finally, the fission of O–O bonds (all reactions are endothermic except the addition of oxygen) in bromophenylperoxy produces BPhxy radicals. Coupling of MBBz and 2-BPhxy radicals evolves pre-PBDF and pre-PBDE structures. In pre-PBDF intermediates (*o*-C/*o*-C), the phenoxy oxygen exists in an *ortho* position relative to the C–C bridge, acting as intermediates to DF and MBDF isomers. Kinetic analysis indicates that the O/*o*-C pre-PBDEs/pre-PBDFs form upon bimolecular pairing of the phenoxy O atoms in 2-BPhxy radicals at three C(H) sites in the MBBz molecule. These adducts self-eject the out-of-plane H atoms to produce PBDEs, rather than undergo a three-step mechanism forming PBDFs. Our calculations predict that, 4-MBDF appears as the viable product of real combustion.

10.2. Recommendations for future work

Despite the great deal of experimental and theoretical work (including results reported in this thesis) that has contributed to a better understanding of the combustion chemistry of BFRs, there are still many unanswered and intriguing questions. In Table 10.1, we highlight selected research gaps and suggested actions for addressing them.

Table 10.1. Knowledge gaps and proposed corrective actions.

Knowledge gap	Proposed action
PBDD/Fs formation	Identify and quantitate PBDD/F congeners (using soxhlet extraction followed by column clean-up and sample preparation for analysis) evolved from the thermal breakdown of major BFRs in gas phase experiments.
Effectiveness of gaseous bromination routes	Investigate the pure gas phase decomposition of benzene under pyrolytic and oxidative environments enriched with Br ₂ and /or HBr. Yields of brominated benzenes and major brominated products will indicate the efficiency of gas phase routes as bromination pathways in their own right, without assistance from surface-catalysed reactions.
Decomposition behaviour of nearly all NBFRs is unknown	Carry out TGA-based experiments on major types of NBFRs.
Decomposition of BFRs in the gas phase	Most studies on the decomposition of BFRs target their decomposition in the condensed medium (apart from TBBA that was covered in the current thesis). To address gas phase decomposition, samples of selected BFRs must be evaporated and introduced into a reactor. Then, samples must be collected and prepared for instrumental analysis.

CHAPTER 10 Conclusion and Recommendations

Effect of polymeric materials on the decomposition of BFRs under different operational conditions	Apart from TBBA, the influence of polymeric resins on the decomposition behaviour of BFRs has not been thoroughly investigated.
Studies on BFR decomposition have provided only qualitative or semi-qualitative product profiles	Provide detailed quantitative measurements of product profiles from the oxidation of neat prominent BFRs.
The contribution of precursor and de novo routes in the formation of PBDD/Fs is unknown	Decomposition of several BFRs (such as HBCD) does not form bromophenols in appreciable amounts, thus, the formation of PBDD/Fs from these BFRs most likely originates from a de novo pathway. Careful temperature monitoring of the formation of PBDD/Fs from TBBA and PBDEs will reveal the contributions of precursor and de novo routes. The former is expected to occur at low temperatures prior to the complete destruction of BFRs.
Kinetic models are not available for the decomposition of most BFRs	Theoretical modelling could readily predict reaction rate constants and formulate mechanistic decomposition steps.
Emissions from BFR-laden materials under fire conditions	Lab-scale combustion experiments are incapable of simulating the hostile combustion conditions of real fires (inadequate oxygen content, presence of metals, random mixing of a large number of reactants, unpredictable pressure and temperature profiles). There is a need to carry out cone-calorimeter and large-scale (both under and over-ventilated) experiments to simulate real fire conditions with BFR-treated materials, and to measure simultaneously the emission of brominated pollutants.

Regarding the fate of BFRs emitted to the environment, our work has indicated unequivocally that certain C-Br bonds are significantly weakened. This will be

instrumental in reporting kinetic rates of debromination processes. It will allow the deduction of photodecay rates for brominated pollutants. Future work along this aspect may also focus on:

1. In a real environment, it has been reported that soil somehow mediates the photodecomposition processes of halogenated pollutants. However, the exact mechanisms are unknown.
2. Several composite materials (such as reduced graphene oxide dropped on transitional metal oxides) display remarkable photocatalytic activity. Thus, it is very interesting to investigate how these materials catalyse the photodegradation of BFRs. This will help to fine tune their properties toward higher removal rates of halogenated molecules.

APPENDICES

APPENDIX A (CHAPTER 3)**Table 3.S1.** Career gas nitrogen flow rates as a function of reaction temperature set in K.

Temperature (K)	Flow rate (mL/min)
573	360.6
623	331.7
673	307.0
723	285.8
773	267.3
823	251.1
873	236.7
923	223.9
973	212.4
1023	202.0
1073	192.6
1123	184.0
1173	176.2
1223	169.0
1273	162.3

APPENDIX C (CHAPTER 6)

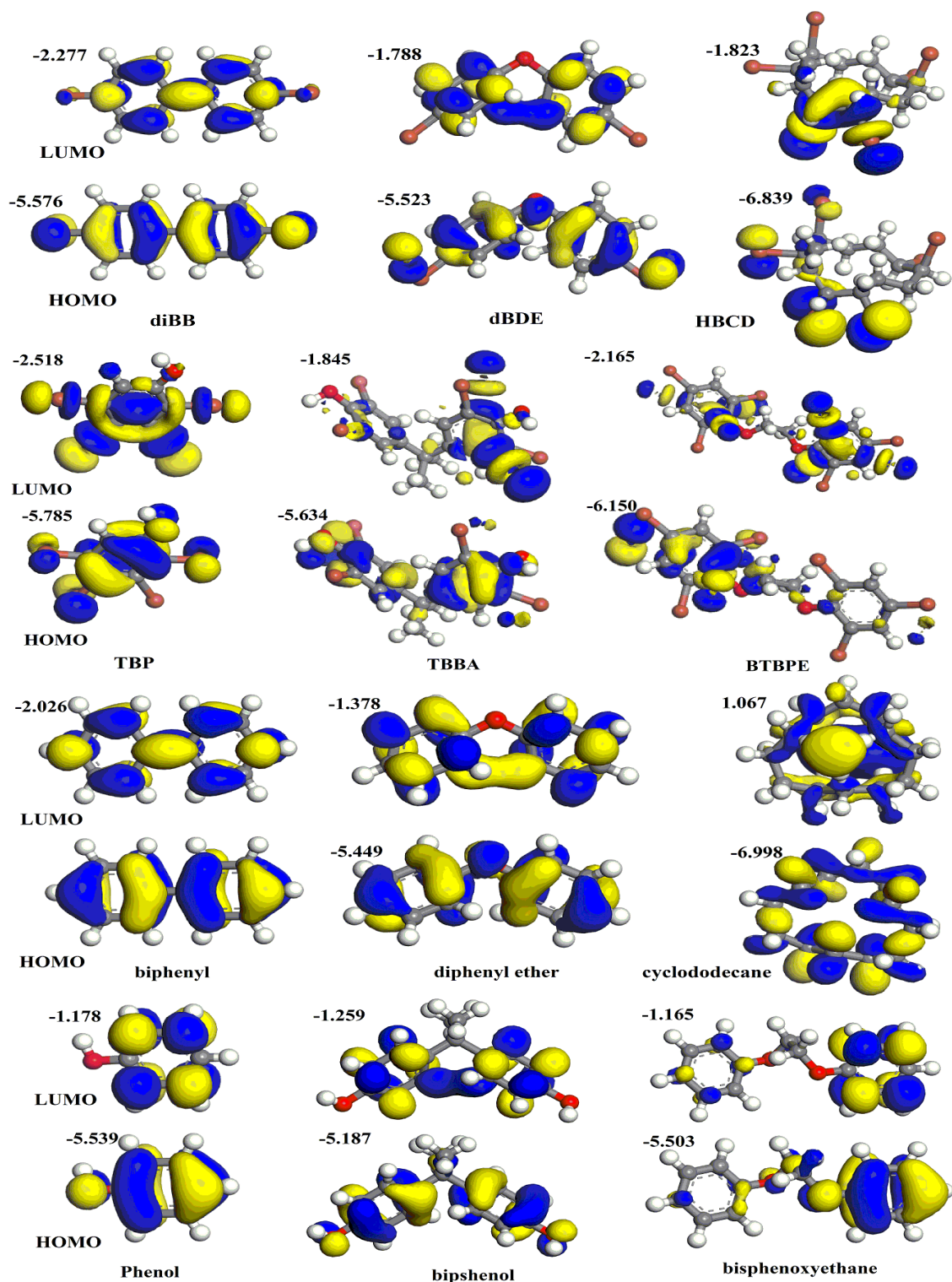


Figure 6.S1. The frontier molecular orbital energies (in eV) calculated using TDDFT method for selected BFRs and their non-brominated molecules in gas phase.

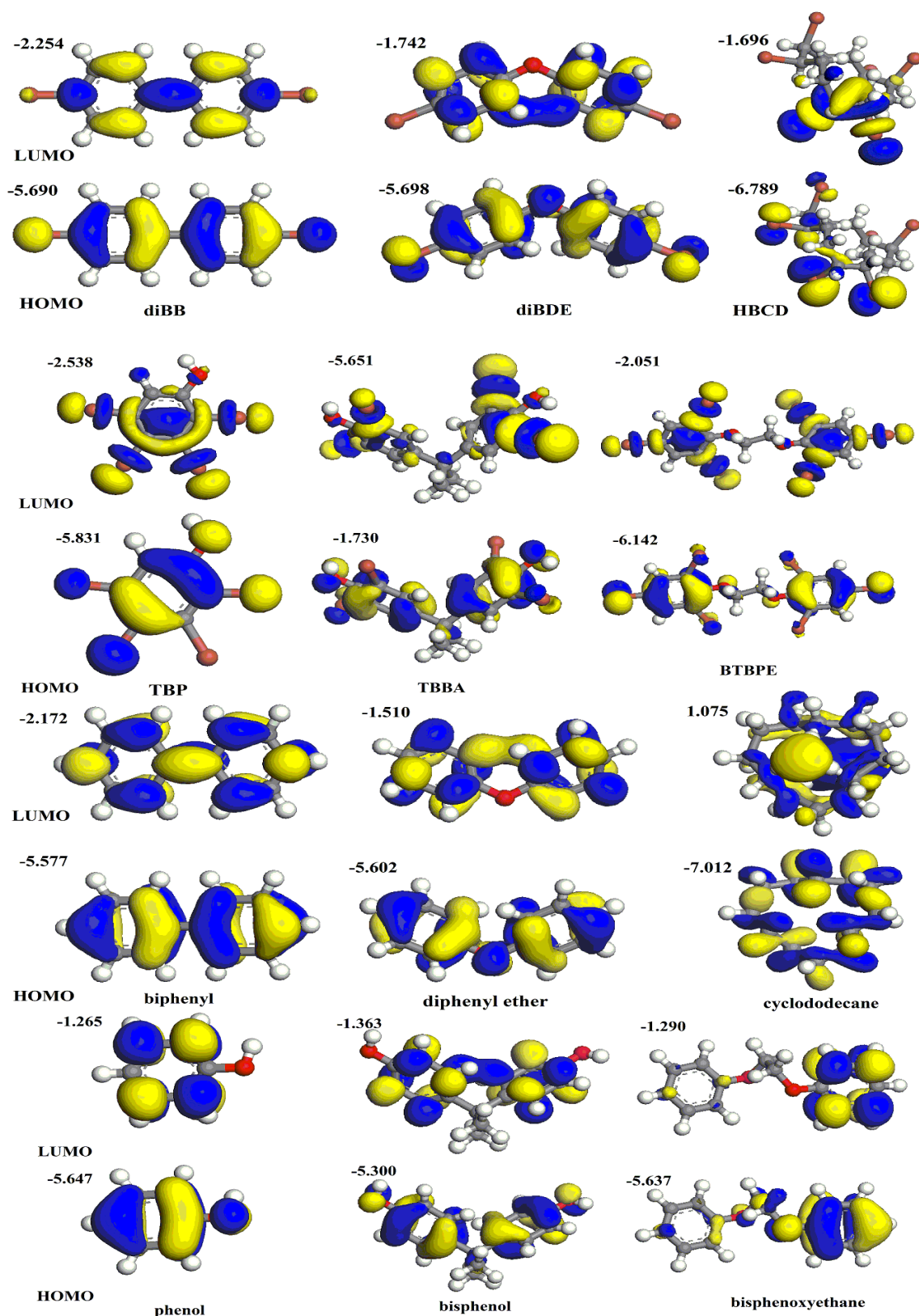


Figure 6.S2. The frontier molecular orbital energies (in eV) calculated using TDDFT method for selected BFRs and their non-brominated molecules in aqueous phase.

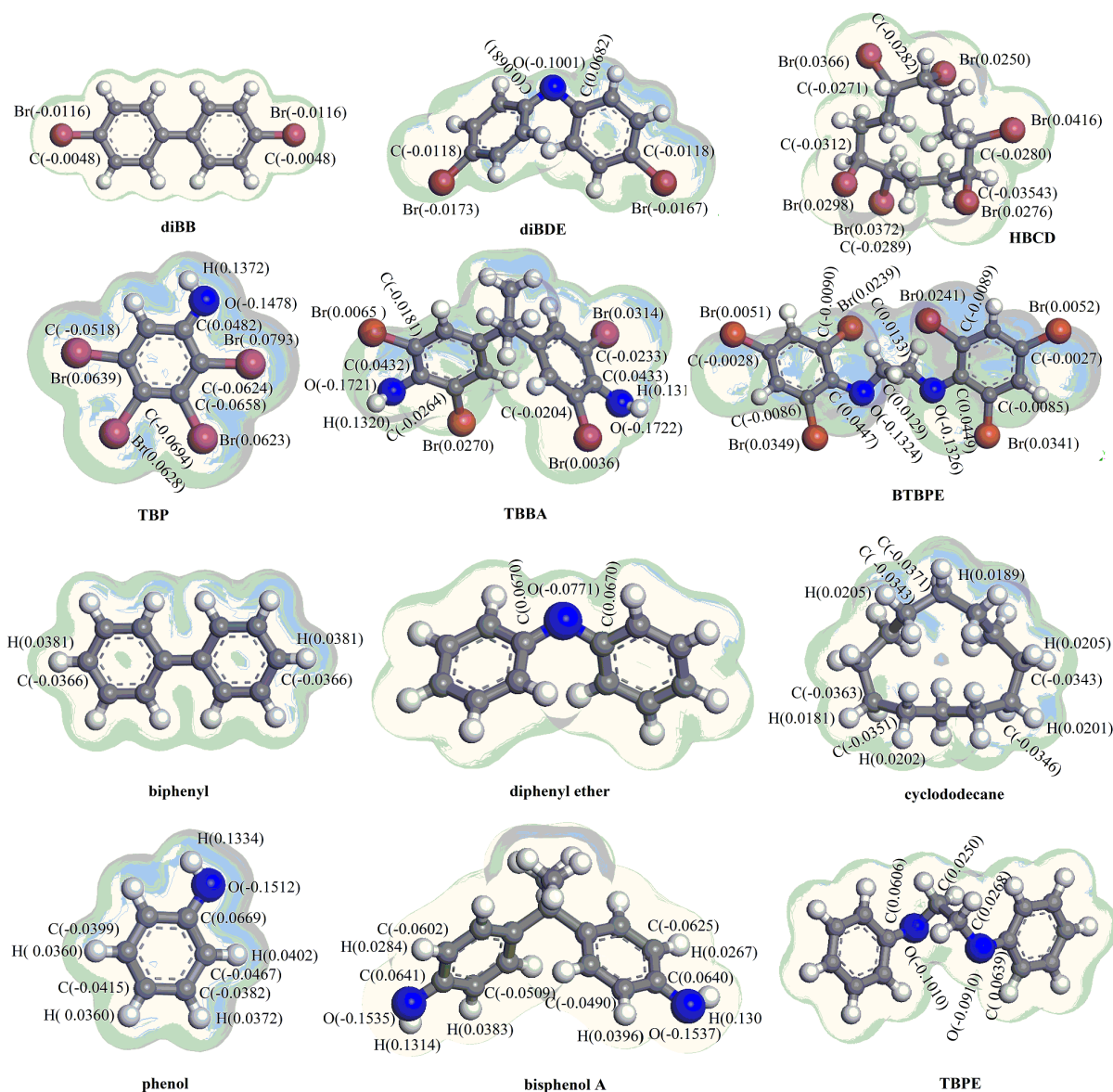


Figure 6.S3. Optimised geometries with electron density distribution for selected BFRs and their non-brominated isomers with net atomic charge presented on selected atoms.

APPENDIX D (CHAPTER 7)

1. Analysis of neat TBBA

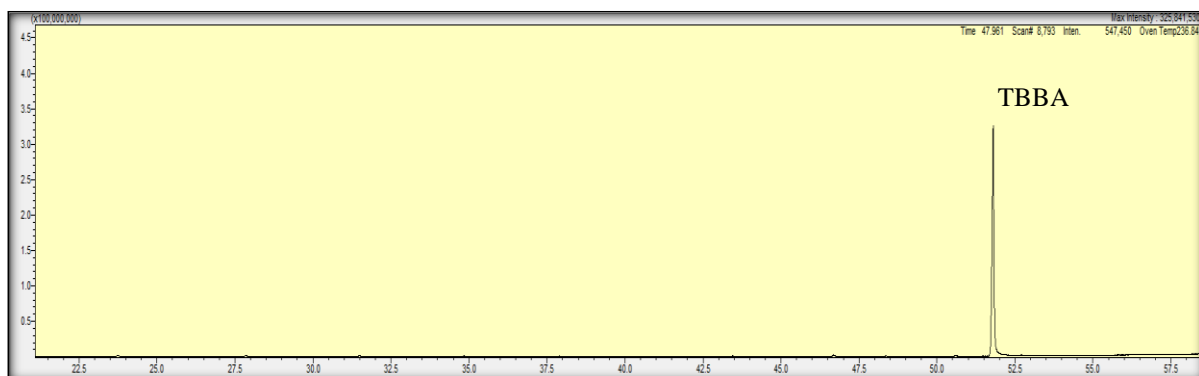
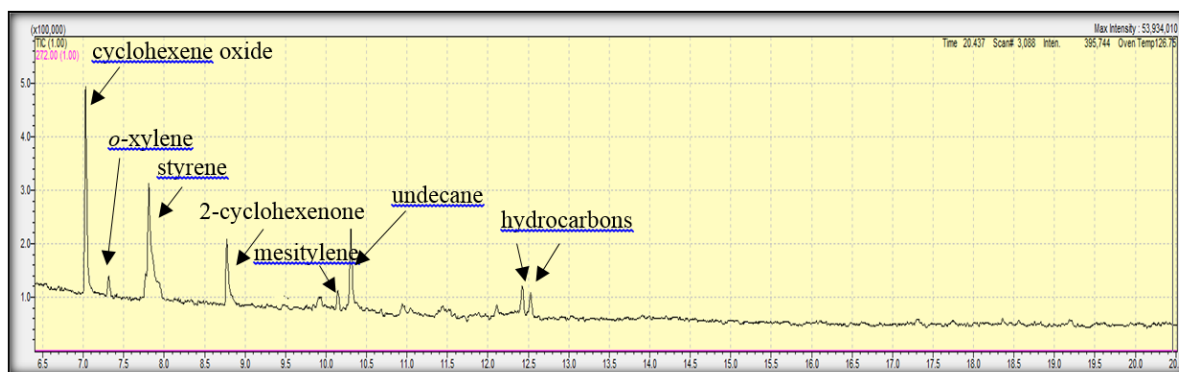


Figure 7.S1. Ion chromatogram of neat TBBA.

2. Analysis of impurities identified in TBBA sample



Total ion current (TIC)

Ion source temperature: 473 K

Transfer line: 523 K

Injector: 523 K

Temperature program: 303 K hold for 3 min, 8 K/min to 373 K hold for 2 min, and 4 K/min to 573 K hold for 2 min

Figure 7.S2. TIC chromatogram of impurities present in TBBA identified by comparing their mass spectra with the spectra available in the NIST library.

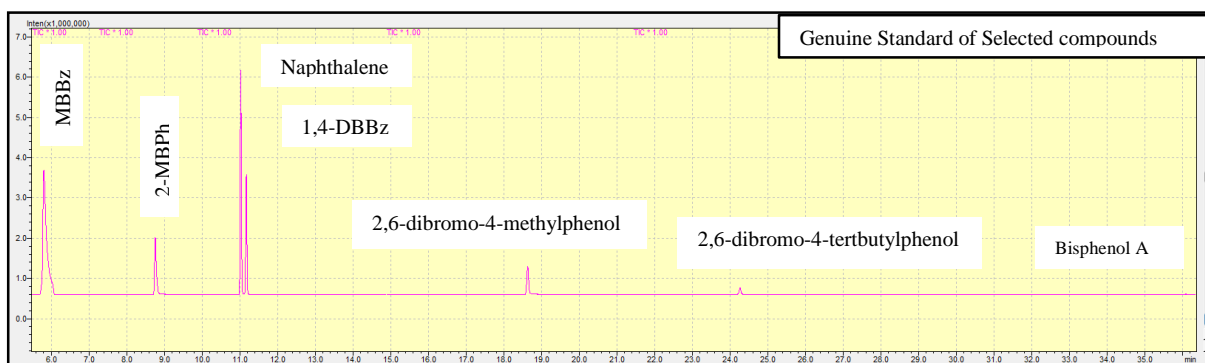
Table 7.S1. Impurities (in ppm) encompass in high purity quartz reactor.

Al	B	As	Ca	Cr	Cd	Cu	K	Fe	Li	Mg	Na	Mn	Ni	P	Sb	Zr	Ti	OH
14	<0.2	<0.002	0.4	<0.05	<0.01	<0.05	0.6	0.2	0.6	0.1	0.7	<0.05	<0.1	<0.2	<0.003	0.8	1.1	<5

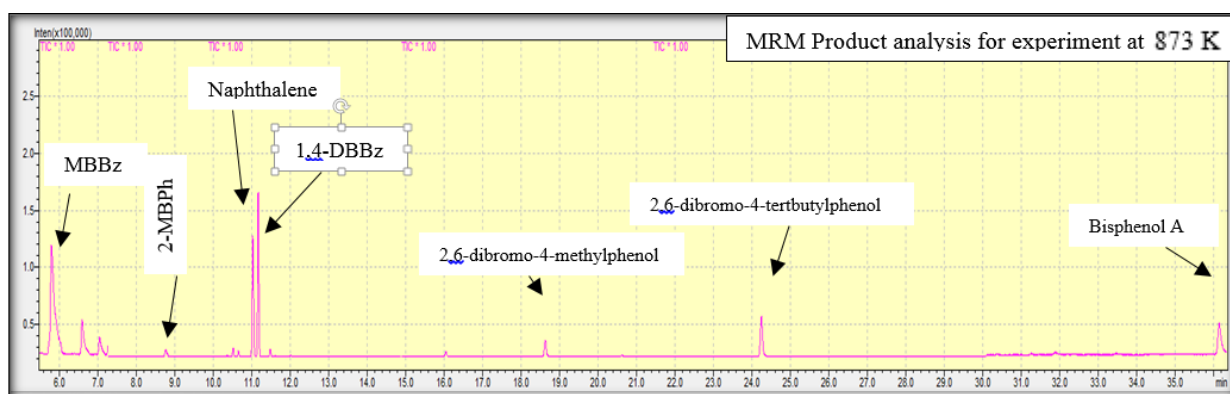
3. Method details and MRM chromatograms for the experiments conducted at 873 K.

Table 7.S2. Detail of the MRM acquisition mode.

Compound Name	Start time (min)	End time (min)	Ch1 m/z	Ch1 CE	Ch2 m/z	Ch2 CE
MBBz	5.50	7.28	156>77.1	21.0	77>51	18.0
2-MBPh	7.28	9.89	172>65.1	21.0	174>65	21.0
Naphthalene	9.89	14.90	128>102	21.0	128>78	24.0
1,4-DBBz	9.89	14.90	236>157	27.0	236>154	27.0
2,6-dibromo-4-methylphenol	14.90	21.45	185>77.1	15.0	187>77	18.0
2,6-dibromo-4-tertbutylphenol	21.45	30.16	295>214	15.0	293>219	12.0
Bisphenol A	30.16	40.0	213>119	9.0	119>91.1	9.0



(a)

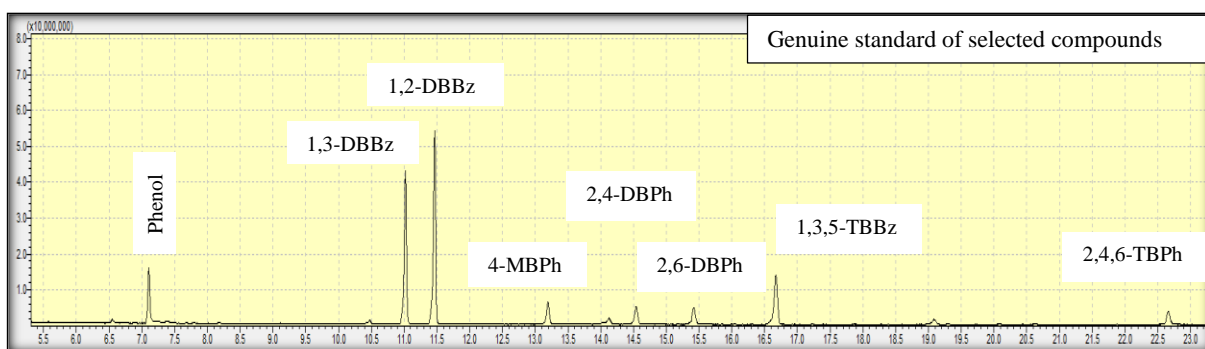


(b)

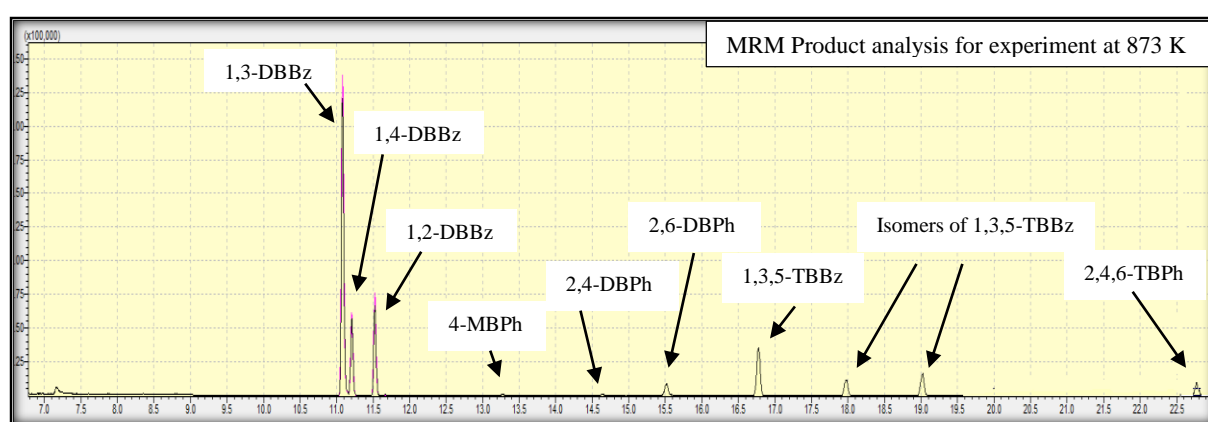
Figure 7.S3. MRM chromatogram of selected compounds (a) genuine standards (b) products generated at reaction temperature of 873 K.

Table 7.S3. Detail of the MRM acquisition mode.

Compound Name	Start time (min)	End time (min)	Ch1 m/z	Ch1 CE	Ch2 m/z	Ch2 CE	Ch3 m/z	Ch3 CE
Phenol	6.79	9.04	94>66.1	9.0	94>55	18.0	94>51	27.0
1,3-DBBz	9.04	12.31	236>155	21.0	236>157	21.0	157>76.1	18.0
1,2-DBBz	9.04	12.31	234>154.9	21.0	236>155	18.0	236>157	18.0
4-MBPh	12.31	13.85	172>65.1	24.0	174>65	24.0	174>93.1	15.0
2,4-DBPh	13.85	14.97	252>63.1	30.0	252>142.9	33.0	252>145	18.0
2,6-DBPh	14.97	16.03	252>63.1	27.0	252>143.1	24.0	252>144.8	27.0
1,3,5-TBBz	16.03	19.65	314>234.8	27.0	316>234.8	24.0	314>232.8	21.0
2,4,6-TBPh	19.65	22.95	330>140.9	27.0	332>142.9	36.0	332>141.1	36.0



(a)

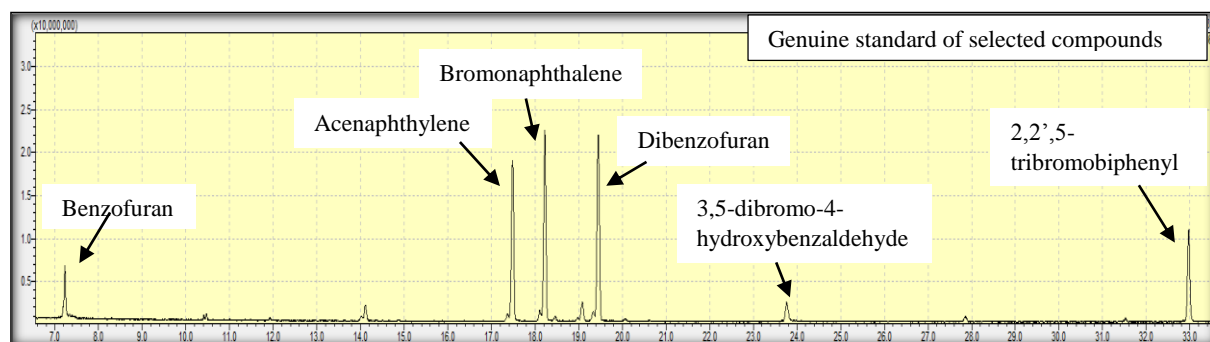


(b)

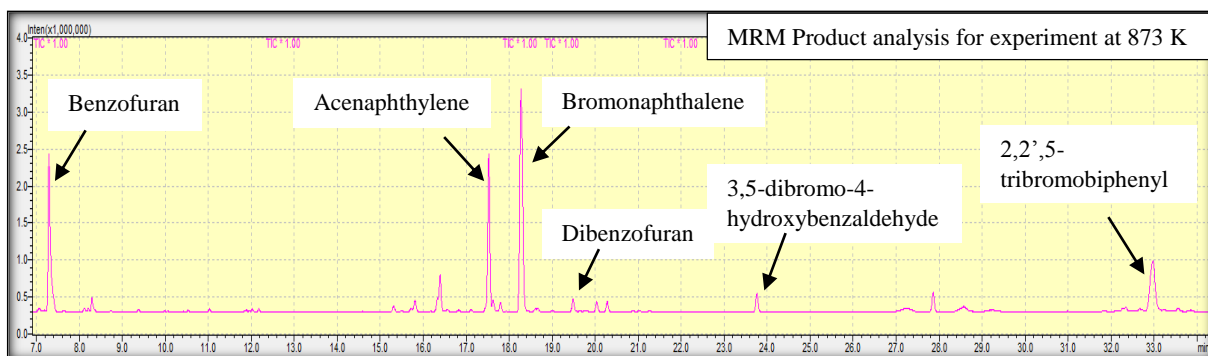
Figure 7.S4. MRM chromatogram of selected compounds (a) genuine standards (b) products generated at reaction temperature of 873 K.

Table 7.S4. Detail of the MRM acquisition mode.

Compound Name	Start time (min)	End time (min)	Ch1 m/z	Ch1 CE	Ch2 m/z	Ch2 CE
Benzofuran	6.93	12.36	118>89.1	21.0	89.00>63.00	21.0
Acenaphthylene	12.36	17.86	152>126	24.0	152.00>150.00	30.0
Bromonaphthalene	17.86	18.84	208>127.1	21.0	206.00>127.10	21.0
Dibenzofuran	18.84	21.60	168>139	24.0	139.00>89.10	21.0
3,5-dibromo-4-hydroxybenzaldehyde	21.60	28.37	355>73.2	12.0	355.00>266.80	18.0
2,2',5-tribromobiphenyl	28.37	34.28	230>151.1	18.0	311.00>231.90	18.0



(a)



(b)

Figure 7.S5. MRM chromatogram of selected compounds (a) genuine standards (b) products generated at reaction temperature of 873 K.

4. Recoveries

We introduced biphenyl-D10 into the solvent trap in the concentration of 2 mm³ prior to the experiment. After a 5 h run, we add benzene-13C (2 mm³) to the sample before its concentration to a final volume of 1 mL in rotary evaporator (4 h run). The concentrated solution is then analysed in GC-QQQMS. The concentration of biphenyl-D10 and benzene-13C in final solution (1 mL) serves to calculate the percentage recovery from (amount = concentration × volume):

$$\% \text{ Recovery} = \left(\frac{\text{amount recovered}}{\text{amount initially present}} \right) \times 100$$

Table 7.S5. Percentage recovery of deuterated biphenyl (D10) and benzene-13C in the thermal decomposition of TBBA.

Temperature (K)	biphenyl-D10 (%)	benzene-13C (%)
673	88.6	99.1
723	87.2	99.3
773	72.5	99.2
823	75.8	98.9
873	94.1	99.1
923	81.2	99.2
973	86.4	99.3
1023	74.1	99.1
1073	85.2	98.7
1123	74.9	98.6

5. Results for blank run

The analysis of product condensate from the experiment performed at 873 K with 0 mg of TBBA input weight (blank) run for 5 h provide the following results for MRM analysis. In TIC chromatogram we detected no VOC and SVOC (signal/noise <3). We estimate the background as based on mass of TBBA fed to a typical experiment:

$$\text{Background} = \frac{\text{(amount of product quantitated in a blank run (in } \mu\text{g))}}{\text{(typical sample input (in g) in an actual experiment)}}$$

$$\begin{aligned} \text{Where the sample input is} &= \text{evaporation rate (in mg min}^{-1}\text{)} \times \text{total run time (in min)} \\ &= 0.06 \times 300 \\ &= 18 \text{ mg} \end{aligned}$$

Table 7.S6. Results of blank experiment conducted at 873 K.

Compound	Blank results (μg)	Background – assuming sample size of 18 mg ($\mu\text{g per g of TBBA}$)
Phenol	0.038	2.1
4-bromophenol	0.029	1.5
2,4-dibromophenol	0.045	2.5
2,6-dibromophenol	0.047	2.5
2,4,6-tribromophenol	0.066	3.5
1,3-dibromobenzene	0.005	0.3
Dibenzofuran	0.030	1.5
Naphthalene	0.016	0.75
Bromonaphthalene	0.026	1.4
3,5-dibromo-4- hydroxybenzaldehyde	0.108	6
2,6-dibromo-4-methylphenol	0.102	5.5


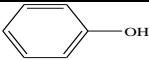
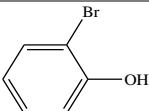
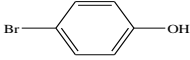
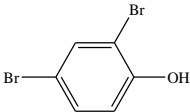
6. Results of replicate experiments

Table 7.S7. The replicates of selected VOCs and SVOCs at important temperatures: *R1* and *R2* denote replicated experiments.

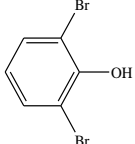
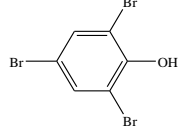
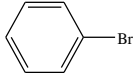
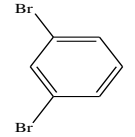
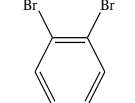
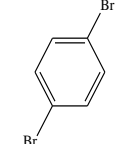
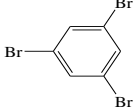
Temperature (K)	873		923		973	
Compounds	Yield (μg of compound per g of sample)					
	<i>R1</i>	<i>R2</i>	<i>R1</i>	<i>R2</i>	<i>R1</i>	<i>R2</i>
Benzene	21	23	32	35	51	48
Phenol	30	34	51	54	53	55
2-bromophenol	37	39	59	54	62	65
4-bromophenol	27	30	49	52	54	53
2,4-dibromophenol	38	44	73	79	71	72
2,6-dibromophenol	175	183	690	698	168	171
2,4,6-tribromophenol	120	130	284	291	238	234
Bromobenzene	19	23	64	69	128	131
1,3-dibromobenzene	7	9	22	29	44	48
1,2-dibromobenzene	1.5	2	14	17	25	28
1,4-dibromobenzene	3	5	5	5	7	8
1,3,5-tribromobenzene	14	17	23	25	29	30
Benzofuran	80	92	490	499	1530	1541
Dibenzofuran	32	39	62	68	95	99
Naphthalene	27	30	62	70	199	187
Bromonaphthalene	39	44	92	85	267	270
Acenaphthylene	9	12	81	87	468	474
2,6-dibromo-4-methylphenol	450	460	162	169	240	249
2,6-dibromo-4-tertbutylphenol	208	220	204	210	98	105
3,5-dibromo-4-hydroxybenzaldehyde	1111	1170	1200	1230	330	321
2,2',5-tribromobiphenyl	48	53	75	79	340	349
Bisphenol	684	690	490	499	520	509

7. Yield of products of gas phase pyrolysis of TBBA estimated using MRM acquisition mode

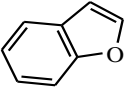
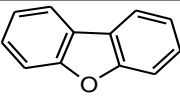
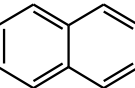
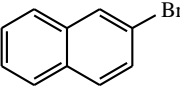
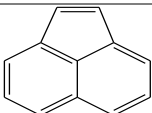
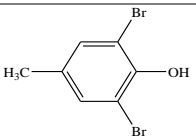
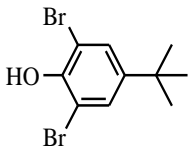
Table 7.S8. Yields of VOCs and SVOCs (in $\mu\text{g (g TBBA)}^{-1}$) measured on GC-QQMS operated in MRM mode as a function of temperature. During the analyses, we used three dominant ions m/z ratios and their relative abundance to identify the species, whereas, quantitation involved the most abundant/dominant ions (peak area) listed in the table.

Species	Elution time (min)	Structures	Ions (m/z) with relative abundance	Temperature (K)									
				723	773	823	873	923	973	1023	1073	1123	
1 Benzene	0.92		78(100); 77(26); 52(17)	-	0.5	13	21	32	51	60	34	24	
2 Phenol	7.08		94(100); 66(39); 65(27)	-	-	16	30	51	53	38	14	3	
3 2-bromophenol	8.78		172(100); 174(96); 65(72)	-	-	16	37	59	62	45	13	2	
4 4-bromophenol	13.17		172(100); 65(97); 93(87)	-	-	17	27	49	54	38	12	-	
5 2,4-dibromophenol	14.53		252(100); 63(56); 250(52)	-	-	22	38	73	71	46	12	-	

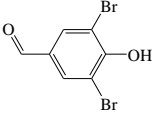
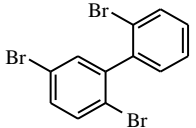
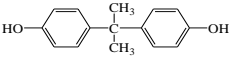
APPENDIX D Chapter 7

6	2,6-dibromophenol	15.41		252(100); 63(56); 250(53)	6	32	113	175	690	168	111	95	23
7	2,4,6-tribromophenol	22.65		330(100); 332(98); 328(34)	2	27	90	120	284	238	104	6	21
8	Bromobenzene	5.28		77(100); 156(77); 158(74)	-	2	13	19	64	128	100	87	13
9	1,3-dibromobenzene	11.00		236(100); 155(77); 157(75)	-	1	2	7	22	44	28	8	4
10	1,2-dibromobenzene	11.45		236(100); 157(74); 155(77)	-	0.3	1	1.5	14	25	15	5	2
11	1,4-dibromobenzene	11.20		236(100); 155 (57); 234(56)	-	0.5	1	3	5	7	4	2.7	2
12	1,3,5-tribromobenzene	16.65		314(100); 74(62); 75(48)	-	0.5	10	14	23	29	10	5	2
13	Isomer of 1,3,5-tribromobenzene	17.87	N.A	314(100); 74(62); 75(48)	-	0.3	1	2	2.5	6	2	1.8	1

APPENDIX D Chapter 7

14	Isomer of 1,3,5-tribromobenzene	18.92	N.A	314(100); 74(62); 75(48)	-	0.5	1	1.5	2.5	5	2	1.5	1
15	Benzofuran	7.23		118(100); 89 (86); 90(80)	-	5	28	80	490	153	137	144	120
16	Dibenzofuran	19.44		139(100); 169(99); 168(95)	-	2	22	32	62	95	82	60	21
17	Naphthalene	11.03		128(100); 129(39); 127(28)	1	2	21	27	62	199	276	450	322
18	2-Bromonaphthalene	18.22		127(100); 206 (96); 208(96)	0.5	2	24	39	92	267	403	400	178
19	Acenaphthylene	17.48		152(100); 151 (81); 150(77)	-	2	4	9	81	217	468	97	-
20	2,6-dibromo-4-methylphenol	18.60		185(100); 187 (94); 266(87)	7	32	364	450	162	184	240	310	-
21	2,6-dibromo-4-tertbutylphenol	24.30		293(100); 291(52); 295(50)	10	42	174	208	204	98	105	19	-

APPENDIX D Chapter 7


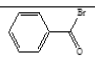
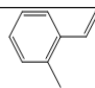

22	3,5-dibromo-4-hydroxybenzaldehyde	23.75		266(100); 280 (73); 281(61)	11	40	370	111	120	330	240	318	208
23	Isomer of 3,5-dibromo-4-hydroxybenzaldehyde	27.2	N.A	266(100); 280 (73); 281(61)	4	14	130	170	76	65	82	98	44
24	Isomer of 3,5-dibromo-4-hydroxybenzaldehyde	27.8	N.A	266(100); 280 (73); 281(61)	6	18	200	290	220	240	302	295	130
25	2,2',5-tribromobiphenyl	32.96		311(100); 230 (92); 232(91)	-	22	27	48	75	340	26	18	-
26	Bisphenol A	36.2		213(100); 119(38); 91(22)	2	24	690	684	490	520	420	464	-

Species quantitation in Table 7.S9 involved injecting genuine standards

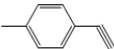
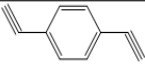
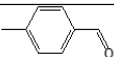
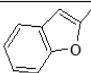
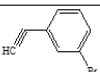
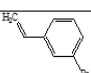
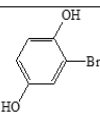
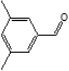
(-): not detected

8. Peak areas of products of gas phase pyrolysis of TBBA estimated using TIC mode

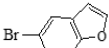
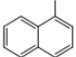
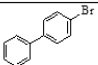
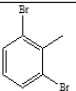
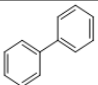
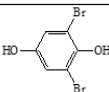
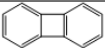
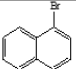
Table 7.S9. Peak areas of VOCs and SVOCs estimated in GC-QQQMS operated in TIC modes as a function of temperature. The identification of each compound is performed by comparing their mass spectra with NIST library database or the mass spectra available in literature.

Products	Elution time (min)	Structures	Ion (m/z)	Temperature(K)								
				723	773	823	873	923	973	1023	1073	1123
1 Phenylethyne ¹	4.6		102(100);76(26);50(11)	-	-	-	-	-	247369	9845269	14521169	1330209
2 Benzoyl bromide ¹	6.65		105(100);77(67);51(23)	-	99709	247369	75098	50489	-	-	-	-
3 1-ethenyl-2-methylbenzene ¹	7.4		117(100); 118(81);115(39)	-	-	-	-	764179	296589	188139	75021	50489
4 1-bromo-4-methylbenzene ¹	8.12		91(100);65(17);170(8)	-	-	-	25879	222759	246967	267389	246489	198431

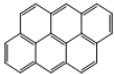
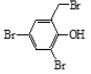
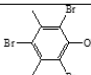
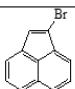
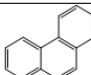
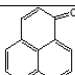
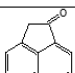
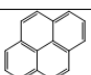
APPENDIX D Chapter 7

5	1-ethynyl-4-methylbenzene ¹	8.3		115(100);116(69);89(8)	-	-	-	-	345909	246967	1697789	2304709	739569
6	1,4-diethynylbenzene ¹	8.9		126(100);76(10);74(9)	-	-	-	-	-	1084109	1808241	1417639	1407521
7	Methylbenzaldehyde ¹	9.23		91(100);119(85);120(70)	-	364514	99709	50488	25879	-	-	-	-
8	Methylbenzofuran ¹	9.6		131(100);132(97);104(25)	-	13573	936449	493469	395029	222759	360418	75018	-
9	1-bromo-3-ethynyl benzene ¹	10.05		101(100);180(82);182(80)	-	-	-	25879	1576309	911839	1501689	1500111	312199
10	1-Bromo-3-ethynylbenzene ¹	10.4		180(100);182(99);101(72)	-	6191	50489	75098	395029	247369	221659	199249	188141
11	2-bromohydroquinone ¹	10.9		188(100);53(96);79(91)	-	148929	247369	518079	591909	237349	230651	-	-
12	3,5-dimethylbenzaldehyde ¹	11.72		133(100);134(67);105(56)	-	8652	25878	33262	173539	247349	74096	-	-

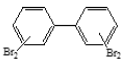
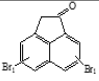
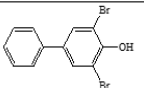
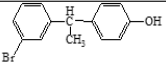
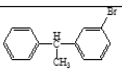
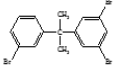
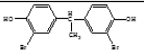
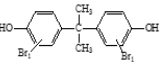
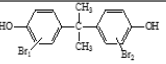
APPENDIX D Chapter 7

13	5-bromobenzofuran ¹	13.05		196(100);198(83);89(82)	-	8651	62794	75099	99701	124319	189047	148729	74086
14	Methylnaphthalene ¹	13.31		142(100);141(90.8);115(46)	-	30801	198149	247369	419631	222754	389021	247265	293589
15	Bromobiphenyl ¹	13.40		152(100);232(90);234(88)	-	-	-	-	-	25879	542191	229801	-
16	1,3-dibromo-2-methylbenzene ¹	13.44		169(100);171(94);115(86)	-	25879	75099	50489	50469	24654	229642	20879	-
17	Biphenyl ¹	15.76		154(100);153(39);152(39)	-	-	-	-	148929	173421	5593671	4950162	17904361
18	2,6-dibromohydroquinone ¹	16.95		268(100);267(61);53(51)	-	3729	11113	13574	123421	75099	-	-	-
19	Biphenylene ¹	17.50		152(100);151(20);150(15)	-	-	-	-	74021	77531	12760684	13405121	5049064
20	1-Bromonaphthalene ¹	18.25		206(100);127(89);208(74)	-	-	275597	551194	1207154	680351	24031464	4307454	3122041

APPENDIX D Chapter 7

21	Anthanthren ¹	19.85		276(100);277(20);274(17)	-	-	-	-	24991	51129	8906424	9548134	1193904
22	2,4-dibromo-6-(bromomethyl)phenol ¹	21.2		264(100);262(56);267(56)	-	99709	3122032	1193904	217759	189321	1092690	-	-
23	3,5-dimethyl-2,4,6-tribromophenol ¹	21.8		279(100);277(52);89(47)	-	8651	551193	1193904	221759	163549	-	-	-
24	Bromoacenaphthylene ¹	25.4		151(100);230(67);232 (63)	-	-	-	-	24876	37289	1836514	2469324	551192
25	Phenanthrene ¹	26.4		178(100);176(23);179(16)	-	-	-	-	13774	24897	2379321	3022033	1193901
26	Phenalenone ¹	29.3		152(100);180(59);151(28)	-	-	-	-	123419	74091	16904364	18992494	-
27	Acenaphthenone ¹	32.2		168(100);140(86);139(76)	-	-	-	-	-	23999	550192	519032	-
28	Pyrene ¹	34.1		202(100);203(17);200(15)	-	-	-	-	-	-	265498	530462	223461

APPENDIX D Chapter 7

29	Tetrabromobiphenyl ¹	32.3		470(100);150(88);468(65)	-	-	-	-	532194	1786612	1092859	541099	-
30	Dibromoacenaphthenone ¹	33.9		326(100);217(51);324(50)	-	-	-	-	22641	25832	863592	1194002	254987
31	3,5-dibromo-[1,1'-biphenyl]-4-ol ¹	35.2		328(100);326(52);139(45)	-	679735	2479323	1193621	552156	993904	-	-	-
32	4-[1-(3-bromophenyl)ethyl]phenol	37.4		N.A	9215414	8549129	10191839	13405394	9536134	8168104	-	-	-
33	1-bromo-3-(1-phenylethyl)benzene	41.8		N.A	8263710	6193909	551193	25651	4207531	-	-	-	-
34	1,3-dibromo-5-[2-(3-bromophenyl)propan-2-yl]benzene	42.5		N.A	8220450	1193803	872549	531254	4950164	-	-	-	-
35	2-bromo-4-[1-(3-bromo-4-hydroxyphenyl)ethyl]phenol	43.0		N.A	8906419	551193	229838	254591	9137	-	-	-	-
36	Dibromobisphenol A ²	44.05		N.A	26457338	26259581	25616872	23974163	13590219	2466424	-	-	-
37	Tribromobisphenol A ²	46.5		N.A	42790313	33972097	32686678	29758564	18832495	6878321	-	-	-

(-): not detected

References:

1. Linstrom, P.J., Mallard, W.G. NIST Chemistry WebBook, NIST Standard Reference Database Number 69, National Institute of Standards and Technology, Gaithersburg, MD, June 2005, <http://webbook.nist.gov/chemistry>.
2. Barontini, F., Cozzani, V., Marsanich, K., Raffa, V., Petarca, L. An experimental investigation of tetrabromobisphenol A decomposition pathways. *J. Anal. Appl. Pyrolysis* **2004**, 72, 41

9. Full scan chromatogram for the product analysis at 973 K

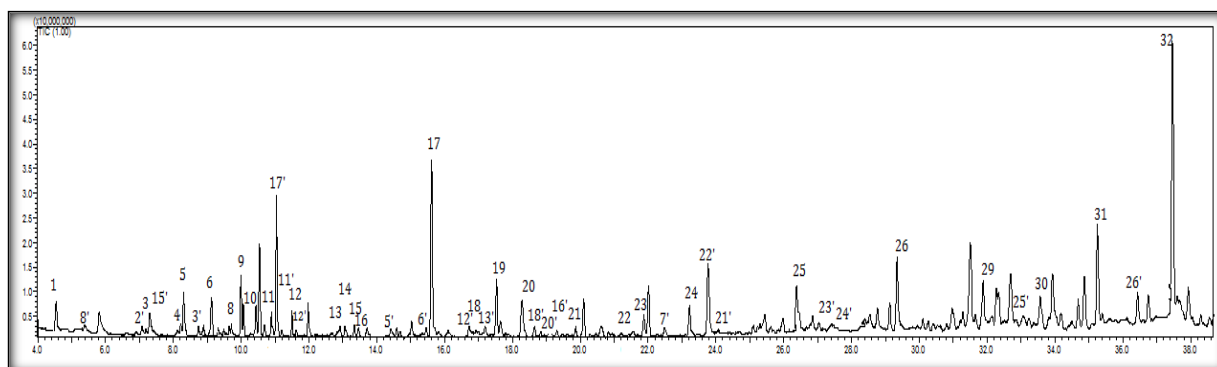


Figure 7.S6. TIC chromatogram for the products identified at 973 K for the retention time between 4.0 min to 38 min given in Table 7.S8 and 7.S9. The species of Table 7.S8 are depicted using X'. X represents the species number in Table 7.S10.